Flow Science Incorporated
723 E. Green Street, Pasadena CA 91101
(626) 304-1134 • Fax (626) 304-9427

WHOLE LAKE MEAD ELCOM-CAEDYM MODEL
ADDITION OF YEARS 2006 AND 2007

Prepared for

National Park Service

and

Clean Water Coalition

and

Southern Nevada Water Authority

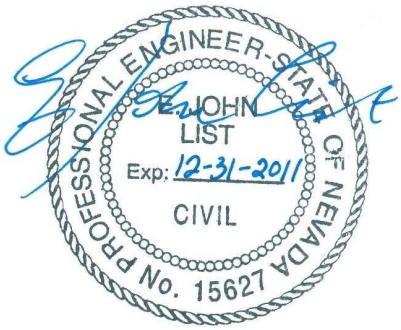

Exp: 6/30/2011

Reviewed By
E.John List, Ph.D., P.E.

Reviewed By
Imad A. Hannoun, Ph.D., P.E.

Prepared By
Al Preston, Ph.D.

FSI V064081 & V084015 Task 1
December 9, 2010

Table of Contents

List of Figures

1 INTRODUCTION

2 DATA ANALYSIS

3 MODELING APPROACH

4 MODEL CALIBRATION RESULTS

APPENDIX A

APPENDIX B

SUMMARY

Flow Science previously developed the three-dimensional ELCOM/CAEDYM "Whole Lake Model", comprising the entire Lake Mead, from Hoover Dam to the mouths of the Muddy, Virgin, and Colorado Rivers. The Whole Lake Model was originally calibrated for years 2000 through 2005. In the present work Flow Science has expanded the calibration period to include years 2006 and 2007. The addition of year 2006 was performed under contract with the National Park Service, while the addition of year 2007 was performed under a separate contract with the CWC, and was sponsored equally by the CWC and SNWA. For the sake of clarity and completeness, the additions of both years are presented in this single report.

The Whole Lake Model uses the ELCOM/CAEDYM computer code. The Estuary Lake and Coastal Ocean Model (ELCOM) is a fully three-dimensional computational fluid dynamics program designed for practical numerical simulation of hydrodynamics and thermodynamics for inland and coastal waters. The Computational Aquatic Ecosystem Dynamics Model (CAEDYM) is a biogeochemical, water quality model that computes interactions between biological organisms and the chemistry of their nutrient cycles. The coupling of these two models allows for an integrated approach with feedback between the biogeochemical and hydrodynamic systems so that a complete representation of all appropriate processes can be included in an analysis. The ELCOM/CAEDYM models were originally developed at the Centre for Water Research (CWR) at the University of Western Australia. The following parameters describing the water quality are included in the model: temperature, conductivity, perchlorate, bromide, chlorophyll *a*, total phosphorus (various species), nitrate, ammonium, total organic carbon, pH, and dissolved oxygen.

MODEL ENHANCEMENTS

During the original 2000 through 2005 modeling a number of possible modeling refinements were identified that could lead to potential enhancements in the model calibration and utility. Many of these enhancements, as well as additional subsequently identified enhancements, have been implemented in the present work. These enhancements are summarized as follows:

- Continuous model simulation over three years (2005 through 2007). This demonstrates the ability of the model to be used for multiple-year simulations, as well as enabling subtleties such as complete or incomplete destratification in each winter to be examined using the model.

- Use of wind data from multiple locations within Lake Mead in 2006 and 2007. This results in a more realistic representation of the on-lake wind patterns and wind speeds and their effect on lake dynamics.

- Use of more accurate Virgin River flow rate due to availability of flow rate data from a location close to Lake Mead from April 2006 onwards. Based upon these new data, additional corrections were also made to the summer flows in years 2000 through 2005.

- Use of spatially variable initial conditions for phosphorus and nitrogen. This enabled different initial concentrations to be specified in Boulder Basin and the Upper Basins, which improved the calibration results.

- Use of spatially-variable sediment oxygen demand. This enabled higher sediment oxygen demand rates to be specified near the inflows, which resulted in a vastly improved DO simulation.

- Re-calibration of phosphorus and algae computational routines. This was motivated by the more recent phosphorus data measured within Lake Mead. Specifically, the USBR samples collected in 2007 were analyzed for phosphorus by the High Sierra Laboratory, using methods with low detection limits. This altered the understanding of the phosphorus processes in the lake, which necessitated a re-calibration.

- Model calibration over an eight-year period. The present calibration spans eight years (2000 through 2007), compared to six years for the previous Whole Lake Model, and four years for the earlier Boulder Basin Model. The longer calibration period provides more confidence in the model.

MODEL CALIBRATION AND VALIDATION

The performance of the ELCOM/CAEDYM model was evaluated by comparing the simulation results with data collected at stations near the CR inflow (CR394.0), near the VR and MR inflows (VR25.1), in Overton Arm (VR12.9/13.0), near the Narrows (CR360.7), near the LVW inflow in the LVB (LVB3.5), in the open water of Boulder Basin (CR346.4), at the SNWA intakes, and at the Hoover Dam outlets. In certain instances, comparisons at additional locations were made in order to illustrate the simulated and measured spatial trends. In general, the model adequately reproduced most of the observed water quality features within the entire lake and provided added insight into lake mixing processes. In the following, a summary of the calibration/validation process is provided.

ELCOM Results

Overall, the results of the ELCOM calibration are summarized as follows:

- ELCOM captures the lake water temperature variation, including stratification and thermocline depth, reasonably well over the eight year model period. Overall, time series comparisons of the simulated and measured data show good agreement at all of the measuring stations.

- ELCOM is able to capture the incomplete lake destratification in the winter of 2006 and the complete destratification in the winter of 2007.

- The intrusion (insertion) depths of all the inflows (i.e., CR, VR, MR and LVW) are generally well predicted, indicating that the simulation is ultimately able to predict the fate of each inflow with regard to their relationship to the epilimnion and hypolimnion.

- The spatial and temporal distributions of conductivity throughout the reservoir are well-predicted by the simulation.

- ELCOM captures the variation of perchlorate and bromide concentrations well. Overall, time series comparisons of the simulated and measured data show good agreement at all of the measuring stations.

CAEDYM Results

The CAEDYM calibration process focused on identifying and reproducing the key water quality characteristics within Lake Mead related to the timing of algal blooms (represented by chlorophyll *a*), nutrient concentrations (phosphorus and nitrogen), TOC concentrations, DO concentrations, and pH.

During the calibration process for the previous 2000 through 2005 model, Dr. David Hamilton, Professor of Biological Sciences at the University of Waikato, New Zealand, and the author of CAEDYM, was consulted to assist and review the model calibration and provide ranges of accepted values of the parameters for Lake Mead. In the present work, the parameters used in the re-calibration of the phosphorus and algae routines were determined to fall within the provided range of accepted values for Lake Mead. Overall, the results of the CAEDYM calibration are summarized as follows:

- The model is able to capture the general temporal trends of algae growth and decay during the growing season. The algal growth in the winters is often under-predicted by the simulation, although the measured chlorophyll *a* concentrations are near the method detection limit and may not be representative of the true (but low) concentrations in the winters.

- The simulated chlorophyll *a* results indicate reasonable agreement when plotted directly against the measured field data. There is considerable data scatter, but much of this can be attributed to substantial variation within the field data.

- The model is able to capture the spatial trends and overall magnitudes of the chlorophyll *a* growing season average. In particular, the large spatial gradients near the LVW and VR, and the differences in concentrations between Boulder Basin and the Upper Basins, are generally well replicated. However, the model overestimates the chlorophyll *a* levels in 2000, and underestimates them in 2001.

- The simulated chlorophyll *a* growing season average indicates good agreement when plotted directly against growing season averages computed directly from the field data. There is substantial scatter between the simulation and field data, which has been quantified as illustrated by error bars. Additionally, the variation among the field data of the different agencies (i.e., USBR, COLV and SNWA), has been quantified and illustrated by error bars. While the simulation error bars are larger than the error bars for the field data, they are of similar magnitude, which indicates that the variation among field data impacts the error of the simulation.

- Due to the difficulty of measuring phosphorus at extremely low concentrations, direct phosphorus concentration comparisons between the data and the model results were difficult. Still, CAEDYM captured the primary characteristics of the spatial variation of phosphorus in the lake, as well as some seasonal trends in the FRP concentrations within the epilimnion.

- The agreement between the simulated and measured NO3 concentrations is good in Boulder Basin. The NO3 simulation was vastly improved in the Upper Basins compared with the previous 2000 through 2005 simulation, as a result of the implementation of spatially variable initial conditions.

- The agreement between the simulated and measured TOC concentrations is reasonable throughout the lake.

- The agreement between the simulated and measured pH is good throughout the lake.

- The agreement between the simulated and measured DO concentrations is good throughout the lake. The DO simulation was vastly improved compared with the previous 2000 through 2005 simulation, as a result of the implementation of spatially-variable sediment oxygen demand.

- The simulation is able to capture the replenishment of the DO in the hypolimnion of Boulder Basin by the CR underflow in winter. This is particularly important in the simulation of the winter of 2006, when the lake did not completely destratify.

Overall, there is good agreement between model results and measured field data. The discrepancies tend to be attributed to difficulties in data sampling, uncertainties in chemical analysis, highly variable biochemical and aquatic processes, and limited model spatial resolution.

LIMNOLOGICAL CONCLUSIONS

Many limnological conclusions may be drawn from the analysis of the gathered field data. The simulation results can complement these conclusions (e.g., through the use of animations) as well as lead to new conclusions and understanding.

Many of the general limnological conclusions that were drawn from the present study were also identified in the previous 2000 through 2005 modeling effort. For completeness these are provided here as follows:

- The LVW, VR and MR flow insertion elevations vary from season to season. Between April and October these inflows generally enter the lake as interflows and travel along the thermocline, where they can be vertically mixed within the epilimnion by strong winds. In winter, these inflows generally enter as underflows that travel along the bottom of the reservoir. In November and March, the density currents are in a transition period and can intrude into both the epilimnion and the hypolimnion.

- The CR inflow is colder and generally tends to insert lower in the water column than the other inflows. However, there are times when it can insert near the surface. When the CR inserts at mid-depths during the stratified period, a "double thermocline" structure near the inflow can result.

- Typically, the LVW inflow has the highest conductivities and constituent concentrations (i.e., bromide, perchlorate, TP, NO3, and TOC), followed by the VR and MR. The CR has the lowest conductivities and constituent concentrations. In particular, the CR inflow FRP concentrations are typically an order of magnitude lower than those for the other inflows.

- During most winters the lake is vertically mixed, although on occasion a weak thermocline may persist at depth in the lake, particularly within Boulder Basin.

- The insertion elevations, and the relative conductivities and constituent concentrations of the inflows, result in spatial distributions of conductivity and constituent concentrations that are generally consistent from year to year. In the winters there are higher conductivities/concentrations in Boulder Basin (and near the LVW in particular) and in the northern half of Overton Arm (near the VR and MR). During the stratified period the higher

conductivities/concentrations remain at these locations, but are also mainly confined to the epilimnion.

- When the lake is stratified persistent winds prevailing from the southeast can drive the warm surface waters to the northwest portions of the lake, resulting in upwellings of cold water on the southeastern shores.

- DO is lower at the lake bottom near each of the inflows (i.e., LVW, CR, VR and MR), most likely as a result of deposition and decay of particulate organic matter.

- Chlorophyll *a* concentrations are generally higher in Boulder Basin than in the Upper Basins.

- Chlorophyll *a* concentrations are generally higher near the inflows, particularly the LVW.

The addition of model years 2006 and 2007, as well as the availability of additional data sources enabled new general limnological conclusions to be drawn. These are summarized here as follows:

- The wind speeds in the Upper Basins are consistently lower than in Boulder Basin.

- The DO in the bottom of Boulder Basin can be directly replenished by inflow from the CR in the winter. This was identified in the measured field data, and highlighted by the simulation through animations. This mechanism of DO replenishment is particularly important in the years that Lake Mead does not completely destratify.

- There is a correlation between the fluorescence measured at the USGS platform in the LVB, and the chlorophyll *a* data measured at Station LVB3.5. However, this correlation seemed to shift in mid-2007. Additional analysis of the data-sets over longer time periods is required.

POSSIBLE FUTURE MODELING REFINEMENTS

The model is generally capable of adequately reproducing the water quality in the lake, and a number of modeling refinements have been implemented since the original 2000 through 2005 model. Nevertheless, additional refinements have been identified that could further improve the calibration and model utility.

The possible modeling refinements are identified as follows:

1. Continuous multiple year simulations over the *entire* modeling period. At present the model is initialized in year 2000, and again in years 2001, 2002, 2004 and 2005. Ideally the model would be initialized only once in year 2000, and then run continuously through all simulation years.

2. Improved treatment of particulate phosphorus settling in CAEDYM. Measurements of the particle size distributions of the inflows would be useful to aid in the understanding of particulate settling within Lake Mead, and to enable modifications to CAEDYM in order to improve the settling of particulate phosphorus.

3. Finer grids (e.g., CAEDYM on 300-m grid, or increased vertical resolution) as computational power increases. This would improve the resolution near to the inflows.

4. Statistical metrics of "goodness-of-fit" between the simulation results and measured field data. The error analysis of the model error in chlorophyll *a* concentrations needs to be extended to include other parameters of interest.

In summary, the ELCOM/CAEDYM modeling package has been shown to be a powerful tool that can provide an accurate analysis of the hydrodynamics and water quality within Lake Mead. Many model enhancements have been made since the original 2000 through 2005 modeling, including the addition of years 2006 and 2007. Despite the fact that, as noted, there are some improvements that can further enhance the model's utility, in its current form it still provides the capability of comprehensive resolution of spatial and temporal predictions of the lake response to future changes in inputs or operations.

1 INTRODUCTION

1.1 PROJECT SETTING

Lake Mead was formed in 1935 by the construction of Hoover Dam on the Colorado River. Hoover Dam is located approximately 25 miles southeast of the City of Las Vegas, Nevada. The lake extends upstream along approximately 60 miles of the Colorado River and straddles the States of Nevada and Arizona. The lake comprises four large basins: Boulder, Virgin, Temple, and Gregg. At full capacity, the lake contains 26 million acre-ft (28 billion cubic meters) of water and has a surface area of 163,000 acres (200 square kilometers). The two principal outflows include releases through Hoover Dam to supply the lower Colorado River and withdrawals by the Southern Nevada Water Authority (SNWA) from the east side of Saddle Island in Boulder Basin to supply municipal, irrigation, and industrial demand in the Las Vegas metropolitan area. The major inflows to Lake Mead include the Colorado River (CR) at the upstream (eastern) end, the Muddy River (MR) and Virgin River (VR) in the Overton Arm (northern boundary), and the Las Vegas Wash (LVW) in the northwestern corner of Boulder Basin (**Figure 1.1**).

Historically, LVW was an ephemeral stream that reached the Colorado River system only as a result of large storms producing significant runoff events. However, effluent from the City of Las Vegas (COLV), the City of Henderson (COH), and the Clark County Water Reclamation District (CCWRD) wastewater treatment plants (WWTPs) is now discharged into Boulder Basin via the LVW.

1.2 PROJECT HISTORY

In the 1990s population growth within the Las Vegas Valley and the associated increase in effluent flow rates were identified as likely to result in decreasing water quality in Boulder Basin if the effluent continued to be discharged as a surface flow via the LVW. Thus, in the late 1990s, COLV, COH, and CCWRD, collectively referred to as the Clean Water Coalition (CWC), commissioned an assessment of future wastewater treatment needs. Following this, in 1999, the CWC commissioned an Alternate Discharge Study (ADS) to investigate alternatives to the discharge of effluent to the LVW. The CWC selected a team of consultants, with Black & Veatch as the prime and managing consultant, to conduct a study of discharge alternatives. Since then, the ADS has become known as the Systems Conveyance and Operations Plan (SCOP).

In 2001, Flow Science Incorporated (Flow Science), working under contract with Black & Veatch, used the one-dimensional DYnamic REServoir Model – Water Quality (DYRESM-WQ) to evaluate the fate of the effluent discharged below the lake thermocline. Subsequently, a three-dimensional model was sought to provide a more complete picture of mixing and algal growth in the entire Boulder Basin of Lake Mead. The selected three-dimensional model was the Estuary Lake and Coastal Ocean Model

(ELCOM) coupled with the Computational Aquatic Ecosystem Dynamics Model (CAEDYM).

In the spring of 2002, Flow Science, in conjunction with Black & Veatch, began setting up the ELCOM/CAEDYM three-dimensional model for predicting transport, mixing, and water quality within Boulder Basin. ELCOM is a fully three-dimensional computational fluid dynamics program designed for practical numerical simulation of hydrodynamics and thermodynamics for inland and coastal waters. CAEDYM is a biogeochemical, water quality model that computes interactions between biological organisms and the chemistry of their nutrient cycles. The coupling of these two models allows for an integrated approach with feedback between the biogeochemical and hydrodynamic systems so that a complete representation of all appropriate processes can be included in an analysis. The ELCOM/CAEDYM models were originally developed at the Centre for Water Research (CWR) at the University of Western Australia. The models are discussed in more detail in Section 3, and a detailed discussion of prior applications is included in Appendix B.

The ELCOM/CAEDYM model of Boulder Basin was initially calibrated for the period 2000 to 2003 for various water quality parameters including temperature, conductivity, perchlorate, chloride, sulfate, bromide, fecal coliform, dissolved oxygen, nutrients, and chlorophyll *a*. The goal of the study was to determine, in detail, the impacts of discharging the WWTP effluent at the three possible effluent discharge locations as identified by a Citizens Advisory Committee (CAC). The modeling considered the reservoir at different water levels and various operational scenarios and also addressed the possible impact of the effluent discharge on the existing SNWA intakes in the basin. The results of that evaluation are discussed in a report titled "Lake Mead ELCOM/CAEDYM Modeling" (Flow Science, 2005Flow Science Incorporated, 2005). Many of the results from that report were subsequently used in the water quality sections of that project's Environmental Impact Report (EIR). Subsequently, the calibration period was extended to include 2004, and also expanded to include total organic carbon.

As part of a separate project, the calibrated ELCOM/CAEDYM model of Boulder Basin was also used to evaluate the water quality impacts on a proposed third SNWA drinking water intake at an alternate location within Lake Mead. The results of that work are included in the report "Lake Mead ELCOM/CAEDYM Joint Modeling Study, Alternative SNWA Intake Locations" (Flow Science, 2006).

The ELCOM/CAEDYM model of Boulder Basin was also used to evaluate and pre-design diffuser port sizes, locations and orientations, for the SCOP discharge diffuser, as well as to determine operation plans. The results of that work are included in the report "Lake Mead Pre-Design Lake Diffuser" (Flow Science, 2007a).

Since that work, Flow Science expanded the ELCOM/CAEDYM model of Boulder Basin to encompass the entire Lake Mead from Hoover Dam to the mouths of the Muddy,

Virgin, and Colorado Rivers. This "Whole Lake Model" was calibrated for the period 2000-2005 for the following parameters: temperature, conductivity, perchlorate, bromide, chlorophyll *a*, total phosphorus (various species), nitrate, ammonium, total organic carbon, pH, and dissolved oxygen.

The objectives of the Whole Lake Model were to:

- Develop a calibrated tool for use in assessing the impacts of Muddy and Virgin River flows (e.g., from flooding or upstream development) on water quality in Boulder Basin.

- Develop a calibrated tool that can be used in the future management of the reservoir operations as part of the Boulder Basin Adaptive Management Plan (BBAMP). The operations include the operation of the SCOP diffusers and the various SNWA intakes.

- Obviate the need for estimating the inflow rates and water quality at the Narrows as was done for the Boulder Basin model, thereby removing a source of uncertainty that existed in the prior model.

- Develop a calibrated tool for use in assessing the impacts of proposed operational changes at Lake Powell (e.g., changes in Colorado River inflow temperatures) on water quality in Lake Mead and Boulder Basin.

- Understand the water quality impacts of lower lake water surface elevations due to drought conditions throughout the lake.

- Better understand general water quality and transport processes throughout the lake, especially in the Upper Basins where field data are historically less dense or non-existent.

- Develop a calibrated tool for future use in for evaluating water quality conditions at potential new intake or discharge locations.

These objectives were accomplished with the development of the original Whole Lake Model as detailed in the report "Lake Mead ELCOM-CAEDYM Model, Extension to Entire Lake" (Flow Science, 2007). The present work further develops and improves the original Whole Lake Model, as described in the next section.

1.3 ADDITION OF YEARS 2006 AND 2007 AND OTHER ENHANCEMENTS

In the current project, Flow Science has expanded the calibration period of the ELCOM/CAEDYM Whole Lake Model to include years 2006 and 2007. The addition of year 2006 was performed under contract with the National Park Service, while the addition of year 2007 was performed under a separate contract with the CWC, and was

sponsored equally by the CWC and SNWA. For the sake of clarity and completeness, the additions of both years are presented in this single report.

While the main motivation of the present work was to add the two additional years to the calibration period, other model enhancements were also called for.

The objectives of the present work are thus summarized as follows:

- Extend the calibration period of the Whole Lake Model to include years 2006 and 2007, which will inherently provide more confidence in the model.
- Perform the calibration simulation continuously for three years, from 2005 through 2007.
- Implement wind data from multiple locations within Lake Mead in 2006 and 2007.
- Implement spatially variable sediment oxygen demand.
- Re-calibrate phosphorus and algae computational routines to improve the model and reflect the latest understanding of the phosphorus processes in the lake.

1.4 REPORT ORGANIZATION

This report describes the methodology, assumptions and the results of the investigations that were performed to add years 2006 and 2007 to the calibration period for the ELCOM/CAEDYM Whole Lake Model of Lake Mead.

Section 2 of this report presents graphical plots and an analysis of the salient field data that were used as model inputs or to calibrate the model. Since significant data analysis has been presented in previous work associated with the development of the original Whole Lake Model, the analysis presented here focuses upon new data sets and observations that have arisen as a result of adding years 2006 and 2007 to the calibration period.

Section 3 discusses the modeling approach. It provides a brief description of the ELCOM/CAEDYM models and details of the computational grids and model inputs used in the calibration simulations, as well as descriptions of the enhancements that have been added to the model since the previous modeling work.

The ELCOM/CAEDYM calibration results are presented in Section 4. This section presents comparisons of the model calibration simulations with measured field data for the 2000 through 2007 modeling period. The focus is primarily on how well the model is

able to match the field data. Additional attention is given to the calibration of the model in years 2006 and 2007, since that is the primary focus of this work.

Section 5 presents brief discussions and descriptions of animations of the simulated variables, which are in included in the DVD that accompanies this report.

The report concludes with Section 6, which summarizes the major findings of the modeling study.

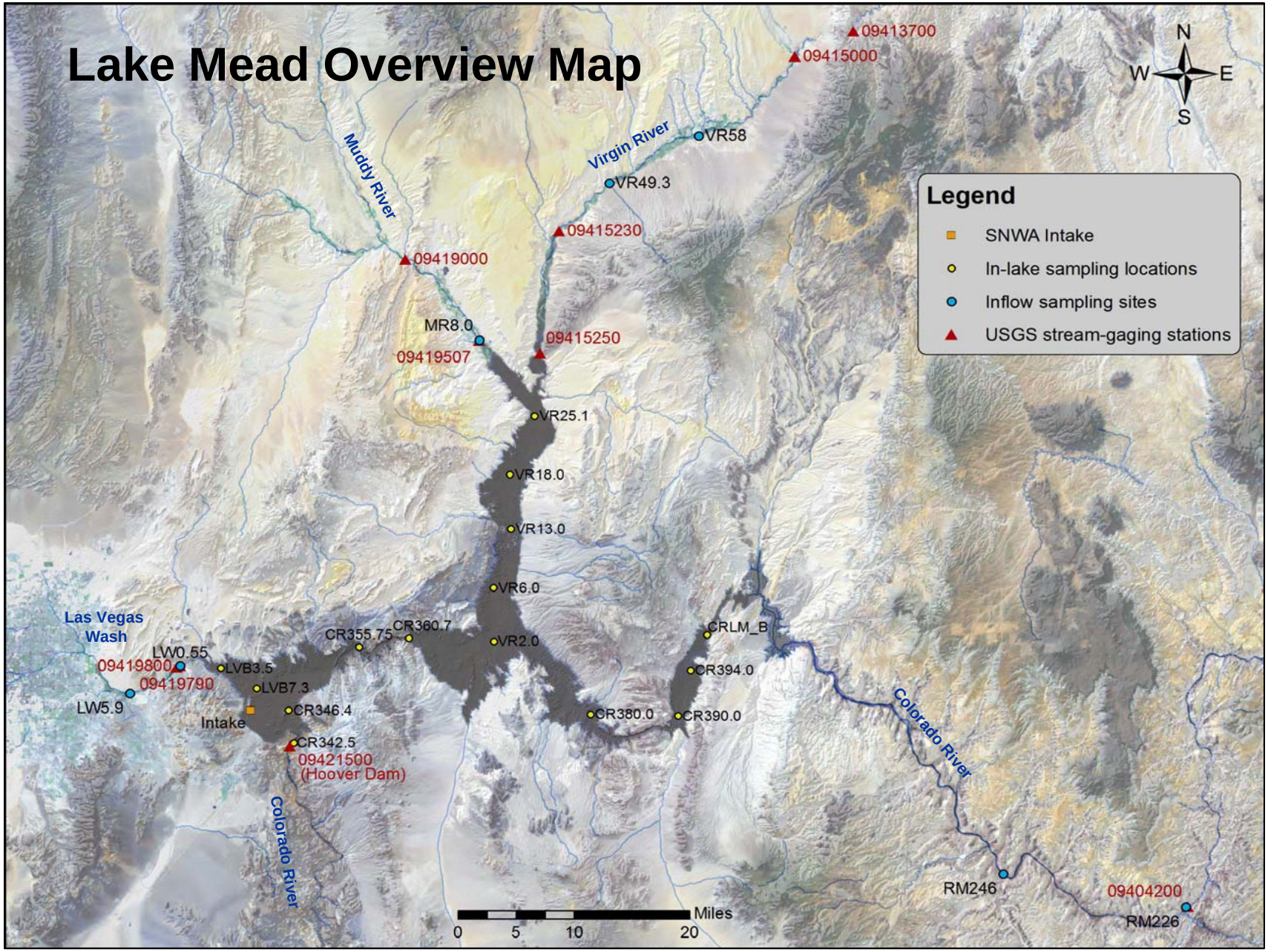

Ch1_Figures.ppt
FSI V064081 & V084015 Task 1
December 9, 2010

Figure 1.1

FLOW SCIENCE

2 DATA PRESENTATION AND ANALYSIS

This section presents plots and analysis of the field data that were gathered in and around Lake Mead. Much data analysis has been presented in previous work associated with the development of the original 2000 through 2005 Whole Lake Model (Flow Science, 2007). The analysis presented here is not intended to duplicate any of that effort; instead, the new analysis focuses upon new data sets and observations that have arisen as a result of extending the modeling period to include years 2006 and 2007. The reader is encouraged to refer to the earlier report (Flow Science, 2007) for more complete presentations and analysis of years 2000 through 2005, as well the Boulder Basin modeling report (Flow Science, 2005) for a more complete analysis of the general limnology of Boulder Basin, in particular.

Much of the data analyses performed during the present work is directly related to the set-up of input files for the simulation. However, these analyses are not presented in this section. Instead, the focus of this section is discussion and analysis of the data in an overall context. The specific details of the set-up of the simulation input files are presented in Appendix A.

2.1 DATA SOURCES

The numerous data sources used in the original 2000 through 2005 Whole Lake Model were also used for the present modeling. Previous reports provide extensive details of the data sources that were used and the data that were obtained (Flow Science, 2005 and Flow Science, 2007). The existing data sets were updated to include years 2006 and 2007. In some instances new or better data sources became available. These are summarized below.

- River flow rate data for the VR from U. S. Geological Survey (USGS) gauging Station 0941520 became available from April 21, 2006. This station is located much closer to Lake Mead than the previously used station, and as such the model input switched to using these data (see Section A.1.2).

- Profiles of temperature, conductivity, pH and DO nominally measured every six hours at four USGS platforms (Las Vegas Bay [LVB], Sentinel Island, Virgin Basin, and Overton Arm) were obtained. The locations of these platforms are indicated on **Figure 2.1**. While these data were also obtained during the previous modeling effort they were not presented in that report (Flow Science, 2007) due to the relatively short time-span of available data at that time.

- Profiles of fluorescence nominally measured every six hours at four USGS platforms (Las Vegas Bay [LVB], Sentinel Island, Virgin Basin, and Overton

Arm) were obtained from January 2006 onwards. The locations of these platforms are indicated on **Figure 2.1**.

- Between 2005 and early 2007, nutrient samples collected within and around Lake Mead by U. S. Bureau of Reclamation (USBR) and Southern Nevada Water Authority (SNWA) switched to using the High Sierra Lab for analysis. These more recent data have lower phosphorus detection limits than earlier data, and have lead to a better understanding of phosphorus processes in Lake Mead (see Sections 2.3.6 and A.2.2), and a re-calibration of the Whole Lake Model (Section 3.4.6). The re-calibration was also motivated by the availability of a longer data set (2000 to 2007).

The following sections present plots and discussions of the collected data, including meteorology, water inflow and outflow data and in-reservoir data. Focus is primarily on the new data-sets as well as instances where the updated 2006 and 2007 data indicate different trends than the earlier 2000 through 2005 data. The reader is encouraged to refer to the earlier report (Flow Science, 2007) for more complete descriptions of years 2000 through 2005.

2.2 METEOROLOGY

The meteorological data obtained from the USGS stations located at Sentinel Island, Virgin Basin and Overton Arm (**Figure 2.1**), were analyzed in a manner similar to that used in the previous modeling (Flow Science, 2007). Particular emphasis was placed upon the wind speed data, since the wind is the primary driver of mixing in Lake Mead.

Annual average wind speeds in the Lake Mead area are presented in **Figure 2.2**. The year-to-year trends were consistent among most of the various data-sets. However, from 2005 onwards, the annual wind speeds at Sentinel Island appeared to have decreased significantly more than at most other locations. This is due to new instrumentation that was installed at a lower height on the Sentinel Island platform, in August 2004.

Figure 2.2 illustrates that the annual average wind speeds at Virgin Basin were lower than at Overton Arm, and wind speeds in both of these upper basins were lower than at Sentinel Island. This trend is further illustrated in **Figure 2.3**, which plots monthly average wind speeds at the three in-reservoir locations (Sentinel Island, Virgin Basin and Overton Arm). This figure also indicates that there is a reasonable correlation of seasonal trends in wind speed at the three locations.

2.3 WATER INFLOW AND OUTFLOW DATA

This section primarily consists of graphical plots of inflow and outflow rates, inflow temperatures, conductivities, pH and concentrations of various constituents for the 2000 through 2007 modeling period. Each plot typically includes all four inflows (LVW, CR, VR and MR) and, in the case of flow-rates, the two outflows (Hoover Dam outlets and SNWA intakes). For clarity, the raw data from numerous sources are not shown. Instead, the data used for the model inputs are presented. This is based upon the premise that the model input is the best possible interpretation of all the field data, since it was obtained through careful cleansing and reconstruction methods. The details of this cleansing and reconstruction, together with plots including the raw data, are presented in Appendix A.

Similar plots spanning only 2000 through 2005 were presented in the previous modeling report (Flow Science, 2007), along with detailed discussions. The discussion here is limited to new trends that are observed due to the addition of the 2006 and 2007 model years, as well as to any changes that may have been made to the 2000 through 2005 data. For more detailed discussions the reader is encouraged to refer to the previous modeling report (Flow Science, 2007).

2.3.1 Flow Rates and Water Surface Elevation

The flow rates for the four inflows (LVW, CR, VR and MR) and the two outflows (Hoover Dam outlets and SNWA intakes [also including the smaller Basic Water Company (BWC) intake flow rate]) are presented in **Figure 2.4** for the 2000 through 2007 modeling period. In this figure, some data gaps have been filled, and the flow rates for the VR and MR have been adjusted to account for water use between the gauging stations and the lake (see Appendix A).

The flow rate magnitudes, diurnal and seasonal variations for 2000 through 2005 have been discussed in the previous modeling report (Flow Science, 2007). For the most part these trends are continued in 2006 and 2007. In particular, both the SNWA intakes outflow and LVW inflow were increasing over time as a result of population growth in the Las Vegas Valley. However, more recent 2009 data (not shown here) indicate that this trend has ceded, which may be a result of strict water conservation policies as well as a decreased population.

As discussed in the previous modeling report (Flow Science, 2007), the flow rate of the VR was particularly high in the winter and spring of 2005 (**Figure 2.4**) as a result of large winter storms and persistent spring snow melt in the upper reaches of the VR. **Figure 2.4** indicates that the flow rate in the winter and spring of 2006 was much lower than in 2005, but higher than in the years prior to that. In the winter and spring of 2007, the flow rate of the VR was comparable to the flow rates in 2000 through 2004.

Prior to April 2006 the flow rate for the VR entering Lake Mead was estimated using data from a gauging station located approximately 40 miles upstream of Lake Mead. In the original modeling a simple correlation was used to account for water usage between this station and the lake (Flow Science, 2007). Since April 2006, new data from a location close to Lake Mead have been available, and have been used directly (see Section A.1.2). Analysis of the new data together with observations from USGS personnel, indicate that the summer flow rates of the VR into Lake Mead are close to zero in most years. Thus, in the present modeling, the VR flow rate was set to zero from July through September of 2000 through 2005, as illustrated in **Figure 2.4**.

The water surface elevation (WSEL) of Lake Mead is plotted in **Figure 2.5**. The persistent drought in the Upper CR Basin, coupled with increased demand for water from users both in the Las Vegas Valley and downstream, lead to a decrease in the WSEL of Lake Mead over the 2000 through 2004 period. In the first few months of 2005 the WSEL increased, in part as a result of the large storm inflow in the VR. However, in 2006 and 2007, the WSEL continued to decrease in a manner generally similar to years 2000 through 2004.

2.3.2 Temperature

The respective temperatures of the four inflows (LVW, CR, VR and MR) are presented in **Figure 2.6** for the 2000 through 2007 modeling period. In this figure, some data gaps have been filled, and some erroneous data removed as discussed in Appendix A. Years 2006 and 2007 showed similar general trends to the previous years, which were discussed in the previous modeling report (Flow Science, 2007).

There are some differences in the inflow temperatures in the winter of 2006/2007, when the CR and VR temperatures were colder than in other years (**Figure 2.6**).

It is also noted that maximum summer time temperatures of the CR inflow in 2006 and 2007 are lower than in 2005, and are comparable to most other years. The higher temperatures in 2005 are thought to be related to changes in the WSEL of Lake Powell (Flow Science, 2007).

2.3.3 Conductivity

The conductivities of the four inflows (LVW, CR, VR and MR) are presented in **Figure 2.7** for the 2000 through 2007 modeling period. Years 2006 and 2007 showed similar general trends to the previous years (Flow Science, 2007). In this figure, some data gaps have been filled, and some erroneous data removed as discussed in

Appendix A. In particular the conductivity in the VR prior to late 2004 has been reconstructed using a simple dilution model (Flow Science, 2007).

2.3.4 Perchlorate

The perchlorate concentration in the LVW inflow is plotted in **Figure 2.8** for the 2000 through 2007 modeling period. The concentrations of perchlorate in the LVW decreased considerably over the 2000 through 2005 period as a result of the ongoing clean-up effort. The perchlorate concentrations plateaued in 2006, before further decreasing in 2007.

The perchlorate concentrations in the other three inflows (CR, VR and MR) were all assumed to be zero, since the perchlorate all originated in the LVW (Flow Science, 2005).

2.3.5 Bromide

The bromide concentrations for the four inflows (LVW, CR, VR and MR) are presented in **Figure 2.9** for the 2000 through 2007 modeling period.

For the CR and LVW, years 2006 and 2007 showed similar general trends to the previous years, which were discussed in the previous modeling report (Flow Science, 2007).

The bromide concentrations in the VR and MR in years 2006 and 2007 were generally lower than those in years 2000 through 2004. This is likely a result of the flushing of those watersheds by the unusually high flow rates in 2005.

2.3.6 Phosphorus

The filterable reactive phosphorus (FRP) concentrations for the four inflows (LVW, CR, VR and MR) are presented in **Figure 2.10** for the 2000 through 2007 modeling period. It should be noted that prior to 2005 most of the FRP concentrations in the CR were below the method detection limits. The concentrations plotted for the CR up to 2005 have thus been reconstructed as detailed in Section A.2.2.

Figure 2.10 indicates that the CR inflow FRP concentrations were typically an order of magnitude lower than the other inflows. The VR and MR inflow FRP concentrations were of comparable magnitude to each other. The lower FRP concentrations in these inflows in 2005 were due to dilution by the large storm and snow-melt flows. It is not

clear why the VR inflow FRP concentration is low in the summer of 2007, but it is noted that the summer concentrations in the VR have little impact on the lake due to the very low inflow rate (**Figure 2.4**).

The highest FRP inflow concentrations were typically in the LVW. As discussed in the previous modeling report (Flow Science, 2007), this was due to the LVW consisting primarily of waste-water that, although highly treated, still contained higher concentrations of phosphorus than the river flows. **Figure 2.11** plots the FRP concentrations and mass loadings in the LVW and in the combined effluent stream from the three WWTPs (flow-weighted averaging of the CCWRD, COLV and COH WWTPs effluent data was used). **Figure 2.11** indicates that the FRP concentration and loading in the LVW were strongly correlated with the WWTP effluent concentration and loading.

The measured total phosphorus (TP) concentrations in the three river inflows (i.e., CR, VR and MR) indicate large variability (see Section A.2.2). This is due to the influence of particulate phosphorus in the inflows (resulting in a non-homogenous inflow) coupled with the small (relative to the spatial scale of the non-homogeneities in the inflow) sample volumes and infrequent (relative to the time-scale for changes in concentration) sampling. As a result of the large variability trends in the data are difficult to identify. Additionally it is evident from in-reservoir data that much of the particulate phosphorus in the inflows settles within the first few miles of the lake (Flow Science, 2009), and as such has relatively little impact on the lake as a whole. Due to the large variability and rapid settling of particulate phosphorus, plots of TP concentration in the three river inflows are not provided in this section. Rather, detailed plots are provided in Section A.2.2, which also provides additional discussion as to how the model was adapted to deal with the rapid settling of particulate phosphorus in these inflows.

The measured TP concentrations in the LVW do not exhibit the large variability of the other inflows, due to the influence of the discharges from the WWTPs. **Figure 2.12** is similar to **Figure 2.11**, except that TP concentrations and loads are plotted rather than FRP. Note that **Figure 2.12** uses log-scales on the vertical axes, which enable the isolated large peaks in the LVW data to be plotted. These peaks were not present in the WWTP values, indicating that they were likely a result of storm water run-off, which added additional phosphorus to the LVW.

The longer-term temporal trends in the LVW phosphorus load from the WWTPs are better illustrated in **Figures 2.13** and **2.14**, which plot the annual average and growing season (April through September) average FRP and TP loads, respectively. The trends in FRP load (**Figure 2.13**) closely follow those for the TP load (**Figure 2.14**), with the TP loads being higher than the FRP load by a relatively consistent amount each year. This indicates that changes in treatment processes at the WWTPs have similar impacts on both the FRP and TP loads.

Figures 2.13 and **2.14** indicate that from 1999 through 2003 the annual average phosphorus load steadily decreased, while the growing season average phosphorus load

remained relatively constant. This implies that most of the reduction in the annual phosphorus load was due to increased treatment in the winter months (i.e., not in the growing season). From 2003 through 2005, both the annual and growing season average loads decreased, due to increased year-round treatment. The phosphorus loads were at a minimum in 2005, as a result of plant optimization experiments, and returned to 2004 levels in 2006 and 2007.

2.3.7 Nitrate

The nitrate (NO3) concentrations for the four inflows (LVW, CR, VR and MR) are presented in **Figure 2.15** for the 2000 through 2007 modeling period.

Generally, years 2006 and 2007 showed similar trends to the previous years, which were discussed in the previous modeling report (Flow Science, 2007). An exception is the NO3 concentration for the CR inflow. The concentrations in the CR in 2006 and 2007 are generally a little lower than those in late 2005, which reverses the 2000 through 2005 trend of increasing NO3 concentrations in the CR.

2.3.8 Total Organic Carbon

The total organic carbon (TOC) concentration data for the four inflows (LVW, CR, VR and MR) are presented in **Figure 2.16** for the 2000 through 2007 modeling period.

The TOC concentrations in the LVW were typically higher than in the other inflows. In this figure the concentrations in the LVW prior to July 2003 were reconstructed from data within Lake Mead, as discussed in Appendix A. The concentration in the LVW appears lower in 2006 and 2007, due to switching to a more representative data source (see Section A.2.5). The new data source is from a station that is closer to the lake than the previously used station.

As discussed in the previous modeling report (Flow Science, 2007), the TOC concentrations of the upstream inflows (i.e., CR, VR and MR) were higher from late 2003 through early 2005, than they were during the rest of the modeling period. The TOC concentrations in 2006 and 2007, likely due to the increased number of erosion control structures in the LVW, and improvements at the WWTPs.

2.3.9 pH

The pH levels for the four inflows (LVW, CR, VR and MR) are presented in **Figure 2.17** for the 2000 through 2007 modeling period. The pH levels of the four inflows typically ranged between 7.5 and 8.5.

2.3.10 Dissolved Oxygen

The DO concentration data for the four inflows (LVW, CR, VR and MR) are presented in **Figure 2.18** for the 2000 through 2007 modeling period. Years 2006 and 2007 showed similar general trends to the previous years. Specifically, each of the inflows exhibited seasonal variations, with higher DO concentrations in the winters than in the summers. This seasonality was primarily related to the dependence of oxygen solubility on water temperature: the colder water in the winters had higher oxygen solubility than the warmer water in the summers.

2.4 IN-RESERVOIR DATA

This section presents plots and analysis of the physical and water quality data collected within Lake Mead, with an emphasis on the 2006 and 2007 data. For completeness full suites of plots are provided for years 2006 and 2007, even though discussion is generally limited to trends that are different to those presented in the previous 2000 through 2005 modeling effort (Flow Science, 2007).

2.4.1 Inflow Insertion Levels

The insertion levels of the four inflows (i.e., the LVW, CR, VR and MR) were discussed extensively in the previous 2000 through 2005 modeling report (Flow Science, 2007). Additional analyses of the LVW insertion level, including calculations of densities (determined by temperature and salinity) of the LVW inflow water and the receiving lake water, were presented in an earlier report on the modeling effort of Boulder Basin (Flow Science, 2005).

The insertion levels of the four inflows in the lake in 2006 and 2007 are best illustrated by presenting graphical snapshots of the conductivity measured in Lake Mead. Since the LVW, VR and MR inflow conductivities were higher than ambient lake values, the conductivity can be used as a tracer and the inflows can readily be identified in such snapshots. Similarly, the lower conductivity CR inflow can be identified.

Figures 2.19 through **2.30** present twelve snapshots of the conductivity measured in Lake Mead by the USBR in 2006 and 2007, with approximately two months between each figure. Each snapshot consists of color contours of conductivity as a function of elevation and distance along the thalweg of the CR (upper frame), the LVW (lower left frame) and the VR (lower right frame). Isotherms are also shown on the snapshots as white lines, in order to illustrate the thermal stratification. For clarity, the data at Stations CR346.4 and CR342.5 are included as an extension of the LVB (LVW thalweg), in addition to being plotted as part of the CR thalweg. The approximate location that the Overton Arm (VR thalweg) joins the CR thalweg in Virgin Basin is also indicated. The locations of the station names where the measurements were made are indicated on each figure and illustrated in **Figure 2.1**.

The twelve snapshots in **Figures 2.19** through **2.30** display overall trends that were similar to those presented as a *typical* year in the previous modeling report (Flow Science, 2007). The LVW, VR and MR inflows can be identified as regions of higher conductivity, while the CR inflow can be identified as a region of lower conductivity.

In February 2006 and 2007 (**Figures 2.19** and **2.25**, respectively), the lake was of relatively uniform temperature, with the positions of the isotherms being strongly influenced by the inflows (particularly the CR and VR inflows). All three inflows (LVW, CR and VR) entered the lake as underflows, and remained primarily near the lake bottom. There were some subtle, yet important, differences in the manner in which the CR underflow progresses into Boulder Basin in the winters of 2006 and 2007, but discussion of these impacts is delayed until Section 2.4.3.

By April (**Figures 2.20** and **2.26**) some thermal stratification was established in the lake as the surface waters were warmed. The cold CR inflow remained primarily as an underflow, although there was some indication of transition to an interflow near the surface in 2006 (**Figure 2.20**). The shallow LVW and VR inflows warmed up more quickly than the receiving lake water, and as such entered the lake as surface flows or interflows near the surface.

In June (**Figures 2.21** and **2.27**) thermal stratification was well established throughout the lake. The CR was entering as an interflow, centered about the 20°C isotherm in 2006 (**Figure 2.21**), and appeared to be transitioning from an underflow to an interflow in 2007 (**Figure 2.27**). The LVW and VR inflows were entering as surface flows or interflows near the surface in both years.

The transition of the CR inflow from an underflow to an interflow was complete by August of both years (**Figure 2.22** and **2.28**). The remaining regions of low conductivity in the hypolimnion near the CR inflow are the remnants from the earlier underflows. This region is larger in 2007 (**Figure 2.28**) than in 2006 (**Figure 2.27**), which is an indication that the transition took longer in 2007. The LVW and VR inflows continued to enter as surface flows or interflows near the surface in both years.

By October (**Figures 2.23** and **2.29**) the thermal stratification was weakening as the surface of the lake cooled. The CR continued to enter as an interflow near the elevation of the thermocline. The LVW and VR inflows were also entering as interflows, but at elevations just above the thermocline. On occasions these interflows were mixed upwards into the epilimnion by wind events.

The lake was only weakly stratified by December (**Figures 2.24** and **2.30**). The CR entered as an underflow in December 2006 (**Figure 2.24**), but the stronger thermocline resulted in the CR continuing to enter as an interflow along the thermocline (albeit close to the bottom of lake) in 2007 (**Figure 2.30**). In both years the LVW entered the lake initially as an underflow, but was then impeded by the weak thermocline and continued as an interflow at the thermocline elevation. The VR also initially entered the lake as an underflow in both years. In 2006 it was dense enough to penetrate the weak thermocline and remain as an underflow (**Figure 2.24**), whereas in 2007 the underflow was impeded by the stronger thermocline (**Figure 2.30**).

As discussed in the previous 2000 through 2005 modeling report (Flow Science, 2007), the large inflow volumes of the CR can result in a "double thermocline" structure in the region near the CR inflow. **Figure 2.31** plots the measured temperature profiles at Station CR394.0, which is near the CR inflow (see **Figure 2.1**), for selected months from years 2004 through 2007. The trends that were identified in previous years were generally repeated in 2006 and 2007. In particular, the double thermocline structure in July and August was repeated in 2006 and 2007.

However, the temperature profiles in February and April of 2007 were quite different to previous years. This was a result of a colder than usual CR inflow temperature in the winter of 2007 (see Section 2.3.2).

2.4.2 General Water Quality Observations

This section presents analysis of the measured data collected from Lake Mead. An exhaustive presentation of all the available data has not been made. Rather, selected data have been plotted to present the new 2006 and 2007 data, and to compare the data-trends of these years to those of 2000 through 2005. It should be noted that more complete sets of plots of in-reservoir conditions are presented in relation to the model calibration in Section 4.

2.4.2.1 Conductivity

Figure 2.32 plots the surface and bottom conductivities measured at Stations CR394.0, CR360.7 and CR346.4 for the 2000 through 2007 modeling period. Station

CR394.0 is located near the CR inflow (see **Figure 2.1**) and thus is primarily representative of water from the CR. Station CR360.7 is located at the downstream end of Virgin Basin, just upstream of the Narrows, and is representative of the water from the CR mixed with water from the VR and MR (although it may also be impacted by water from the LVW due to reverse flow at the surface through the Narrows [Flow Science, 2007]). Station CR346.4 is located in Boulder Basin, and is thus representative of water from all four inflows (CR, VR, MR and LVW).

As discussed in the previous modeling report (Flow Science, 2007), the increase in conductivity within Lake Mead from 2000 through 2004 was primarily driven by changes in the CR inflow, resulting in increased conductivities at all locations in **Figure 2.32**. In early 2005 large storms in the VR and MR resulted in a cold, high-salinity (conductivity) and dense underflow traveling down the Overton Arm, through the Narrows and into the bottom of Boulder Basin (Flow Science, 2007). This manifests itself in **Figure 2.32** as a rapid rise in the conductivity at Stations CR360.7 and CR346.4, particularly at the lake bottom. At the same time in 2005, the conductivity of the CR inflow began to decrease as indicated by the conductivity at Station CR394.0. Thus the conductivities at Stations CR360.7 and CR346.4 became separated from those at Station CR394.0 in 2005, as illustrated in **Figure 2.32**.

In 2006 and 2007 the conductivities at all locations in **Figure 2.32** decreased in response to the lower CR inflow conductivity. However, the separation between the conductivities at Station CR394.0 and Stations CR360.7 and CR346.4 remained. The magnitude of the separation in 2007 is smaller than in 2005, and would be expected to continue to decrease in the future under normal circumstances. The residence time of Lake Mead is approximately two to four years, which is an indication of the time-scale for these changes to take place.

2.4.2.2 Perchlorate

Figure 2.33 plots the surface and bottom perchlorate concentrations measured at Station CR343.3 for the 2000 through 2007 modeling period. The perchlorate concentrations appeared to have plateaued in 2006 and 2007, following the 2000 through 2005 period of decreasing concentrations. This trend closely follows the trend in concentrations of the LVW inflow, although the inflow concentrations in the LVW continued to decrease in 2007 after plateauing in 2006 (Section 2.3.4).

2.4.2.3 Chlorophyll a

Figures 2.34 and **2.35** illustrate the top 5 m and growing season average chlorophyll *a* concentrations as a function of location in Lake Mead, for years 2006 and

2007, respectively. In the plots the chlorophyll *a* concentration is represented at each location measured in the lake by a symbol, whose color represents the concentration value. Note that the color scale is logarithmic (i.e., for each change in color the concentration goes up by a constant ratio, rather than by a constant increment), a result of the wide range of concentrations present in the lake.

The general spatial trends of chlorophyll *a* concentrations in 2006 and 2007 closely followed those in previous typical years (Flow Science, 2007). That is, the concentrations immediately near each of the inflows were noticeably higher than the general open water concentrations, and the highest concentrations were in the inner LVB near the LVW.

Figure 2.36 plots the chlorophyll *a* concentrations measured at Station LVB3.5 (upper frame) and Station CR346.4 (lower frame) for the 2000 through 2007 modeling period. It should be noted that there are no COLV chlorophyll *a* measurements at Station LVB3.5 from 2005 onwards, due to the switch to movable stations.

The chlorophyll *a* concentrations in 2000 and 2005 in the inner LVB (represented in **Figure 2.36** by Station LVB3.5) were lower than other years. The low chlorophyll *a* concentrations in 2005 may be a result of increased phosphorus removal by the WWTPs in 2005 (see Section 2.3.6) resulting in lower phosphorus loads (**Figures 2.13** and **2.14**) in the LVW. Indeed, in some instances, the phosphorus load in the LVW may have a direct impact on the chlorophyll *a* concentrations in the LVB, as evidenced when the phosphorus loads from the WWTPs were increased in 2006 and 2007 (**Figures 2.13** and **2.14**) the chlorophyll *a* concentrations at Station LVB3.5 also increased (although some of the increase may be related to lowering WSEL resulting in the LVW inflow becoming closer to Station LVB3.5).

However, the chlorophyll *a* concentrations in the inner LVB may also be significantly impacted by other factors, some of which may not be entirely understood. For example, the chlorophyll *a* concentrations in 2000 are similar to those in 2005 (**Figure 2.36**), yet year 2000 has the highest phosphorus loading of the years modeled, while year 2005 has the lowest phosphorus loading of the years modeled (**Figures 2.13** and **2.14**). Additionally, year 2001 has a similar, and slightly lower, phosphorus loading as year 2000, yet the chlorophyll *a* concentrations in 2001 are higher than any other year. The unusually low chlorophyll *a* concentrations in 2000 and unusually high concentrations in 2001 illustrate the large degree of natural variation that exists within the observed data.

Yet the annual and growing season averaged phosphorus loadings from the WWTPs in 2000 were lower than in 2001 (**Figures 2.13** and **2.14**). This is a result of the natural variability in the lake, which can dramatically impact algae growth.

The temporal trends in chlorophyll *a* concentrations in the open water of Boulder Basin (represented in **Figure 2.36** by Station CR346.4) did not generally follow those of the inner LVB. In particular, the concentrations in 2005 were comparable to those in years 2002 through 2004. The concentrations decreased in 2006 and 2007. Year 2007 is

particularly noticeable for the vastly reduced magnitude of the fall bloom (second chlorophyll *a* peak in each calendar year). This manifested in a lower growing season average chlorophyll *a* concentration at Station CR346.4 in 2007, as evidenced by comparing **Figure 2.35** (2007) with **Figure 2.34** (2006).

The lower chlorophyll *a* concentrations in 2007 were also observed in the upper basins and throughout the open water of Lake Mead (**Figure 2.35**). The lower concentrations may be a result of changes in phosphorus loading from upstream, different algae types, or the impact of quagga mussels.

2.4.2.4 Phosphorus

Figure 2.37 plots the surface and hypolimnion FRP concentrations measured at Station CR346.4 for the 2000 through 2007 modeling period. The variability of the FRP measurements between the three agencies (SNWA, COLV and USBR) is apparent. From about 2004 onwards the USBR data-set at the surface is relatively consistent without unexplained outliers. From about mid-2005 onwards the COLV data-set at the surface is also relatively consistent without unexplained outliers and in reasonable agreement with the USBR data-set. Some seasonal trends can sometimes be identified in these data. In particular the FRP concentrations are low in the summer, due to uptake of FRP by algae, and higher in most winters (with 2006 being an exception). The SNWA data-set is consistently higher than the other two data-sets, and does not exhibit the seasonal trends.

In the hypolimnion there are limited USBR and COLV data at Station CR346.4 within the range of elevations plotted (**Figure 2.37**). The SNWA data-set is relatively consistent without unexplained outliers, but appears consistently higher than the limited USBR and COLV data that are available.

Figure 2.38 plots the surface and hypolimnion TP concentrations measured at Station CR346.4 for the 2000 through 2007 modeling period. There are significant differences between the USBR, SNWA and COLV data-sets, which is probably a result of the method detection limits being higher than the concentrations that are in the lake at this location. For these data, the concentrations were plotted as half of the detection value and it should be noted that the actual value could vary from zero to twice that plotted (i.e., from zero to the detection limit). As a result of the relatively high detection limits, trends in TP concentrations are difficult to identify.

A limited number of samples collected between 2000 and 2003 were analyzed for TP using inductively-coupled plasma mass spectrometry (ICP-MS), which has lower detection limits. These data are plotted on **Figure 2.38**, and indicate TP concentrations ranging from approximately 0.004 mg P/L to 0.012 mg P/L in the epilimnion, and from approximately 0.003 mg P/L to 0.007 mg P/L in the hypolimnion.

In early 2007 the USBR phosphorus samples began to be analyzed by the High Sierra Laboratory, using methods with a detection limit of 0.001 mg P/L. Thus the USBR data plotted in **Figures 2.37** and **2.38** can be considered more reliable in 2007. Additionally, the SNWA samples began to be analyzed by the High Sierra Laboratory from late October 2007. Thus, it is anticipated that future data-sets for years 2008 and onwards will indicate better agreement, and enable trends in phosphorus concentrations to be more easily identified.

2.4.2.5 Total Organic Carbon

Figure 2.39 plots the surface and hypolimnion TOC concentrations measured at Station CR346.4 for the 2000 through 2007 modeling period.

The seasonal trends and elevated TOC concentrations in 2001 and from mid-2003 through 2005 have been discussed in the previous modeling report (Flow Science, 2007). The TOC concentrations in 2006 and 2007 decreased back to the levels that occurred in 2000 and 2002, which reflects the lower CR inflow concentrations (see Section 2.3.8).

2.4.2.6 Dissolved Oxygen

Figure 2.40 plots the surface and bottom DO concentrations measured at Station CR346.4 for the 2000 through 2007 modeling period. Station CR346.4 is representative of the open water in Boulder Basin, and is located in deep water such that the impacts at the reservoir bottom can be gauged.

As discussed in the previous modeling report (Flow Science, 2007), the trends in DO concentrations from year to year were similar, except in 2003. In 2003 there was not the characteristic rise in DO concentration at the lake bottom at the beginning of the year. This indicates that the deepest portions of Boulder Basin did not completely destratify, and were not re-oxygenated by the CR inflow, during the winter of 2002/2003.

In 2006 and 2007 the DO increased sharply at the beginning of each year. This re-oxygenation can be due to top-down vertical mixing of the lake, direct inflow of the CR, or both. This is discussed further in Section 2.4.3.

Figures 2.41 through **2.52** present twelve snapshots of the DO concentrations measured in Lake Mead by the USBR, in 2006 and 2007. These snapshots are similar to those presented for conductivity in Section 2.4.1, except that the June 2006, August 2006 and August 2007 plots are replaced with other months due to some unusual and likely erroneous readings from the DO probe.

Figures 2.41 through **2.52** indicate that the DO distributions in 2006 and 2007 are similar to previous typical years, which were thoroughly discussed in the previous modeling report (Flow Science, 2007) and are briefly summarized below.

In the summers the lake is stratified, and the decomposition of organic material in the hypolimnion results in lower DO concentrations. Additionally, the sediment oxygen demand (SOD) further lowers the DO concentration near the lake bottom, particularly near each of the inflows where the SOD is higher (see Section 3.4.5). The DO in the epilimnion remains high due to direct aeration from the atmosphere and oxygen production by algae photosynthesis.

In the winters the lake is re-oxygenated, through a combination of vertical mixing bringing oxygen from the epilimnion, and the CR inflow bringing in oxygen directly. The impact of the CR inflow on the DO in the deepest portions of Boulder Basin, are further discussed in the next section.

2.4.3 Mechanisms for Oxygen Replenishment of Boulder Basin

As discussed in Section 2.4.2.6 the DO in the hypolimnion of Lake Mead was replenished in most years between 2000 and 2007. This is evident in **Figure 2.40**, where the DO concentration at the bottom of Station CR346.4 (located in deep water in Boulder Basin) exhibited rapid rises at the beginning of each calendar year, except 2003. In the winter of that year, Lake Mead did not completely de-stratify, with the deepest portions of Boulder Basin remaining isolated from the DO in the epilimnion by a weak thermocline (Flow Science, 2007).

In the years where the DO at the bottom of Station CR346.4 did rise, it is widely accepted that the replenishment of the DO was from the winter mixing of the epilimnion (with higher DO concentrations) with the water at depth. Thus the DO was replenished by a "top-down" mixing process. However, further analysis of the in-reservoir field data indicates that the CR inflow is a second possible mechanism for DO replenishment in Boulder Basin. Both of these mechanisms are illustrated using the 2006 and 2007 in-reservoir data.

Figures 2.53, **2.54** and **2.55** plot contours of measured field data in January, February and March of 2006, respectively. Each plot has four frames, respectively corresponding to temperature, conductivity, density (as computed from temperature and salinity) and DO. Each of the frames plots contours as a function of elevation and distance along the thalweg of the CR, from CR342.5 (near Hoover Dam) to CR394.0 (near the CR inflow).

In January 2006 (**Figure 2.53**), Lake Mead was stratified, particularly in Boulder Basin. The warmer water in the epilimnion (first frame of **Figure 2.49**) resulted in stable density stratification (third frame). The stratification resulted in higher conductivity

(from the LVW inflow) remaining in the epilimnion (second frame), and low DO in the hypolimnion (fourth frame). The CR inflow is visible at the right of each frame as a cold, low-conductivity, dense and high-DO, underflow, extending almost to CR380.0 from CR394.0.

By mid-February the CR underflow has progressed into Boulder Basin and beyond CR355.75, as is visible in all four frames of **Figure 2.54**. The CR inflow has directly replenished the DO in the hypolimnion from VR2.0 downstream to CR355.75 (fourth frame of **Figure 2.54**). A region of low DO remains at the bottom between Stations CR342.5 (near Hoover Dam) and CR346.4. The stable density stratification in Boulder Basin remains (third frame), indicating that the DO replenishment was not from a top-down mixing event.

By mid-March the CR underflow has progressed beyond Stations CR346.4 and CR342.5, and the region of low DO has been replaced with higher DO water from the CR (third frame of **Figure 2.55**). This manifests as the sharp rise in DO concentration at the bottom of Station CR346.4 in **Figure 2.40**. Again, the stable density stratification in Boulder Basin remains (third frame of **Figure 2.55**), indicating that the DO replenishment was not from a top-down mixing event.

The stratification and DO replenishment in the winter of 2007 was different, as indicated in **Figures 2.56**, through **2.59**, which respectively plot data from December 2006, and January, February and March 2007.

In December 2006 (**Figure 2.56**) the density structure of Lake Mead was qualitatively similar to that in January 2006 (**Figure 2.53**). There was stable density stratification throughout the lake and low DO in the hypolimnion of Boulder Basin (**Figure 2.52**).

However, by January 2007 (**Figure 2.57**) there were minimal vertical density gradients in Boulder Basin (third frame of **Figure 2.57**), as a result of vertical mixing. Additionally, the DO concentration in the hypolimnion of Boulder Basin had increased. At the same time, the CR inflow was visible as an underflow that had progressed beyond Station CR380.0, but not as far as Station VR2.0 (all four frames of **Figure 2.57**). This indicated that the increase in DO concentration at the bottom of Boulder Basin through January 2007 was caused only by the top-down mixing, and not the CR inflow.

By February and March 2007 (**Figures 2.58** and **2.59**, respectively) the CR inflow had progressed all the way into Boulder Basin. This is most evident in the plots of temperature (upper frames of **Figures 2.58** and **2.59**) that show layers of cold water from the CR inflow extending along the reservoir bottom all the way to Station CR342.5 (near Hoover Dam). It is noted that the inflow temperature of the CR in the winter of 2007 was colder than in most other years (Section 2.3.2).

The DO concentrations at the bottom of Boulder Basin indicate that there was an additional rise in DO from January (**Figure 2.57**) to February (**Figure 2.58**). This indicates that CR inflow also contributed to the DO replenishment in 2007. That is, the

initial DO replenishment was a result of top-down vertical mixing between December and January, and then there was additional DO replenishment due to the CR inflow between January and February.

In summary, the 2006 and 2007 field data have indicated that the CR inflow can directly transport DO into the deepest portions of Boulder Basin, regardless of whether Boulder Basin completely destratifies. Thus, it is possible for the DO in Boulder Basin to be replenished even in years where the reservoir does not completely destratify (as occurred in the winter of 2006). As a result of this phenomenon, it is possible to increase the DO levels at the bottom of the lake if the flow from the CR is increased during the winter months.

2.4.4 USGS Platform Data

The USGS maintains four sampling platforms within Lake Mead. These platforms are located at Las Vegas Bay, Sentinel Island, Virgin Basin, and Overton Arm, as indicated on **Figure 2.1**. At each of the platforms vertical profiles of temperature, conductivity, pH, DO and fluorescence are measured nominally every six hours.

Figures 2.60 through **2.64** respectively plot the measured temperature, conductivity, pH, DO and fluorescence data measured at the USGS platforms in 2006 and 2007. Each figure plots contours as a function of depth and time for all four platforms: Las Vegas Bay (first frame), Sentinel Island (second frame), Virgin Basin (third frame), and Overton Arm (fourth frame). It should be noted that the vertical scales for Las Vegas Bay and Overton Arm (first and fourth frames) are different to those for Sentinel Island and Virgin Basin (second and third frames), a result of the different depths. It should also be noted that the data at Sentinel Island and Virgin Basin do not extend all the way to the reservoir bottom, with approximately one-third of the depth being excluded.

The data presented in **Figures 2.60** through **2.64** were of good quality and generally had only minimal gaps. The largest data gap occurred over the last quarter of 2007, where the conductivity, pH and DO data at Sentinel Island appeared to be missing or erroneous.

At the time-scale presented in these figures, the sub-daily changes in the data are not apparent. Instead, the plots of temperature, conductivity, DO and pH (**Figures 2.60** through **2.63**), simply illustrate the annual and seasonal changes in water quality that have been discussed fully in previous reports (Flow Science, 2005 and Flow Science, 2007). Years 2006 and 2007 appear to be consistent with earlier years discussed in those reports, and are not discussed further here.

Section 4 presents additional plots and discussion of the USGS data in relation to model validation on a sub-daily basis. In addition, correlations of the USGS fluorescence data with chlorophyll *a* data are developed in the next section.

2.4.5 Fluorescence and Chlorophyll *a* Correlation

Fluorescence measurements, such as those presented in **Figure 2.64**, are often used to obtain quick and inexpensive estimates of chlorophyll concentrations. These estimates are dependent upon the existence of correlations, which are generally different for different algal species and different water bodies. This section explores possible fluorescence and chlorophyll *a* correlations that may be useful for Lake Mead.

As a first step in examining possible correlations, chlorophyll *a* field data that were collected from locations near to each of the four USGS platforms were identified. **Table 2.1** summarizes the chlorophyll *a* sampling stations that were used for comparison to the fluorescence data for each of the four USGS platforms. The locations of the sampling stations and USGS platforms are shown in **Figure 2.1**. **Table 2.1** also indicates which agency and how frequently the chlorophyll *a* data were collected.

Table 2.1: Sampling Stations used for Fluorescence – Chlorophyll *a* Correlations

USGS Platform	Sampling Station	Agency	Data Frequency	Figure number
Las Vegas Bay	LVB3.5	USBR SNWA	monthly weekly	Figure 2.65 Figure 2.66
Sentinel Island	CR346.4	USBR SNWA	monthly weekly	Figure 2.67 Figure 2.68
Virgin Basin	CR360.7	USBR	monthly	Figure 2.69
Overton Arm	VR25.1	USBR	monthly	Figure 2.70

For each of the six chlorophyll *a* data sets listed in **Table 2.1**, a plot of measured chlorophyll *a* overlaid with measured fluorescence, were made as functions of time. The specific figure numbers are listed in **Table 2.1**.

For example, **Figure 2.65** plots chlorophyll *a* data as measured at Station LVB3.5 by USBR (left vertical axis) and measured fluorescence as measured at the USGS platform in the Las Vegas Bay (right vertical axis) as functions of time (horizontal axis) in 2006

through 2008. The upper frame plots data near the surface (within the top 1 m), and the lower frame plots data between 2 and 6 m depth (including the top 5-m average for chlorophyll *a*).

Figures 2.66 through **2.70** present similar plots for the other chlorophyll *a* data-sets as listed in **Table 2.1**. The SNWA chlorophyll *a* data do not include near surface measurements, and as such **Figures 2.66** and **2.70** only include a single frame (plotting data between depth of 2 and 6 m).

Of all the locations, the correlation between chlorophyll *a* and fluorescence was most discernable within the Las Vegas Bay (**Figures 2.65** and **2.66**). This is likely due to the Las Vegas Bay having chlorophyll *a* concentrations that were significantly higher than at the other locations. Therefore, the main peaks in both chlorophyll *a* and fluorescence were more distinguishable from the general measurement "noise" than at the other locations. As a result of this observation, the correlation was only explored for the Las Vegas Bay data. Additionally, the SNWA chlorophyll *a* data (**Figure 2.66**) were used, since the data was collected weekly (compared to the monthly USBR data).

Figure 2.66 plots the weekly SNWA chlorophyll *a* data and the sub-daily fluorescence data from the Las Vegas Bay on the same plot. The different frequencies of sampling can impact the appearance of the data-sets. Thus, **Figure 2.71** re-plots the same data-sets as **Figure 2.66**, except that the fluorescence data have been interpolated (or re-sampled) onto the same weekly sampling as the chlorophyll *a* data-set.

Figure 2.71 indicates that there was a good correlation between fluorescence data and chlorophyll *a* data up until about May 2007. That is, up until May 2007, the plots of fluorescence and chlorophyll *a* closely followed each other (on their respective axes). After May 2007, the fluorescence data became much higher than the chlorophyll *a* data (relative to their respective axes), although both data-sets still appeared to follow similar temporal trends.

The fluorescence and chlorophyll *a* data in **Figure 2.71** were compared directly in **Figure 2.72** by plotting the fluorescence as a function of chlorophyll *a* concentration. Different colored symbols were used depending upon the date of the data, as indicated in the legend of the figure. Plotting the data in this manner illustrates that there were two correlations, depending upon the time the data were collected. From March 15, 2005 through May 30, 2007 (blue symbols), the correlation was,

fluorescence (%) = 0.1642 x chlorophyll *a* (µg/L) with an R^2 of 0.3278.

From August 27, 2007 through June 2, 2008 (green symbols) the correlation was,

fluorescence (%) = 0.7394 x chlorophyll *a* (µg/L) with an R^2 of 0.7716.

Between these periods (red symbols) there appeared to be no correlation.

The most likely explanation for the changes in the correlation is that the USGS fluorometer at the Las Vegas Bay platform was re-calibrated in mid-2007. Another possible explanation would be that the algae types may have shifted and thus changed the relative relationship between fluorescence and chlorophyll *a* concentration. Future analysis of additional data measured since June 2008 is required to determine if the second correlation (above) has held true over more recent times.

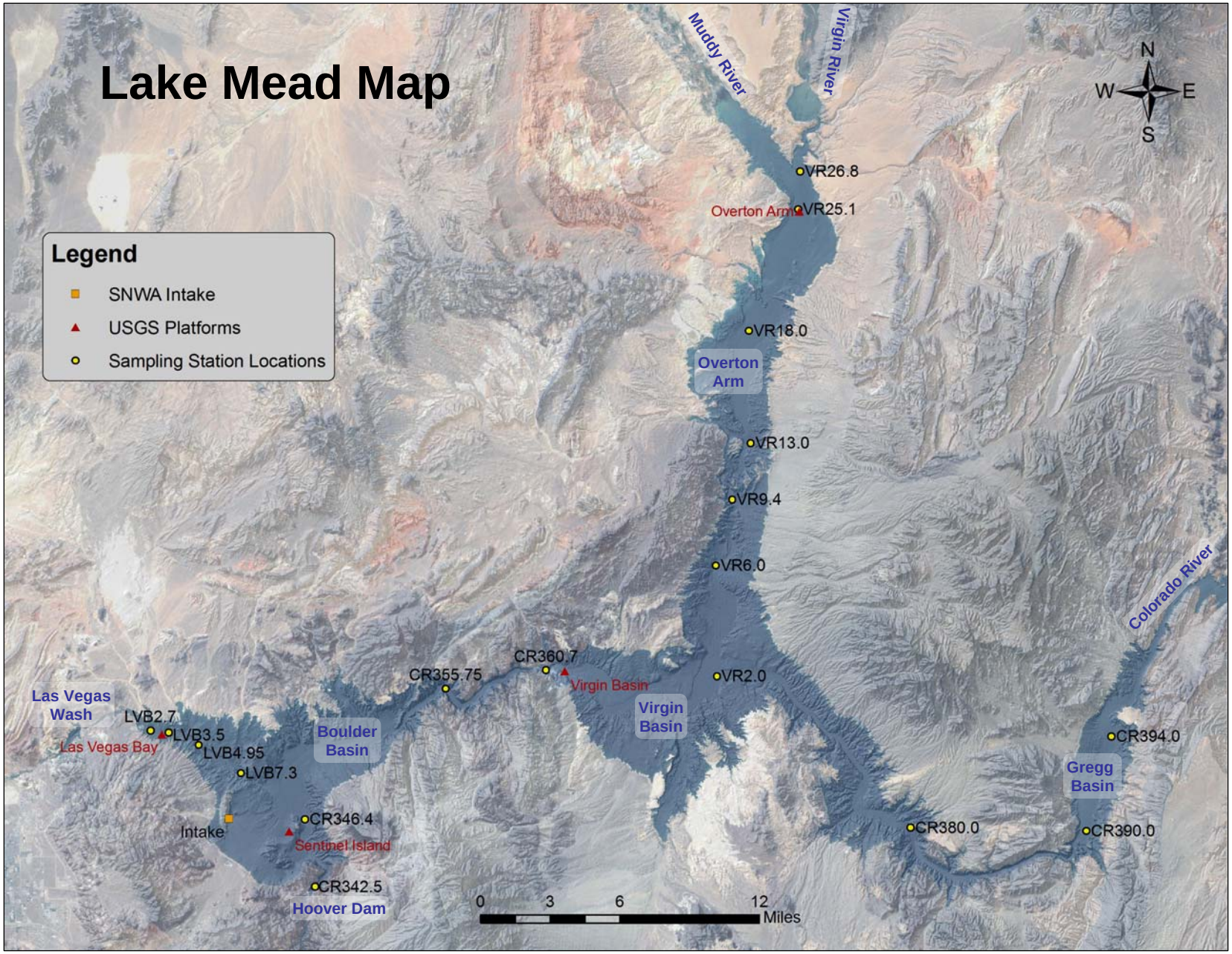

Ch2_Figures.ppt
FSI V064081 & V084015 Task 1
December 9, 2010

Figure 2.1

FLOW SCIENCE

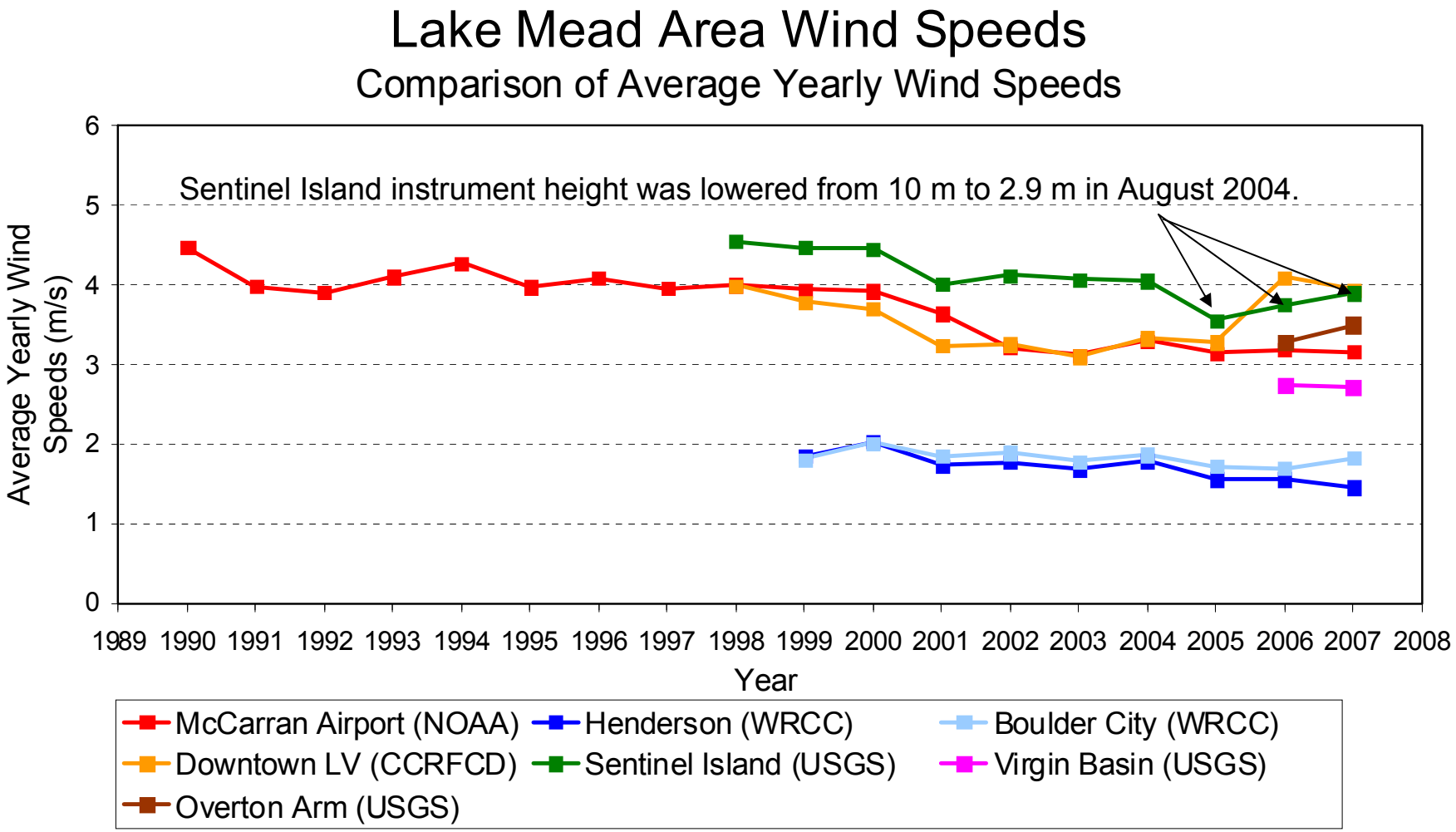
Lake Mead Area Wind Speeds
Comparison of Average Yearly Wind Speeds
Sentinel Island instrument height was lowered from 10 m to 2.9 m in August 2004.
Average Yearly Wind Speeds (m/s)
0
1
2
3
4
5
6
1989 1990 1991 1992 1993 1994 1995 1996 1997 1998 1999 2000 2001 2002 2003 2004 2005 2006 2007 2008
Year
McCarran Airport (NOAA)
Henderson (WRCC)
Boulder City (WRCC)
Downtown LV (CCRFCD)
Sentinel Island (USGS)
Virgin Basin (USGS)
Overton Arm (USGS)

Figure 2.2

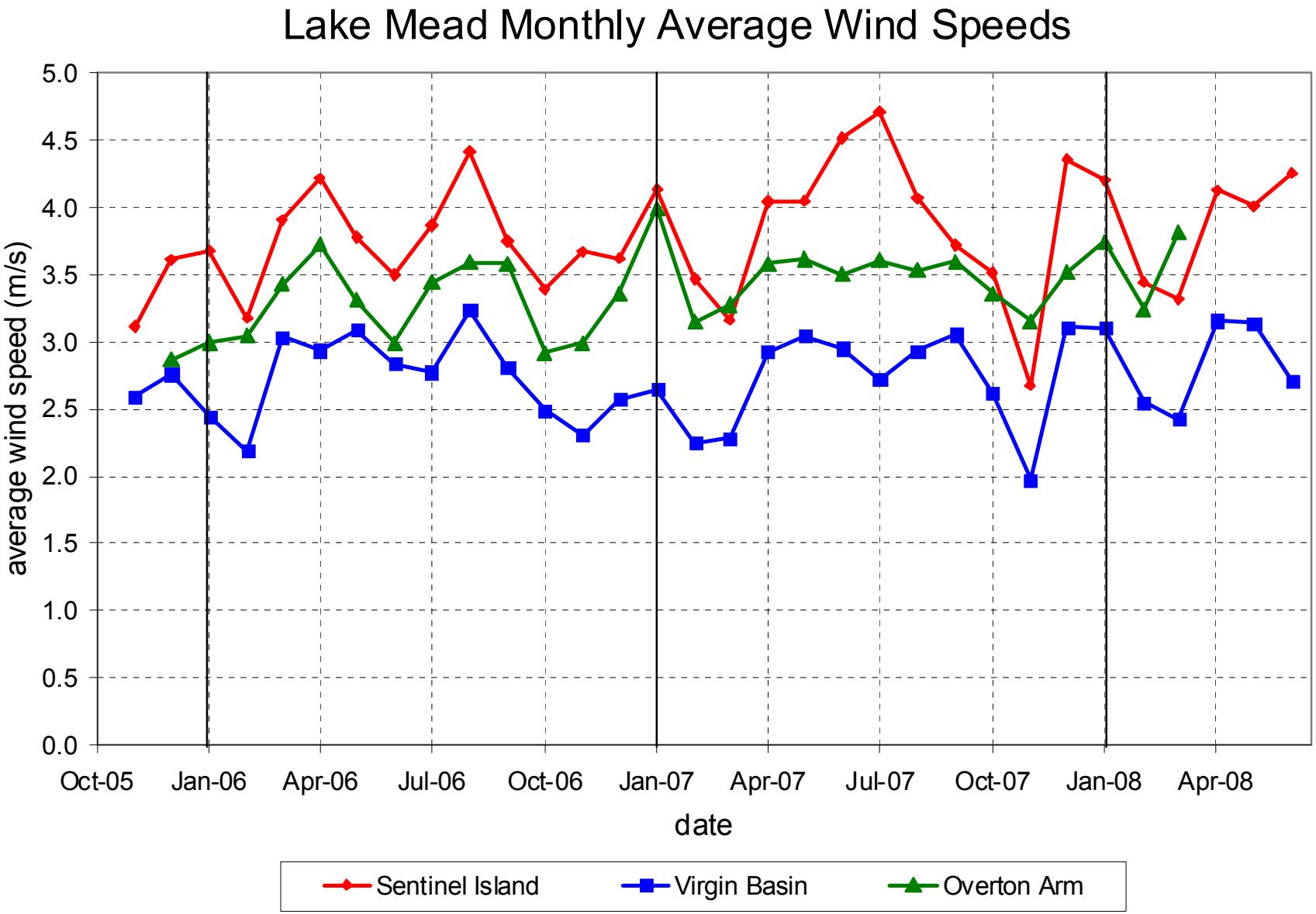
Lake Mead Monthly Average Wind Speeds
average wind speed (m/s)
5.0
4.5
4.0
3.5
3.0
2.5
2.0
1.5
1.0
0.5
0.0
Oct-05
Jan-06
Apr-06
Jul-06
Oct-06
Jan-07
Apr-07
Jul-07
Oct-07
Jan-08
Apr-08
date
Sentinel Island
Virgin Basin
Overton Arm

Figure 2.3

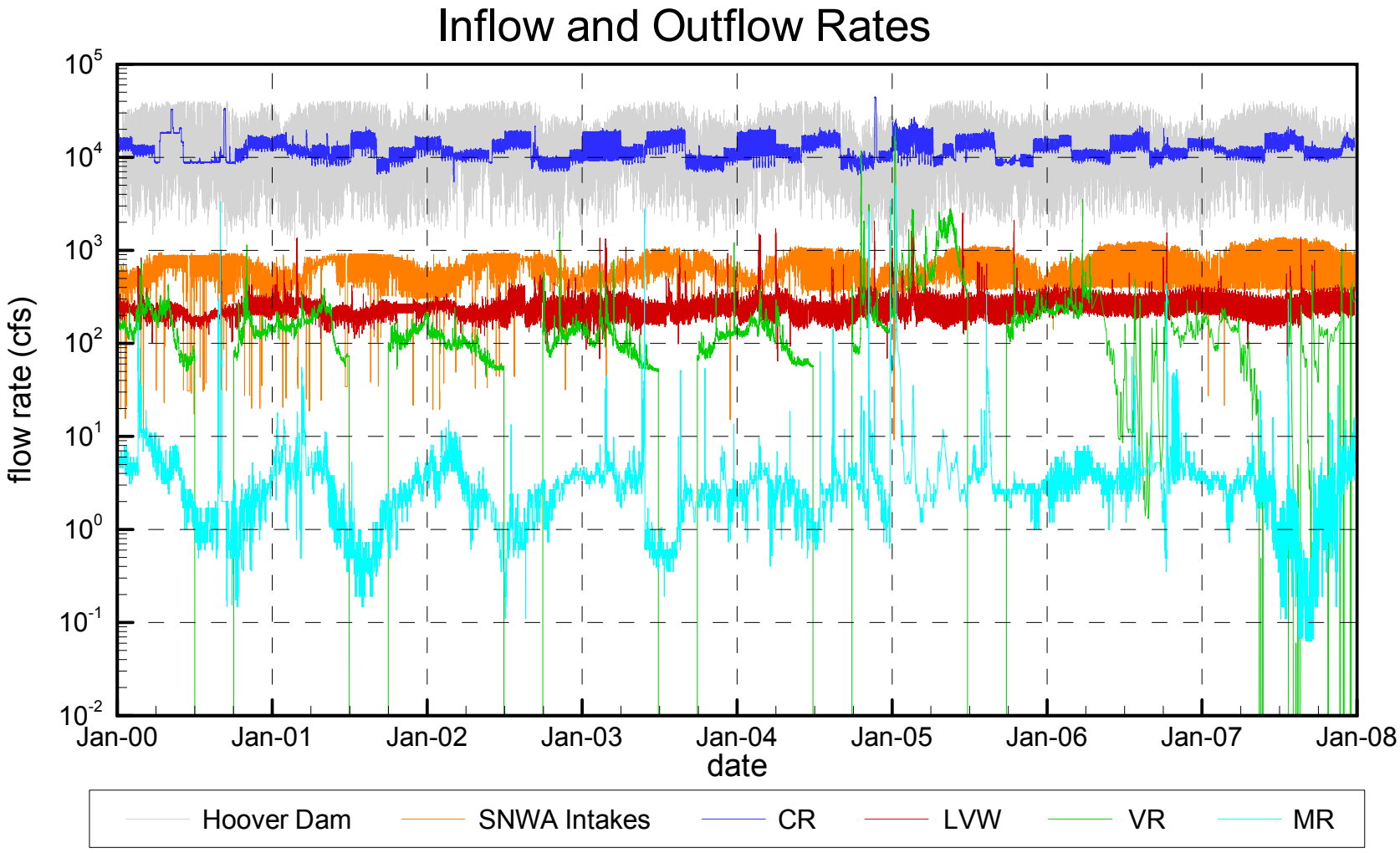
Inflow and Outflow Rates
flow rate (cfs)
10^5
10^4
10^3
10^2
10^1
10^0
10^{-1}
10^{-2}
Jan-00
Jan-01
Jan-02
Jan-03
Jan-04
Jan-05
Jan-06
Jan-07
Jan-08
date
Hoover Dam
SNWA Intakes
CR
LVW
VR
MR

Figure 2.4

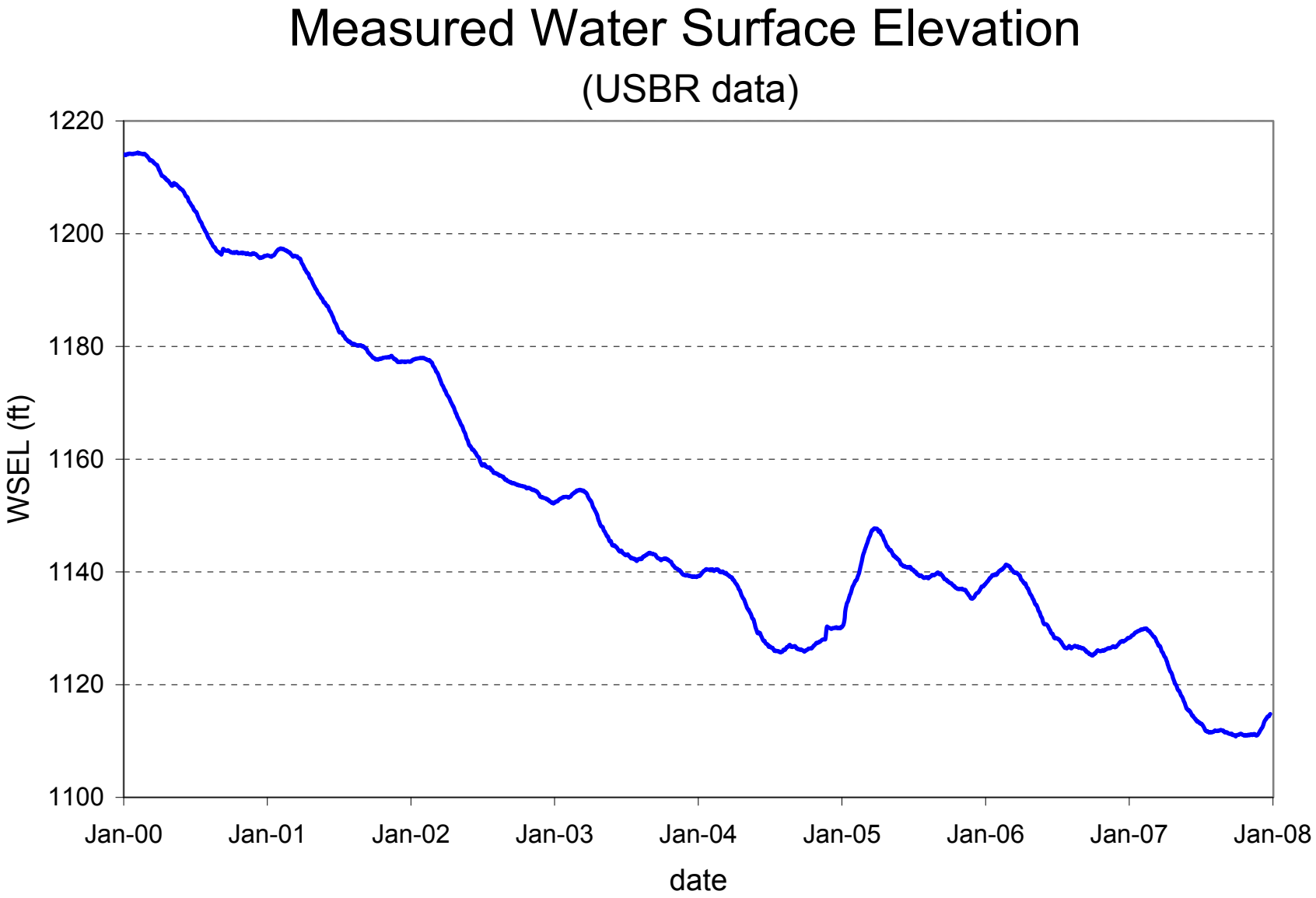
Measured Water Surface Elevation
(USBR data)
WSEL (ft)
1220
1200
1180
1160
1140
1120
1100
Jan-00
Jan-01
Jan-02
Jan-03
Jan-04
Jan-05
Jan-06
Jan-07
Jan-08
date

Figure 2.5

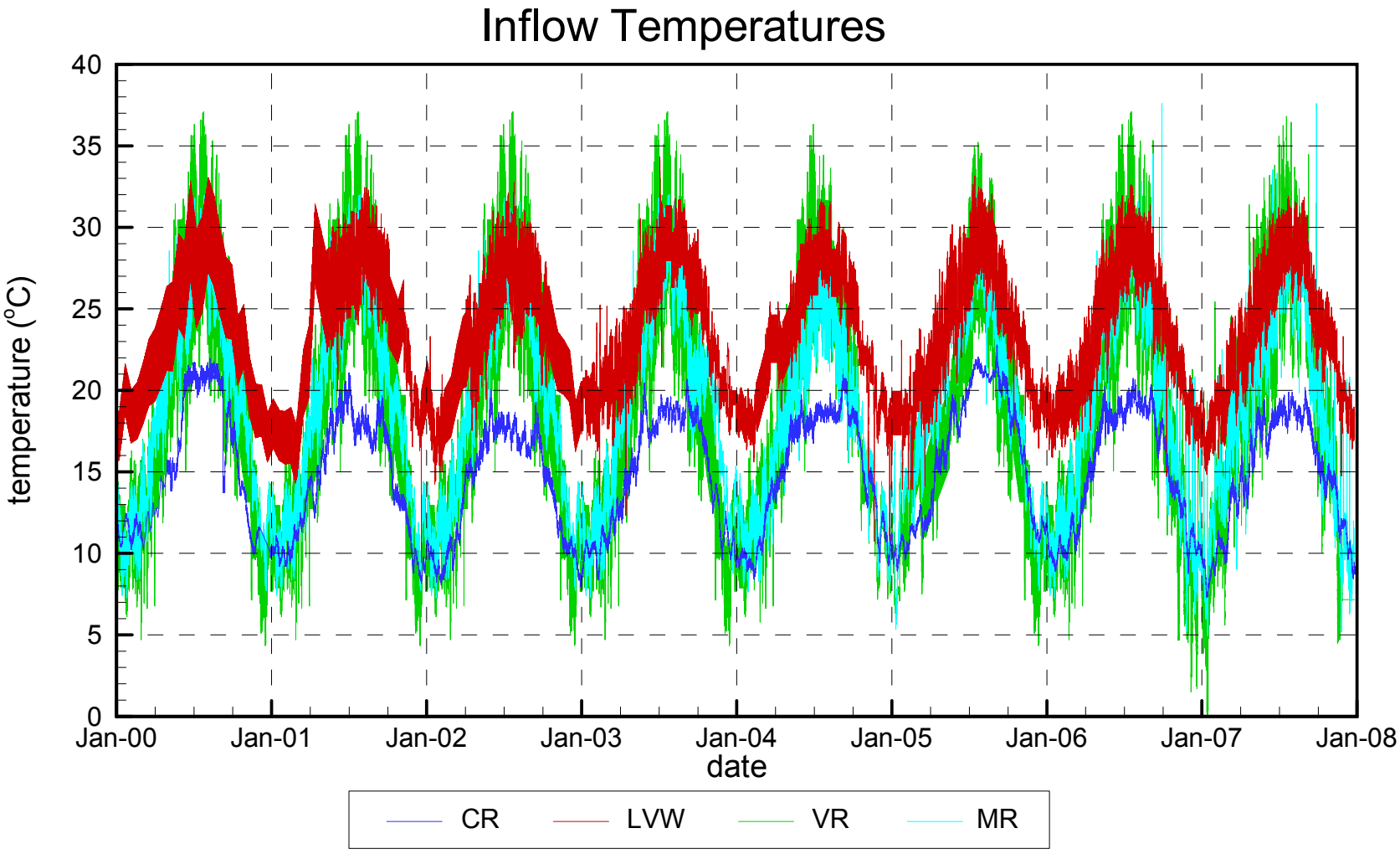
Inflow Temperatures
temperature (°C)
40
35
30
25
20
15
10
5
0
Jan-00
Jan-01
Jan-02
Jan-03
Jan-04
Jan-05
Jan-06
Jan-07
Jan-08
date
CR
LVW
VR
MR

Figure 2.6

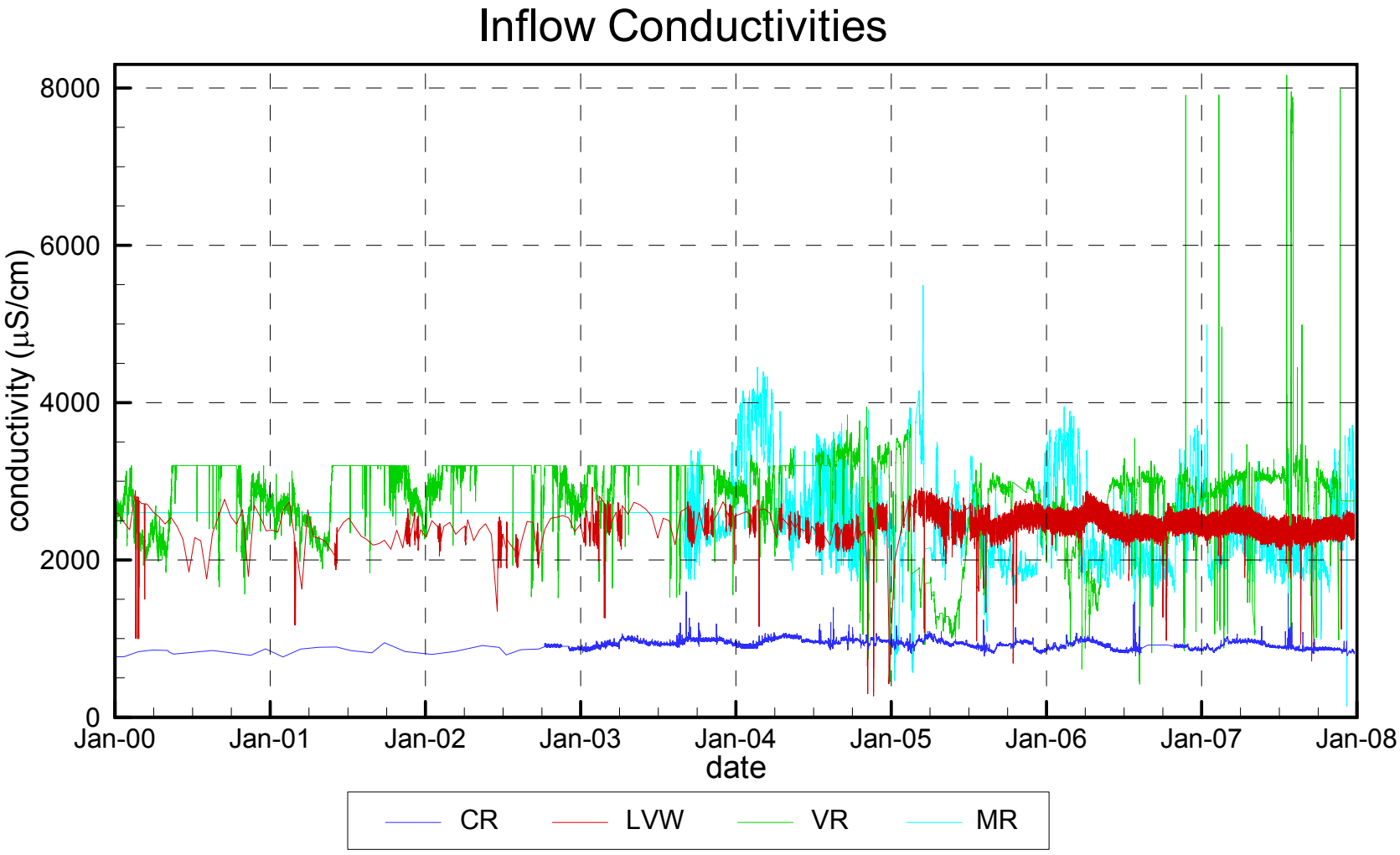
Inflow Conductivities
conductivity (µS/cm)
8000
6000
4000
2000
0
Jan-00
Jan-01
Jan-02
Jan-03
Jan-04
Jan-05
Jan-06
Jan-07
Jan-08
date
CR
LVW
VR
MR

Figure 2.7

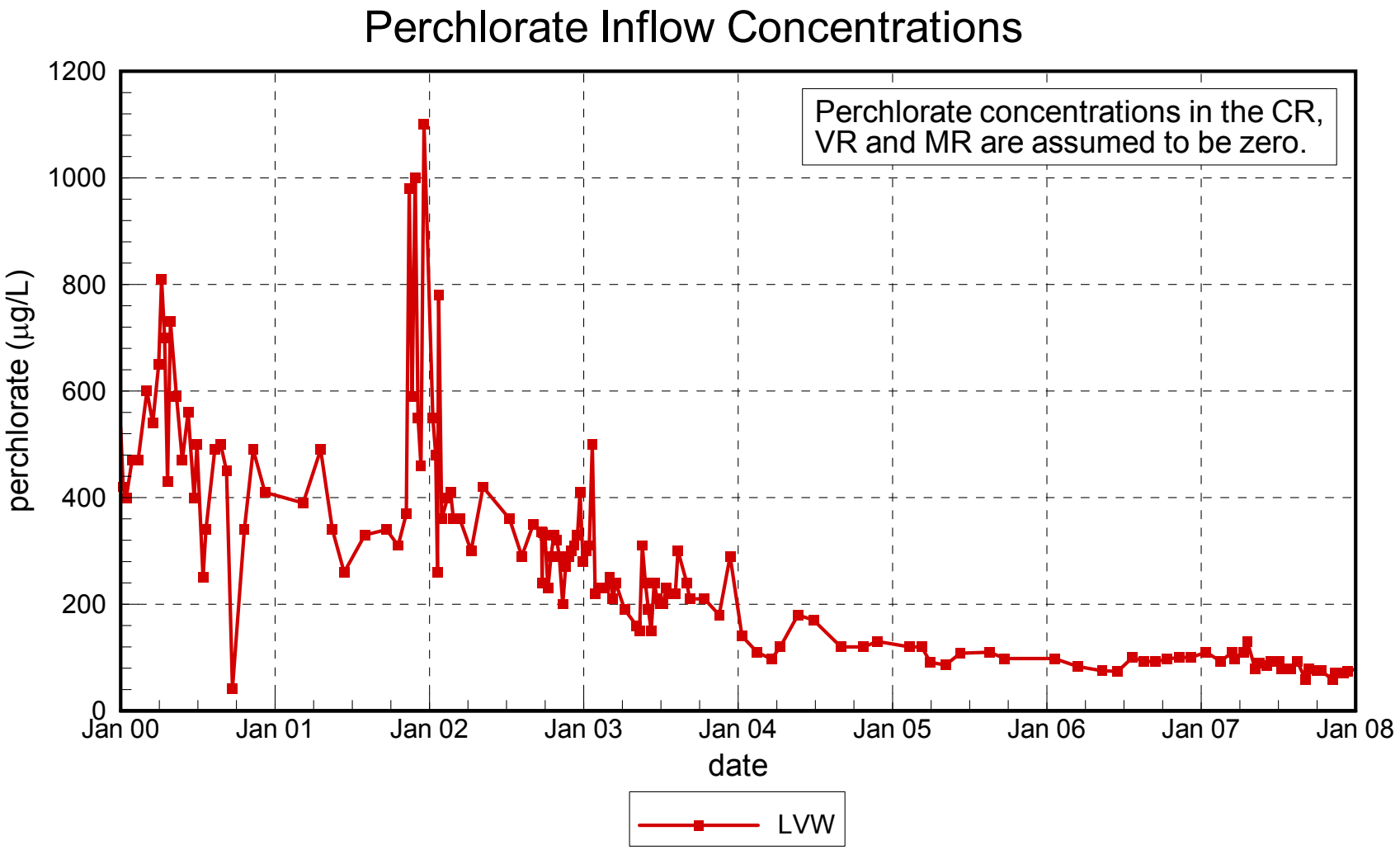
Perchlorate Inflow Concentrations
Perchlorate concentrations in the CR, VR and MR are assumed to be zero.
perchlorate (µg/L)
1200
1000
800
600
400
200
0
Jan 00
Jan 01
Jan 02
Jan 03
Jan 04
Jan 05
Jan 06
Jan 07
Jan 08
date
LVW

Figure 2.8

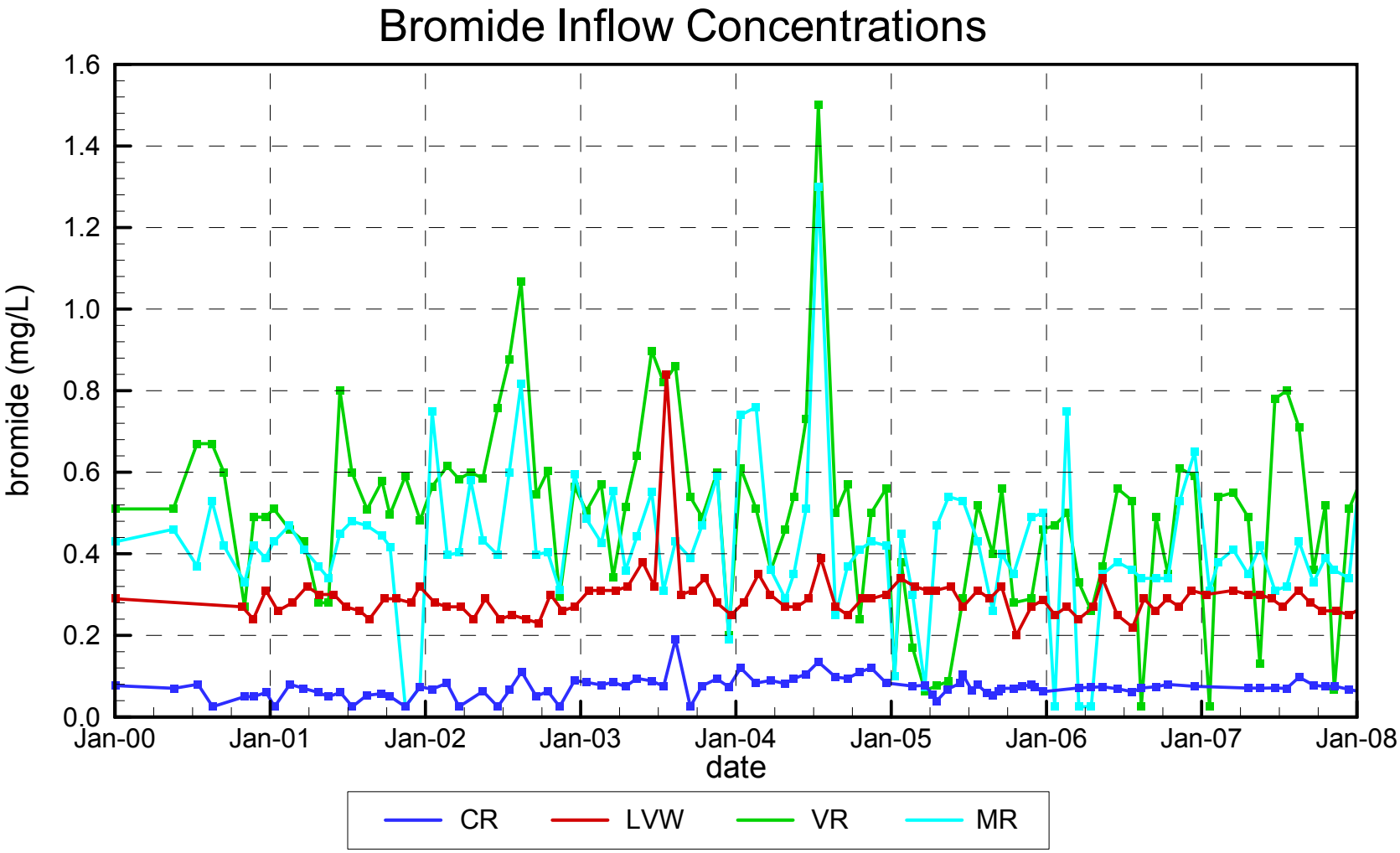
Bromide Inflow Concentrations
bromide (mg/L)
1.6
1.4
1.2
1.0
0.8
0.6
0.4
0.2
0.0
Jan-00
Jan-01
Jan-02
Jan-03
Jan-04
Jan-05
Jan-06
Jan-07
Jan-08
date
CR
LVW
VR
MR

Figure 2.9

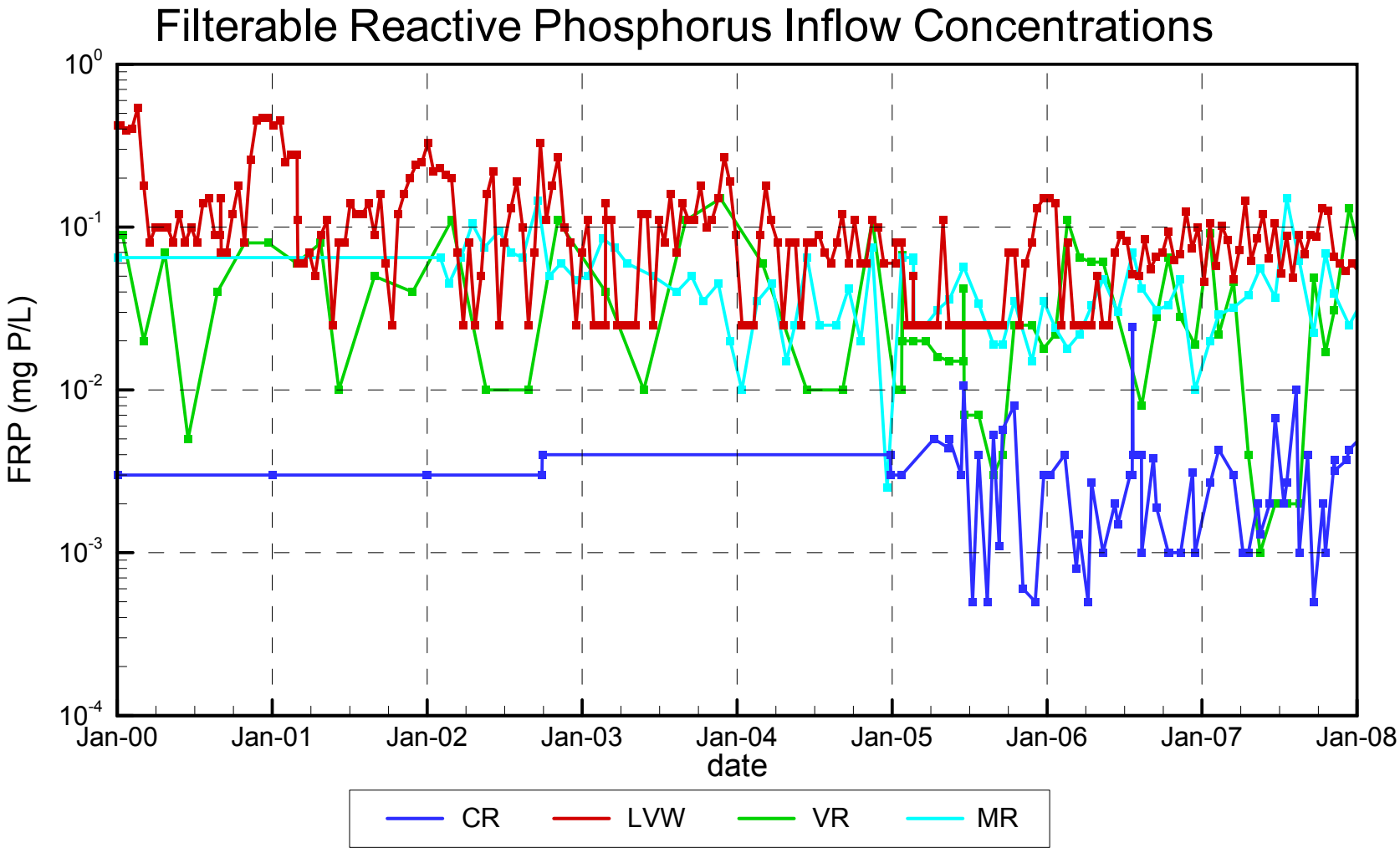
Filterable Reactive Phosphorus Inflow Concentrations
FRP (mg P/L)
10^0
10^-1
10^-2
10^-3
10^-4
Jan-00
Jan-01
Jan-02
Jan-03
Jan-04
Jan-05
Jan-06
Jan-07
Jan-08
date
CR
LVW
VR
MR

Figure 2.10

Filterable Reactive Phosphorus in Las Vegas Wash

(Data Source: COH and WWTPs)

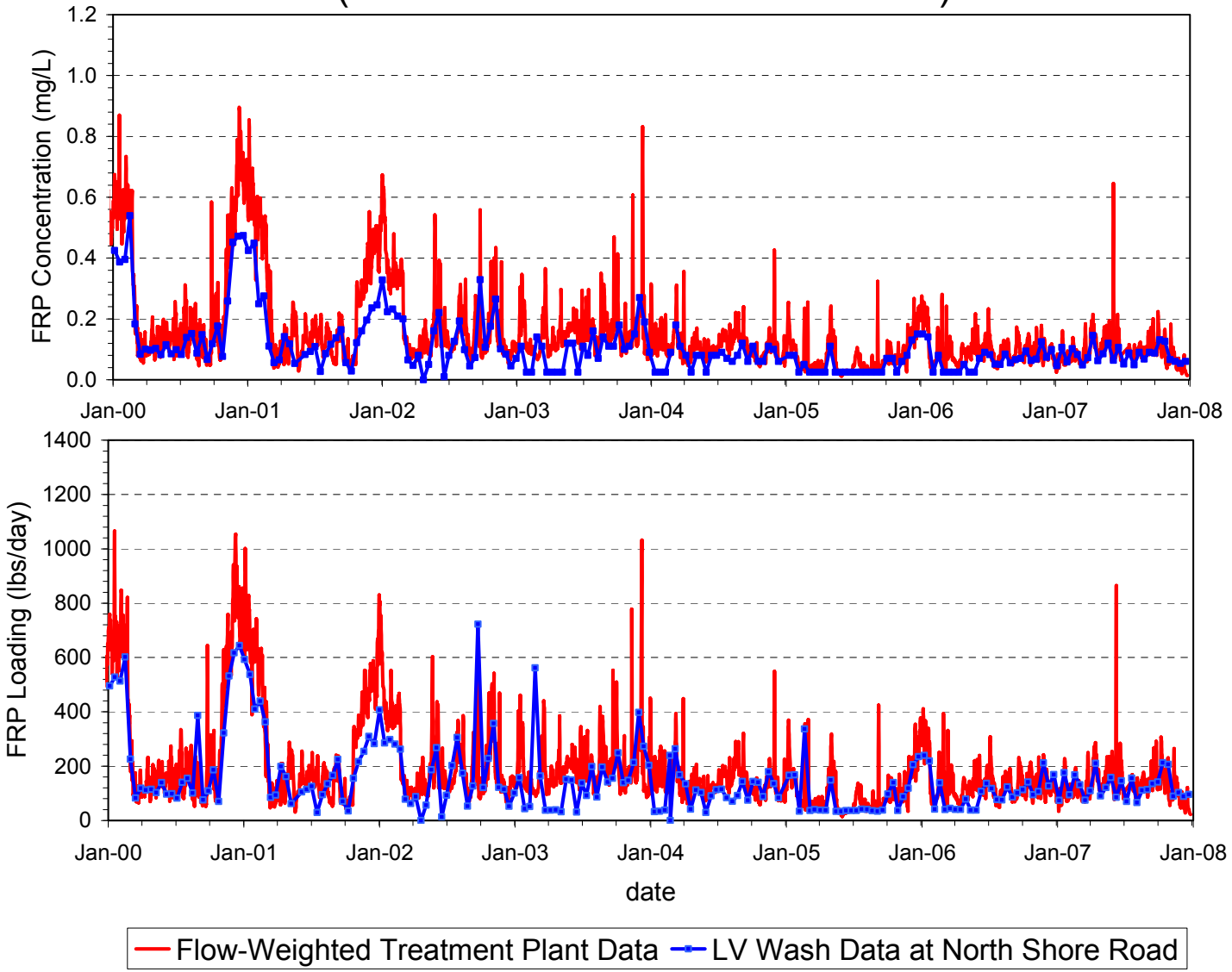

Figure 2.11

Total Phosphorus in Las Vegas Wash

(Data Source: COH and WWTPs)

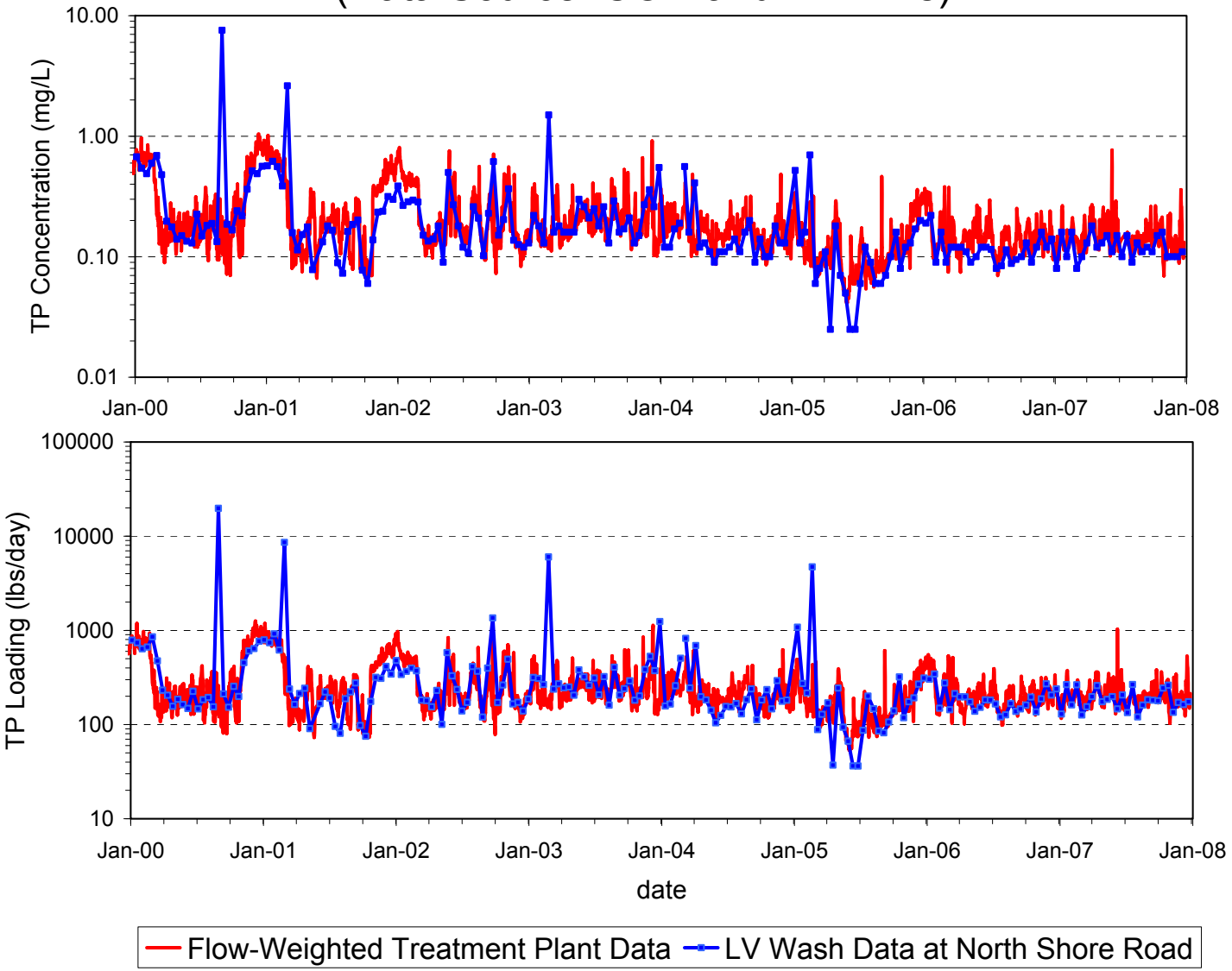

Figure 2.12

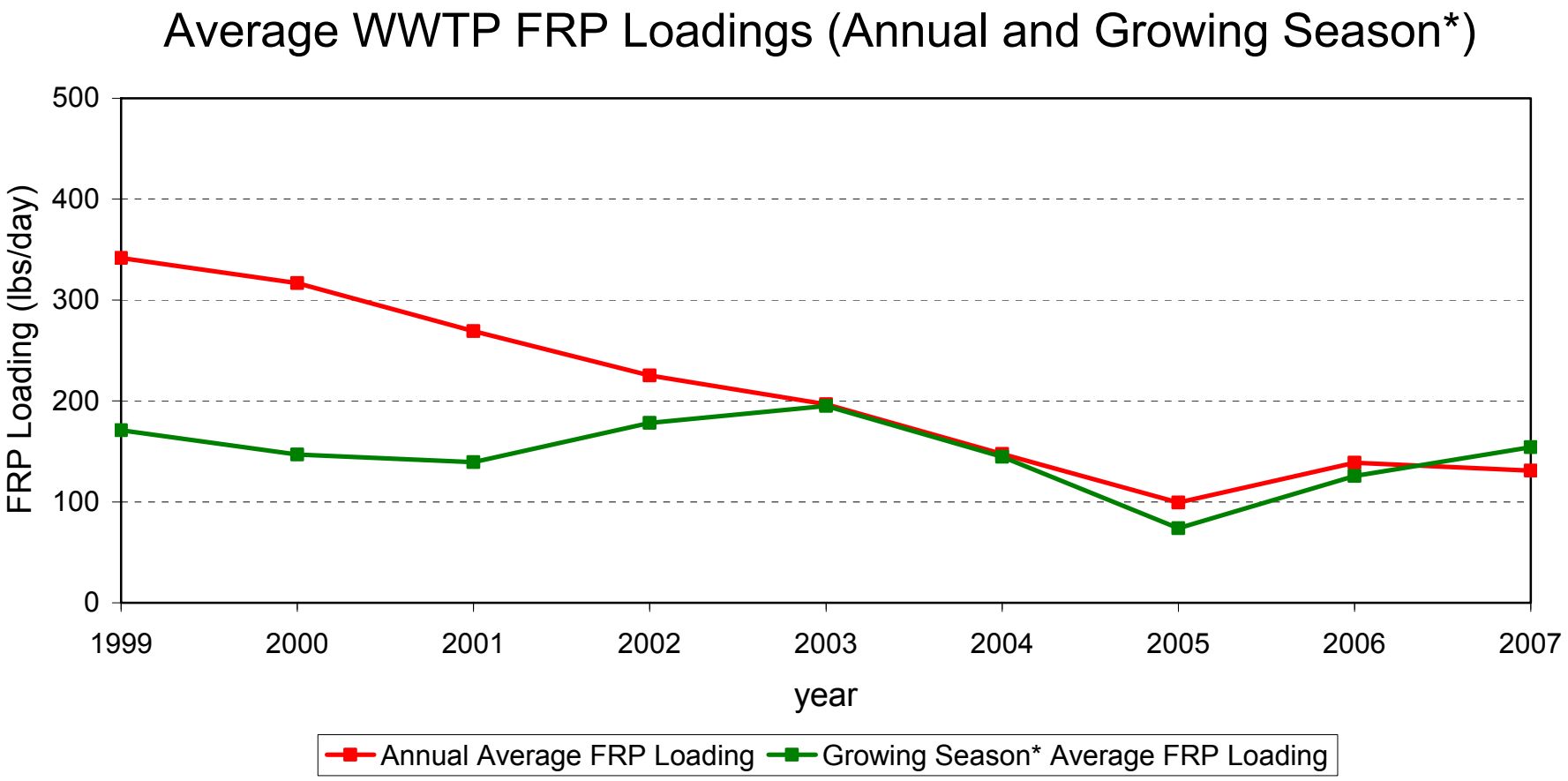
Average WWTP FRP Loadings (Annual and Growing Season*)
FRP Loading (lbs/day)
500
400
300
200
100
0
1999
2000
2001
2002
2003
2004
2005
2006
2007
year
Annual Average FRP Loading
Growing Season* Average FRP Loading
* Growing Season is from April 1 through September 30

Figure 2.13

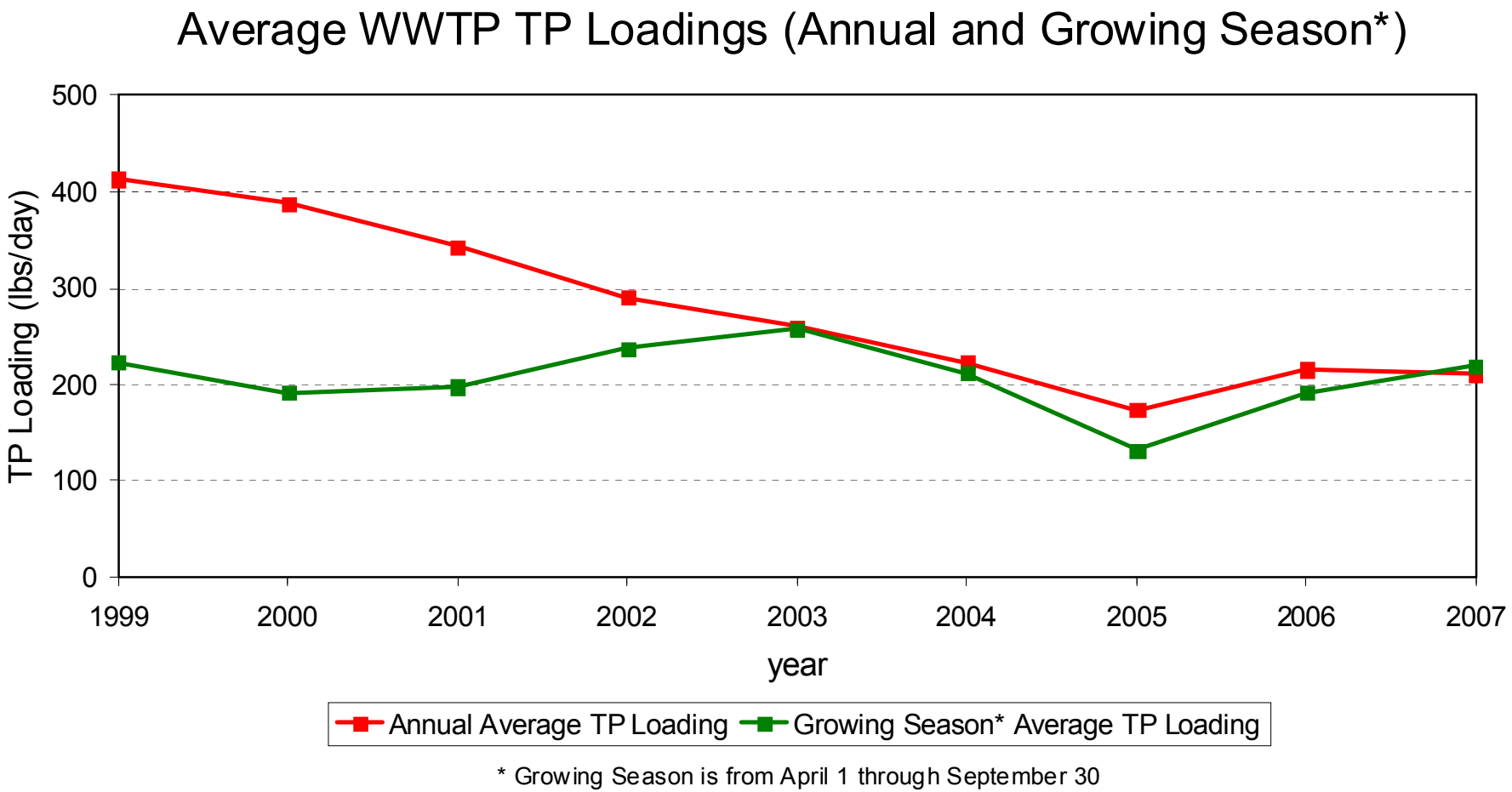
Average WWTP TP Loadings (Annual and Growing Season*)
TP Loading (lbs/day)
500
400
300
200
100
0
1999
2000
2001
2002
2003
2004
2005
2006
2007
year
Annual Average TP Loading
Growing Season* Average TP Loading
* Growing Season is from April 1 through September 30

Figure 2.14

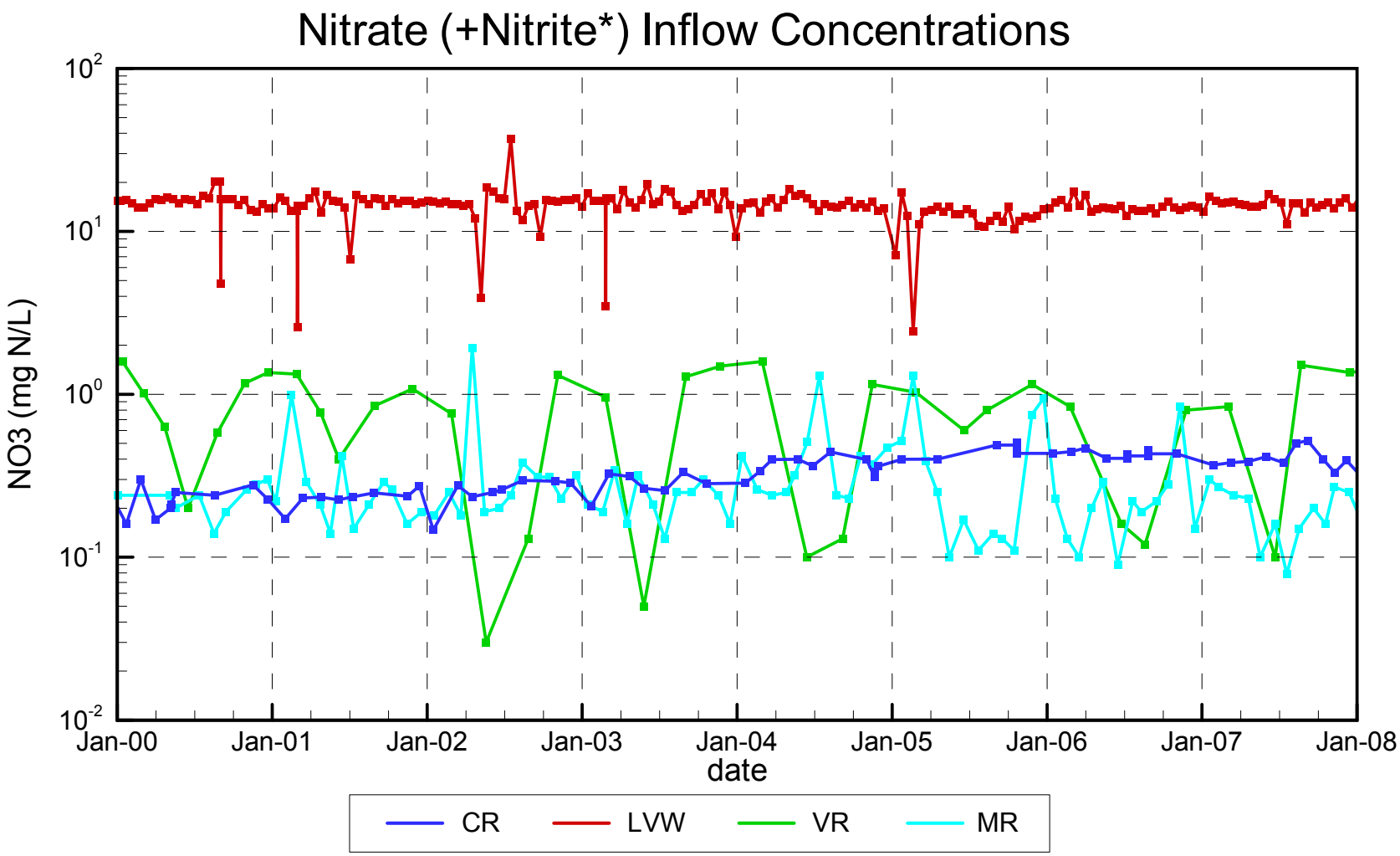

* The model treats nitrate + nitrite as a single combined variable, denoted as NO3.

Figure 2.15

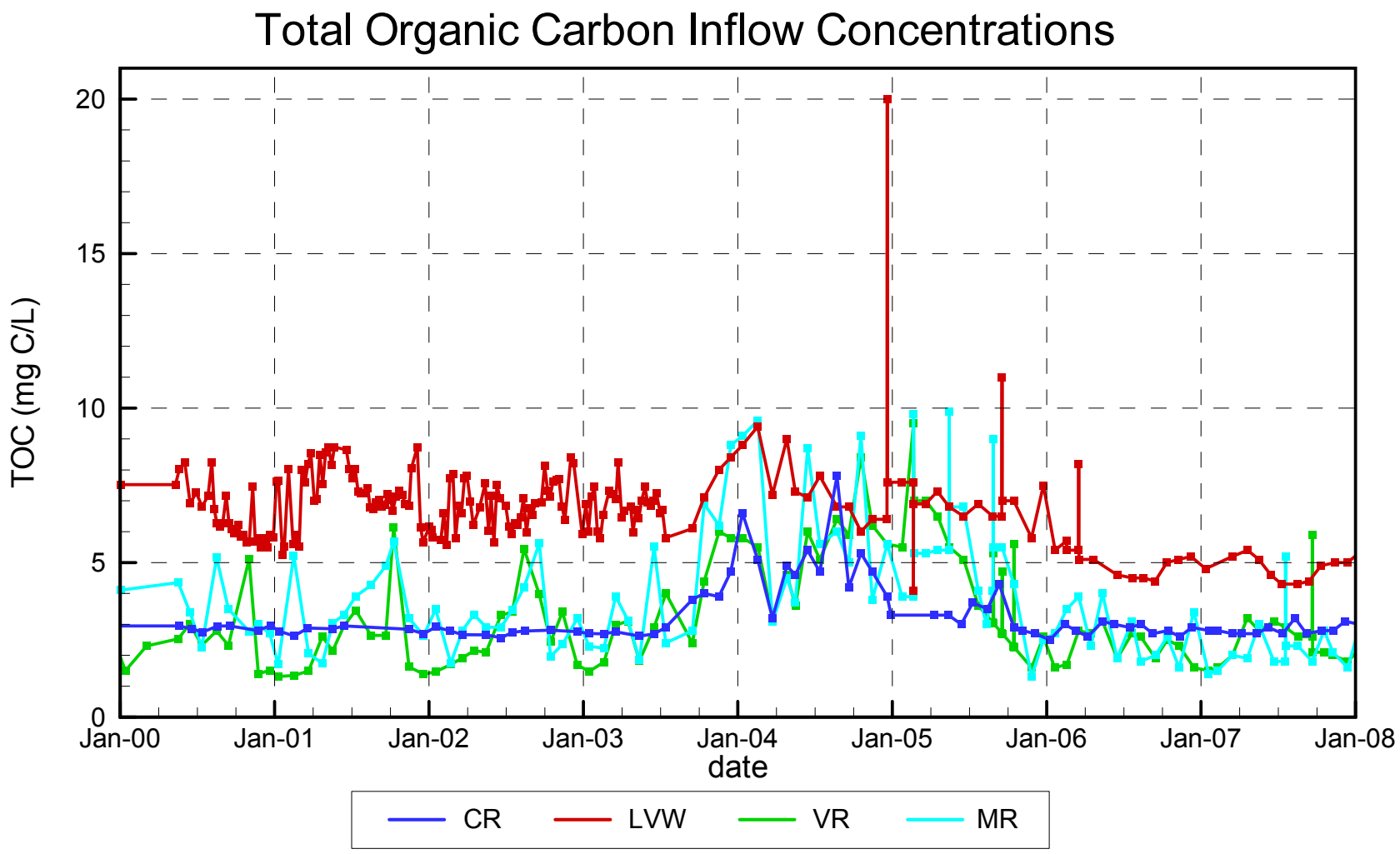
Total Organic Carbon Inflow Concentrations
TOC (mg C/L)
20
15
10
5
0
Jan-00
Jan-01
Jan-02
Jan-03
Jan-04
Jan-05
Jan-06
Jan-07
Jan-08
date
CR
LVW
VR
MR

Figure 2.16

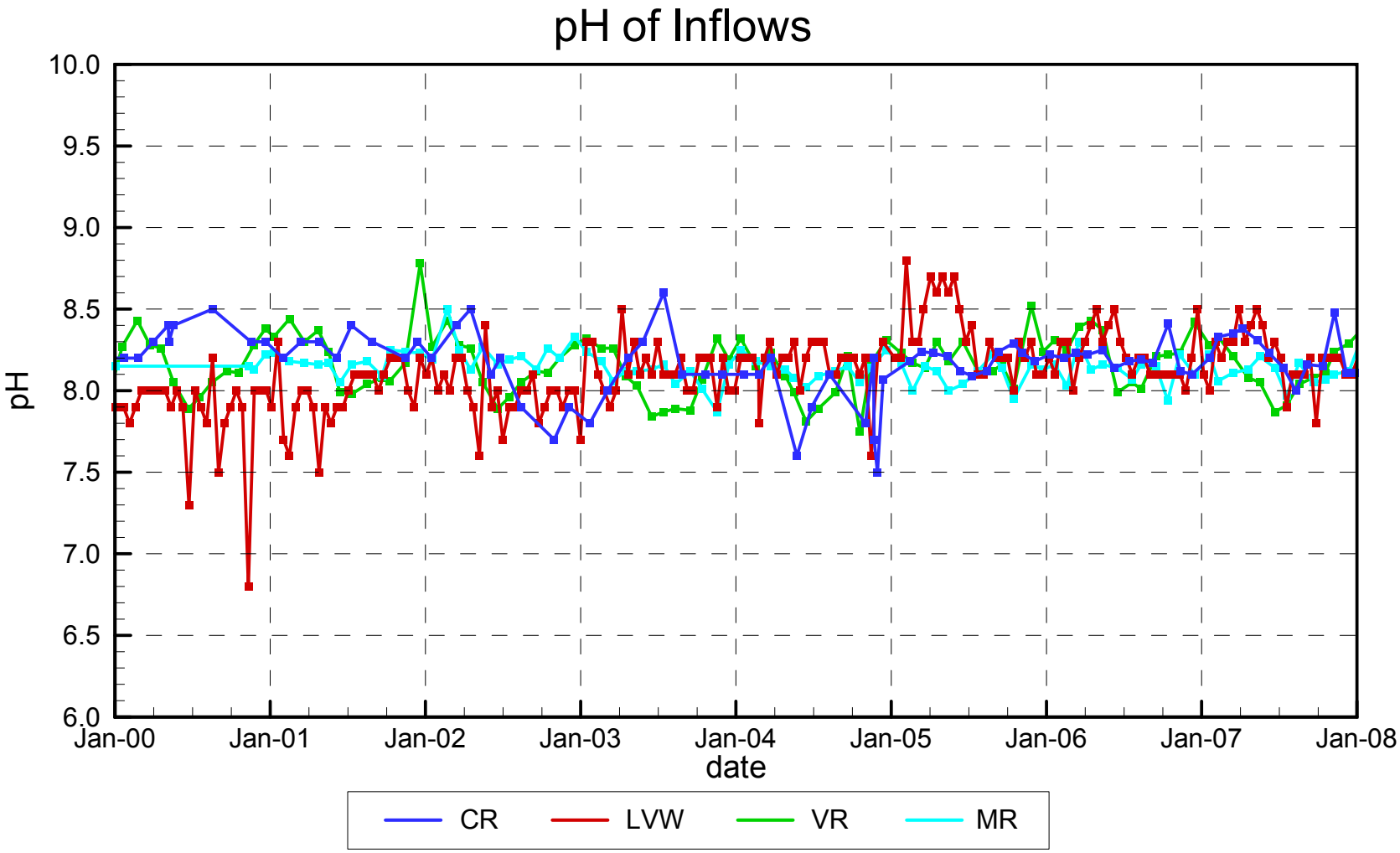
pH of Inflows
10.0
9.5
9.0
8.5
8.0
7.5
7.0
6.5
6.0
pH
Jan-00
Jan-01
Jan-02
Jan-03
Jan-04
Jan-05
Jan-06
Jan-07
Jan-08
date
CR
LVW
VR
MR

Figure 2.17

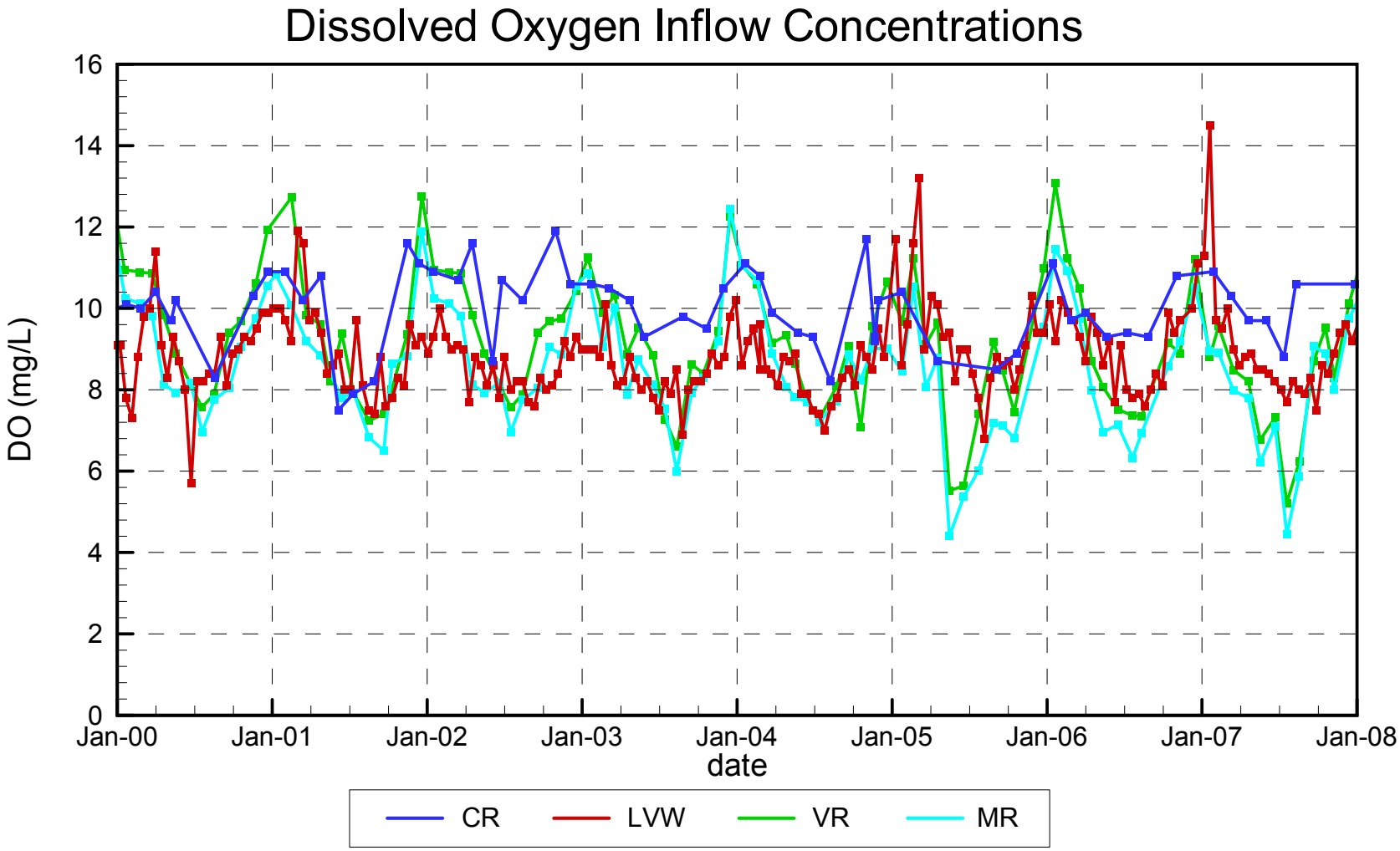
Dissolved Oxygen Inflow Concentrations
DO (mg/L)
16
14
12
10
8
6
4
2
0
Jan-00
Jan-01
Jan-02
Jan-03
Jan-04
Jan-05
Jan-06
Jan-07
Jan-08
date
CR
LVW
VR
MR

Figure 2.18

Measured Conductivity in Lake Mead : February 13 - 16, 2006

(USBR data)

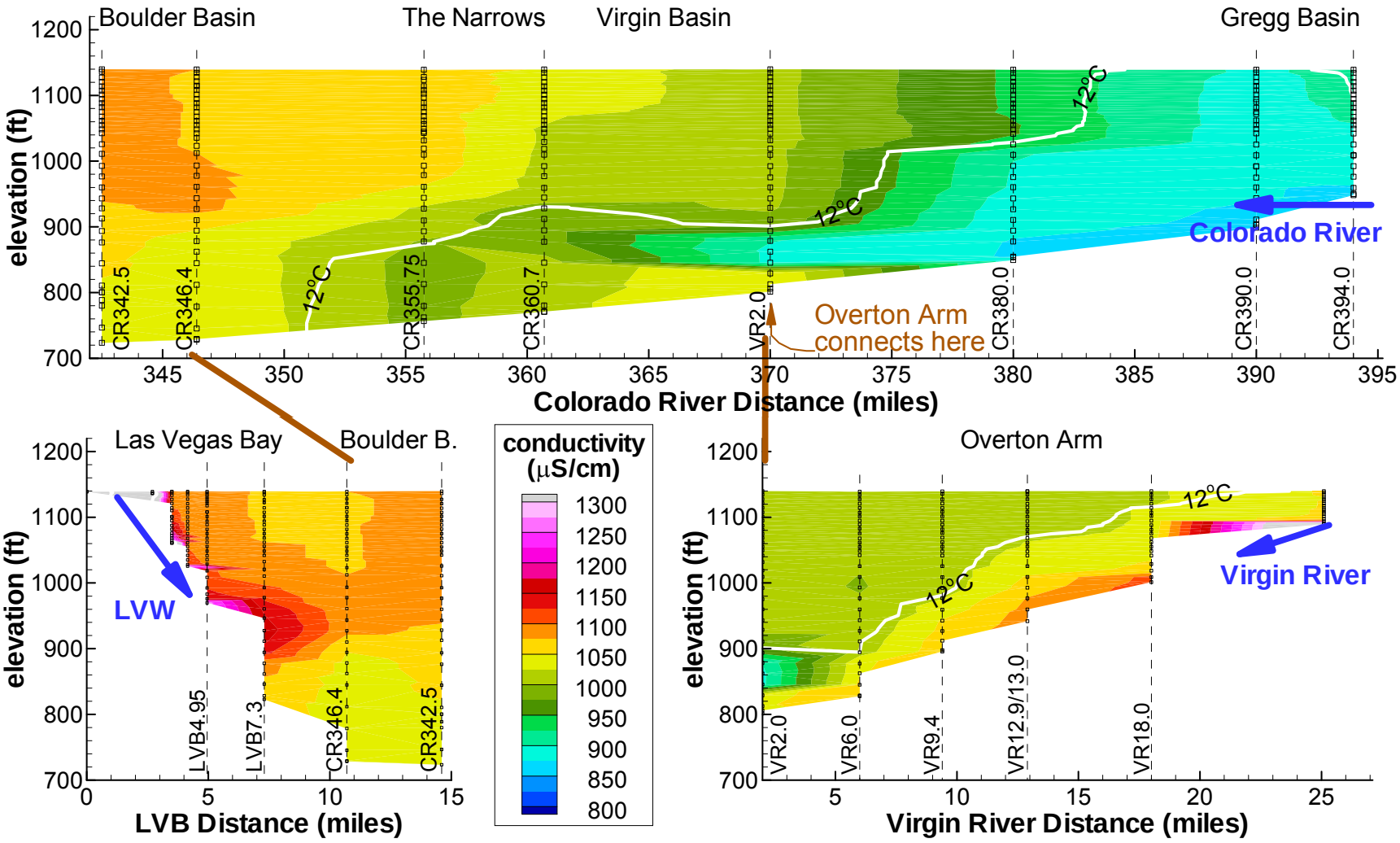

Figure 2.19

FLOW SCIENCE

Measured Conductivity in Lake Mead : April 11 - 13, 2006

(USBR data)

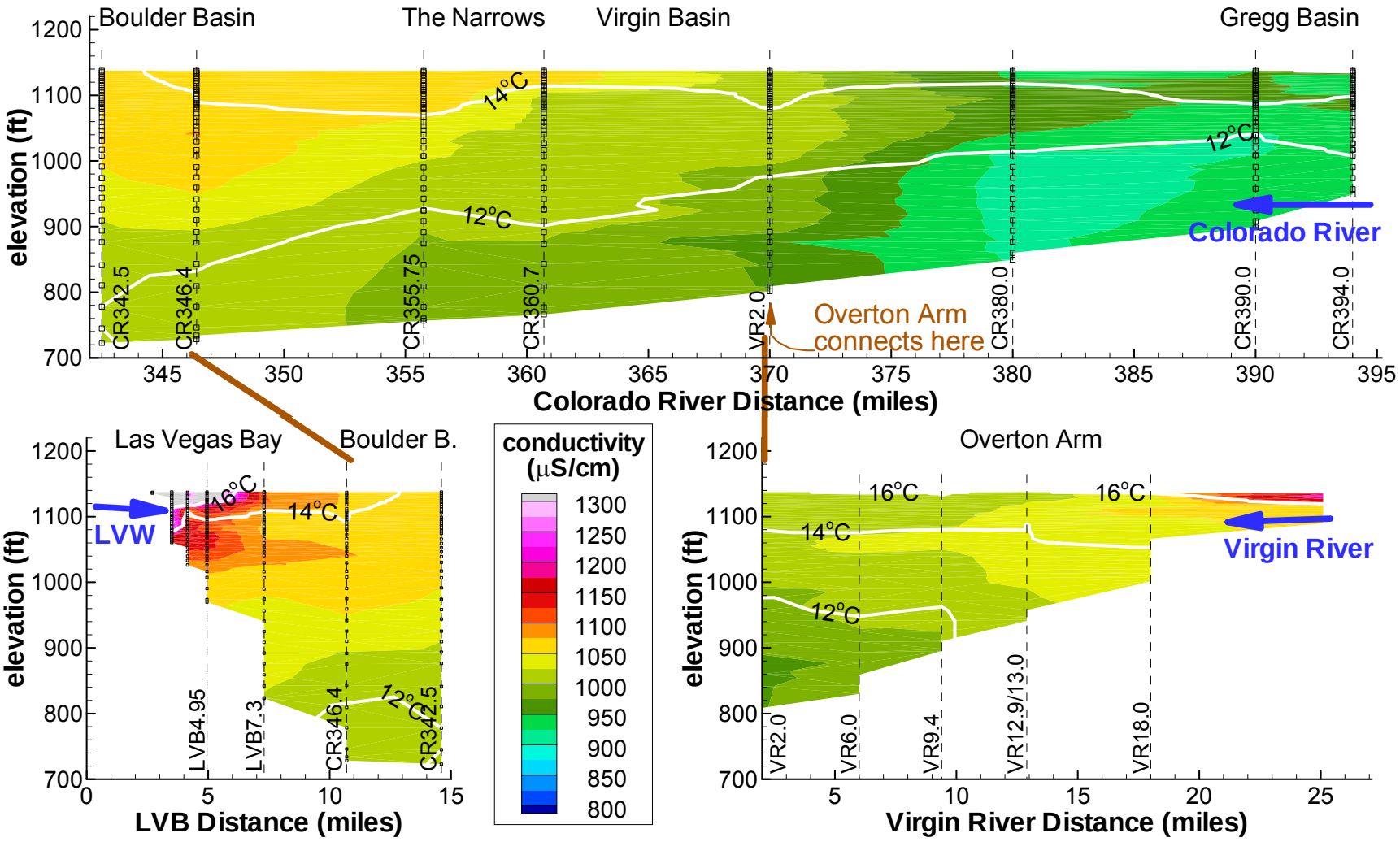

Figure 2.20

FLOW SCIENCE

Measured Conductivity in Lake Mead : June 13 - 15, 2006

(USBR data)

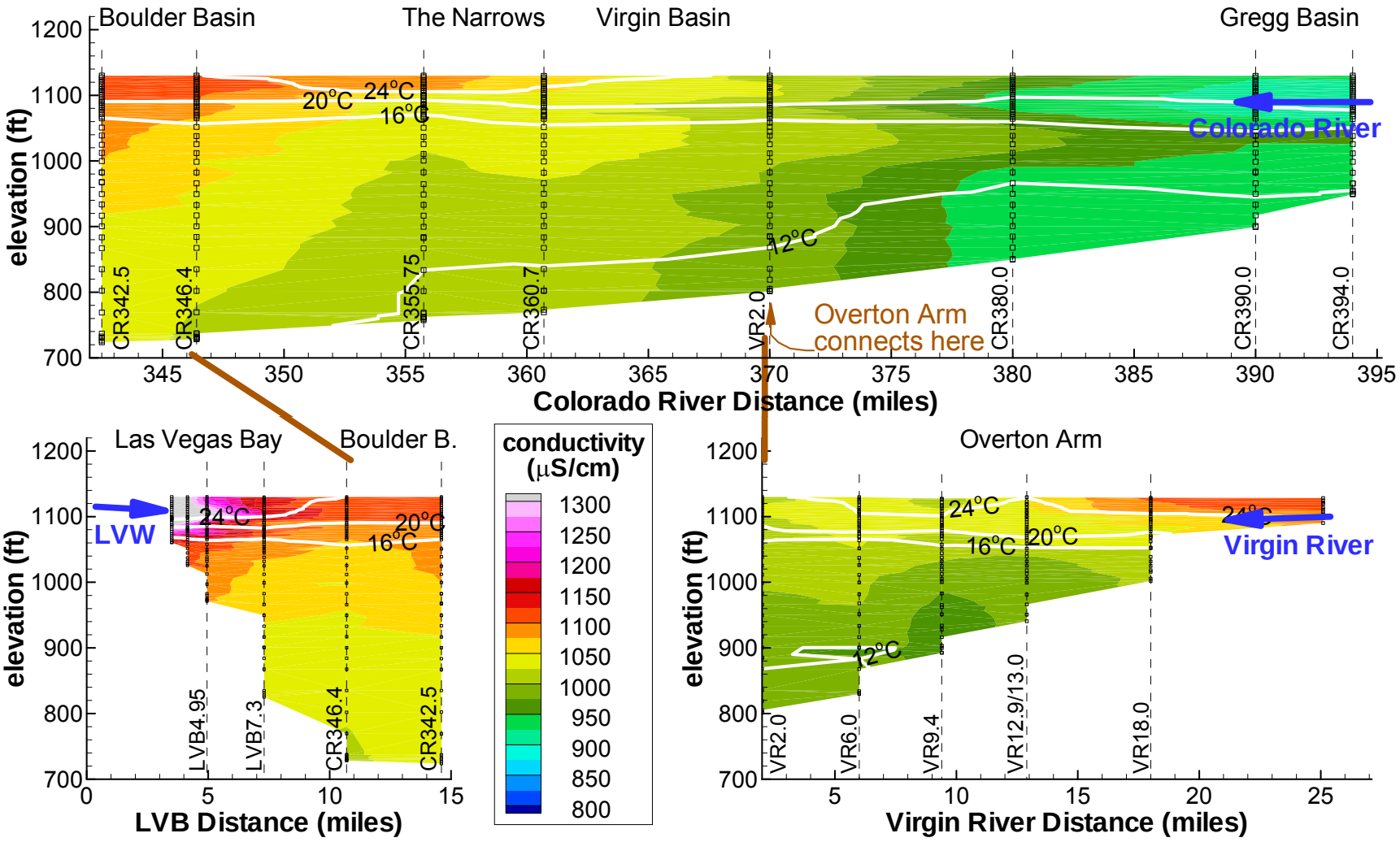

Figure 2.21

FLOW SCIENCE

Measured Conductivity in Lake Mead : August 15 - 17, 2006

(USBR data)

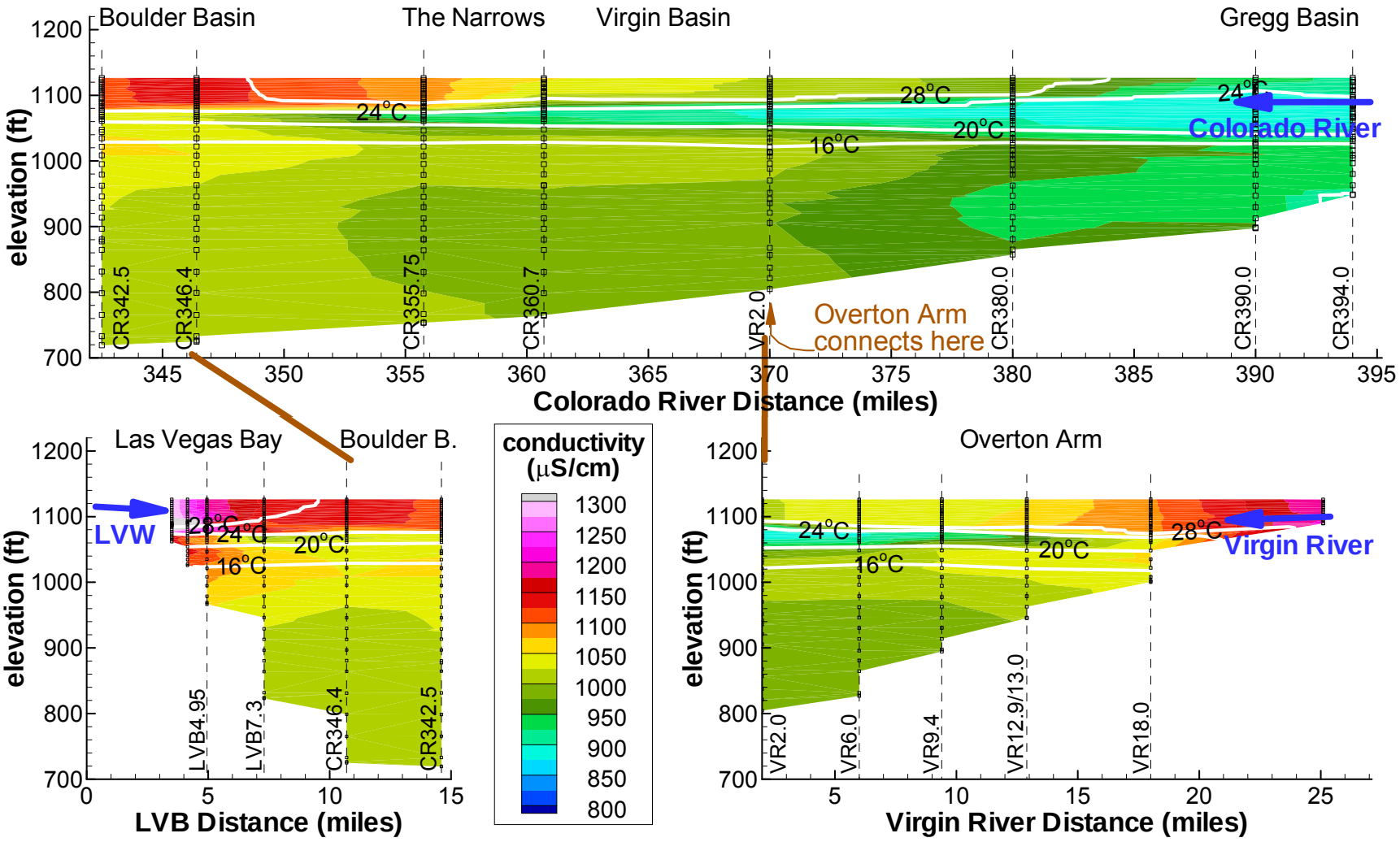

Figure 2.22

FLOW SCIENCE

Measured Conductivity in Lake Mead : October 17 - 19, 2006

(USBR data)

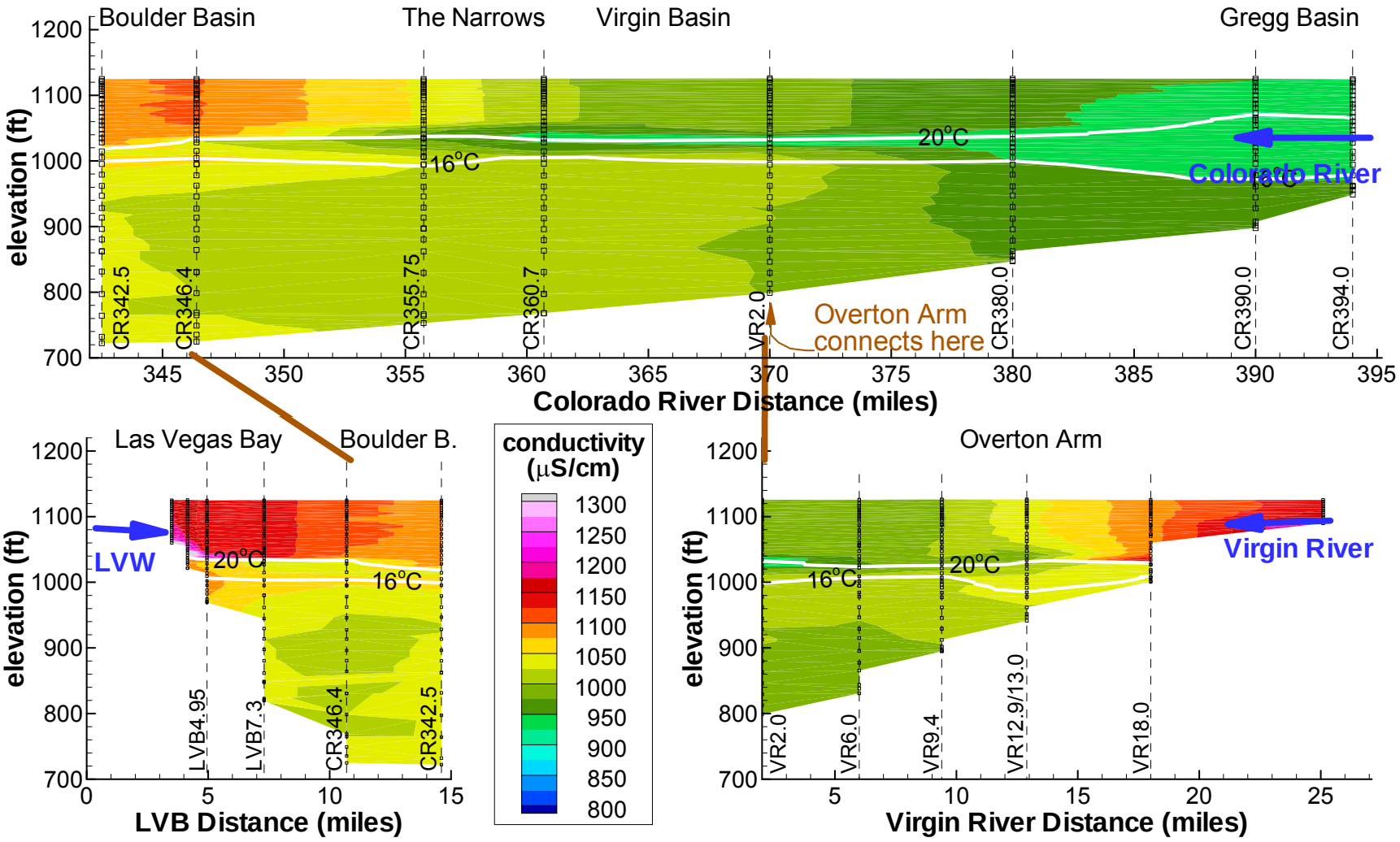

Figure 2.23

FLOW SCIENCE

Measured Conductivity in Lake Mead : December 12 - 14, 2006

(USBR data)

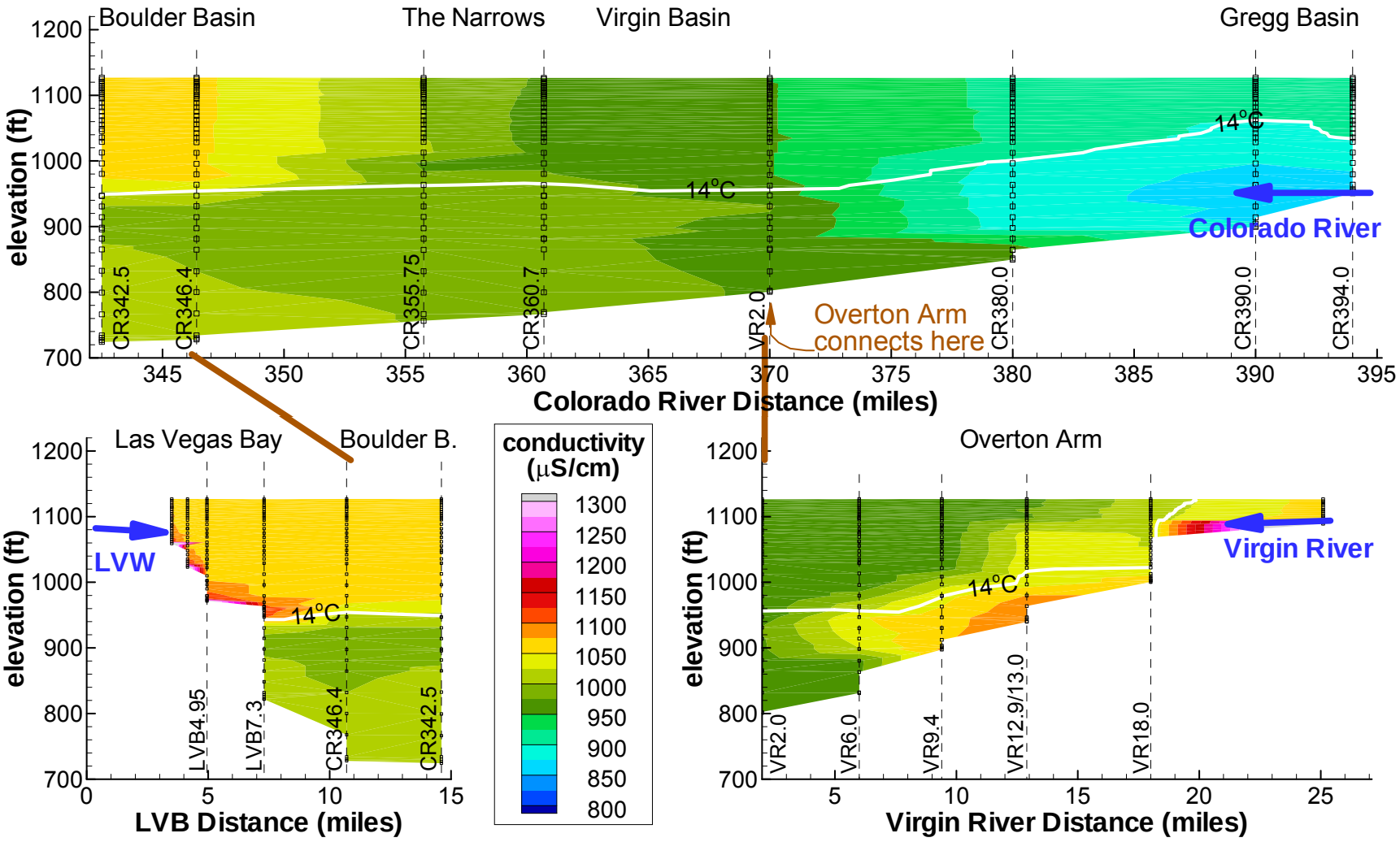

Figure 2.24

FLOW SCIENCE

Measured Conductivity in Lake Mead : February 13 - 15, 2007

(USBR data)

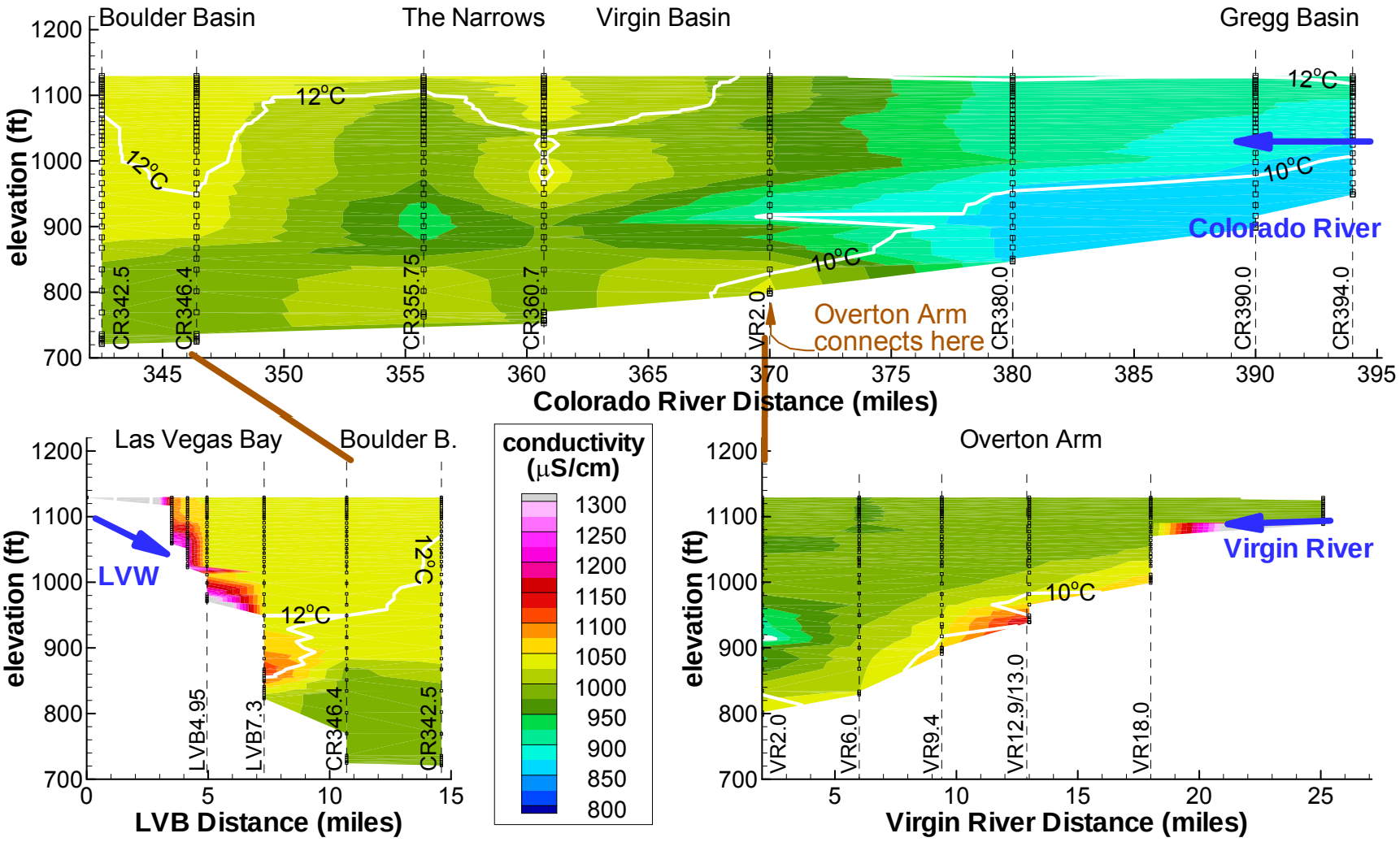

Figure 2.25

Measured Conductivity in Lake Mead : April 10 - 12, 2007

(USBR data)

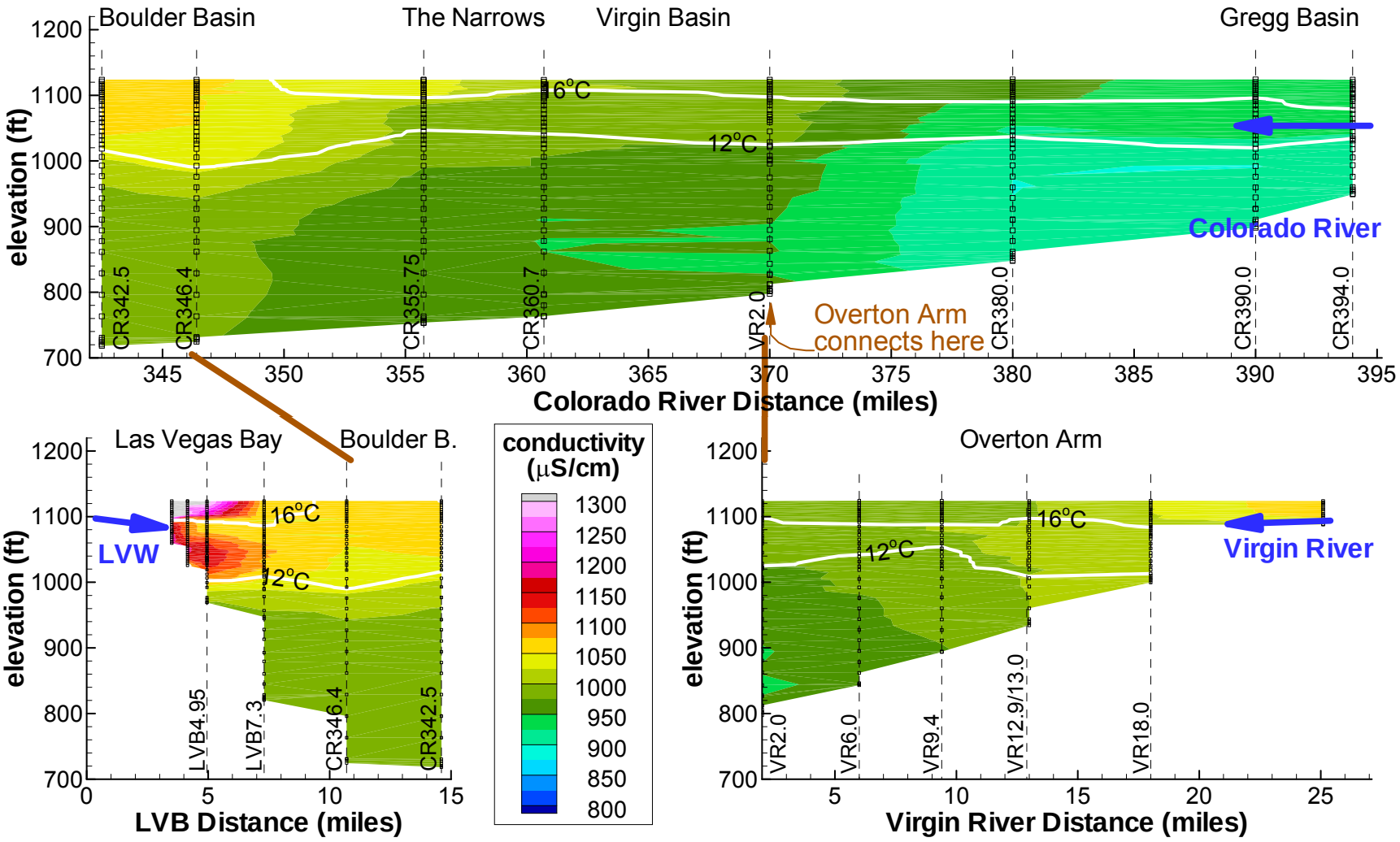

Figure 2.26

Measured Conductivity in Lake Mead : June 12 - 14, 2007

(USBR data)

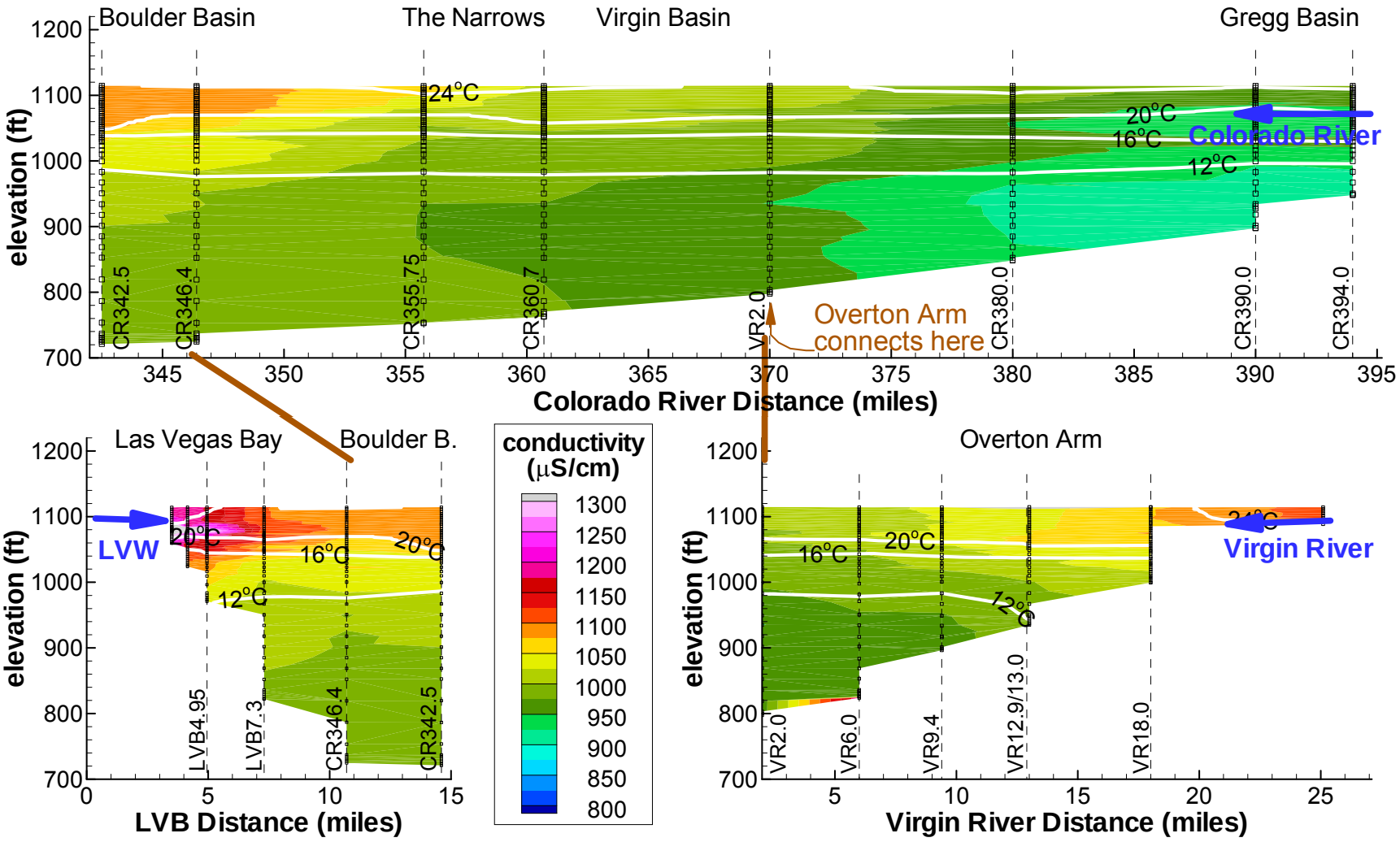

Ch2_Figures.ppt
FSI V064081 & V084015 Task 1
December 9, 2010

Figure 2.27

FLOW SCIENCE

Measured Conductivity in Lake Mead : August 14 - 16, 2007

(USBR data)

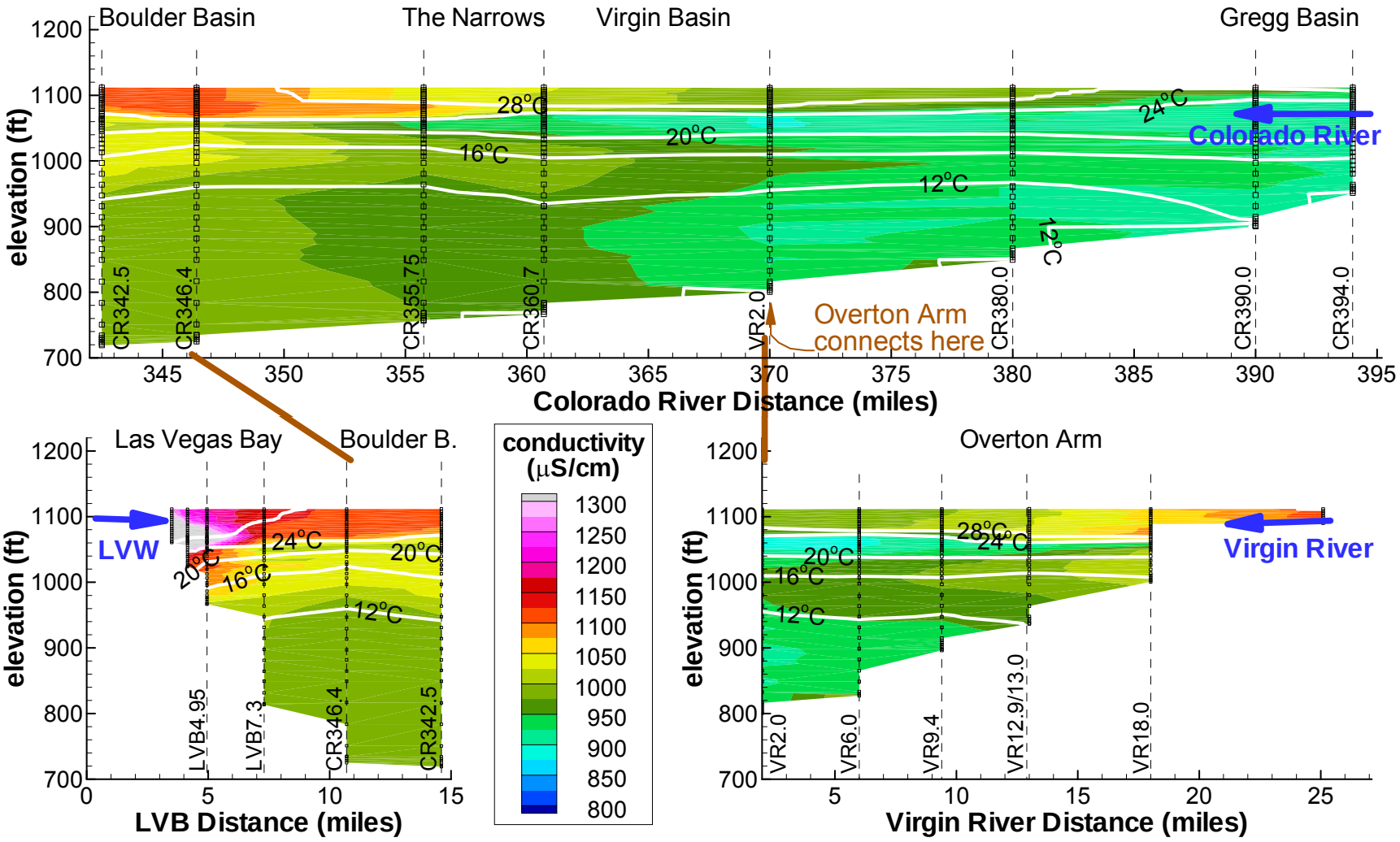

Figure 2.28

FLOW SCIENCE

Measured Conductivity in Lake Mead : October 16 - 18, 2007

(USBR data)

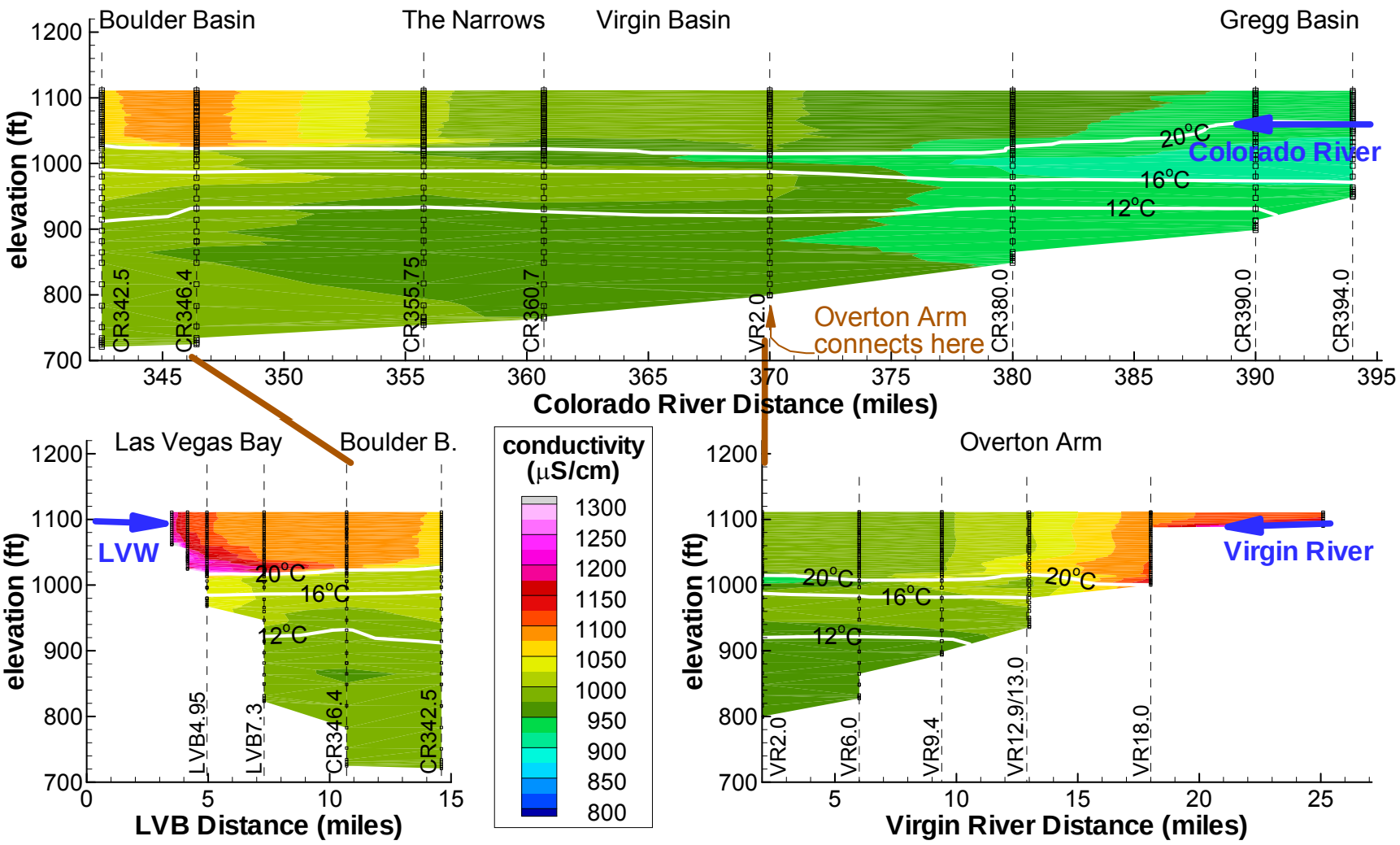

Figure 2.29

FLOW SCIENCE

Measured Conductivity in Lake Mead : December 11 - 13, 2007

(USBR data)

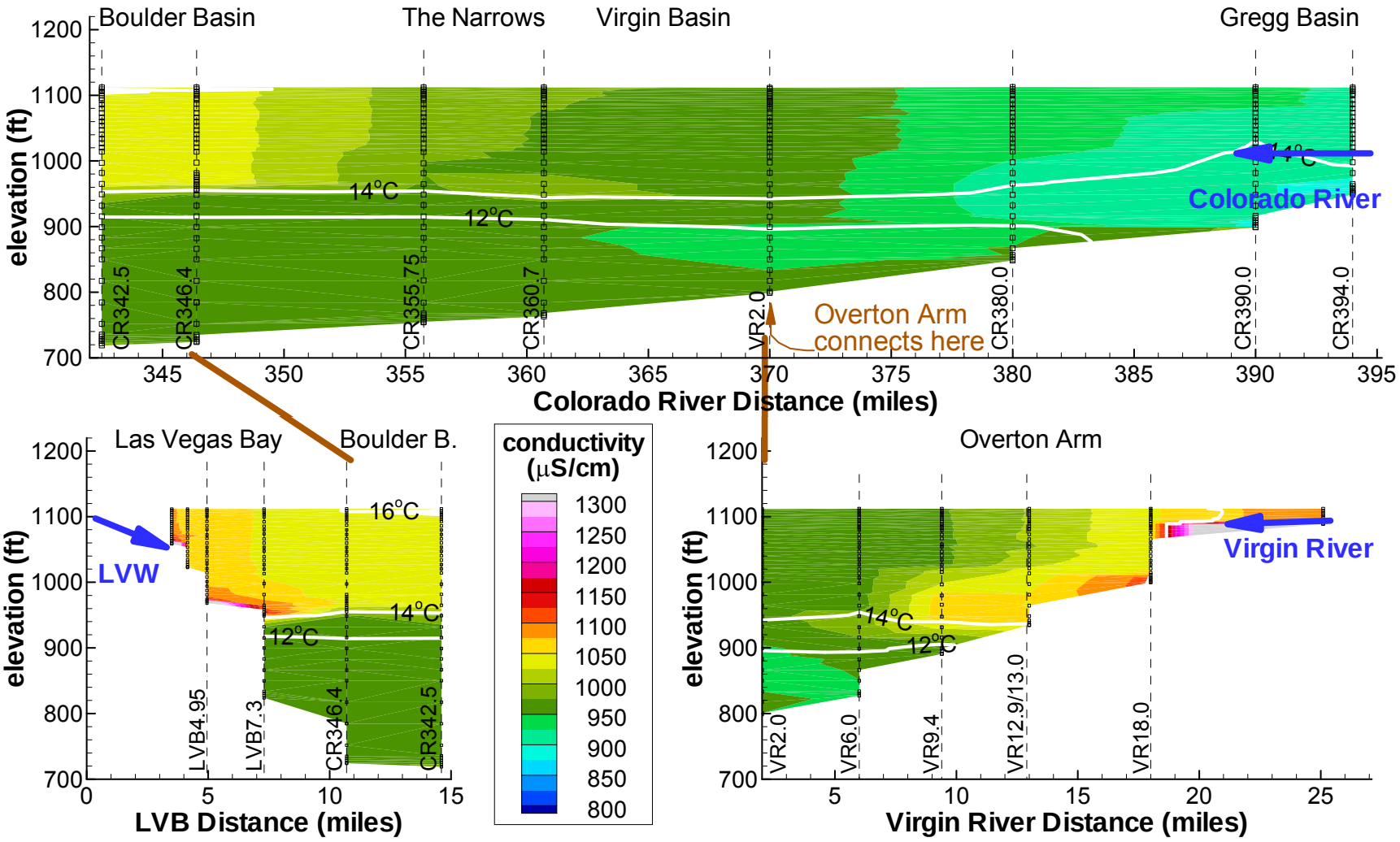

Figure 2.30

FLOW SCIENCE

Measured Temperature Profiles at Station CR394.0 2004 - 2007 (USBR data)

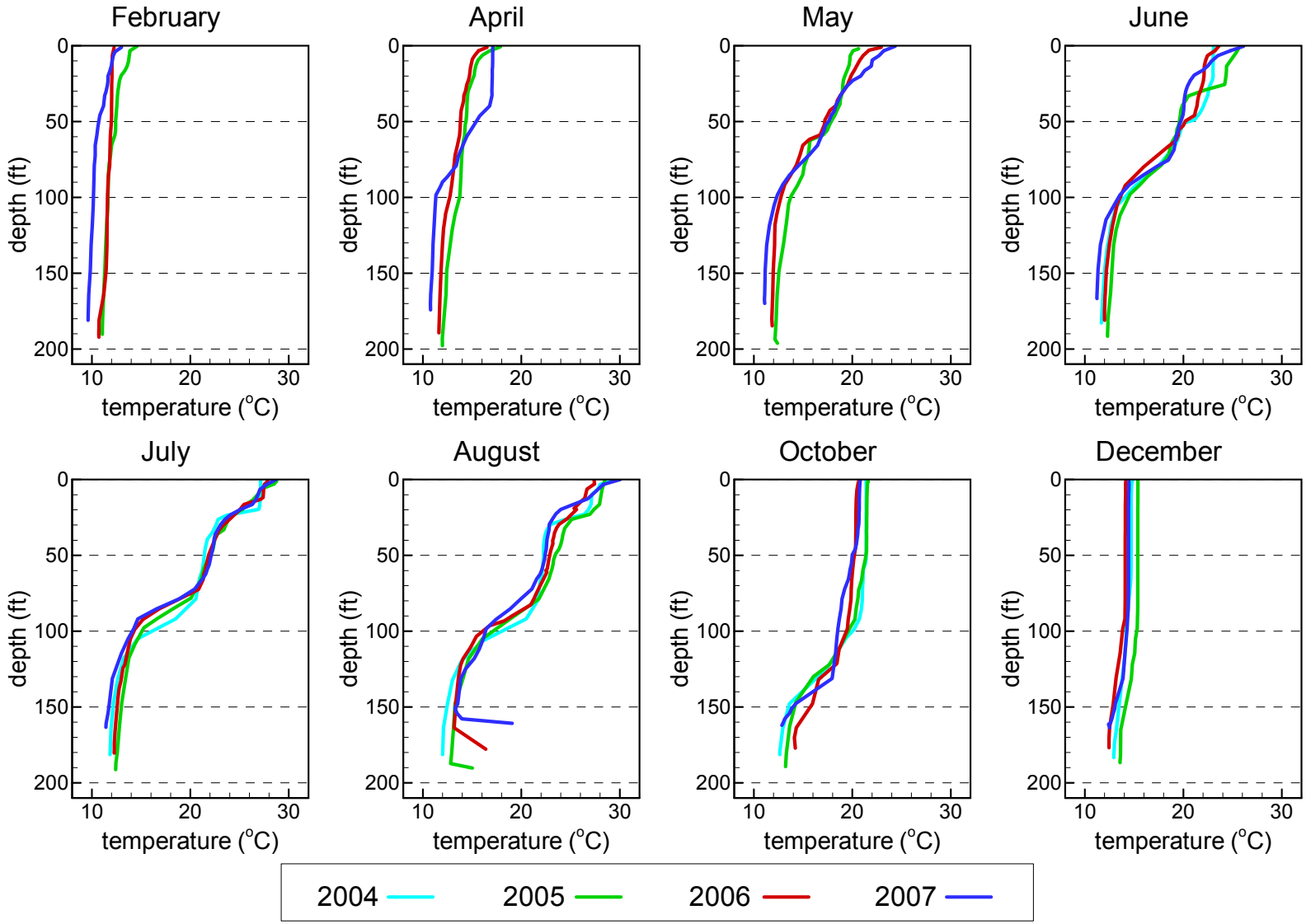

Figure 2.31

FLOW SCIENCE

Measured Conductivity in Lake Mead (USBR data)

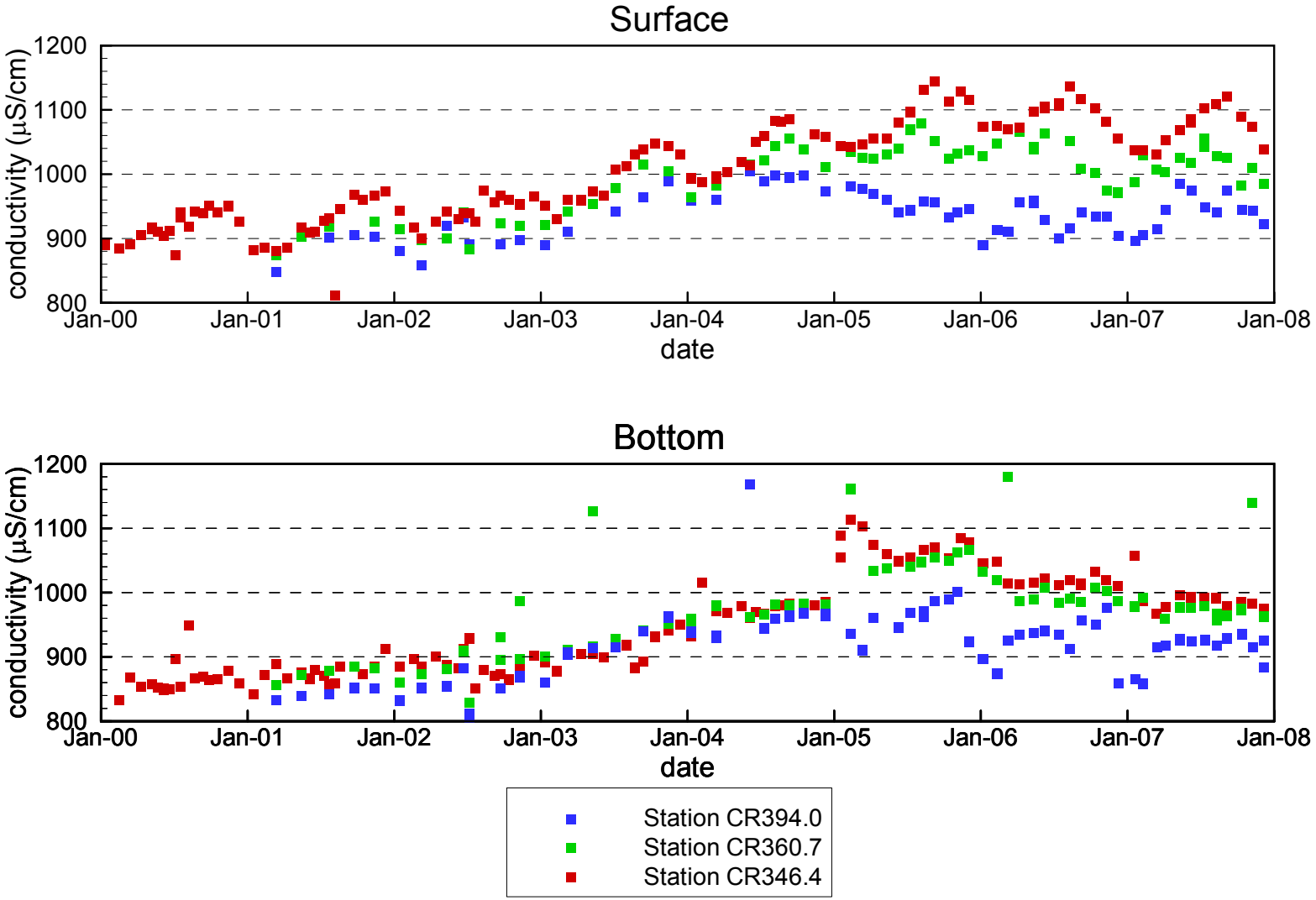

Figure 2.32

Measured Perchlorate at Station CR343.3

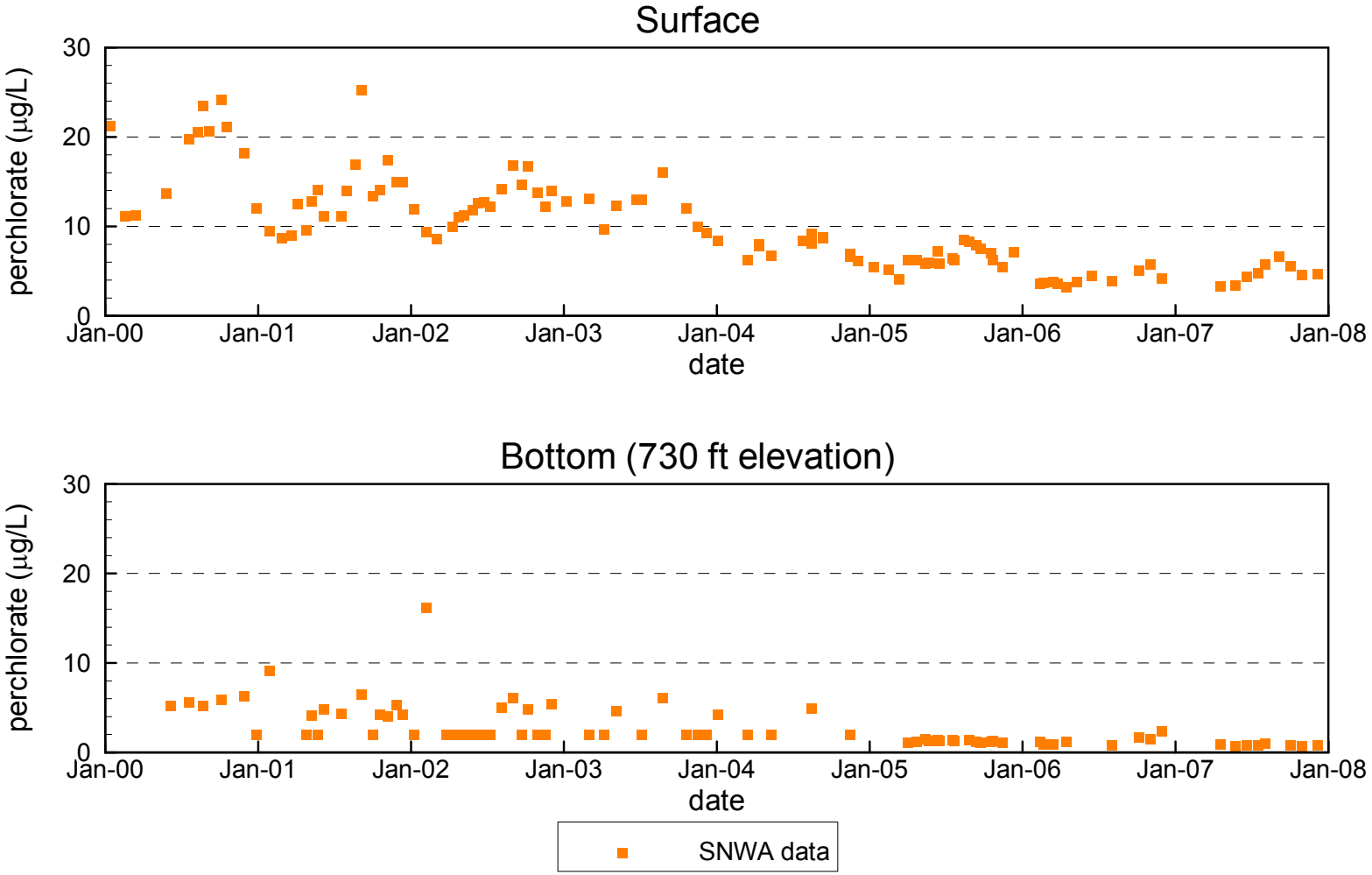

Figure 2.33

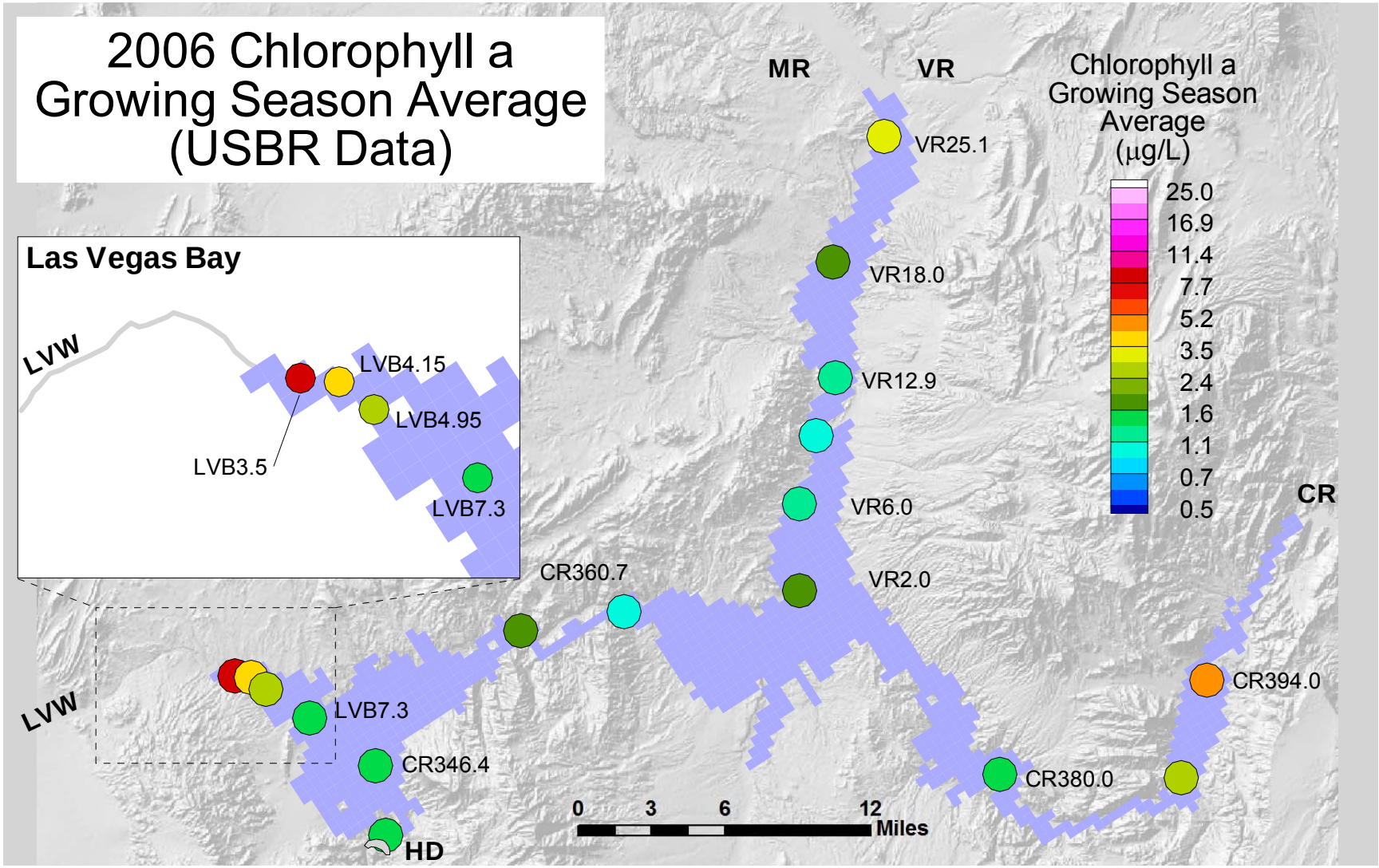

Notes: Growing season is April 1 - September 30.
Circles denote the average over the growing season of USBR 0-5 m composite field data.
Field data averages are only provided if there are three or more measurements in the growing season.

2007 Chlorophyll a Growing Season Average (USBR Data)

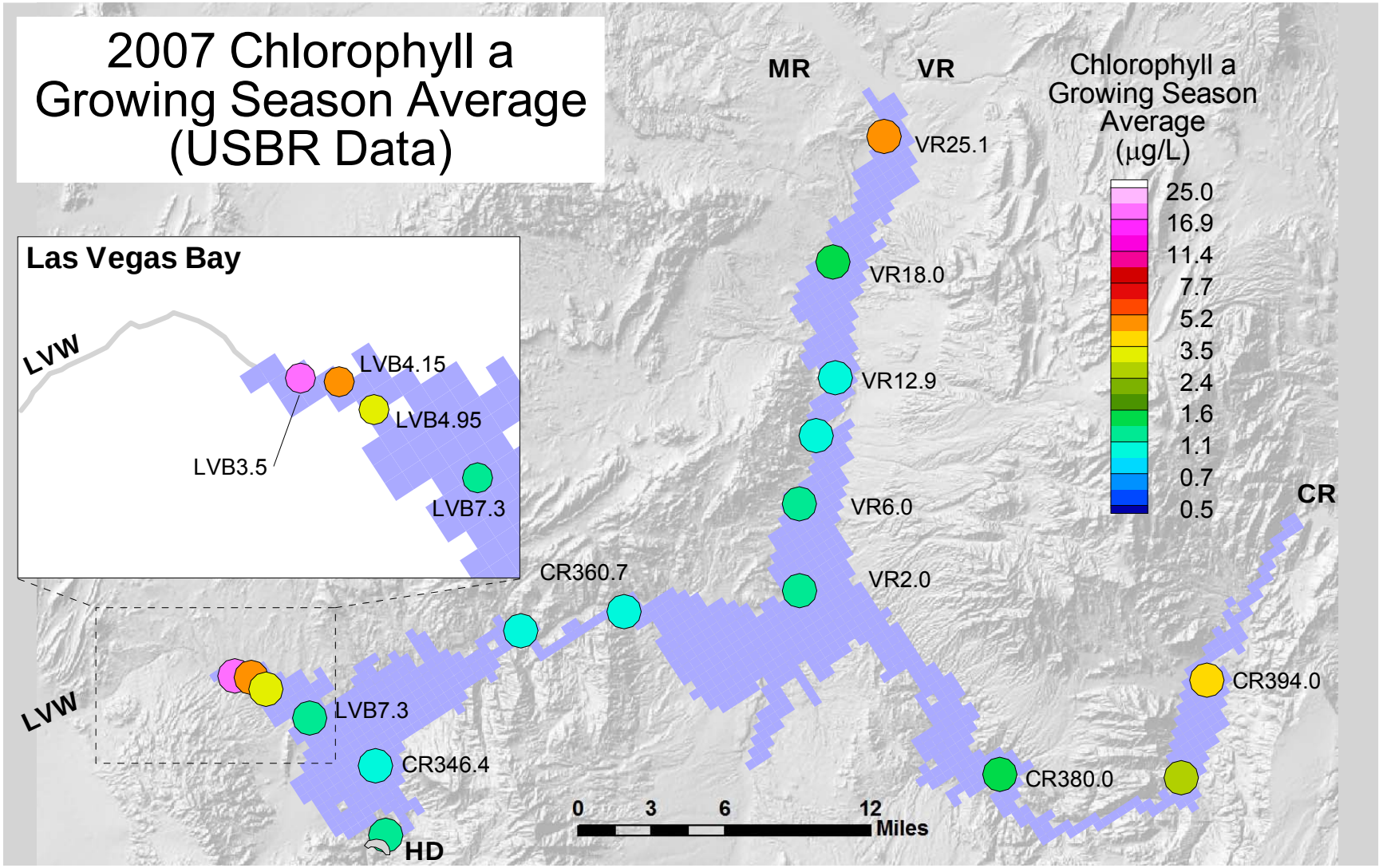

Notes: Growing season is April 1 - September 30.
Circles denote the average over the growing season of USBR 0-5 m composite field data.
Field data averages are only provided if there are three or more measurements in the growing season.

Measured Chlorophyll a at Stations LVB3.5 and CR346.4 (Top 5-m Average)

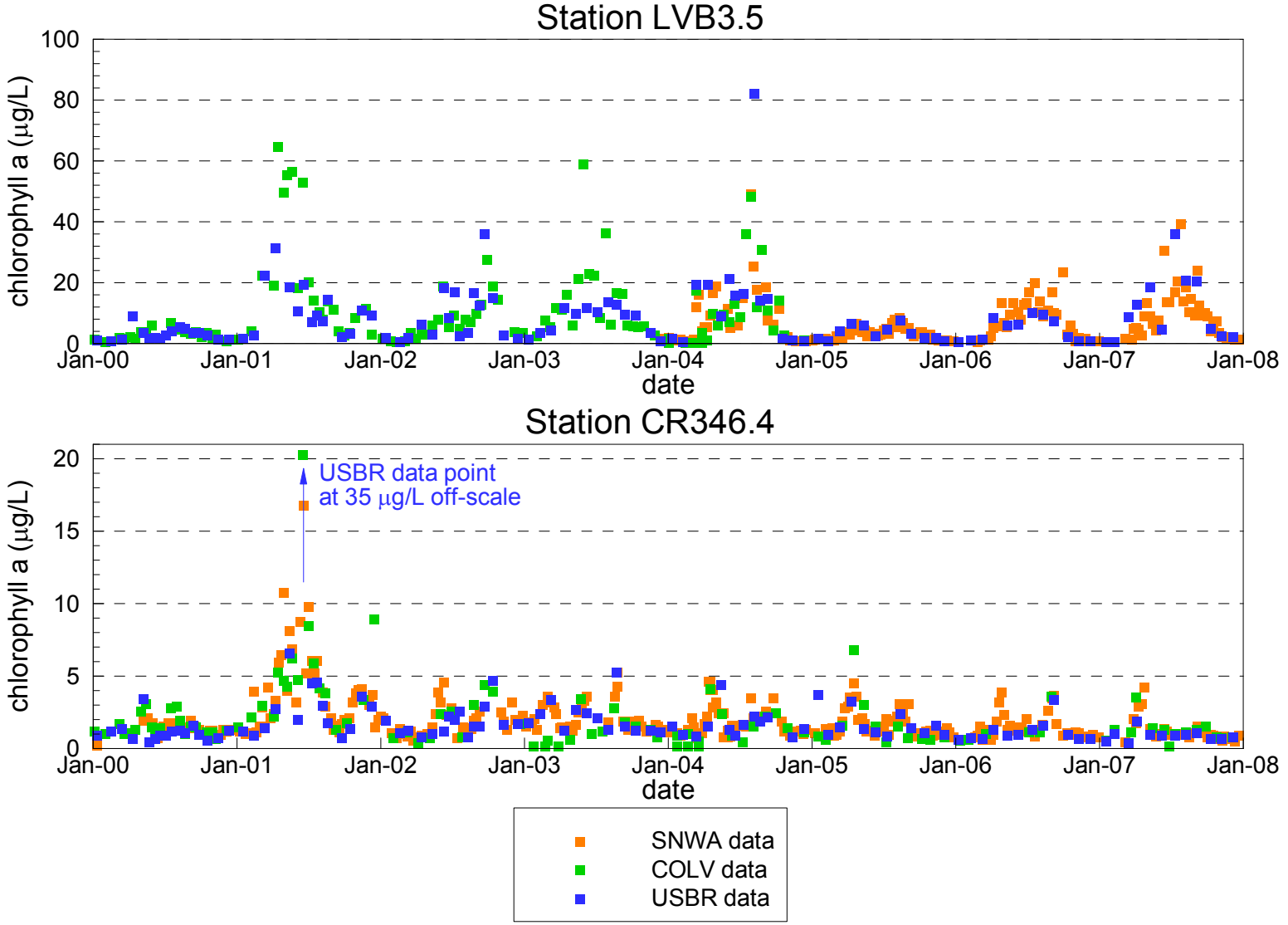

Figure 2.36

Measured Filterable Reactive Phosphorus at Station CR346.4

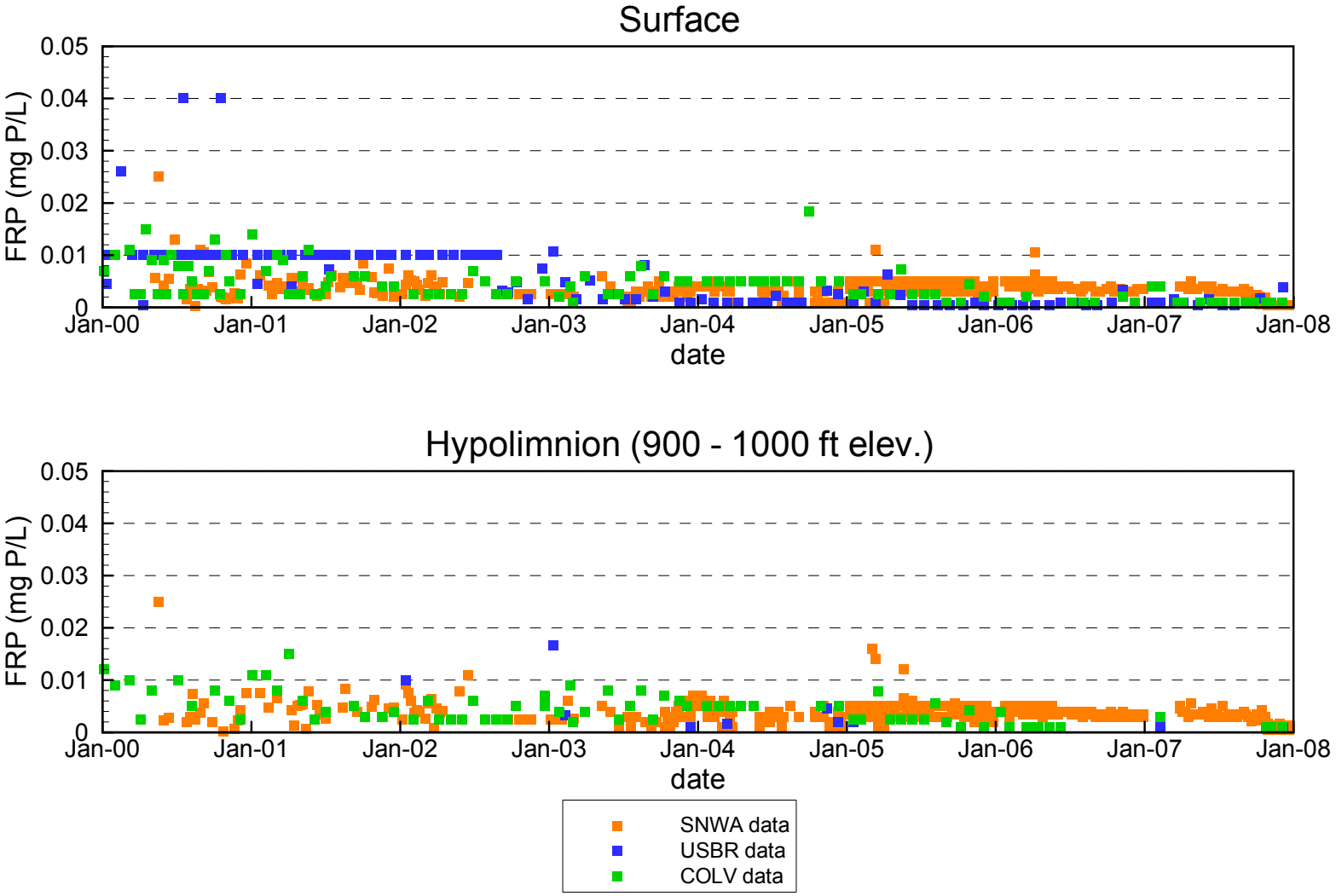

Figure 2.37

Measured Total Phosphorus at Station CR346.4

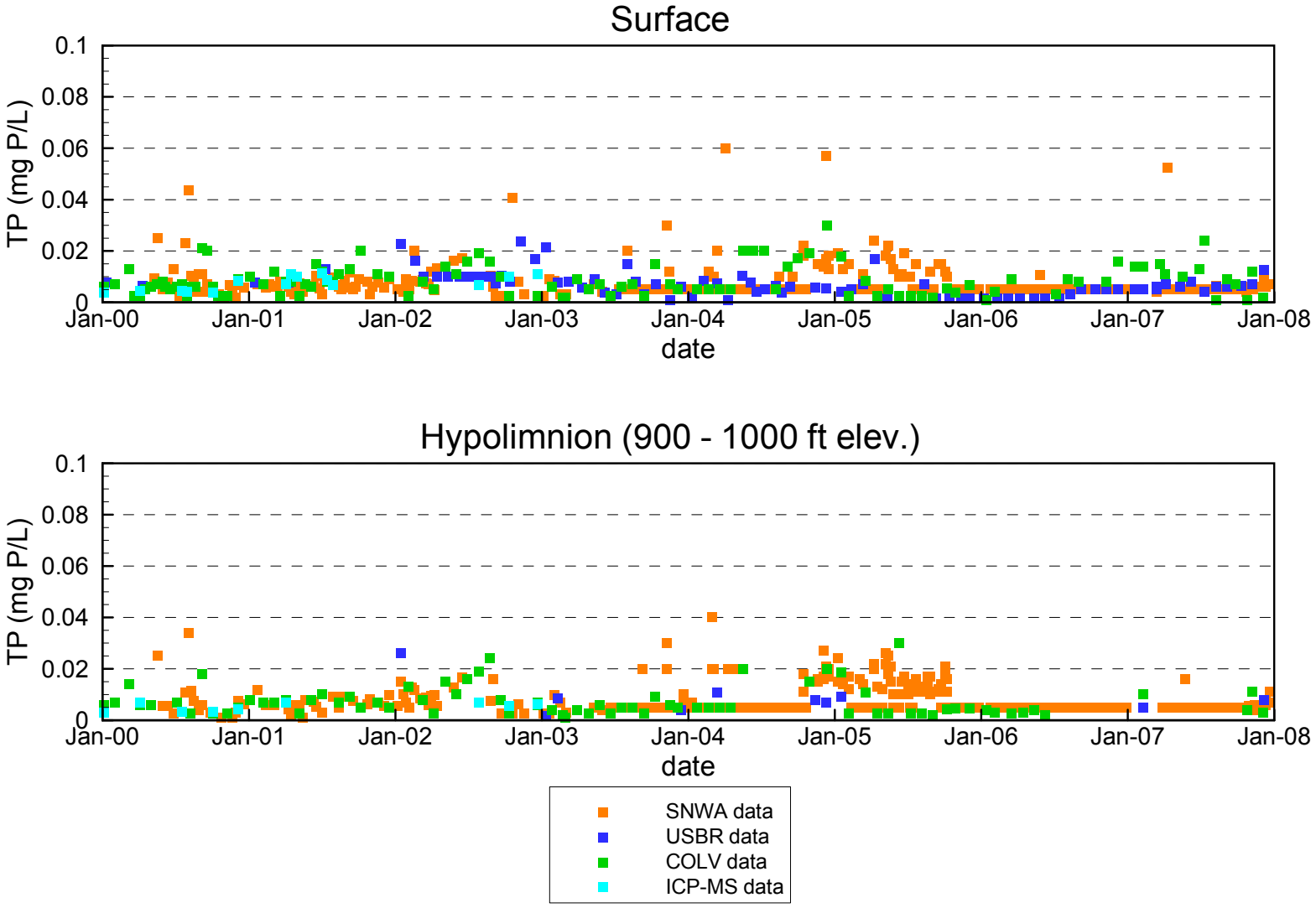

Figure 2.38

Measured Total Organic Carbon at Station CR346.4

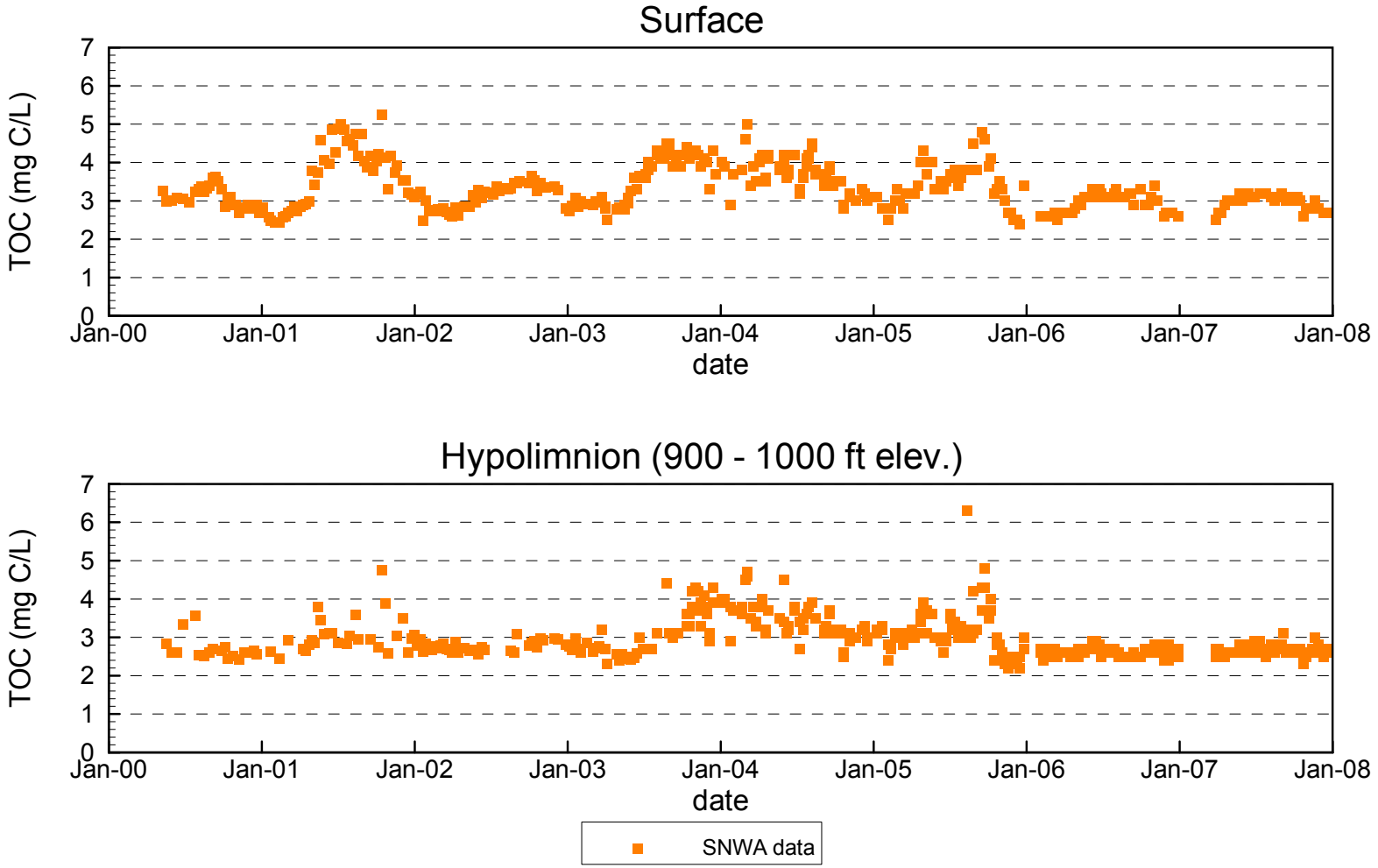

Figure 2.39

Measured Dissolved Oxygen at Station CR346.4

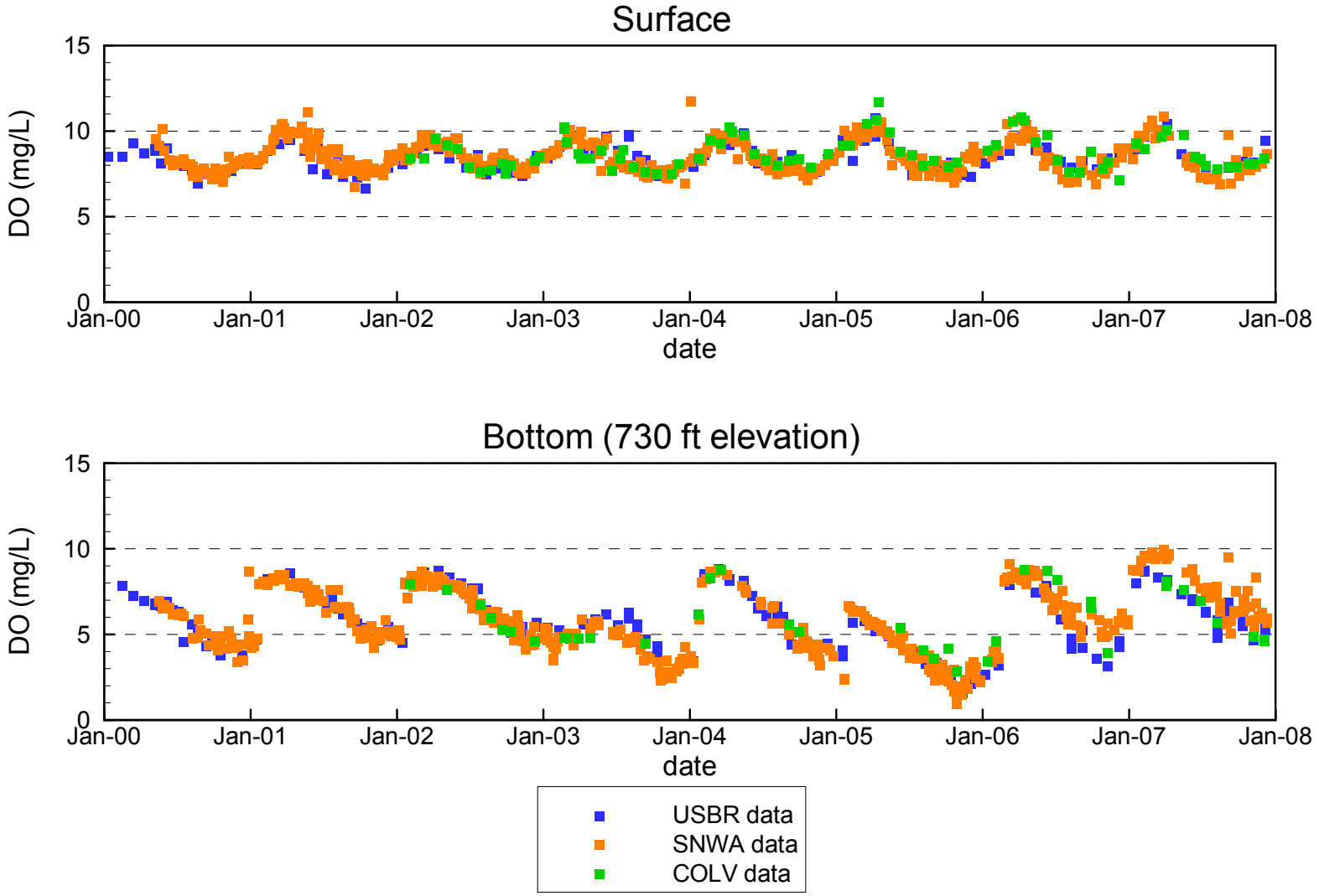

Figure 2.40

Measured Dissolved Oxygen in Lake Mead : February 13 - 16, 2006

(USBR data)

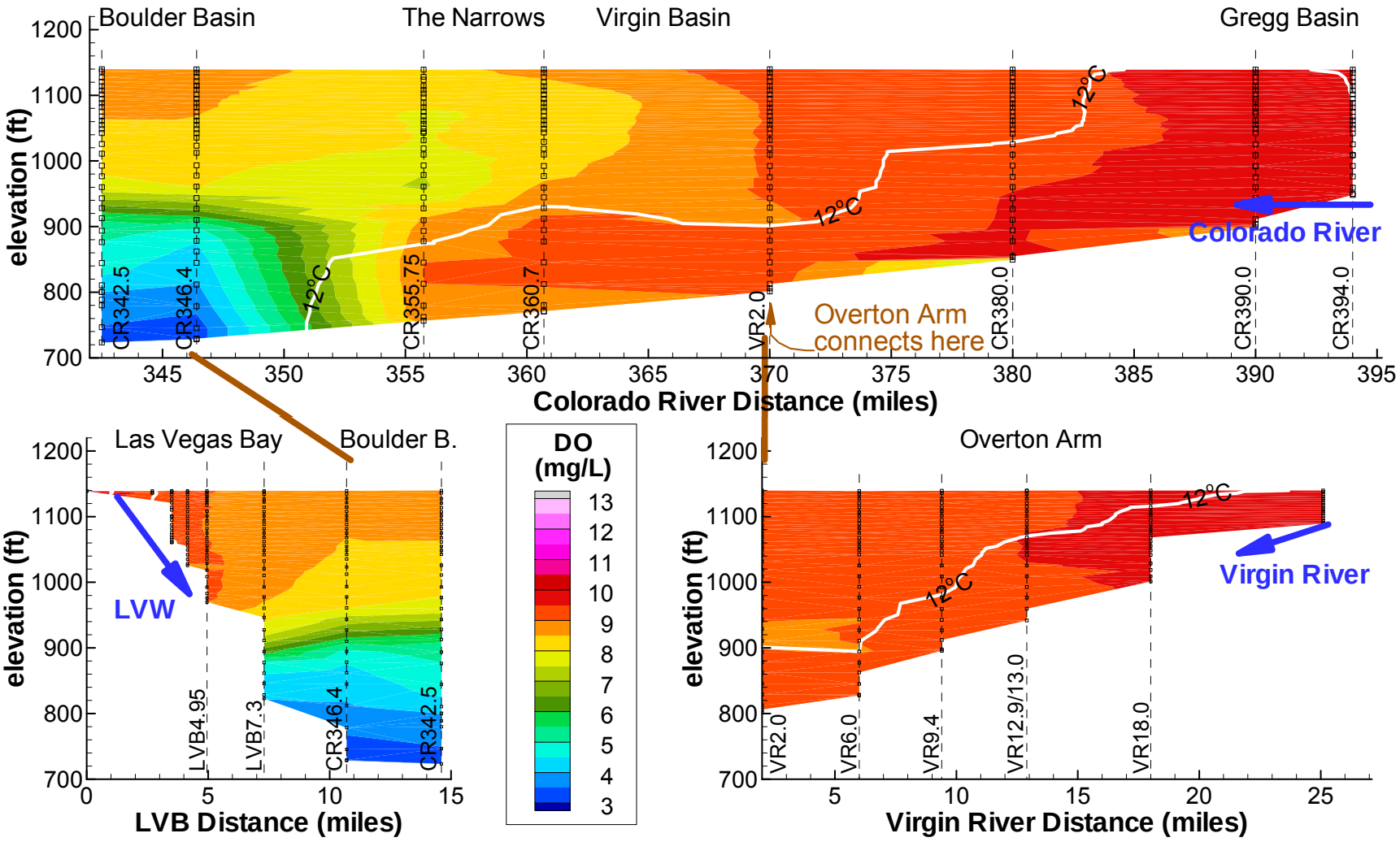

Figure 2.41

FLOW SCIENCE

Measured Dissolved Oxygen in Lake Mead : April 11 - 13, 2006

(USBR data)

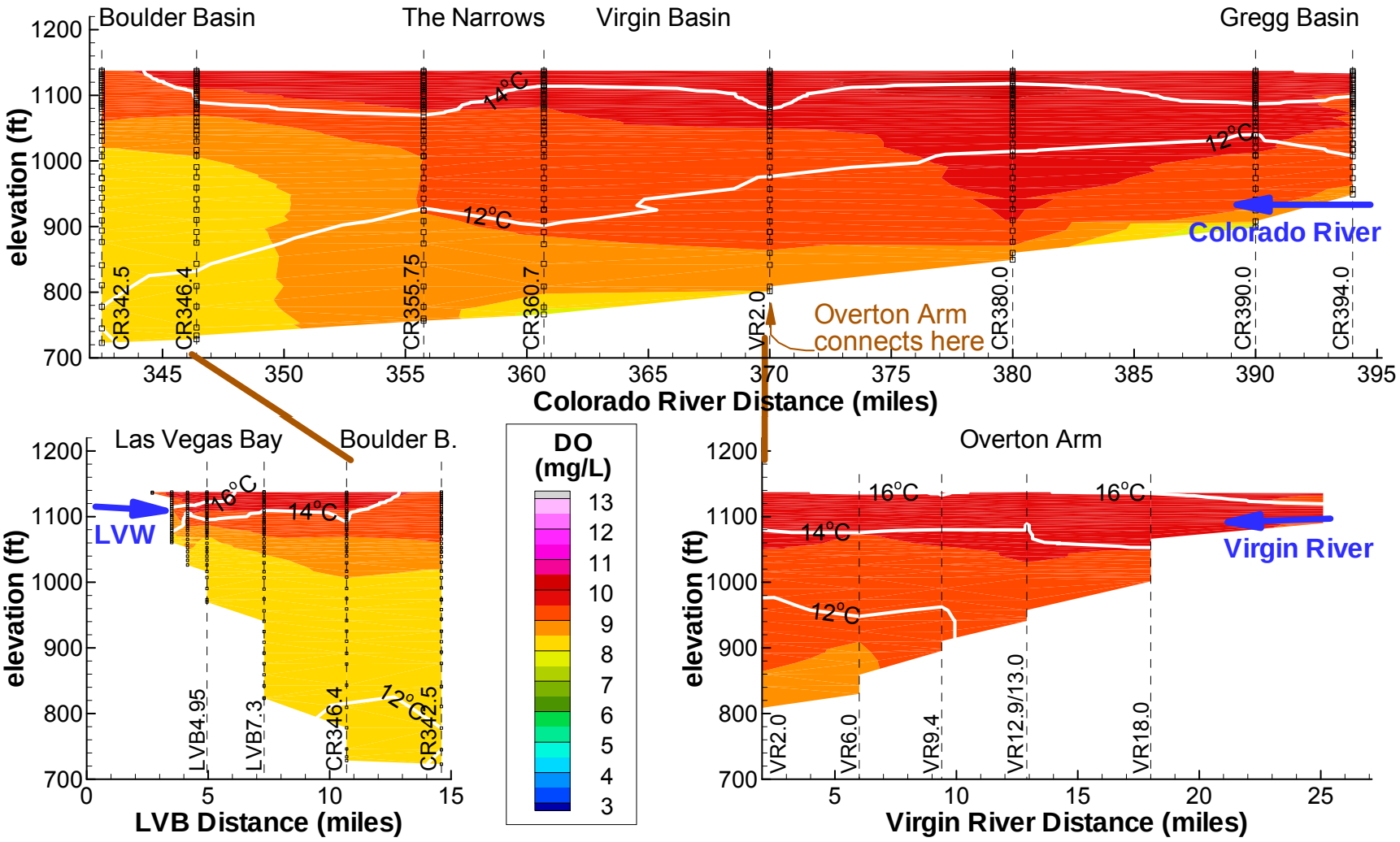

Figure 2.42

FLOW SCIENCE

Measured Dissolved Oxygen in Lake Mead : May 16 - 18, 2006

(USBR data)

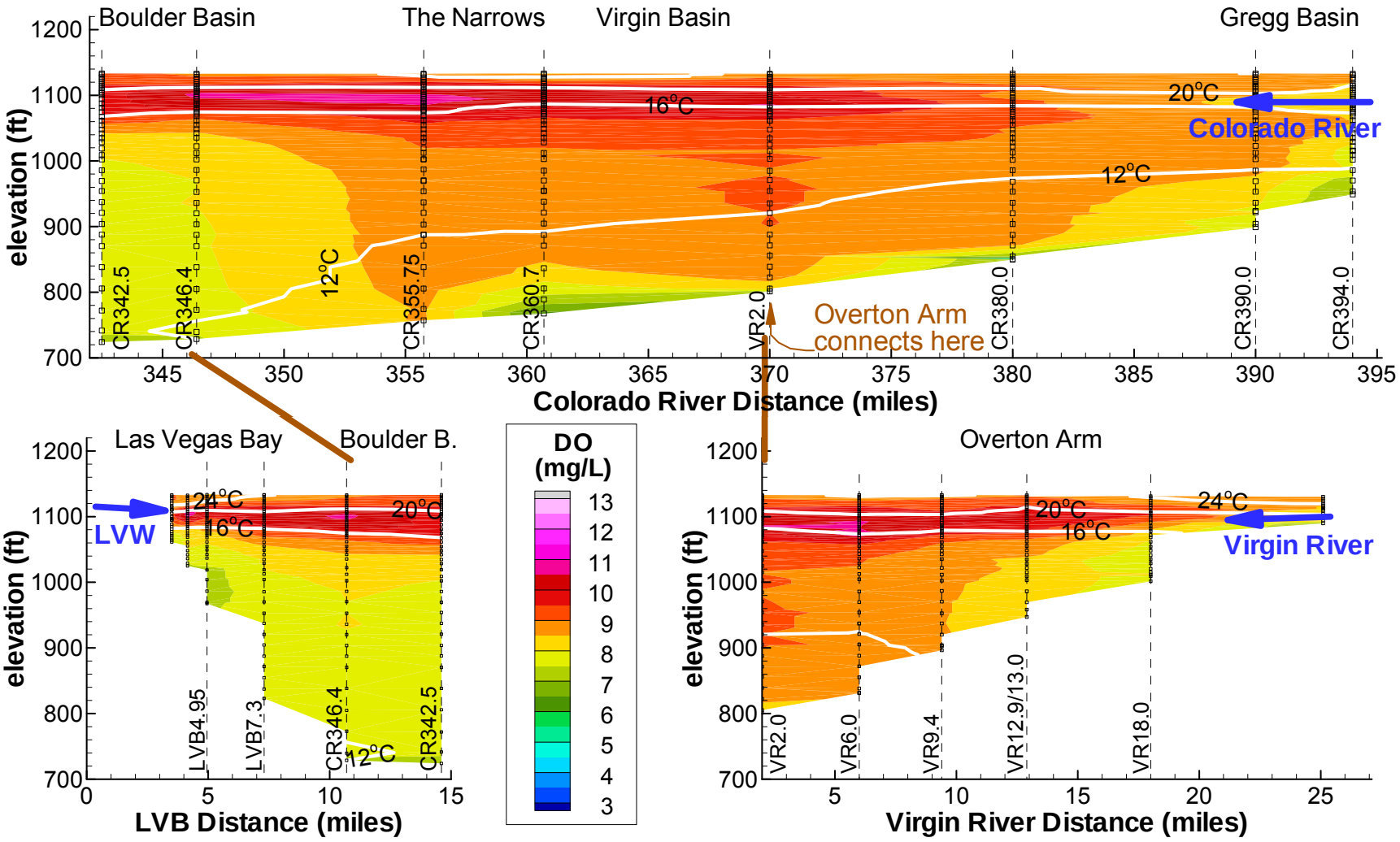

Ch2_Figures.ppt
FSI V064081 & V084015 Task 1
December 9, 2010

Figure 2.43

FLOW SCIENCE

Measured Dissolved Oxygen in Lake Mead : July 18 - 20, 2006

(USBR data)

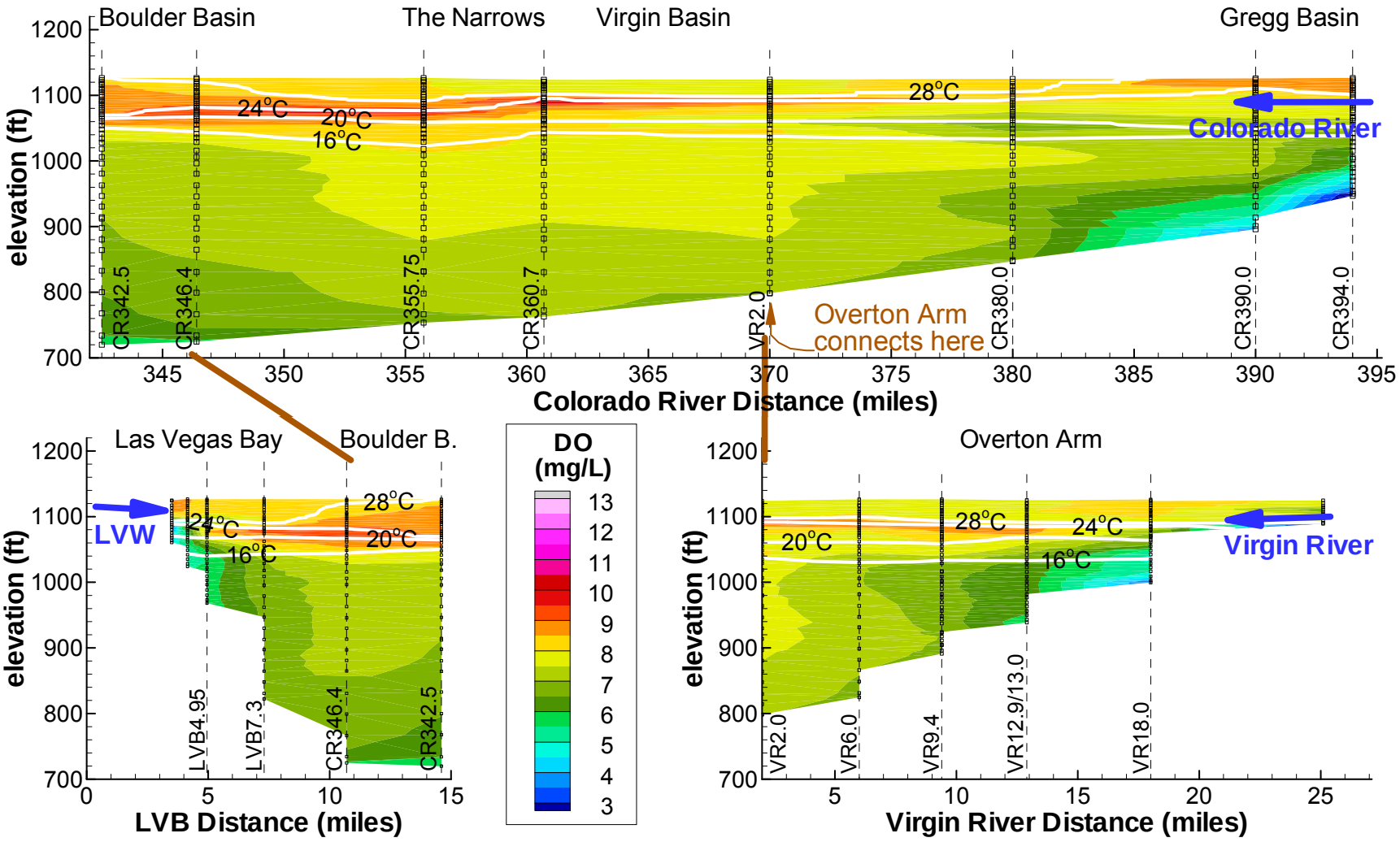

Figure 2.44

Measured Dissolved Oxygen in Lake Mead : October 17 - 19, 2006

(USBR data)

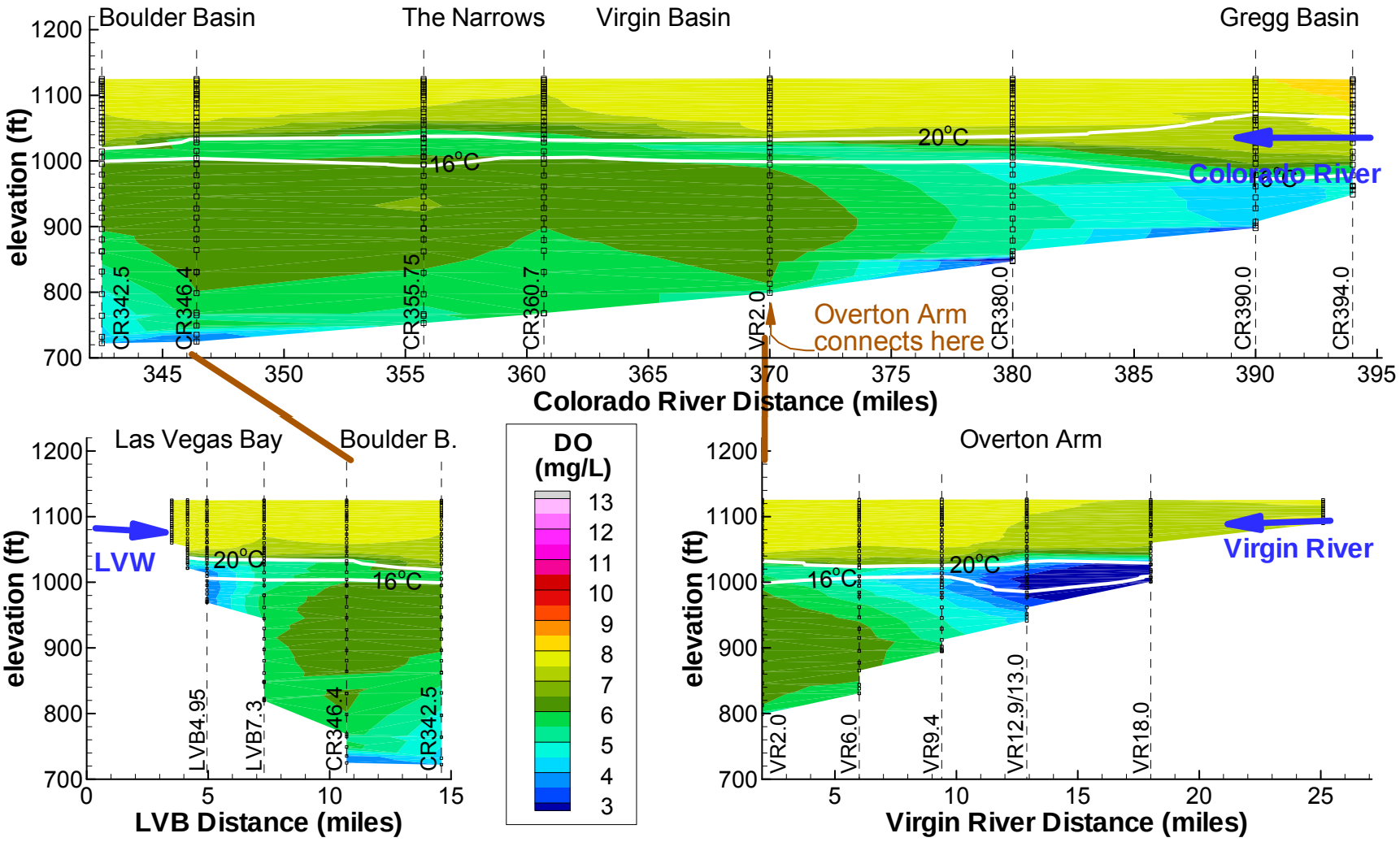

Figure 2.45

FLOW SCIENCE

Measured Dissolved Oxygen in Lake Mead : December 12 - 14, 2006

(USBR data)

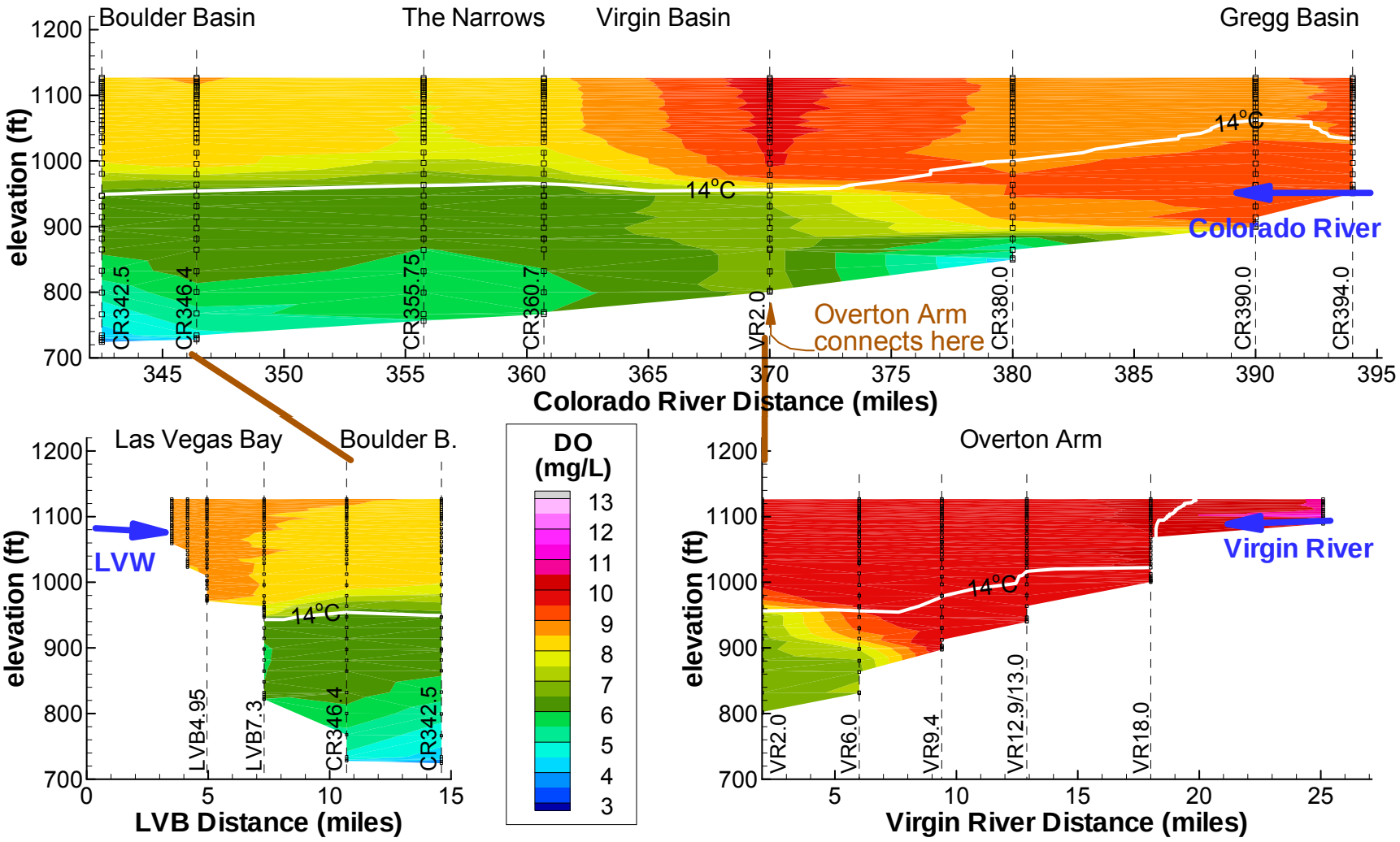

Figure 2.46

Measured Dissolved Oxygen in Lake Mead : February 13 - 15, 2007

(USBR data)

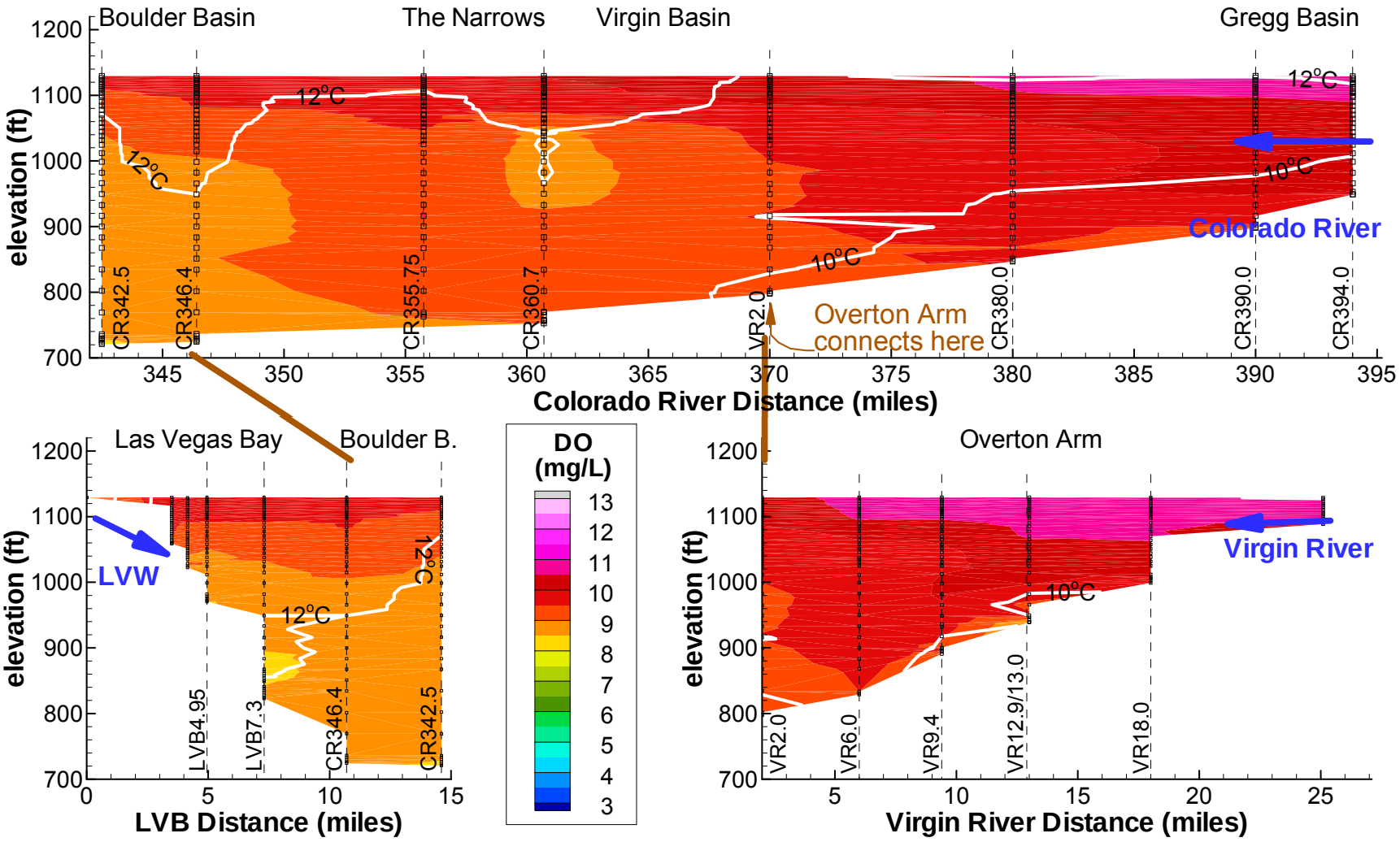

Figure 2.47

Measured Dissolved Oxygen in Lake Mead : April 10 - 12, 2007

(USBR data)

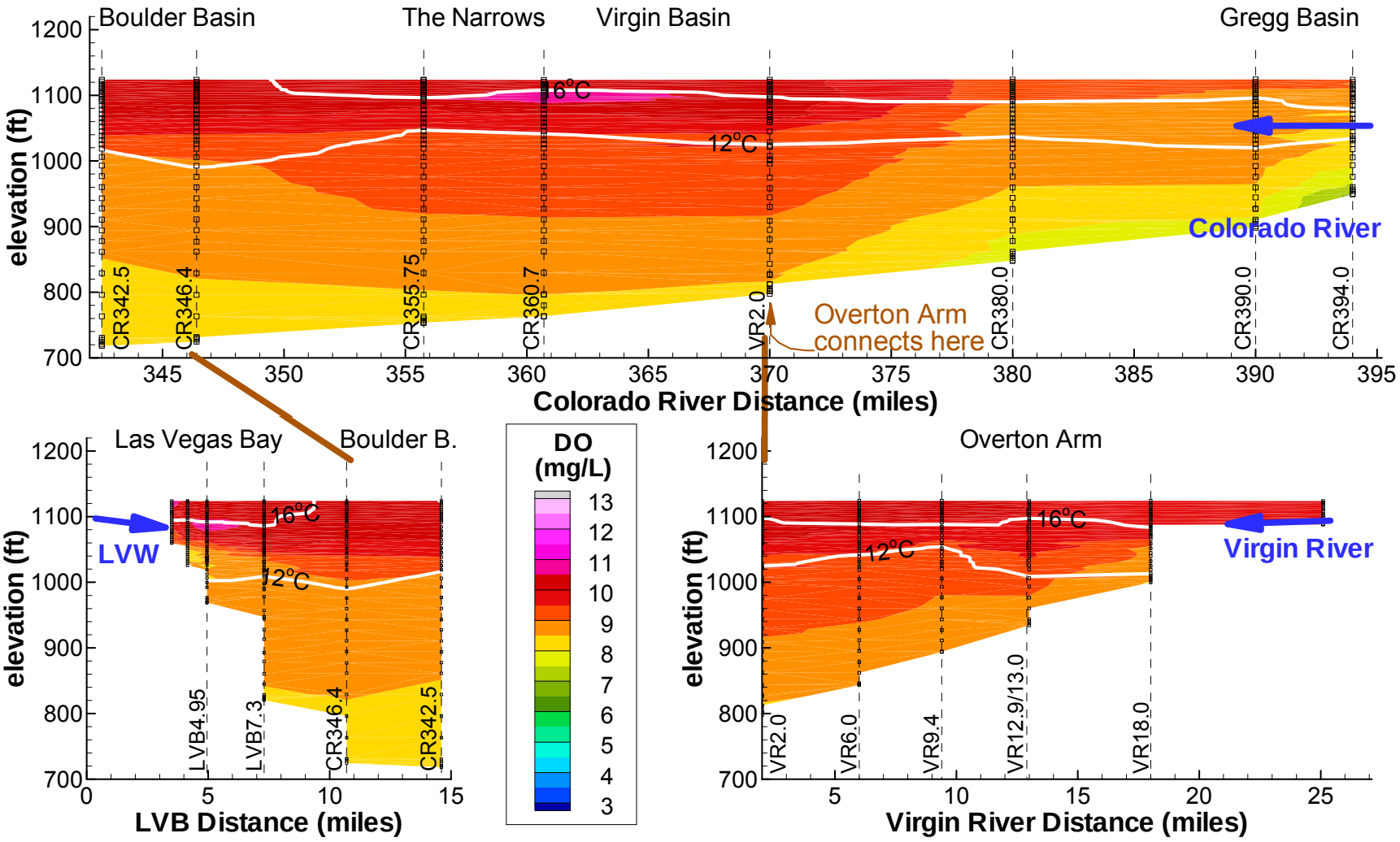

Figure 2.48

Measured Dissolved Oxygen in Lake Mead : June 12 - 14, 2007

(USBR data)

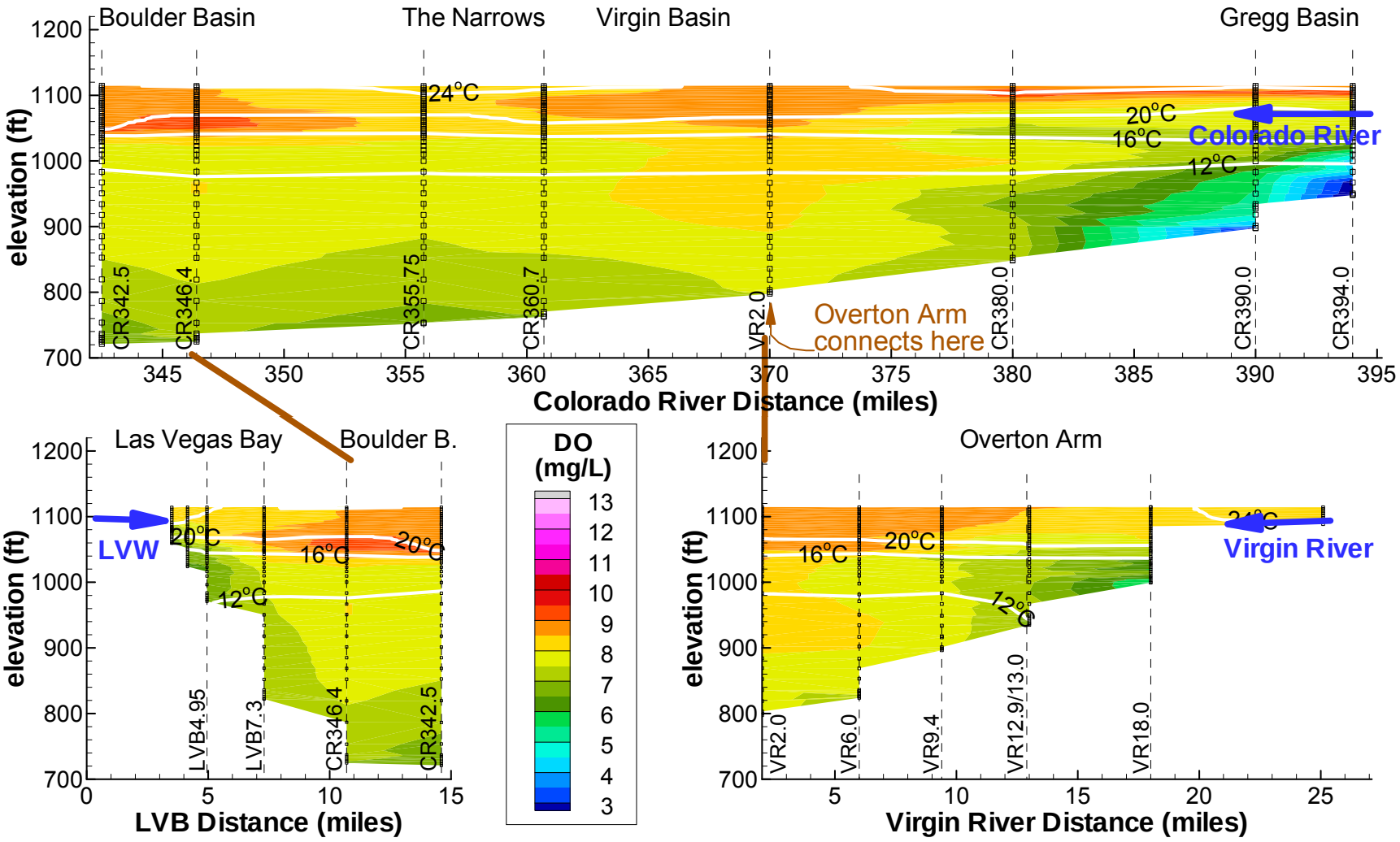

Figure 2.49

Measured Dissolved Oxygen in Lake Mead : July 16 - 18, 2007

(USBR data)

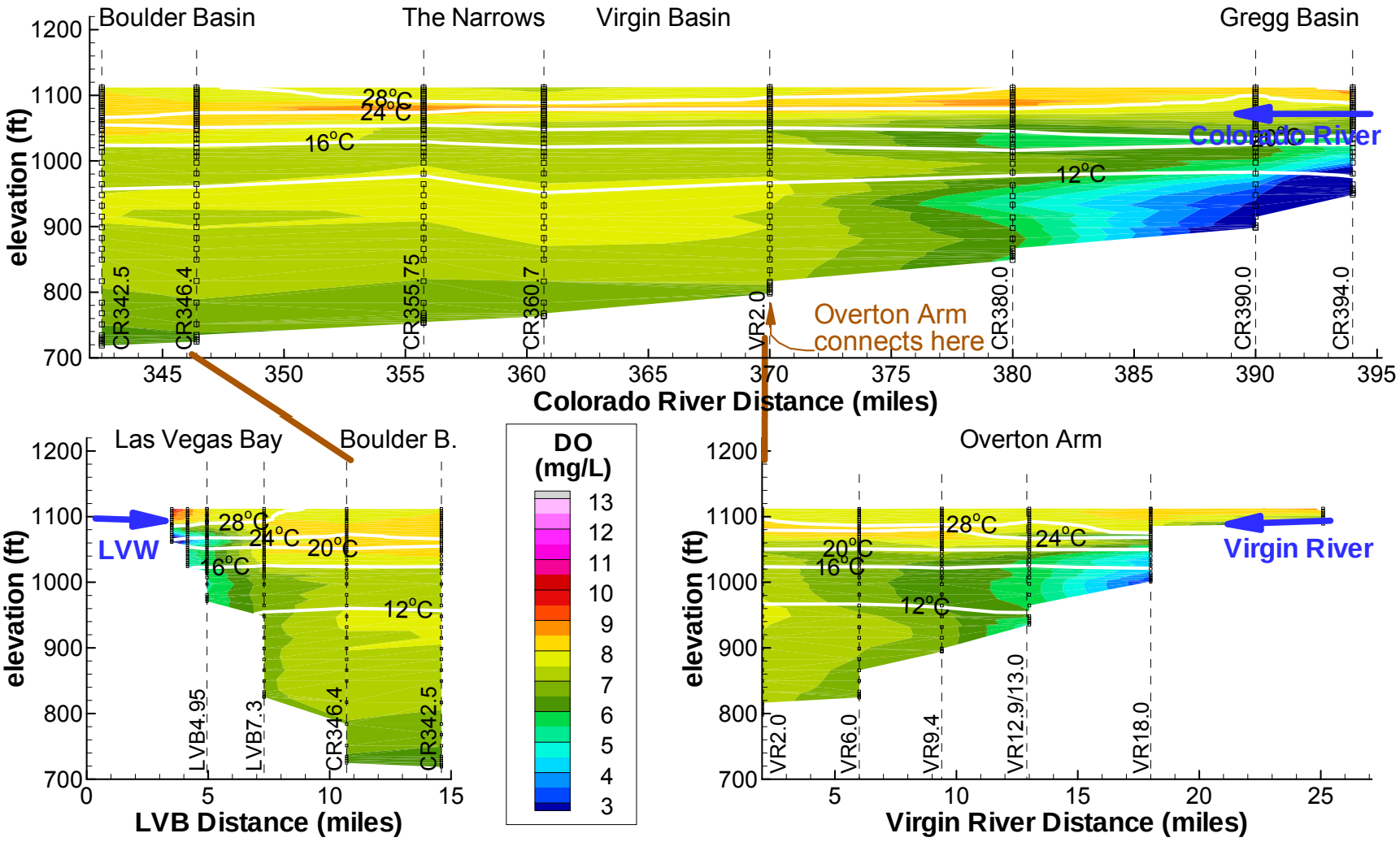

Figure 2.50

Measured Dissolved Oxygen in Lake Mead : October 16 - 18, 2007

(USBR data)

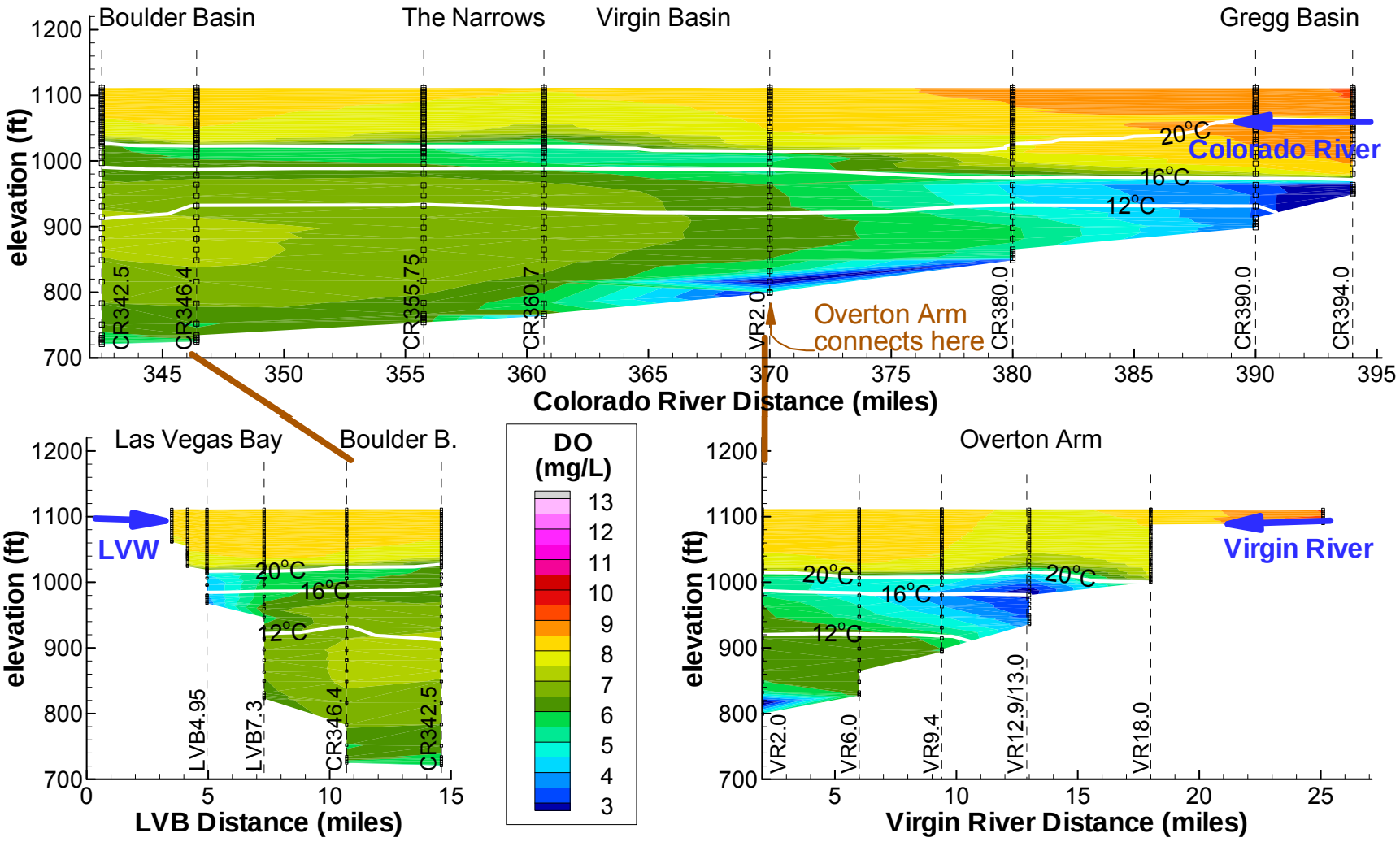

Figure 2.51

FLOW SCIENCE

Measured Dissolved Oxygen in Lake Mead : December 11 - 13, 2007

(USBR data)

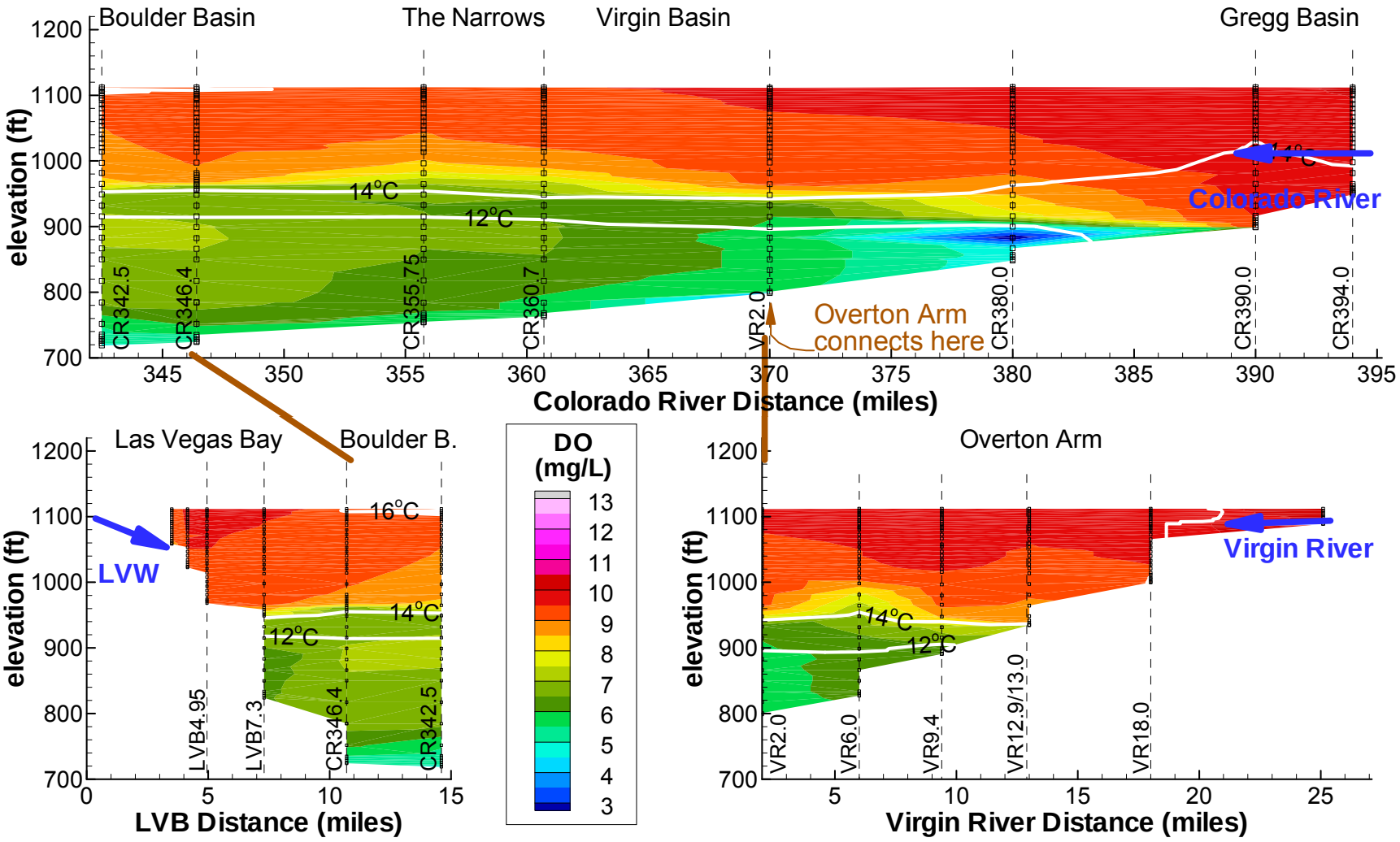

Figure 2.52

FLOW SCIENCE

Measured Data (USBR) in Lake Mead : January 10 - 12, 2006

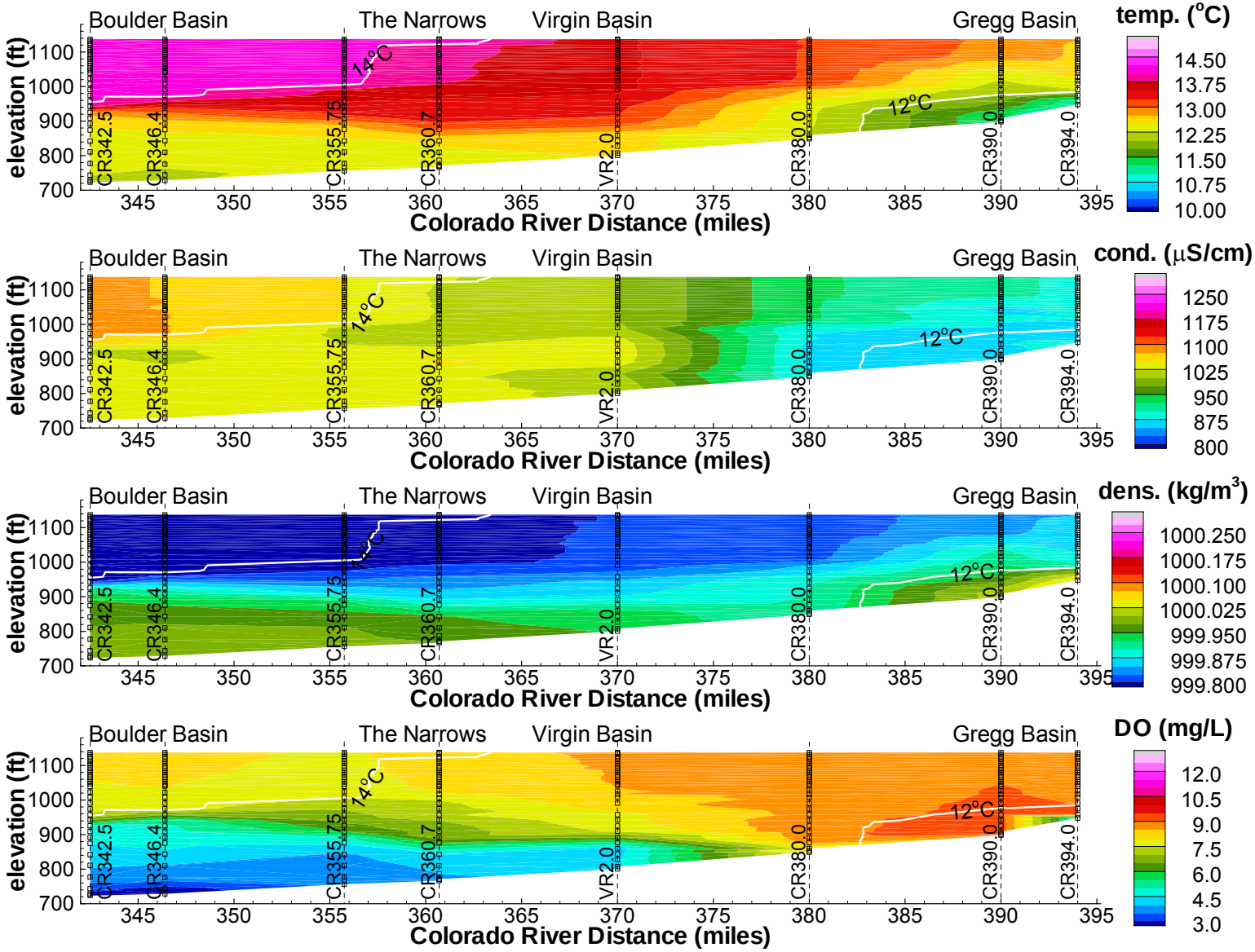

Figure 2.53

FLOW SCIENCE

Measured Data (USBR) in Lake Mead : February 13 - 16, 2006

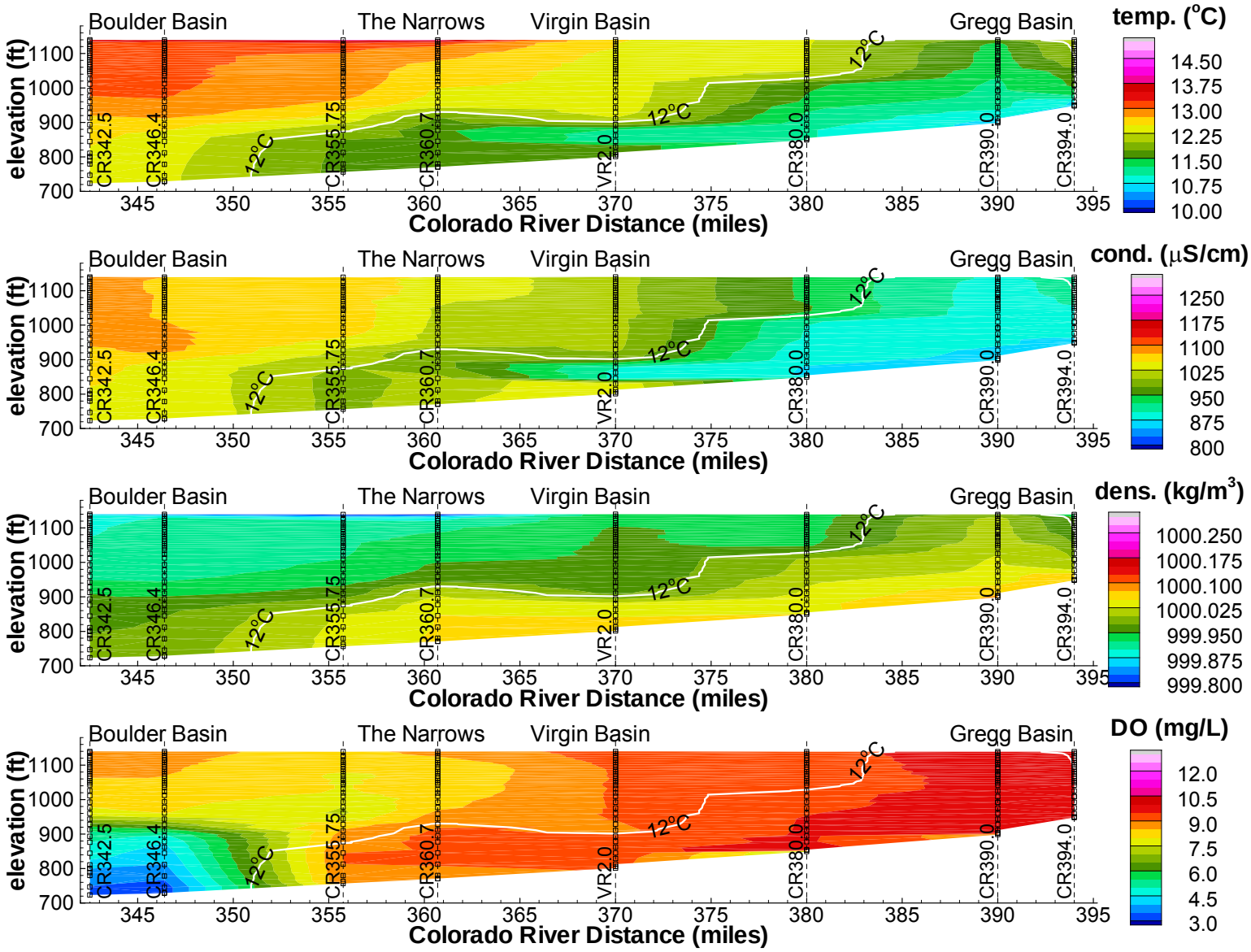

Figure 2.54

FLOW SCIENCE

Measured Data (USBR) in Lake Mead : March 10 - 15, 2006

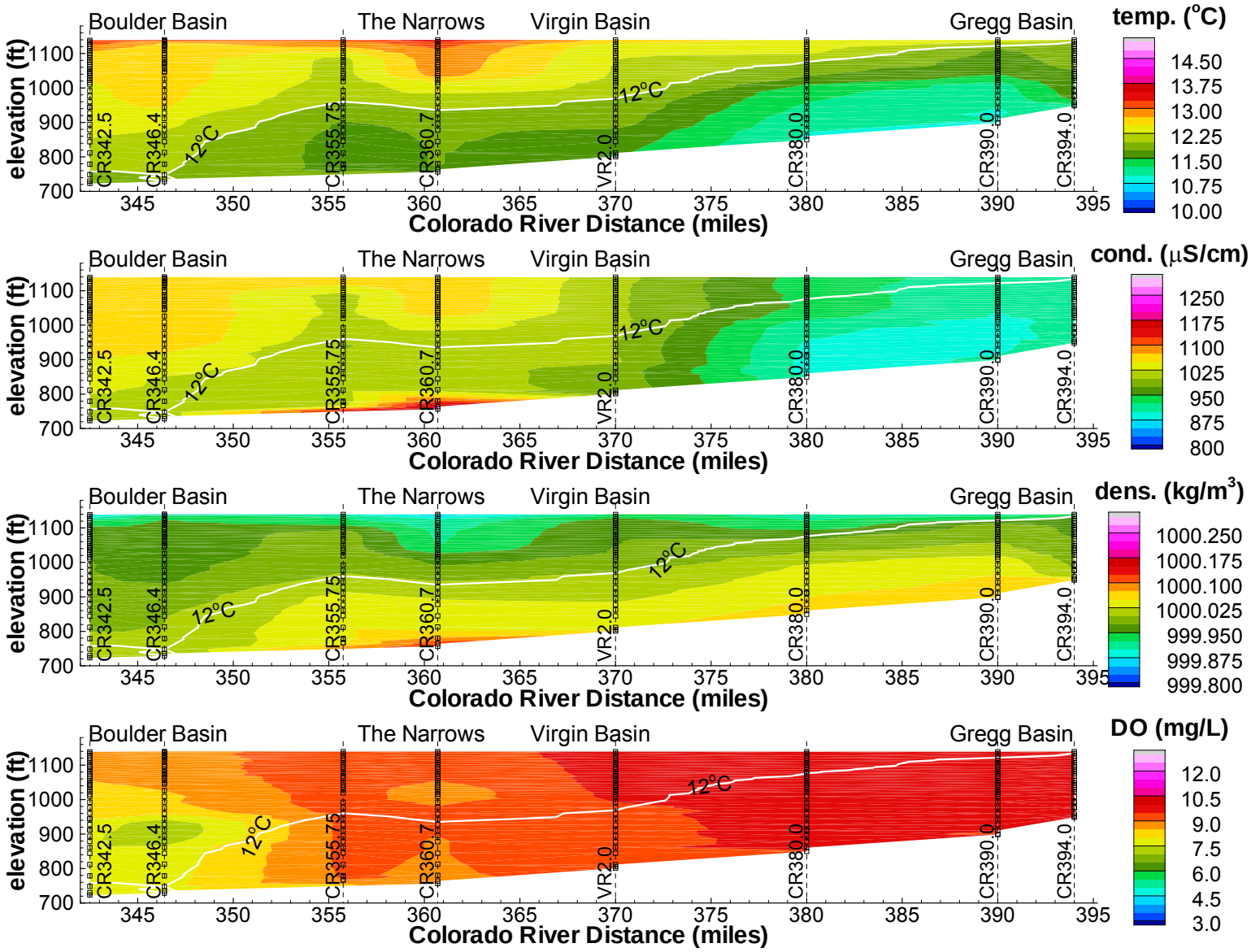

Figure 2.55

FLOW SCIENCE

Measured Data (USBR) in Lake Mead : December 12 - 14, 2006

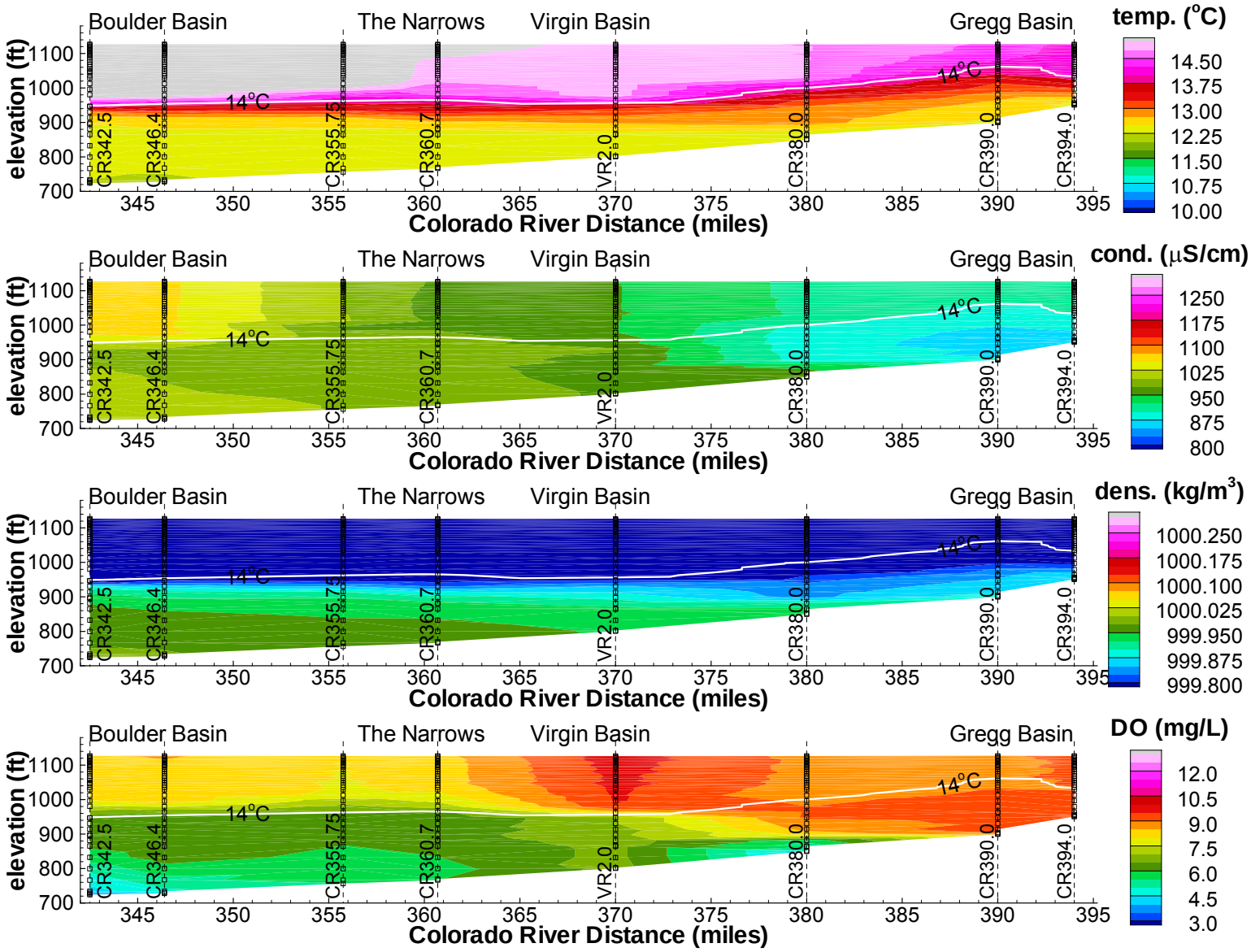

Figure 2.56

Measured Data (USBR) in Lake Mead : January 23 - 25, 2007

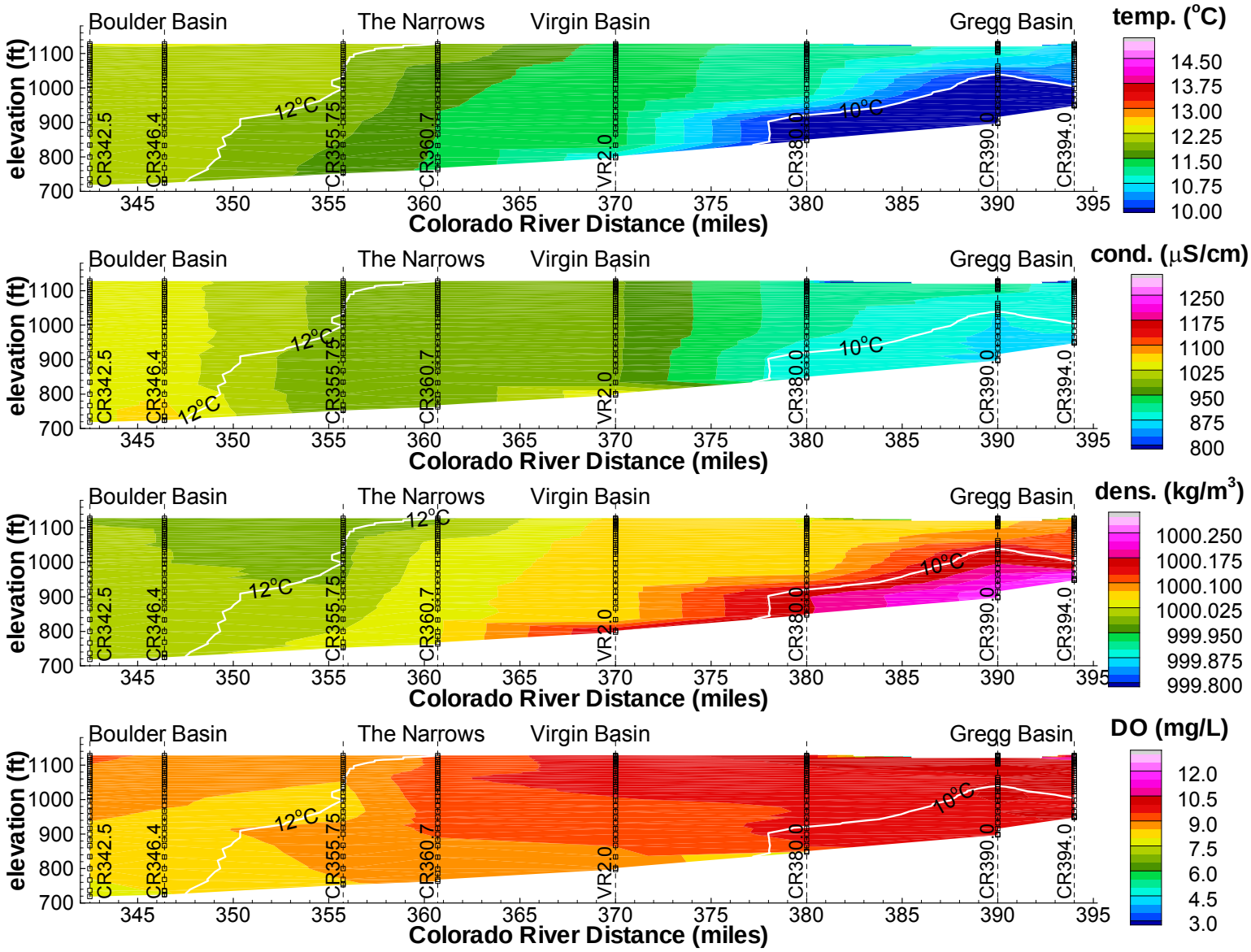

Figure 2.57

FLOW SCIENCE

Measured Data (USBR) in Lake Mead : February 13 - 15, 2007

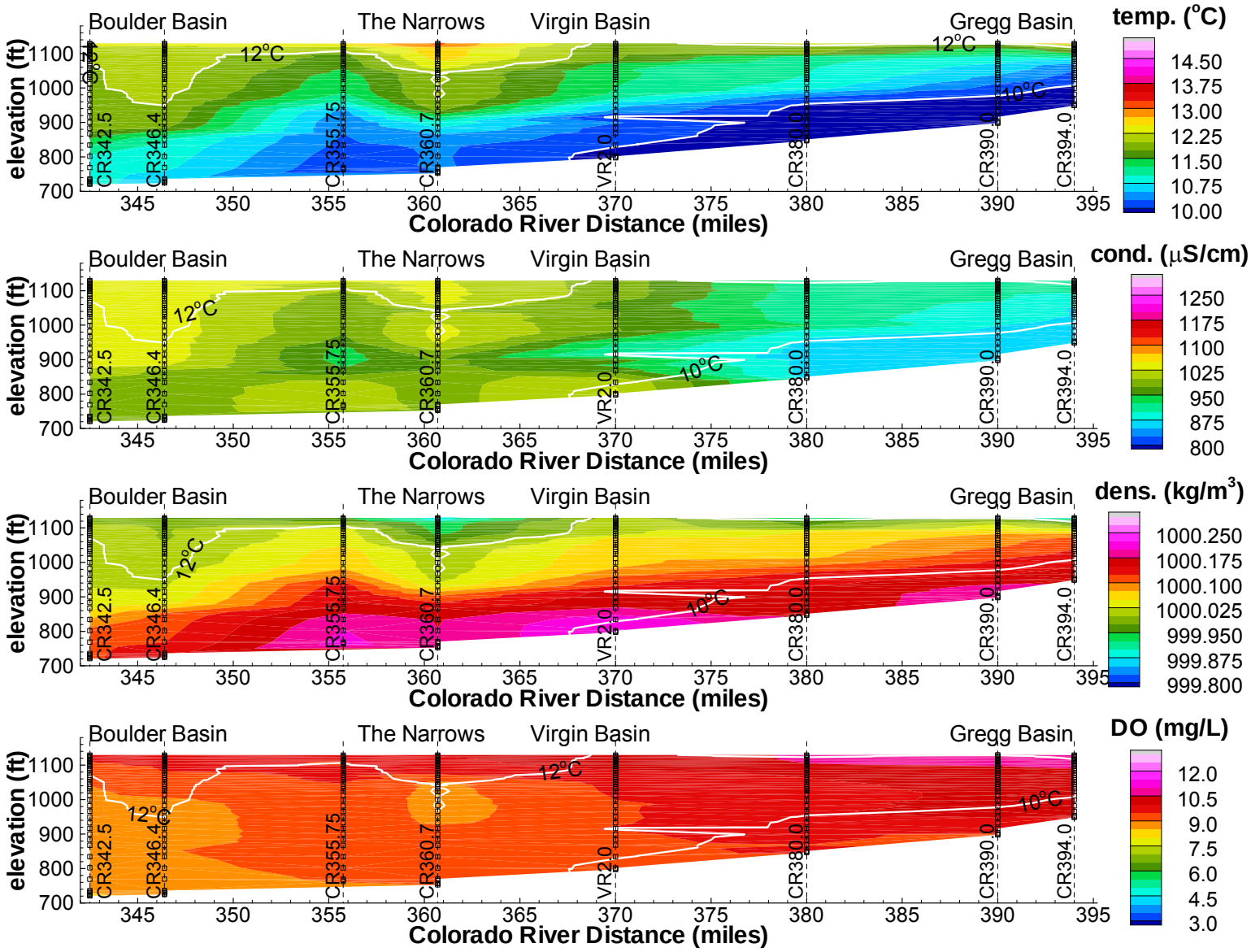

Ch2_Figures.ppt
FSI V064081 & V084015 Task 1
December 9, 2010

Figure 2.58

FLOW SCIENCE

Measured Data (USBR) in Lake Mead : March 20 - 22, 2007

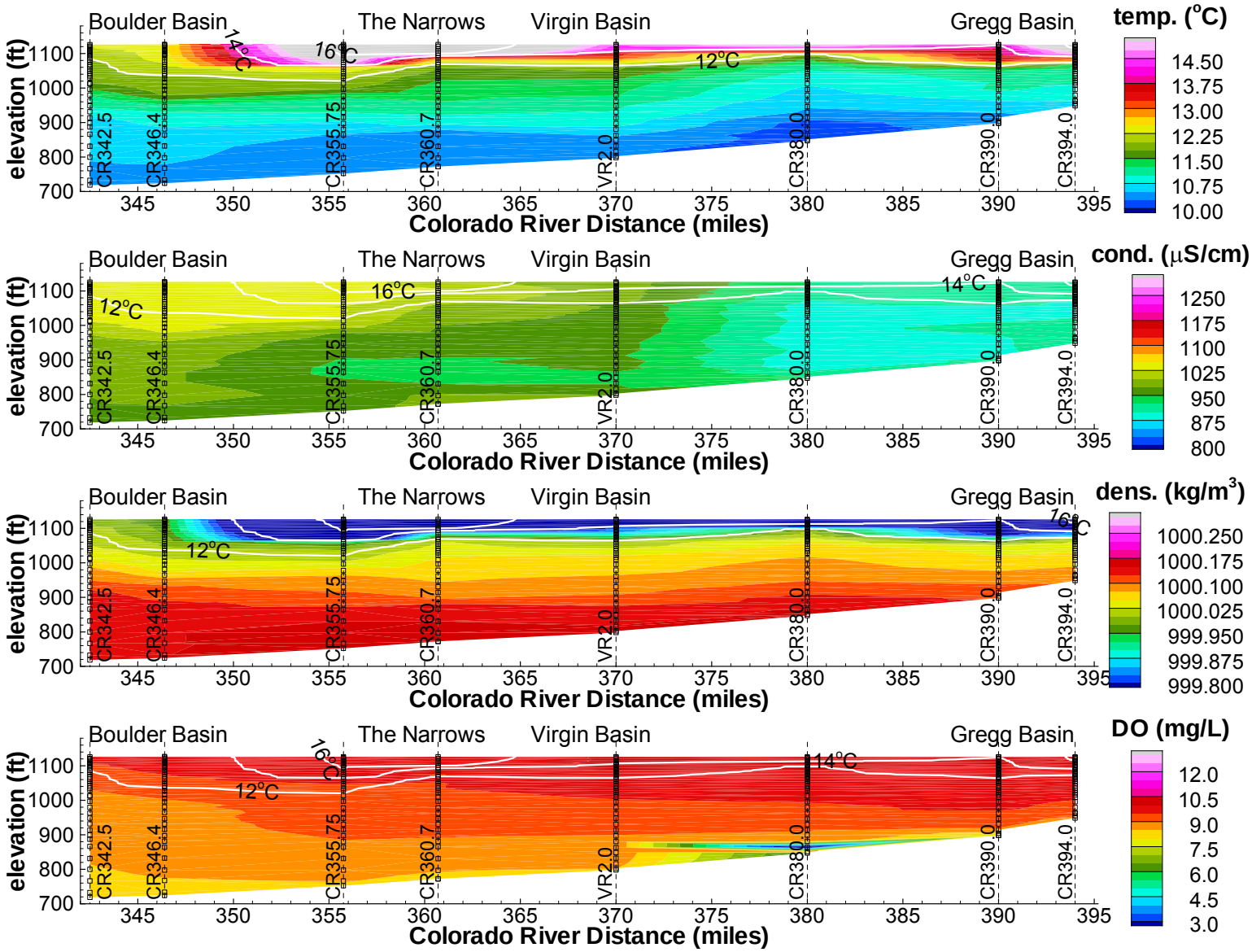

Figure 2.59

FLOW SCIENCE

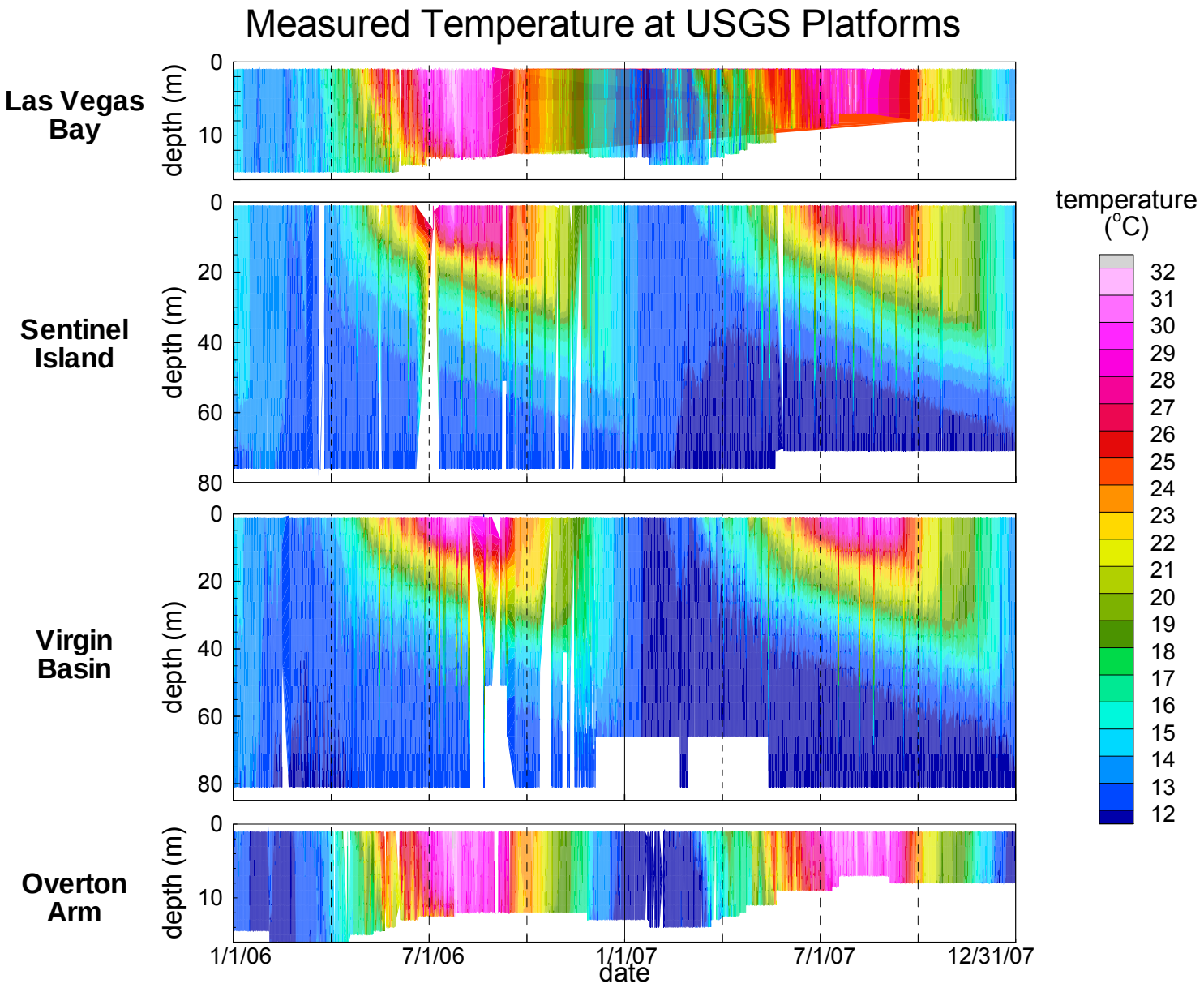
Measured Temperature at USGS Platforms
Las Vegas Bay
Sentinel Island
Virgin Basin
Overton Arm
depth (m)
0
10
20
40
60
80
1/1/06
7/1/06
1/1/07
7/1/07
12/31/07
date
temperature (°C)
32
31
30
29
28
27
26
25
24
23
22
21
20
19
18
17
16
15
14
13
12

Figure 2.60

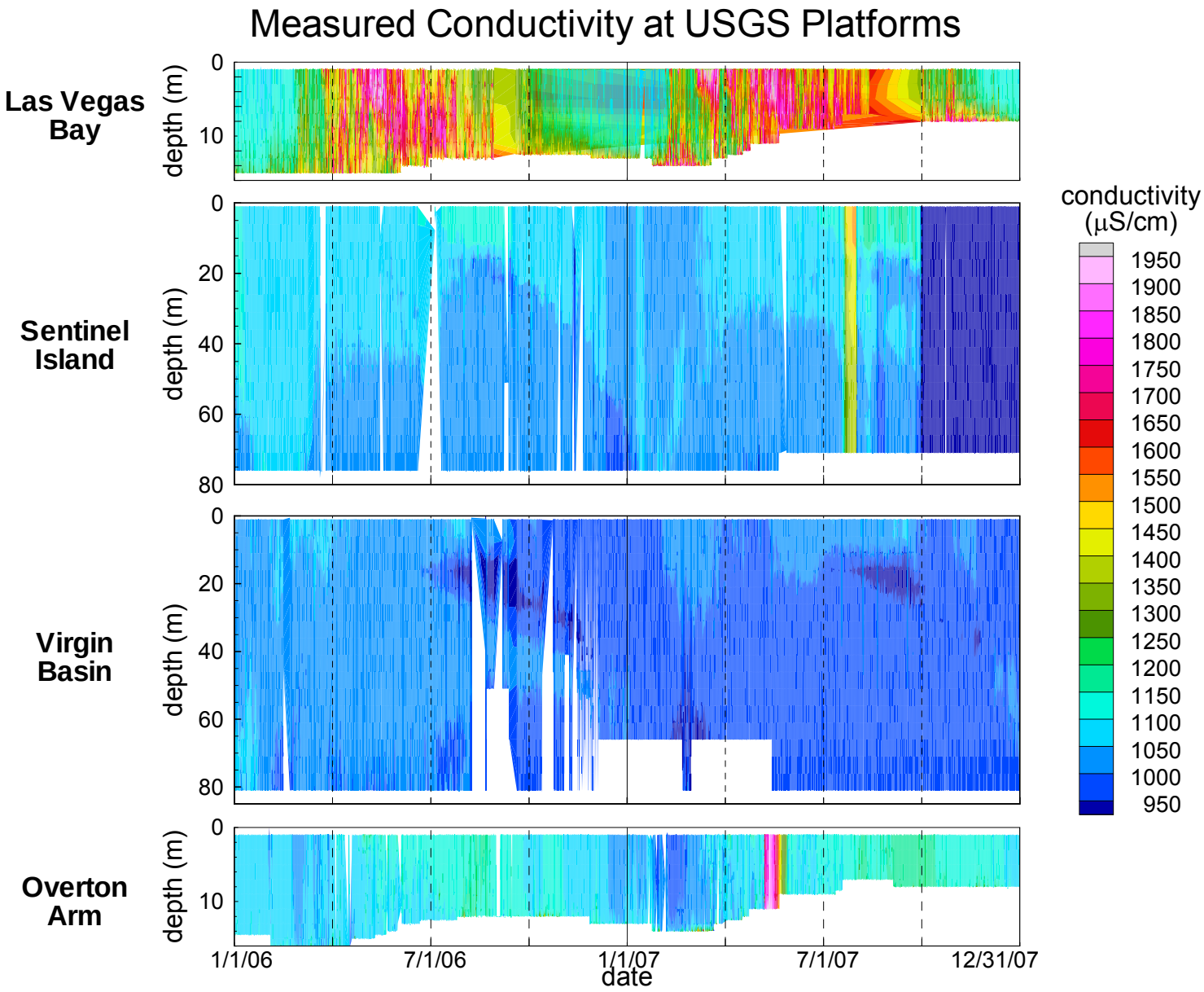
Measured Conductivity at USGS Platforms
Las Vegas Bay
Sentinel Island
Virgin Basin
Overton Arm
depth (m)
0
10
20
40
60
80
1/1/06
7/1/06
1/1/07
7/1/07
12/31/07
date
conductivity (µS/cm)
1950
1900
1850
1800
1750
1700
1650
1600
1550
1500
1450
1400
1350
1300
1250
1200
1150
1100
1050
1000
950

Figure 2.61

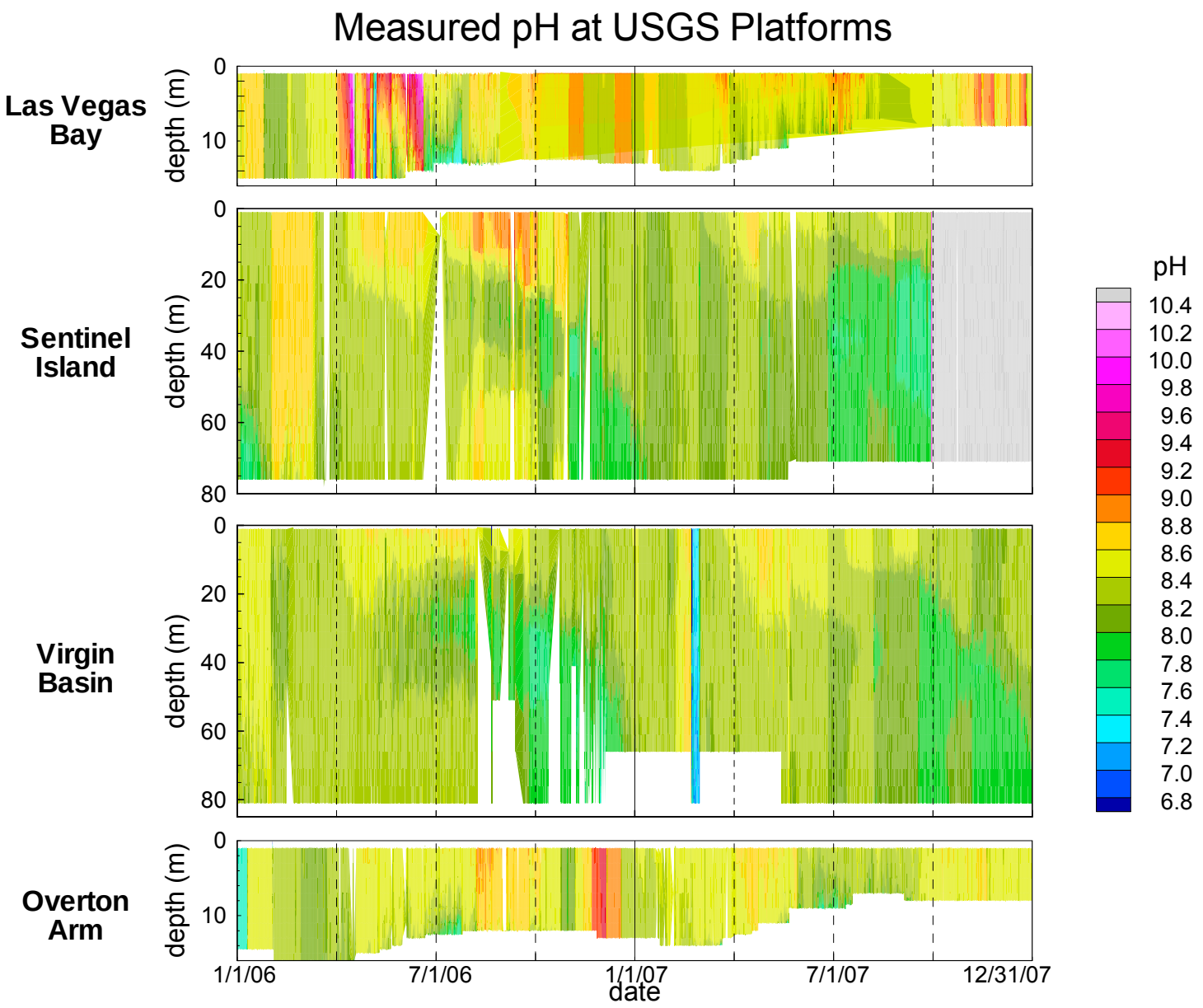
Measured pH at USGS Platforms
Las Vegas Bay
Sentinel Island
Virgin Basin
Overton Arm
depth (m)
0
10
20
40
60
80
1/1/06
7/1/06
1/1/07
7/1/07
12/31/07
date
pH
10.4
10.2
10.0
9.8
9.6
9.4
9.2
9.0
8.8
8.6
8.4
8.2
8.0
7.8
7.6
7.4
7.2
7.0
6.8

Figure 2.62

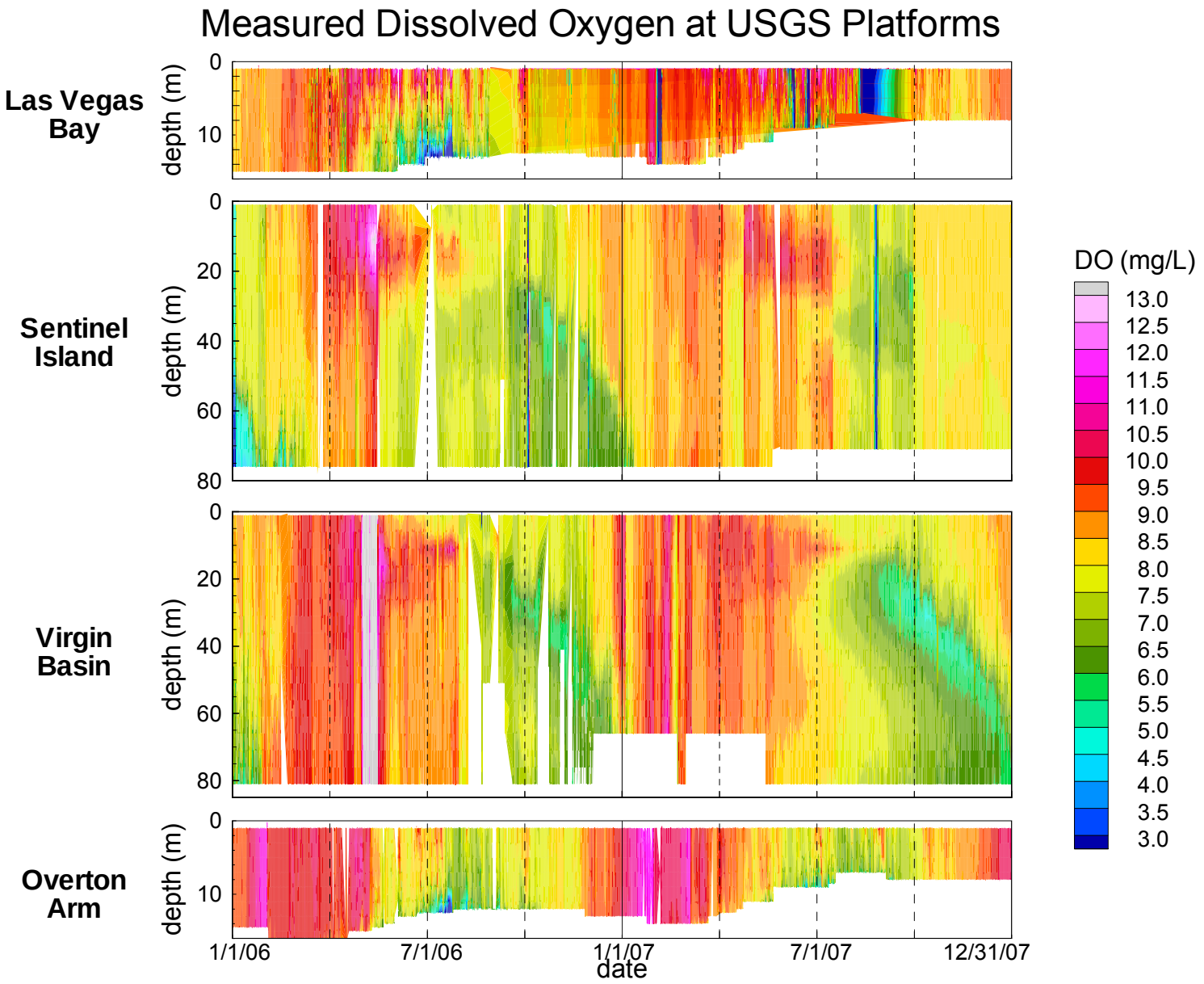
Measured Dissolved Oxygen at USGS Platforms
Las Vegas Bay
Sentinel Island
Virgin Basin
Overton Arm
depth (m)
0
10
20
40
60
80
1/1/06
7/1/06
1/1/07
7/1/07
12/31/07
date
DO (mg/L)
13.0
12.5
12.0
11.5
11.0
10.5
10.0
9.5
9.0
8.5
8.0
7.5
7.0
6.5
6.0
5.5
5.0
4.5
4.0
3.5
3.0

Figure 2.63

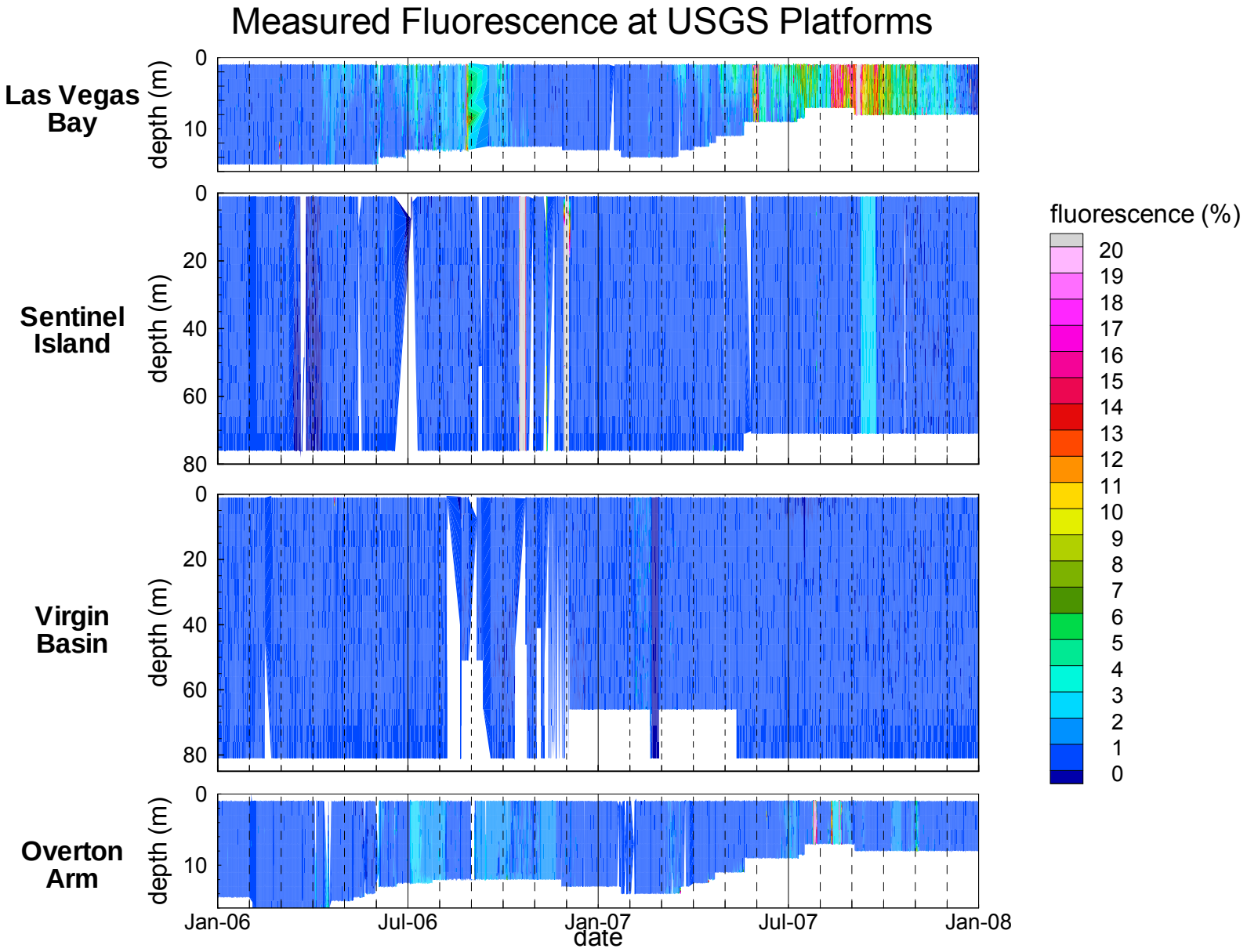
Measured Fluorescence at USGS Platforms
Las Vegas Bay
Sentinel Island
Virgin Basin
Overton Arm
depth (m)
0
10
20
40
60
80
Jan-06
Jul-06
Jan-07
Jul-07
Jan-08
date
fluorescence (%)
20
19
18
17
16
15
14
13
12
11
10
9
8
7
6
5
4
3
2
1
0

Figure 2.64

Measured Chlorophyll a and Fluorescence

USBR Station LVB3.5and USGS Platform Las Vegas Bay Site 3

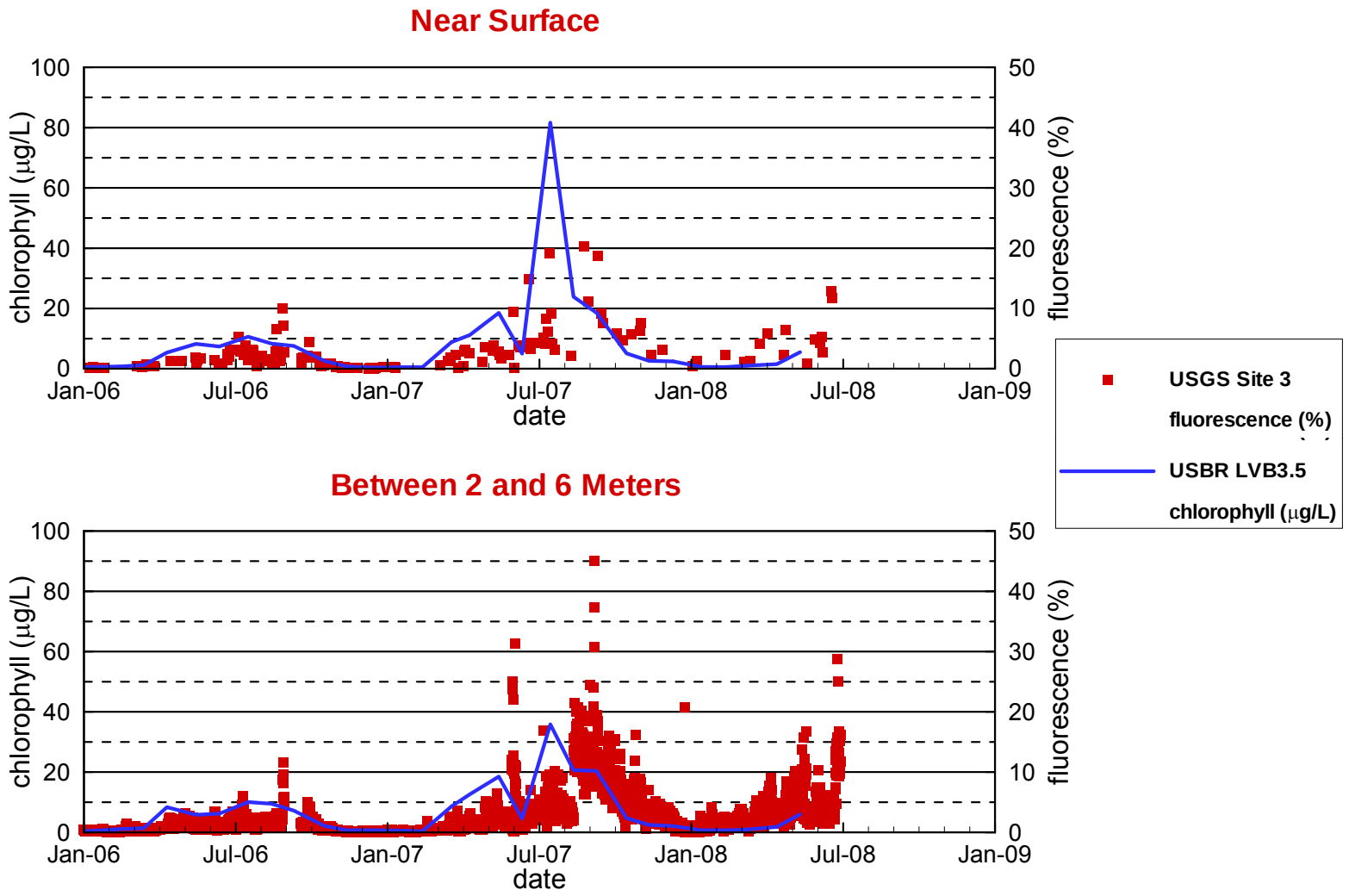

Figure 2.65

FLOW SCIENCE

Measured Chlorophyll a and Fluorescence

SNWA Station LVB3.5and USGS Platform Las Vegas Bay Site 3

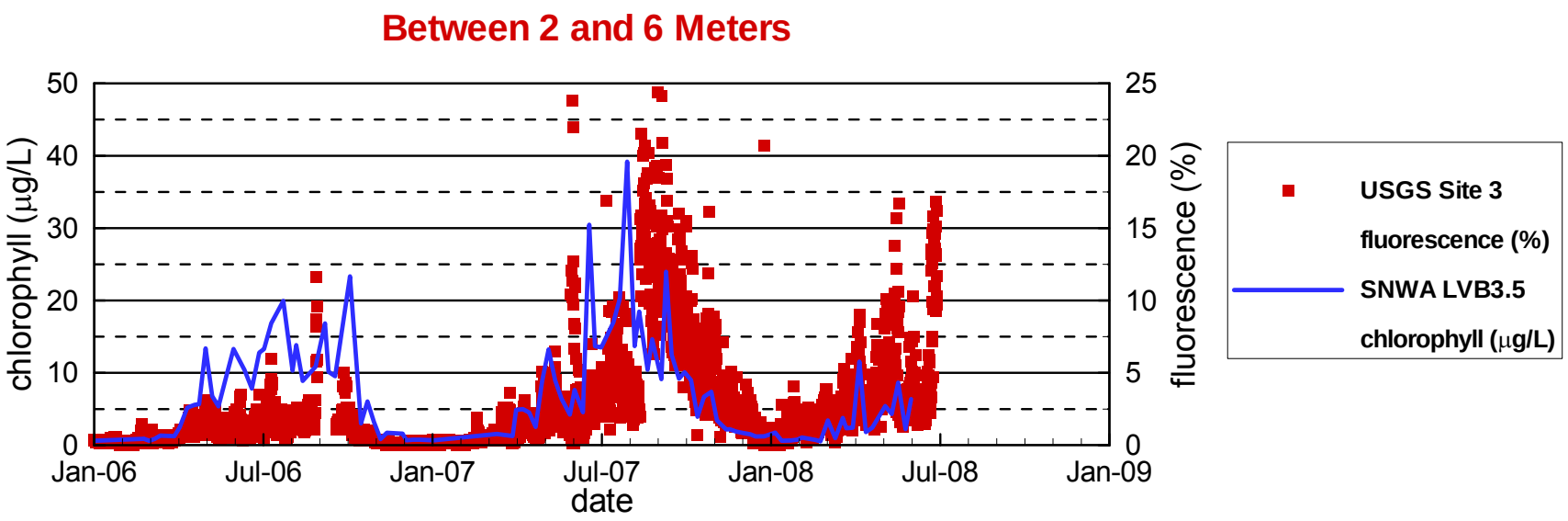

Figure 2.66

Measured Chlorophyll a and Fluorescence

USBR Station CR346.4 and USGS Platform Sentinel Island

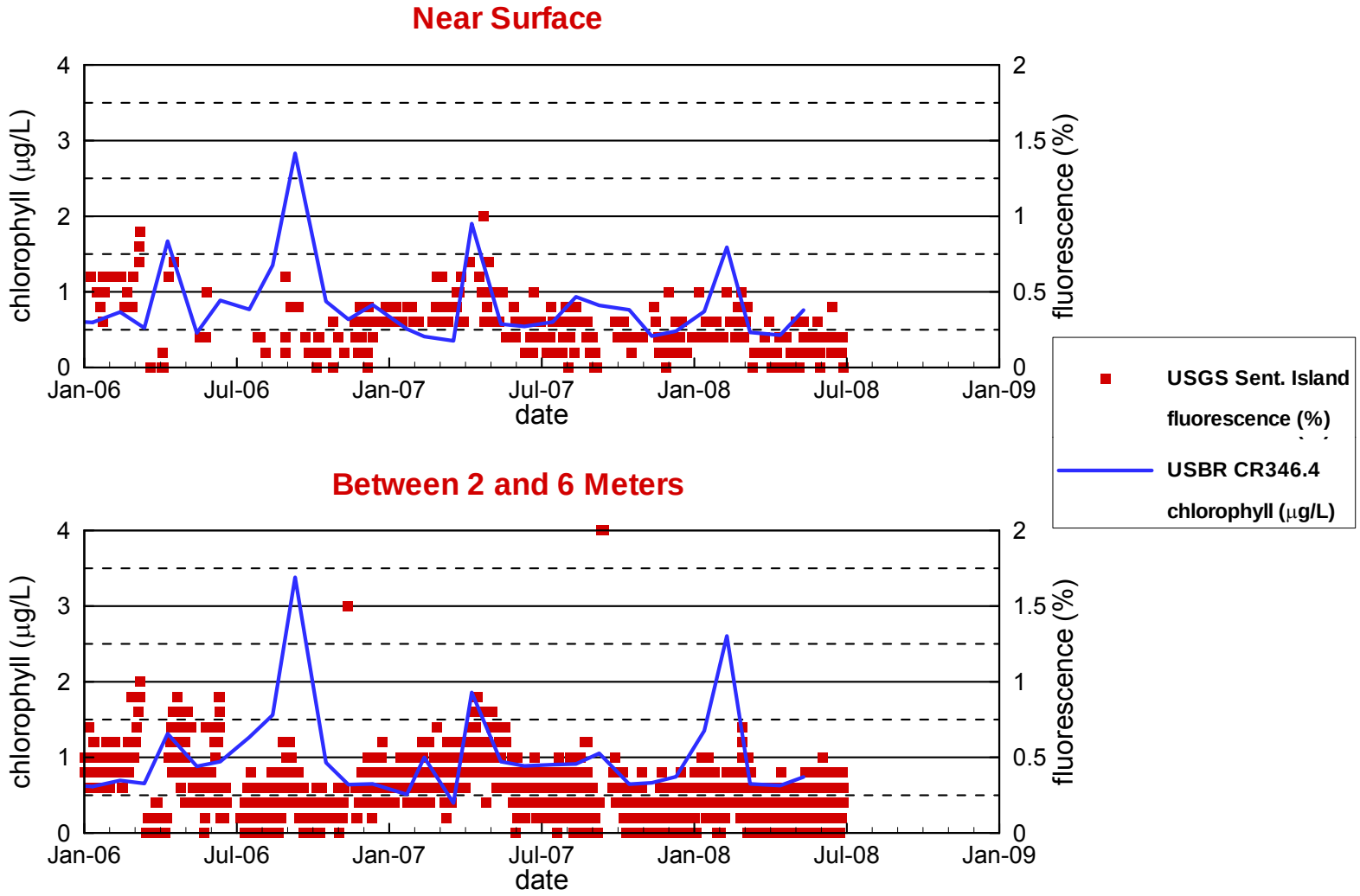

Figure 2.67

FLOW SCIENCE

Measured Chlorophyll a and Fluorescence

SNWA Station CR346.4 and USGS Platform Sentinel Island

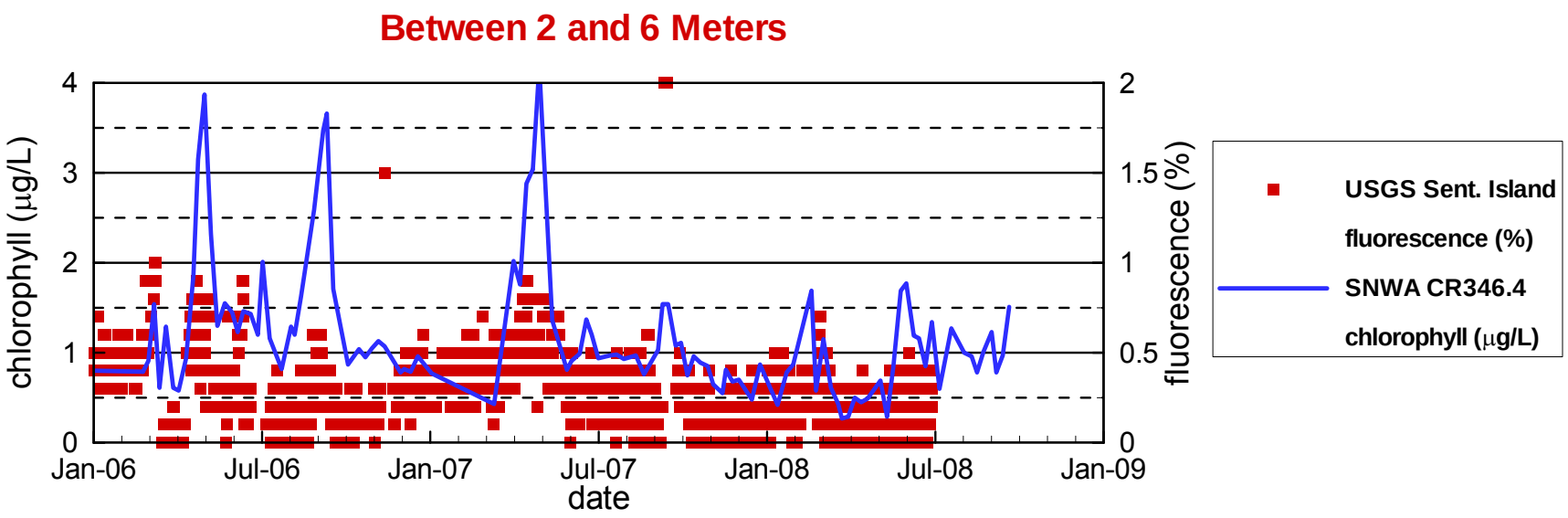

Figure 2.68

Measured Chlorophyll a and Fluorescence

USBR Station CR360.7 and USGS Platform Virgin Basin

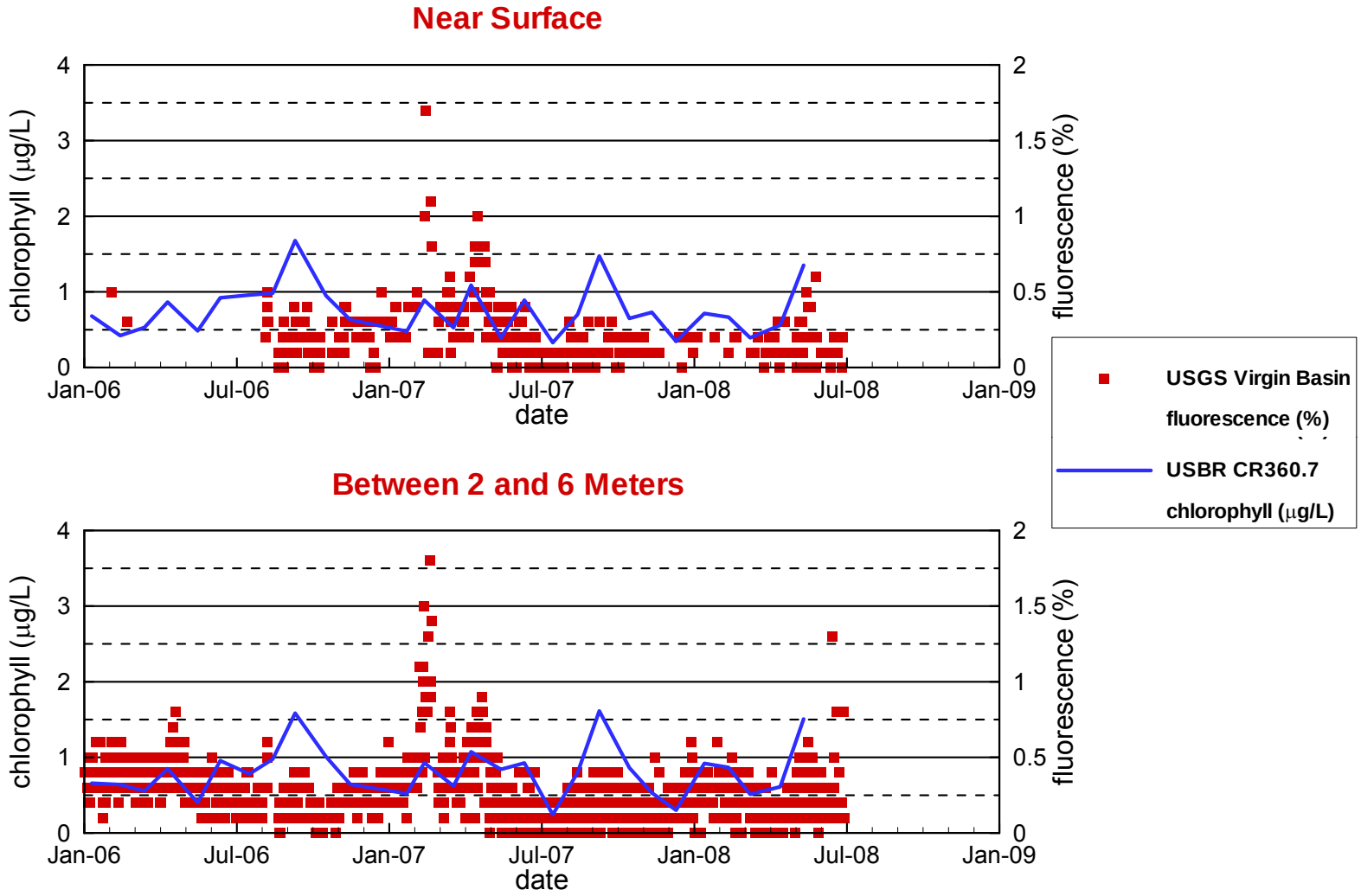

Figure 2.69

Measured Chlorophyll a and Fluorescence

USBR Station VR25.1 and USGS Platform Overton Arm

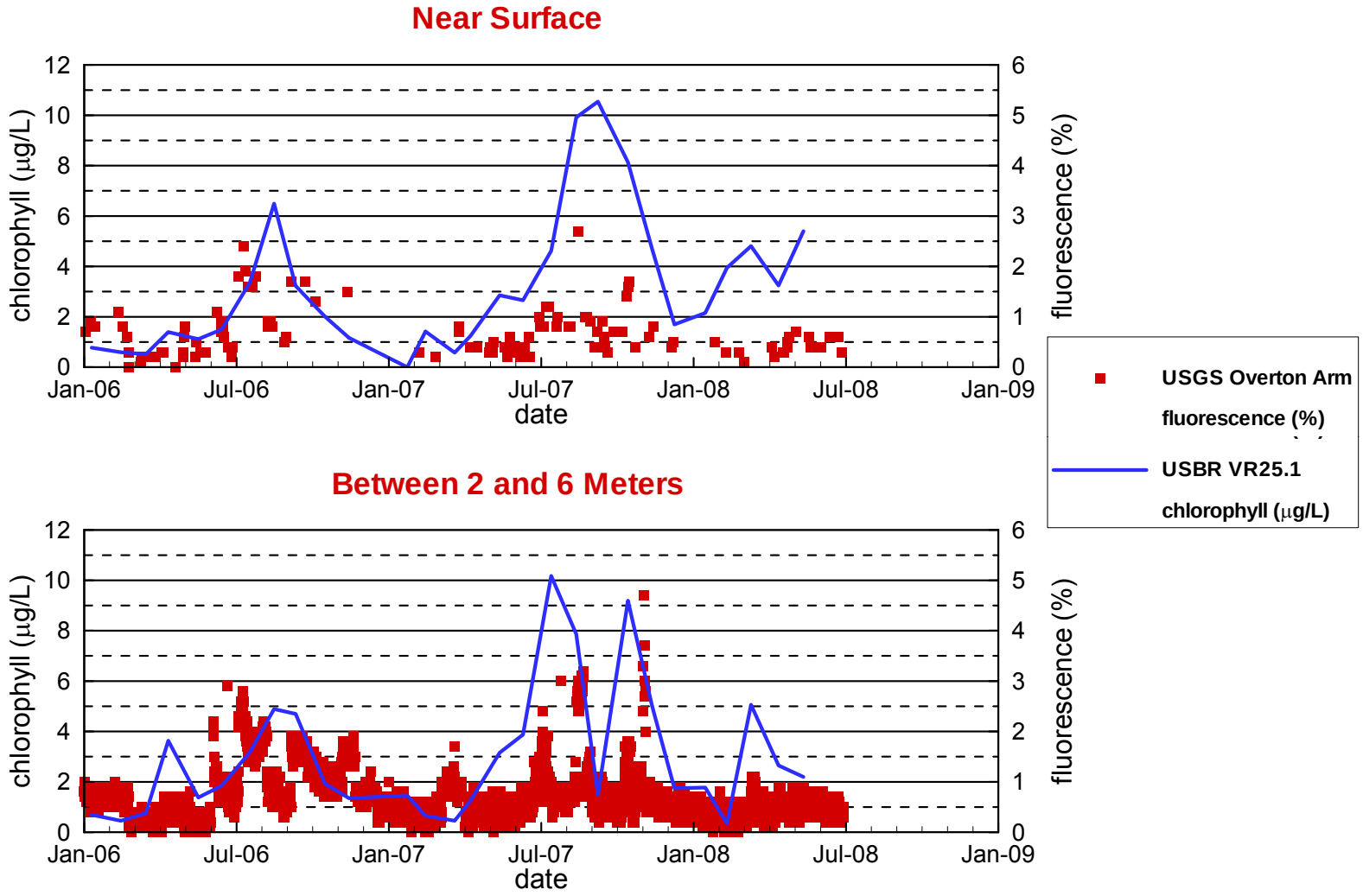

Figure 2.70

Measured Chlorophyll a and Fluorescence

SNWA Station LVB3.5 and USGS Platform Las Vegas Bay Site 3

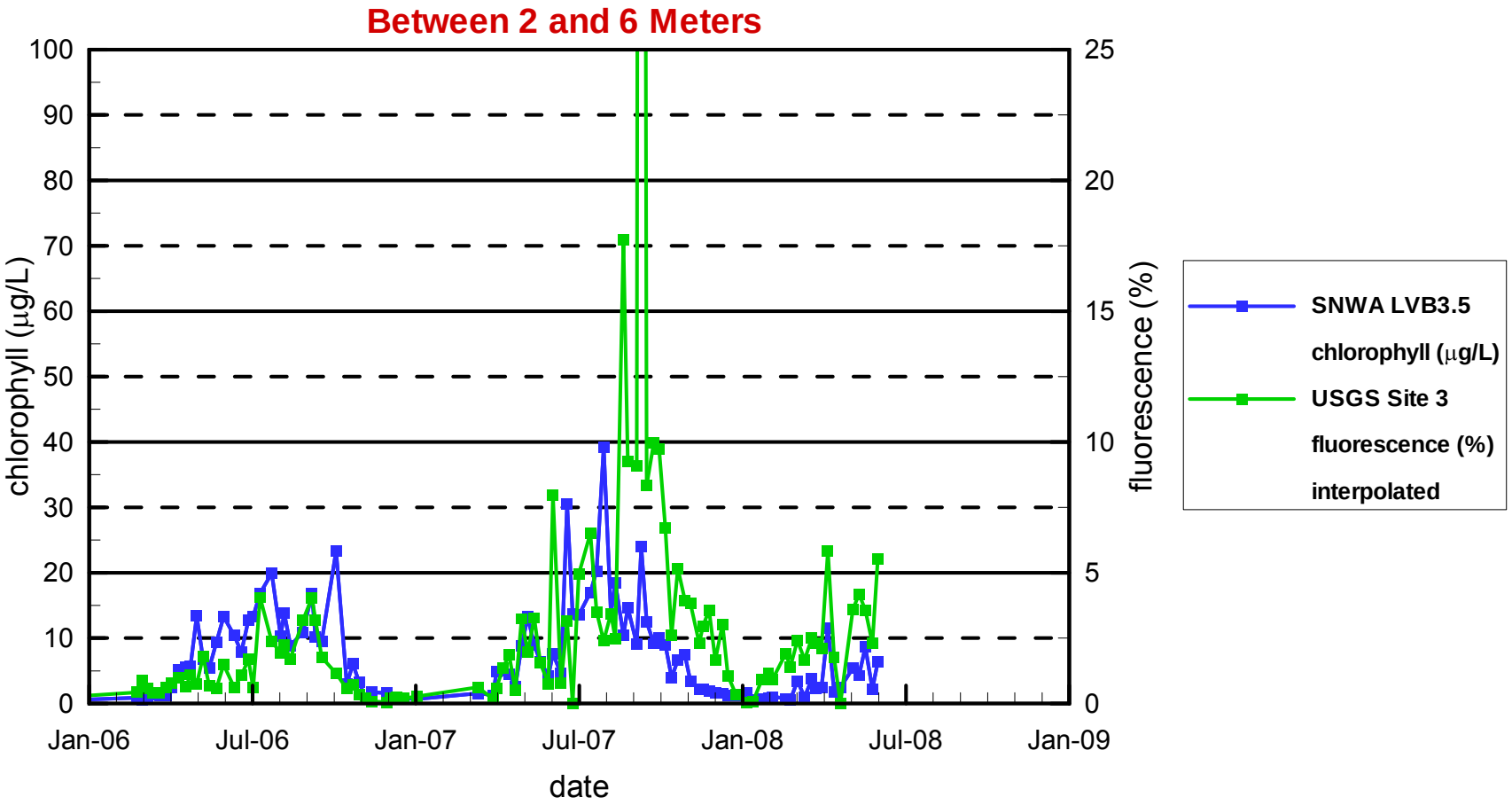

Figure 2.71

Chlorophyll a at LVB3.5 versus Fluorescence at Site 3*

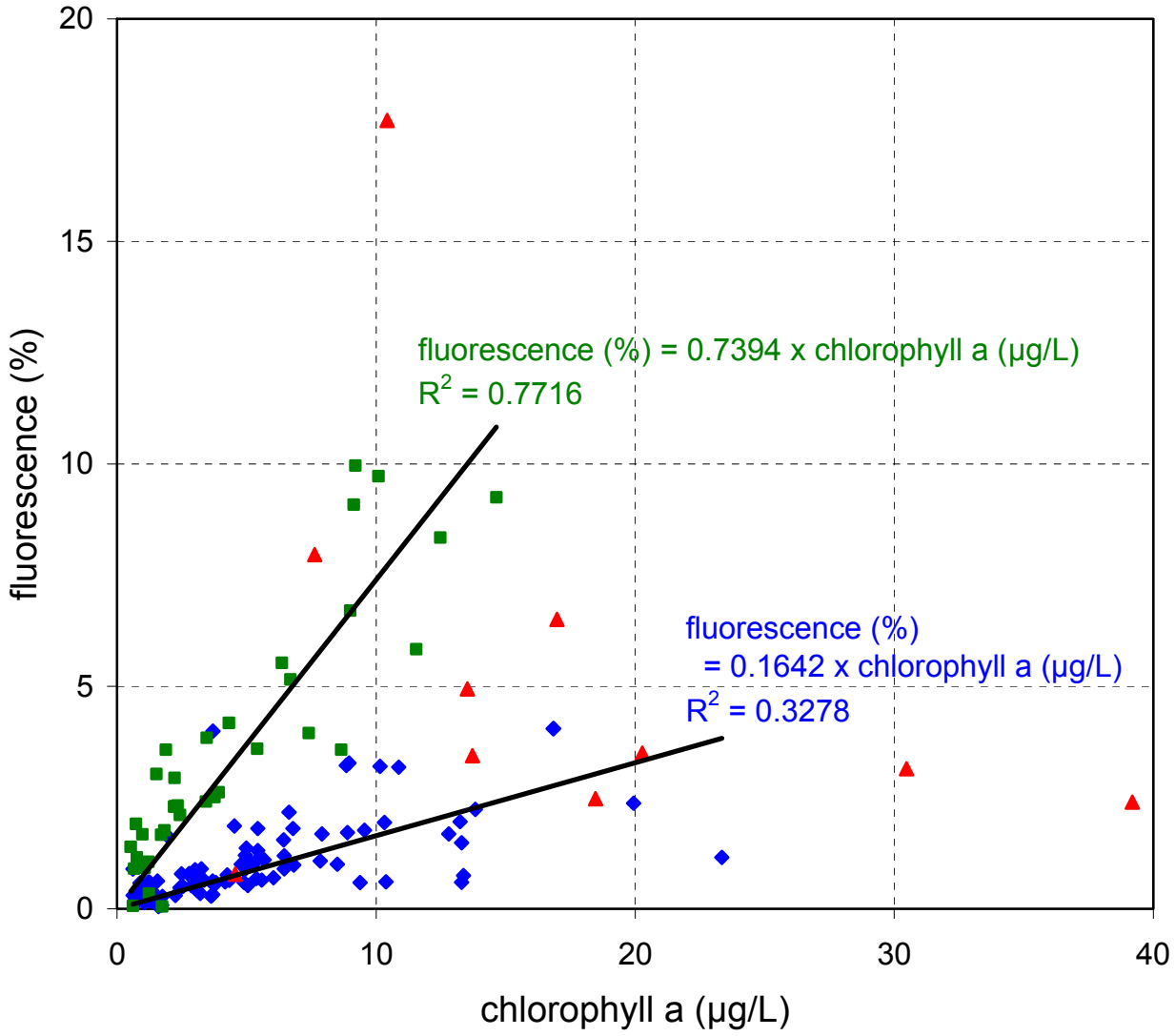

◆ 3/15/2005 - 5/30/2007

▲ 6/4/2007 - 8/22/2007

■ 8/27/2007 - 6/2/2008

* Notes:

Fluorescence data are measured by USGS every six hours at Las Vegas Bay platform at Site 3.

Chlorophyll a data are measured by SNWA weekly at Station LVB3.5

For plotting purposes, the 6-hourly fluorescence data are interpolated onto the same sample dates and times as the weekly chlorophyll a data.

Figure 2.72

3 MODELING APPROACH

This section provides a brief general description of the ELCOM/CAEDYM models, and details of the computational grids and model inputs used in the calibration simulations. Many of the details of this section are the same as in a previous report on the original 2000 through 2005 Whole Lake Model (Flow Science, 2007). Specifically, the same versions of ELCOM/CAEDYM (Section 3.1) and the same model grids (Section 3.2) are used. However, adding 2006 and 2007 to the modeling period required updates and changes to the model inputs (Section 3.3). In addition, several refinements were made to the model, as discussed in Section 3.4.

3.1 DESCRIPTION OF ELCOM AND CAEDYM

The Center for Water Research at the University of Western Australia has developed a modeling system for aquatic ecosystems that combines a three-dimensional hydrodynamic simulation method with a suite of water quality modules that compute interactions between biological organisms and the chemistry of their nutrient cycles. This integrated approach allows for the feedback and coupling between biogeochemical and hydrodynamic systems so that a complete representation of all appropriate processes can be included in an analysis. The hydrodynamic simulation code is the Estuary Lake and Coastal Ocean Model (ELCOM), and the biogeochemical model is the Computational Aquatic Ecosystem DYnamics Model (CAEDYM).

ELCOM allows the user to define boundary conditions, physical inputs, and bathymetry in a grid structure to simulate a body of water. It is used to predict variations in water temperature, salinity, and the concentration of conservative tracers in space and time within the body of water. This is accomplished by solving the unsteady Reynolds-averaged Navier-Stokes equations and scalar transport equations. CAEDYM can be linked to ELCOM (or any another appropriate hydrodynamic model) to predict aquatic ecological behavior within the same body of water. Biogeochemical inputs are defined similar to the physical inputs in ELCOM. CAEDYM uses parameter-specific algorithms to calculate the variations in aquatic ecology. Detailed information concerning the history, methodology, and validation of ELCOM and CAEDYM, as well as technical descriptions of each, are included in Appendix B.

The calibration simulations documented in this report were performed using ELCOM v2.1.1 and CAEDYM v2.2.1.

3.2 COMPUTATION DOMAIN AND GRID

The computational domain and model grids were the same as were used in the original 2000 through 2005 Whole Lake Model (Flow Science, 2007). For completeness, the domain and grid descriptions are repeated here.

The model domain consisted of the entire Lake Mead, including the Boulder, Virgin and Gregg Basins and Overton Arm (see **Figure 2.1**). The bathymetric data set used for the model grids consisted of elevation data at a horizontal spacing of 10 m (**Figure 3.1**). This data set was provided by the USGS, and was based upon a survey in 2001. The data set included the relatively-recent effects of sediment deposition in the basins by the inflows. **Figure 3.2** illustrates the sediment depth in Gregg Basin near the CR inflow, as determined from the 2001 survey. It should be noted that sediment deposition is an ongoing process, and as such the lake bottom elevations may change over time. The modeling does not attempt to capture this process and uses the same grids for all simulation years considered herein.

Two grid resolutions were used during simulations: a 600-m horizontally-spaced grid and a 300-m horizontally-spaced grid. In general, the finer 300-m grid provides more accurate results as it can better resolve finer bathymetric details. However, the use of this grid requires longer model run times and more computer memory resources. These limitations rendered the 300-m grid impractical for simulations that consider non-conservative parameters (i.e., ELCOM coupled with CAEDYM), which have a significantly longer run time and require more computer memory resources than comparable simulations that only consider conservative parameters (i.e., ELCOM only). Therefore, all of the non-conservative parameter simulations used the 600-m grid while all of the conservative parameter simulations used the 300-m grid. It is noted that an ELCOM run takes approximately three days per one year of simulation on an Intel Core 2 (2.93 GHz) processor (300-m grid), whereas CAEDYM runs on the 600-m grid require two days per year of simulation.

The horizontal discretizations of the 600-m and 300-m grids are shown in **Figures 3.3** and **3.4**, respectively. Note that both grids are rotated 33 degrees with respect to north. This rotation aligns the Narrows with the axes of the grid, which enables better resolution of the narrow flow channels between Virgin and Boulder Basins.

The elevations for each of the grid points were obtained directly from the 10-m data set using the "nearest-neighbor" sampling technique. Plots of the resulting grids indicated that some of the narrow channels that existed in the 10-m bathymetry were blocked in the 300-m and 600-m grids, as a result of the discretization. An example of such a situation is illustrated in **Figure 3.5**, which shows a close up of the 300-m grid in the vicinity of Station VR9.4 in the Overton Arm. It is clear in **Figure 3.5** that there is a lack of a clear path for the water to travel down the VR thalweg (note that water can only move between the faces of adjacent cells, and not from cell corner to cell corner).

Inspection of the 10-m data set clearly showed that there should be a clear channel (with monotonically decreasing elevation in the downstream direction) in this region.

Manual adjustments were made to open the channels along all the thalwegs (i.e., LVW, CR and VR) for both 300-m and 600-m grids. In order to ensure the manually altered grids were accurate, comparisons of elevations along the manually opened channels to elevations extracted directly from the 10-m data along the thalwegs of the river channels were made. **Figure 3.6** shows the 300-m grid in the vicinity of VR9.4, after the channels were manually opened. There is now an unimpeded downslope through the thalweg. The manual changes can be clearly seen by comparing **Figures 3.5** and **3.6**.

A constant vertical grid spacing of 2 m was used for both the 300-m and 600-m horizontal grids. **Figure 3.7** plots the 300-m horizontal grid along a vertical profile along the VR thalweg from Virgin Basin to the VR. Note that while ELCOM/CAEDYM is capable of using stretched grids (in both horizontal and vertical directions), a constant vertical grid size was found to be necessary in order to properly resolve the underflows into the lake from the VR, MR and LVW. **Figure 3.7** also illustrates that the elevation of the thalweg in the discretized model decreased monotonically in the downstream direction, which was a result of manually opening the channels as discussed above.

3.3 MODEL INPUTS

Input data files are required to define the conditions at the model boundaries. Model boundary conditions include inflow quantities, outflow quantities, inflow water quality, and meteorological forcing functions (air temperature, solar radiation, wind, etc.) during the simulation period. These model input data files were constructed using field data that were collected from various sources. In most cases the data and methodologies used to set-up model input for years 2006 and 2007 were the same as used and detailed in the previous modeling report (Flow Science, 2007). In some instances new and more representative field data have become available since the previous modeling, and these different data-sets were used for 2006 and 2007 input. Occasionally the original 2000 through 2005 input was also updated with new and more representative data. Additional details of these changes and plots of the model input data and raw field data for all model years are provided in Appendix A.

Simulations also require initial conditions for all water quality variables at all non-land grid cells within the domain to begin the simulation. Following the original modeling (Flow Science, 2007) the 2000, 2001, 2002, 2004 and 2005 simulation years were initialized using measured in-reservoir data. Due to the subtleties that resulted from the incomplete destratification in the winter of 2002/03, the 2003 simulation year was computed as a continuation of the 2002 simulation, and as such did not require initial conditions to be specified. The 2006 and 2007 simulations were also computed

continuously from the 2005 simulation (see Section 3.4.1), and as such did not require any other initial conditions to be specified.

The initial conditions were spatially non-uniform (i.e., used measured data at multiple locations in the lake) for the ELCOM variables (temperature, conductivity, perchlorate and bromide). In the original modeling (Flow Science, 2007) the initial conditions were horizontally-uniform for the CAEDYM variables (chlorophyll *a*, nutrients, DO and pH), with the measured field data at Station CR346.4 being used to initialize the CAEDYM variables throughout the lake. However, spatially variable initial conditions for phosphorus and nitrogen have been implemented into the more recent work to improve model results (see Section 3.4.4).

3.4 MODEL ENHANCEMENTS

In additional to adding years 2006 and 2007 to the original 2000 through 2005 modeling period, numerous enhancements have been made to the model. These enhancements are results of direct improvements to the ELCOM/CAEDYM routines, as well as the more recent availability of additional and better field data.

3.4.1 Continuous Simulation

The original 2000 through 2005 modeling (Flow Science, 2007) simulated each calendar year as separate simulations. That is, the simulation was started at the beginning of each calendar year using initial conditions derived from measured field data (Section 3.3). An exception to this was year 2003, which was computed as a continuation of the 2002 simulation. This was done in order to capture the subtleties that resulted from the incomplete destratification in the winter of 2002/03 (Flow Science, 2007).

In the present modeling, years 2006 and 2007 were each added onto the 2005 simulation in a continuous manner. That is, the simulation was run as a continuous three-year simulation, starting from the 2005 initial condition and continuing through 2006 and 2007. This approach demonstrates the ability of the model to be used for multiple-year simulations, as well as enabling subtleties such as complete or incomplete destratification in each winter to be examined using the model.

3.4.2 Multiple Wind Areas

The original 2000 through 2005 modeling used meteorological data from the USGS platform at Sentinel Island in Boulder Basin. In late 2005 the USGS installed additional meteorological stations in the upper basins of Lake Mead at Virgin Basin and Overton Arm (**Figure 3.8**). Analysis of wind data from these locations indicated consistently lower wind speeds in the upper basins than in Boulder Basin (Section 2.2).

In years 2006 and 2007 the additional wind data (both speed and direction) were implemented into the model. The surface of Lake Mead was divided into three wind areas, as illustrated in **Figure 3.8**, and the three sets of wind data were applied to the different areas. Specifically, the Sentinel Island wind data were applied to the Las Vegas Bay and Boulder Basin, the Overton Arm wind data were applied to the upper portion of Overton Arm, and the Virgin Basin wind data were applied to Virgin Basin, Gregg Basin and the lower portion of Overton Arm (**Figure 3.8**). The use of multiple wind-areas on Lake Mead results in a more realistic representation of the on-lake wind patterns and wind speeds and their effect on lake dynamics.

3.4.3 Virgin River Flow Rate

Prior to April 2006 the flow rate for the VR entering Lake Mead was estimated using data from a gauging station located approximately 40 miles upstream of Lake Mead. In the original 2000 through 2005 modeling a simple correlation was used to account for water usage between this station and the lake (Flow Science, 2007). Since April 2006, new data from a location close to Lake Mead have been available, and have been used directly for model input (see Section A.1.2). Analysis of the new data together with observations from USGS personnel, indicate that the summer flow rates of the VR into Lake Mead are close to zero in most years. Thus, in the present modeling, the VR flow rate was set to zero from July through September of 2000 through 2005. No such adjustments were required in the summers of 2006 and 2007, due to the direct use of flow rate data from the gauging station located close to Lake Mead.

3.4.4 Spatially Variable Initial Conditions for Phosphorus and Nitrogen

The original 2000 through 2005 modeling used horizontally-uniform initial conditions for each of the CAEDYM variables (chlorophyll *a*, nutrients, DO and pH), with the measured field data at Station CR346.4 (in Boulder Basin) being used to initialize the CAEDYM variables throughout the lake. However, field data from the upper basins indicate that the concentrations of phosphorus and nitrogen are lower in the upper basins than in Boulder Basin.

In the present modeling, spatially variable initial conditions for phosphorus and nitrogen were implemented for all years that required initialization (i.e., for 2000, 2001, 2002 and 2004 [see Section 3.3]). For each parameter, a simple binary spatial distribution was used, with one concentration defined for all locations downstream of the Narrows (i.e., Boulder Basin and the Las Vegas Bay), and a second concentration defined for all locations upstream of the Narrows. The downstream concentrations were determined from data measured at Station CR346.4, while the upstream concentrations

were based on an aggregate of observed field data at Stations CR360.7, VR2.0 and VR12.9/13.0.

The implementation of spatially variable initial conditions directly improved the simulation results for nitrogen, and indirectly improved the simulation results for chlorophyll *a*. The improvement to the phosphorus simulation was difficult to gauge due to the relatively high detection limits for the data that existed prior to 2005.

3.4.5 Spatially Variable Sediment Oxygen Demand

The original 2000 through 2005 modeling used a sediment oxygen demand (SOD) that was a constant value throughout Lake Mead. The use of a constant value throughout the lake was cited in the previous report (Flow Science, 2007) as the primary reason why the model did not fully predict the level of DO depletion at the lake bottom near each of the inflows.

The version of CAEDYM used for the modeling (v2.1.1) was not configured to allow spatially variable SOD. Therefore, Flow Science modified the CAEDYM source code "in house", to enable the SOD to be specified as a function of horizontal position in the lake. The SOD values near each of the inflows were then adjusted in an iterative manner, to achieve good agreement with measured DO data from within the lake. **Figure 3.9** illustrates the final distribution of SOD values (in $g/m^2/day$) that was used in the simulations. The single SOD value used in the original modeling was 0.7 $g/m^2/day$, which is retained for much of the open-water domain in the present modeling. The SOD values were increased near each of the inflows, with the maximum value of 4.9 $g/m^2/day$ being used near the LVW (**Figure 3.9**). The SOD rates used by the model were determined to give the best agreement between field data and model results.

The use of variable SOD vastly improved the DO simulation at the reservoir bottom near the inflows. For example, **Figure 3.10** plots measured and simulated DO at Station LVB3.5 from 2000 through 2007. The upper frame plots DO at the surface, while the lower frame plots DO at the bottom. For this figure, the spatially variable SOD was only implemented in the 2005 through 2007 simulation. Simulation results from 2000 through 2004 use the constant SOD value of 0.7 $g/m^2/day$. The DO simulation is clearly improved by the implementation of spatially variable SOD.

It should be noted that **Figure 3.10** does not represent the final model calibration results. The final results (presented in Section 4.2.8) were re-simulated with the spatially variable SOD implemented for all eight years (2000 through 2007). The purpose of **Figure 3.10** is to clearly illustrate the impact and benefit of implementing spatially variable SOD on the model results.

3.4.6 Recalibration of Phosphorus and Algae Routines

The original 2000 through 2005 Whole Lake Model calibration (Flow Science, 2007) was based largely upon understanding of the phosphorus and algae cycles developed during the initial Boulder Basin modeling (Flow Science, 2005). At that point in time, most of the phosphorus data collected in the upstream inflows and within the open water of Lake Mead was below the method detection limit. The phosphorus calibration and the directly related algae calibration were primarily based upon some limited TP data collected within Boulder Basin between 2000 and 2002, as part of a special phosphorus sampling program. These limited data were analyzed using inductively-coupled plasma mass spectrometry (ICP-MS) with detection limits that were low enough to accurately measure the TP concentrations. However, none of the samples were analyzed for FRP using this method, and no samples from the upper basins were analyzed.

Since 2007 the routine samples collected within and around Lake Mead by the USBR and SNWA have been analyzed at the High Sierra Lab using lower detection limits than the previous routine sampling. Flow Science performed a detailed analysis of the new data-sets, and developed a phosphorus budget for Lake Mead (Flow Science, 2009). The budget evaluated the phosphorus fluxes into and out of each basin in Lake Mead, including settling and uptake by algae within the basins, and included separate analyses of both TP and FRP data.

Results of the phosphorus budget altered the understanding of the phosphorus in Lake Mead in the following ways;

- Particulate phosphorus concentrations in Boulder Basin were *higher* than previously thought.
- FRP concentrations in Boulder Basin were *lower* than previously thought.
- Particulate phosphorus concentrations in the CR inflow were higher than previously thought.
- Most of the particulate phosphorus in the CR inflow settled within the first few miles of the lake.

The altered understanding of the phosphorus in Lake Mead necessitated changes to the phosphorus routines in the model and some of the model input. The main changes involved fine-tuning the FRP concentration and increasing the TP concentration of the CR inflow (see Section A.2.2), and decreasing the rate of decomposition of particulate phosphorus to dissolved phosphorus.

Following the changes to the phosphorus cycling, additional changes were made to parameters related to the algae routines to correct the simulated chlorophyll *a*

concentrations. These changes included modifications to the internal phosphorus ratios and temperature limitation functions.

Additionally, minor adjustments were made to parameters related to the nitrogen and carbon routines to improve the NO3, TOC and pH simulations.

In all cases, the modified parameters remained within the range of accepted values. The new calibration spans eight years (2000 through 2007), compared to six years for the previous Whole Lake Model, and four years for the earlier Boulder Basin Model. The longer calibration period provides more confidence in the model.

Lake Mead 10-m Bathymetric Data

(2001, data source: USGS Open-File Report 03-320)

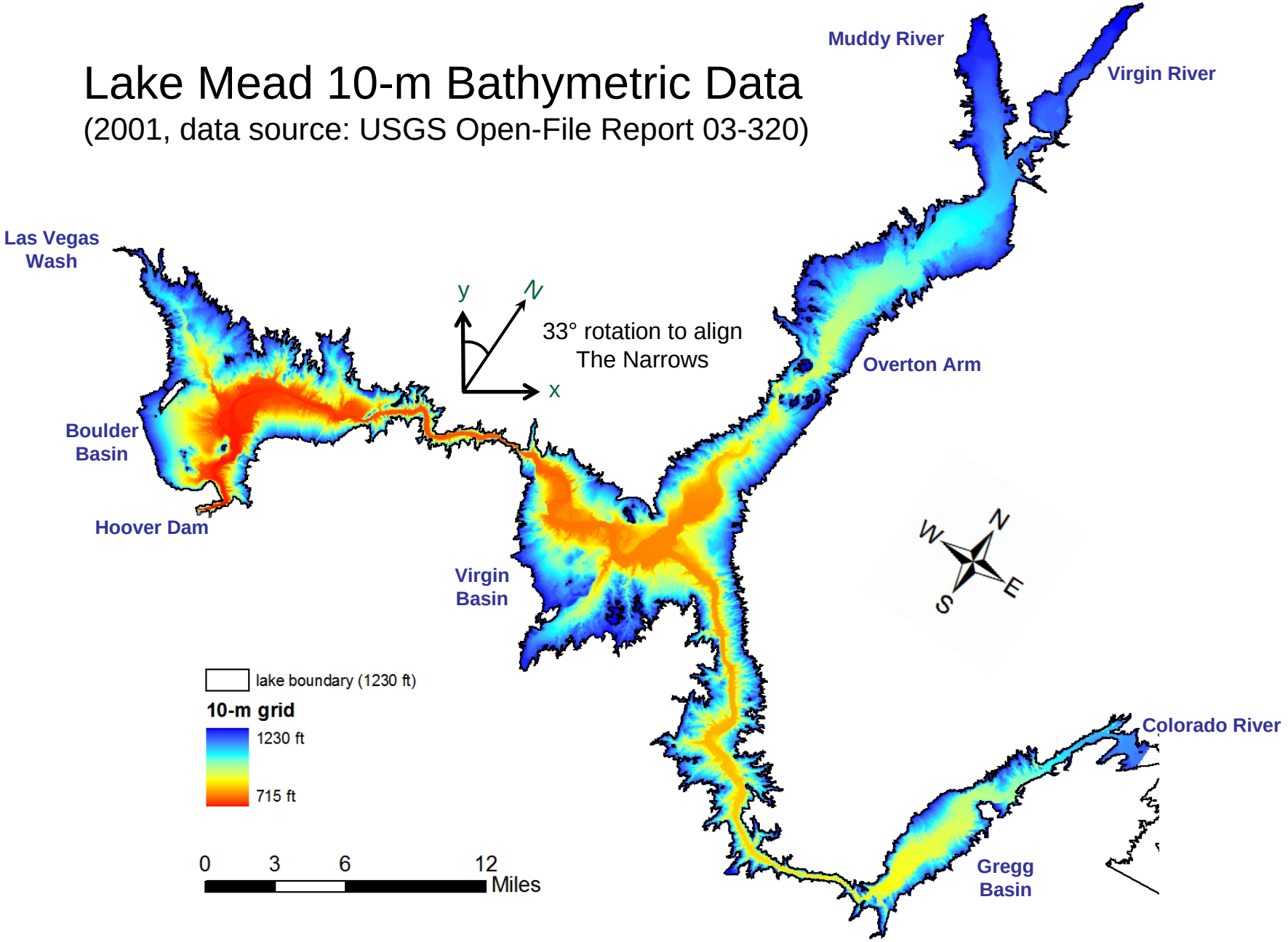

Ch3_Figures.ppt
FSI V064081 & V084015 Task 1
December 9, 2010

Figure 3.1

FLOW SCIENCE

Gregg Basin Sediment

(2001, data source: USGS Open-File Report 03-320)

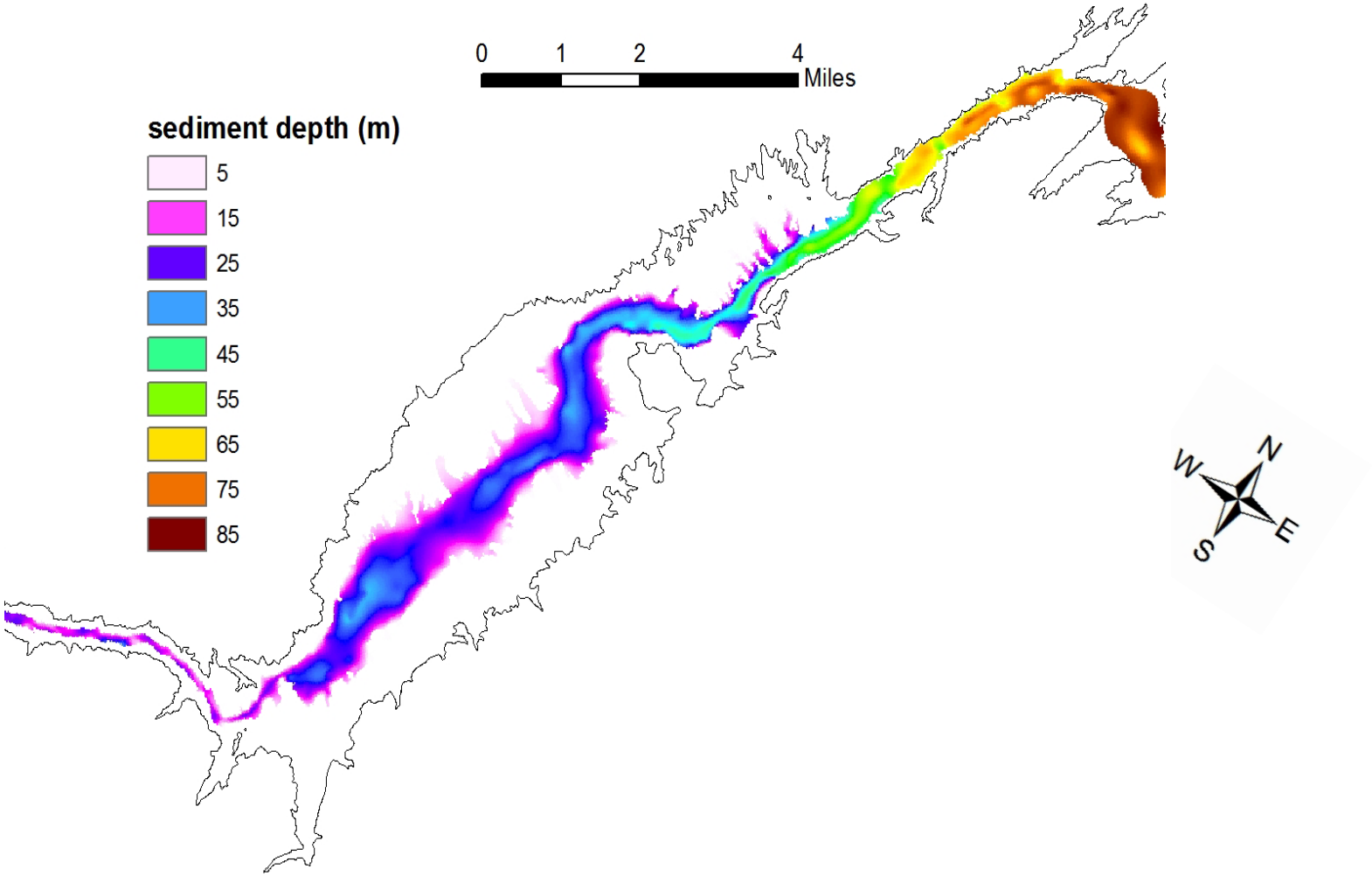

Figure 3.2

600-m Horizontal Grid

(Sampled from 10-m data using “nearest neighbor”)

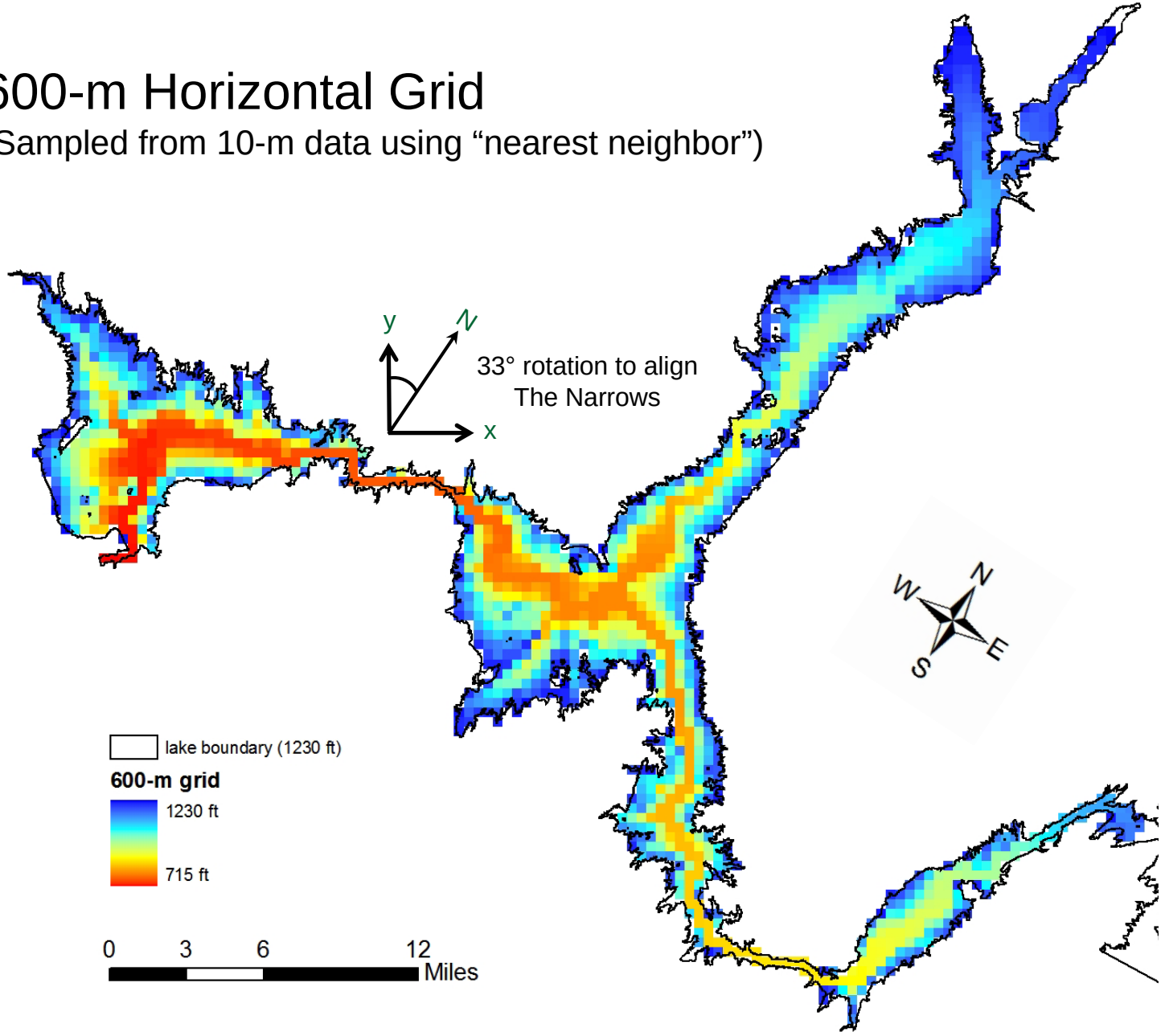

Figure 3.3

300-m Horizontal Grid

(Sampled from 10-m data using “nearest neighbor”)

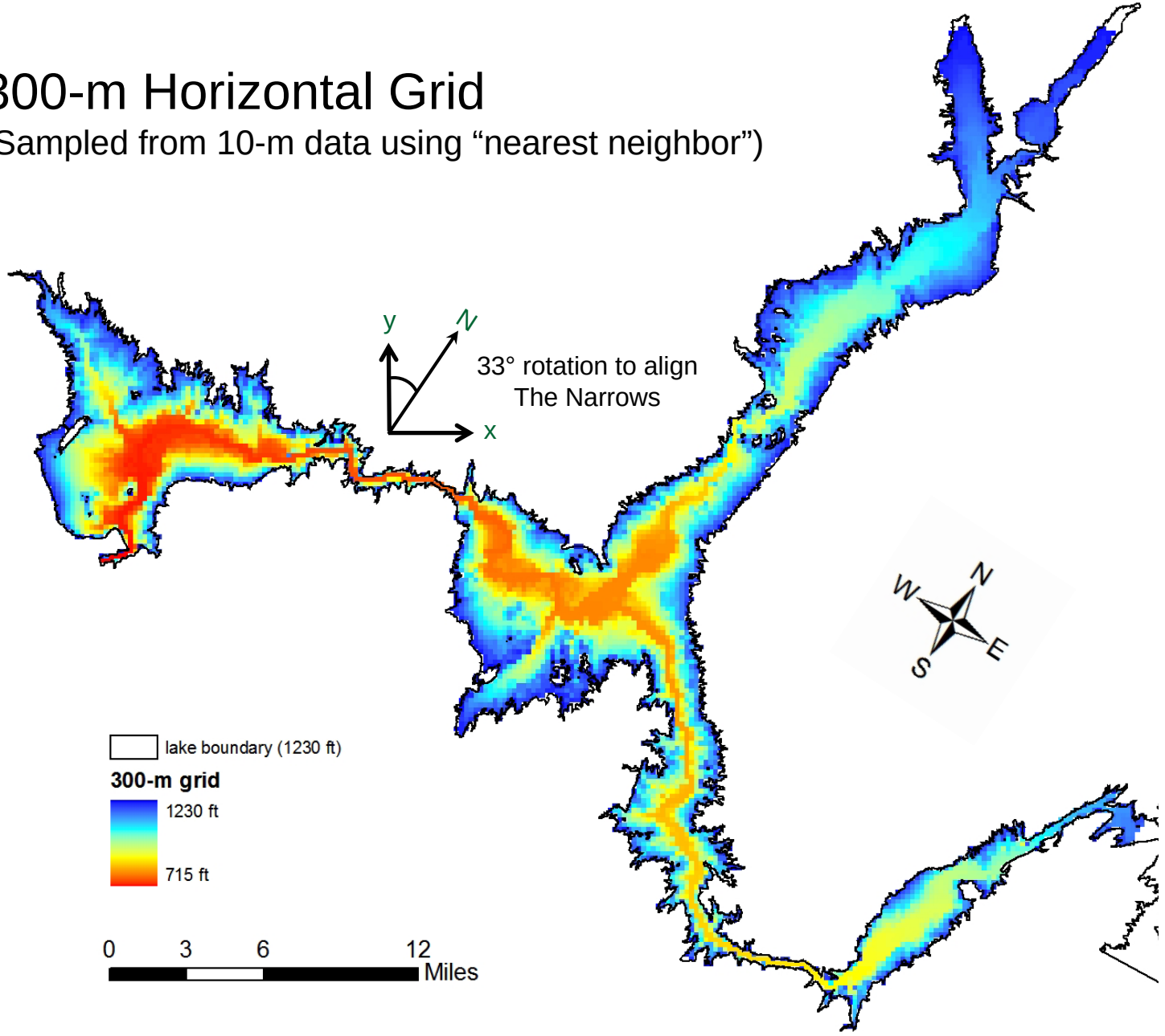

Figure 3.4

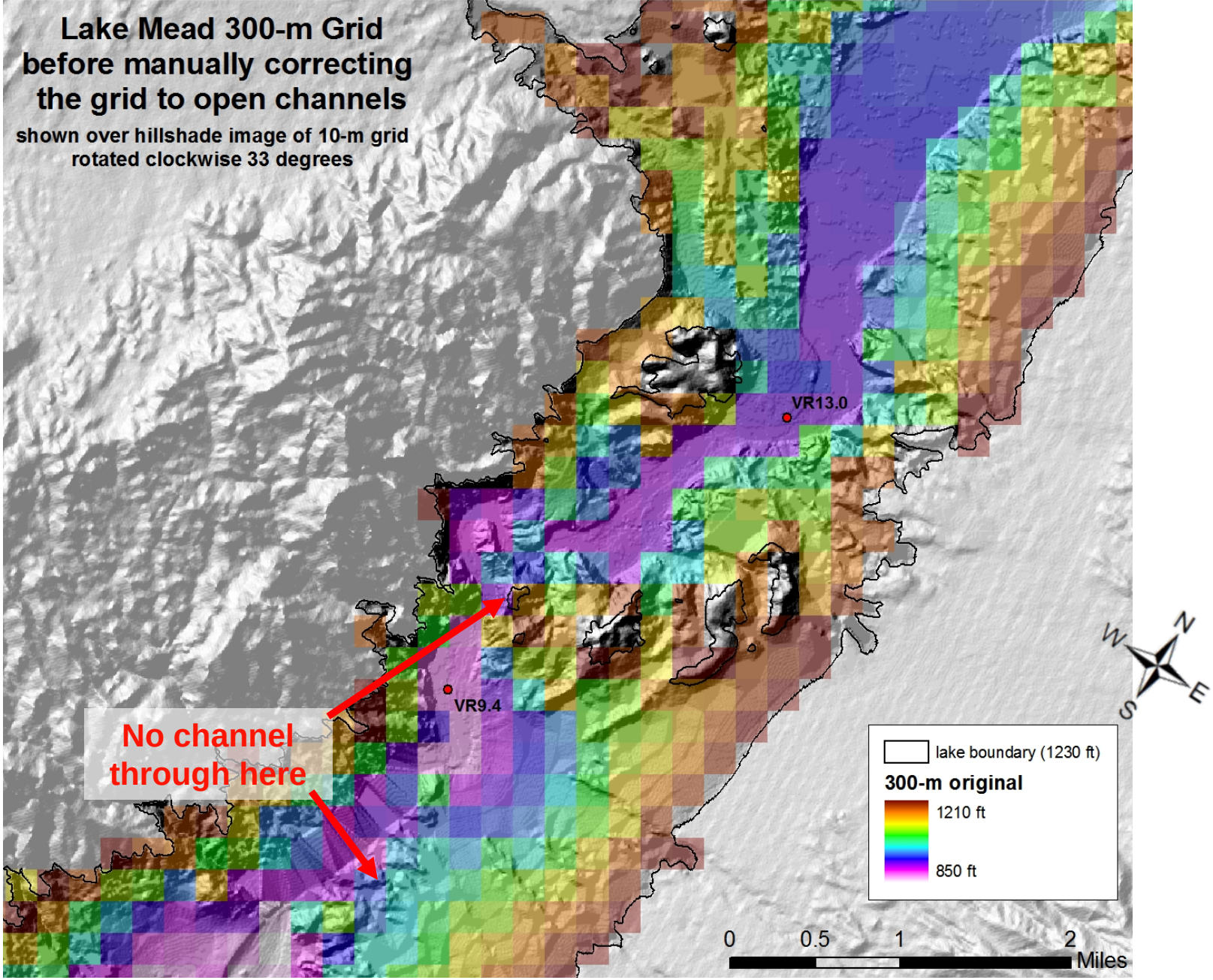
Lake Mead 300-m Grid
before manually correcting
the grid to open channels
shown over hillshade image of 10-m grid
rotated clockwise 33 degrees
VR13.0
VR9.4
No channel
through here
N
W
E
S
lake boundary (1230 ft)
300-m original
1210 ft
850 ft
0
0.5
1
2
Miles

Figure 3.5

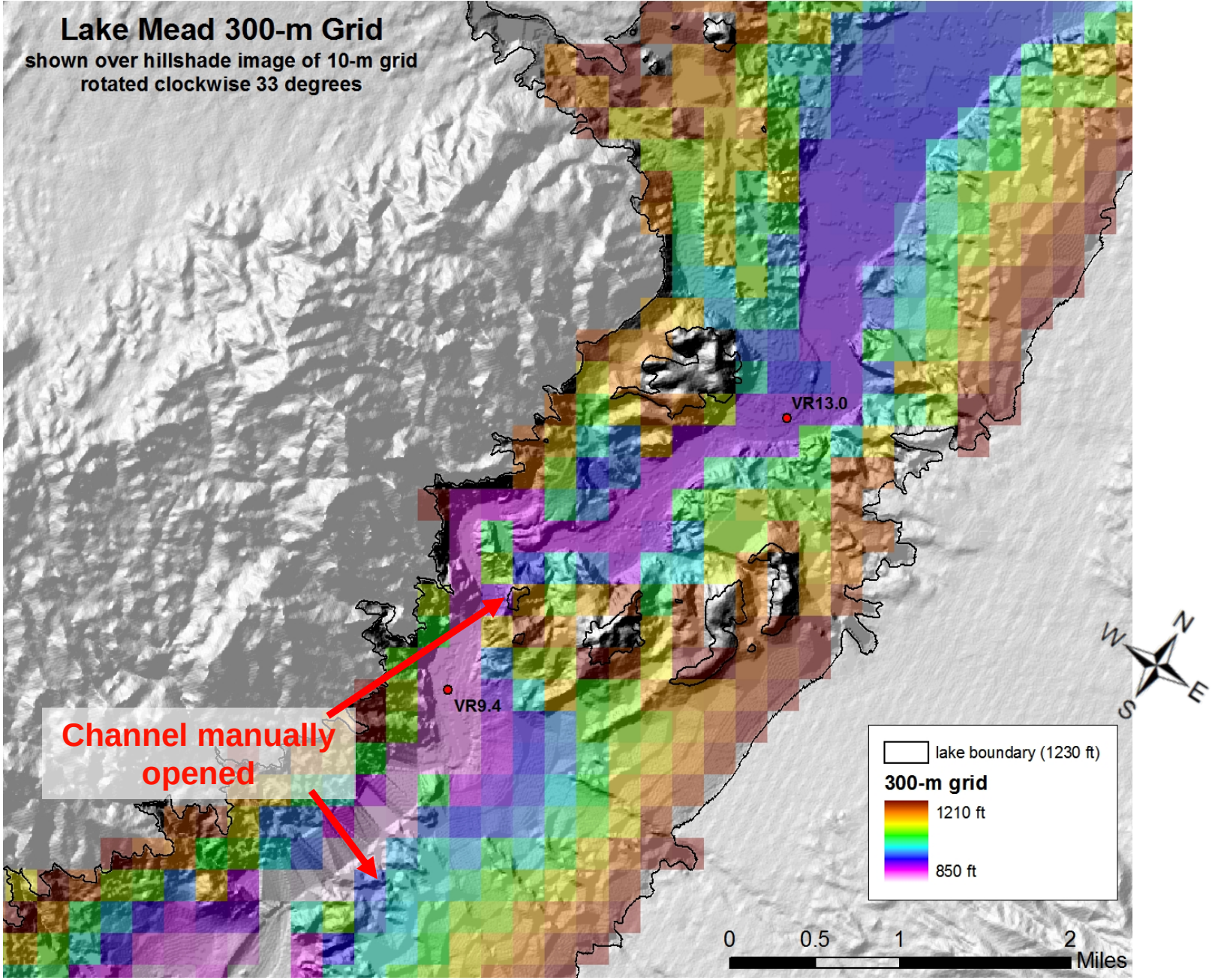

Ch3_Figures.ppt
FSI V064081 & V084015 Task 1
December 9, 2010

Figure 3.6

FLOW SCIENCE

300 x 2 m Computational Grid along Overton Arm Thalweg

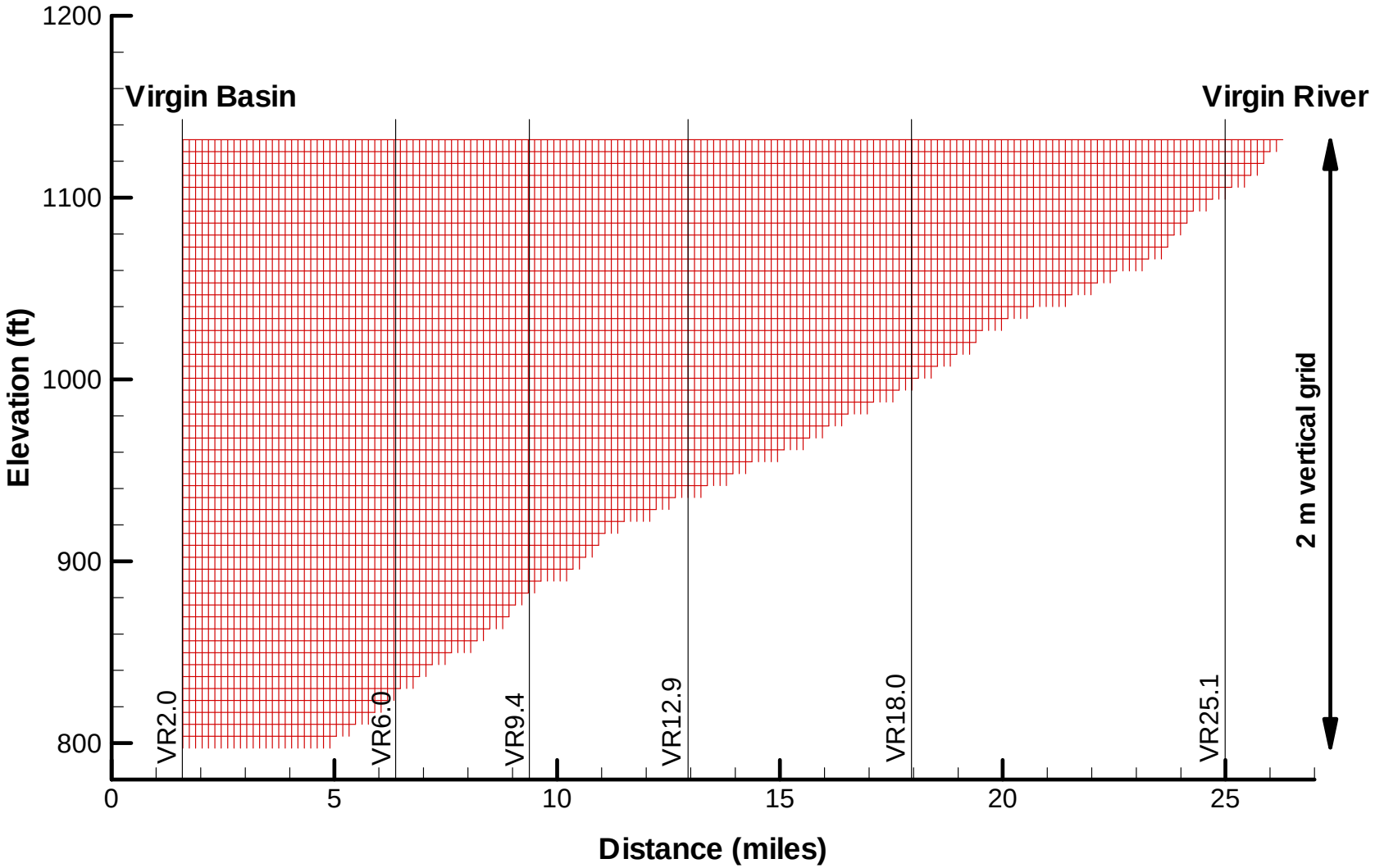

Figure 3.7

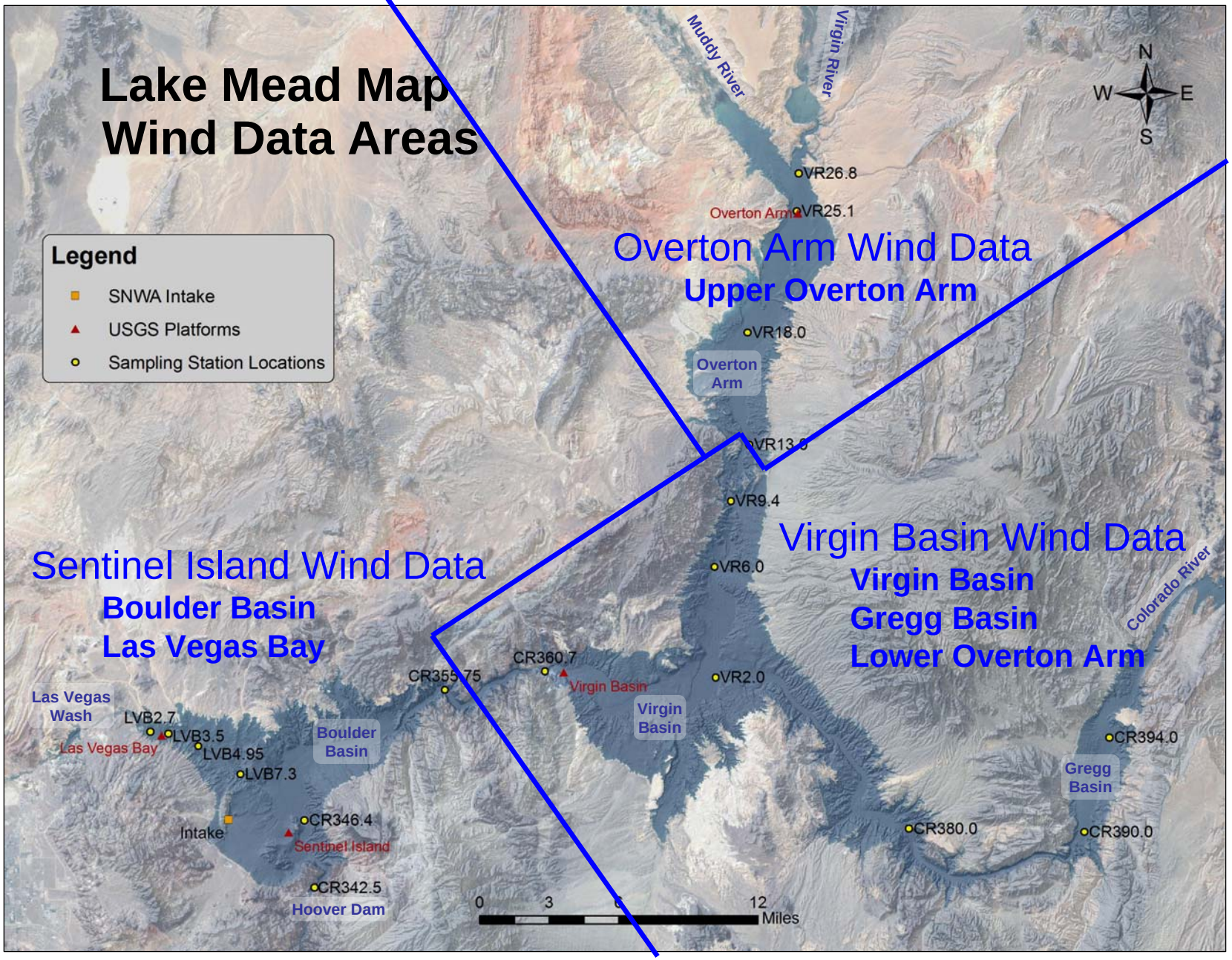

Ch3_Figures.ppt
FSI V064081 & V084015 Task 1
December 9, 2010

Figure 3.8

FLOW SCIENCE

Sediment Oxygen Demand (SOD) Values Used in Lake Mead Modeling

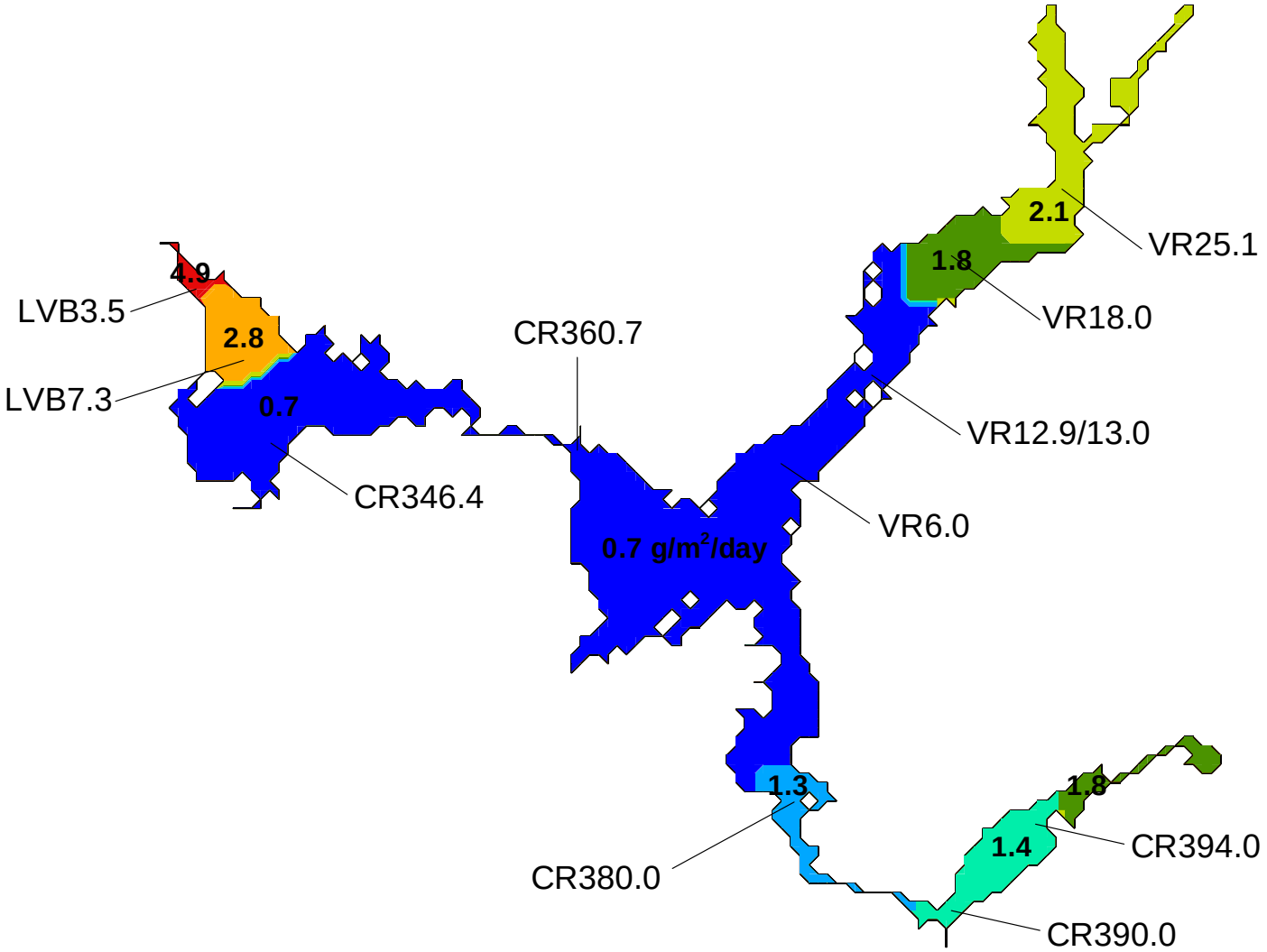

Figure 3.9

Comparison of Measured and Simulated Dissolved Oxygen at Station LVB3.5

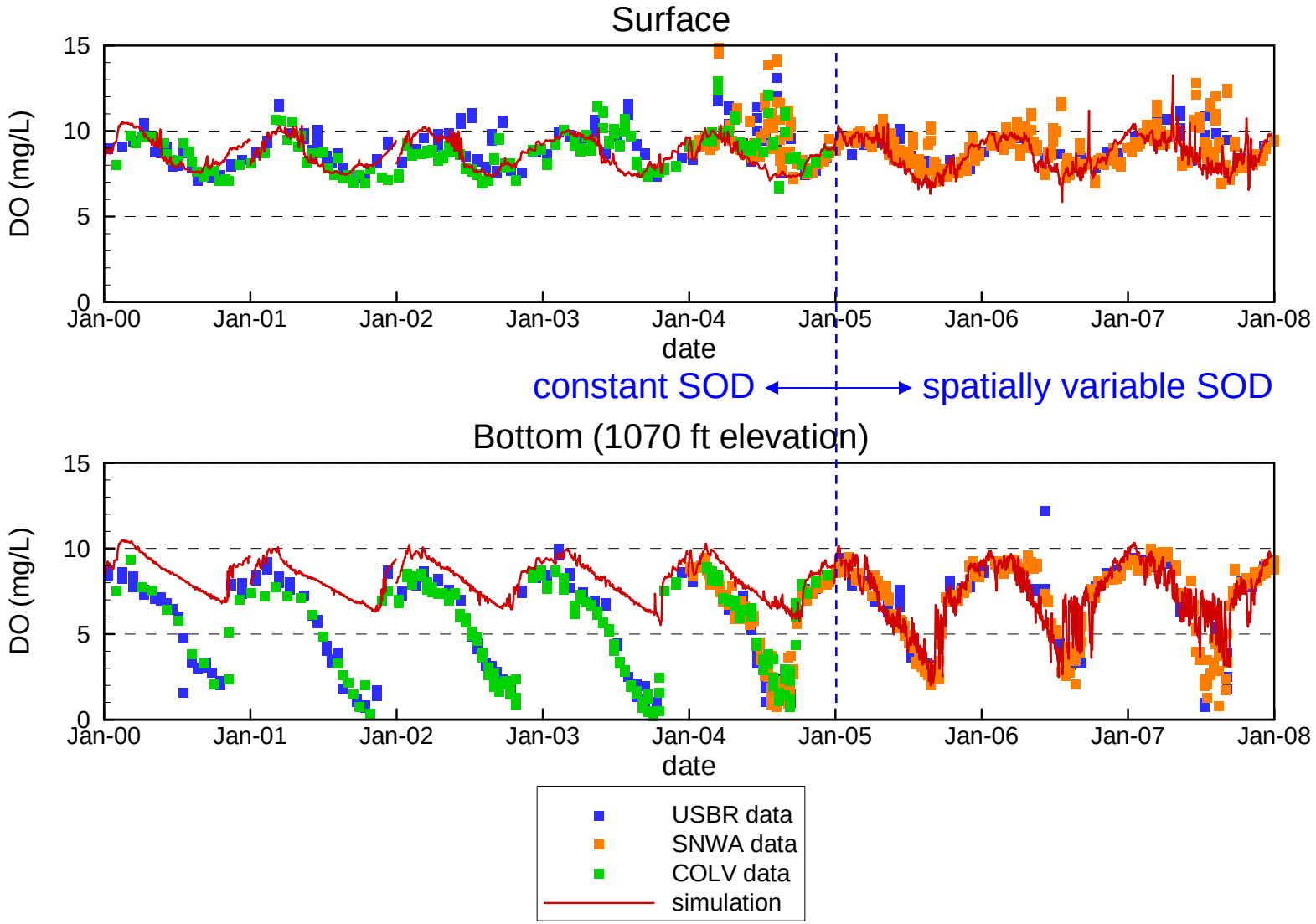

Figure 3.10

4 MODEL CALIBRATION RESULTS

This section presents comparisons of the model calibration simulations with measured field data over the 2000 through 2007 modeling period. It is noted that model calibration results for 2000 through 2005 were presented in a previous report (Flow Science, 2007). However, in the present modeling work, enhancements were made to the model, (Section 3.4) which improved some of the earlier results. Thus comparisons are presented for the entire 2000 through 2007 modeling period. Additional emphasis is placed on comparisons for model years 2006 and 2007, which remain the primary motivation of this work.

The focus of this section is primarily on how well the model is able to match the field data. Discussions of the presented figures are generally kept to a minimum, although elaborations are made in instances where there were discrepancies between the simulation results and field data. In addition, recommendations for future model enhancements are discussed where appropriate. Animations of the model results and additional discussions are presented in Section 5.

In the following sections, comparisons between calibration simulations and field data are presented one water-quality variable at a time, beginning with the ELCOM variables, followed by the CAEDYM variables. Generally, for each variable, time-series plots over the 2000 through 2007 modeling period are provided at the reservoir surface and reservoir bottom (or hypolimnion) at the following six station locations: CR394.0, VR25.1, VR12.9/13.0, CR360.7, LVB3.5 and CR346.4 (see **Figure 4.1**). These locations were selected from all the possible locations since they represent water quality at specific locations: (1) close to each of the inflows (CR394.0, VR25.1 and LVB3.5), (2) in the Overton Arm (VR12.9/13.0), (3) in Boulder Basin (CR346.4), and (4) in Virgin Basin and at the Narrows (CR360.7). Results are presented in order progressing from upstream locations to downstream locations.

Additionally, time-series plots at the SNWA Intakes #1 and #2 and the Hoover Dam outlets are provided where field data are available. The Hoover Dam field data are obtained from Stations CR342.0 and 09421500, which are located in the CR, directly downstream of the dam, as well as the tailrace of the dam. The field data thus represent a combination of water from both the lower (895 ft elevation) and upper (1,045 ft elevation) outlets. The simulation results presented are the average of the simulation results at the two outlet elevations (obtained from the water column directly adjacent to the dam).

For certain variables more descriptive figures are provided as necessary to better illustrate spatial variations (both vertical and horizontal) or other features. These figures are necessarily limited to the variables for which there were sufficiently dense field data available. More emphasis is also placed upon the 2006 and 2007 model years, since the calibration of these years is the primary focus of this work, and these years were not covered in the previous report (Flow Science, 2007).

4.1 ELCOM CALIBRATION

This section presents comparisons of the variables that were simulated by the hydrodynamic model, ELCOM. The ELCOM calibration process primarily involved removing seemingly erroneous out-of-range field data and making improvements to the model inputs (i.e., weather, inflow rates and water quality), as discussed in detail in Appendix A.

Results presented here are from simulations using the 300-m computational grid (see Section 3.2).

4.1.1 Water Surface Elevation

Figure 4.2 plots the simulated and measured WSEL for Lake Mead over the modeling period. The agreement is good, with the maximum discrepancy of approximately 2.5 ft being much lower than either the overall range in WSEL (approximately 100 ft) or the lake depth (approximately 500 ft at full pool). This is indicative that the inflow rates, rainfall data, evaporation model (and associated solar radiation and wind inputs), and neglect of any net loss or gain from groundwater, are reasonably accurate.

It should be noted that the maximum *rate* of discrepancy is approximately 3 ft per year (from 2003 through mid-2004, and again in late 2006 through early 2007). This corresponds to a net river flow rate error of about 400 cfs, which is only three percent of the average CR inflow rate.

4.1.2 Temperature

Figure 4.3 compares the simulated and measured temperature profiles in the reservoir at Station CR346.4 for years 2006 and 2007. For each year, profiles are plotted in winter (January), spring (April), summer (July), and fall (November). The simulation accurately captures the evolution from nearly uniform profiles in the winter through the thermocline development and strengthening in spring and summer, to the cooling and thickening of the epilimnion during the fall turn-over.

Importantly, **Figure 4.3** indicates that the 2005 through 2007 multi-year simulation correctly captures the subtleties related to incomplete destratification in the winter of 2005/2006, and the complete destratification in the winter of 2006/2007. That is, the simulation accurately predicts the depth and strength of the weak thermocline on 1/10/06, as well predicts the lack of such thermocline on 1/23/07. The incomplete versus

complete destratification can have important consequences on the DO concentrations in the deepest portions of Boulder Basin, as discussed in Sections 2.4.2.6 and 2.4.3. Thus, the ability of the model to accurately simulate DO concentrations, inherently depends upon the ability of the model to correctly predict incomplete or complete destratification. Results of the DO calibration are presented in Section 4.2.8.

Contours of measured and simulated temperature as a function of depth and time at Station CR346.4 are plotted in **Figure 4.4**. The simulation accurately captures the thermocline development and destratification each year. The precise location of the 12°C isotherm (shown as a white line) is not always captured by the model, particularly during 2000 through 2004. As discussed in the previous 2000 through 2005 modeling report (Flow Science, 2007) this reflects the inherently difficult nature of accurately capturing the subtle vertical mixing and weak temperature gradients that can occur within the hypolimnion. Nevertheless, and as discussed previously, the simulation is able to capture the important trends in 2005 through 2007: namely the incomplete destratification in the winter of 2005/2006, and the complete destratification in the winter of 2006/2007.

Figure 4.5 compares the simulated and measured temperature profiles at Station CR394.0 for years 2006 and 2007. The simulation is able to replicate the measured profiles throughout the year, including certain aspects of the "double thermoclines" that occur in the summer months (e.g., July) as a result of the CR inflow (see Section 2.4.1).

Figures 4.6 through **4.11** are time-series plots of the measured and simulated temperatures at Stations CR394.0, VR25.1, VR12.9/13.0, CR360.7, LVB3.5 and CR346.4, respectively. The simulation accurately captures the temperatures at the reservoir surface and bottom at all locations.

Figures 4.12 and **4.13** are time-series plots of the measured and simulated temperatures at the SNWA intakes, and the combined Hoover Dam outlets, respectively. The simulation accurately captures the temperature at these locations.

Figure 4.14 plots the depth of selected isotherms at the Sentinel Island USGS platform as a function of time during 2005 through 2007. The measured and simulated isotherm depths are respectively determined from the 6-hourly profiles measured by the USGS, and the simulation daily-output. The upper frame of **Figure 4.14** plots the 18, 23 and 28°C isotherms, while the lower frame plots the 13 and 18°C isotherms. Note that the upper and lower frames have different vertical scales.

While there are some differences between the simulated and measured isotherm depths, particularly in the summer for the 23 and 28°C isotherms, the general agreement illustrated in **Figure 4.14** illustrates the ability of the model to correctly capture the overall seasonal trends in the isotherm depths. In particular, the model accurately captures the timing of the fall destratifications, as evidenced by the agreement of the times when each isotherm hits the surface (zero depth) in the fall of each year.

The 6-hourly temperature measurements from the USGS platforms also enable the simulation to be evaluated on a sub-daily basis. **Figure 4.15** plots the measured and simulated depths of the 18 and 21°C isotherms at the Sentinel Island platform over 20 days in July 2006 (upper frame) and July 2007 (lower frame). For this figure, the simulation was output on a 3-hourly basis, in order to resolve the sub-daily changes. The month of July was chosen due to the frequent prevalence of wind-driven seiching in that month (see Flow Science, 2007), as well as due to the completeness of the measured field data.

Figure 4.15 indicates that the sub-daily trends in the thermocline depths are reasonably well predicted by the simulation. Both the amplitude and the phase of the oscillations are captured by the simulation. Additionally, there are several instances where both the field data and simulation indicate sudden and temporary increases in the amplitude of oscillation (e.g., 7/26/06, 7/29/06, and 7/29/07), indicating the ability of the model to capture responses to specific high-wind events.

4.1.3 Conductivity

Snapshots of measured and simulated conductivity along a vertical profile stretching from Hoover Dam to the CR are shown in **Figures 4.16** (2006) and **4.17** (2007). Generally the simulation correctly replicates the low-conductivity CR underflows, interflows and near-surface flows. There are some subtle differences between the measured and simulated conductivity in the winters of 2006 and 2007, which are related to the simulation of the CR underflow. In February of each year, the measured field data indicate that the CR underflow is mixed upwards over a greater depth than the simulation indicates, particularly at and upstream of Station CR380.0. Less vertical mixing of the inflow in the simulation may also lead to the CR underflow travelling further into the lake, as illustrated in February 2006 (**Figure 4.16**).

The under-estimation of vertical mixing in the simulation is thought to be due to the horizontal grid size. The ELCOM simulation uses a 300-m horizontal grid (Section 3.2), whereas the actual widths of the channels near the CR inflow are substantially smaller. Thus, the simulated inflow velocities are under predicted, which in turn may lead to the vertical mixing being under predicted. In the future simulations may be improved through either a sub-grid model to increase vertical mixing in the regions of narrow channels, or directly through the use of finer computational grids as computer capabilities increase.

Figures 4.16 and **4.17** indicate that the simulation correctly replicates the region of high-conductivity that develops in the epilimnion of Boulder Basin (between Hoover Dam and Station CR355.75) each spring and summer. In both simulation years, the simulation slightly overestimates the conductivity values in the epilimnion of Boulder Basin during the summer and fall. This is discussed later in this section.

Snapshots of measured and simulated conductivity along a vertical profile stretching from Hoover Dam to the VR are shown in **Figures 4.18** (2006) and **4.19** (2007). The simulation correctly replicates the high-conductivity VR underflows, interflows and near-surface flows. In addition, the simulation captures the low conductivity water from the CR that often extends several miles upstream into Overton Arm, below the epilimnion, in the summer and fall.

Snapshots of measured and simulated conductivity along a vertical profile stretching from the LVW to Hoover Dam are shown in **Figures 4.20** (2006) and **4.21** (2007). The simulation correctly replicates the high-conductivity LVW underflows, interflows and near-surface flows. The general distributions of conductivity that result in Boulder Basin are also correctly captured by the simulation.

Figure 4.22 compares the simulated and measured conductivity profiles at Station CR346.4 for 2006 and 2007. For each of the years profiles are plotted in winter (January), spring (April), summer (July) and fall (November). The simulation correctly captures the trends in the vertical variations of the conductivity. In particular, the non-uniform conductivity profile in the winter of 2005/2006 resulting from incomplete destratification (see Section 4.1.2) is captured by the model on 1/10/06. The simulation overestimates the conductivity values in the epilimnion of Boulder Basin during the summer of 2006 and the fall of both years. This is discussed shortly.

Figures 4.23 through **4.28** are time-series plots of the measured and simulated conductivities at Stations CR394.0, VR25.1, VR12.9/13.0, CR360.7, LVB3.5 and CR346.4, respectively. It is noted that conductivity measurements are generally considered to be accurate to within approximately 20 to 40 µS/cm. This range is illustrated by the differences between the field data measured by the three different agencies (i.e., USBR, COLV and SNWA) at Station LVB3.5 (**Figure 4.27**) and Station CR346.4 (**Figure 4.28**). It is also noted that since 2002 the differences between the measurements of the three agencies have decreased as a result of the interagency sampling program.

The simulation, in general, accurately captures the conductivities at the reservoir surface and bottom at most locations as illustrated in **Figures 4.23** through **4.28**.

At times in 2005 through 2007 the peak conductivities at the bottom of Station VR25.1 are not fully captured by the simulation (**Figure 4.24**). As discussed in the previous modeling report (Flow Science, 2007), this is a result of the vertical and horizontal grid size being large relative to the dimensions of the VR inflow, which causes an initial over-dilution of the inflow. Regardless of the initial over-dilution by the simulation, the overall "mass" of conductivity entering the lake is correctly simulated. This is indicated by the good agreement between the simulation and field data at the bottom of Station VR12.9/13.0 (**Figure 4.25**), which is further downstream. At this location, the underflow has entrained more ambient lake water and is thus large enough to be adequately resolved by the simulation. In the future, as computers become faster,

finer vertical grids may be used. This is expected to improve the agreement of the simulation to field data near the VR inflow.

In much of 2005 and early 2006 the conductivity at the bottom of Station CR360.7 is underestimated by the simulation (**Figure 4.26**). However, this phenomenon may be caused by relatively subtle differences between the simulated and actual CR inflow. For example, the measured conductivity shown in **Figure 4.16** indicates that on February 13, 2006 the low-conductivity CR inflow extended along the reservoir bottom beyond Station VR2.0 (CR distance of 370 miles in the figure), but did not reach Station CR360.7. On the same date the simulated conductivity shown in **Figure 4.16** indicates that the simulation predicted the CR inflow to reach Station CR360.7, but only just. This relatively small difference in the prediction of the extent of the CR inflow (illustrated in **Figure 4.16**) causes a more noticeable difference in the time-series plot at Station CR360.7, where the simulated conductivity at the bottom is lower than measurements (**Figure 4.26**). The subtle differences between the simulated and actual CR inflow, as well as possible means to improve the simulation, were discussed earlier in this section.

The simulation tends to over-predict the conductivity in the epilimnion of Boulder Basin during the summer and fall, as indicated at Station CR346.4 (**Figure 4.28**). Reasons for these differences were discussed in the previous modeling report (Flow Science, 2007). Importantly, it is noted that the discrepancies do *not* accumulate over multiple years when the simulation is run continuously from 2005 through 2007. While the discrepancies are noticeably larger in 2006 than in 2005, they have substantially diminished by 2007.

Figures 4.29 and **4.30** are time-series plots of the measured and simulated conductivities at the SNWA intakes, and the Hoover Dam outlets, respectively. The simulation accurately captures the conductivity at these locations.

4.1.4 Perchlorate

Figures 4.31 through **4.35** are time-series plots of the measured and simulated perchlorate concentrations at Stations LVB3.5, CR346.4, and CR343.2, the SNWA intakes, and the Hoover Dam outlets, respectively. The simulation accurately captures the perchlorate concentrations at most locations.

Note that there are no routine measurements of perchlorate in the upper basins, since there are no known significant sources of perchlorate other than from the LVW. In 2003 some limited measurements of perchlorate concentrations were made in the upper basins. These measurements are discussed in an earlier report (Flow Science, 2005) and generally indicated perchlorate concentrations of less than 1 µg/L in the upper basins (an order of magnitude lower than concentrations in Boulder Basin at that time). However, on occasion just upstream of the Narrows concentrations sometimes reached as high as

3 µg/L. This was a result of transport in the upstream direction due to reverse flow through the Narrows. Since 2003 the perchlorate load in the LVW has reduced by a factor of about two to three, and as such the present concentrations in the upper basins are expected to be two to three times lower than in 2003. The upstream transport of perchlorate is illustrated by the animation discussed in Section 5.3, and further details of the reverse flow in the Narrows were discussed in the previous report (Flow Science, 2007).

4.1.5 Bromide

Figures 4.36 through **4.43** are time-series plots of the measured and simulated bromide concentrations at Stations CR394.0, VR25.1, VR13.0, CR360.7, LVB3.5 and CR346.4, the SNWA intakes, and the Hoover Dam outlets, respectively. Note that routine measurements of bromide in the upper basins commenced in 2005.

The simulation accurately captures the bromide concentrations at most locations. Note that many of the plots indicate bromide measurements at and below about 0.025 mg/L. It is believed that these data points are erroneous.

4.2 CAEDYM CALIBRATION

This section presents comparisons of the variables that were simulated by the coupled hydrodynamic-biogeochemical model, ELCOM/CAEDYM. The CAEDYM water quality module requires the specification of many different parameters that control aspects of the simulation including: algae growth and respiration rates, nutrient uptake and release, and decomposition and mineralization rates. The calibration of CAEDYM is thus an iterative process, with changes to specific parameters made until satisfactory agreement with field data is obtained.

The CAEDYM parameter values were held constant over the entire 2000 through 2007 modeling period, even though it is possible that different algae types may occur from year-to-year.

During the course of the original 2000 through 2005 calibration (Flow Science, 2007), Dr. David Hamilton (professor at The University of Waikato, New Zealand, and author of CAEDYM), was consulted to ensure that the resulting calibration parameters were within ranges appropriate for Lake Mead. During the current re-calibration (Section 3.4.6), the parameter variations were again checked to ensure they were within appropriate ranges.

Results presented here are from simulations using the 600-m computational grid, since the computer memory requirements of the CAEDYM water quality module resulted in the simulations on the 300-m grid being impractical (see Section 3.2).

4.2.1 Chlorophyll a

Figures 4.44 through **4.49** are time-series plots of the measured and simulated chlorophyll *a* concentrations at Stations CR394.0, VR25.1, VR12.9/13.0, CR360.7, LVB2.7, LVB3.5 and CR346.4. Note that the plotted concentration is the average over the top 5 m of the water column at each location.

The measured chlorophyll *a* concentrations in the lake are typically low in the winter, increase in the spring, decrease in mid-summer, and sometimes increase again in the fall. The simulation is able to capture these general trends, although the predicted magnitudes and timings of the spring and fall peaks often do not match the data.

The simulation shows generally good agreement with the measured field data at Station CR394.0 in 2005 through 2007 (**Figure 4.44**). The chlorophyll *a* concentrations are likely overestimated in early 2006 at Station VR25.1 (**Figure 4.45**)., This may be due to not accounting for dilution of the phosphorus concentrations during storm flows, resulting in more phosphorus entering the lake from the VR and MR.

The chlorophyll *a* concentration peaks are generally well captured by the simulation at Stations VR12.9/13.0 and CR360.7 (**Figures 4.46** and **4.47**, respectively). The magnitudes of the peaks may appear higher than the field data measurements, but these peaks are of short enough duration that they may not be fully captured by the monthly samples. The field data also indicate chlorophyll *a* concentrations of approximately 1 µg/L in the winters at these (and other) locations. The simulation predicts lower numbers, but it is noted that method detection limits for the chlorophyll *a* measurements are of the same order of magnitude as the field data, and therefore the field data in the winters may not be representative of the true (but low) values in the lake.

The large algae bloom in 2001 is not captured by the simulation at Stations LVB3.5 and CR346.4 (**Figures 4.48** and **4.49**, respectively). As discussed in the previous modeling report (Flow Science, 2007), this may be attributed to the unusual algae species dominant during that year.

The simulation is able to replicate some important longer-term temporal trends within Boulder Basin. As discussed in Section 2.4.2.3, the measured chlorophyll *a* concentrations in 2005 in the inner LVB (represented by Station LVB3.5) were lower than other years, probably as a result of increased phosphorus removal by the WWTPs in 2005 (see Section 2.3.6). The measured chlorophyll *a* concentrations increased in 2006 and further increased in 2007. **Figure 4.48** indicates that the simulation correctly

captures these trends at Station LVB3.5, indicating the ability of the model to correctly respond to changes in phosphorus loads in the LVW.

Additionally, and as discussed in Section 2.4.2.3, the temporal trends in chlorophyll *a* concentrations in the open water of Boulder Basin (represented by Station CR346.4) did not follow those of the inner LVB, with the concentrations in 2005 being comparable to those in other years (excluding 2001). **Figure 4.49** indicates that the simulation bears out these trends at Station CR346.4.

The time-series plots of measured and simulated chlorophyll *a* concentrations presented in **Figures 4.44** through **4.49** are useful to illustrate how the simulation does and does not capture certain temporal trends at each of the locations. However, a more comprehensive comparison between the measurements and simulation is made in **Figure 4.50**, which plots the simulated chlorophyll *a* concentration (vertical axis) directly against the measured field data (horizontal axis). Each point on this plot is obtained by sampling the simulation at 12 noon on the same day that each field measurement was made. This plot includes data from three agencies (as indicated by the different colored symbols) and at all locations in the lake. Comparisons were only made for measurements taken during the growing season (April through September), and only for the top 5-m average samples.

The data points in **Figure 4.50** indicate a cluster that trends around the theoretical perfect model 45-degree line, indicating the general veracity of the model. Nevertheless, there is substantial scatter, which may be quantified by computing the root-mean-square-error (RMSE) between the simulation and field data. This was done using methods developed for the growing season average in the previous modeling (Flow Science, 2007). The RMSE is shown graphically on **Figure 4.50** as the "estimated simulation standard error". Note that the upper and lower error bars are the same length when plotted on the vertical log-scale, which is indicative of the assumed log-normal distribution for the chlorophyll *a* concentrations (Flow Science, 2005 and Flow Science, 2007). The extent of the error bars is comparable to the "width" of the cluster of data points in **Figure 4.50**.

Chlorophyll *a* concentrations at a specific fixed location within Lake Mead are often subject to rapid temporal changes due to advection of algae by wind. This is illustrated in by animation of the simulation results in Section 5.5, and has also been discussed in previous work (Flow Science, 2005). These rapid temporal changes imply that the exact time of sampling may have significant impact on the chlorophyll *a* concentration, for both the field measurements and simulation. Thus, rapid temporal changes may contribute to a substantial amount of the scatter (or apparent model error) illustrated in **Figure 4.50**. In order to determine the impact of the exact sampling time on the model error, the simulation results were re-sampled. For each field data measurement, the simulation was sampled daily at 12 noon from two days prior to the sampling date through two days after the sampling date (for a total of five days). The simulated chlorophyll *a* concentration over these five days that was closest in value to the field data

concentration was then used for model comparison. **Figure 4.51** plots the resulting comparison. The scatter is reduced compared to **Figure 4.50**, and many of the data points fall close to the 45-degree line. Additionally, the estimated simulation standard error is reduced.

4.2.2 Chlorophyll *a* Growing Season Average

The chlorophyll *a* growing season average (i.e., the time average concentration for the top 5 m, between April 1 and September 30), has been identified as a critical parameter in terms of satisfying the Lake Mead WQS for chlorophyll *a* (Flow Science, 2005). Thus, it is important for the simulation to be able to accurately predict this quantity, throughout the lake.

Figures 4.52 through **4.59** present comparisons between the top 5 m chlorophyll *a* growing season averages computed from the measured field data and the simulation, for years 2000 through 2007, respectively. Each figure consists of three sub-figures, corresponding to concentrations along profiles from the LVW to the Hoover Dam (upper sub-figure), from the Hoover Dam to the CR (center), and from the Virgin Basin to the VR (lower). The distances on the horizontal axes of each sub-figure correspond to the appropriate station names (i.e., LVB, CR and VR, respectively). Note that the stations located at LVB distances of 10.8 and 14.7 miles in the upper sub-plot are actually Stations CR346.4 and CR342.25/342.5, respectively, and are also shown on the center sub-plot.

The "error bars" indicated for the measured field data correspond to one standard-deviation of the measurements in the growing season, and are qualitatively indicative of the statistical errors that may be expected as a result of a limited number of samples, and variability in the sampling and measurement techniques (Flow Science, 2007). Note that the upper and lower error bars are the same length when plotted on the vertical log-scale, which is indicative of the assumed log-normal distribution for the chlorophyll *a* concentrations.

In 2000 (**Figure 4.52**) the simulation correctly captures the trend of chlorophyll *a* growing season average concentrations in Boulder Basin, with higher values near the LVW, and lower values in the open water. The overall simulated chlorophyll *a* concentrations are somewhat higher than indicated by the data in parts of the LVB, but are generally within the error bars. There were no measured chlorophyll *a* data in the upper basins in 2000.

In 2001 (**Figure 4.53**) the simulated chlorophyll *a* growing season average concentrations are too low in Boulder Basin (upper sub-figure) and too low in the upper part of the Overton Arm (Stations VR25.1 and VR26.8 in lower sub-figure). The simulated chlorophyll *a* concentrations in the upper part of the CR thalweg (Stations

CR380.0 and CR394.0) are reasonably accurate. Although the simulated concentrations are too low in many locations, they generally lie within the error bars of the measured field data, and also replicate the general spatial trends of concentrations throughout the lake. It is reiterated that 2001 was an atypical year, with an unusually large algae bloom.

The simulation accurately captures the chlorophyll *a* growing season average concentrations throughout the lake in years 2002 through 2007 (**Figures 4.54** through **4.59**). Often the simulated chlorophyll *a* concentrations are slightly low near each of the inflows (i.e., LVW, CR and VR/MR). This may be a result of the inflows initially being artificially over-diluted due to the 600-m grid being larger than the actual width of the channels near the inflows.

A more direct comparison between measured and simulated growing season averages is made in **Figure 4.60**, which plots the chlorophyll *a* growing season average concentrations from the simulation (vertical axis) directly against the growing season average computed from the measured field data (horizontal axis). The plot includes data from all sampling locations in Lake Mead, measured by the USBR, SNWA and COLV (denoted in the figure by symbol shape), and all eight years in the 2000 through 2007 modeling period (denoted in the figure by symbol color).

The data points in **Figure 4.60** indicate a cluster that trends around the theoretical perfect model 45-degree line, indicating the overall veracity of the model. Nevertheless, there is some scatter, which may be quantified by computing the RMSE between the simulation and field data. This was done using methods developed in the previous modeling (Flow Science, 2007). The RMSE is shown graphically on **Figure 4.60** as the *vertical* error bars. The *horizontal* error bars are determined from analysis of the field data from the three different agencies (i.e., USBR, SNWA and COLV). Specifically, the field data from each agency were used to compute the growing season averages for each year and at each location in the lake. At the locations where measurements were made by more than one agency, differences between the computed growing season averages were calculated. These differences were then combined into an overall RMSE, which is shown graphically on **Figure 4.60**, as the horizontal error bars. These horizontal error bars thus reflect the inherent differences and uncertainties that arise in the sampling programs, including the impact of limited sample size, sampling on different dates, and differences in laboratory and analysis techniques.

The amount of scatter indicated in **Figure 4.60** is less than that indicated for the direct point-to-point comparisons made in **Figures 4.50** and **4.51**. Similarly, the size of the model error bars is reduced when comparisons of the growing season averages are made (**Figure 4.60**) rather than direct point-to-point comparisons (**Figures 4.50** and **4.51**). That is, the simulation is able to more accurately replicate the chlorophyll *a* growing season average concentration than the chlorophyll *a* concentration at a specific date. This is a result of the averaging process smoothing out the sampling variations in both the measured field data and the simulation results.

In **Figure 4.60** the vertical error bars are larger than the horizontal error bars, but are of comparable magnitude. In other words, the estimated model error is larger than, but of comparable magnitude, to the estimated uncertainty in the sampling programs.

4.2.3 Phosphorus

Figures 4.61 through **4.68** are time-series plots of the measured and simulated FRP concentrations at Stations CR394.0, VR25.1, VR12.9/13.0, CR360.7, LVB3.5, CR346.4, the SNWA Intakes #1 and #2, and the Hoover Dam outlets, respectively.

The simulation indicates reasonable agreement with the measured field data in the upper basins (**Figures 4.61** through **4.64**). The FRP concentrations at the bottom of Stations VR12.9/VR13.0 and CR360.7 (**Figures 4.63** and **4.64**) are perhaps overestimated in 2006. However, the confidence in the measured field data at that time is not high. During parts of 2005 and 2006 samples were analyzed by multiple laboratories, which often yielded quite different results. This often resulted in the appearance of two (or even three) separate trends in the field data (e.g., the measured field data at the bottom of Station VR12.9/VR13.0 in **Figure 4.63** and the bottom of Station CR360.7 in **Figure 4.64**). From 2007 onwards the field samples collected by the USBR were analyzed by the High Sierra Laboratory using a method detection limit of 0.001 mg P/L. This results in a more representative data-set, with which the simulation has reasonable agreement.

At Station LVB3.5 (**Figure 4.65**) there is significant variability between the measurements of the three agencies (i.e., SNWA, COLV and USBR), particularly between the USBR and SNWA at the bottom of Station LVB3.5 in 2005 through 2007. Note that the COLV ceased the sampling at Station LVB3.5 in 2005, when they switched to using movable station locations. Prior to 2005, the COLV data-set appears to be the most representative, since the USBR data are often below detection limit (e.g., at the surface in 2000 through 2003), and the SNWA data only start in 2004. Since 2005, the USBR data-set appears to be the most representative, since there is large variation among the SNWA data at the bottom of Station LVB3.5. The simulation has reasonable agreement with these data-sets (i.e., the COLV data prior to 2005 and the USBR data from 2005 onwards).

At Station CR346.4 (**Figure 4.66**) there is some variability of the FRP measurements between the three agencies (i.e., SNWA, COLV and USBR). This was discussed in Section 2.4.2.4, where some seasonal trends among the USBR and COLV data were identified. Specifically, from about 2004 onwards these data indicate that the FRP concentrations are low in the summer (due to uptake of FRP by algae), and higher in most winters (with 2006 being an exception). The SNWA data-set is consistently higher than the other two data-sets, and does not exhibit the seasonal trends.

The simulation illustrates the seasonal trends at the surface of Stations CR346.4 reasonably well, and is in reasonable agreement with the USBR and COLV data-sets in the later years (**Figure 4.66**). The simulated FRP concentrations in the winters may be overestimated as a result of the underestimation of algae growth in the winters (see Section 4.2.1).

In the hypolimnion of Station CR346.4 the simulation exhibits reasonable agreement with the SNWA data-set from approximately 2005 onwards (**Figure 4.66**). However, the limited USBR and COLV data at this location are lower than the simulation and the SNWA data.

At the SNWA Intakes (**Figure 4.67**) the simulation has good agreement with the measured field data. However, it is noted that the only field data available at this location are the SNWA data, and these data have not always been in agreement with the USBR and COLV data sets at other locations (i.e., Stations LVB3.5 and CR346.4).

At the Hoover Dam outlets (or immediately downstream of Hoover Dam) there are two sets of FRP measurements (**Figure 4.68**). The simulation is in good agreement with the USGS data-set, but generally higher than the SNWA data-set. It is noted that in 2007 the SNWA samples were analyzed by the High Sierra Laboratory using a method detection limit of 0.001 mg P/L, and thus these data are likely more reliable. If this is the case, then the simulation appears to overestimate the FRP concentration through the Hoover Dam outlets. However, the simulated FRP concentrations through the Hoover Dam outlets are sensitive to the exact location of the thermocline, which is close to the upper outlet (elevation 1,045 ft) for much of 2007. If the simulated thermocline depth is slightly too high, then the water drawn through the upper outlet will be from the hypolimnion, which has higher FRP concentrations than the epilimnion (see **Figure 4.66**). Indeed, extracting FRP concentrations from the simulation one or two cells above the upper outlet elevation results in lower concentrations.

Figures 4.69 through **4.76** are time-series plots of the measured and simulated TP concentrations at Stations CR394.0, VR25.1, VR12.9/13.0, CR360.7, LVB3.5, CR346.4, the SNWA Intakes #1 and #2, and the Hoover Dam outlets, respectively. It should be noted that prior to 2007 much of the measured field data were near or below detection limits (an exception to this is the LVB), and that at low concentrations the TP measurements may be strongly influenced by the presence of particulate phosphorus. These factors can make it difficult to identify trends among the data, especially in open water where TP concentrations are low.

The simulation indicates good agreement with the measured field data at the surface of Station CR394.0 (**Figure 4.69**). At the bottom, the measured field data at Station CR394.0 indicate a wide range of TP concentrations (**Figure 4.69**). The high TP concentrations at this location are likely due to particulate phosphorus that is transported in from the CR. The CAEDYM simulation only accounts for small phosphorus particles,

and as such these larger particles from the CR inflow are considered to settle very quickly in the model (see Section A.2.2).

At Station VR25.1 (**Figure 4.70**) the simulation correctly captures some of the higher TP concentrations that occur during the winter inflows, as well as the lower concentrations in the summer that result from lower inflows and uptake of phosphorus by algae. Not all the features illustrated in the field data are captured, which may be a result of over-mixing and over-dilution in the simulation near to the VR inflow (see Section 4.1.3).

At Station VR12.9/13.0 and CR360.7 (**Figures 4.71** and **4.72**) the simulation at the surface indicates good agreement with the field data. The simulation underpredicts the TP concentration in the hypolimnion in parts of 2006 and much of 2007 at Station VR12.9/13.0 (**Figure 4.71**). However, this does not impact the simulation further downstream at Station CR360.7, where there is good agreement in the hypolimnion (**Figure 4.72**).

The higher TP concentrations from the LVW are reflected by both the measured field data and the simulation at Station LVB3.5 (**Figure 4.73**). The variability in TP measurements by the different agencies at the bottom is likely a result of particulate phosphorus, the presence of which can significantly raise sample concentrations. In particular there are differences between the USBR and SNWA data-sets at the bottom in 2005. At the surface there are generally higher TP concentrations in the spring and summer, and the simulation captures this trend.

At Station CR346.4 (**Figure 4.74**) the variability of the TP measurements between the three agencies (SNWA, COLV and USBR) is apparent. This is due to the low concentrations in the open water being near or below detection limits, and the influence of particulate phosphorus. Between 2000 and 2002, additional special phosphorus sampling was conducted using inductively coupled plasma mass spectrometry (ICP-MS) analysis techniques, which have lower detection limits. The simulation indicates reasonable agreement with these more accurate measurements.

From early 2007 the USBR field samples have been analyzed by the High Sierra Laboratory using methods with a detection limit of 0.001 mg P/L. This detection limit is much lower than the detection limits that were previously used for the routine sampling, which were often around 0.01 mg P/L. The simulation is in reasonable agreement with the lower-detection-limit data set at the surface at Station CR346.4 (**Figure 4.74**), although it is slightly higher during the first half of 2007. This may be related to settling of particulate phosphorus which has not been directly quantified by field measurements. Future simulations would be able to benefit if the particle size distributions of the inflows (particularly the CR and LVW) are measured.

Agreement in the hypolimnion at Station CR346.4 is more difficult to ascertain, due to the lack of low-detection limit measurements at this depth (**Figure 4.74**). SNWA

measurements were made at this depth, but lower detection limits were not used for the SNWA field data until late October 2007. Prior to this, the detection limit was mostly at 0.01 mg P/L, which resulted in the data being plotted as 0.005 mg P/L (half of the detection limit) on **Figure 4.74**. In reality, the actual TP concentration for these points could be anywhere between 0 and 0.01 mg P/L. Indeed, the SNWA data from late October 2007 onwards (which were determined using methods with low detection limits) indicate TP concentrations that are higher than 0.005 mg P/L, and the simulation results are in reasonable agreement with these limited data. Prior to October 2007, it can be argued that the simulation results are also "in agreement" with the SNWA field data on the basis that the simulated TP concentrations are less than the detection limit of 0.01 mg P/L (**Figure 4.74**). In the future, calibration of simulated TP for 2008 and beyond will result in an improved model due to the availability of more low-detection limit phosphorus data.

The TP measurements at the SNWA intake also had a detection limit of 0.01 mg P/L through October 2007, and were thus plotted as 0.005 mg P/L (**Figure 4.75**). From late October 2007 onwards lower detection limits were used, and the simulation results are in reasonable agreement with these data.

The TP measurements at the Hoover Dam outlets (or immediately downstream of Hoover Dam) were also impacted by method detection limits (**Figure 4.76**). Much of the USGS data were below detection limits, in which case they were plotted at half the detection limit value. Thus much of the USGS data in **Figure 4.76** could be up to twice as large as plotted. In addition, much of the temporal variation in the plotted USGS data was due to changes in the detection limits, rather than truly measured values.

Through 2005 the SNWA measurements of TP at Station CR342.0 (located in the CR below the Hoover Dam) used method detection limits of 0.01 mg P/L. Thus, the data plotted in **Figure 4.76** as 0.005 mg P/L (half the detection limit), could actually be as high as 0.01 mg P/L. The simulated TP is below 0.01 mg P/L, and is therefore "in agreement" with these data.

For most of 2006, the TP samples collected by the SNWA from CR342.0 were analyzed by Weck Laboratories. The reporting limit of the analysis was 0.002 mg P/L. However, even with this low reporting limit, there remains much scatter in the field data in 2006 (**Figure 4.76**). The lack of a discernable trend in these data raises questions about the quality of the field data at this location in 2006.

From early 2007, the TP samples collected by the SNWA at CR342.0 were analyzed by the High Sierra Laboratories, using methods with detection limits of 0.001 mg P/L. There is still some scatter among the data, which may be attributable to the presence or absence of particulate phosphorus. Nevertheless, the simulation shows reasonable agreement with the SNWA field data in 2007 (**Figure 4.76**).

It should be reiterated that there has been much recent improvement in the phosphorus sampling programs in and around Lake Mead. From early 2007 the samples collected throughout the lake by the USBR as well as some of the samples collected in the inflows and outflows by the SNWA have been analyzed using low detection limits. From late October 2007 the samples collected within Boulder Basin by the SNWA have also been analyzed using low detection limits. In the future, as the simulation is extended to include 2008 and beyond, the understanding of phosphorus within the lake as well as the veracity of the simulation will greatly benefit from these improved data.

4.2.4 Nitrate

Figures 4.77 through **4.84** are time-series plots of the measured and simulated NO3 concentrations at Stations CR394.0, VR25.1, VR12.9/13.0, CR360.7, LVB3.5, CR346.4, the SNWA intakes, and the Hoover Dam outlets, respectively.

The simulation has reasonable agreement with the field data at the locations in the upper basins, although the depletion of NO3 at the surface in the summers is often underestimated (**Figures 4.77** through **4.80**). However, it should be noted that the NO3 simulation in the upper basins has been greatly improved since the original 2000 through 2005 modeling (Flow Science, 2007). This is primarily a result of the implementation of non-uniform initial conditions as described in Section 3.4.4.

The simulation has better agreement with the field data at the locations within Boulder Basin (**Figures 4.81** through **4.84**).

4.2.5 Ammonium

Figures 4.85 through **4.92** are time-series plots of the measured and simulated ammonium (NH4) concentrations at Stations CR394.0, VR25.1, VR12.9/13.0, CR360.7, LVB3.5, CR346.4, the SNWA intakes, and the Hoover Dam outlets, respectively. At most locations the measured field data is near or below detection limits, and as such agreement of the model is difficult to ascertain.

4.2.6 Total Organic Carbon

Figures 4.93 through **4.100** are time-series plots of the measured and simulated TOC concentrations at Stations CR394.0, VR25.1, VR12.9/13.0, CR360.7, LVB3.5, CR346.4, the SNWA intakes, and the Hoover Dam outlets, respectively. It is noted that measured TOC data in the upper basins were only available from 2005 onwards (**Figures 4.93** through **4.96**).

The simulation correctly matches the field data at most locations in most years, with a few notable exceptions. The higher TOC concentrations measured at the surface of Station CR346.4 in 2001 (**Figure 4.98**) is not captured by the simulation, which is a direct result of the simulation under-predicting the unusual algae bloom (i.e., chlorophyll *a* concentrations) in that year (Section 4.2.1). Additionally the rise in measured TOC concentrations in mid-2003 at Station CR346.4 (**Figure 4.98**), the SNWA Intakes (**Figure 4.99**), and the Hoover Dam outlets (**Figure 4.100**) are not captured by the simulation. The absence of TOC data in the upper basins in the earlier years makes it difficult to determine the cause for this.

At Station LVB3.5 (**Figure 4.97**) the simulation well captures the temporal trends, but the simulated TOC concentrations are consistently higher than the measured data. This discrepancy appears to be limited to within the LVB, since the agreement between simulated and measured TOC concentrations at Station CR346.4 (**Figure 4.98**) is good, particularly in 2006 and 2007.

4.2.7 pH

Figure 4.101 compares the simulated and measured pH profiles at Station CR346.4 for 2006 and 2007. Profiles are plotted in winter (January), spring (April), summer (July) and fall (November). The simulation accurately captures the trends in the vertical variations of the pH throughout the seasons in 2006 and 2007.

Figures 4.102 through **4.109** are time-series plots of the measured and simulated pH at Stations CR394.0, VR25.1, VR12.9/13.0, CR360.7, LVB3.5, CR346.4, the SNWA intakes, and the Hoover Dam outlets, respectively. The simulation accurately models the pH at most locations.

4.2.8 Dissolved Oxygen

Snapshots of measured and simulated DO concentrations along vertical profiles in Lake Mead are shown in **Figures 4.110** through **4.115**. These snapshots are at the same locations and dates as those shown for conductivity in **Figures 4.16** through **4.21**.

The simulation captures most of the general trends of DO concentrations, with higher concentrations near the surface and generally lower concentrations in the deeper portions of the lake, and near to the inflows, throughout most of 2006 and 2007. In February 2007 the simulation predicts a region of low DO around CR360.7 at approximately 100 ft depth that is not evident in the field data (**Figure 4.111**). This discrepancy is thought to be a result of the simulation under-estimating the vertical mixing in the regions of narrow channels, as discussed in Section 4.1.3.

The simulation is much improved over the original 2000 through 2005 simulation (Flow Science, 2007), due to the implementation of spatially variable sediment oxygen demand (see Section 3.4.5). Importantly, the simulation is able to replicate the two mechanisms for DO replenishment of Boulder Basin that were discussed in Section 2.4.3. This is best illustrated by an animation, and further discussion of this is delayed until Section 5.9.

Figure 4.116 compares the simulated and measured DO profiles at Station CR346.4 for 2006 and 2007. For each of the years profiles are plotted in winter (January), spring (April), summer (July) and fall (November). The simulation correctly captures the trends in the vertical variations of the DO concentrations.

Figures 4.117 through **4.124** are time-series plots of the measured and simulated DO concentrations at Stations CR394.0, VR25.1, VR12.9/13.0, CR360.7, LVB3.5, CR346.4, the SNWA intakes, and the Hoover Dam outlets, respectively. The simulation accurately models the DO concentrations at all locations.

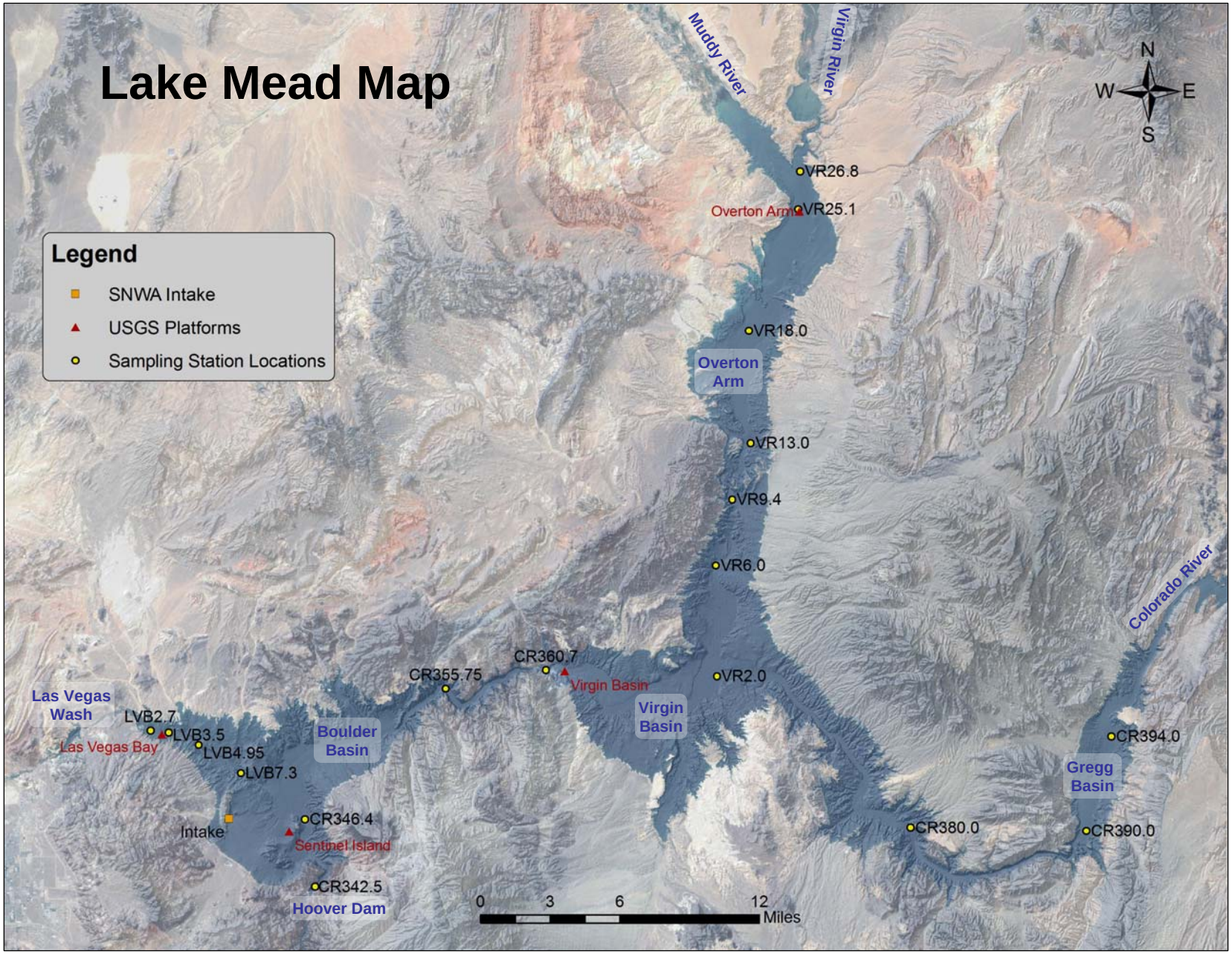

Ch4_Figures.ppt
FSI V064081 & V084015
December 9, 2010

Figure 4.1

FLOW SCIENCE

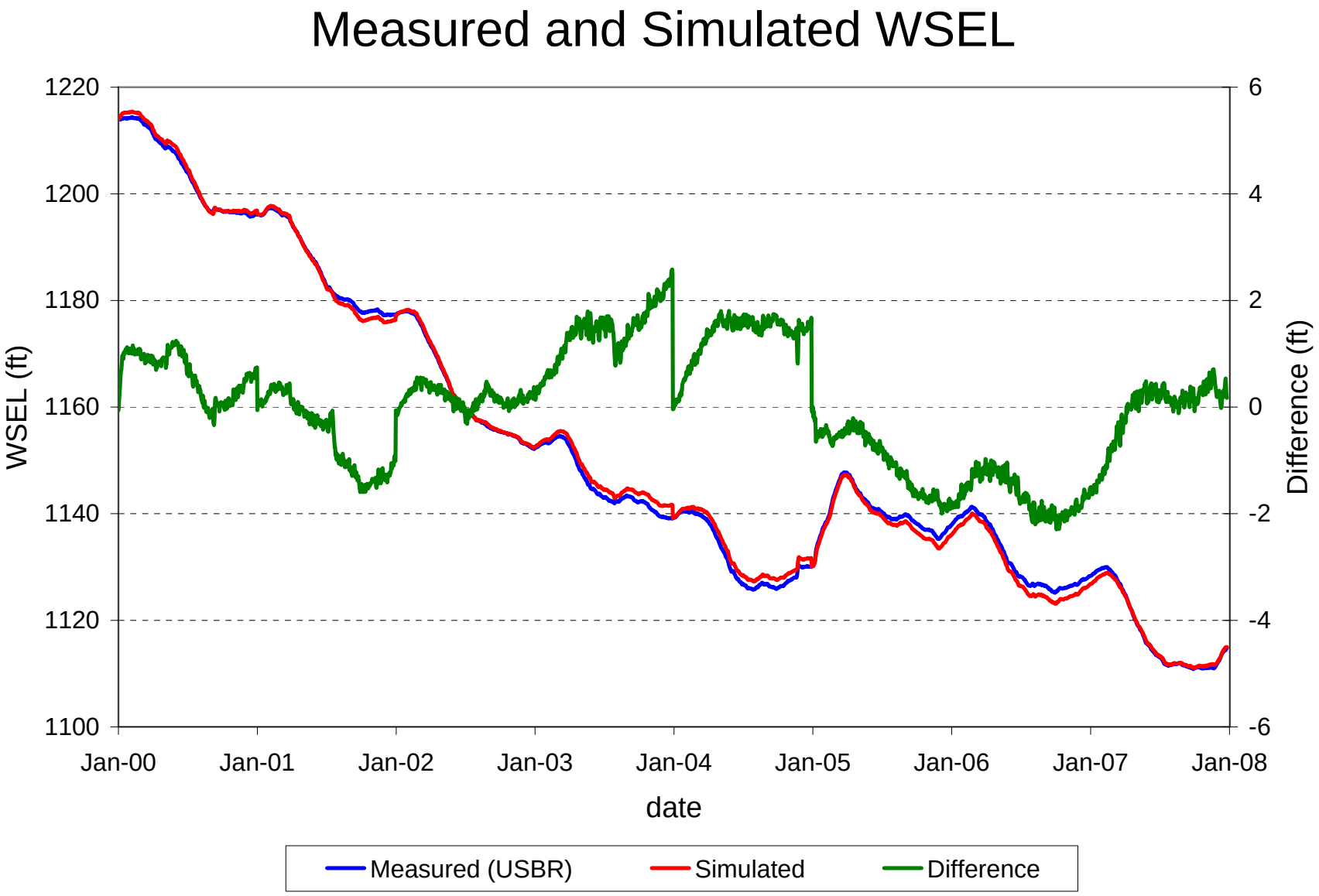
Measured and Simulated WSEL
1220
1200
1180
1160
1140
1120
1100
WSEL (ft)
6
4
2
0
-2
-4
-6
Difference (ft)
Jan-00
Jan-01
Jan-02
Jan-03
Jan-04
Jan-05
Jan-06
Jan-07
Jan-08
date
Measured (USBR)
Simulated
Difference

Figure 4.2

Comparison of Measured and Simulated Temperature Profiles at Station CR346.4 (2006 – 2007)

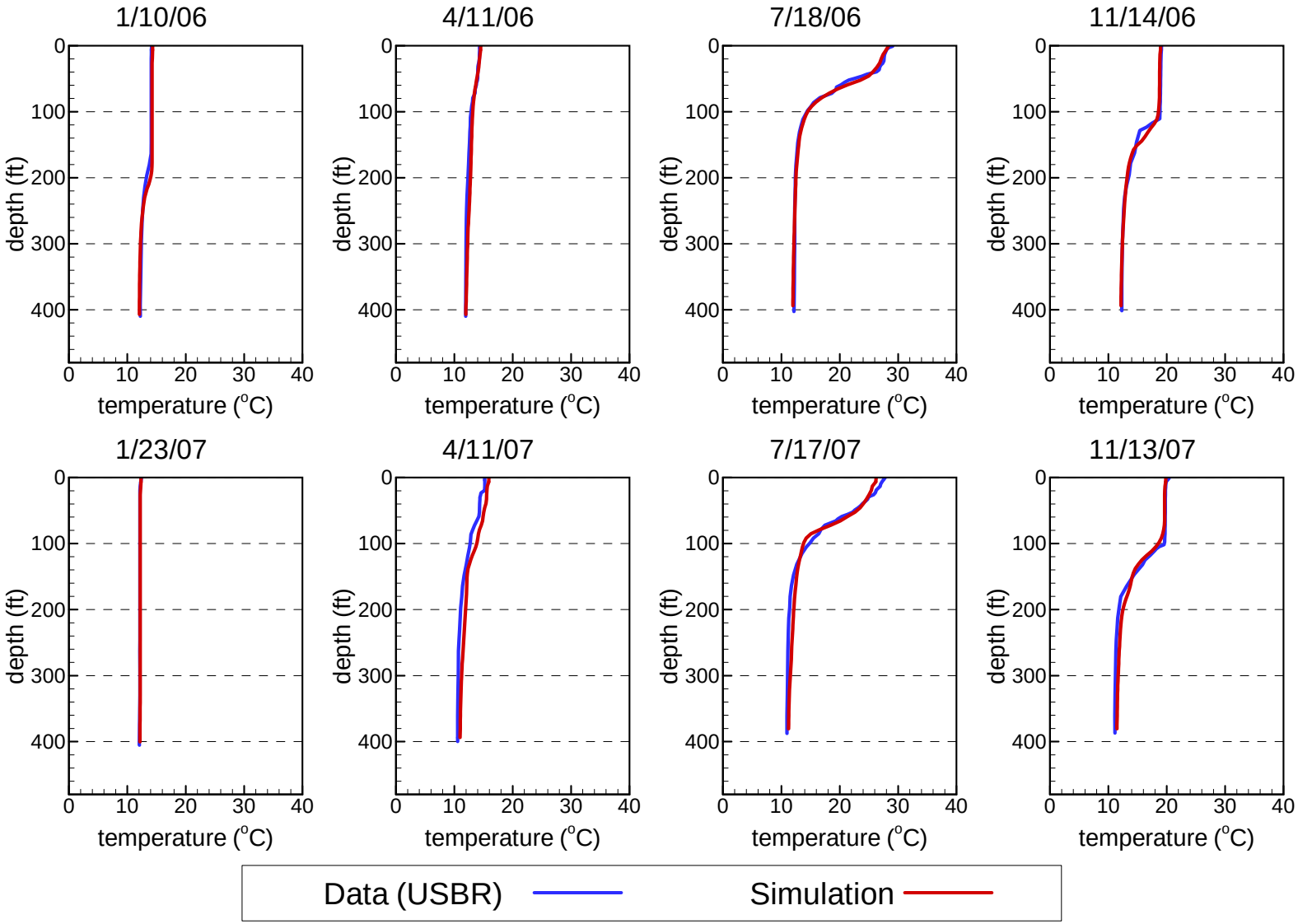

Figure 4.3

Comparison of Measured and Simulated Temperature at Station CR346.4 (2000 - 2008)

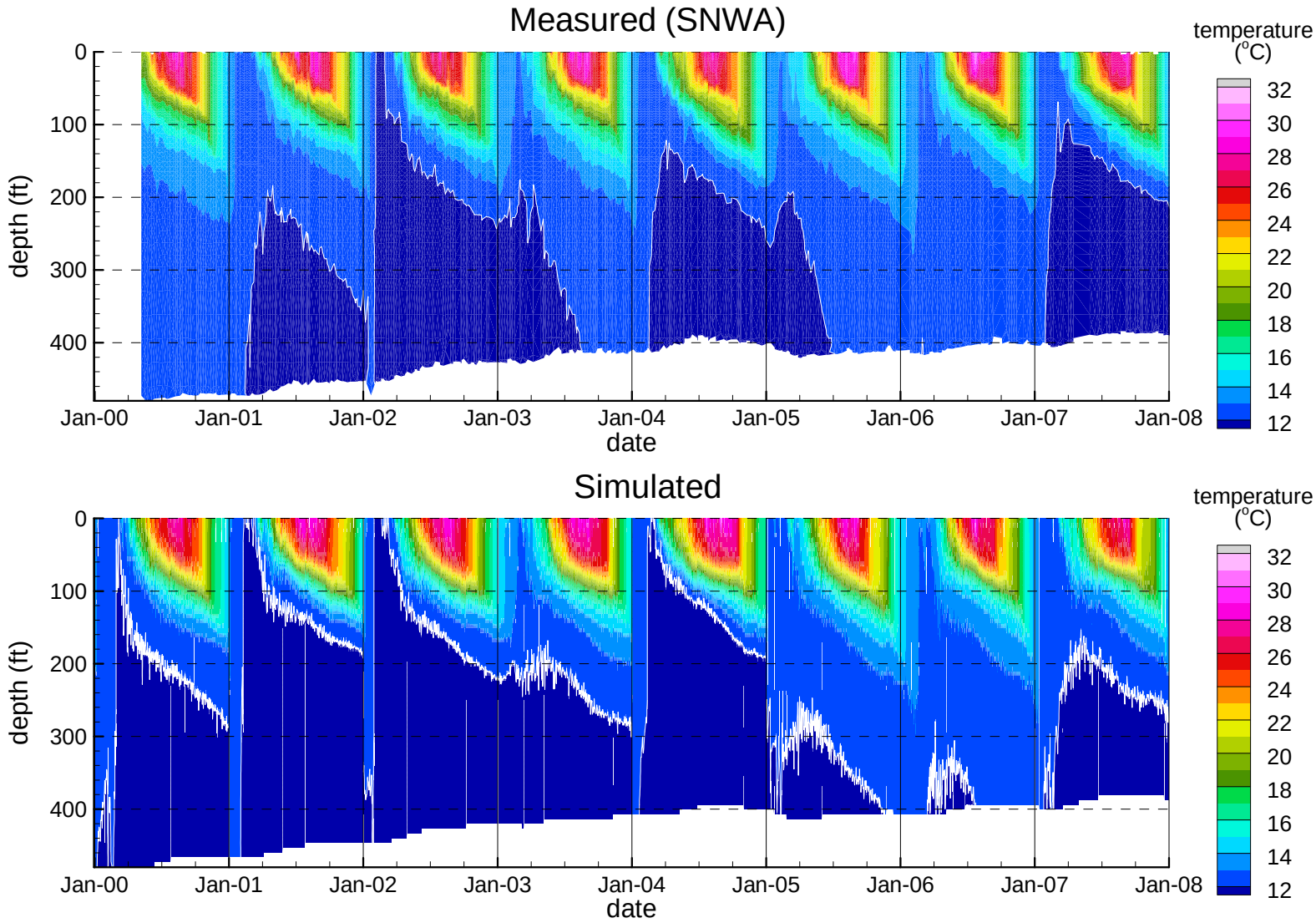

Figure 4.4

Comparison of Measured and Simulated Temperature Profiles at Station CR394.0 (2006 – 2007)

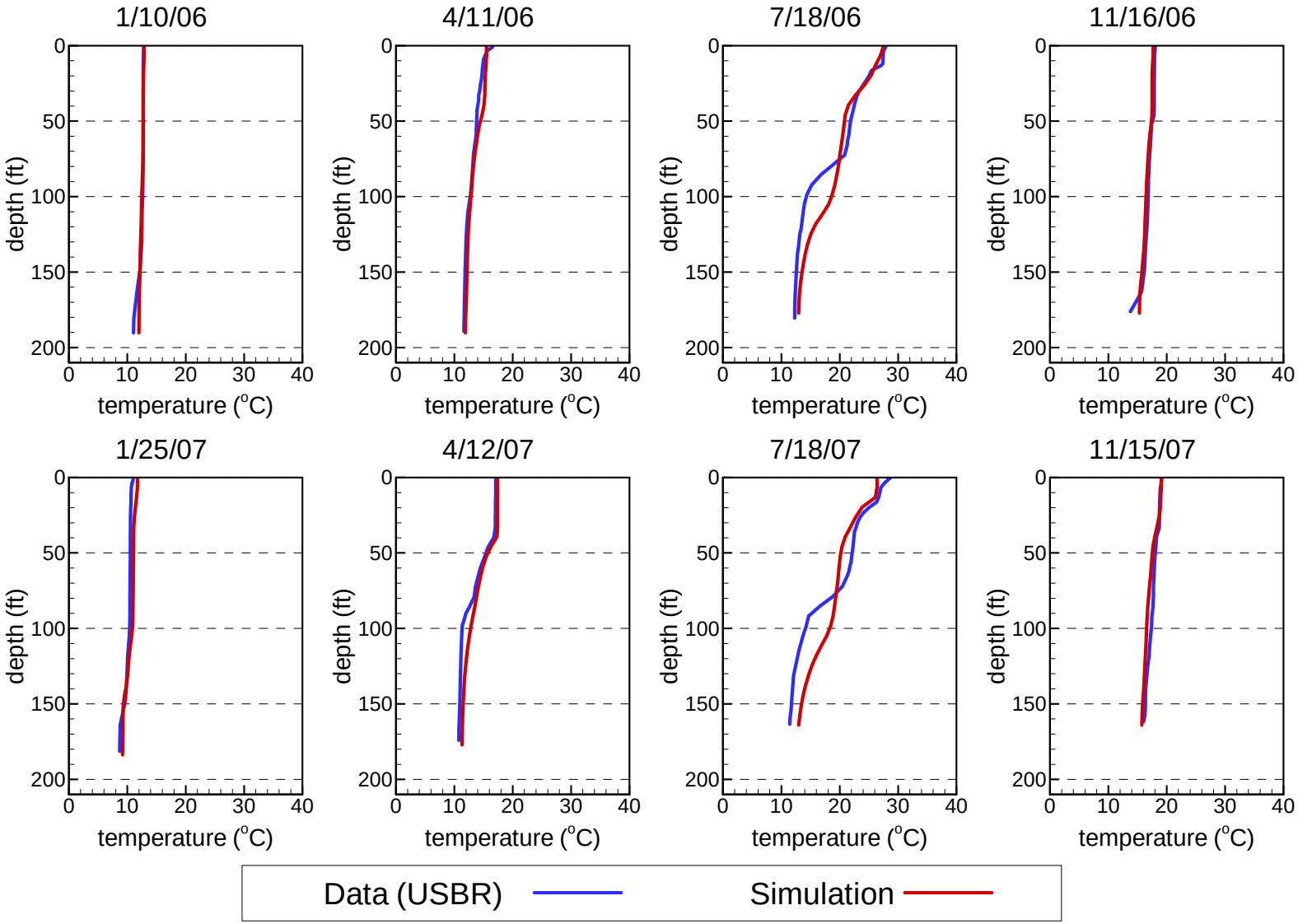

Figure 4.5

Comparison of Measured and Simulated Temperature at Station CR394.0

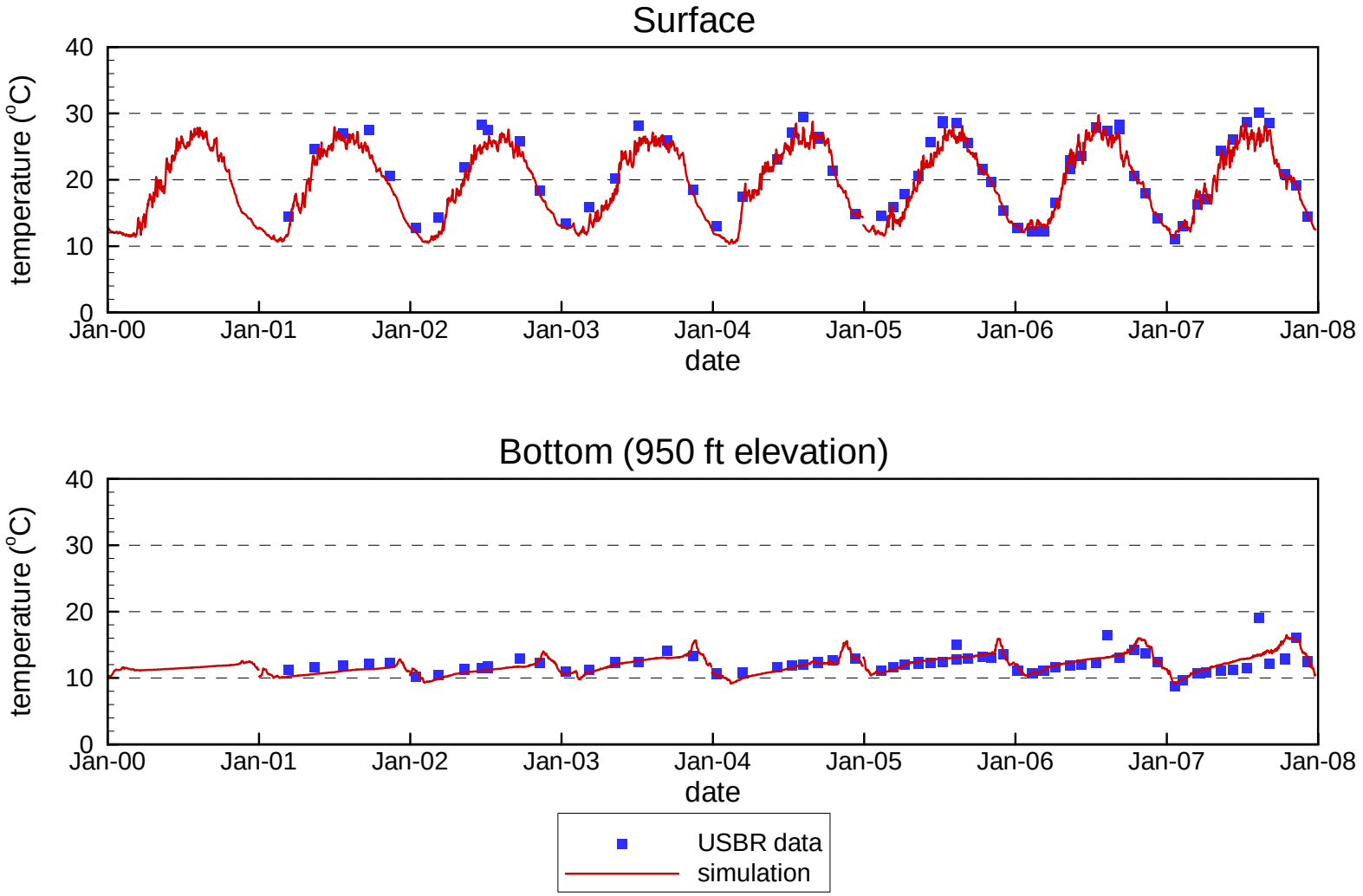

Figure 4.6

Comparison of Measured and Simulated Temperature at Station VR25.1

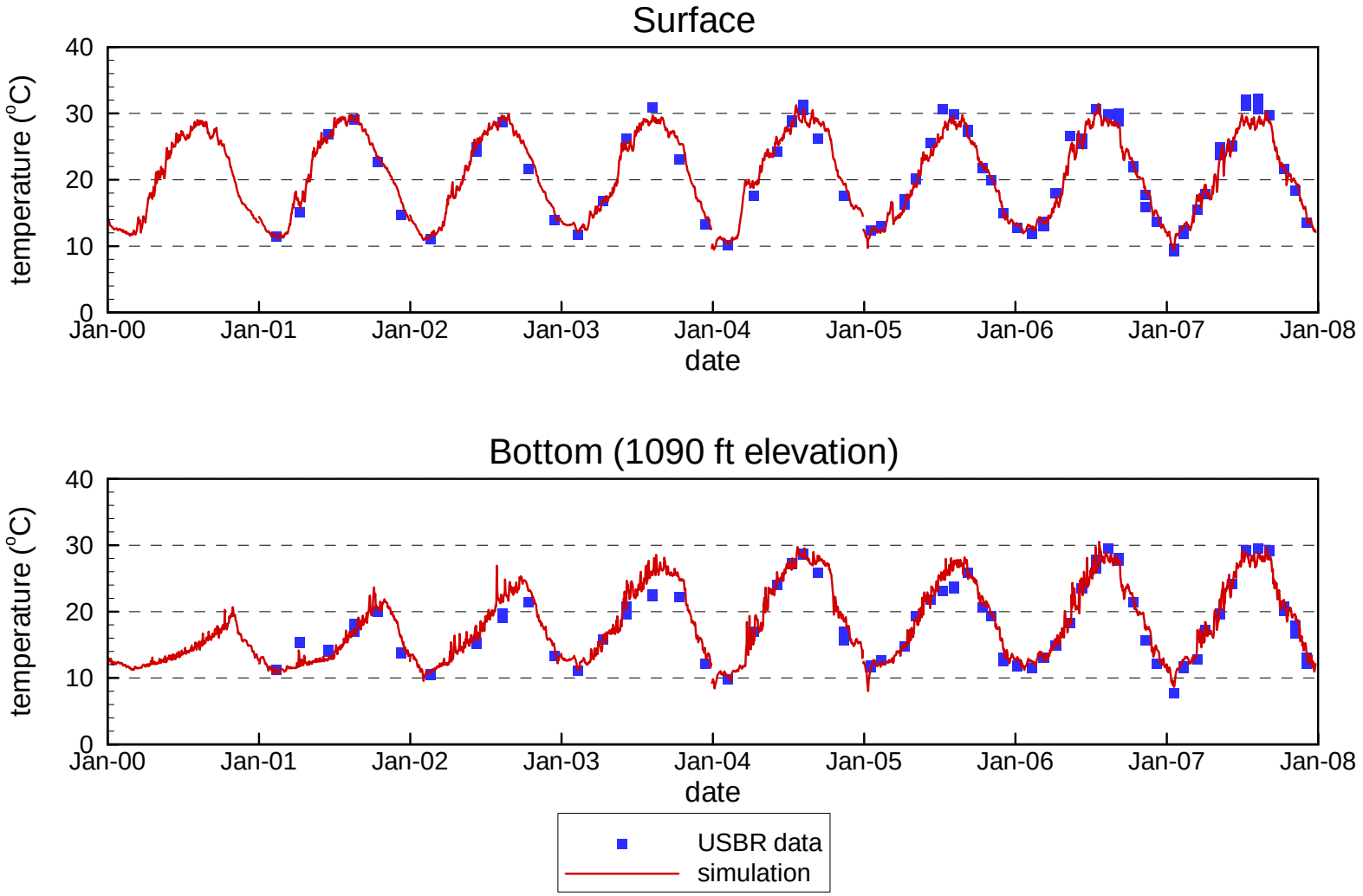

Figure 4.7

Comparison of Measured and Simulated Temperature at Stations VR12.9 / VR13.0

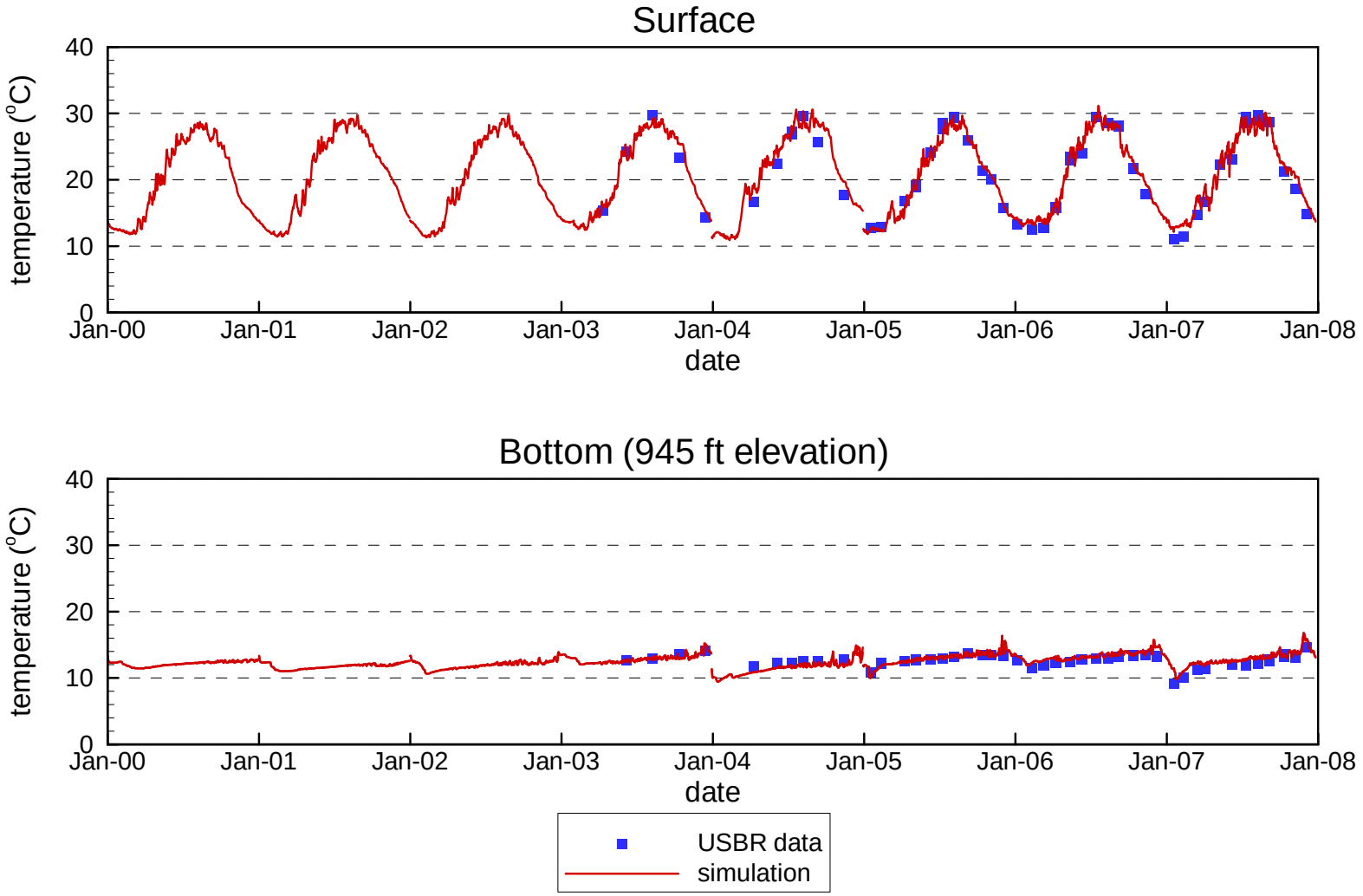

Figure 4.8

Comparison of Measured and Simulated Temperature at Station CR360.7

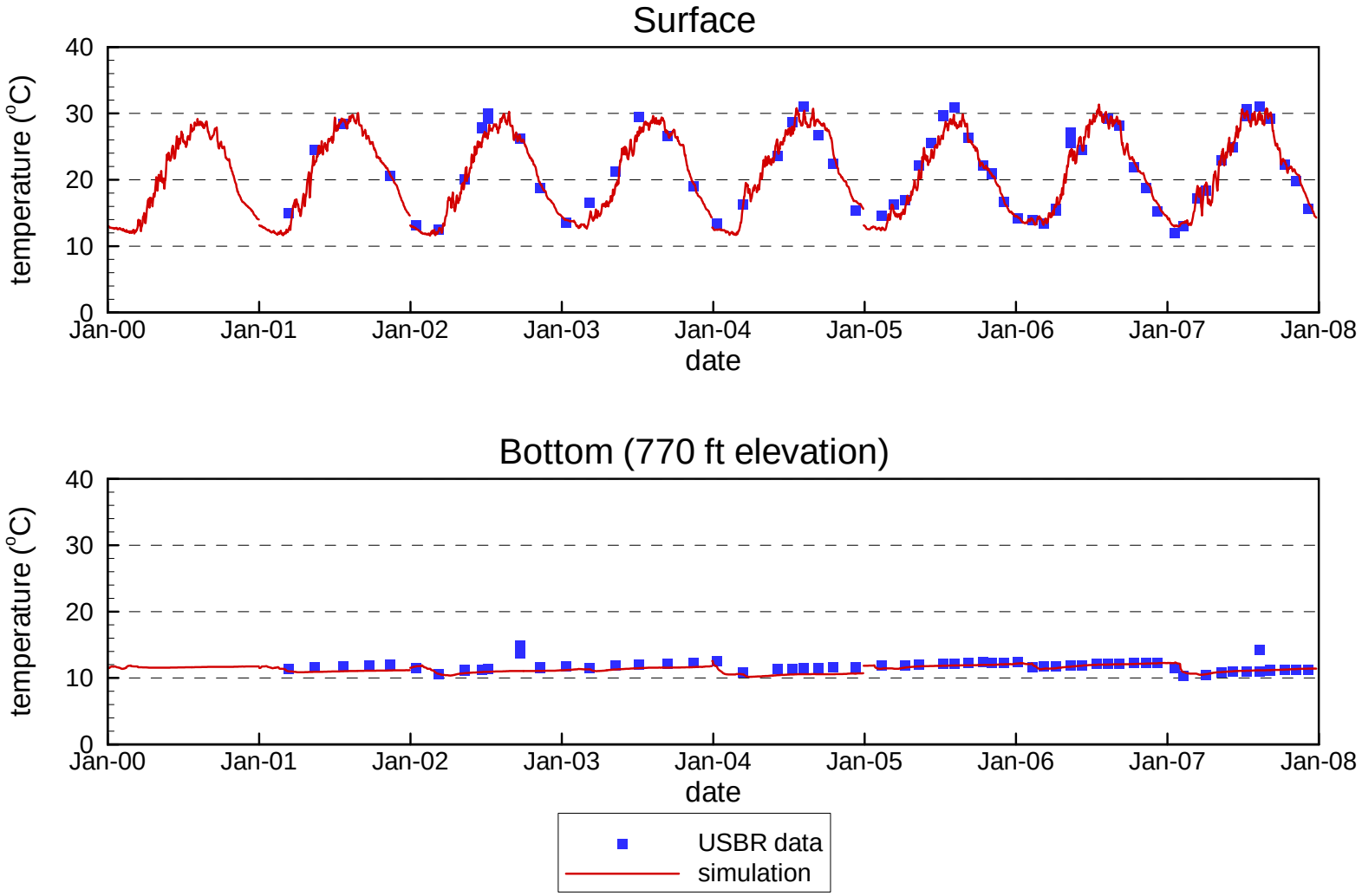

Figure 4.9

Comparison of Measured and Simulated Temperature at Station LVB3.5

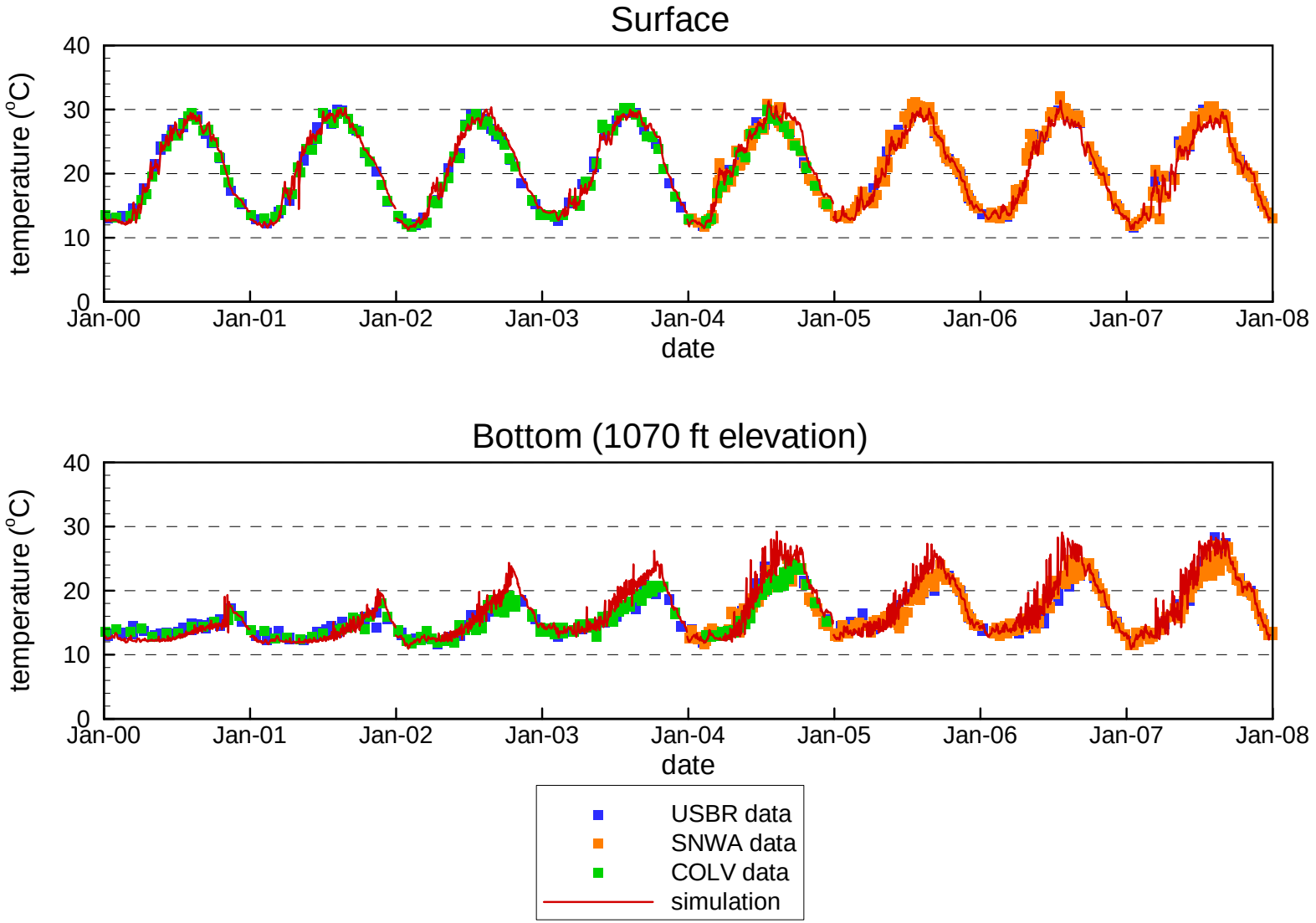

Figure 4.10

Comparison of Measured and Simulated Temperature at Station CR346.4

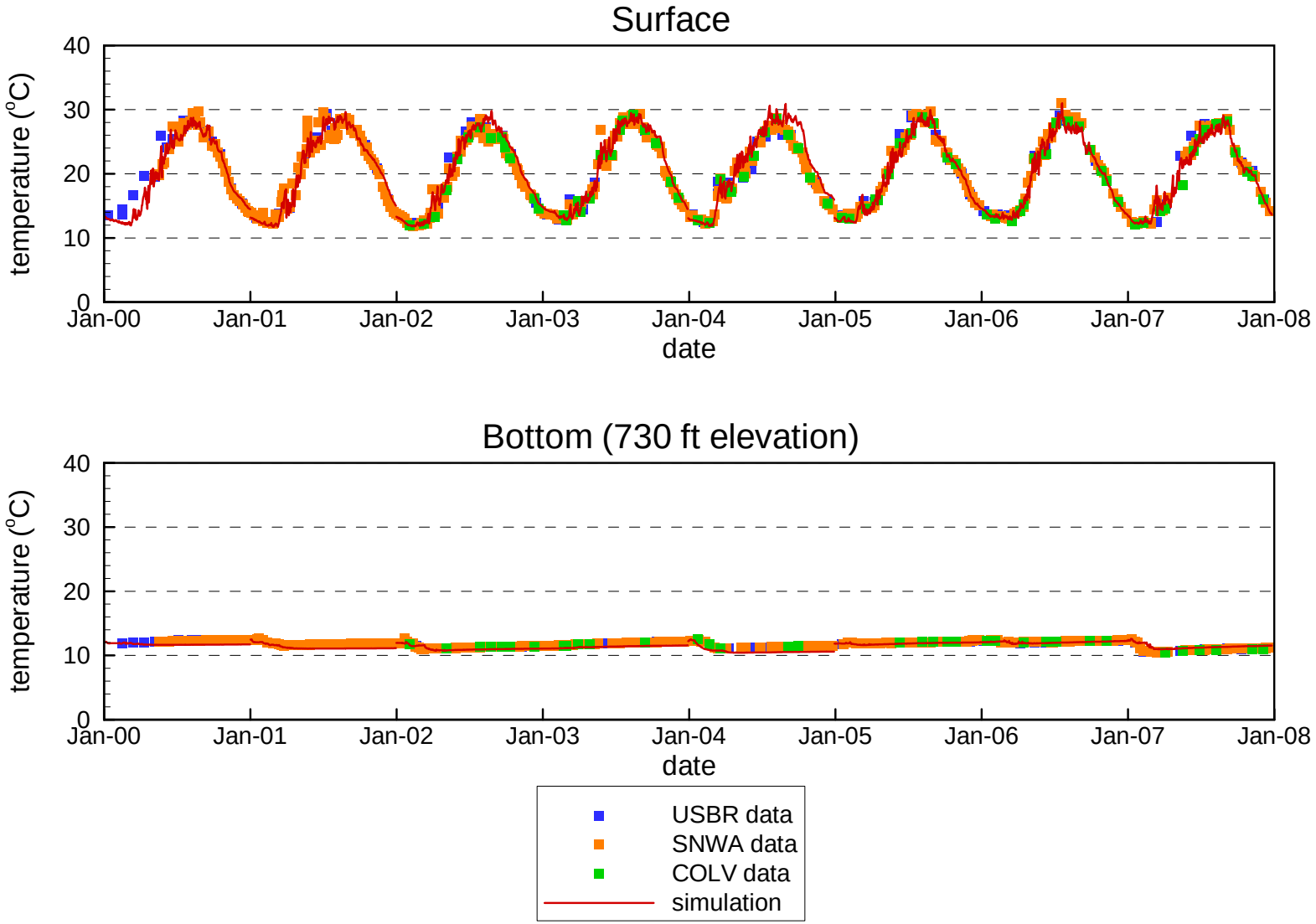

Figure 4.11

Comparison of Measured and Simulated Temperature at SNWA Intakes #1 and #2

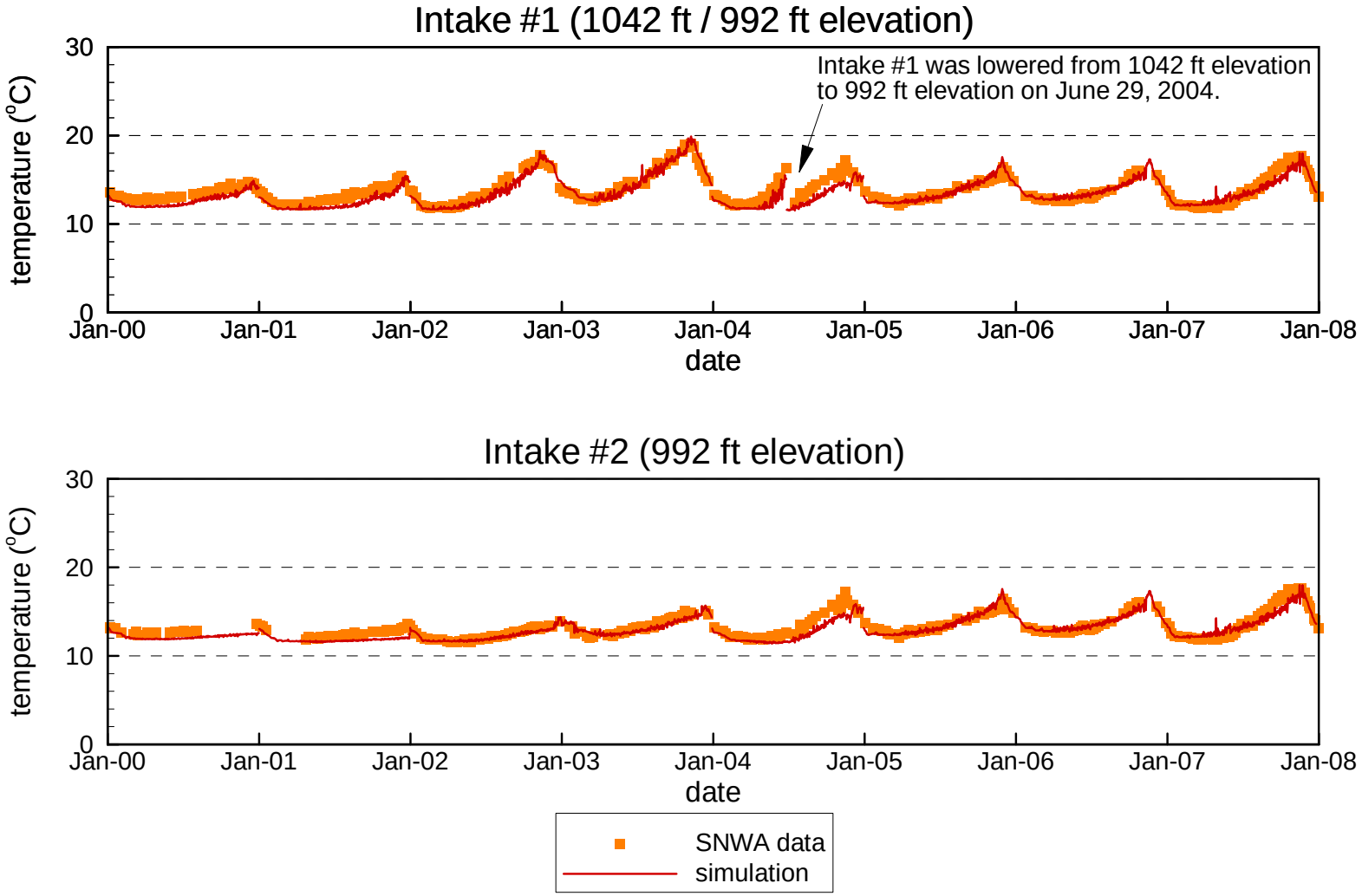

Figure 4.12

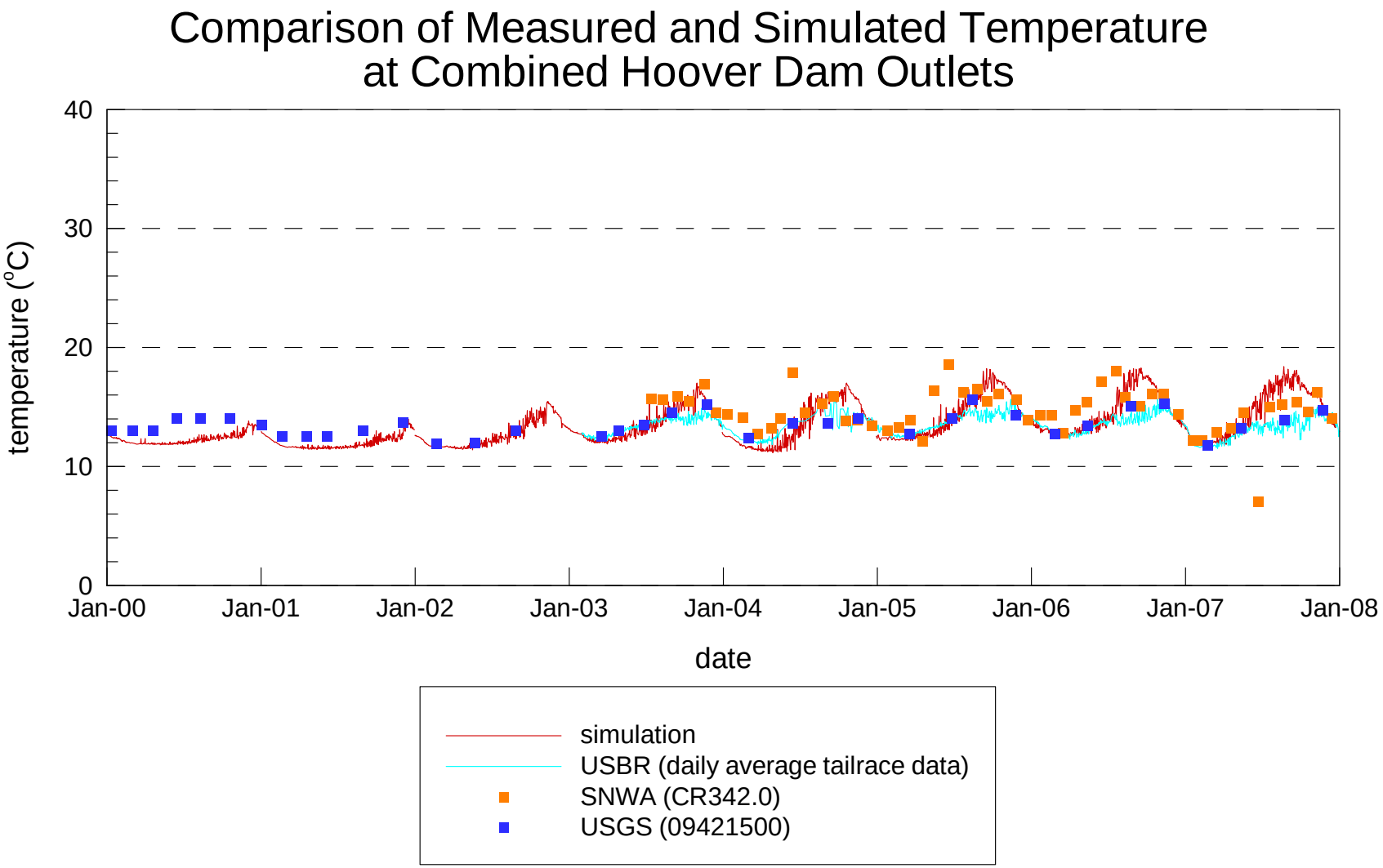
Comparison of Measured and Simulated Temperature
at Combined Hoover Dam Outlets
temperature (°C)
40
30
20
10
0
Jan-00
Jan-01
Jan-02
Jan-03
Jan-04
Jan-05
Jan-06
Jan-07
Jan-08
date
simulation
USBR (daily average tailrace data)
SNWA (CR342.0)
USGS (09421500)

Figure 4.13

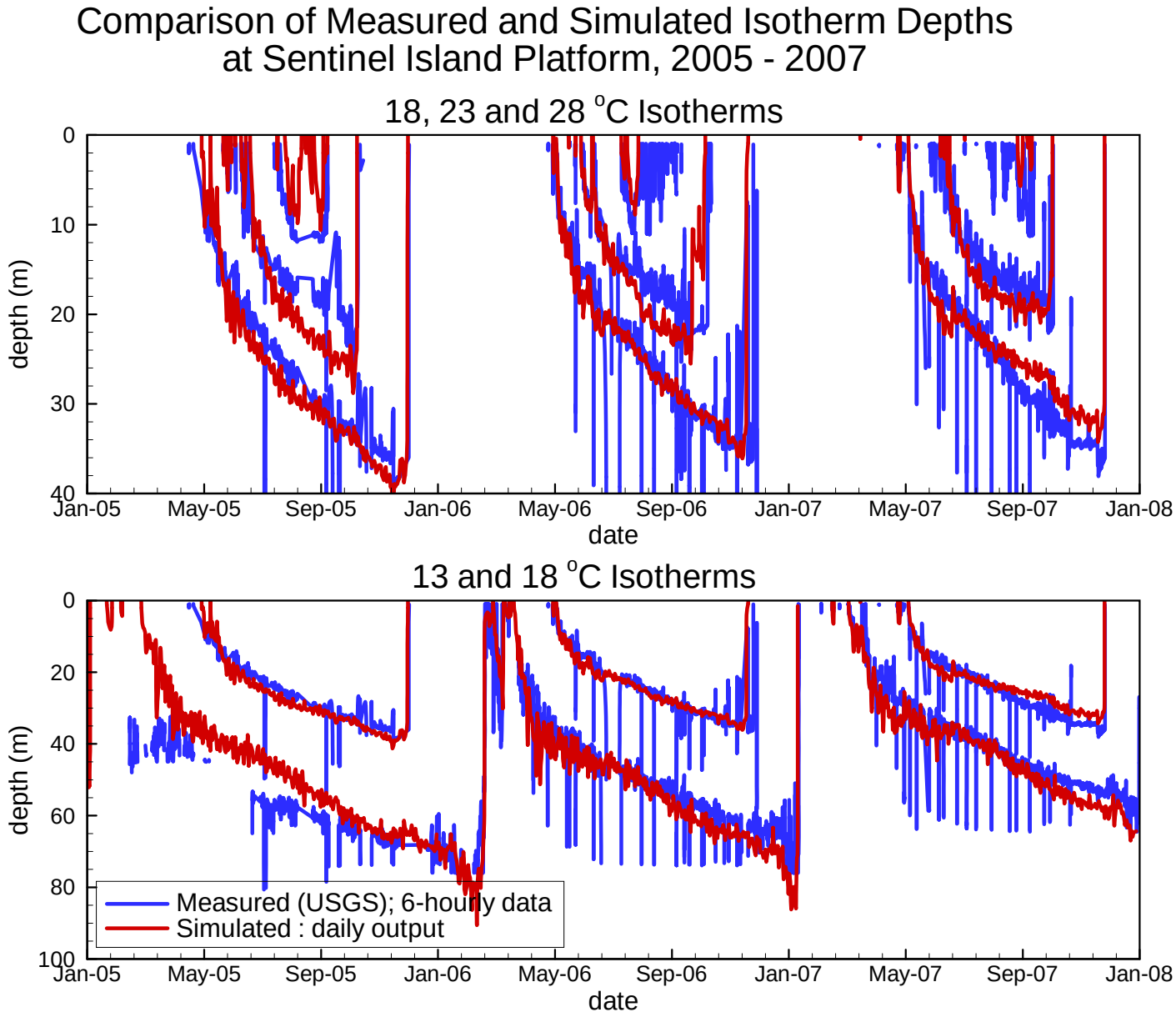
Comparison of Measured and Simulated Isotherm Depths
at Sentinel Island Platform, 2005 - 2007
18, 23 and 28 °C Isotherms
depth (m)
0
10
20
30
40
Jan-05
May-05
Sep-05
Jan-06
May-06
Sep-06
Jan-07
May-07
Sep-07
Jan-08
date
13 and 18 °C Isotherms
depth (m)
0
20
40
60
80
100
Measured (USGS); 6-hourly data
Simulated : daily output
Jan-05
May-05
Sep-05
Jan-06
May-06
Sep-06
Jan-07
May-07
Sep-07
Jan-08
date

Figure 4.14

Comparison of Measured and Simulated Isotherm Depths at Sentinel Island Platform in July 2006 and 2007

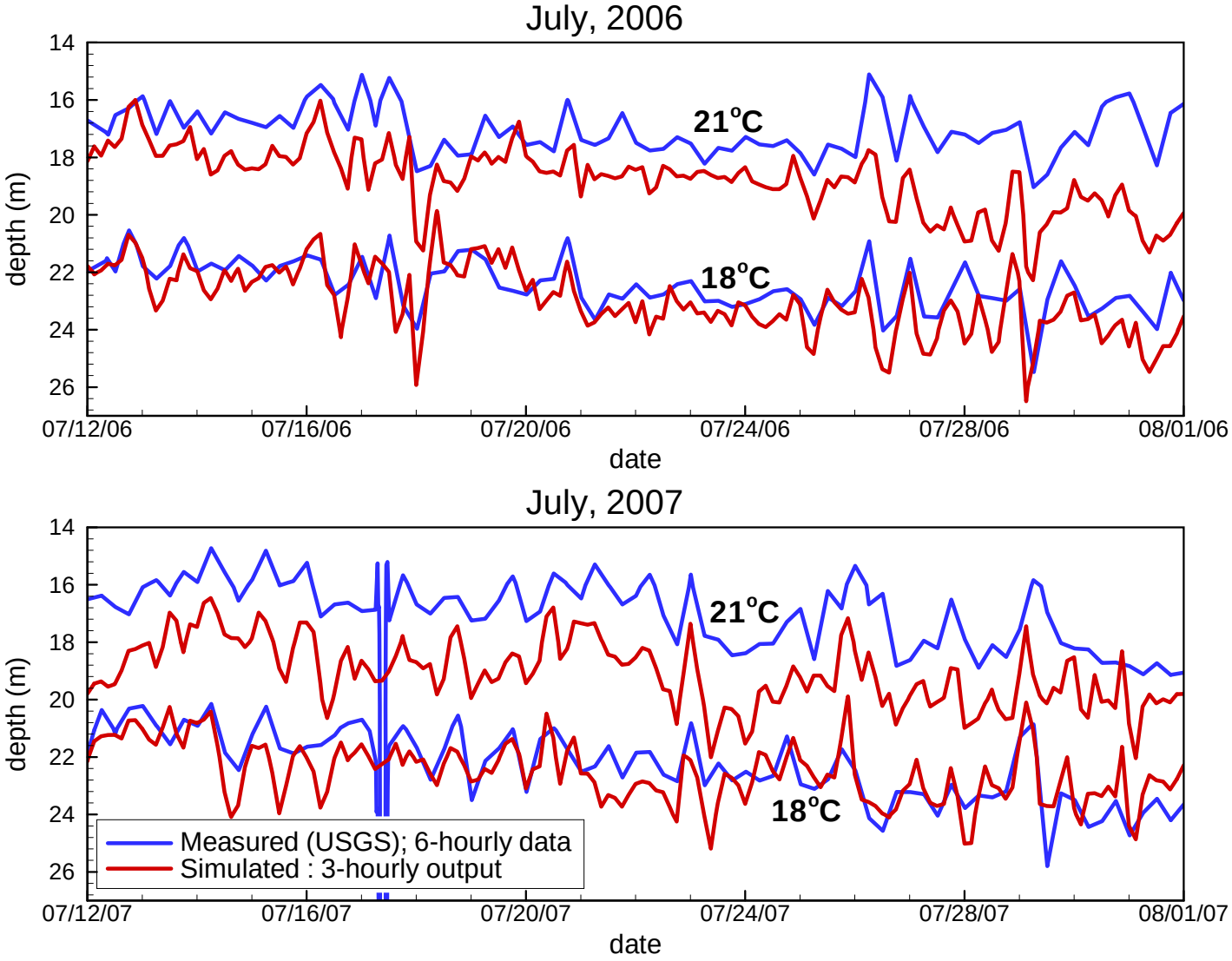

Figure 4.15

Comparison of Measured (USBR) and Simulated Conductivity on Profile from Hoover Dam to Colorado River

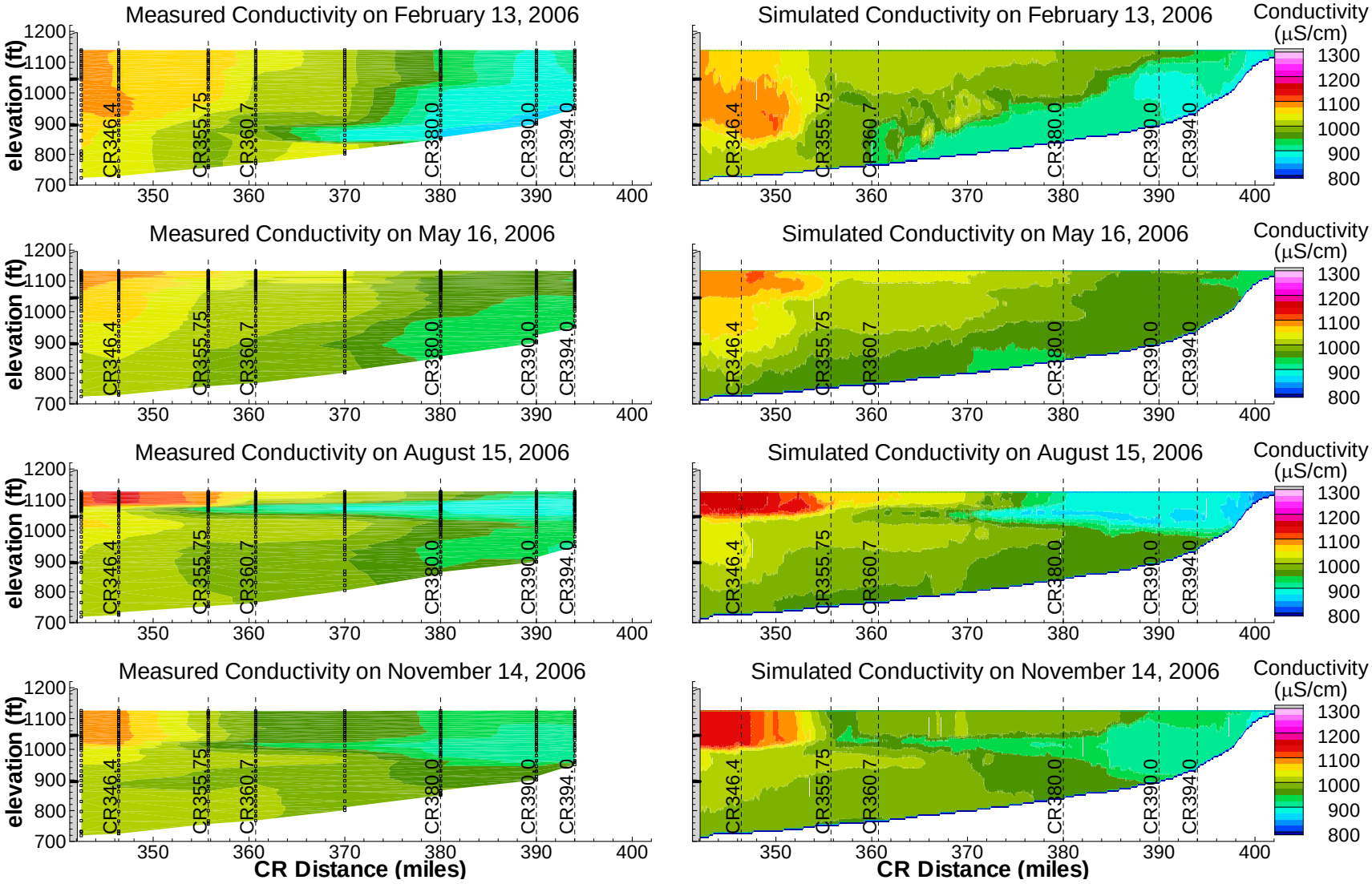

Ch4_Figures.ppt
FSI V064081 & V084015
December 9, 2010

Figure 4.16

FLOW SCIENCE

Comparison of Measured (USBR) and Simulated Conductivity on Profile from Hoover Dam to Colorado River

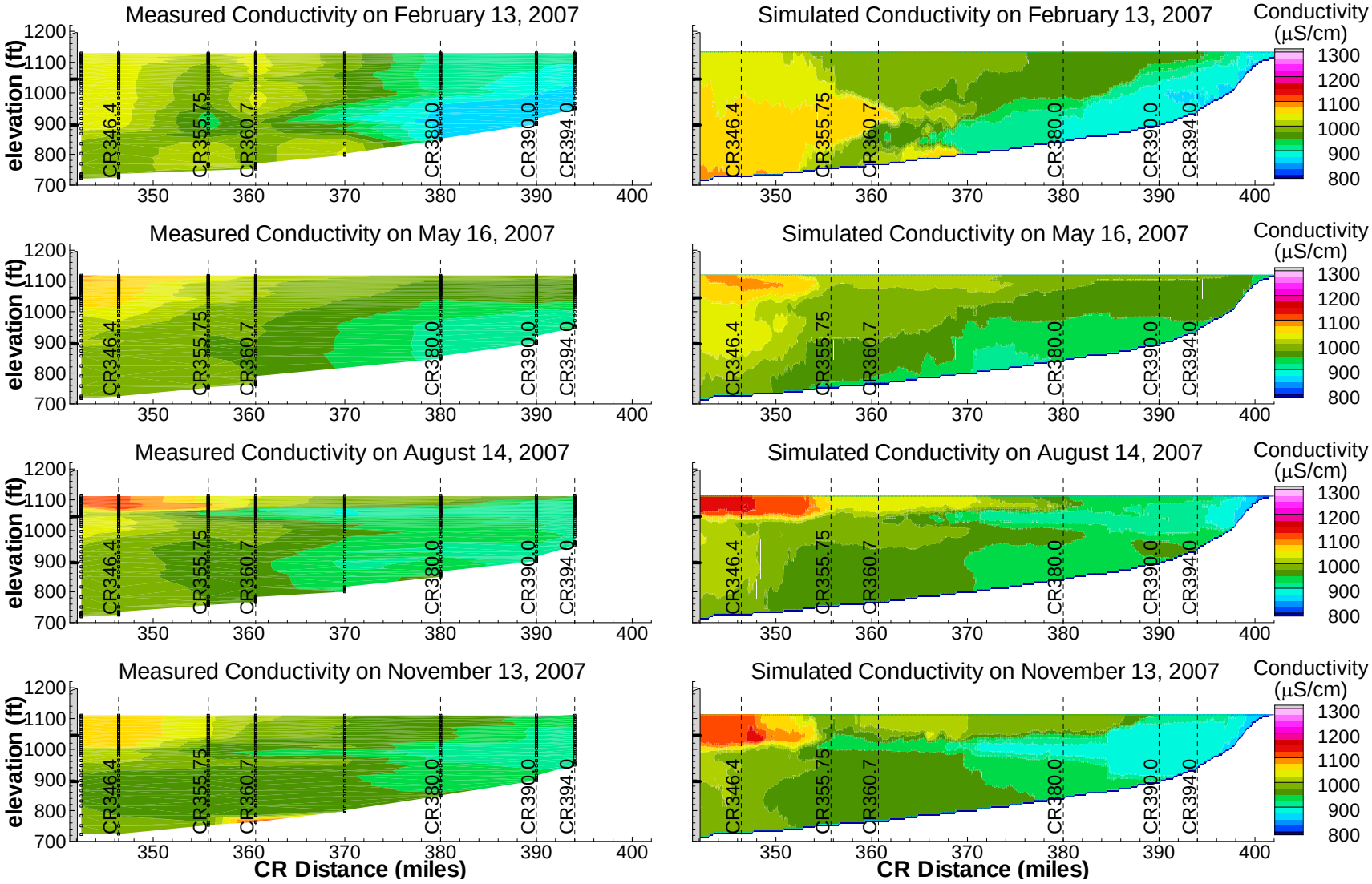

Ch4_Figures.ppt
FSI V064081 & V084015
December 9, 2010

Figure 4.17

FLOW SCIENCE

Comparison of Measured (USBR) and Simulated Conductivity on Profile from Hoover Dam to Virgin River

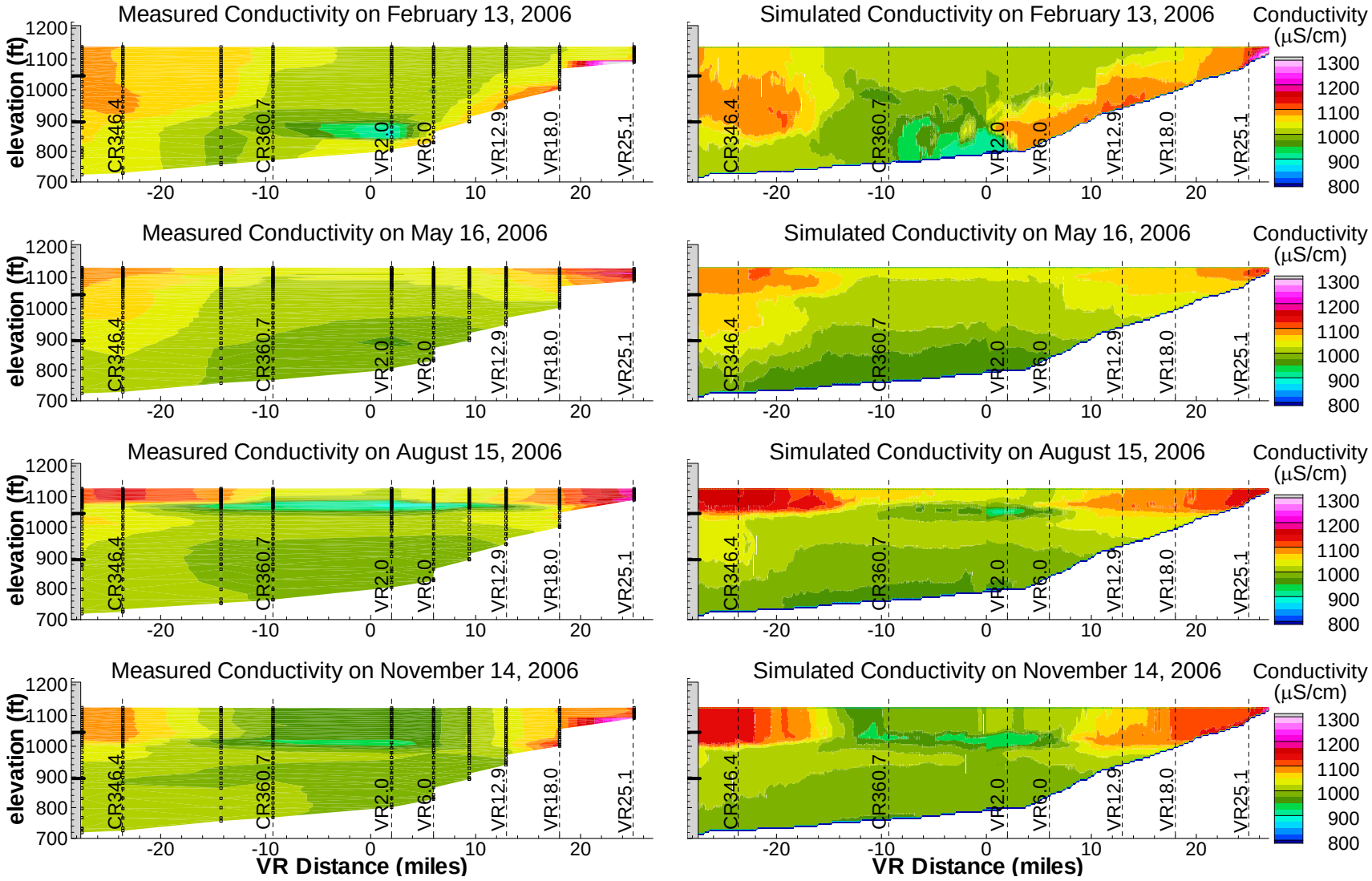

Ch4_Figures.ppt
FSI V064081 & V084015
December 9, 2010

Figure 4.18

FLOW SCIENCE

Comparison of Measured (USBR) and Simulated Conductivity on Profile from Hoover Dam to Virgin River

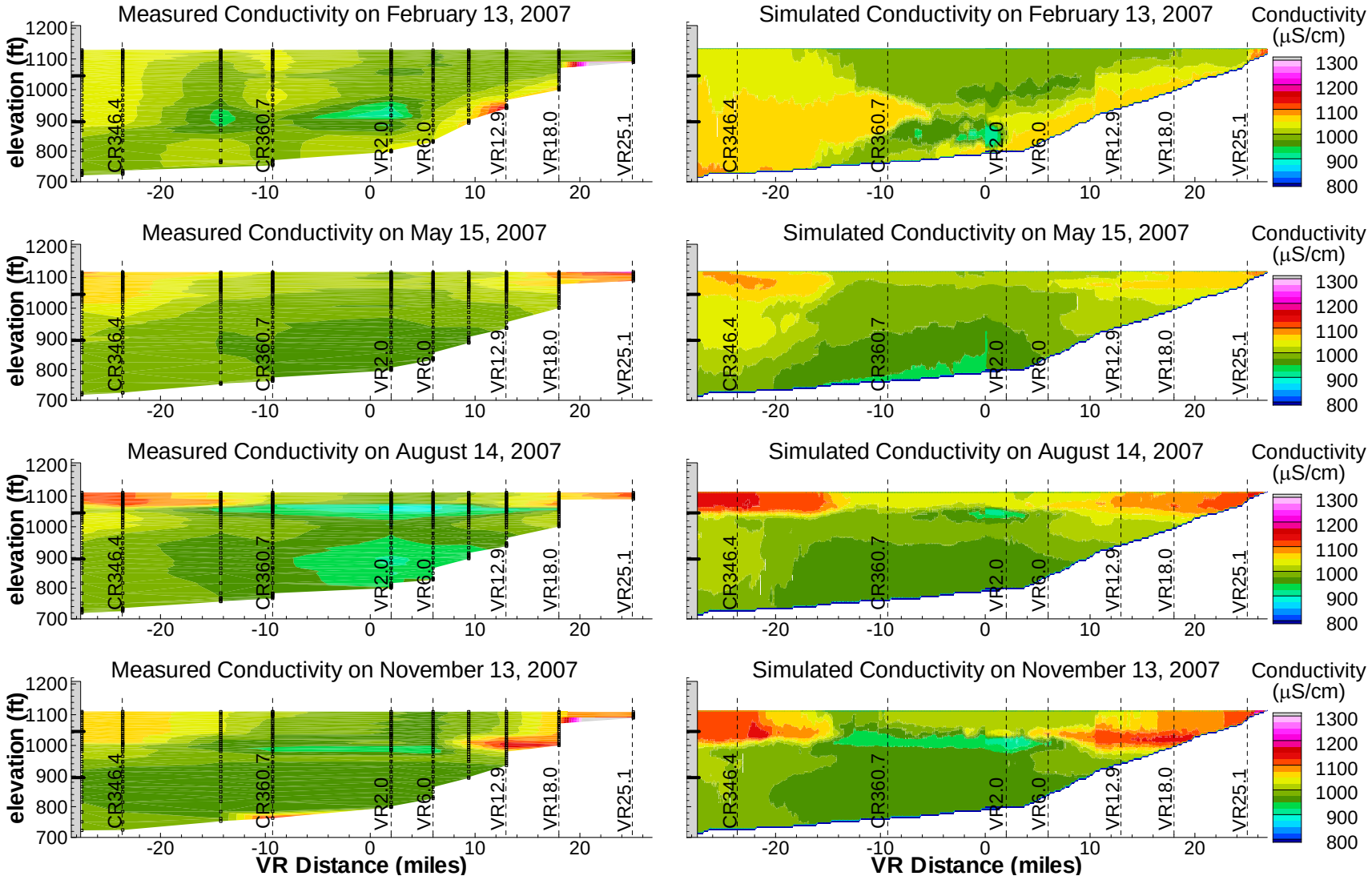

Ch4_Figures.ppt
FSI V064081 & V084015
December 9, 2010

Figure 4.19

FLOW SCIENCE

Comparison of Measured and Simulated Conductivity on Profile from Las Vegas Wash to Hoover Dam

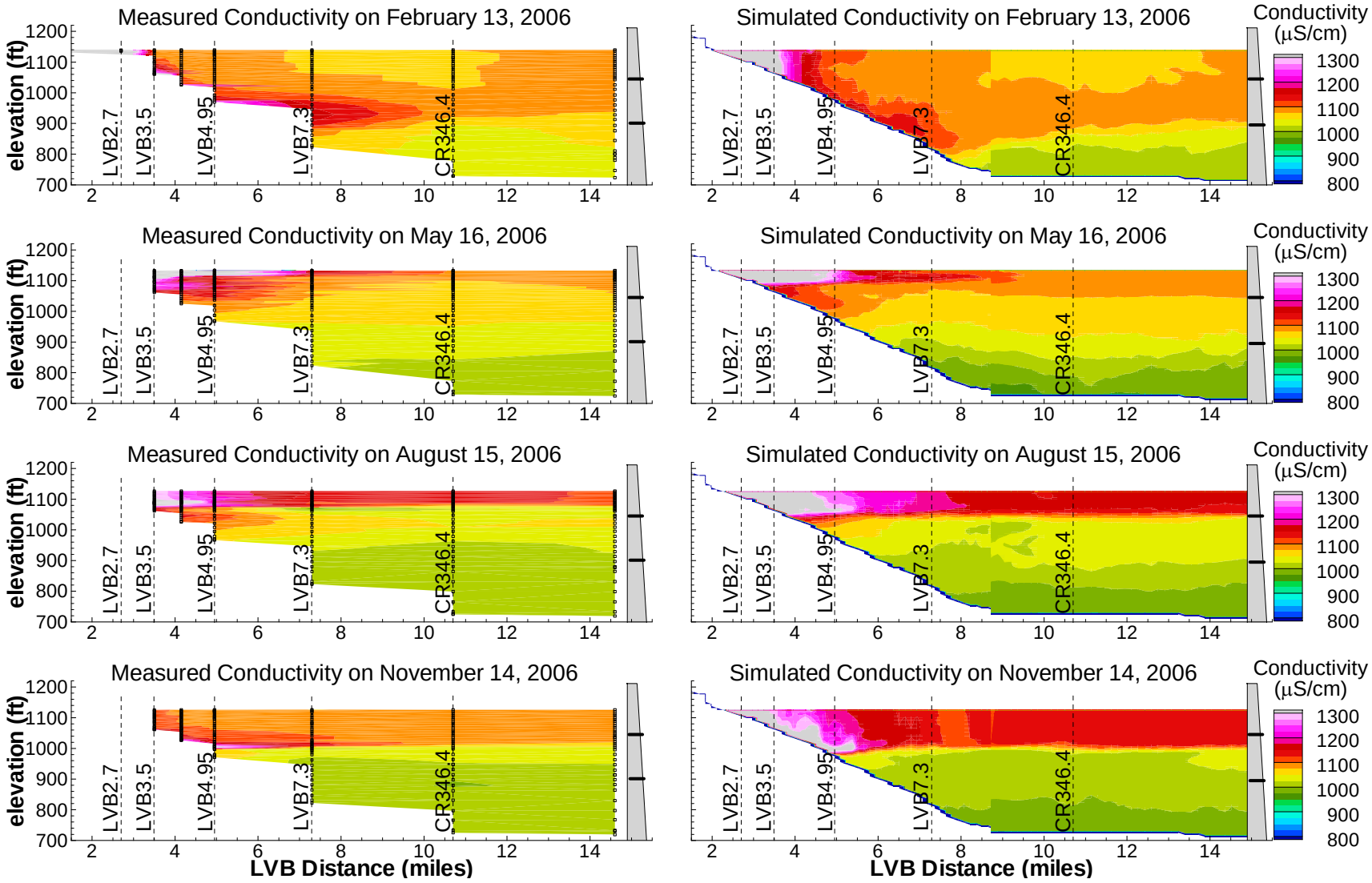

Ch4_Figures.ppt
FSI V064081 & V084015
December 9, 2010

Figure 4.20

FLOW SCIENCE

Comparison of Measured and Simulated Conductivity on Profile from Las Vegas Wash to Hoover Dam

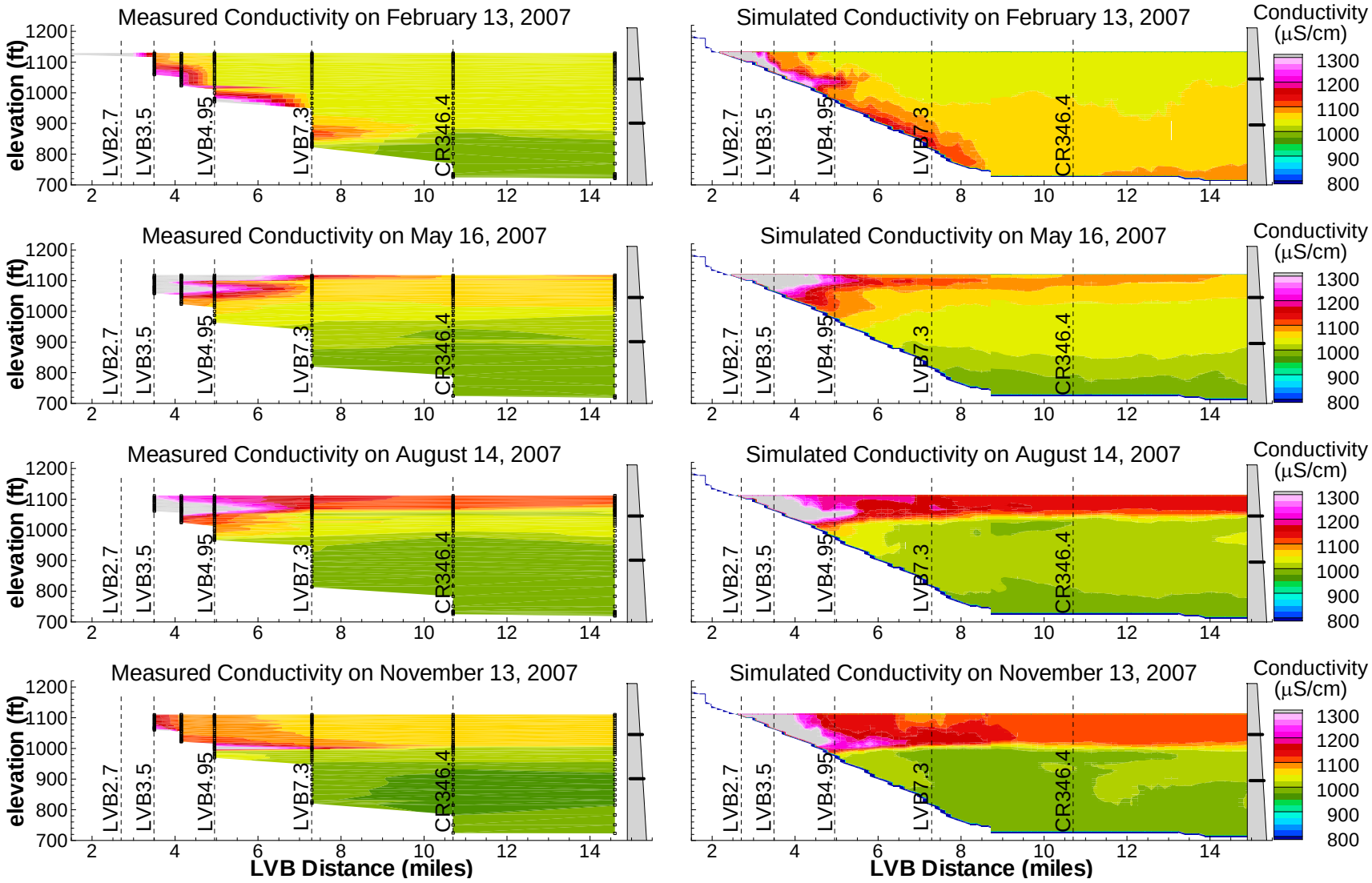

Ch4_Figures.ppt
FSI V064081 & V084015
December 9, 2010

Figure 4.21

FLOW SCIENCE

Comparison of Measured and Simulated Conductivity Profiles at Station CR346.4 (2006 – 2007)

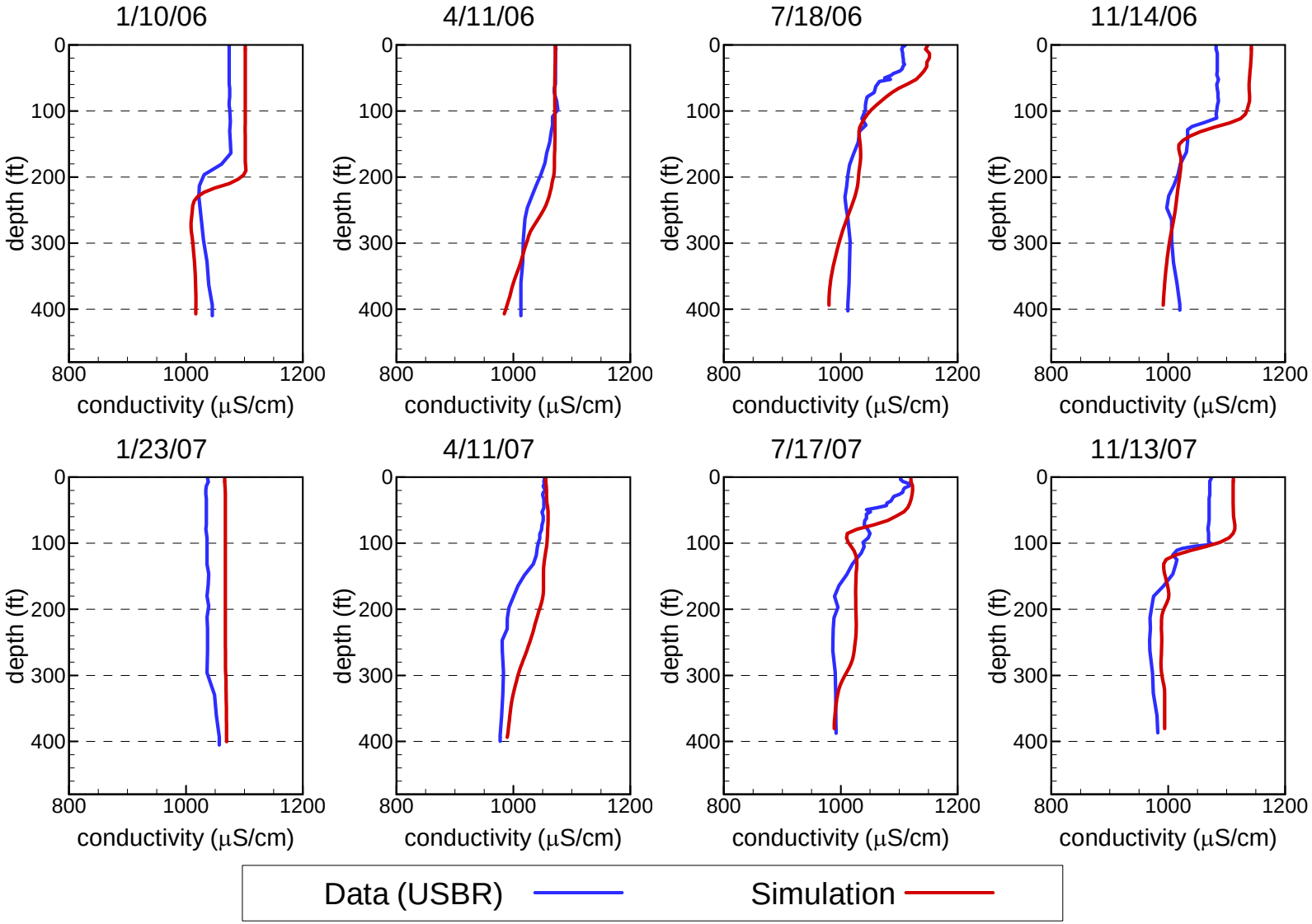

Figure 4.22

Comparison of Measured and Simulated Conductivity at Station CR394.0

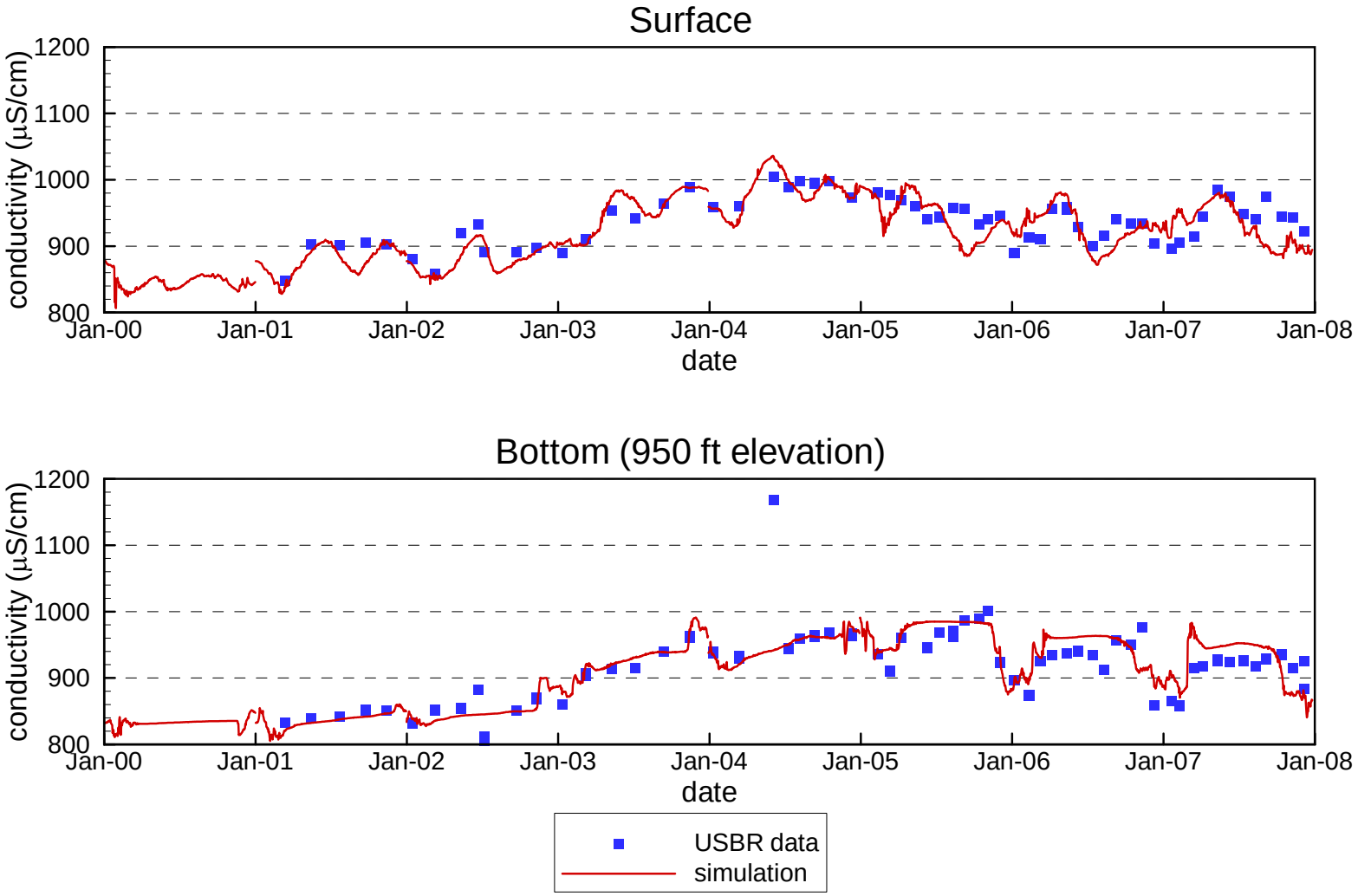

Figure 4.23

Comparison of Measured and Simulated Conductivity at Station VR25.1

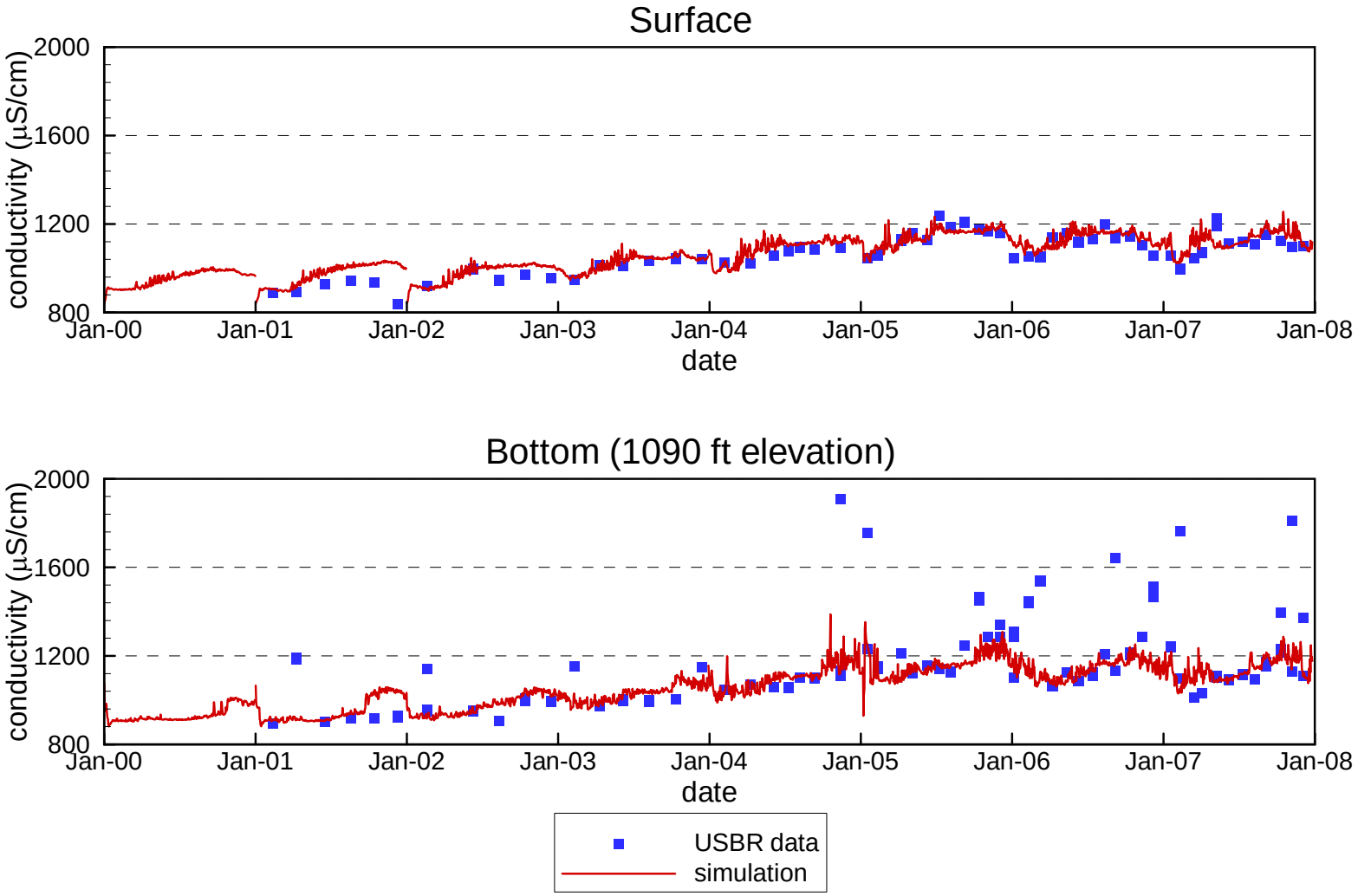

Comparison of Measured and Simulated Conductivity at Stations VR12.9 / VR13.0

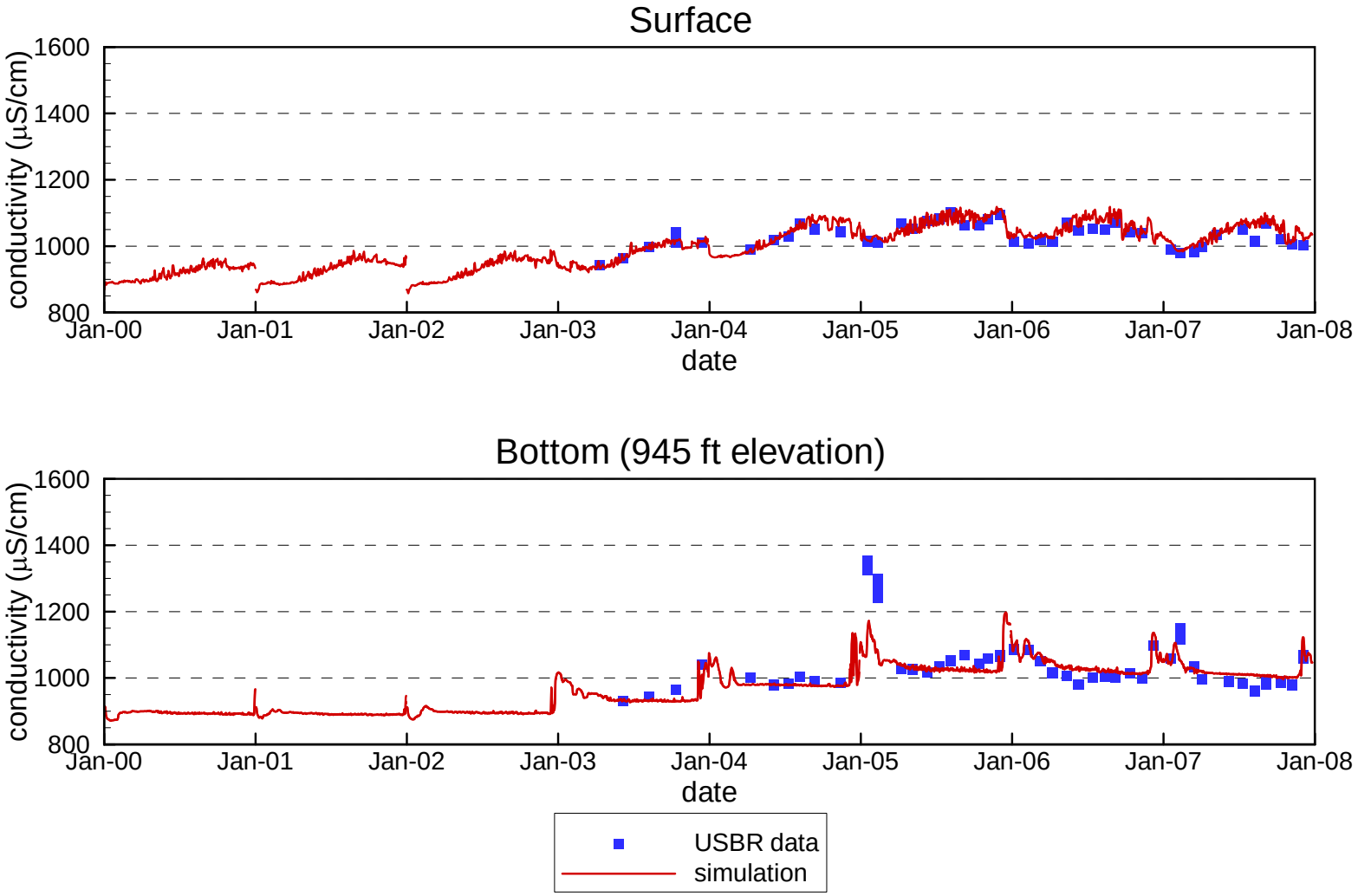

Figure 4.25

Comparison of Measured and Simulated Conductivity at Station CR360.7

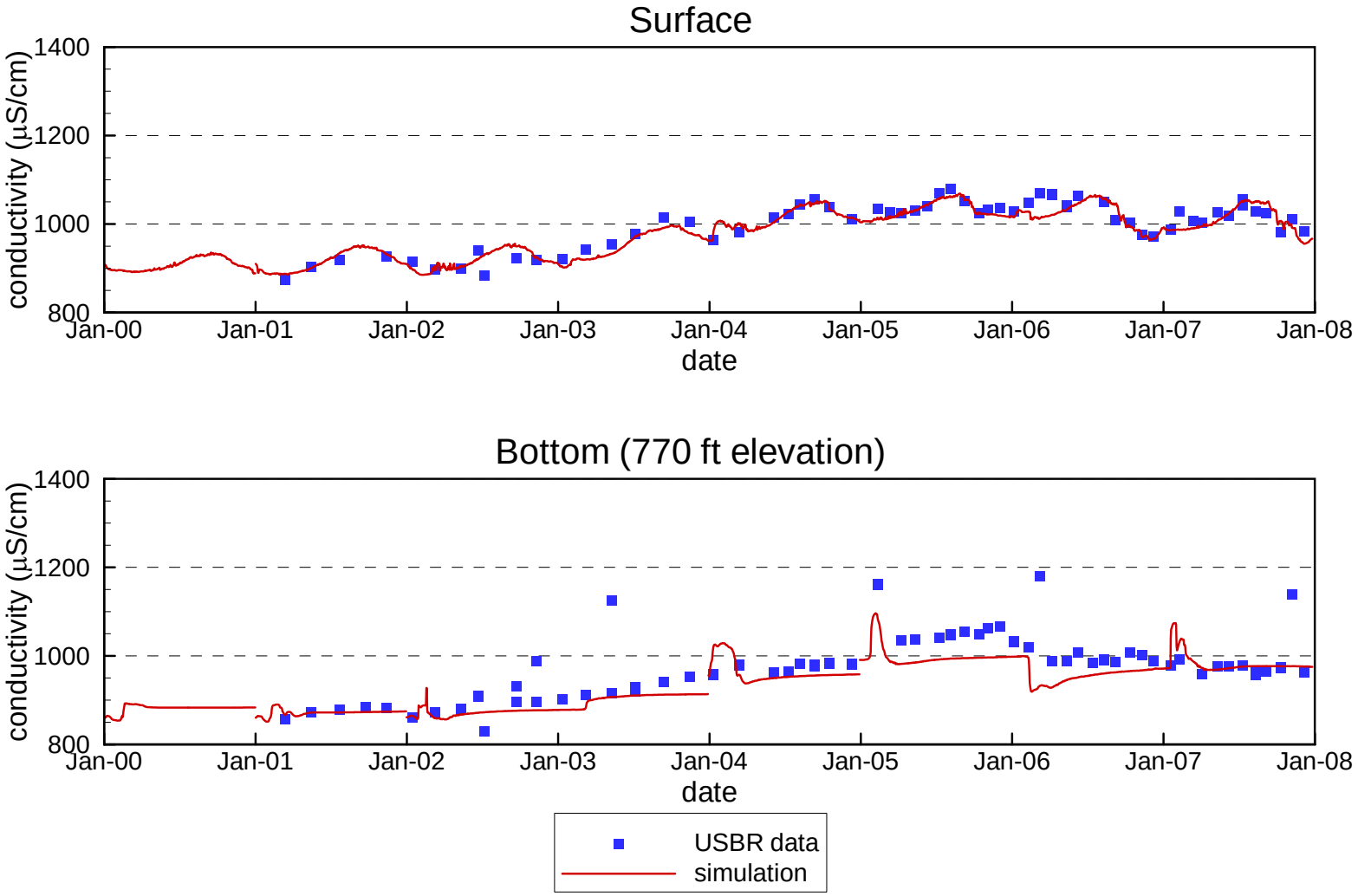

Figure 4.26

Comparison of Measured and Simulated Conductivity at Station LVB3.5

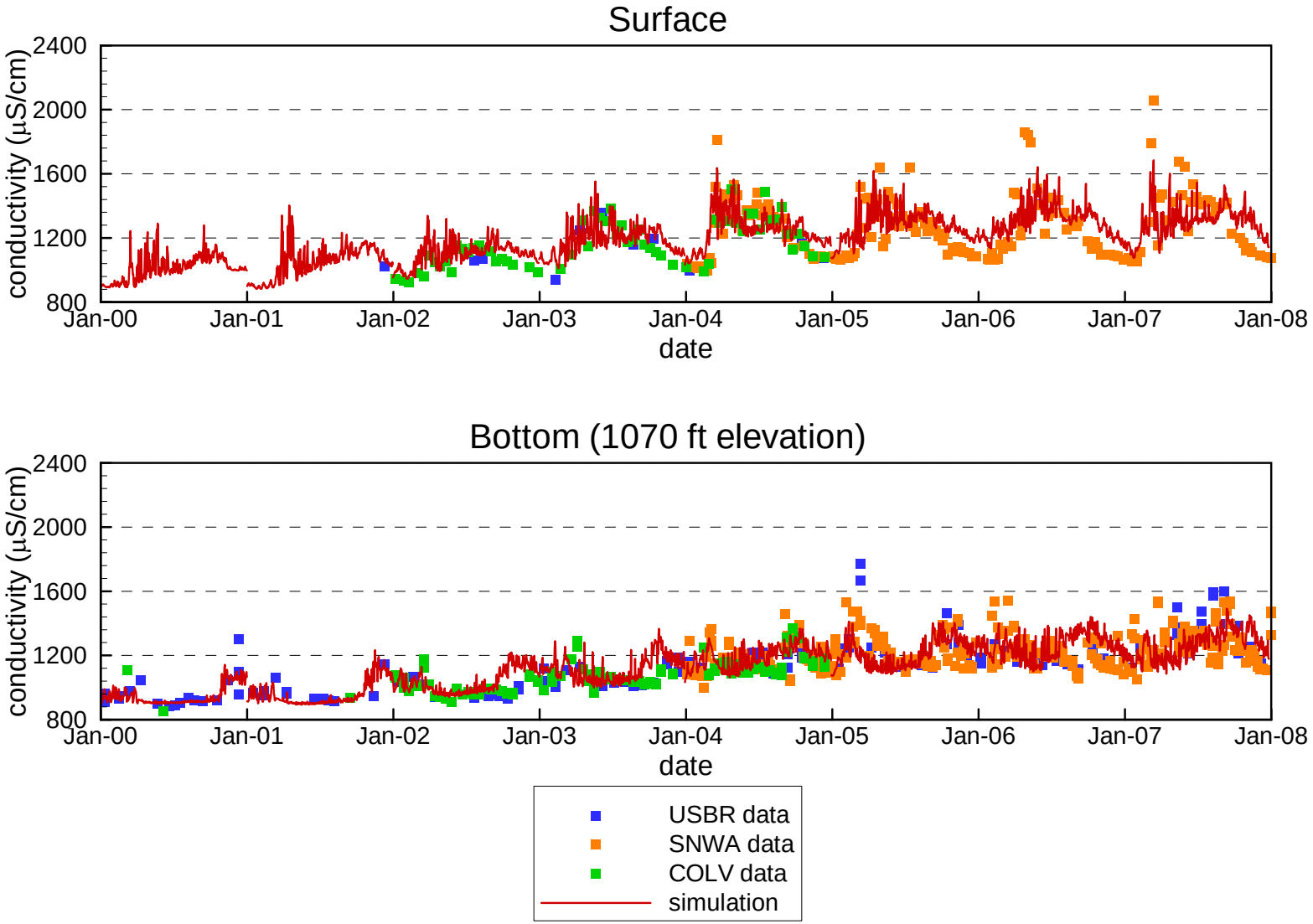

Figure 4.27

Comparison of Measured and Simulated Conductivity at Station CR346.4

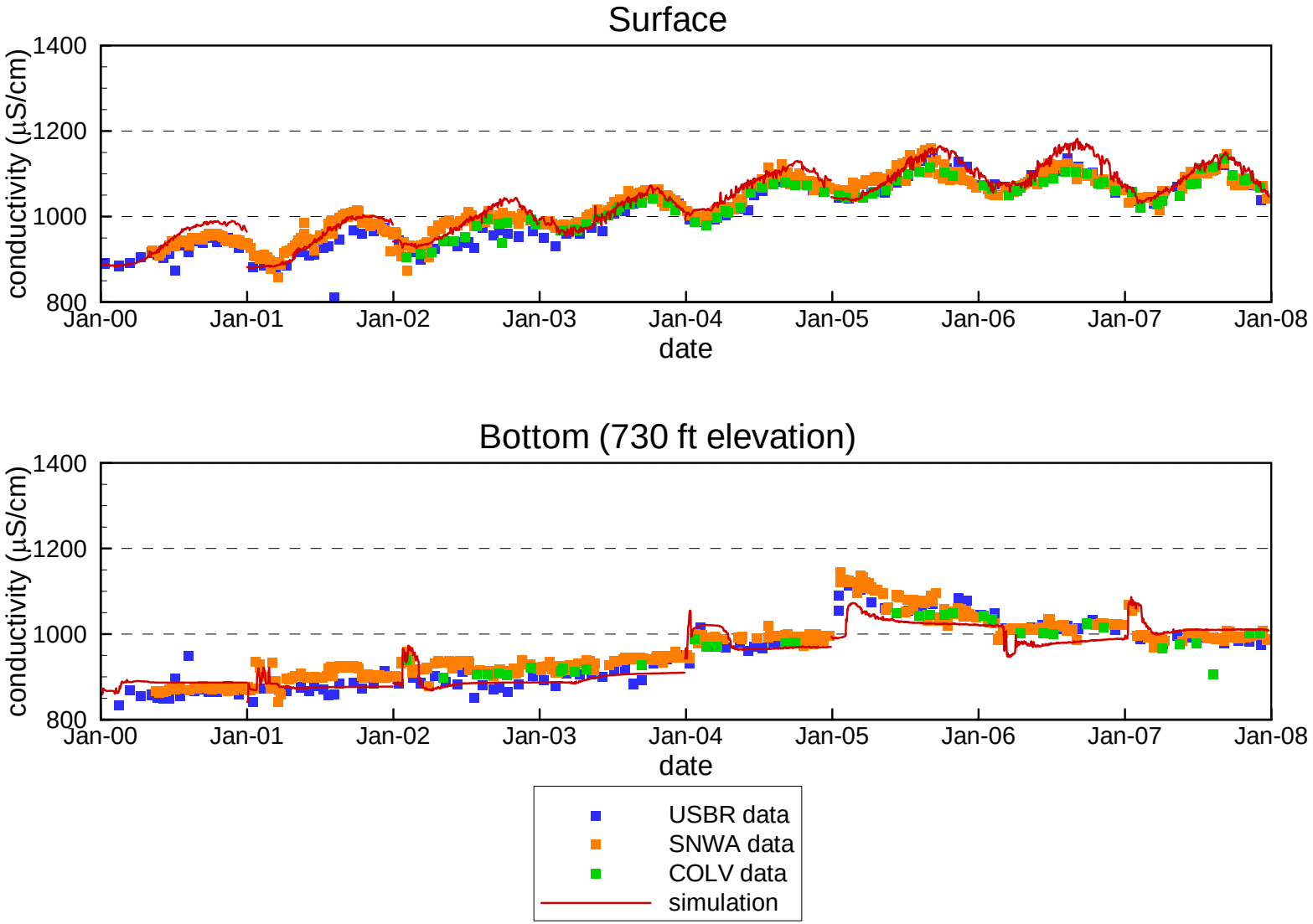

Figure 4.28

Comparison of Measured and Simulated Conductivity at SNWA Intakes #1 and #2

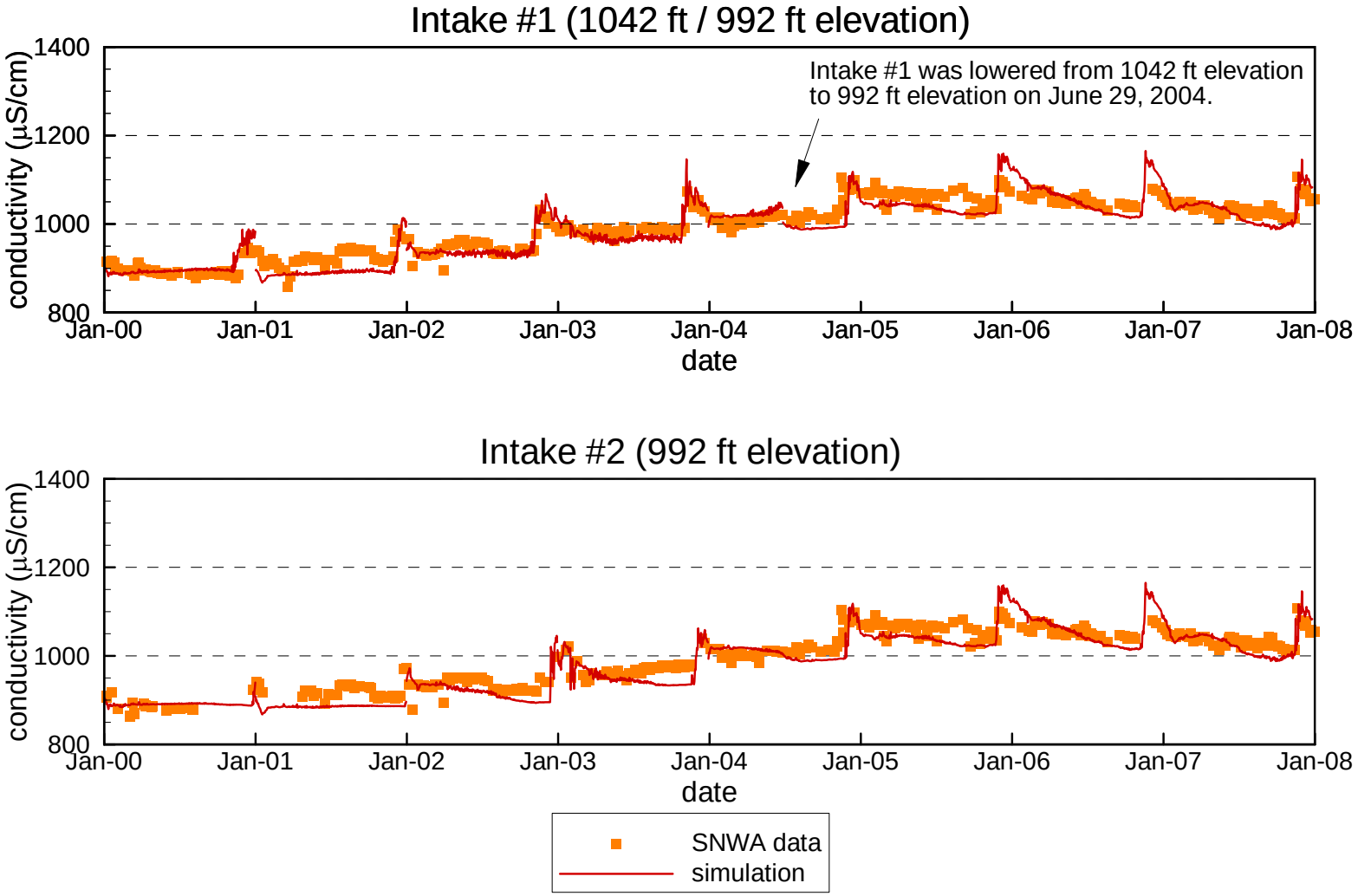

Figure 4.29

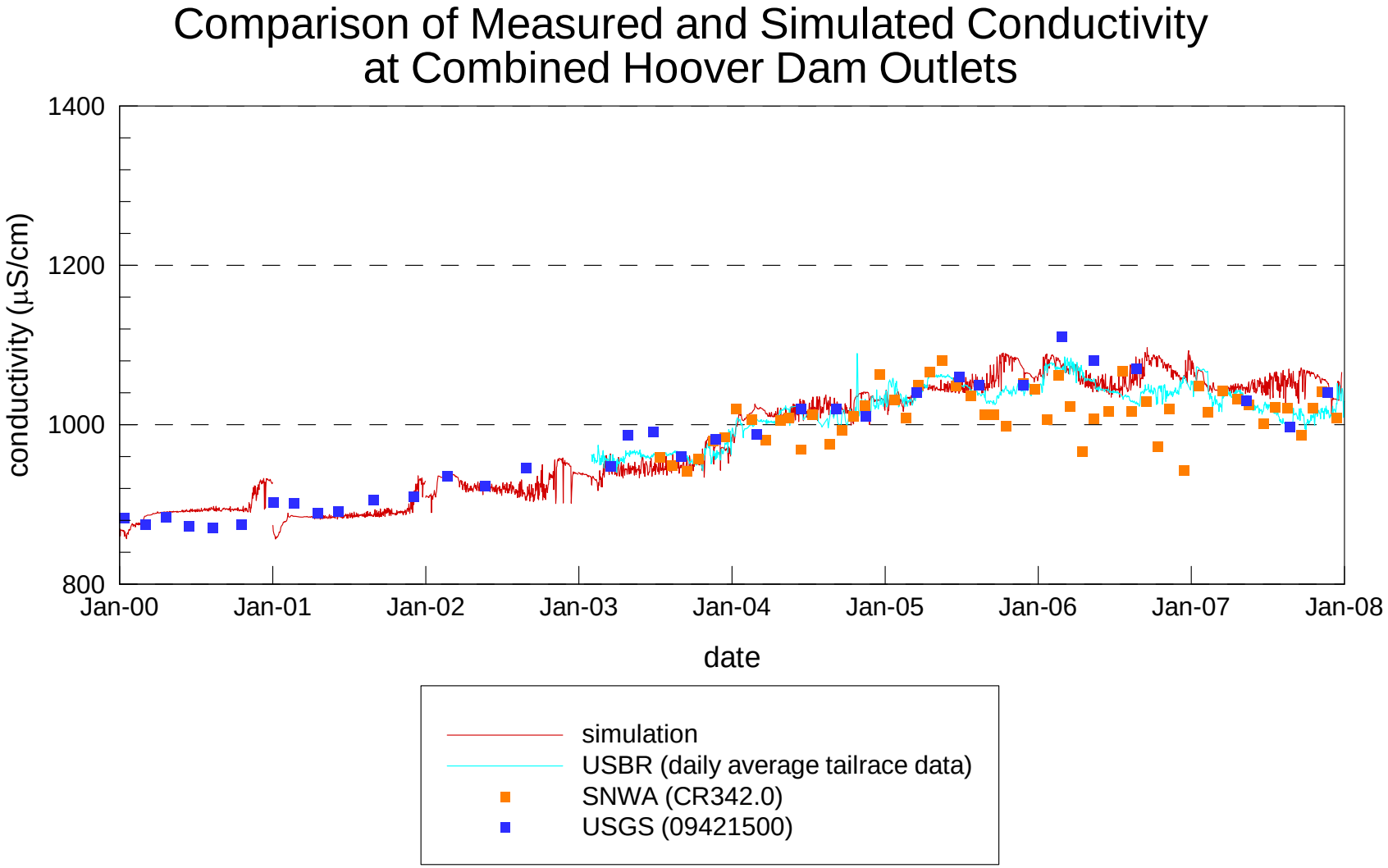
Comparison of Measured and Simulated Conductivity
at Combined Hoover Dam Outlets
conductivity (µS/cm)
1400
1200
1000
800
Jan-00
Jan-01
Jan-02
Jan-03
Jan-04
Jan-05
Jan-06
Jan-07
Jan-08
date
simulation
USBR (daily average tailrace data)
SNWA (CR342.0)
USGS (09421500)

Figure 4.30

Comparison of Measured and Simulated Perchlorate at Station LVB3.5

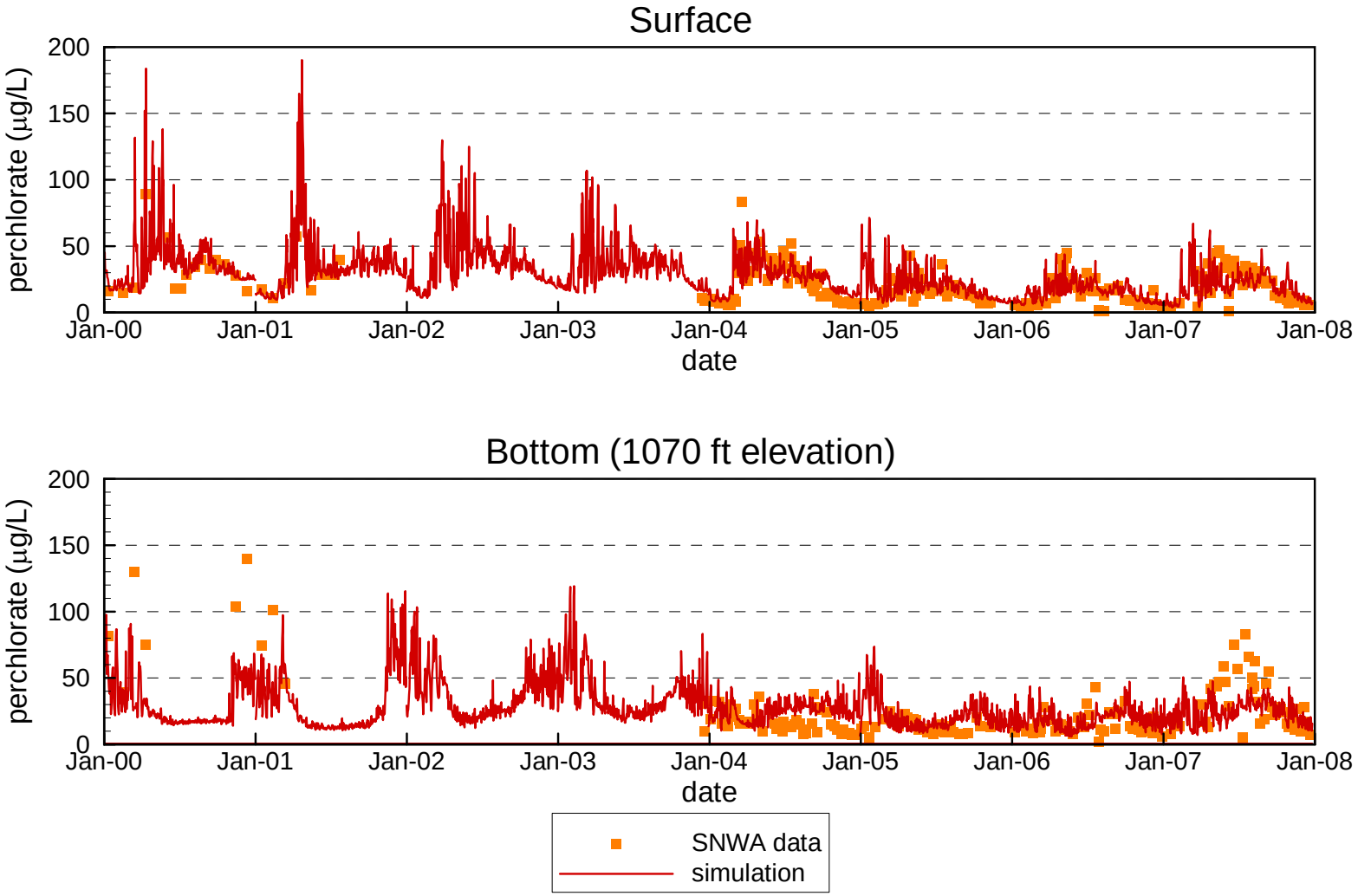

Figure 4.31

Comparison of Measured and Simulated Perchlorate at Station CR346.4

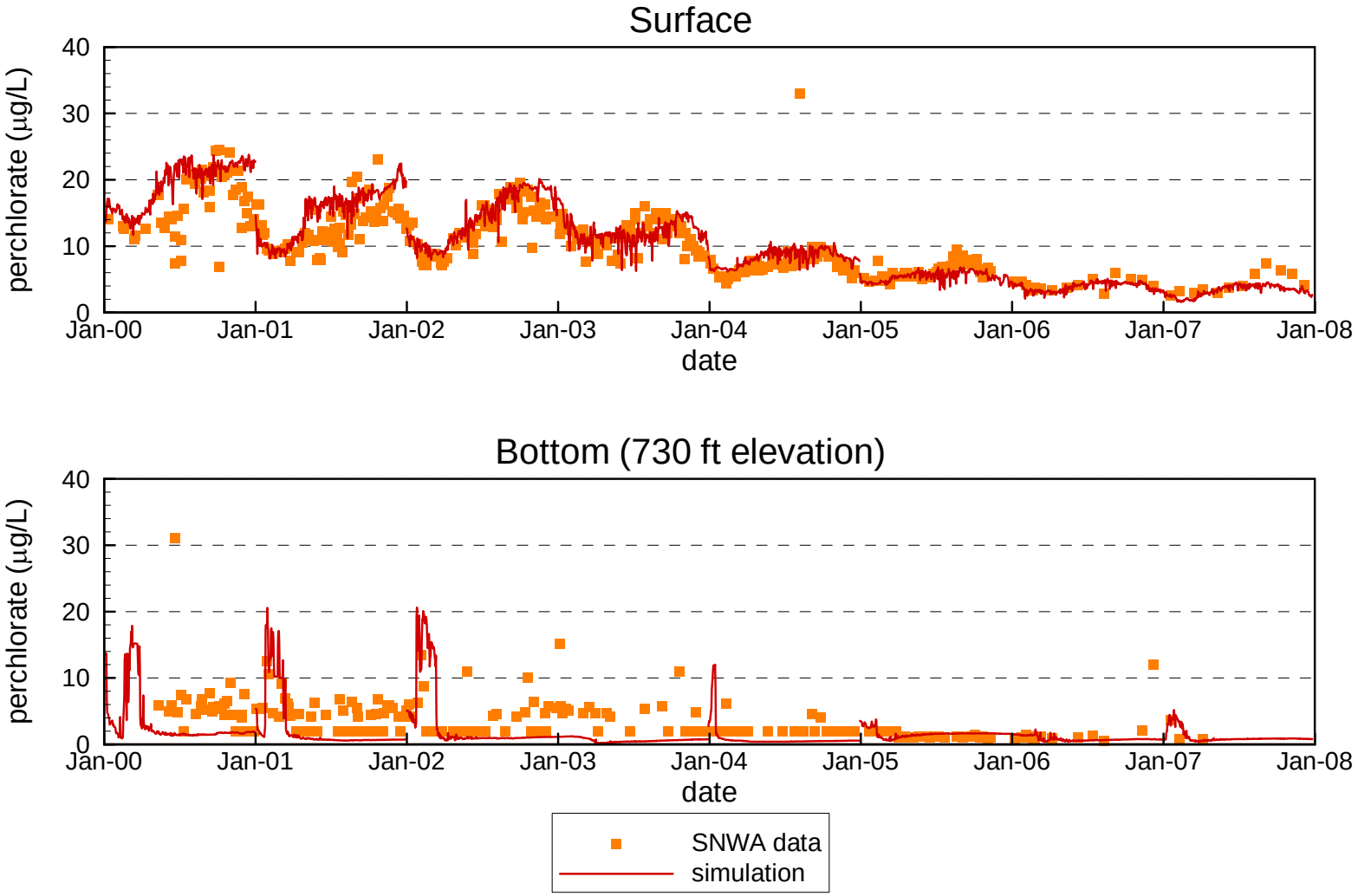

Figure 4.32

Comparison of Measured and Simulated Perchlorate at Station CR343.2

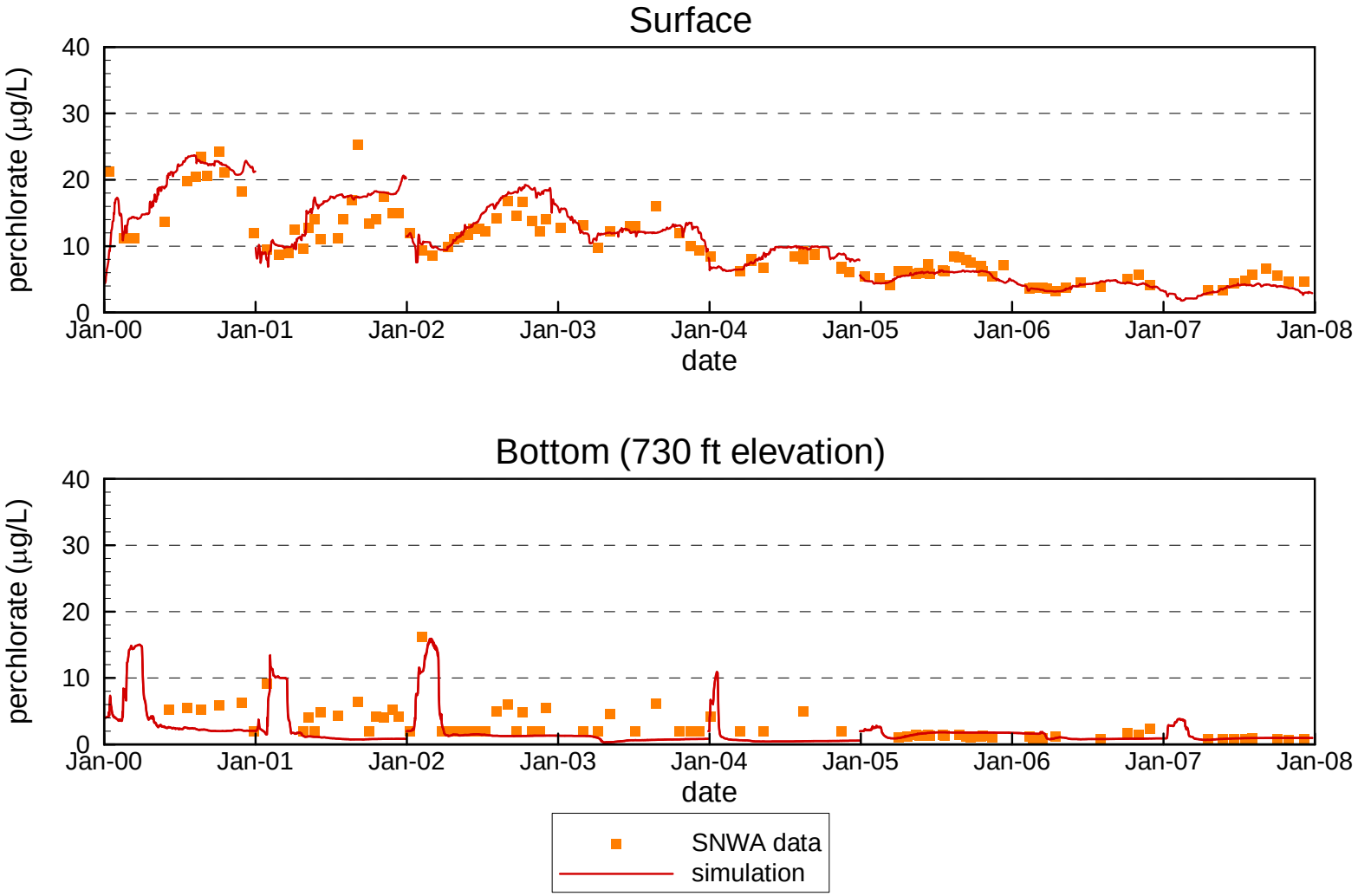

Figure 4.33

Comparison of Measured and Simulated Perchlorate at SNWA Intakes #1 and #2

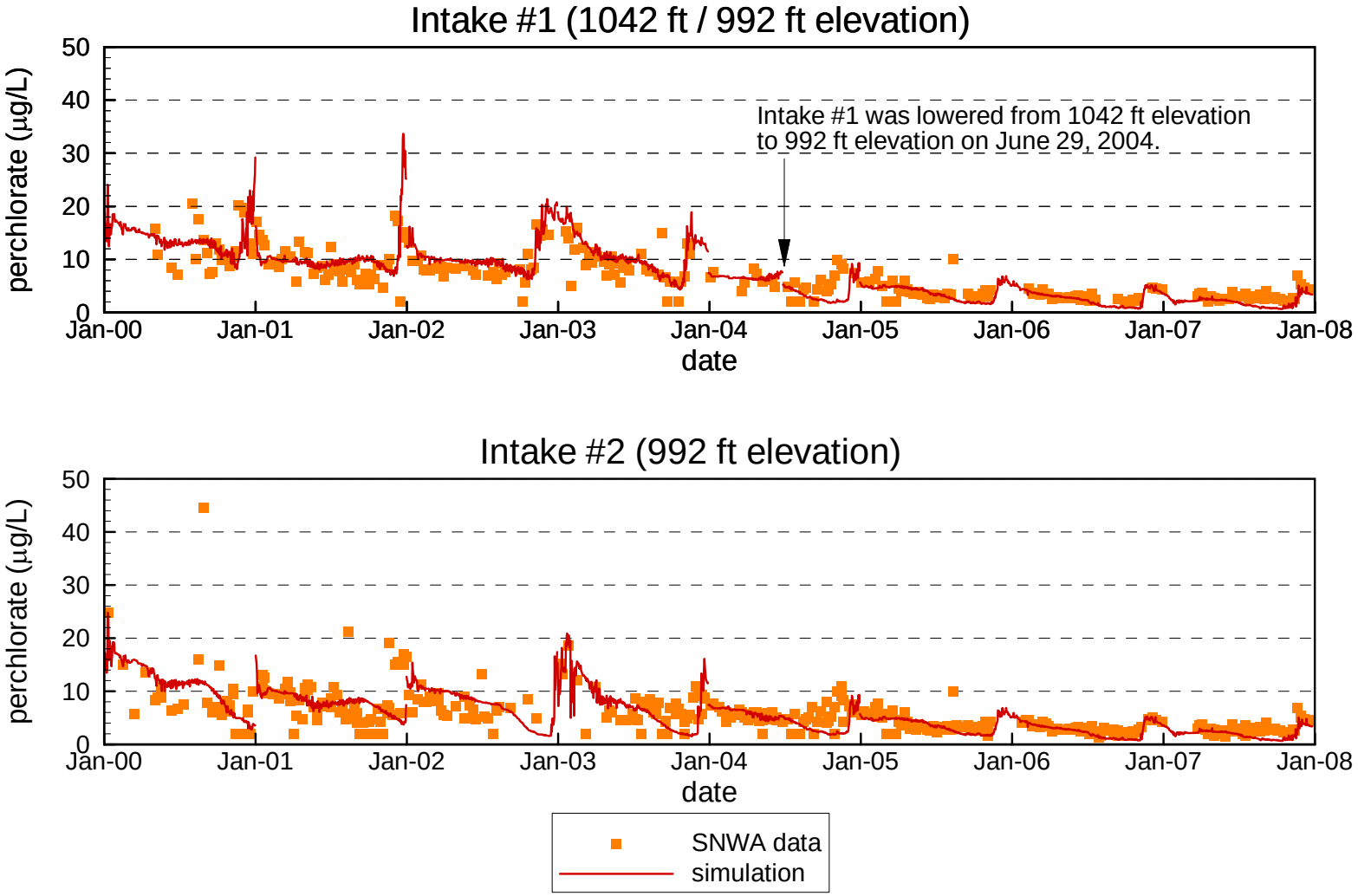

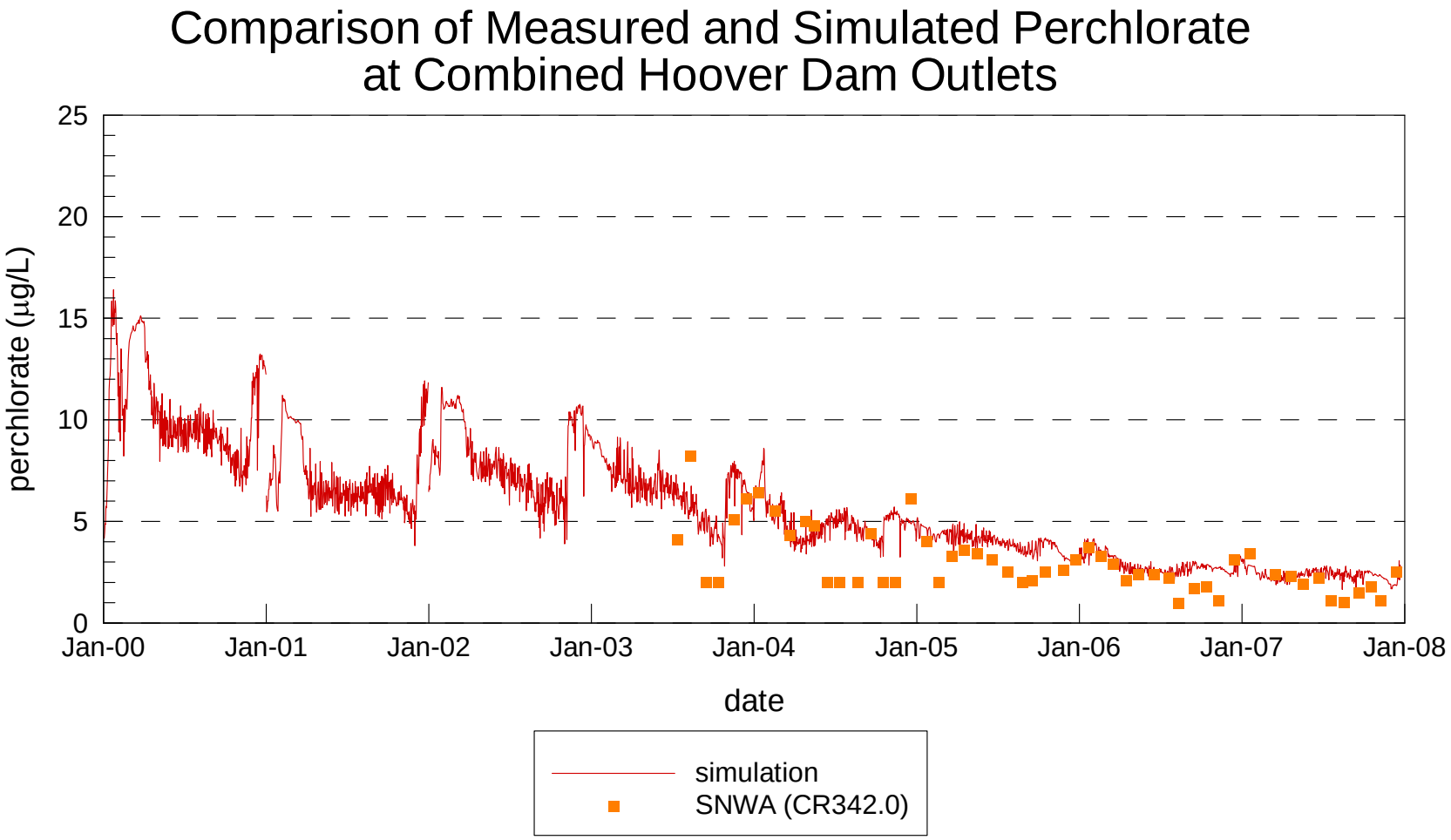
Comparison of Measured and Simulated Perchlorate
at Combined Hoover Dam Outlets
perchlorate (µg/L)
25
20
15
10
5
0
Jan-00
Jan-01
Jan-02
Jan-03
Jan-04
Jan-05
Jan-06
Jan-07
Jan-08
date
simulation
SNWA (CR342.0)

Figure 4.35

Comparison of Measured and Simulated Bromide at Station CR394.0

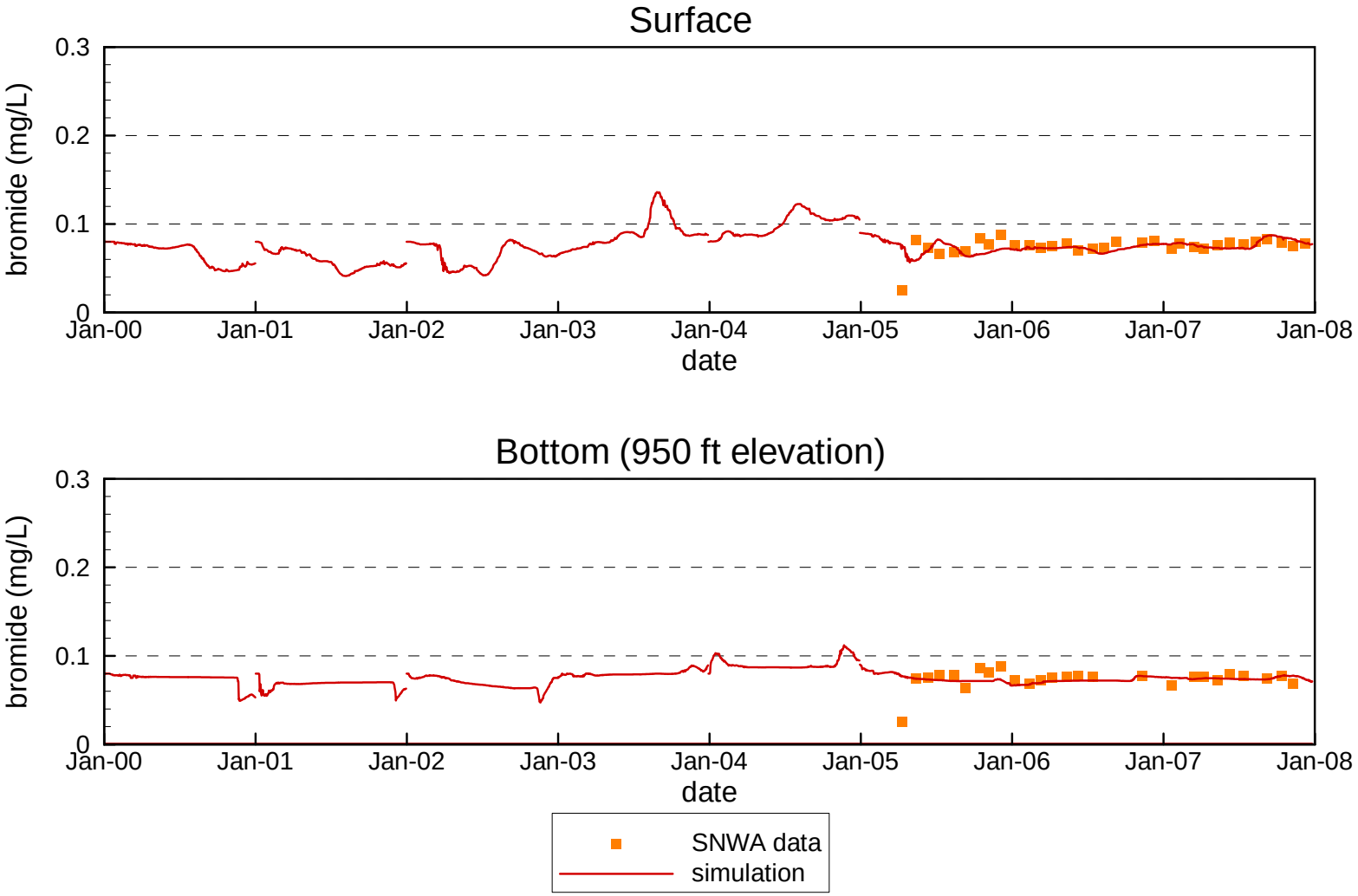

Comparison of Measured and Simulated Bromide at Station VR25.1

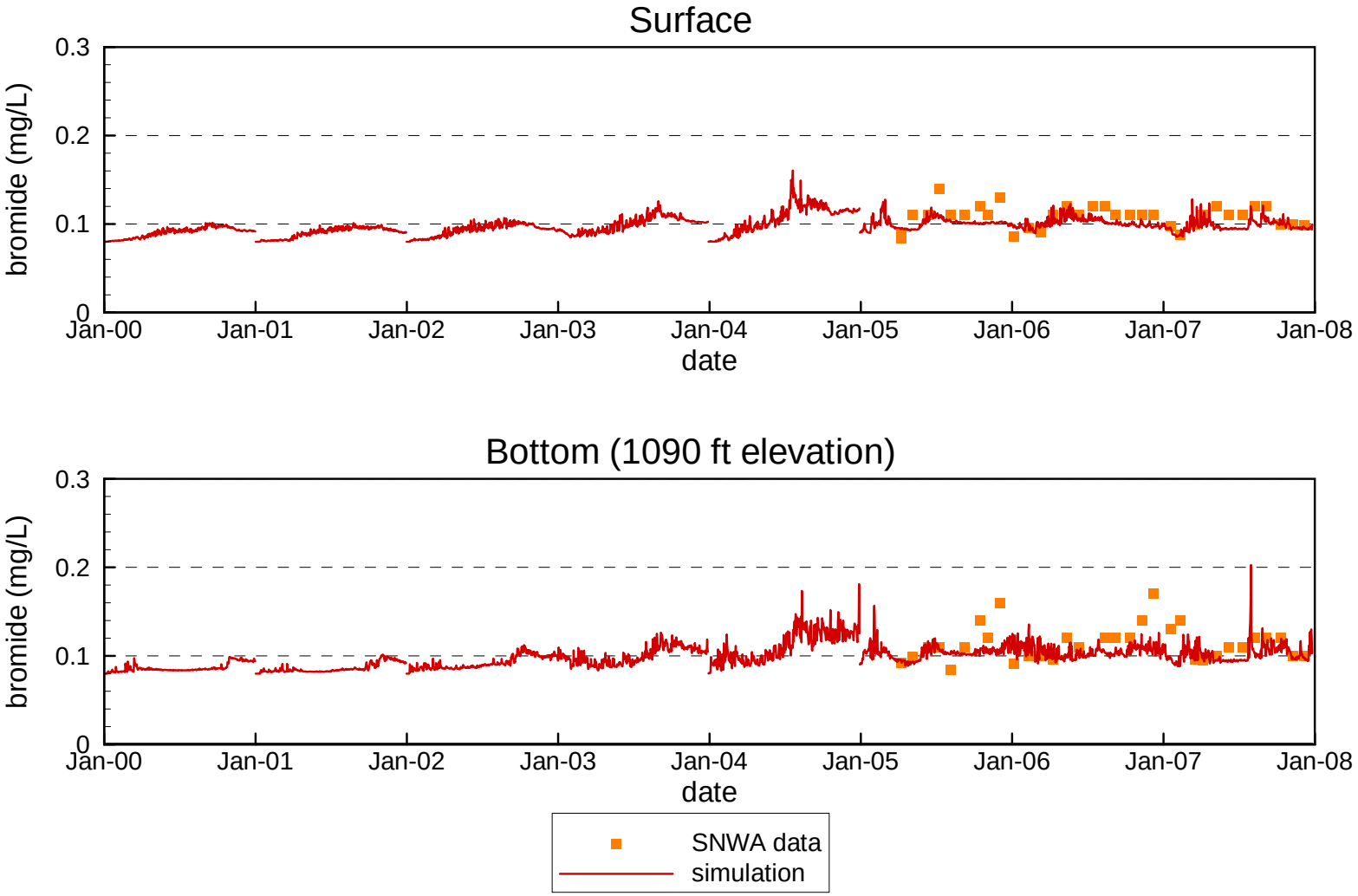

Figure 4.37

Comparison of Measured and Simulated Bromide at Station VR13.0

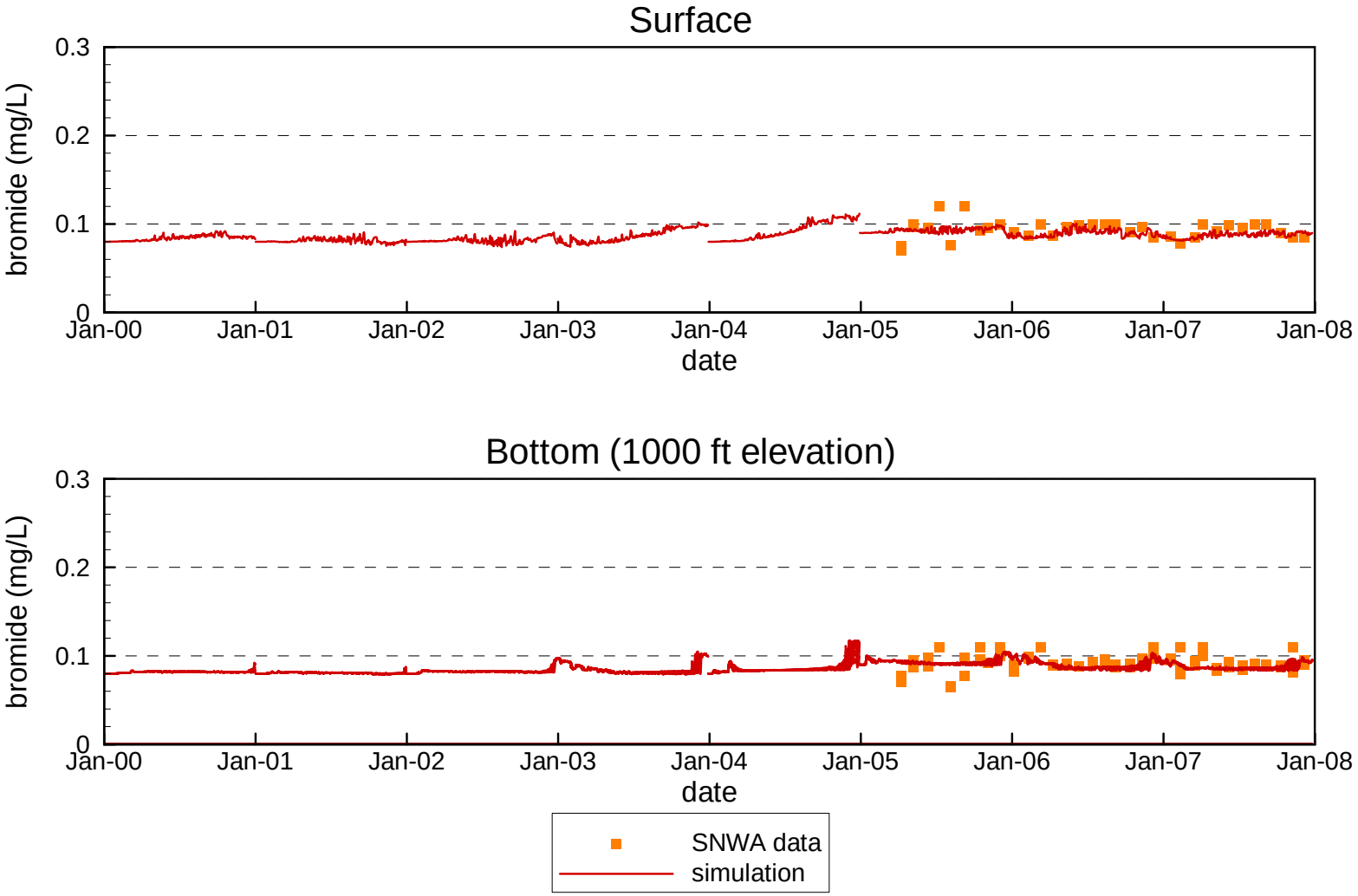

Figure 4.38

Comparison of Measured and Simulated Bromide at Station CR360.7

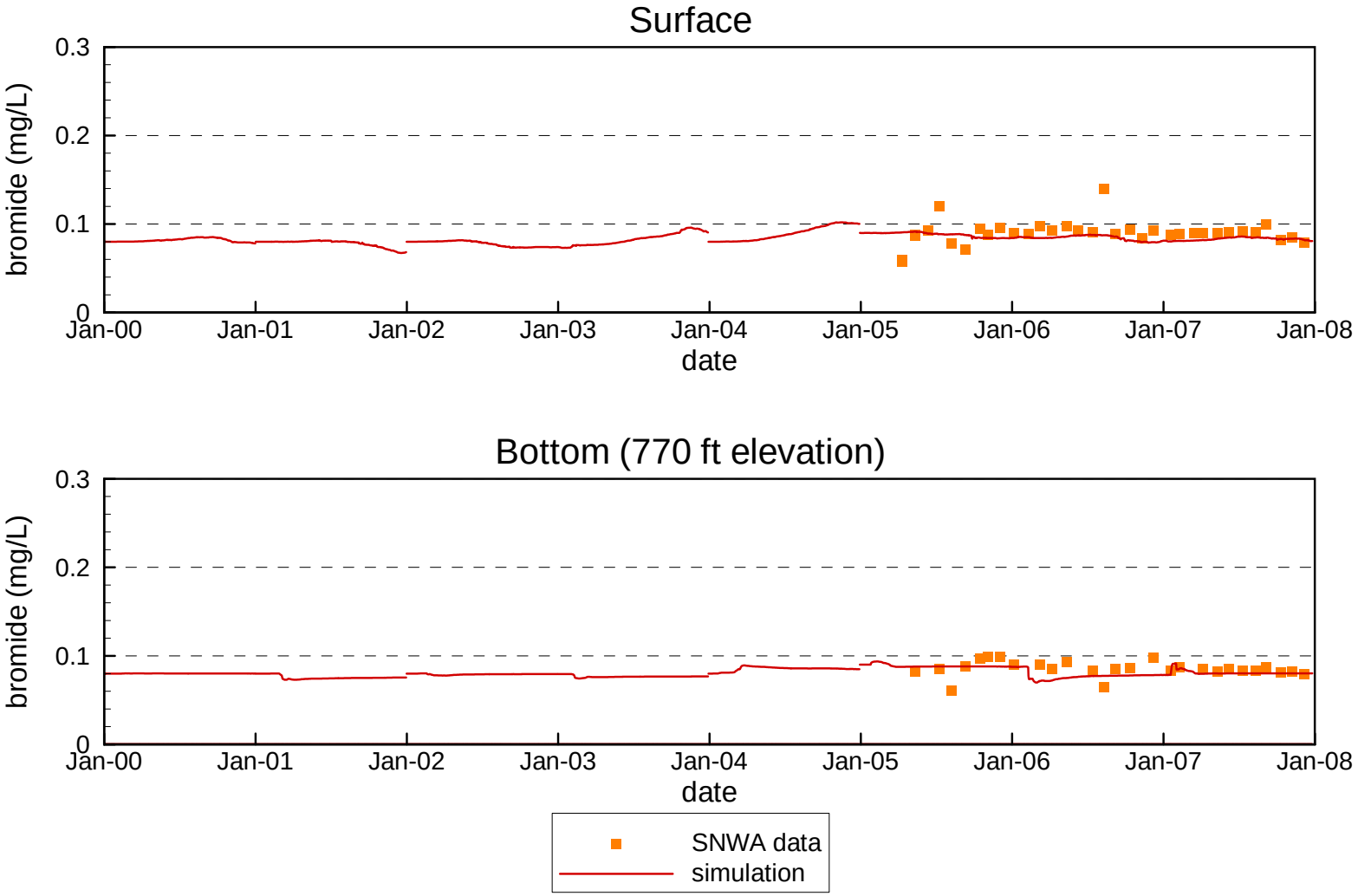

Comparison of Measured and Simulated Bromide at Station LVB3.5

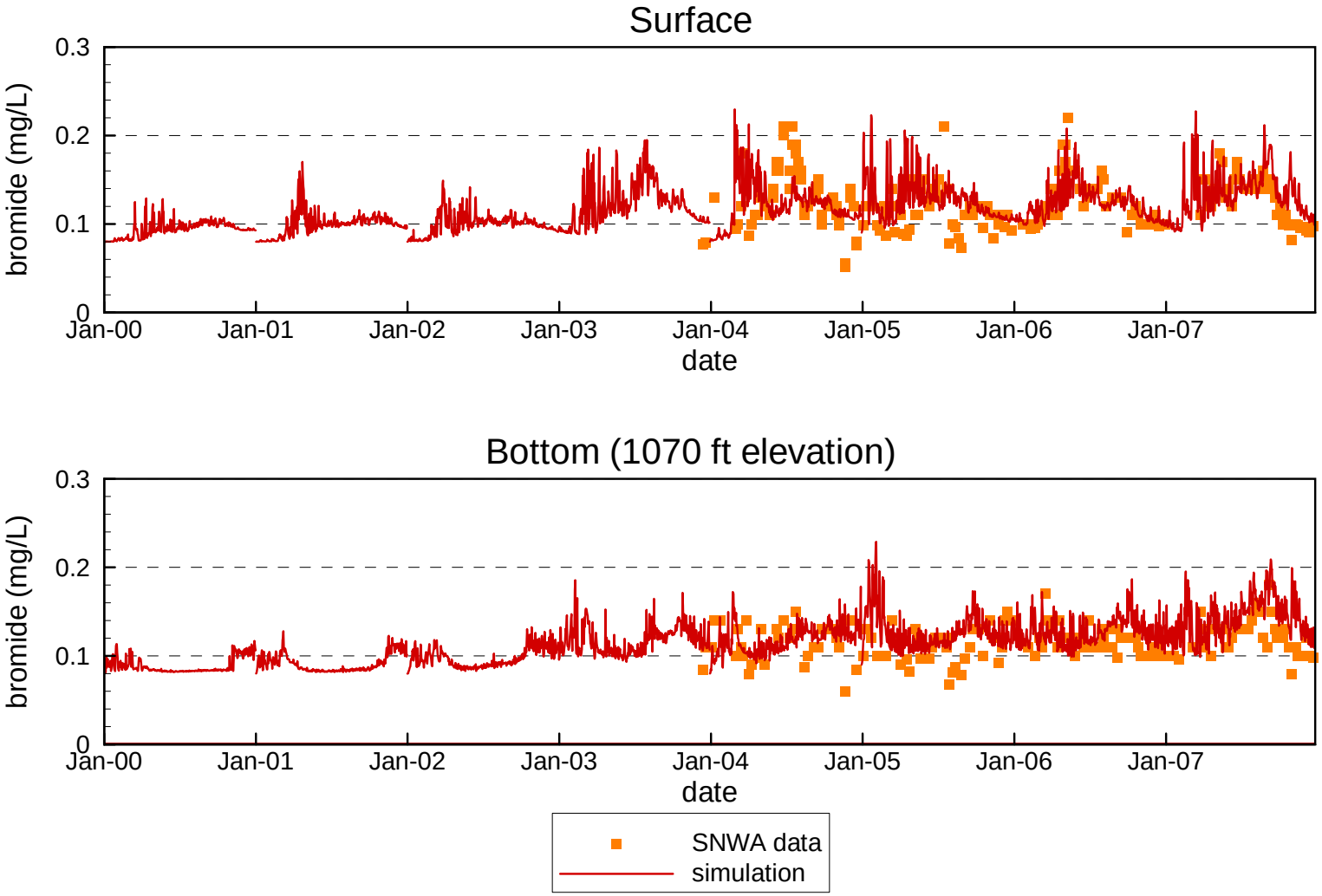

Figure 4.40

Comparison of Measured and Simulated Bromide at Station CR346.4

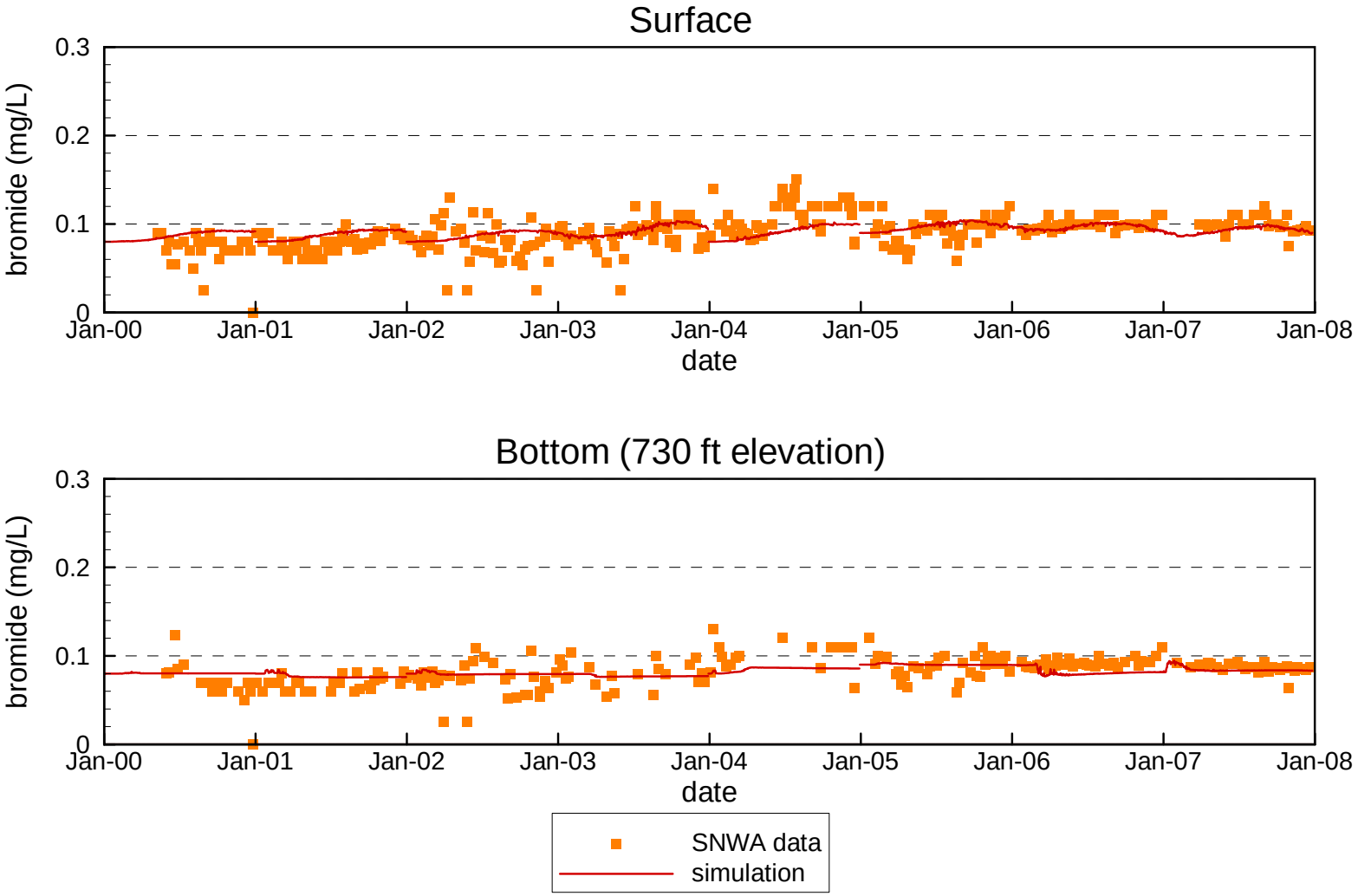

Figure 4.41

Comparison of Measured and Simulated Bromide at SNWA Intakes #1 and #2

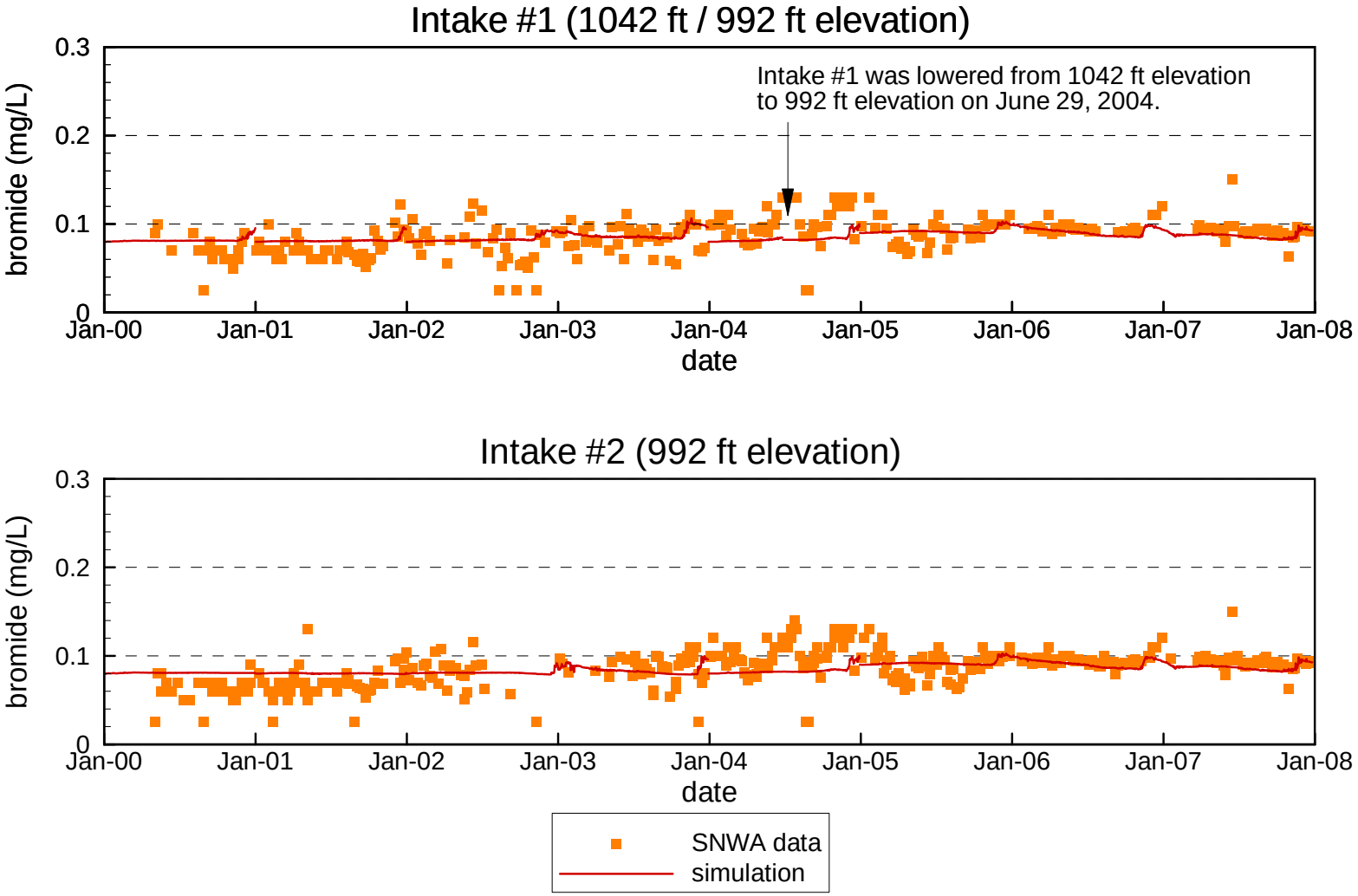

Figure 4.42

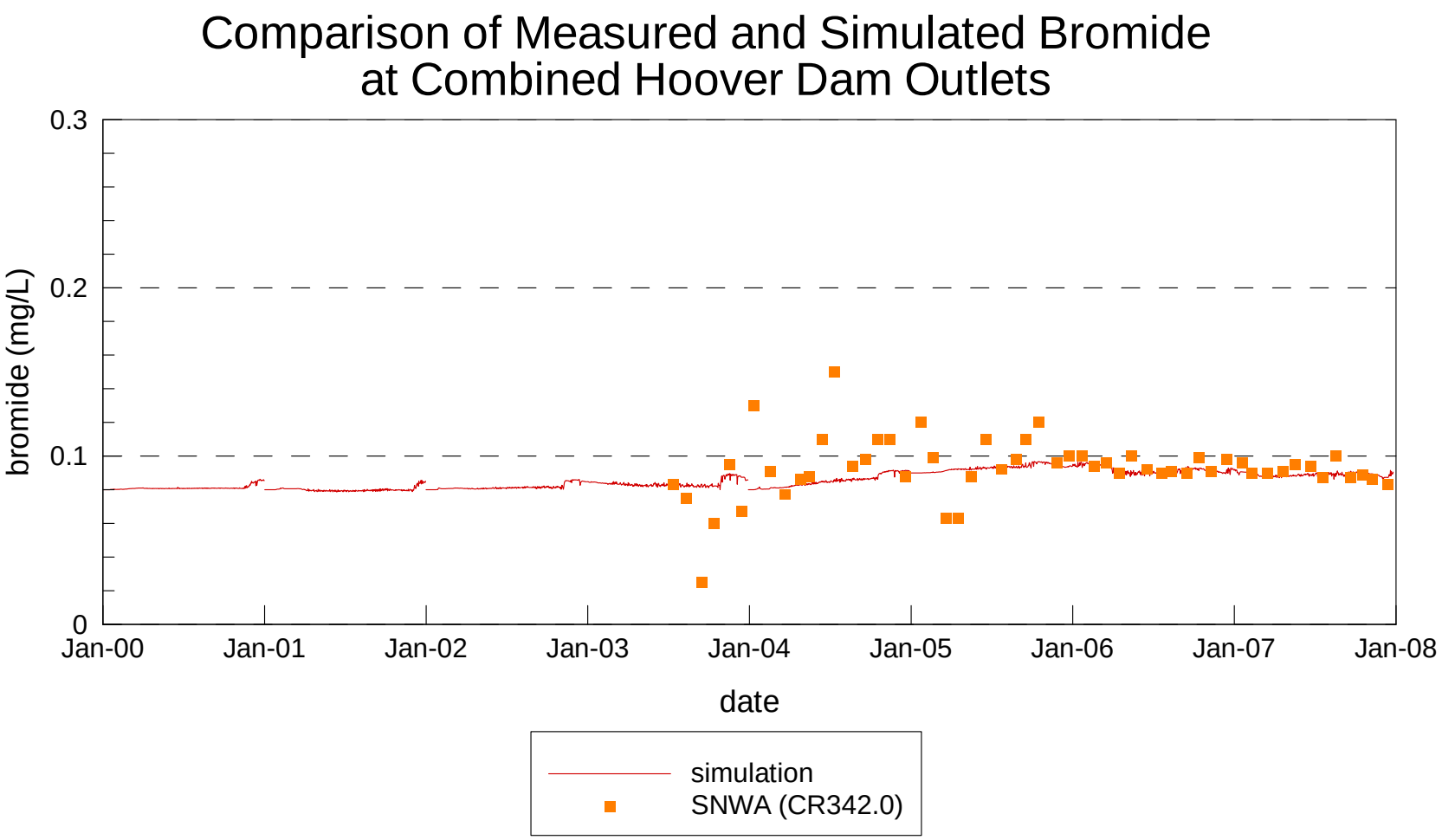
Comparison of Measured and Simulated Bromide
at Combined Hoover Dam Outlets
bromide (mg/L)
0.3
0.2
0.1
0
Jan-00
Jan-01
Jan-02
Jan-03
Jan-04
Jan-05
Jan-06
Jan-07
Jan-08
date
simulation
SNWA (CR342.0)

Figure 4.43

Comparison of Measured and Simulated Chlorophyll a at Station CR394.0

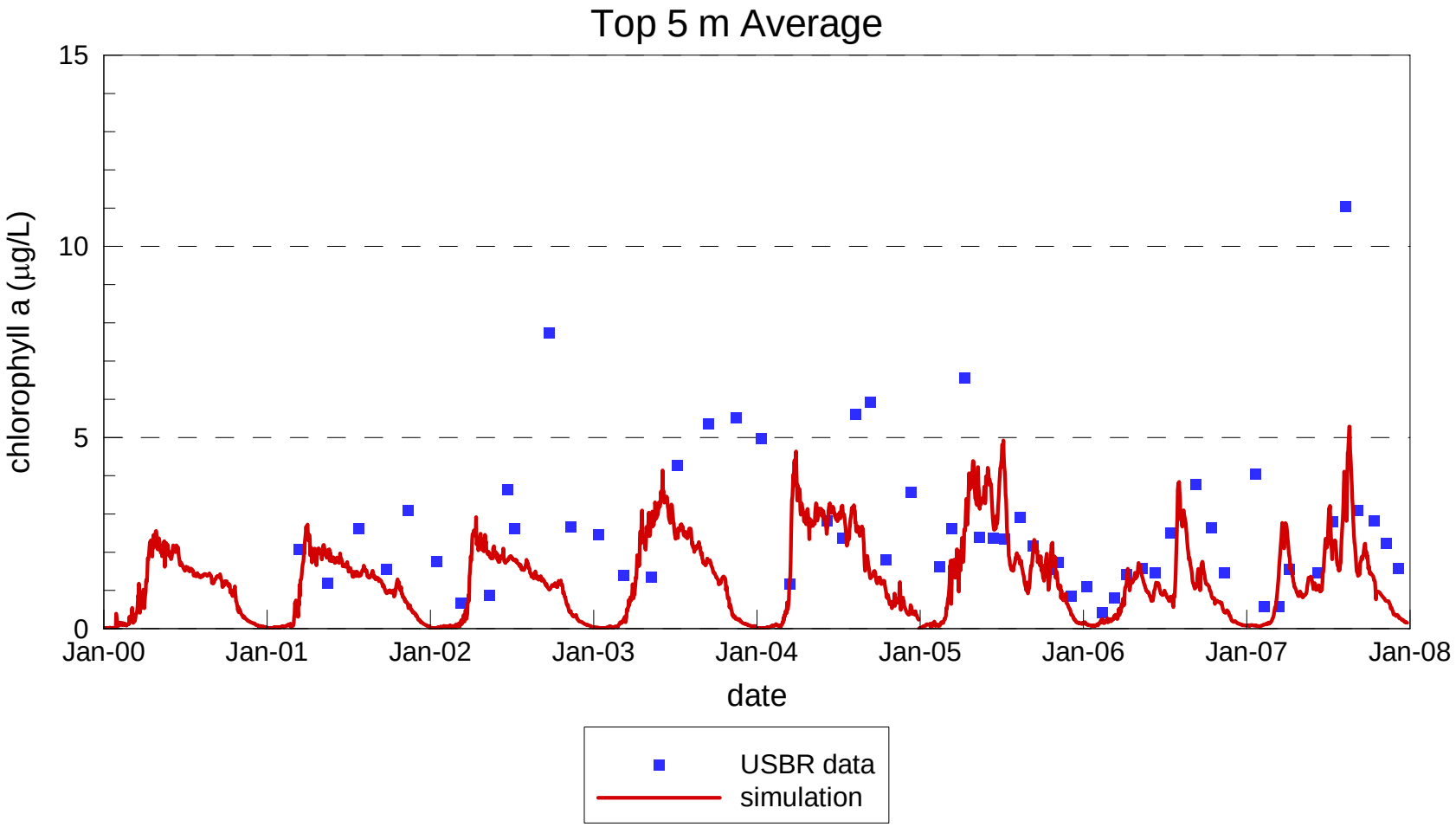

Figure 4.44

Comparison of Measured and Simulated Chlorophyll a at Station VR25.1

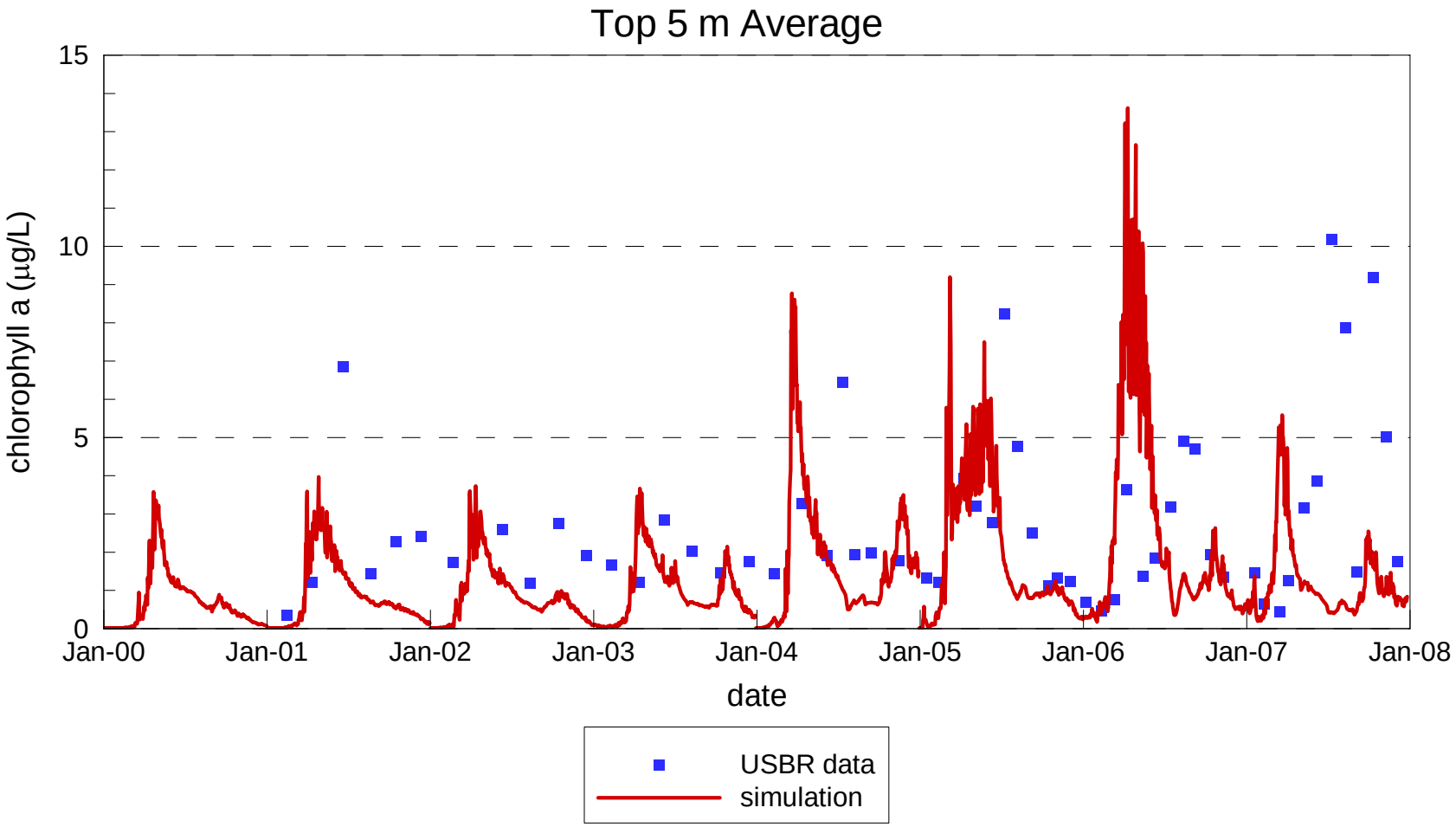

Figure 4.45

Comparison of Measured and Simulated Chlorophyll a at Stations VR12.9 / VR13.0

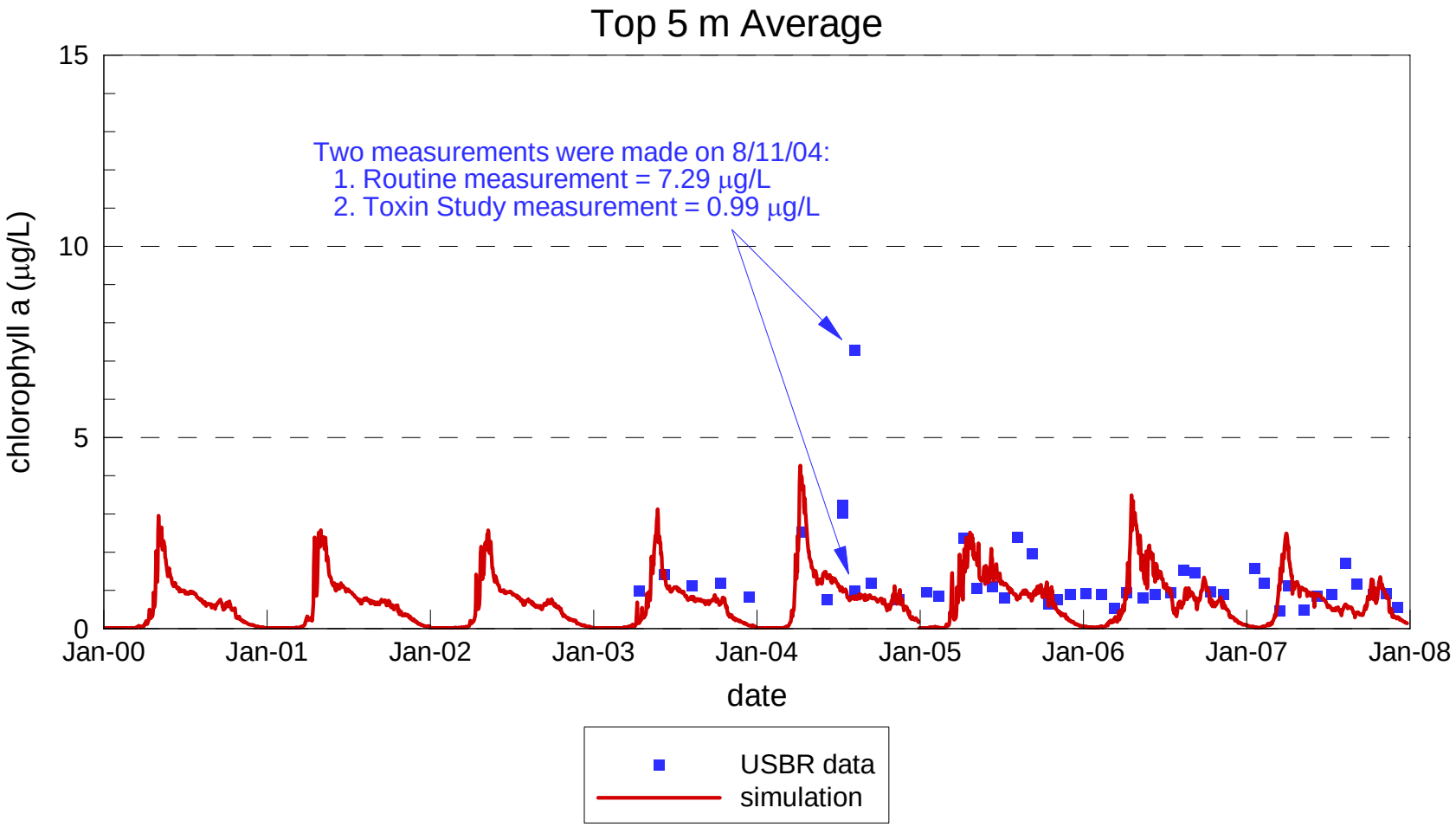

Figure 4.46

Comparison of Measured and Simulated Chlorophyll a at Station CR360.7

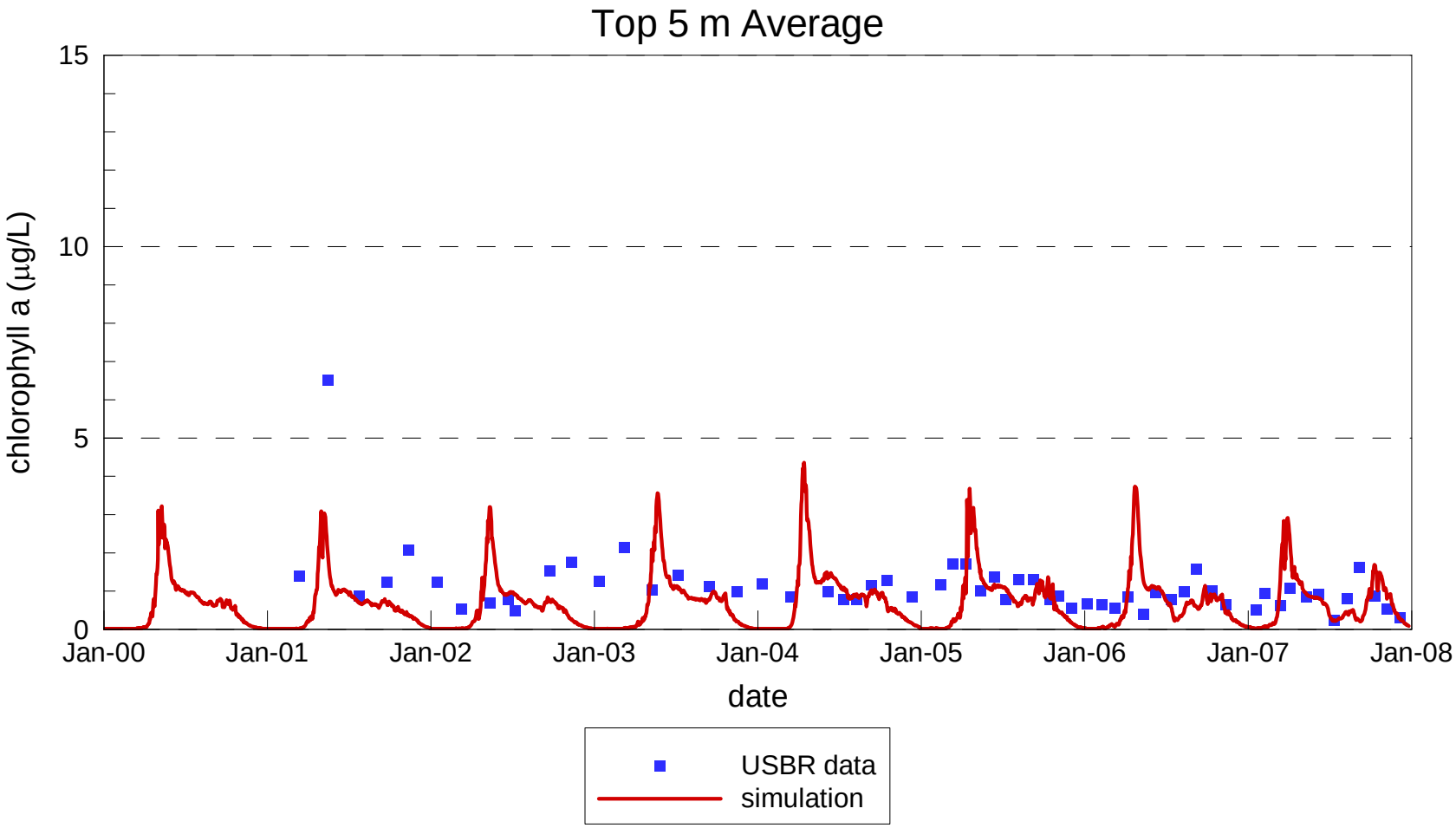

Figure 4.47

Comparison of Measured and Simulated Chlorophyll a at Station LVB3.5

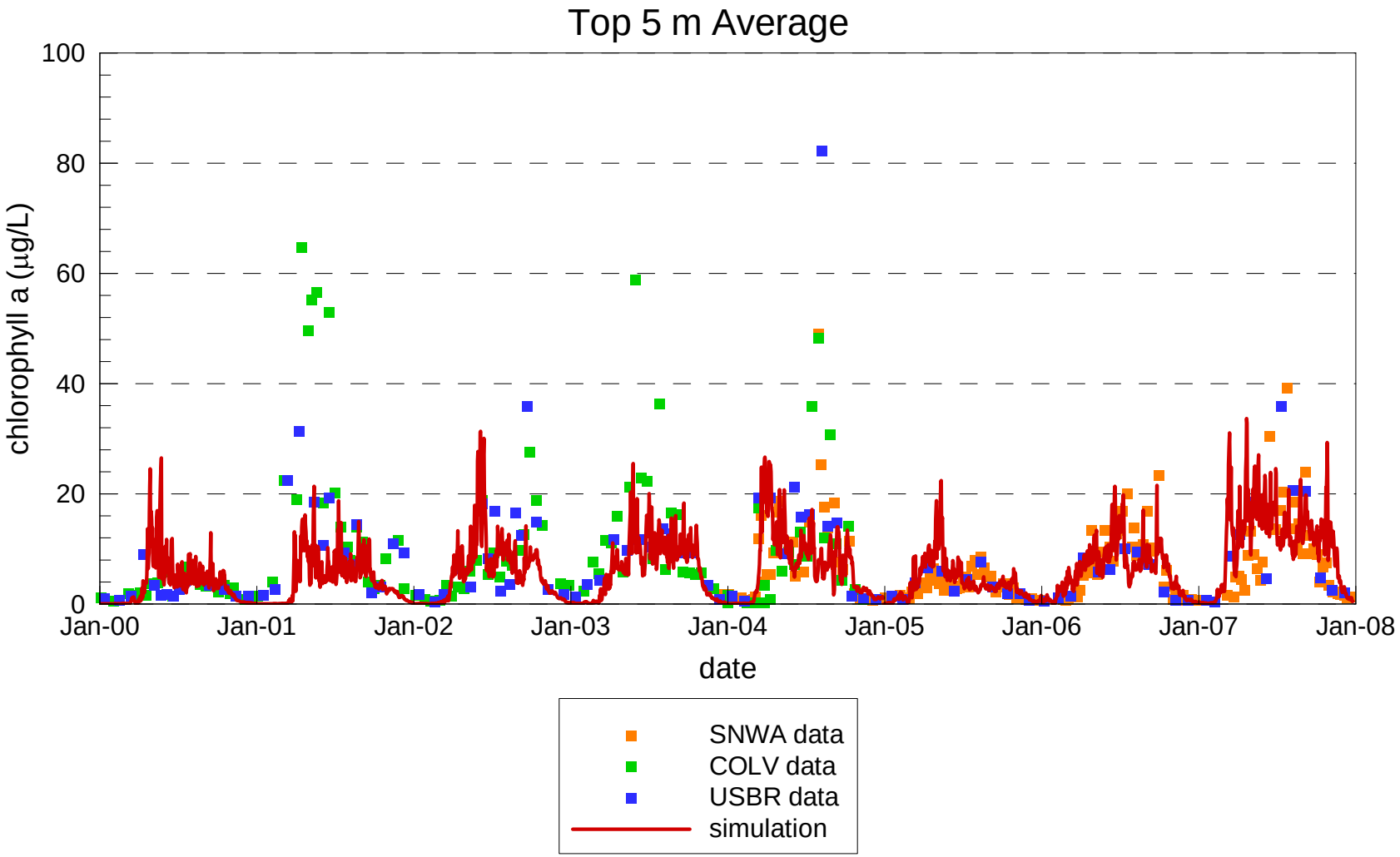

Figure 4.48

Comparison of Measured and Simulated Chlorophyll a at Station CR346.4

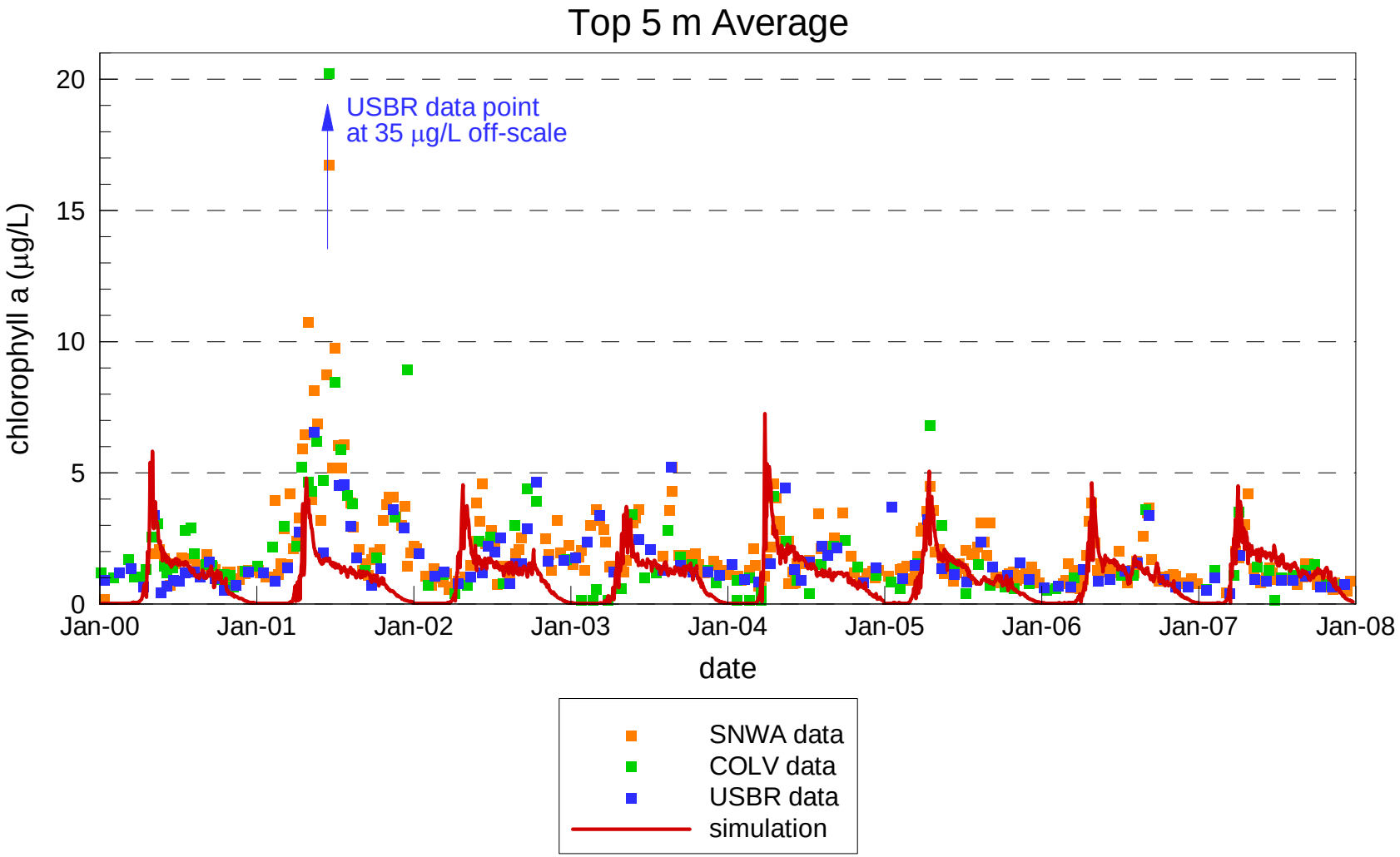

Figure 4.49

2000 – 2007 Simulated versus Measured Chlorophyll a

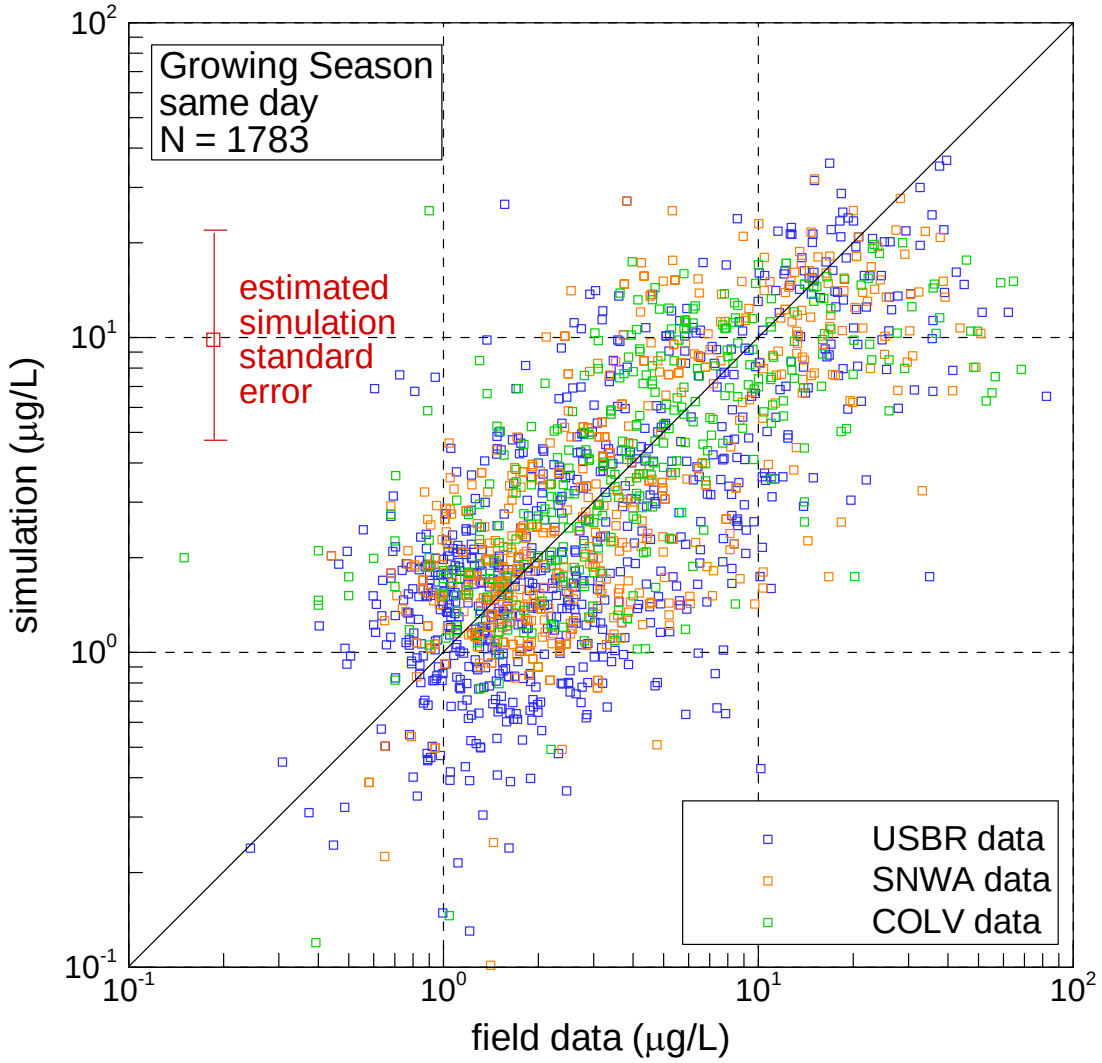

Figure 4.50

2000 – 2007 Simulated versus Measured Chlorophyll a

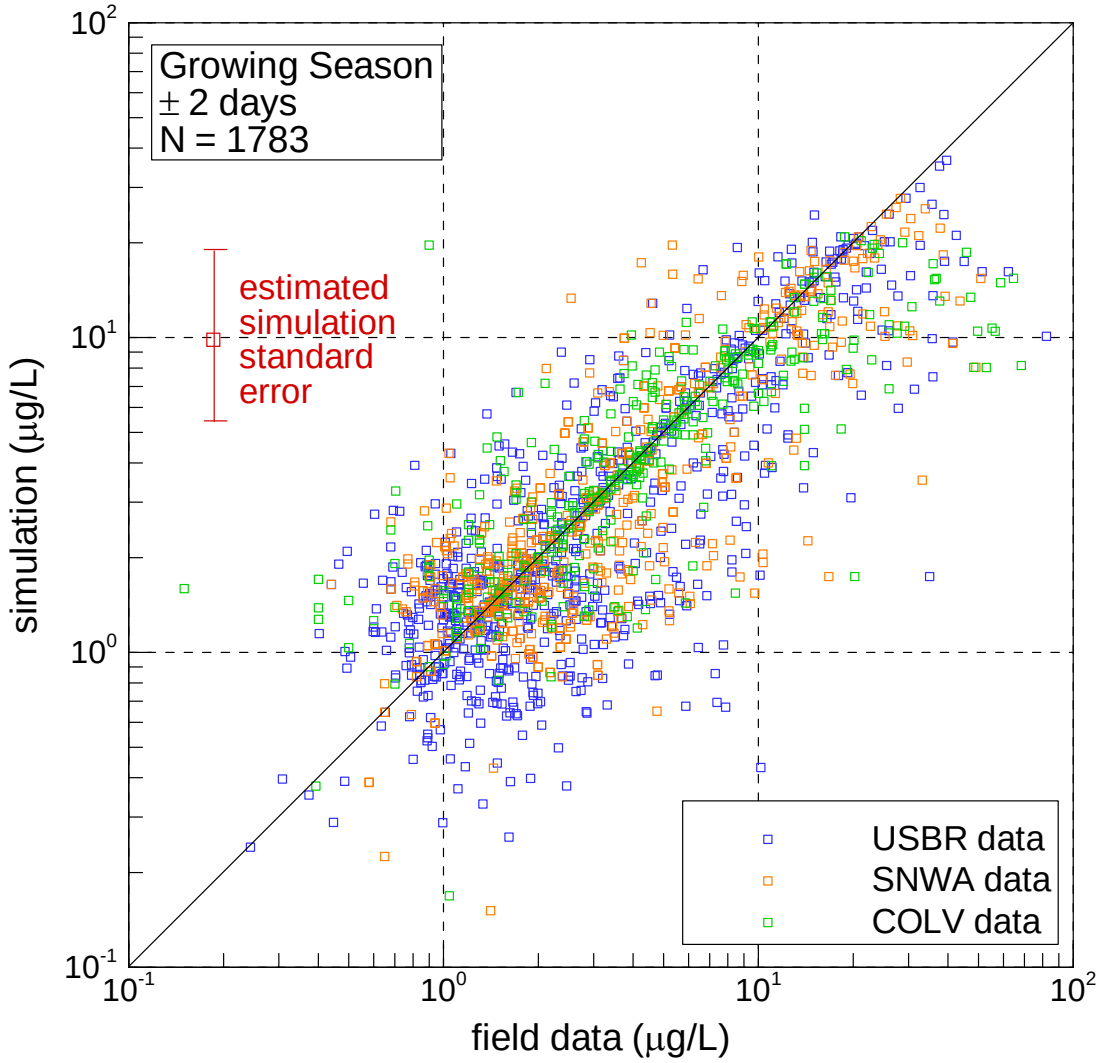

Figure 4.51

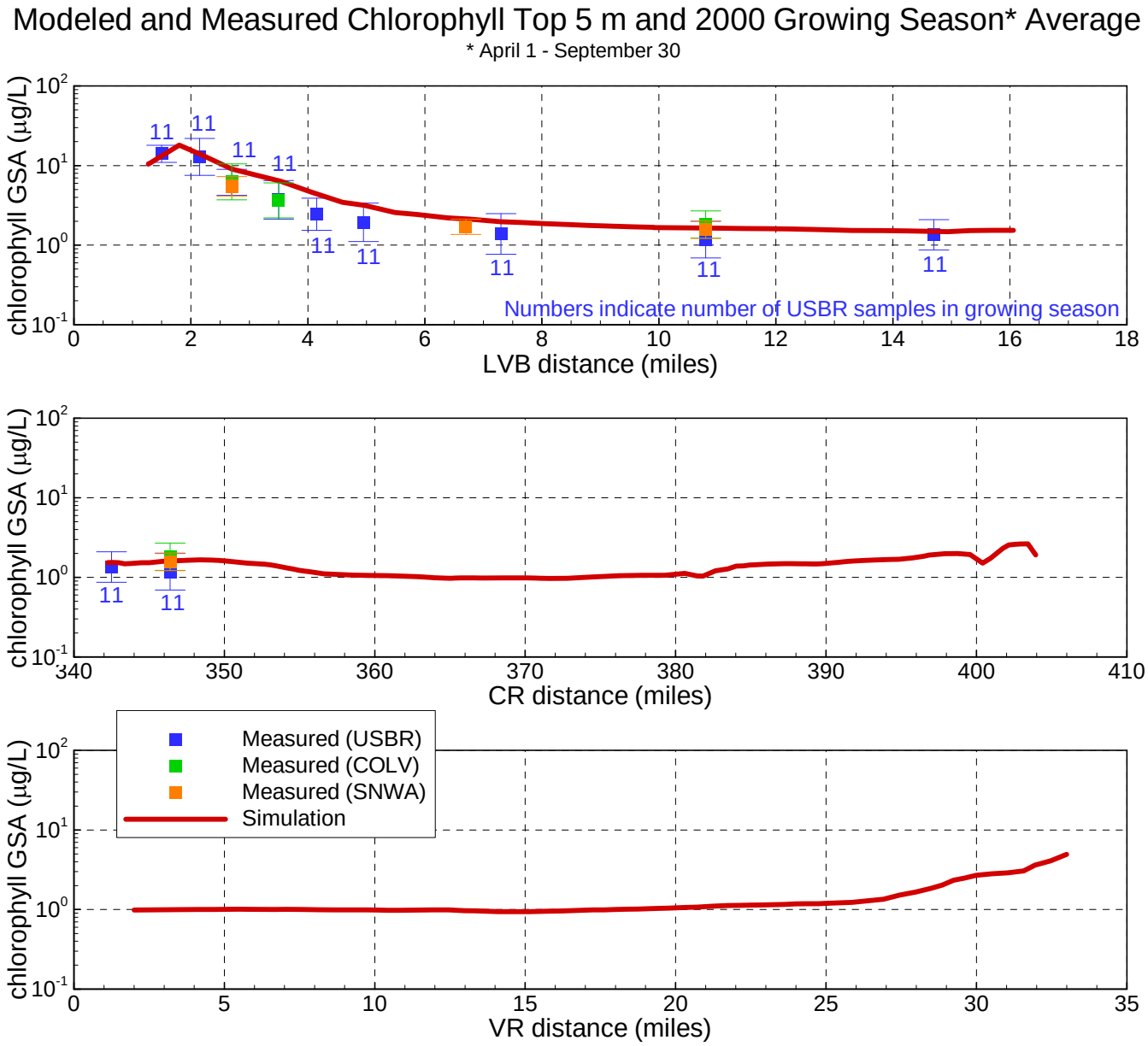

Ch4_Figures.ppt
FSI V064081 & V084015
December 9, 2010

Figure 4.52

FLOW SCIENCE

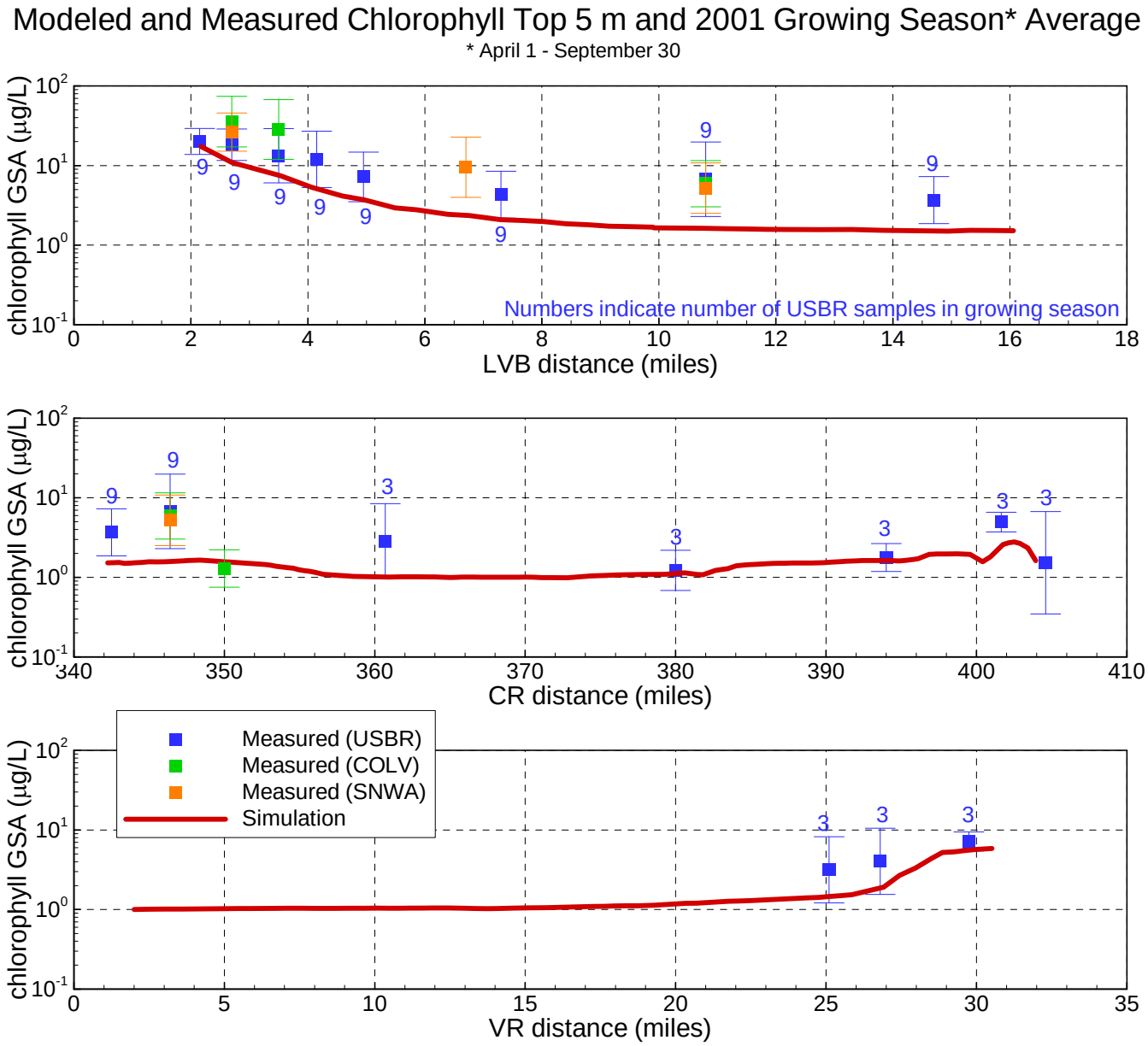

Ch4_Figures.ppt
FSI V064081 & V084015
December 9, 2010

Figure 4.53

FLOW SCIENCE

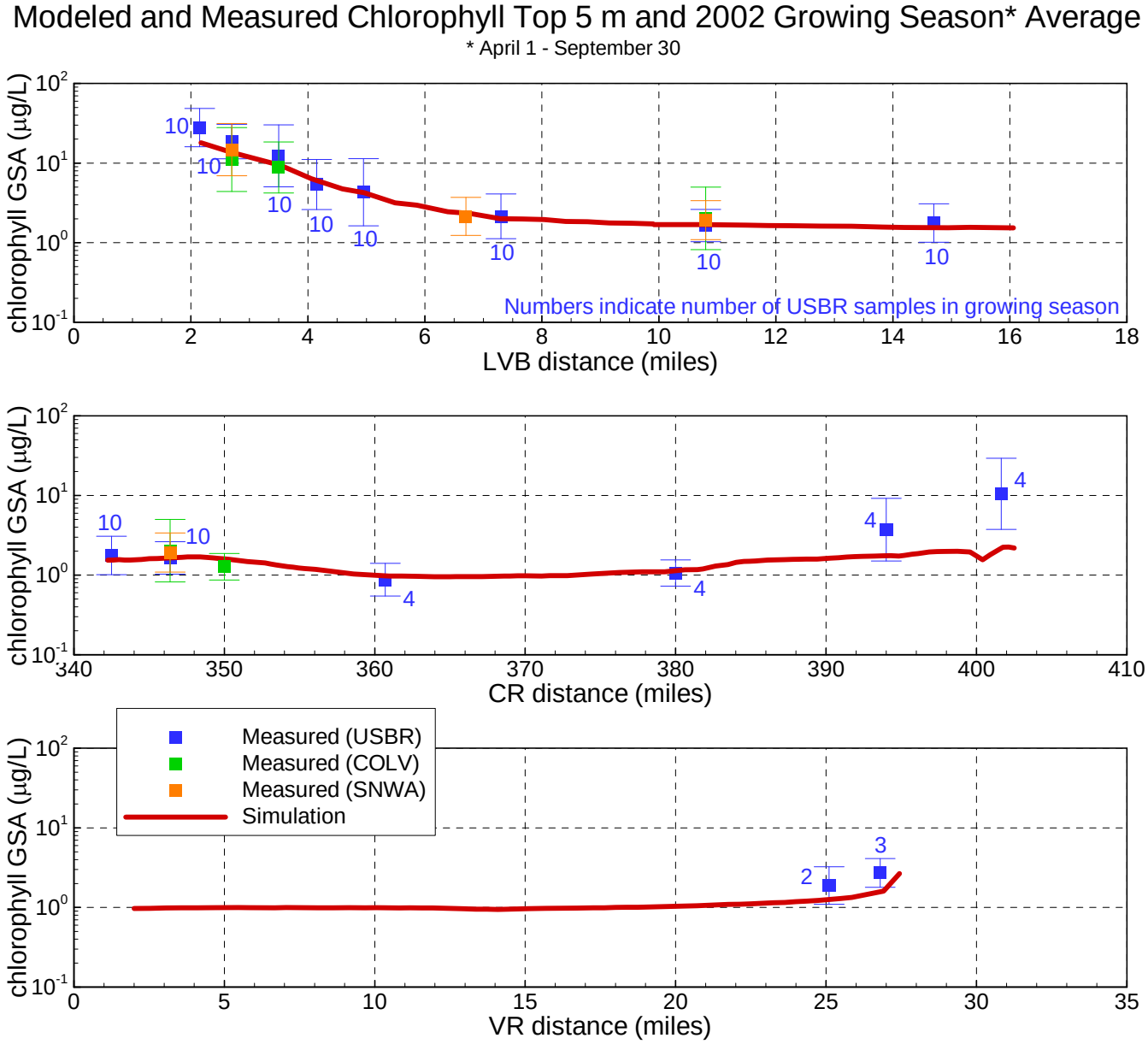

Ch4_Figures.ppt
FSI V064081 & V084015
December 9, 2010

Figure 4.54

FLOW SCIENCE

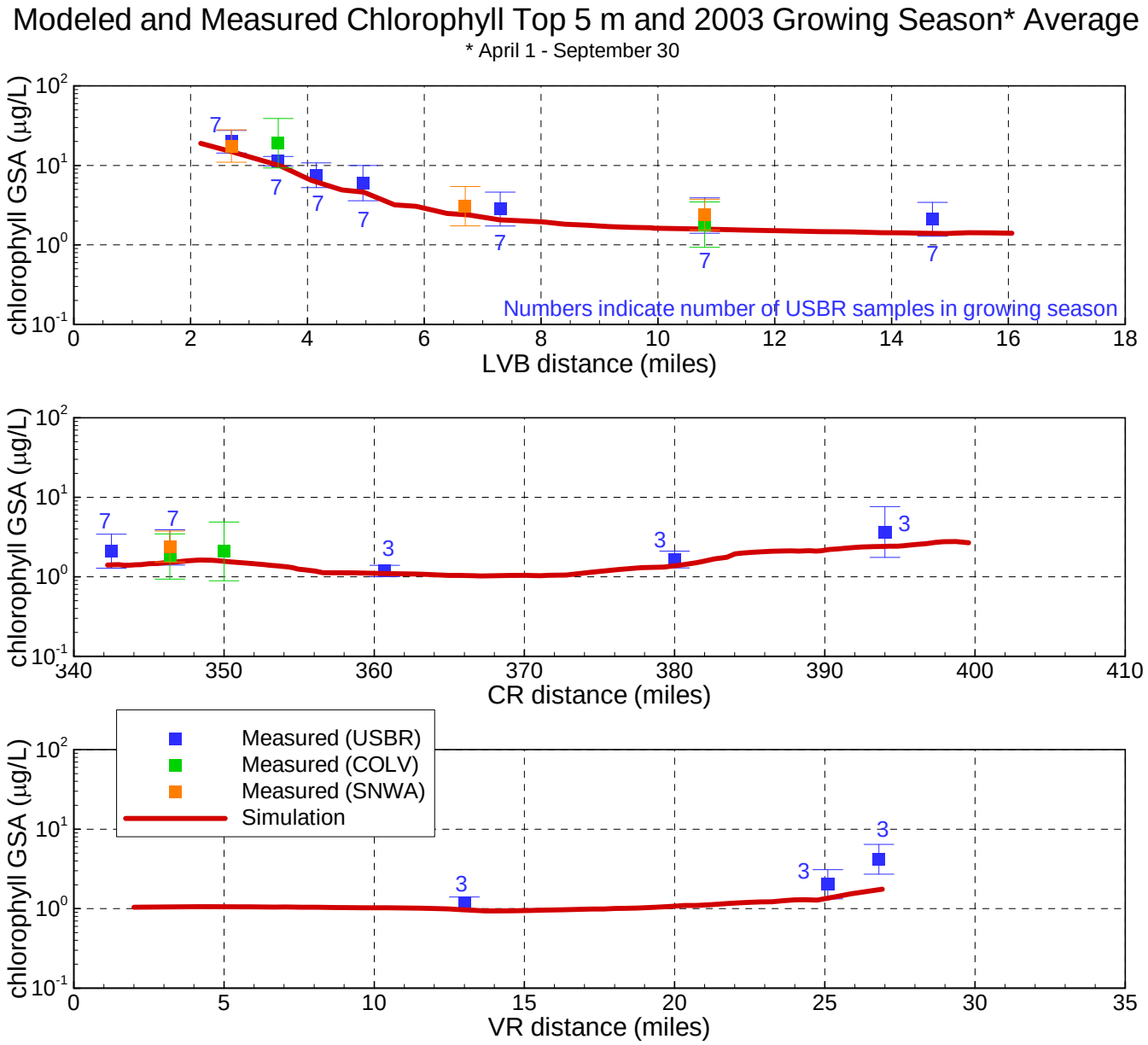

Ch4_Figures.ppt
FSI V064081 & V084015
December 9, 2010

Figure 4.55

FLOW SCIENCE

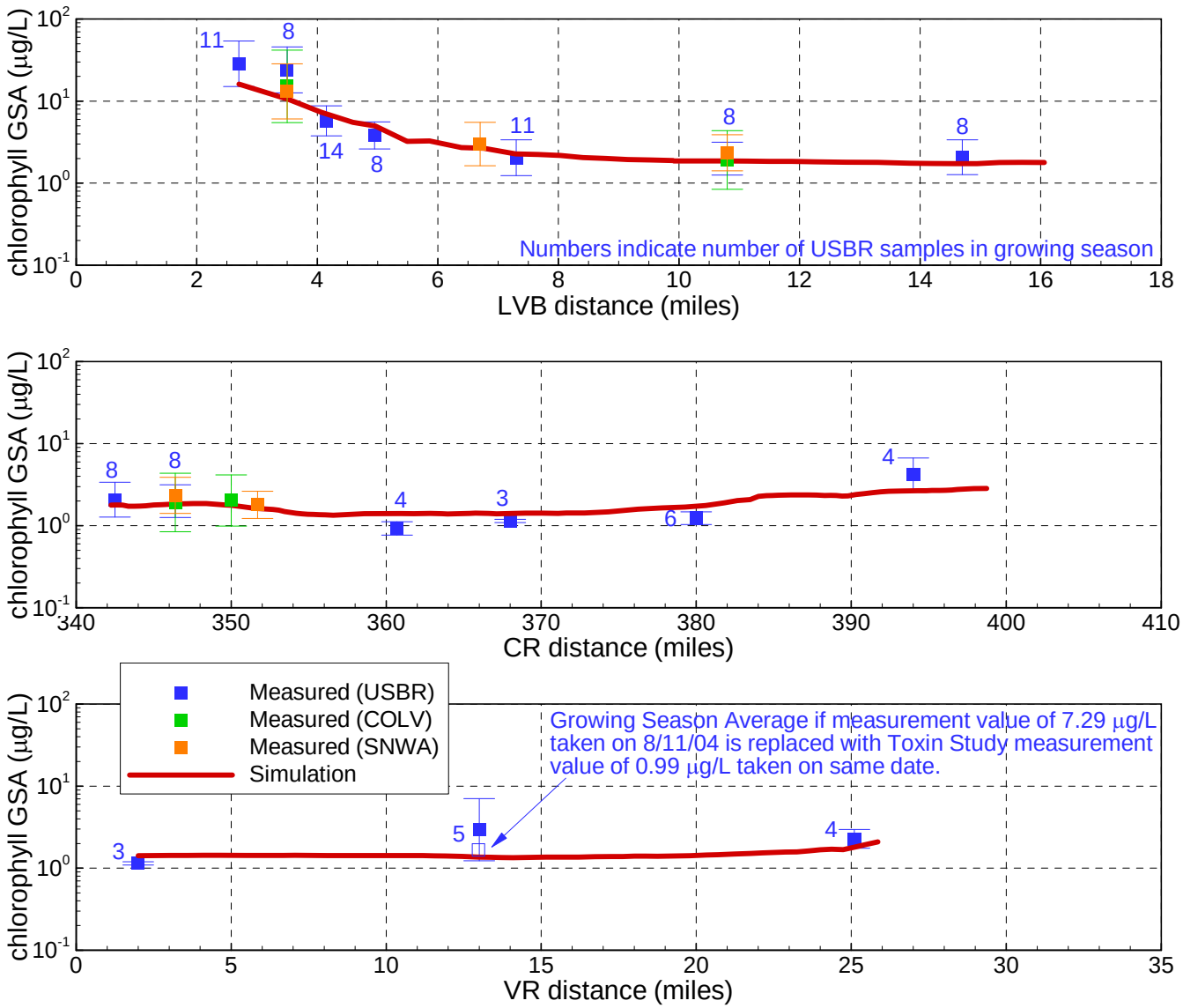
Modeled and Measured Chlorophyll Top 5 m and 2004 Growing Season* Average
* April 1 - September 30
chlorophyll GSA (µg/L)
LVB distance (miles)
Numbers indicate number of USBR samples in growing season
CR distance (miles)
Measured (USBR)
Measured (COLV)
Measured (SNWA)
Simulation
Growing Season Average if measurement value of 7.29 µg/L taken on 8/11/04 is replaced with Toxin Study measurement value of 0.99 µg/L taken on same date.
VR distance (miles)

Figure 4.56

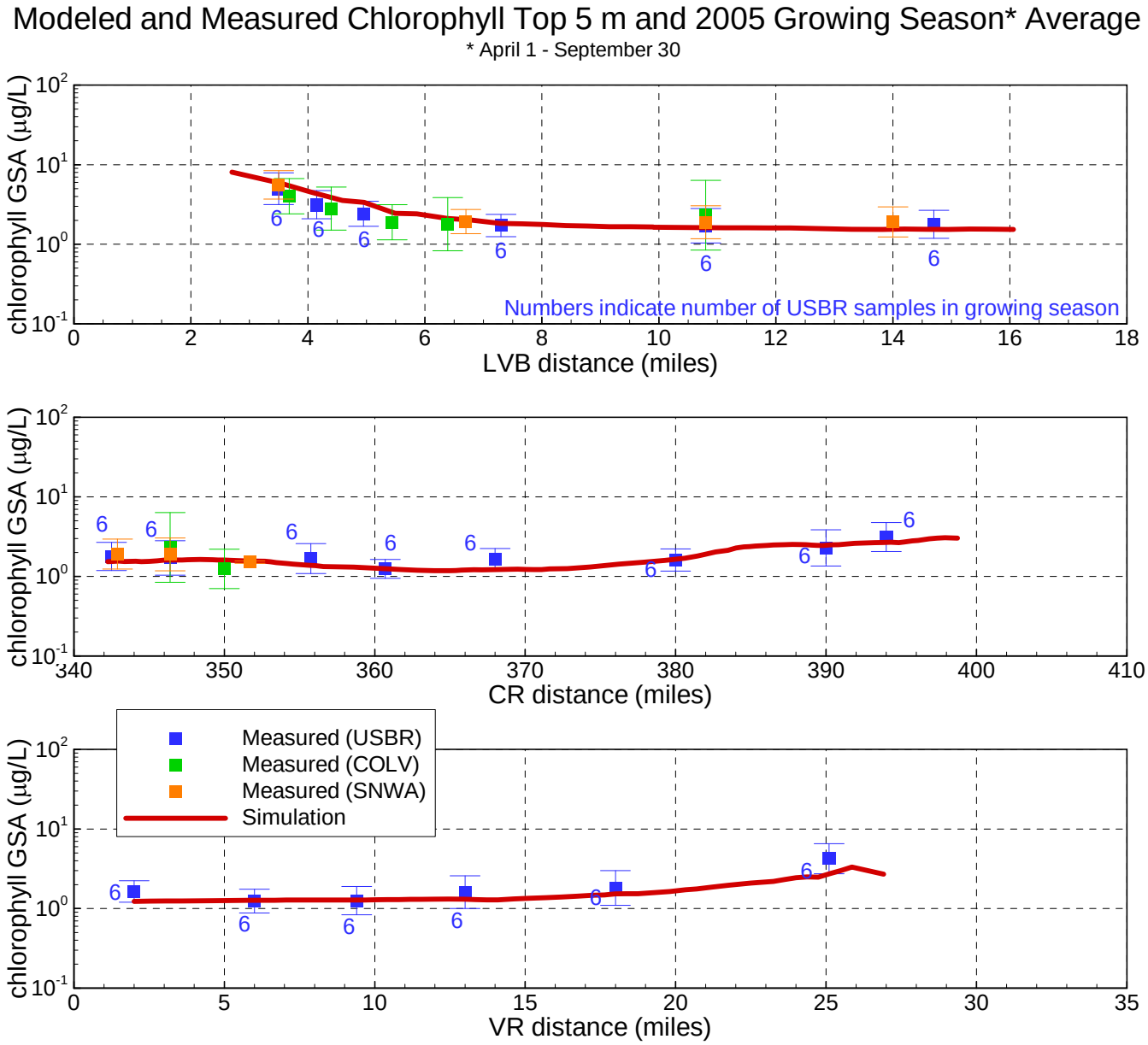

Ch4_Figures.ppt
FSI V064081 & V084015
December 9, 2010

Figure 4.57

FLOW SCIENCE

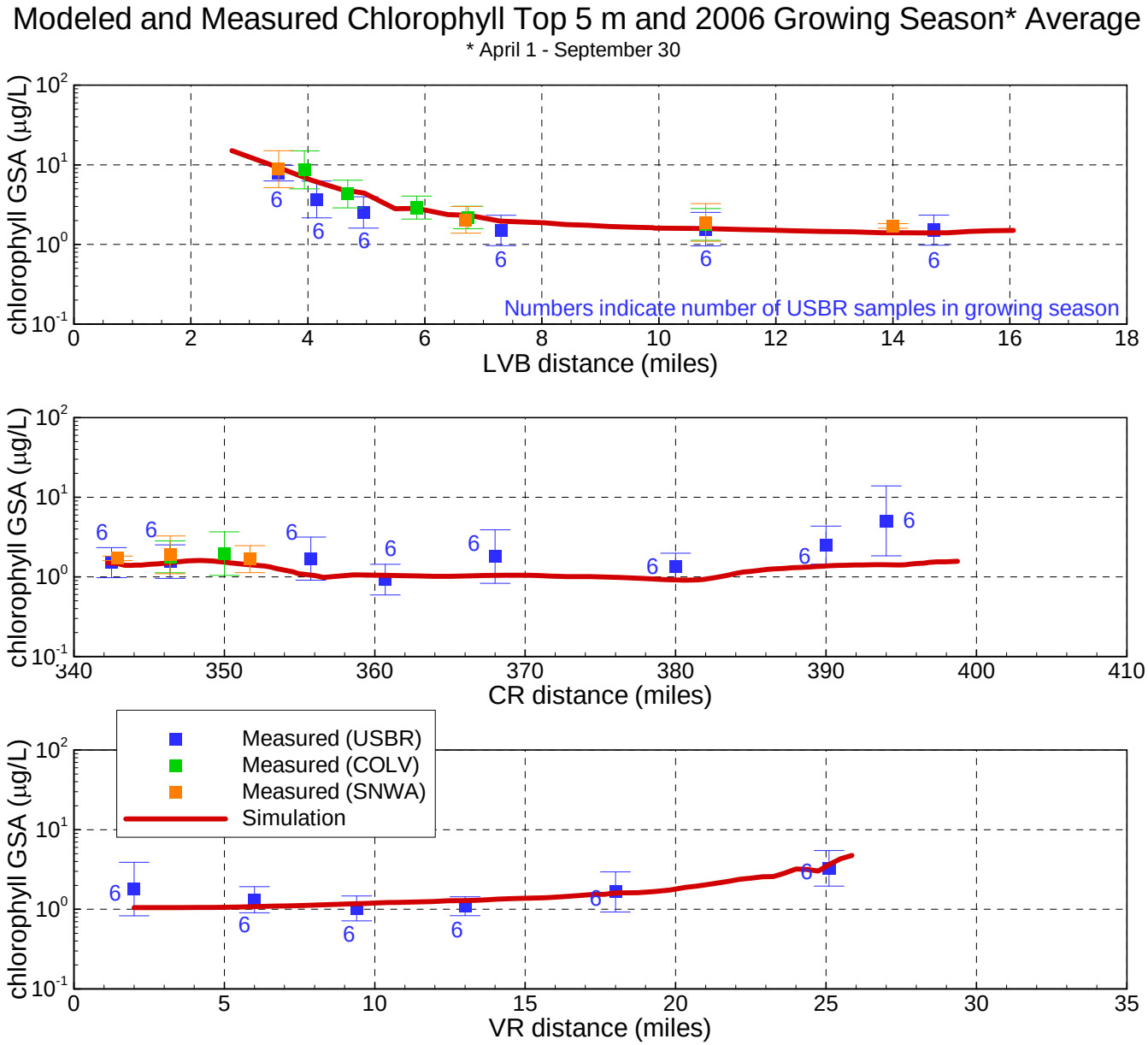

Ch4_Figures.ppt
FSI V064081 & V084015
December 9, 2010

Figure 4.58

FLOW SCIENCE

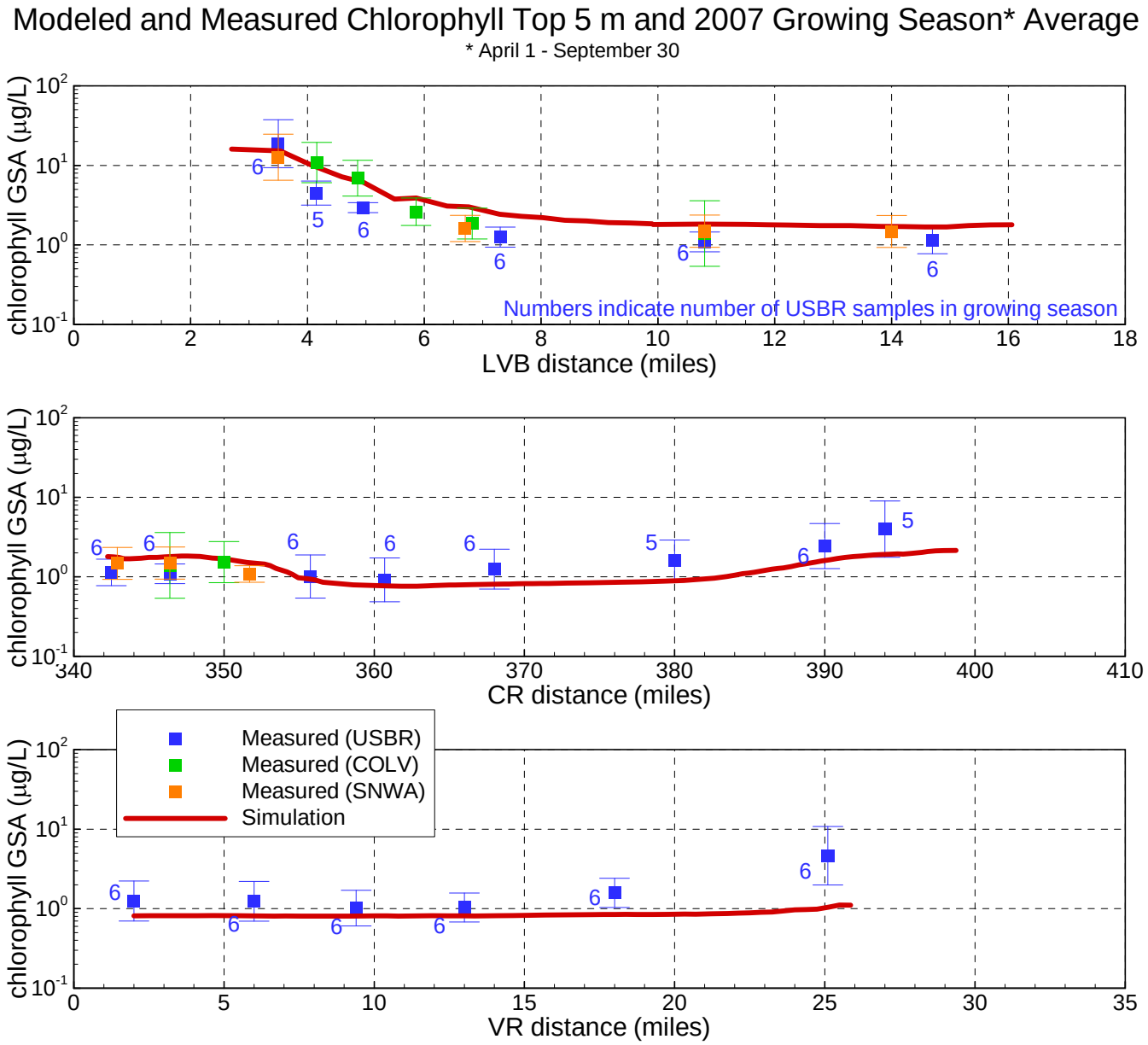

Ch4_Figures.ppt
FSI V064081 & V084015
December 9, 2010

Figure 4.59

FLOW SCIENCE

2000 – 2007 Growing Seasons

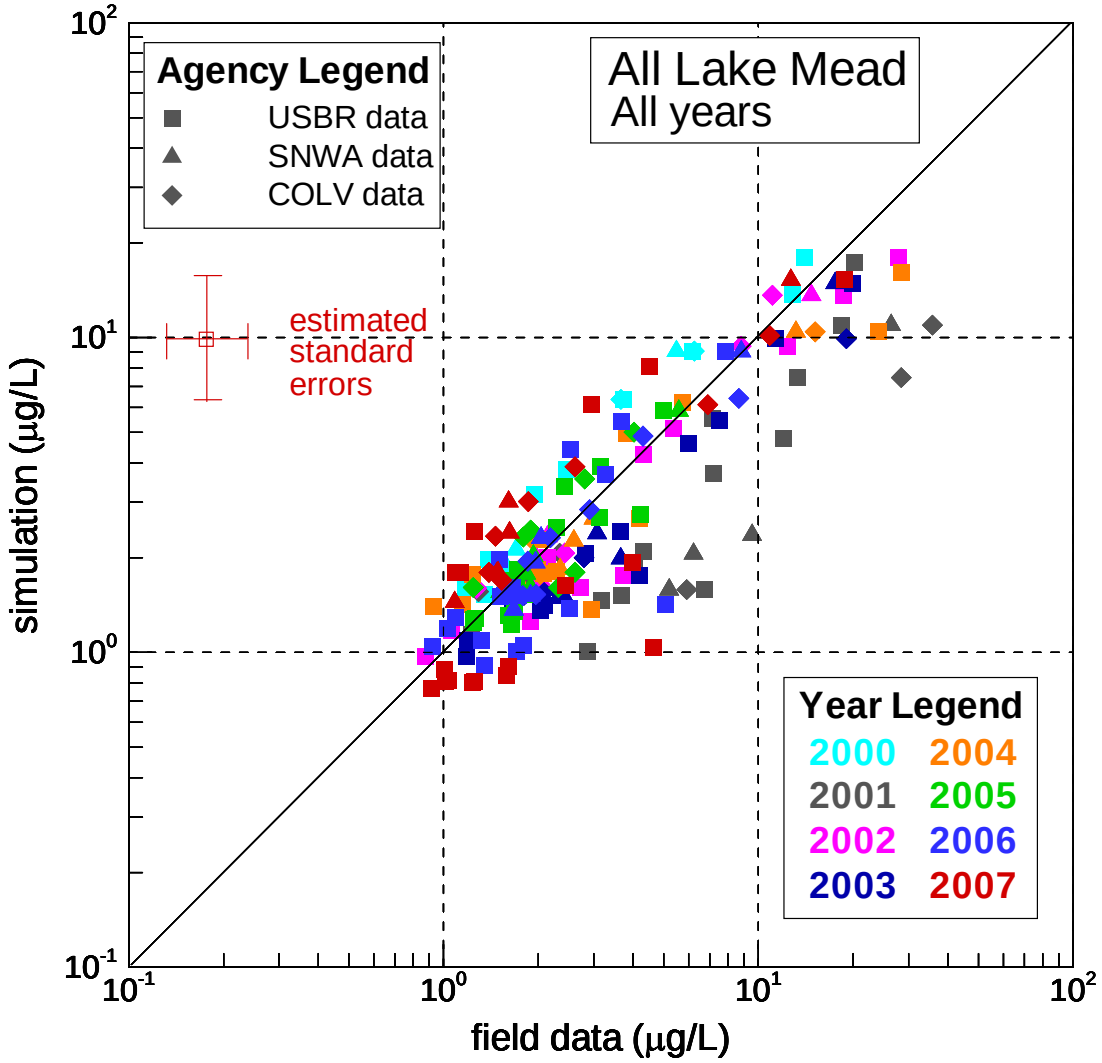

Figure 4.60

Comparison of Measured and Simulated Filterable Reactive Phosphorus at Station CR394.0

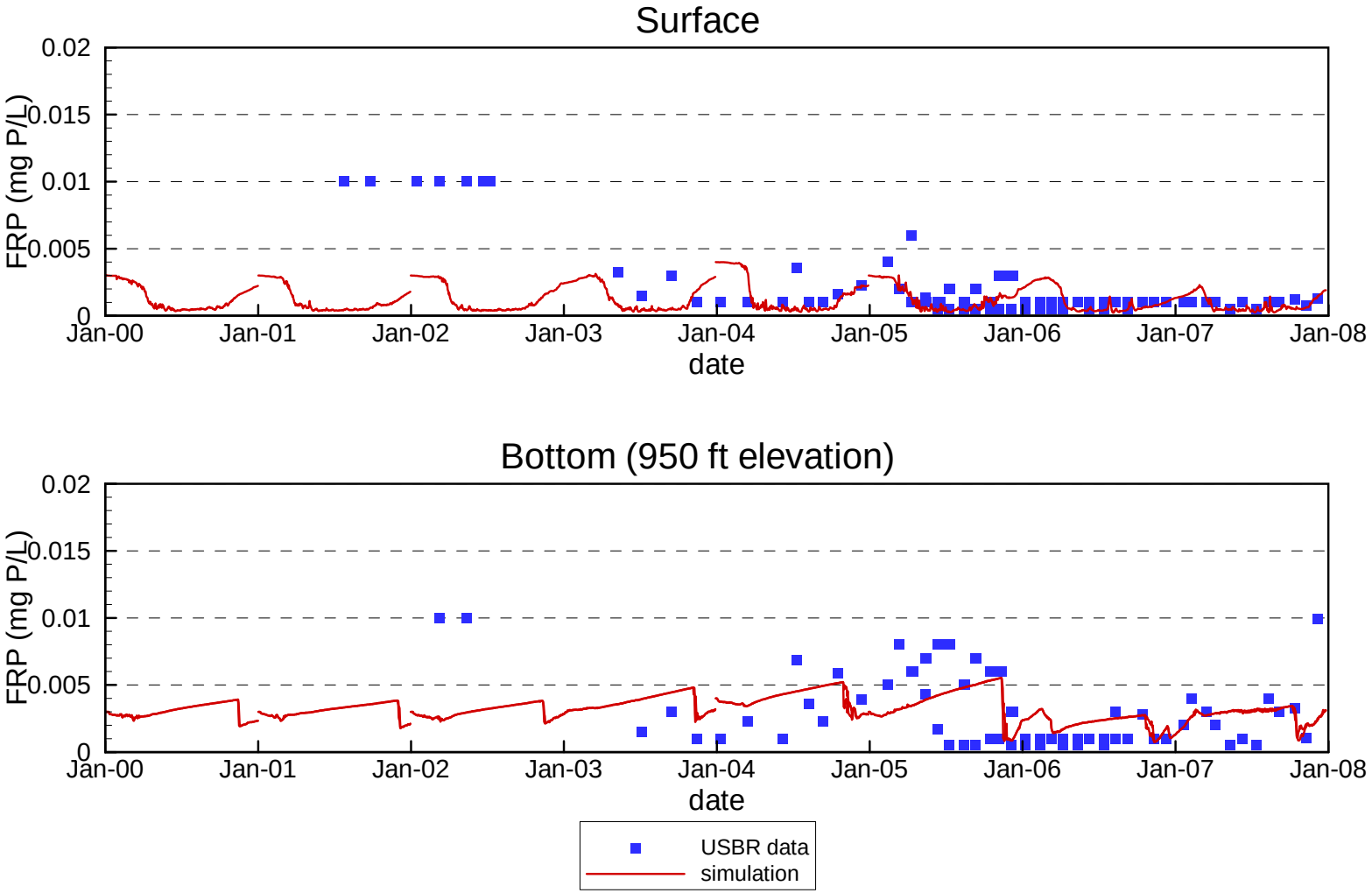

Figure 4.61

Comparison of Measured and Simulated Filterable Reactive Phosphorus at Station VR25.1

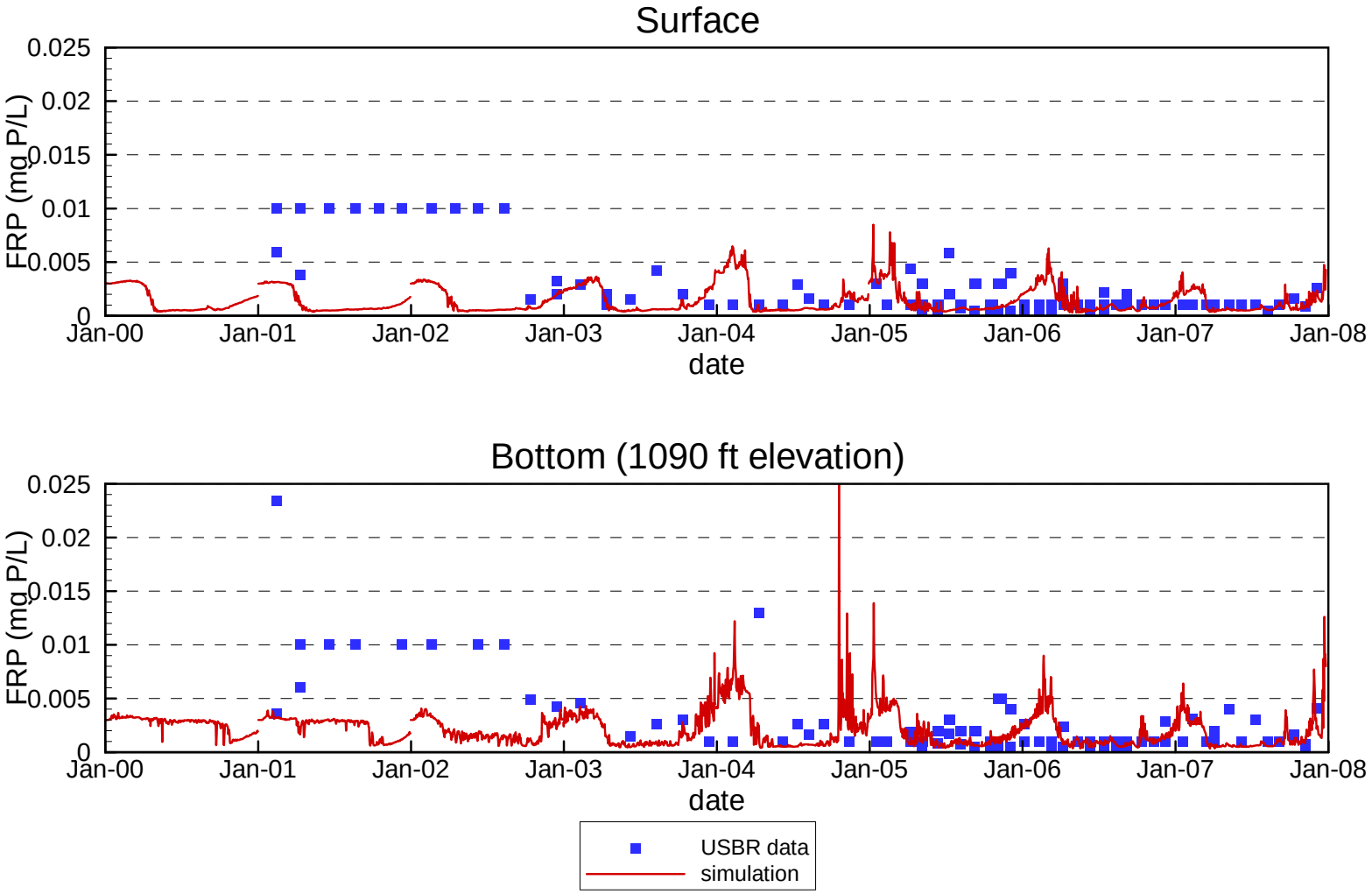

Figure 4.62

Comparison of Measured and Simulated Filterable Reactive Phosphorus at Stations VR12.9 / VR13.0

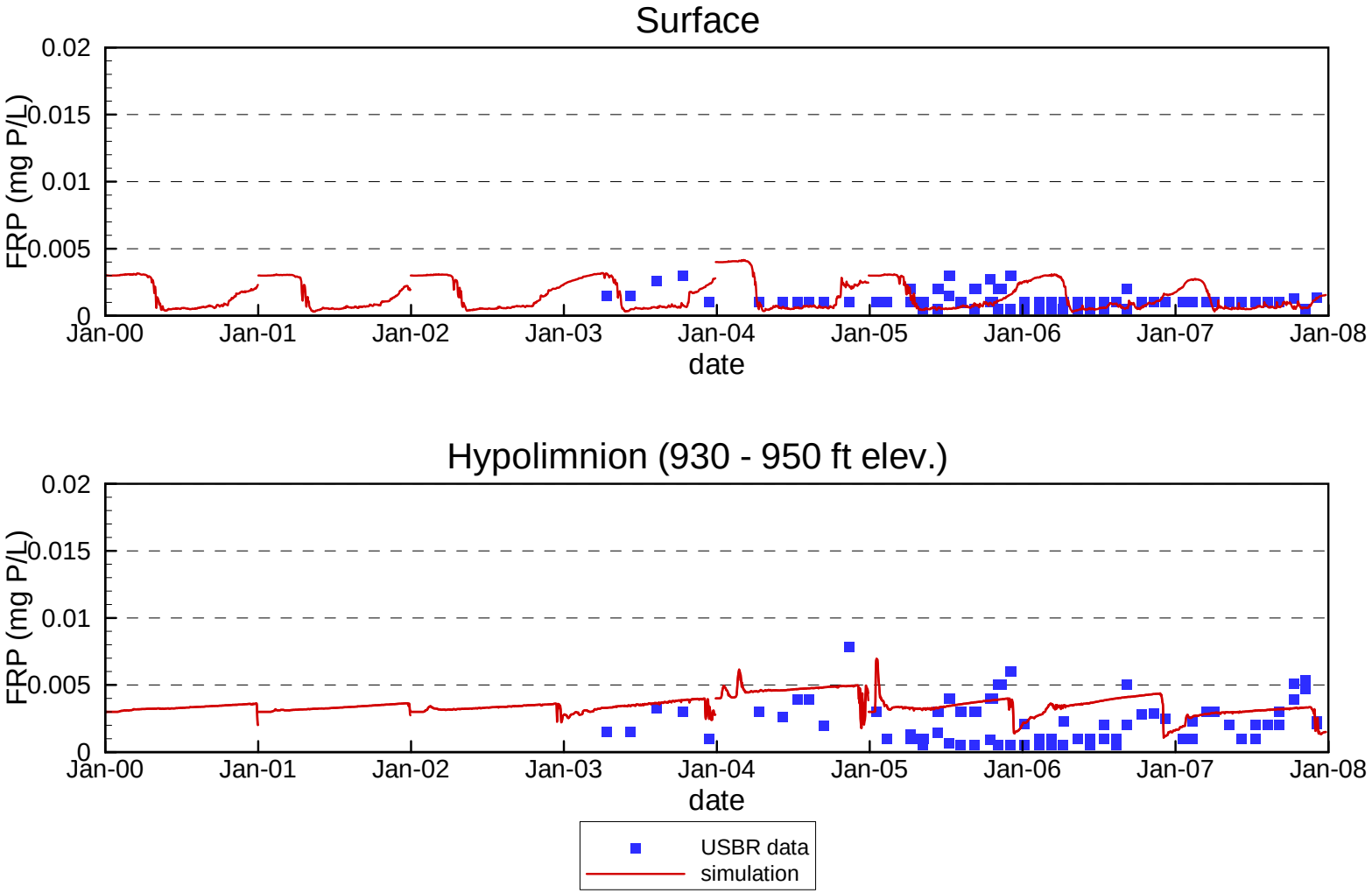

Figure 4.63

Comparison of Measured and Simulated Filterable Reactive Phosphorus at Station CR360.7

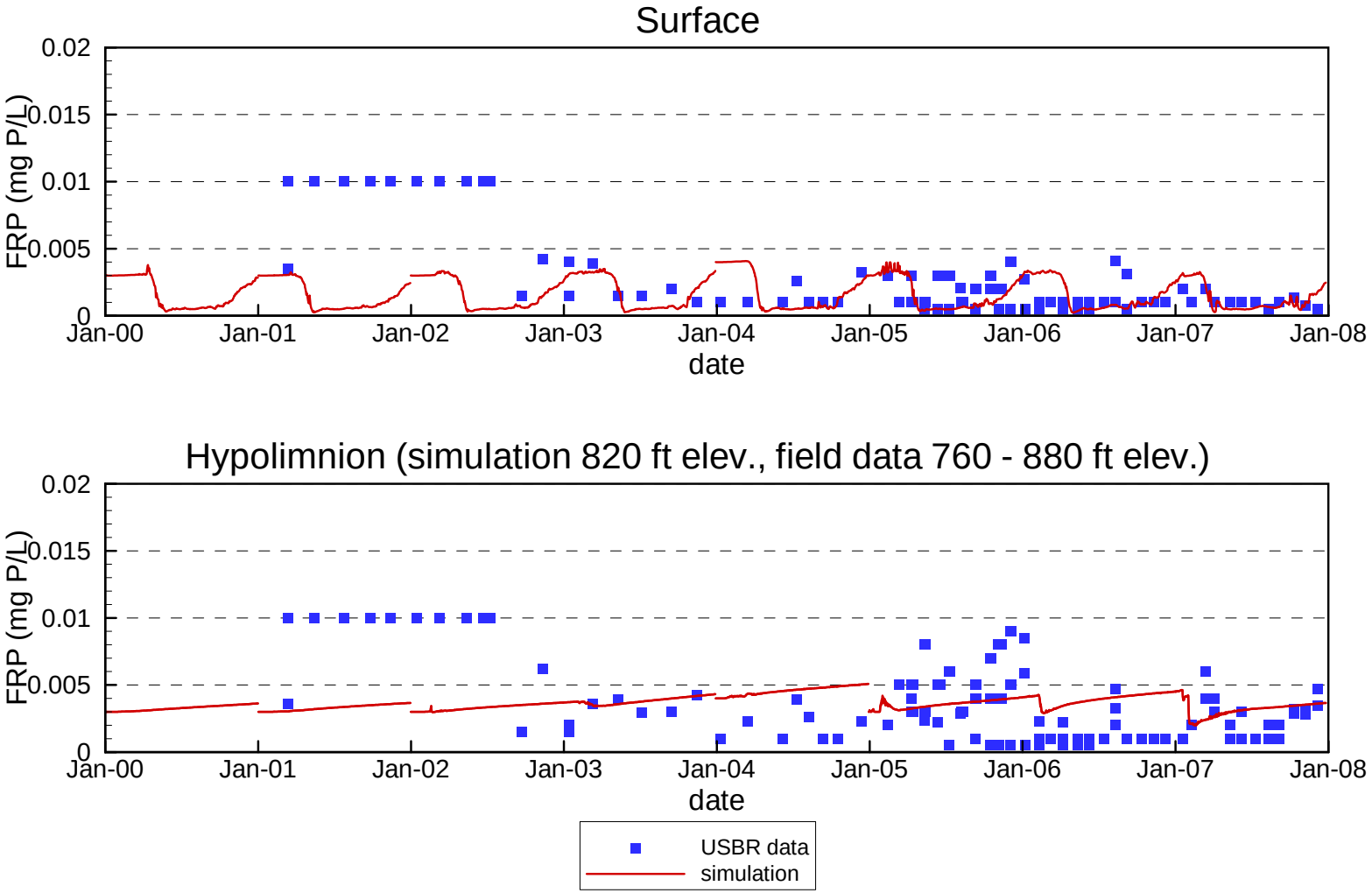

Figure 4.64

Comparison of Measured and Simulated Filterable Reactive Phosphorus at Station LVB3.5

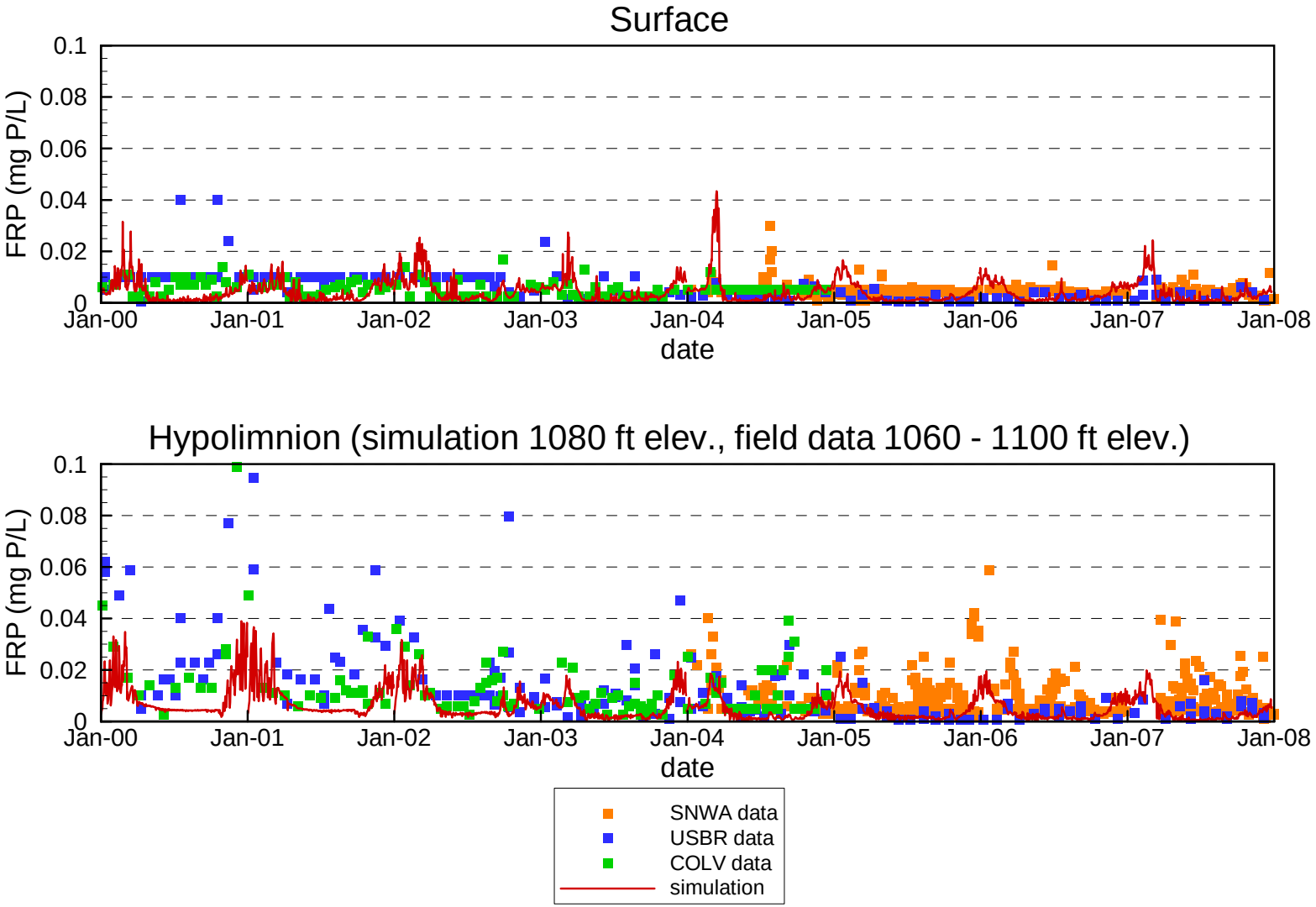

Figure 4.65

Comparison of Measured and Simulated Filterable Reactive Phosphorus at Station CR346.4

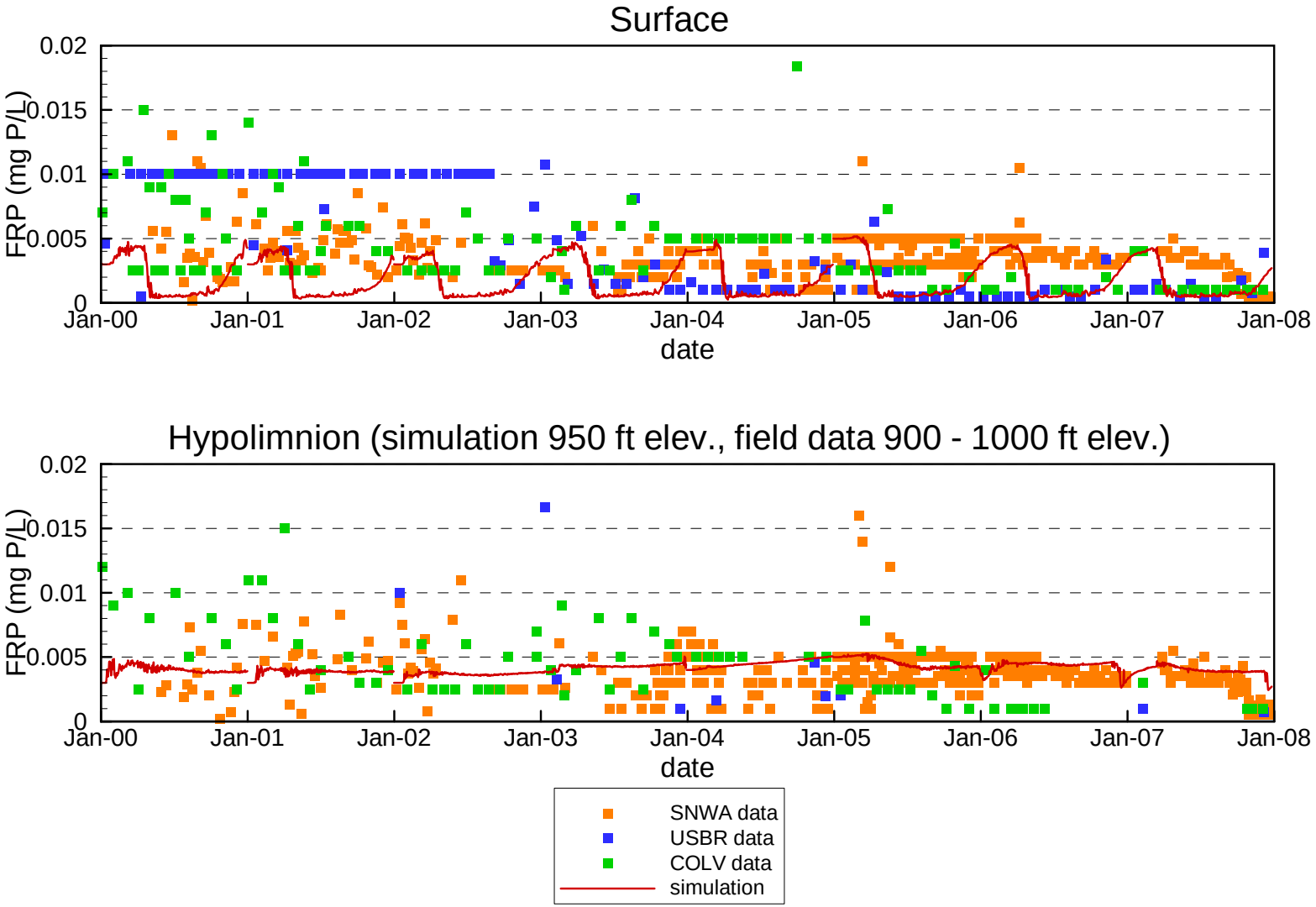

Figure 4.66

Comparison of Measured and Simulated Filterable Reactive Phosphorus at SNWA Intakes #1 and #2

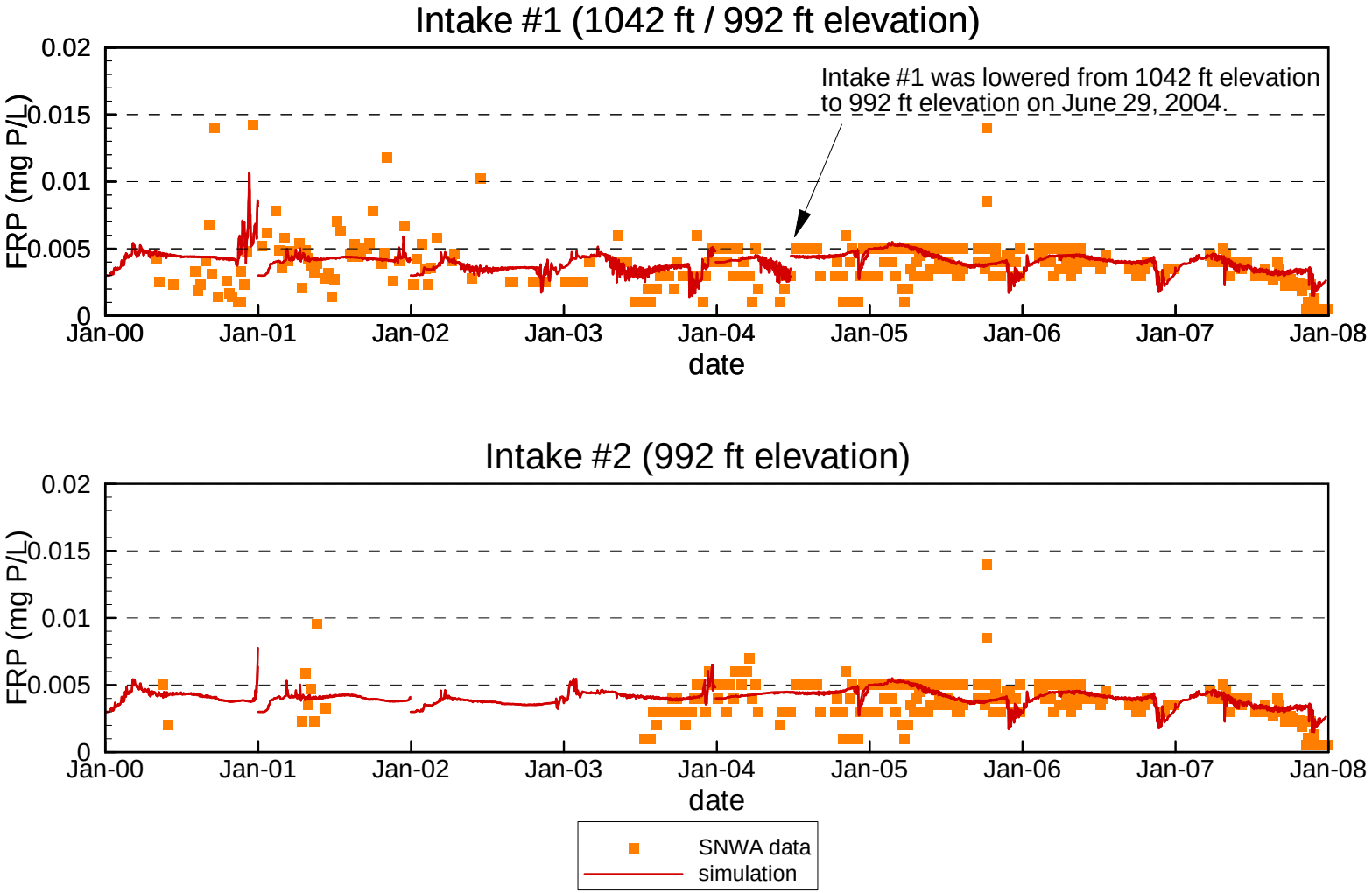

Figure 4.67

Comparison of Measured and Simulated Filterable Reactive Phosphorus at Combined Hoover Dam Outlets

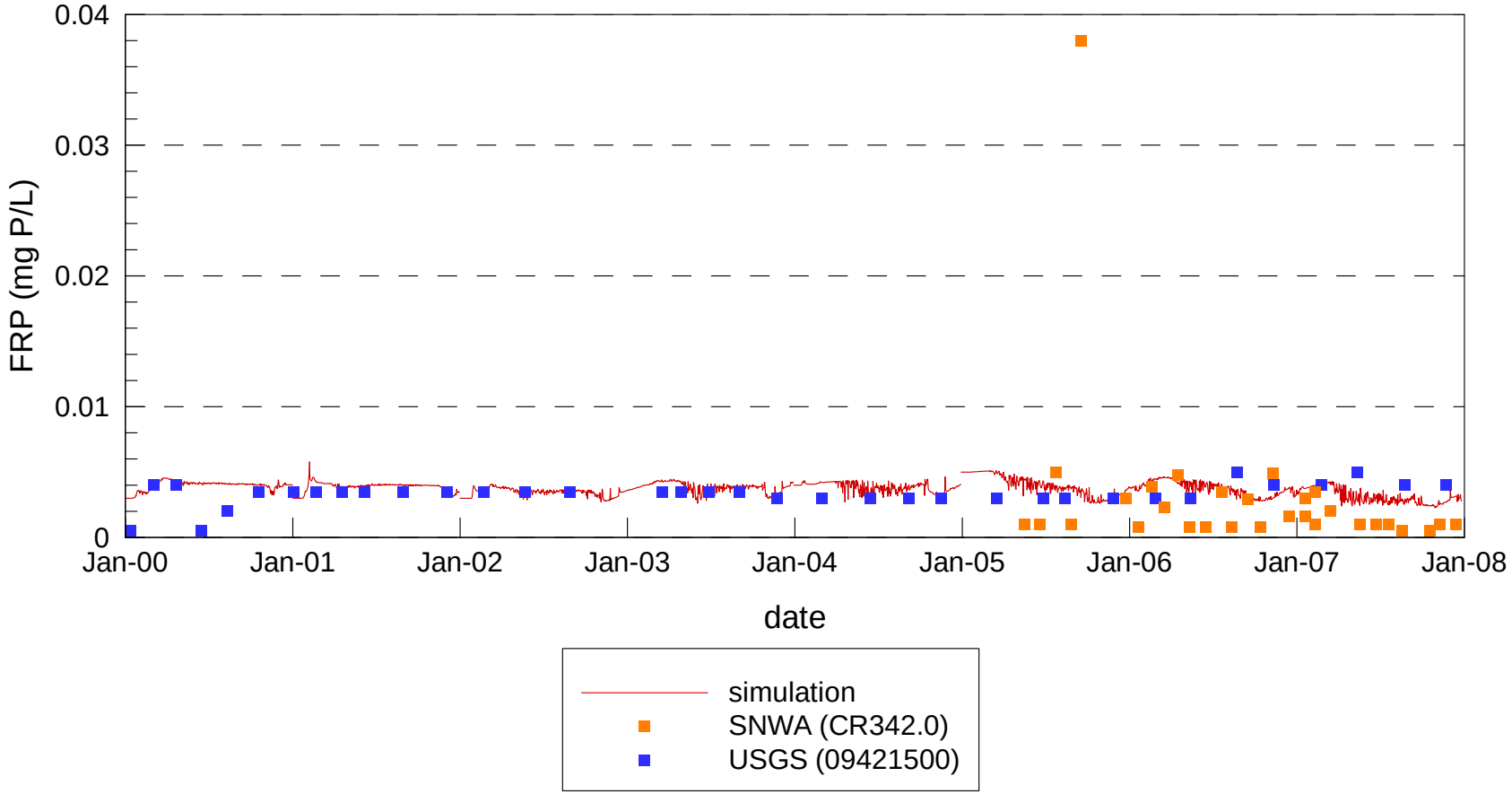

Figure 4.68

Comparison of Measured and Simulated Total Phosphorus at Station CR394.0

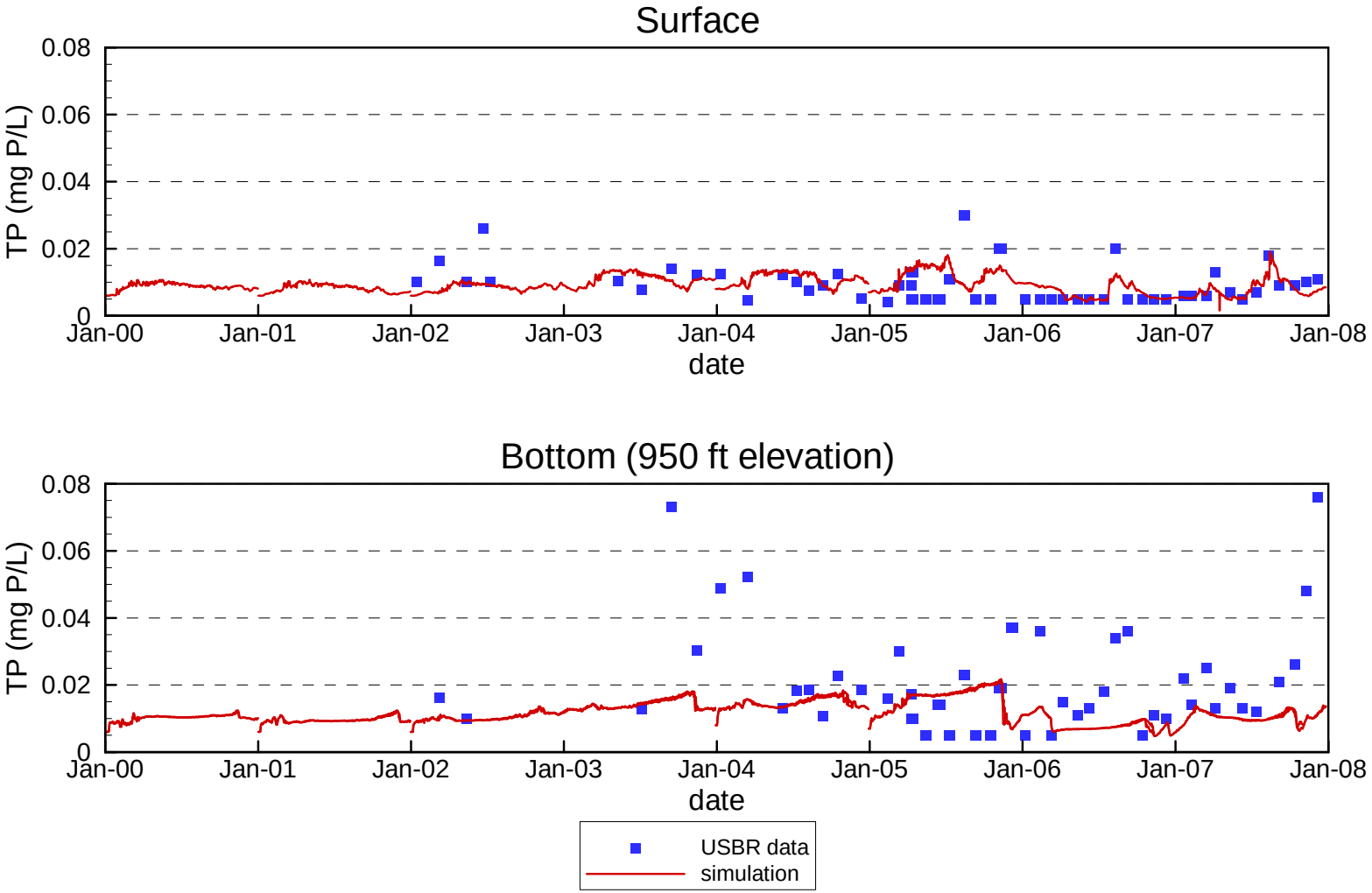

Comparison of Measured and Simulated Total Phosphorus at Station VR25.1

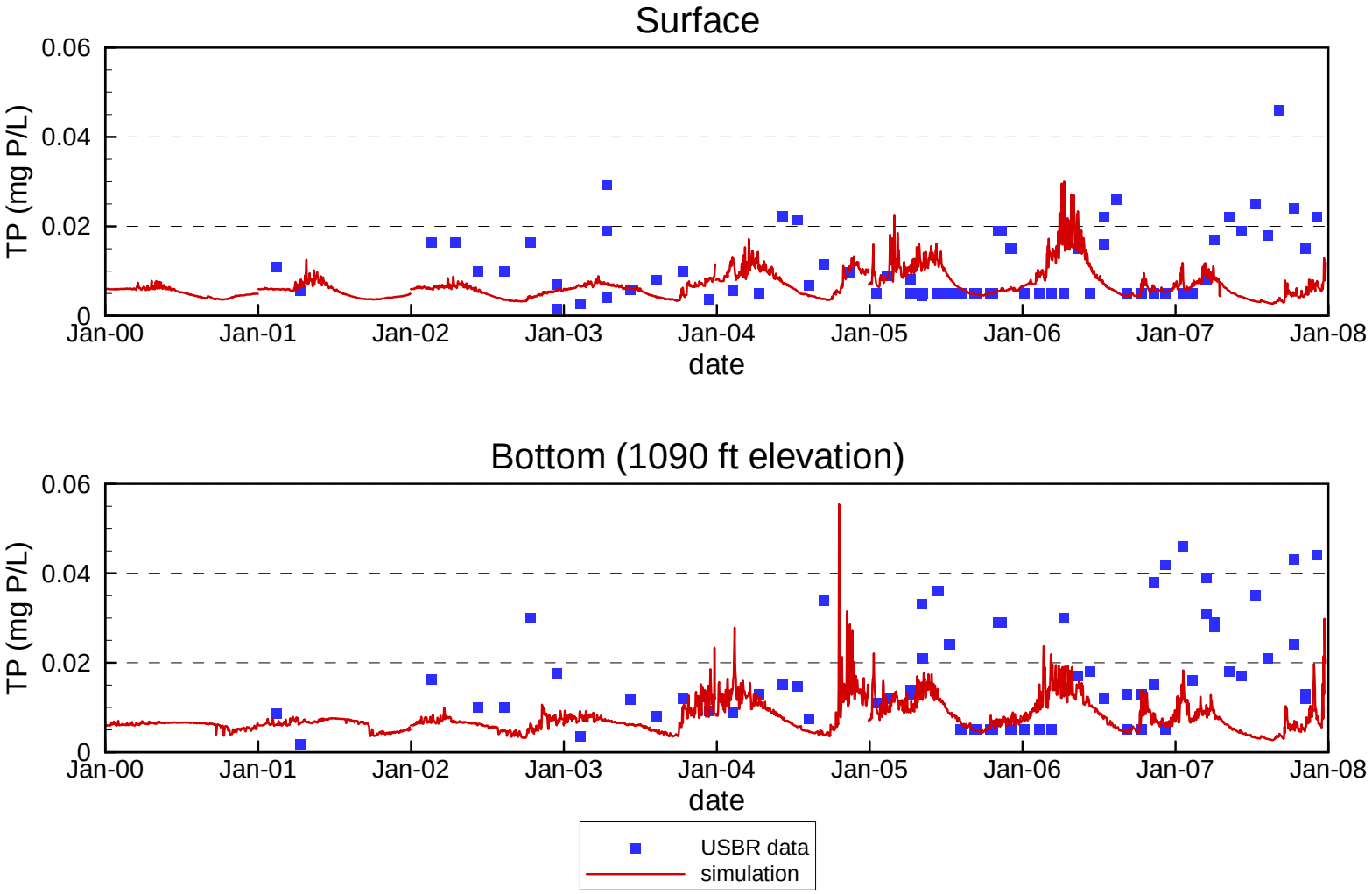

Figure 4.70

Comparison of Measured and Simulated Total Phosphorus at Stations VR12.9 / VR13.0

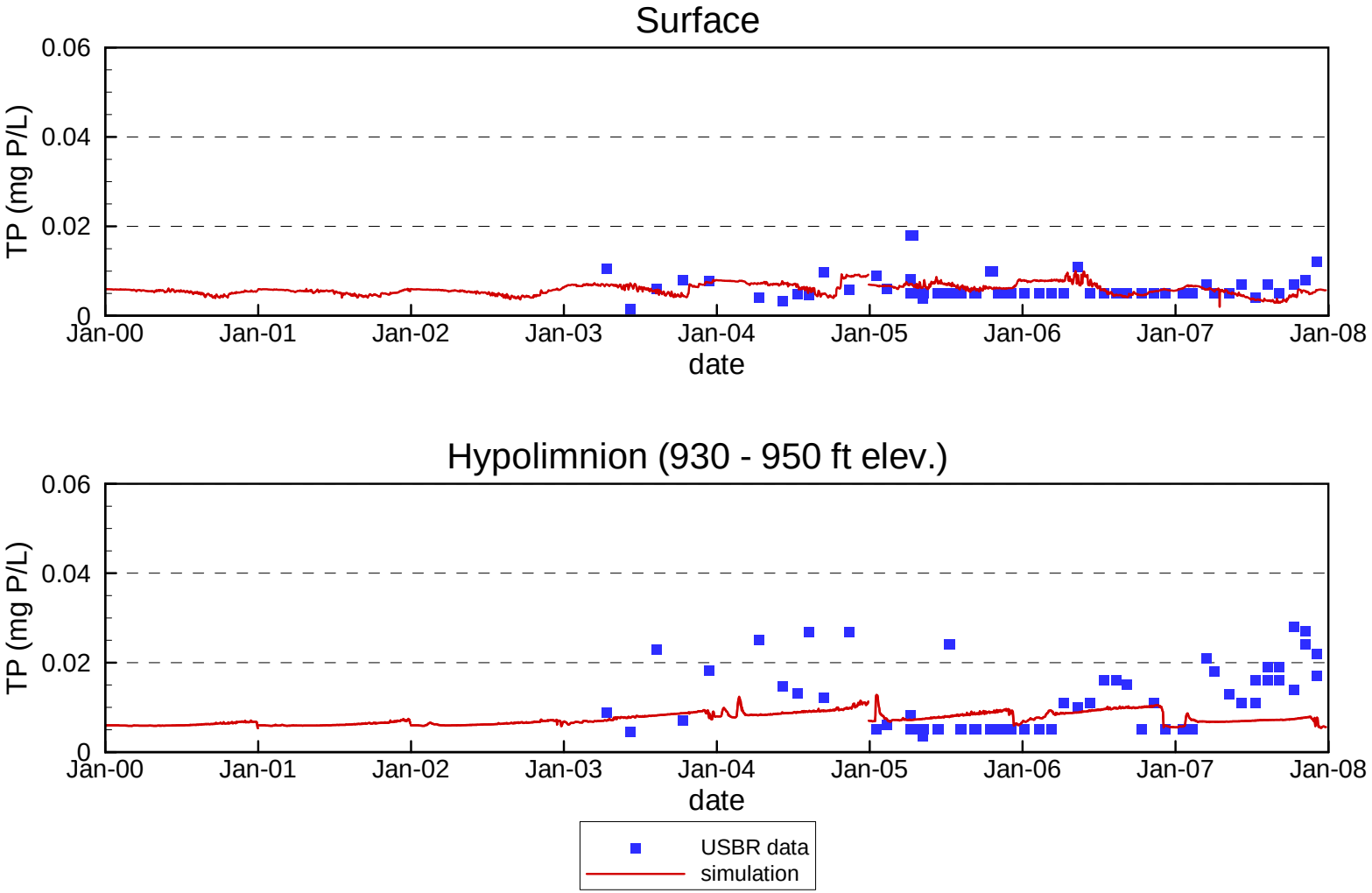

Figure 4.71

Comparison of Measured and Simulated Total Phosphorus at Station CR360.7

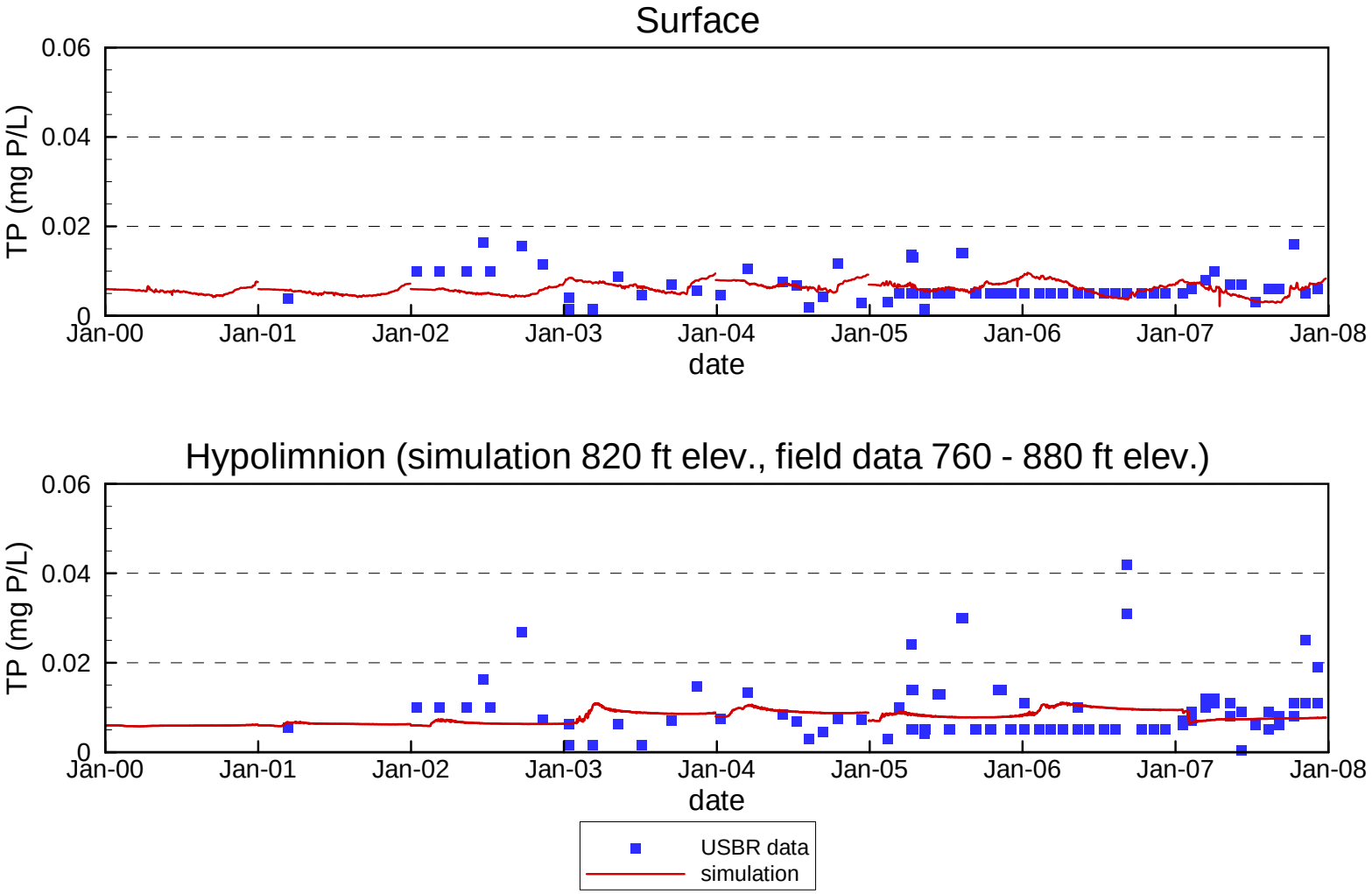

Comparison of Measured and Simulated Total Phosphorus at Station LVB3.5

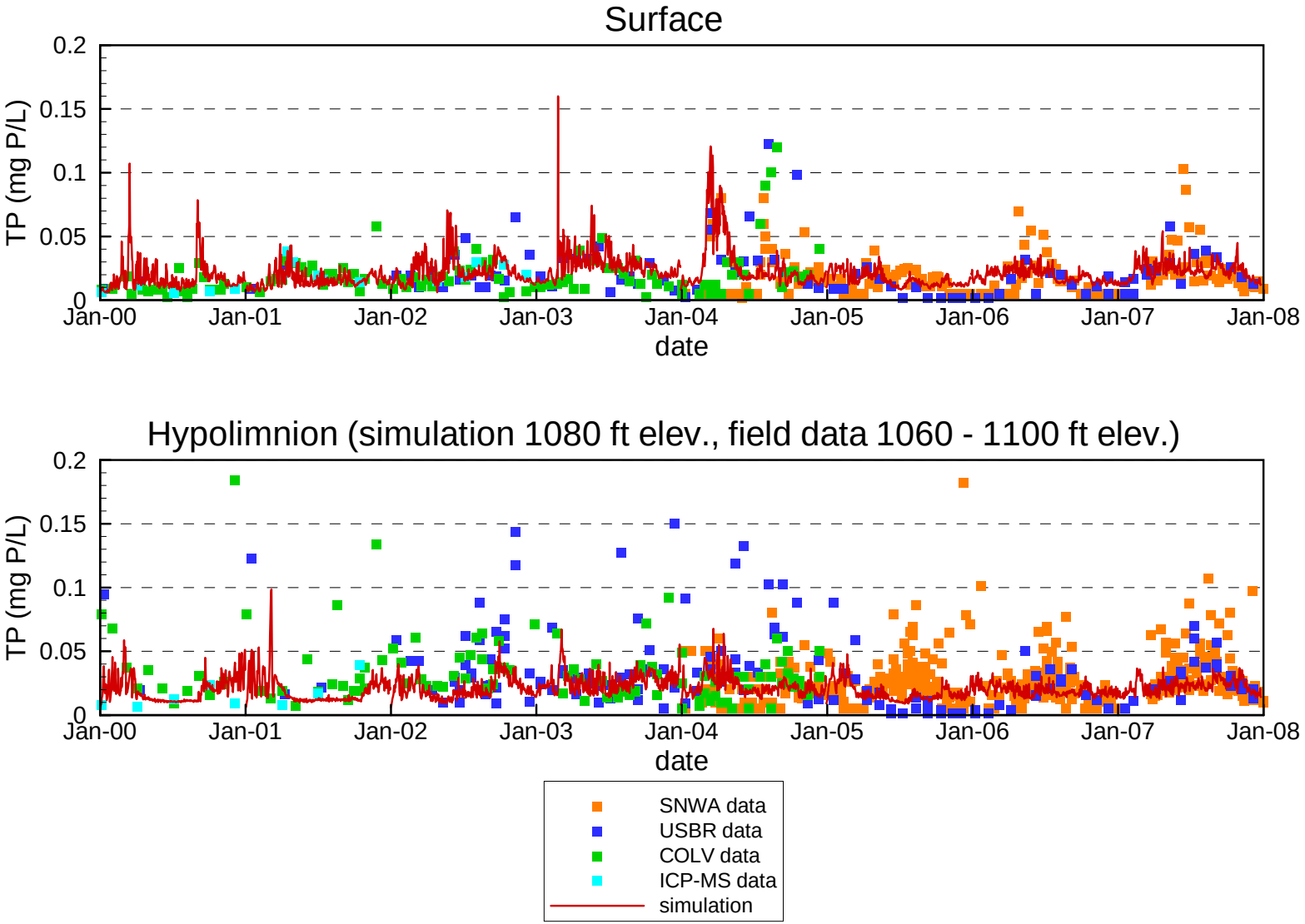

Figure 4.73

Comparison of Measured and Simulated Total Phosphorus at Station CR346.4

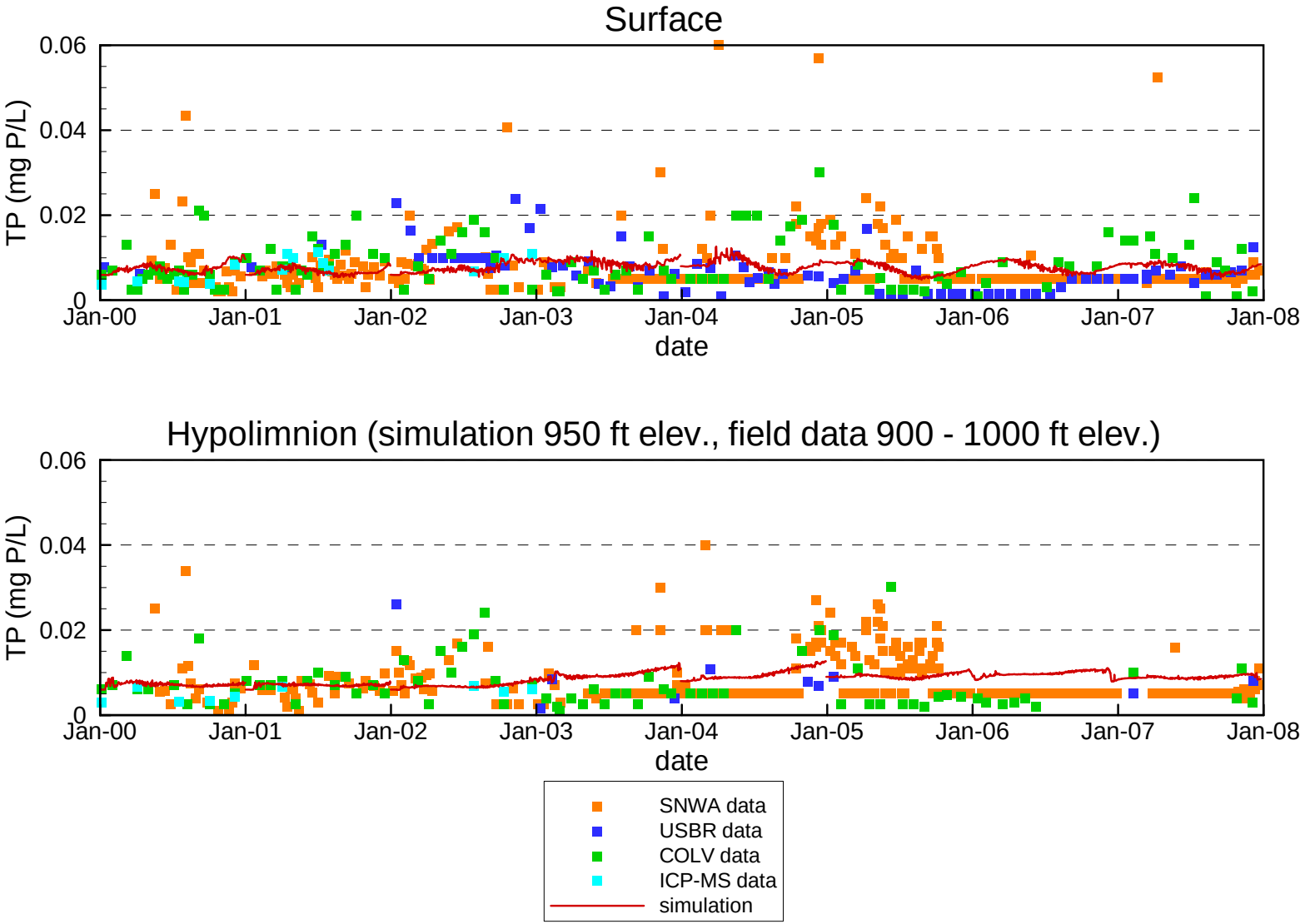

Figure 4.74

Comparison of Measured and Simulated Total Phosphorus at SNWA Intakes #1 and #2

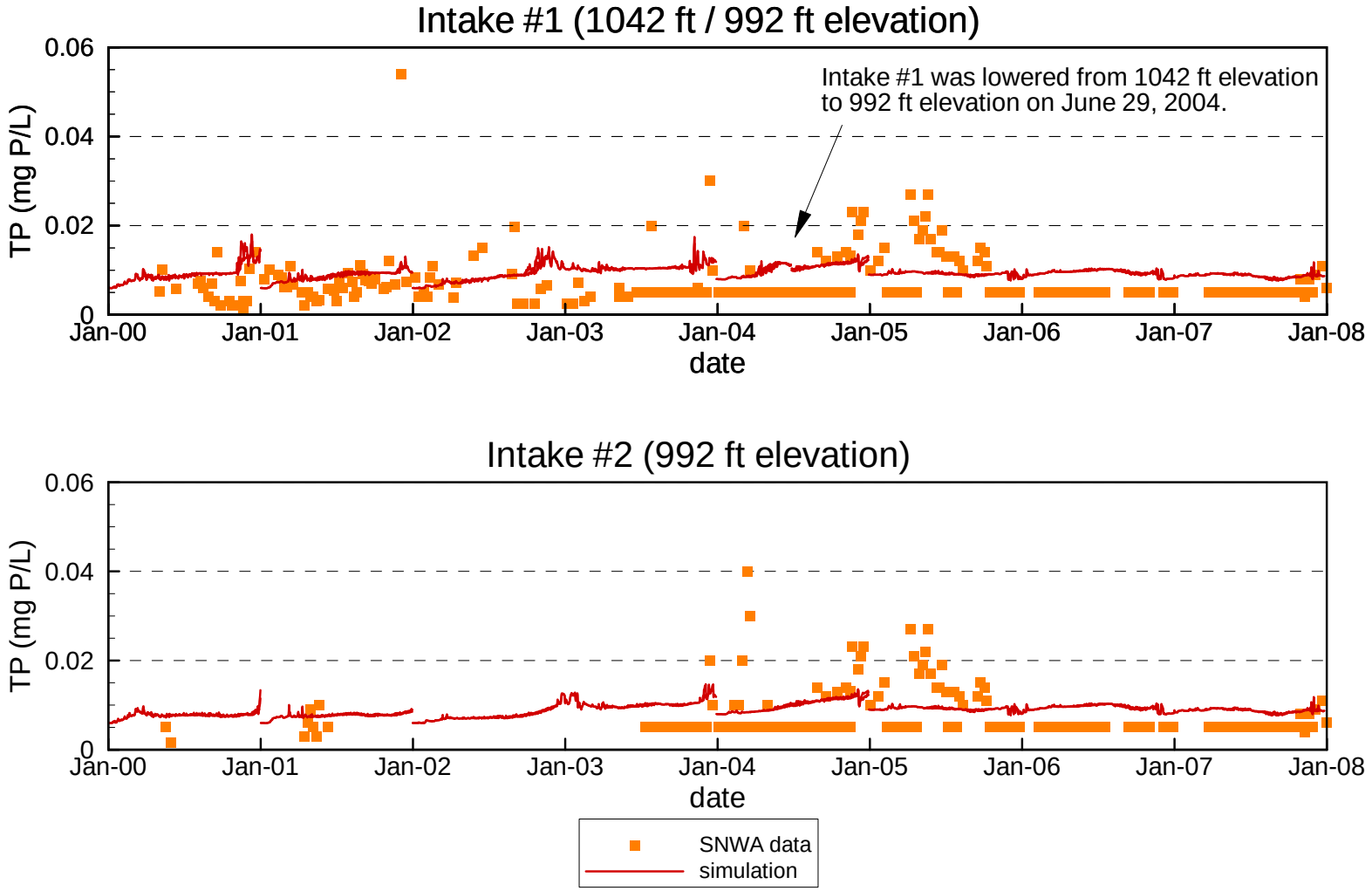

Figure 4.75

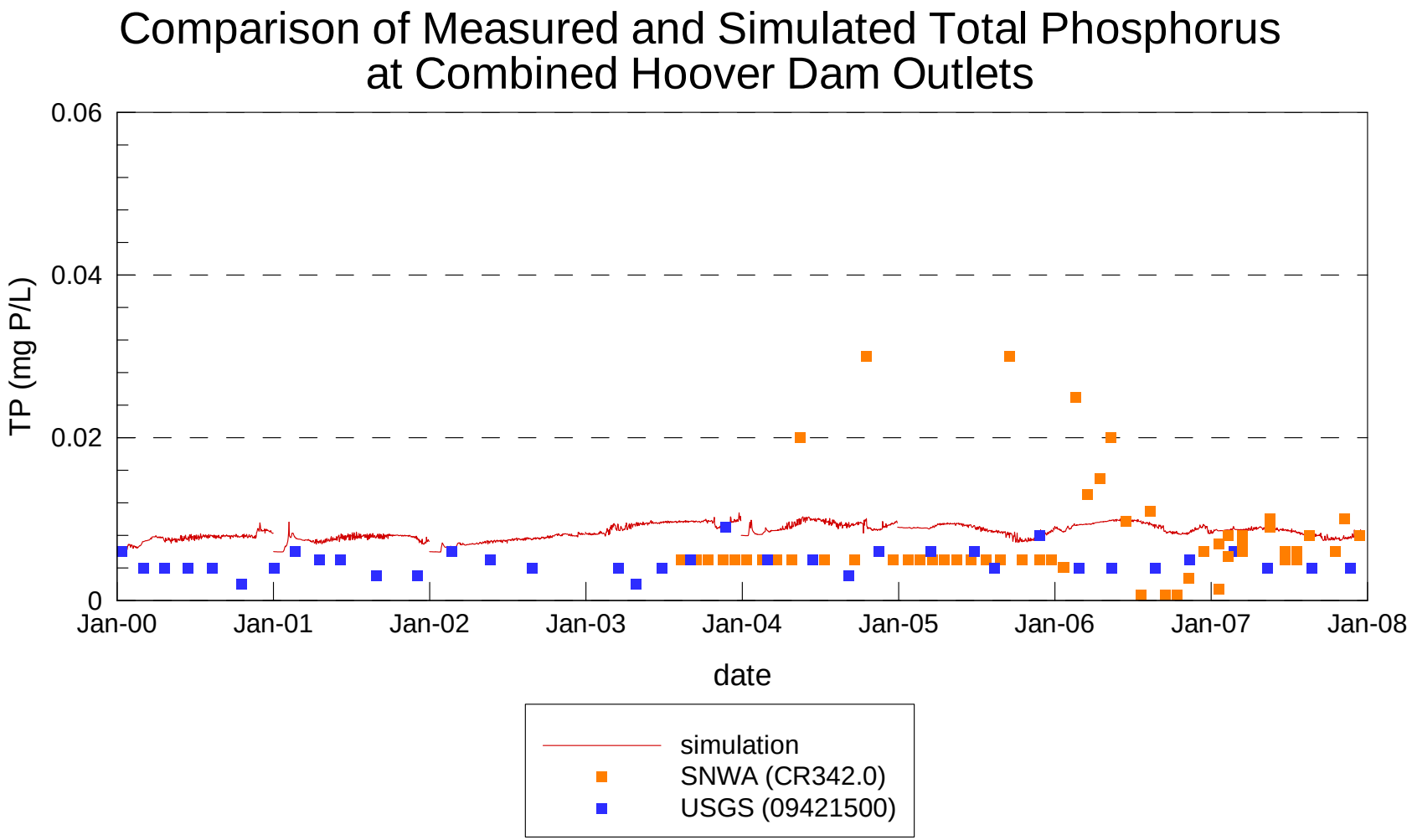
Comparison of Measured and Simulated Total Phosphorus
at Combined Hoover Dam Outlets
TP (mg P/L)
0.06
0.04
0.02
0
Jan-00
Jan-01
Jan-02
Jan-03
Jan-04
Jan-05
Jan-06
Jan-07
Jan-08
date
simulation
SNWA (CR342.0)
USGS (09421500)

Figure 4.76

Comparison of Measured and Simulated Nitrate at Station CR394.0

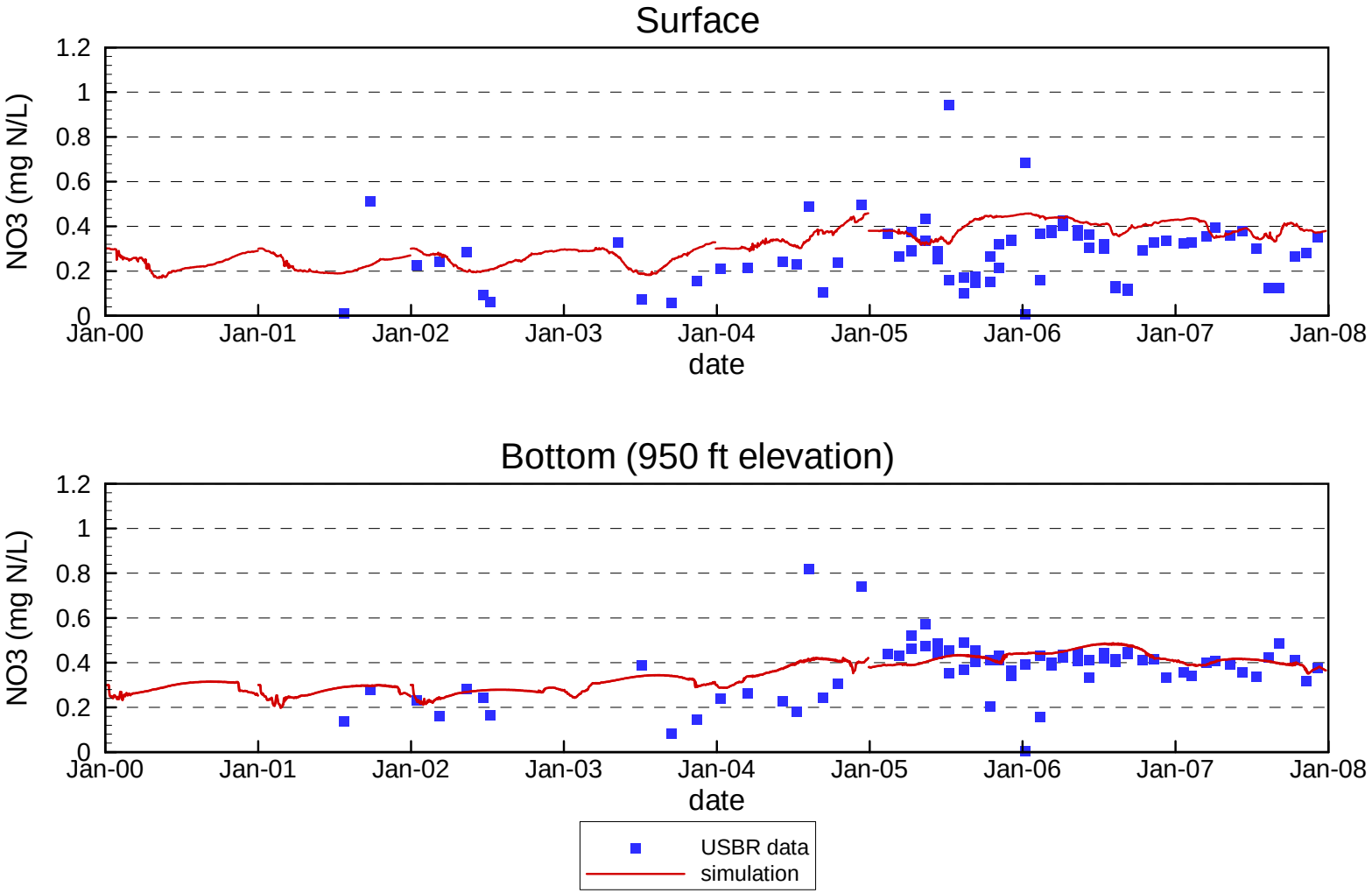

Figure 4.77

Comparison of Measured and Simulated Nitrate at Station VR25.1

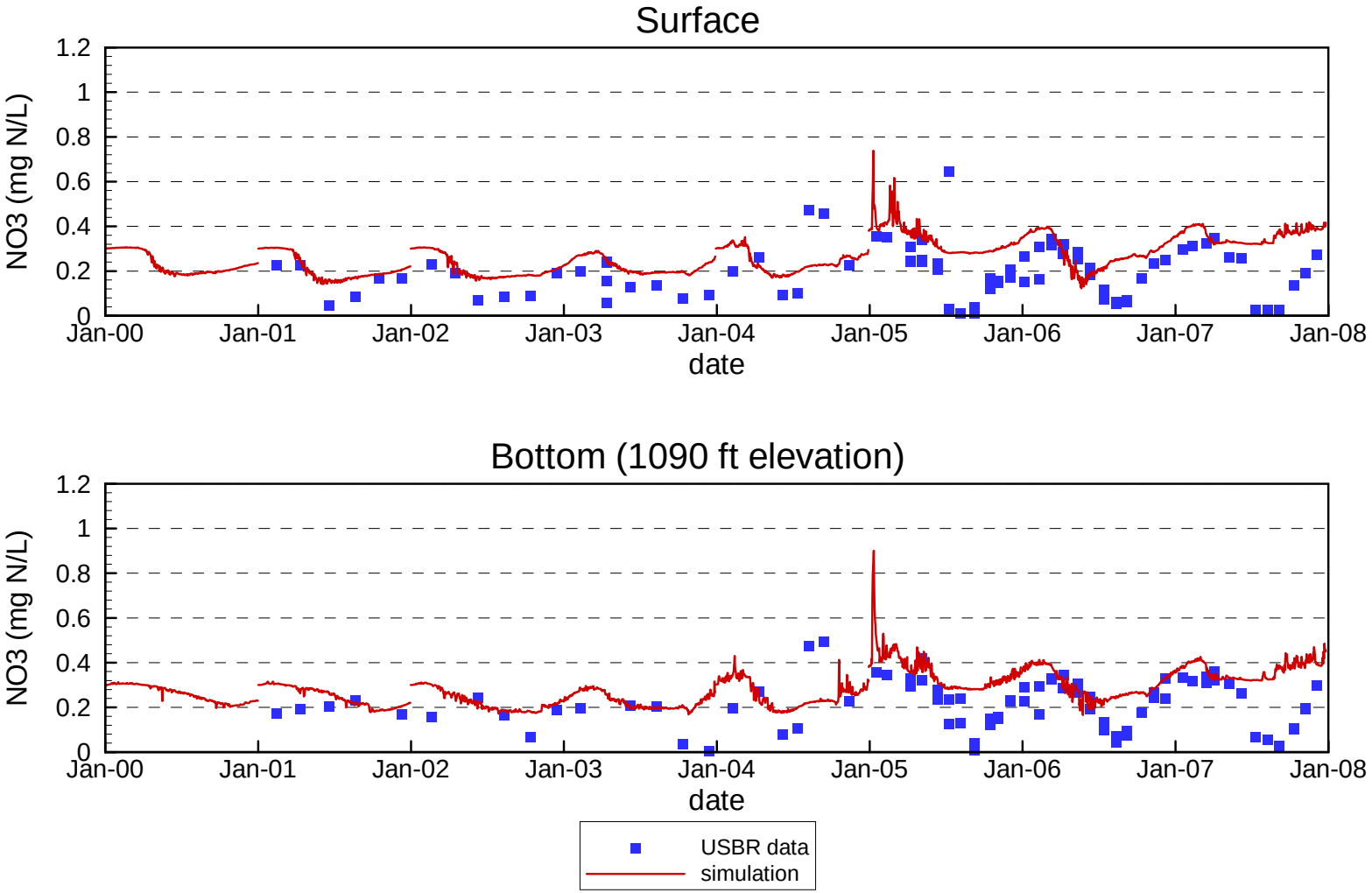

Comparison of Measured and Simulated Nitrate at Stations VR12.9 / VR13.0

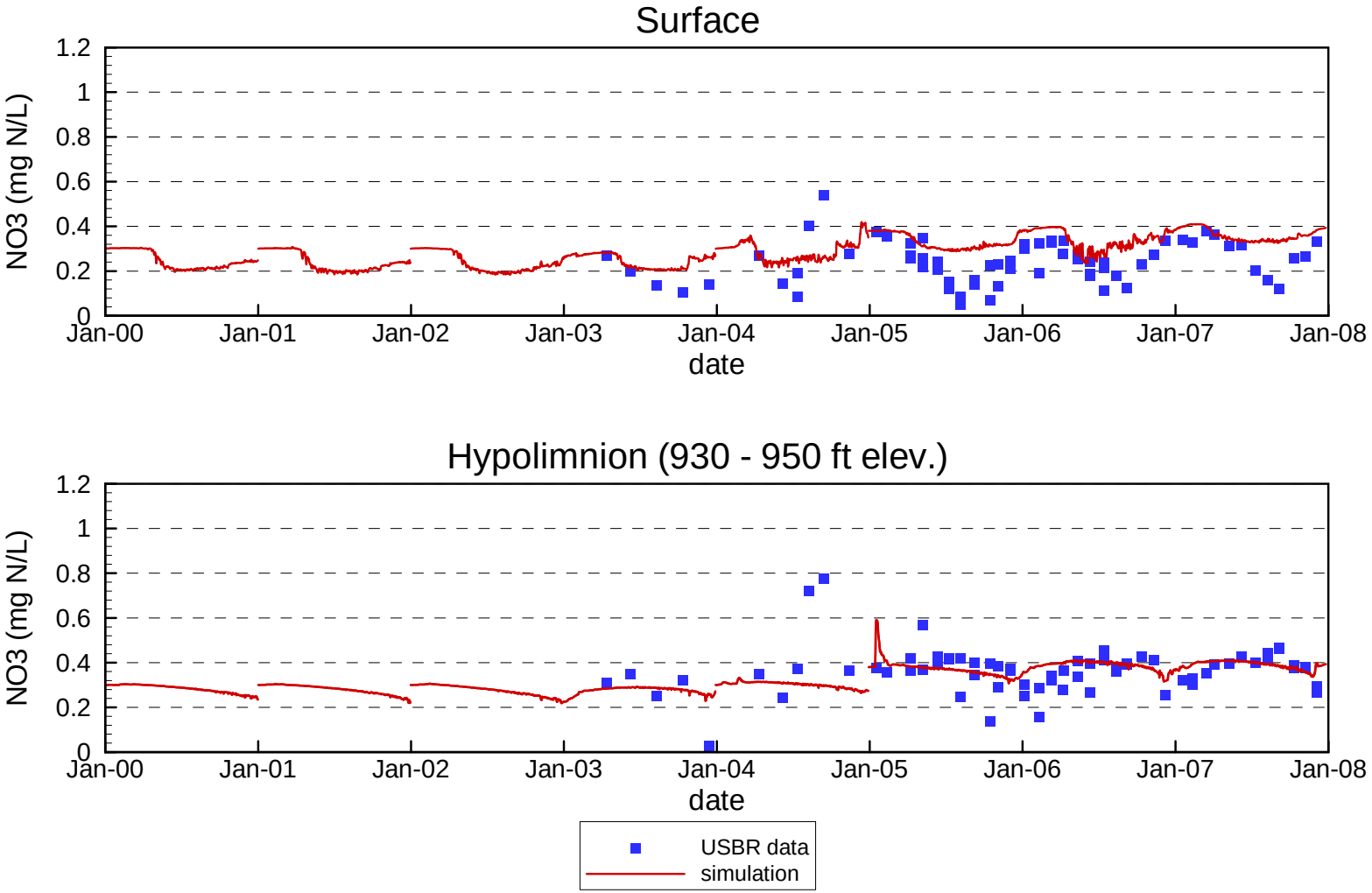

Figure 4.79

Comparison of Measured and Simulated Nitrate at Station CR360.7

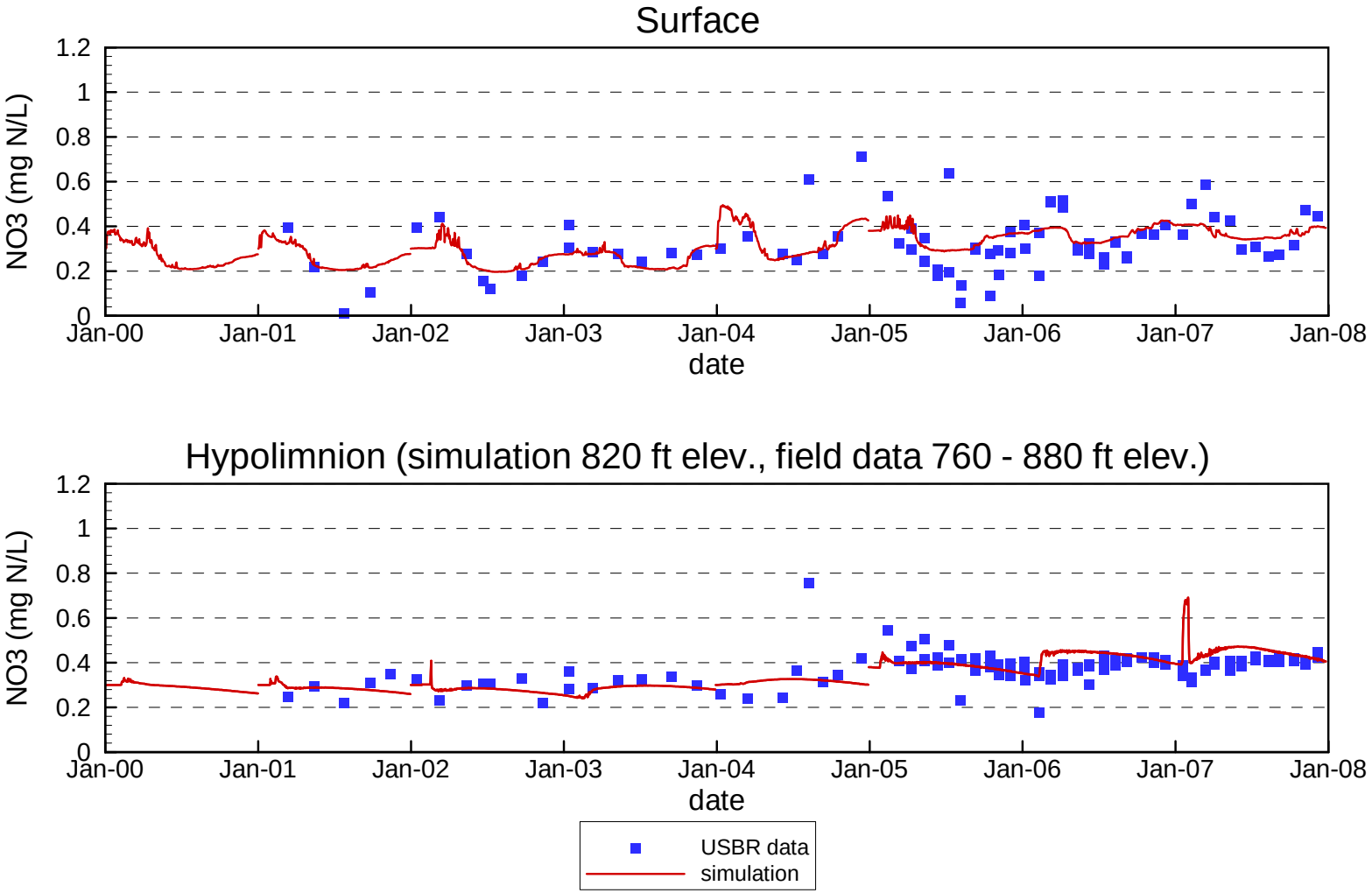

Comparison of Measured and Simulated Nitrate at Station LVB3.5

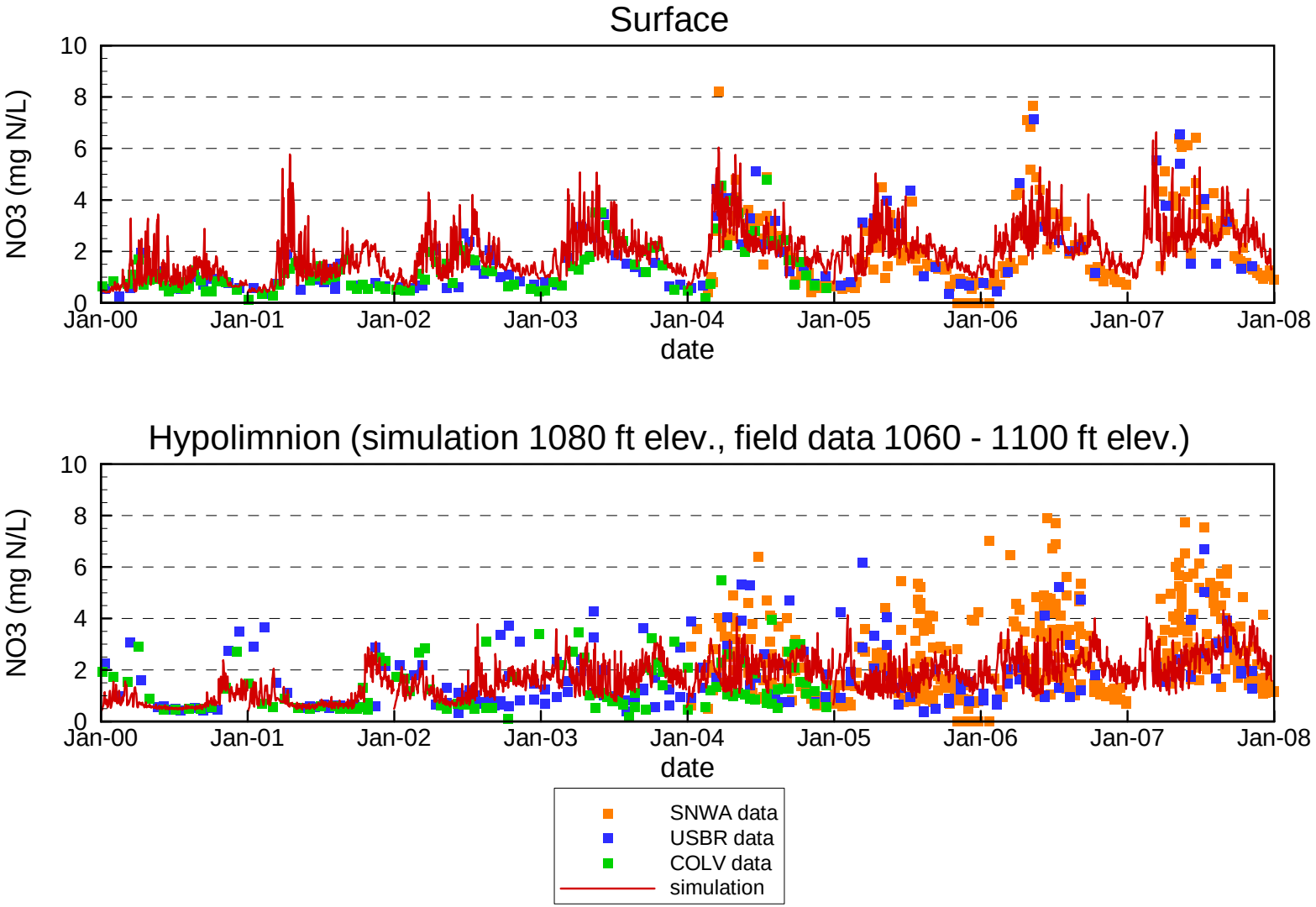

Figure 4.81

Comparison of Measured and Simulated Nitrate at Station CR346.4

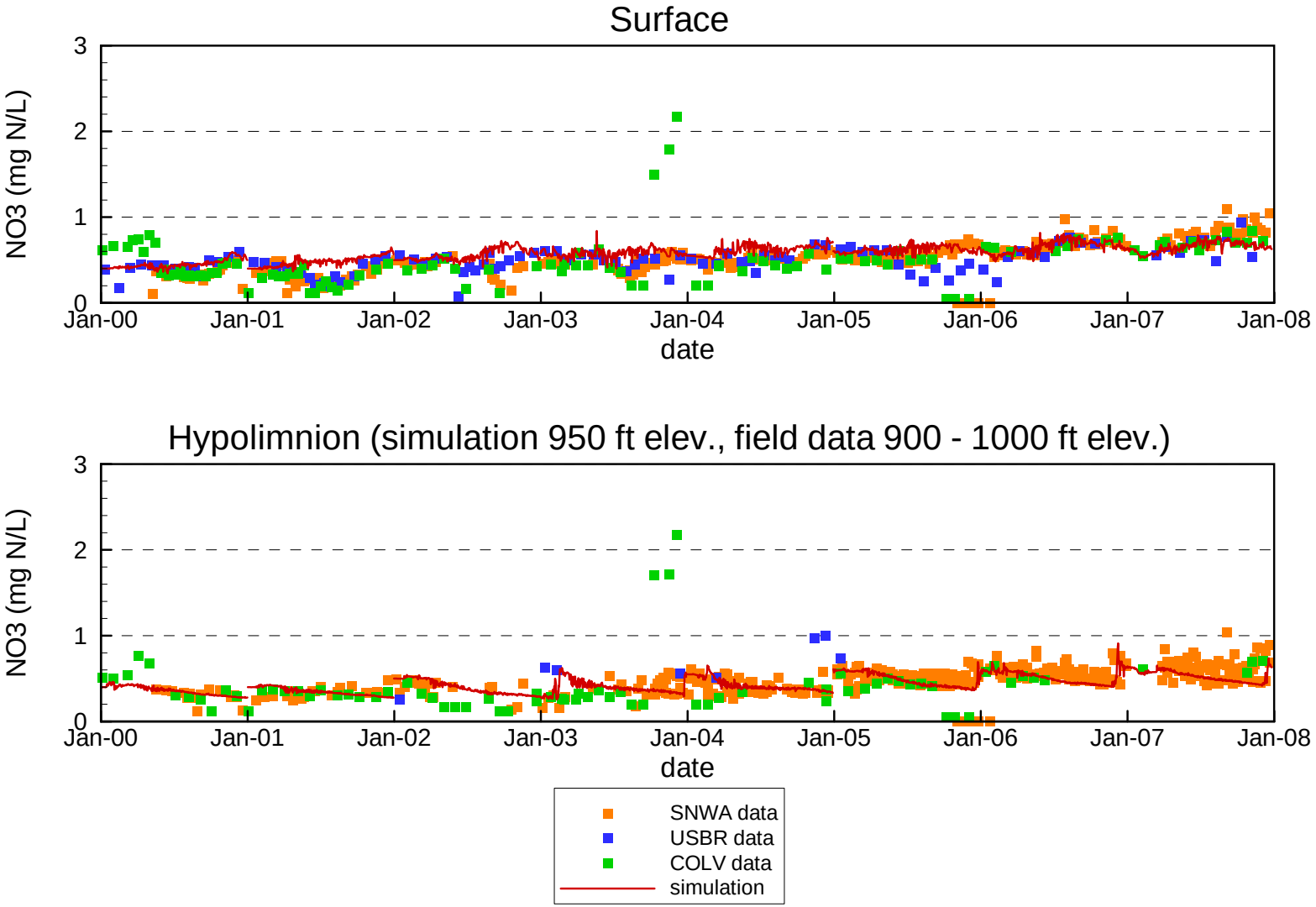

Figure 4.82

Comparison of Measured and Simulated Nitrate at SNWA Intakes #1 and #2

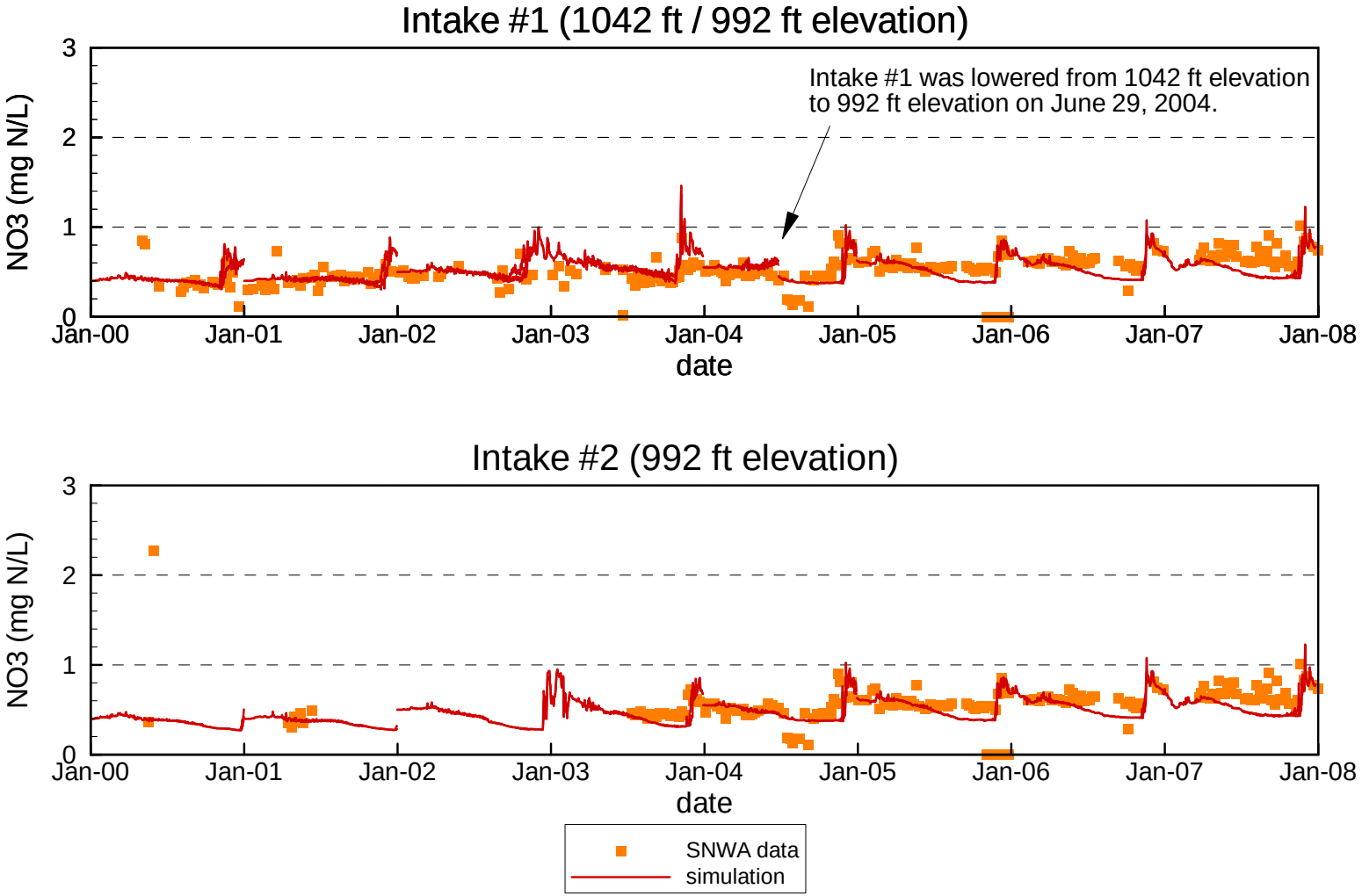

Figure 4.83

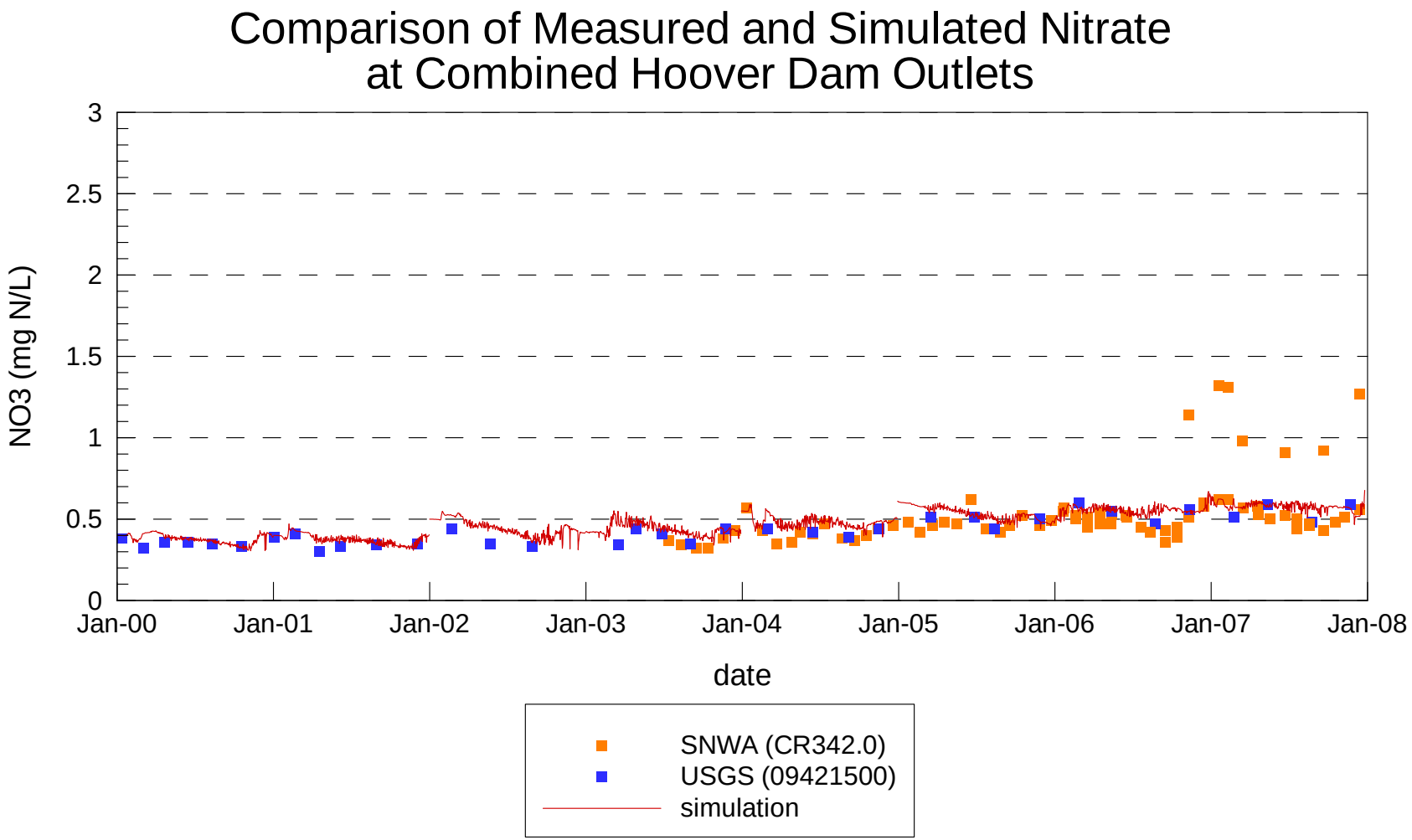
Comparison of Measured and Simulated Nitrate
at Combined Hoover Dam Outlets
NO3 (mg N/L)
3
2.5
2
1.5
1
0.5
0
Jan-00
Jan-01
Jan-02
Jan-03
Jan-04
Jan-05
Jan-06
Jan-07
Jan-08
date
SNWA (CR342.0)
USGS (09421500)
simulation

Figure 4.84

Comparison of Measured and Simulated Ammonium at Station CR394.0

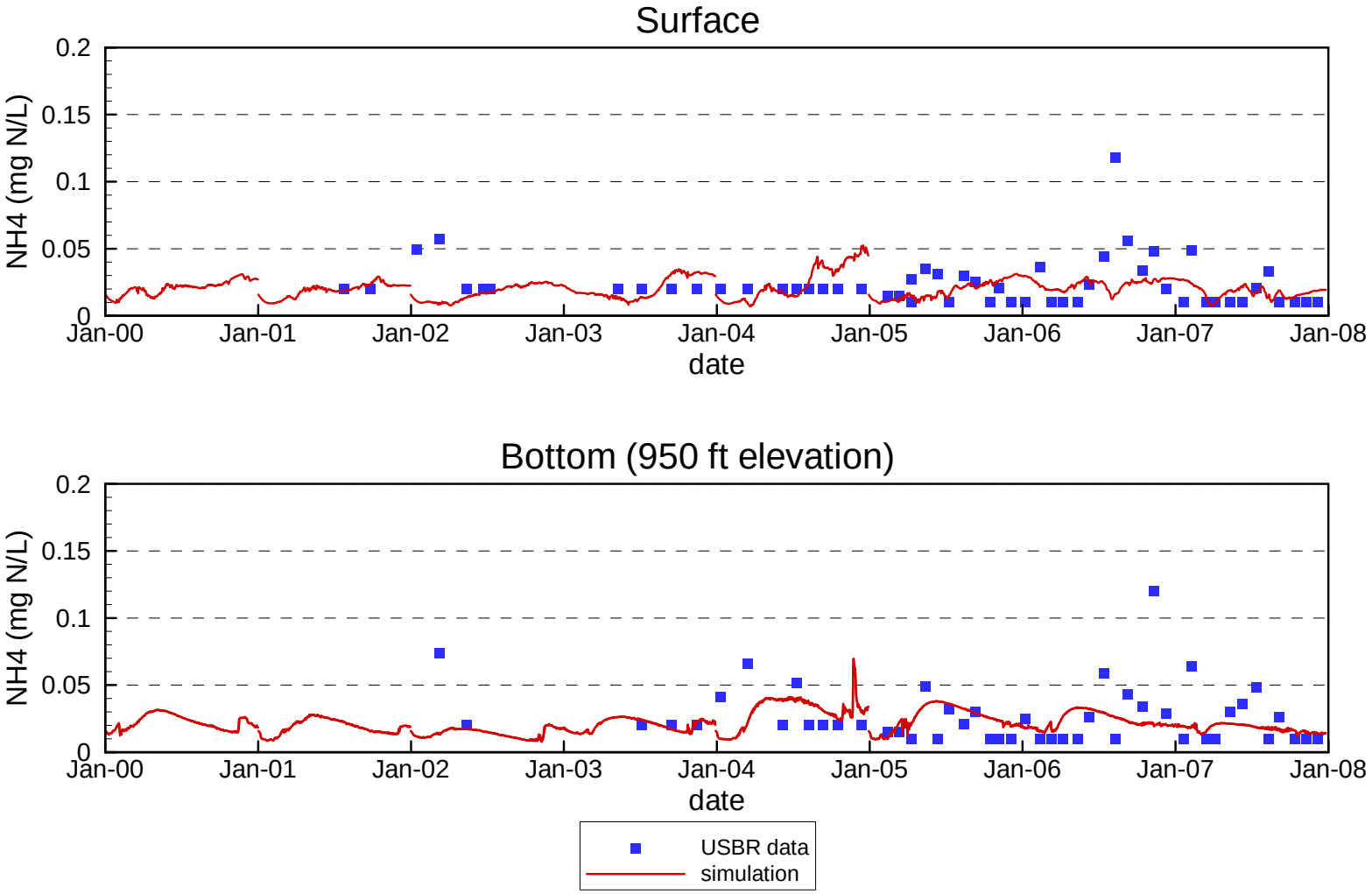

Comparison of Measured and Simulated Ammonium at Station VR25.1

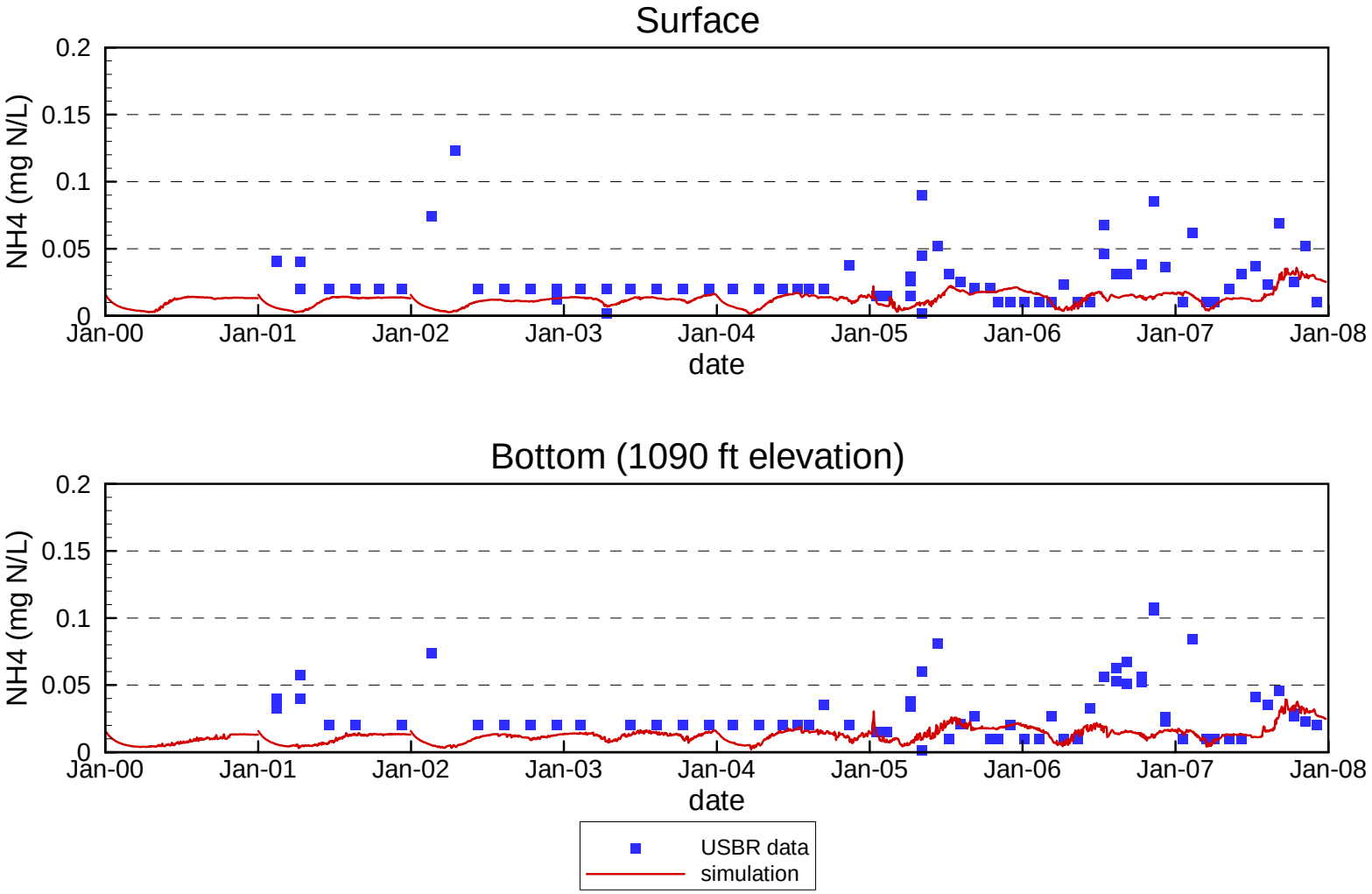

Figure 4.86

Comparison of Measured and Simulated Ammonium at Stations VR12.9 / VR13.0

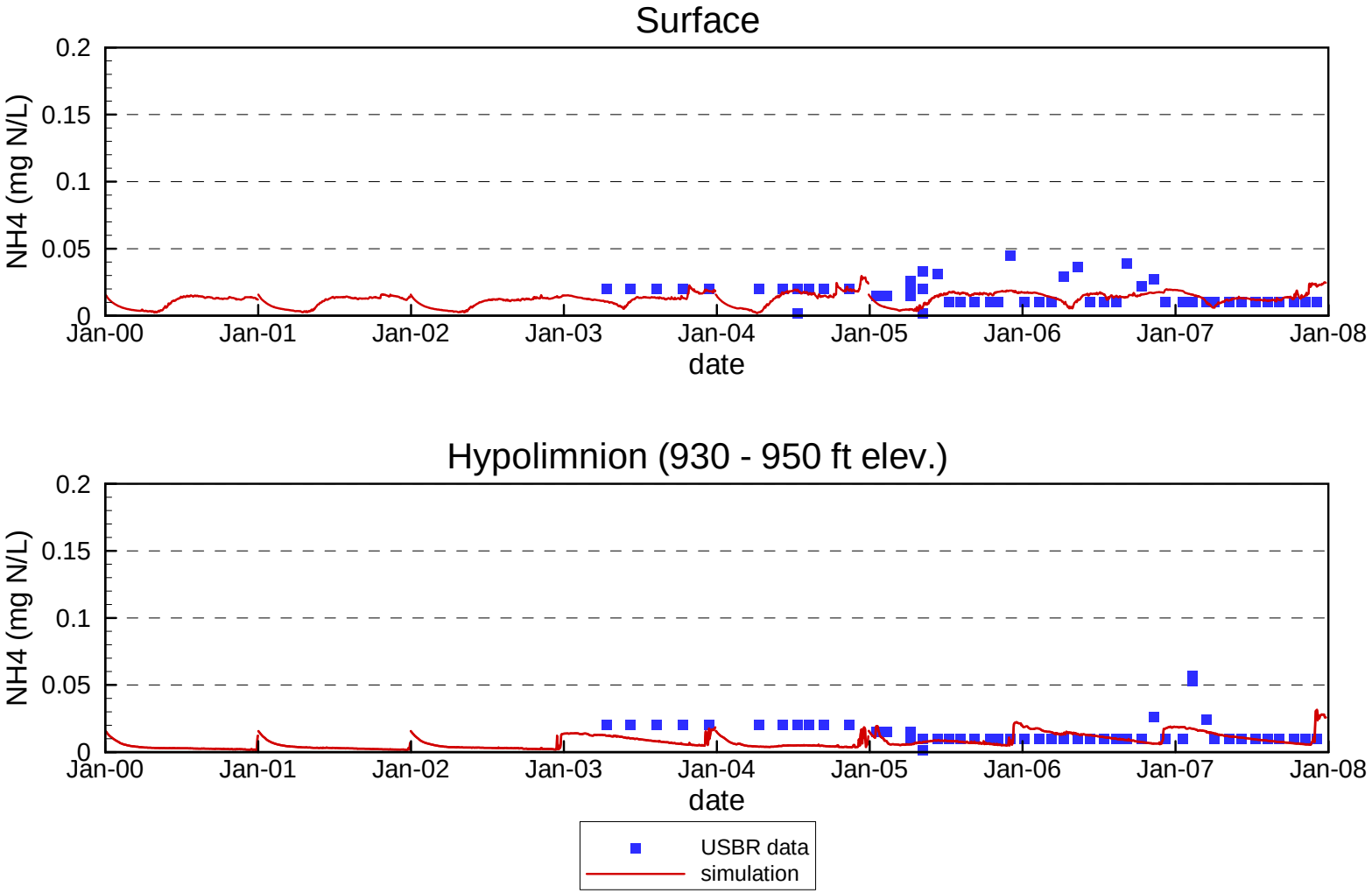

Comparison of Measured and Simulated Ammonium at Station CR360.7

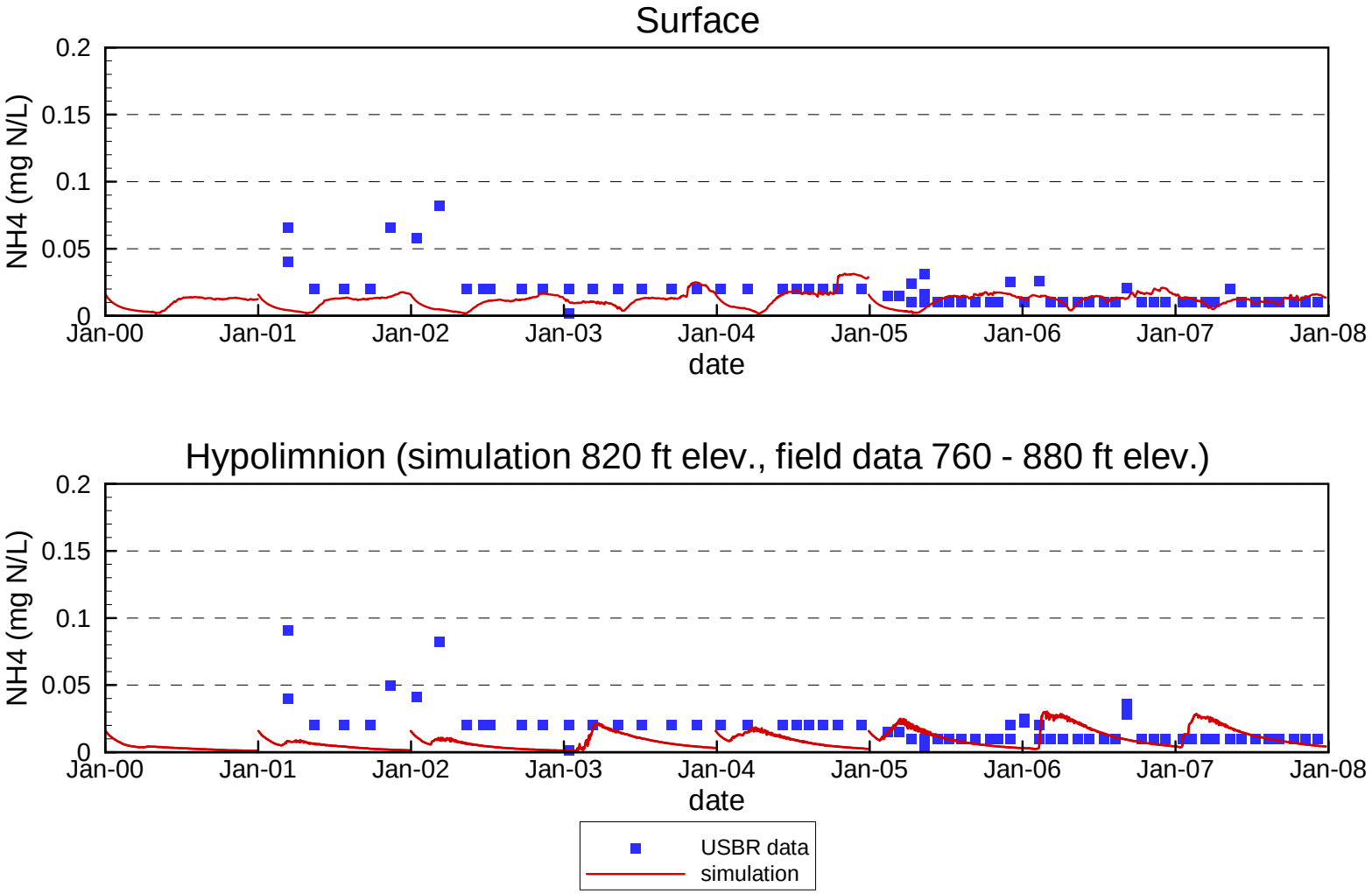

Comparison of Measured and Simulated Ammonium at Station LVB3.5

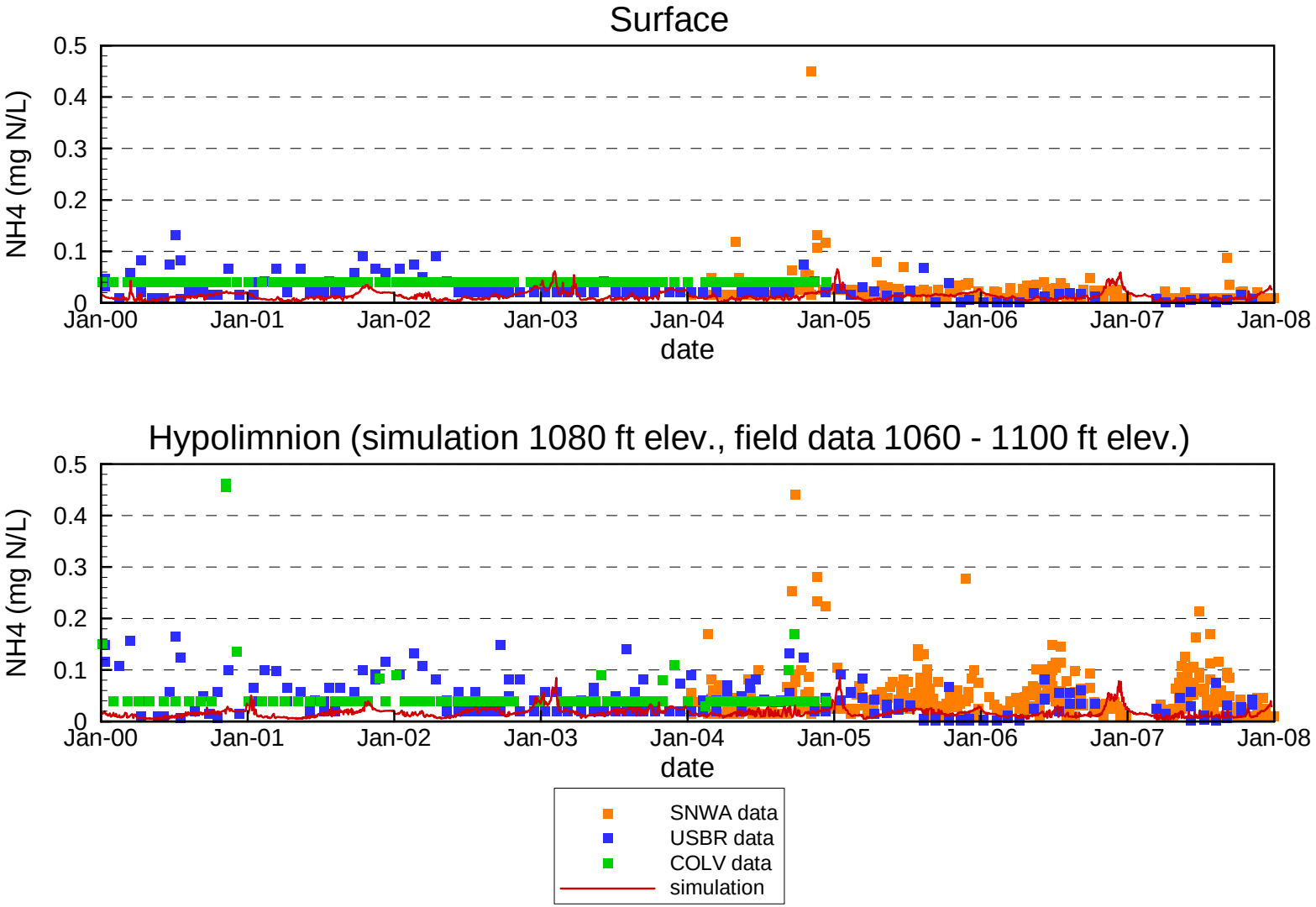

Figure 4.89

Comparison of Measured and Simulated Ammonium at Station CR346.4

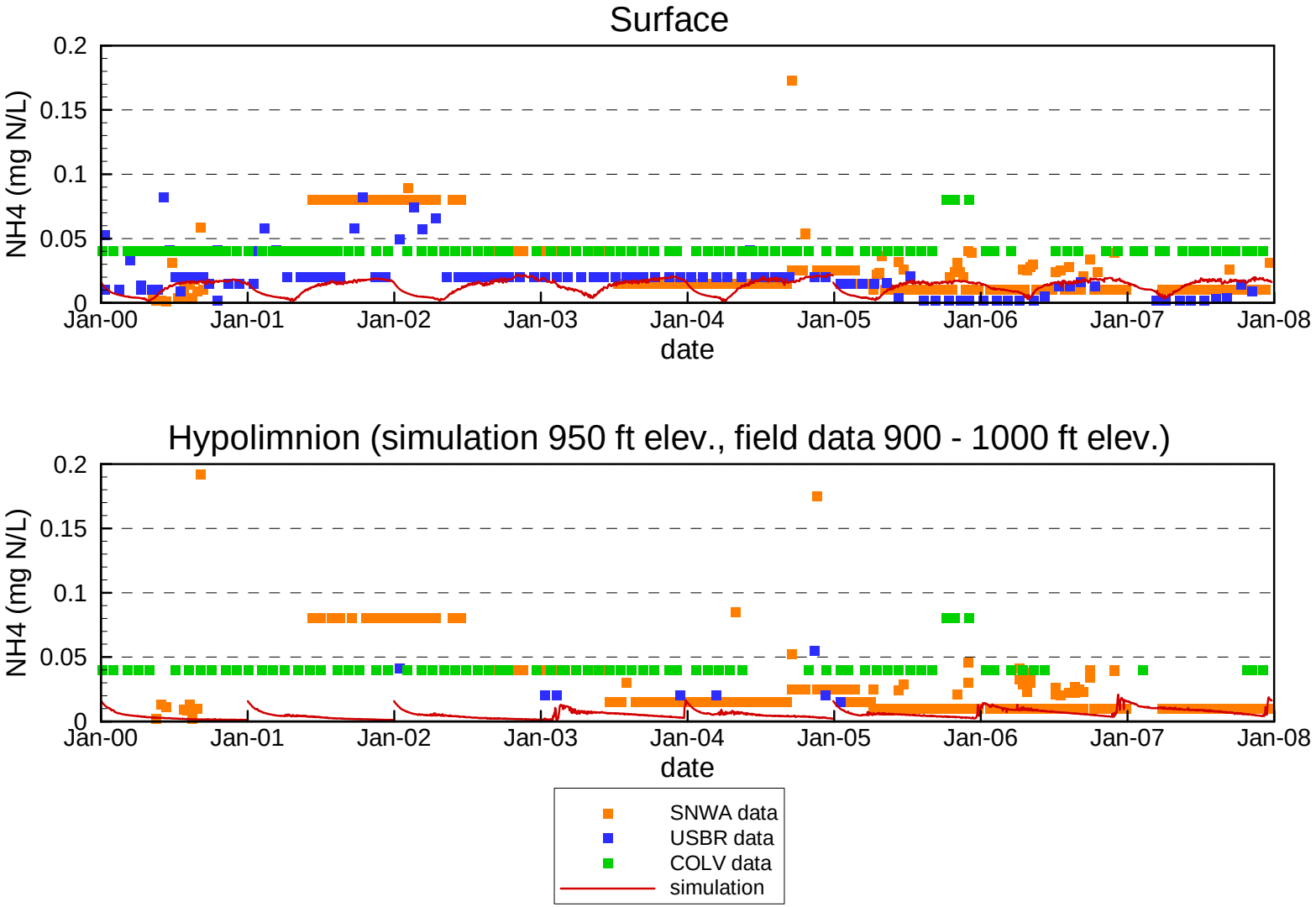

Figure 4.90

Comparison of Measured and Simulated Ammonium at SNWA Intakes #1 and #2

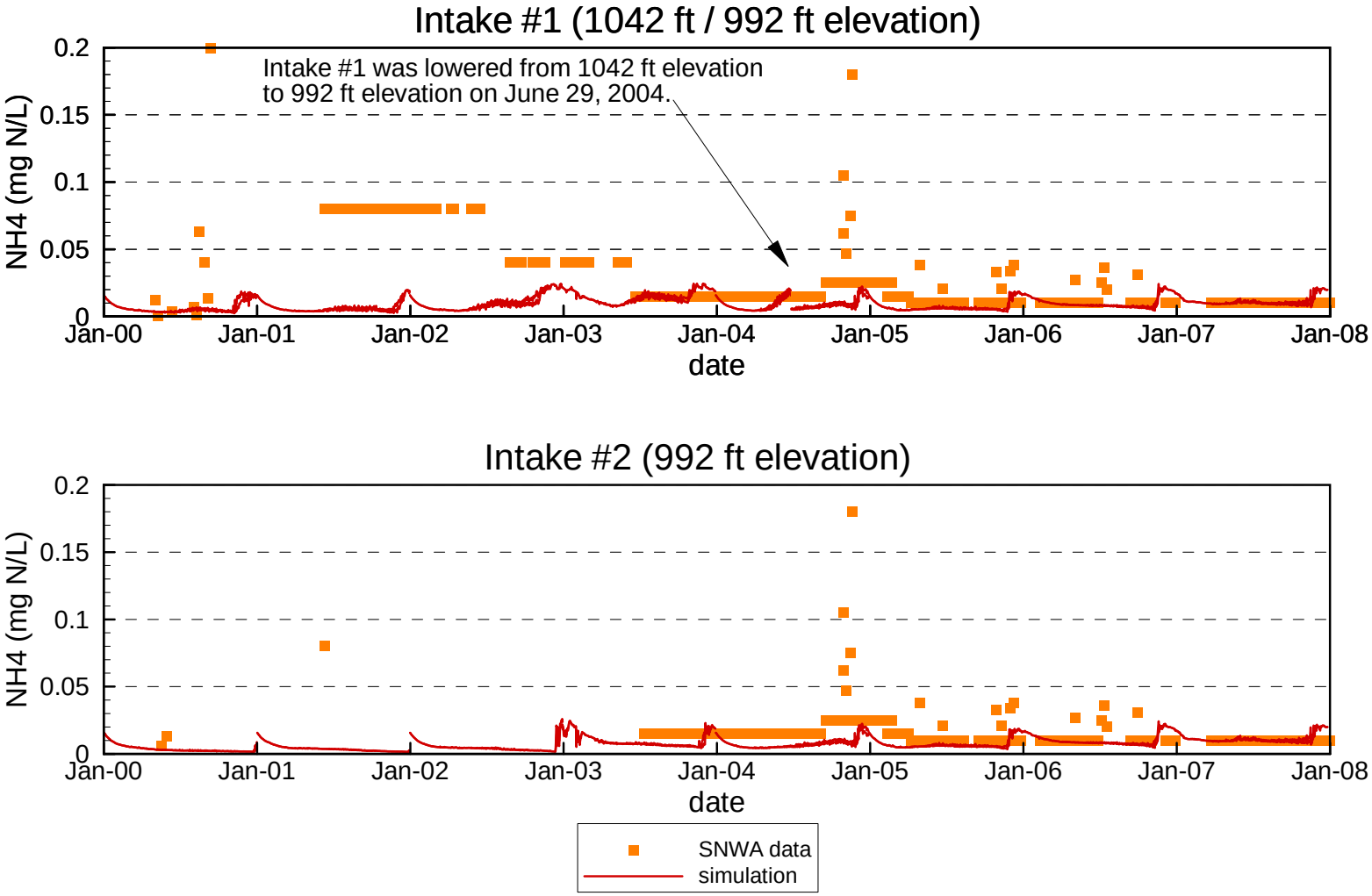

Figure 4.91

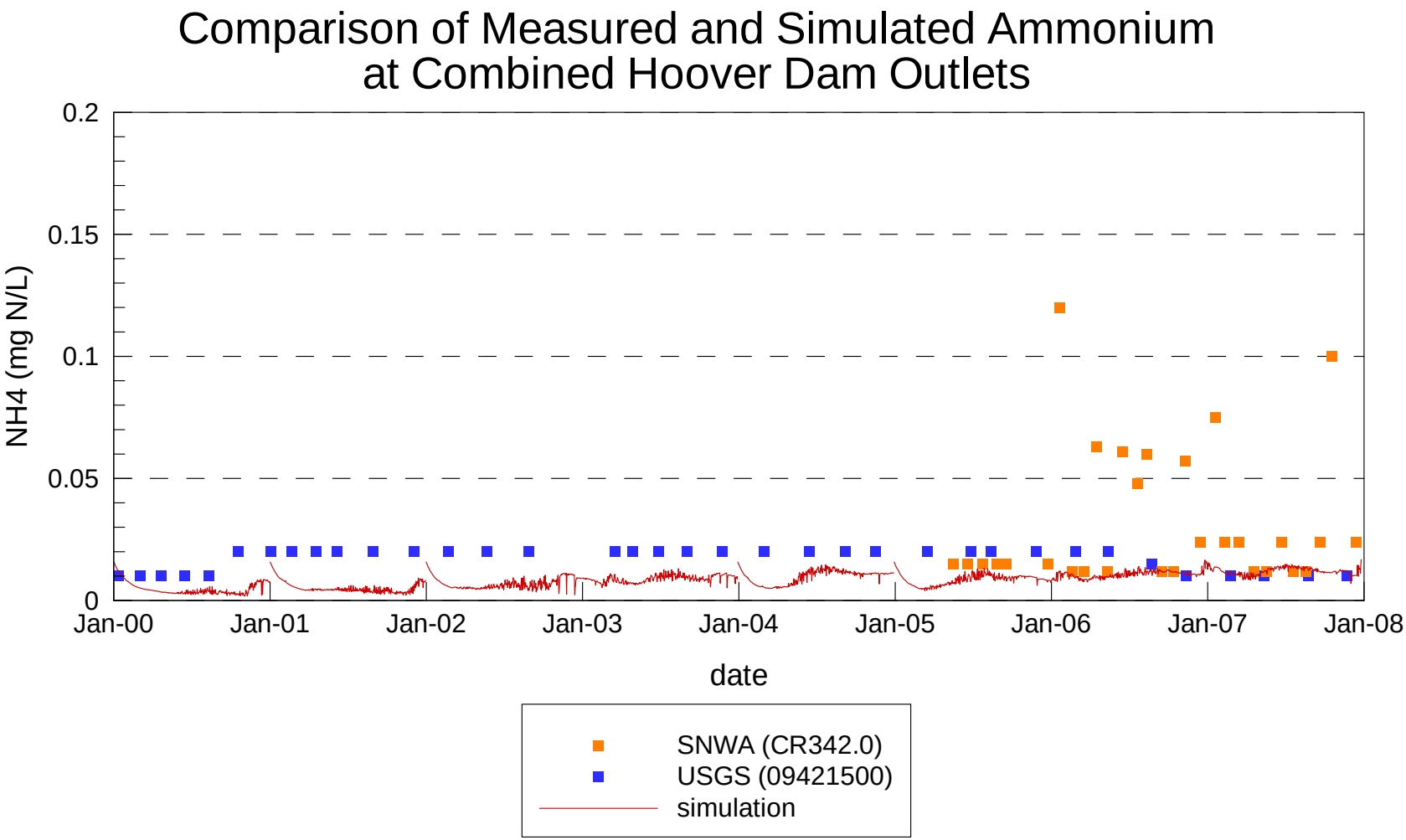
Comparison of Measured and Simulated Ammonium
at Combined Hoover Dam Outlets
NH4 (mg N/L)
0.2
0.15
0.1
0.05
0
Jan-00
Jan-01
Jan-02
Jan-03
Jan-04
Jan-05
Jan-06
Jan-07
Jan-08
date
SNWA (CR342.0)
USGS (09421500)
simulation

Figure 4.92

Comparison of Measured and Simulated Total Organic Carbon at Station CR394.0

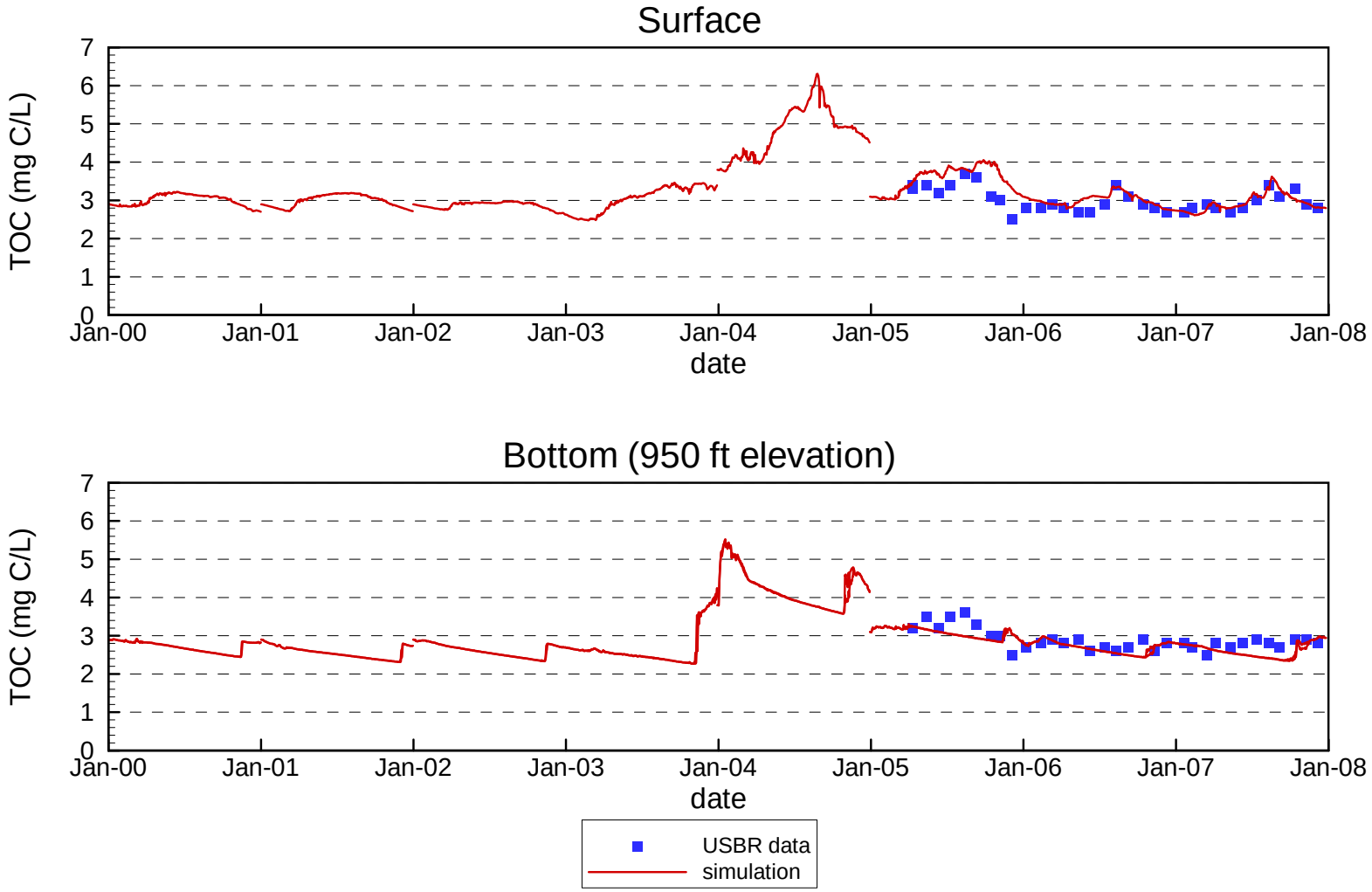

Figure 4.93

Comparison of Measured and Simulated Total Organic Carbon at Station VR25.1

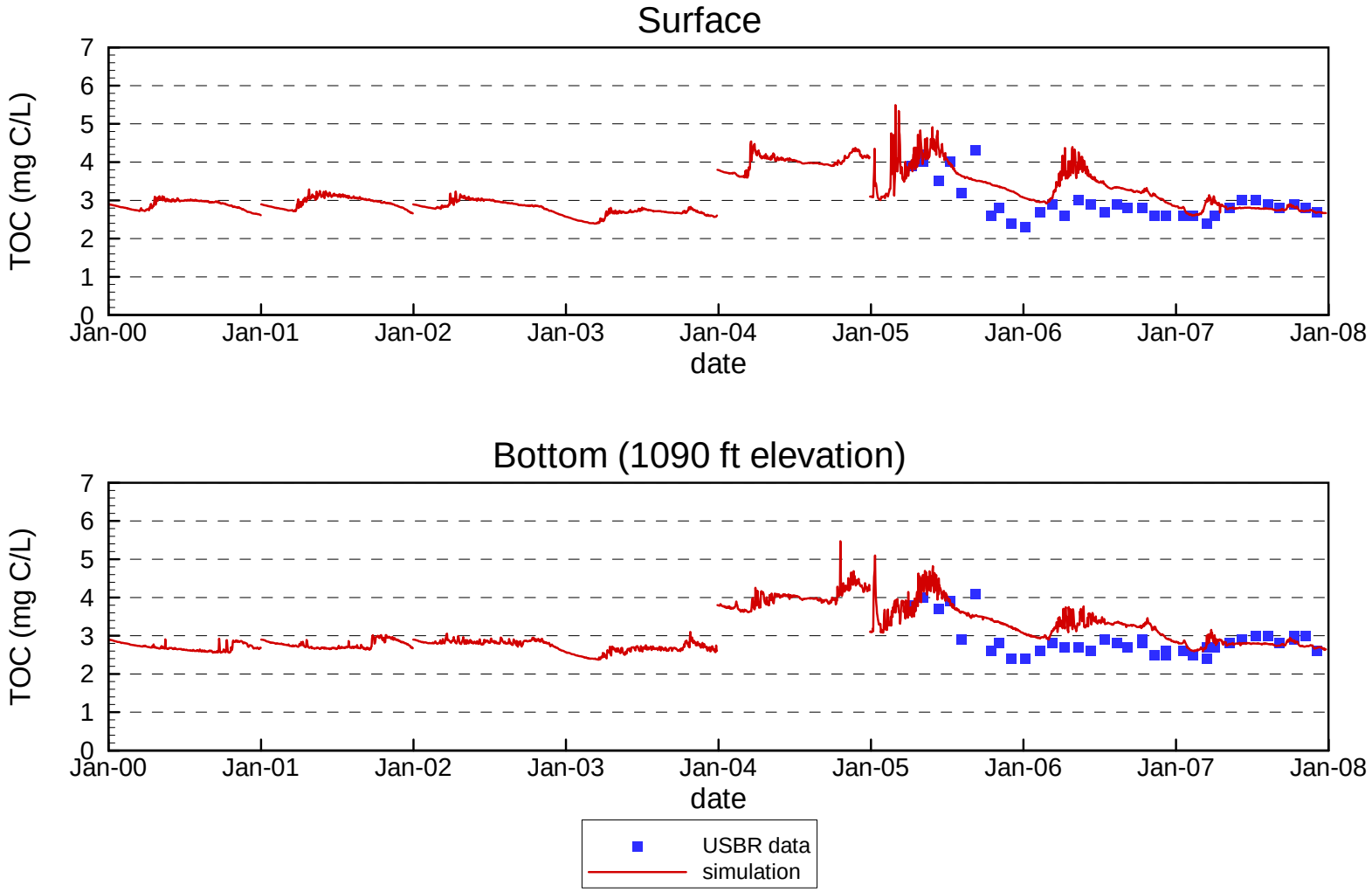

Figure 4.94

Comparison of Measured and Simulated Total Organic Carbon at Stations VR12.9 / VR13.0

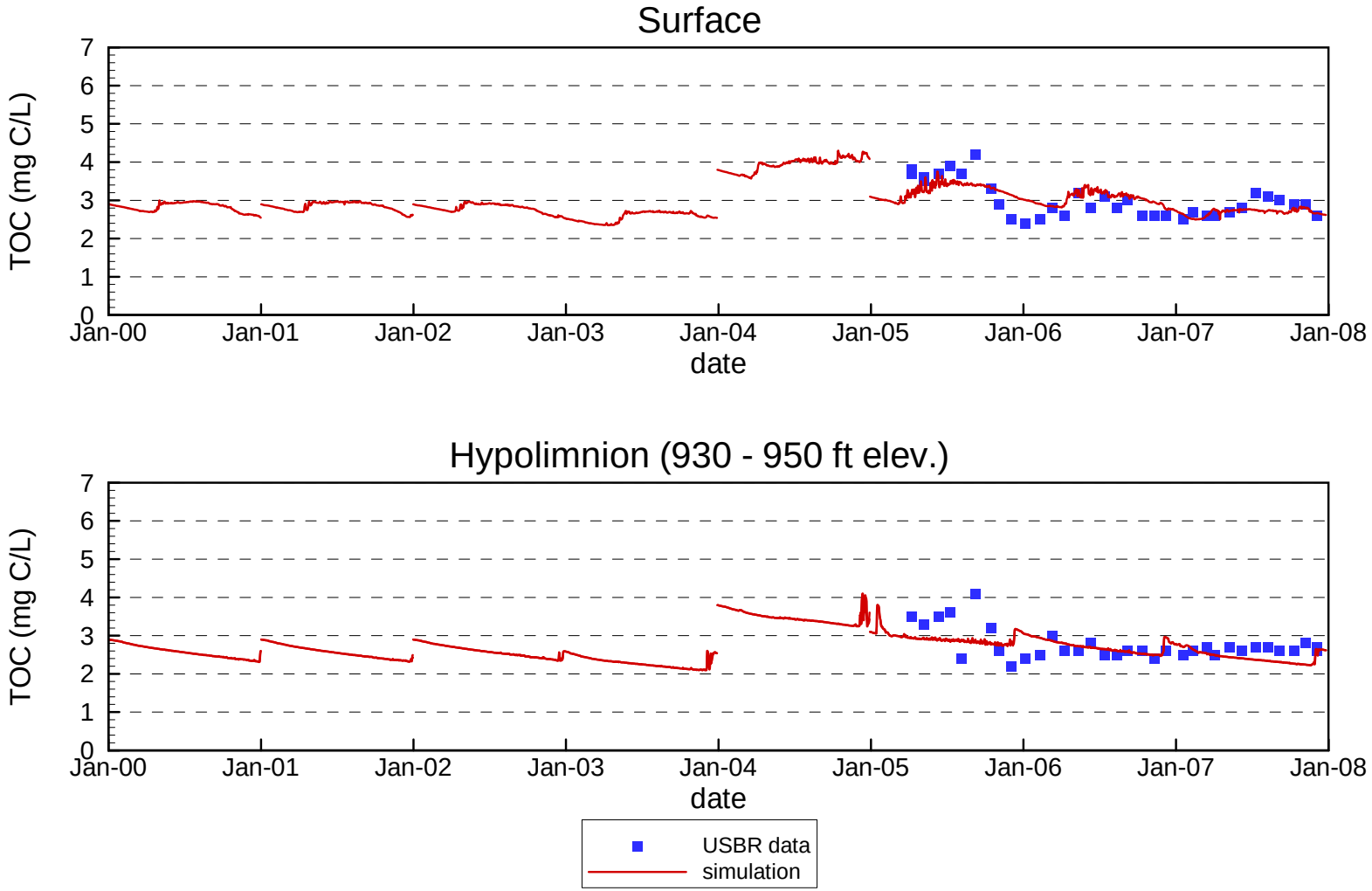

Figure 4.95

Comparison of Measured and Simulated Total Organic Carbon at Station CR360.7

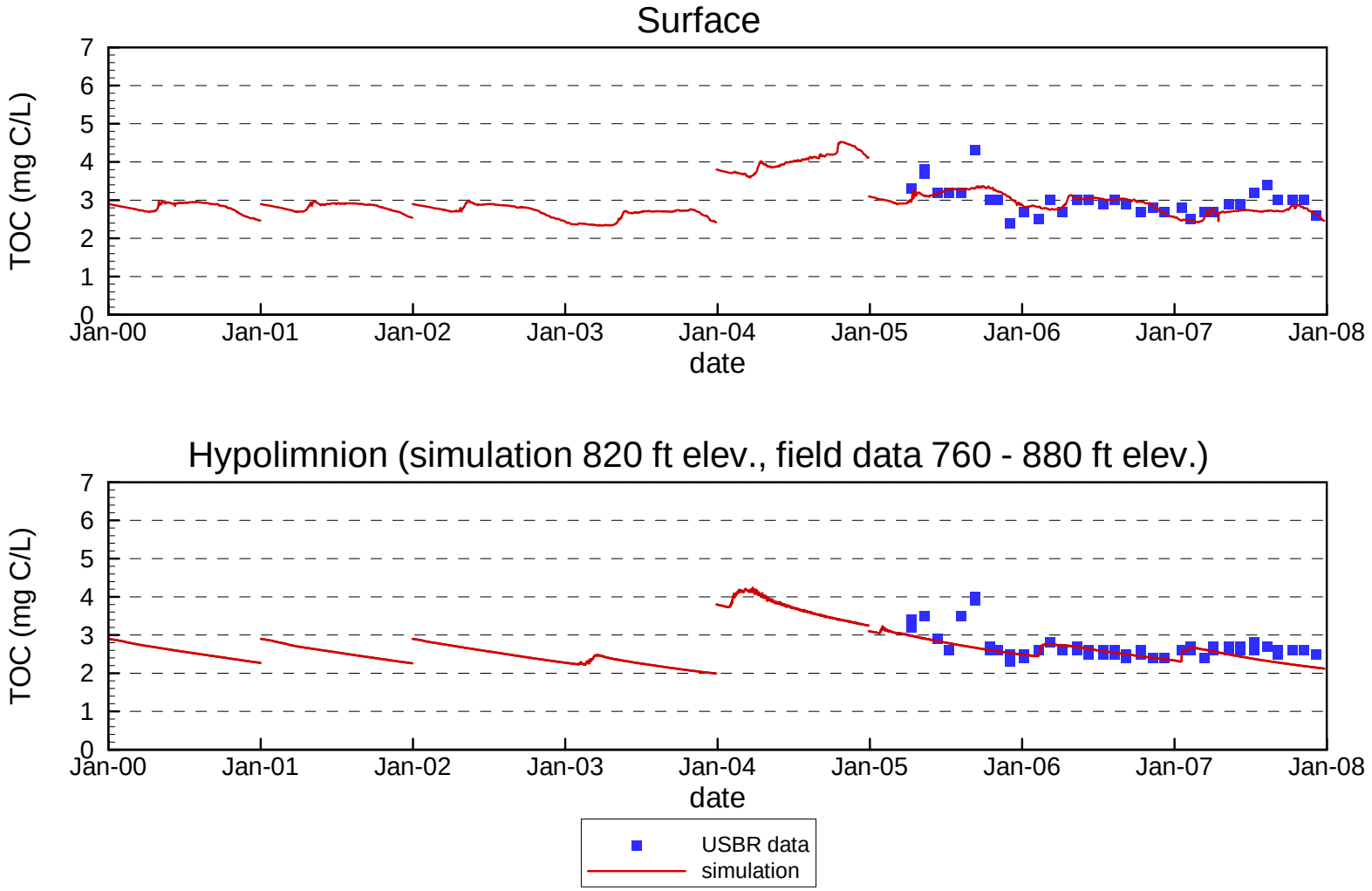

Figure 4.96

Comparison of Measured and Simulated Total Organic Carbon at Station LVB3.5

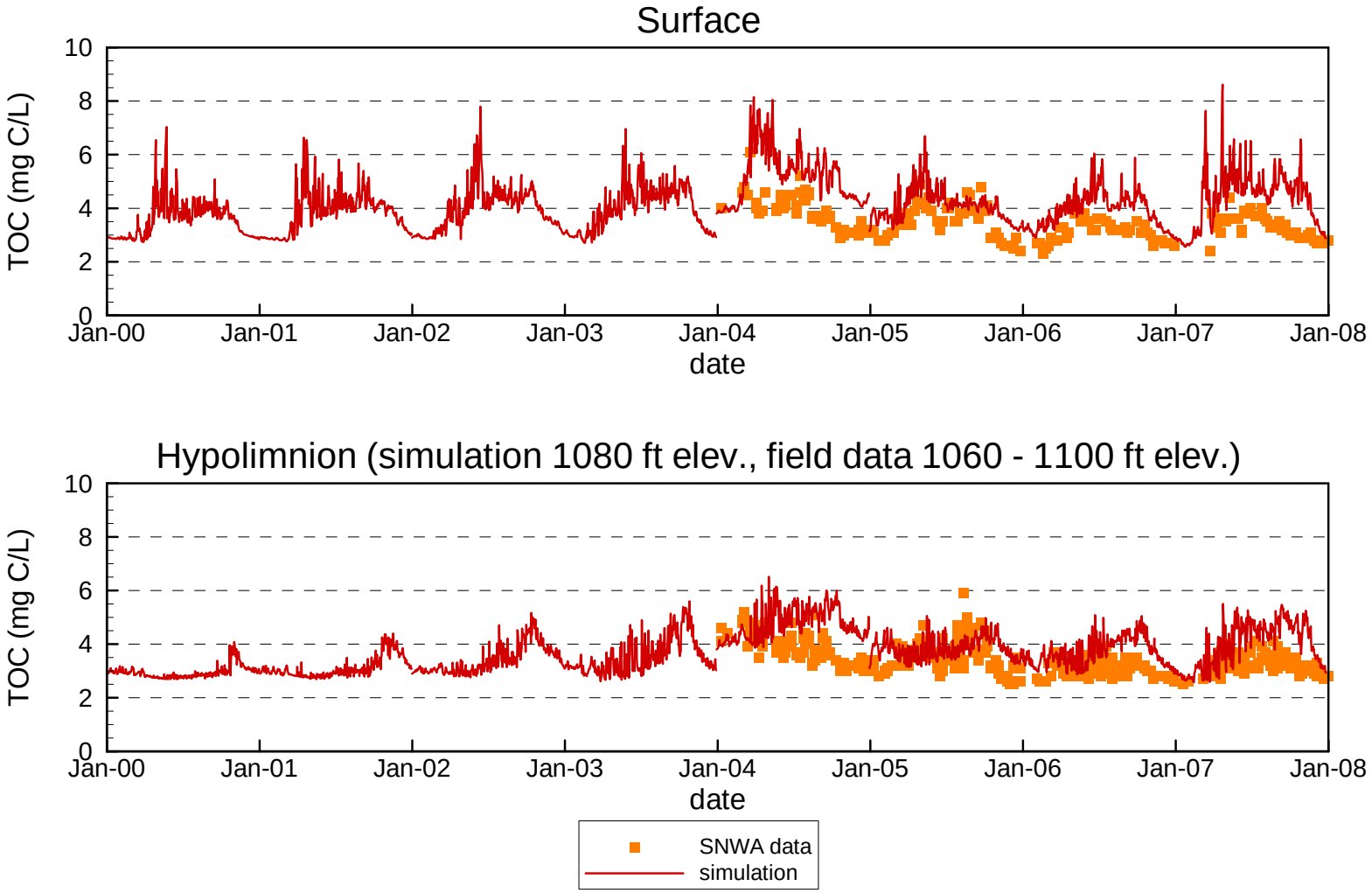

Figure 4.97

Comparison of Measured and Simulated Total Organic Carbon at Station CR346.4

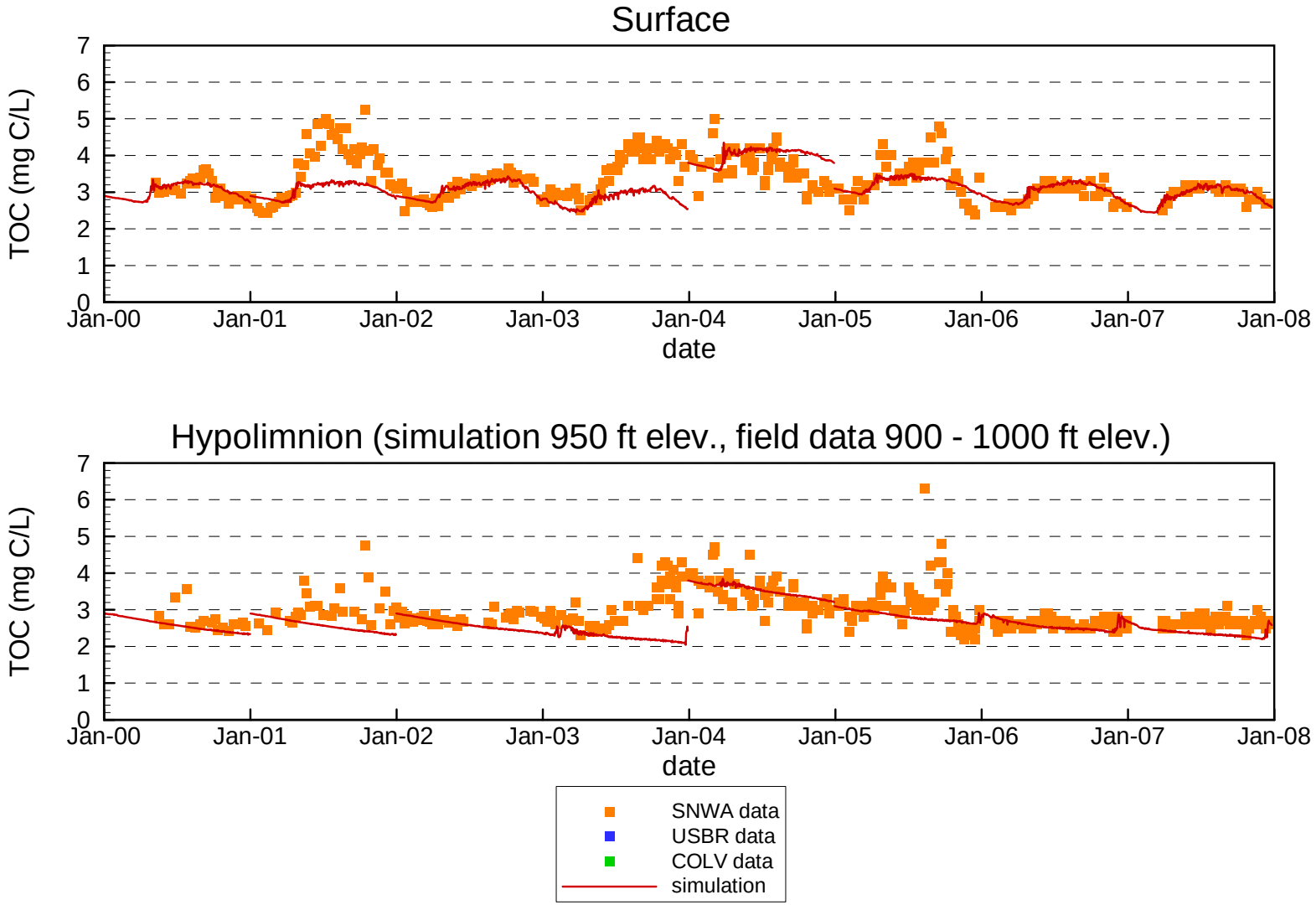

Figure 4.98

Comparison of Measured and Simulated Total Organic Carbon at SNWA Intakes #1 and #2

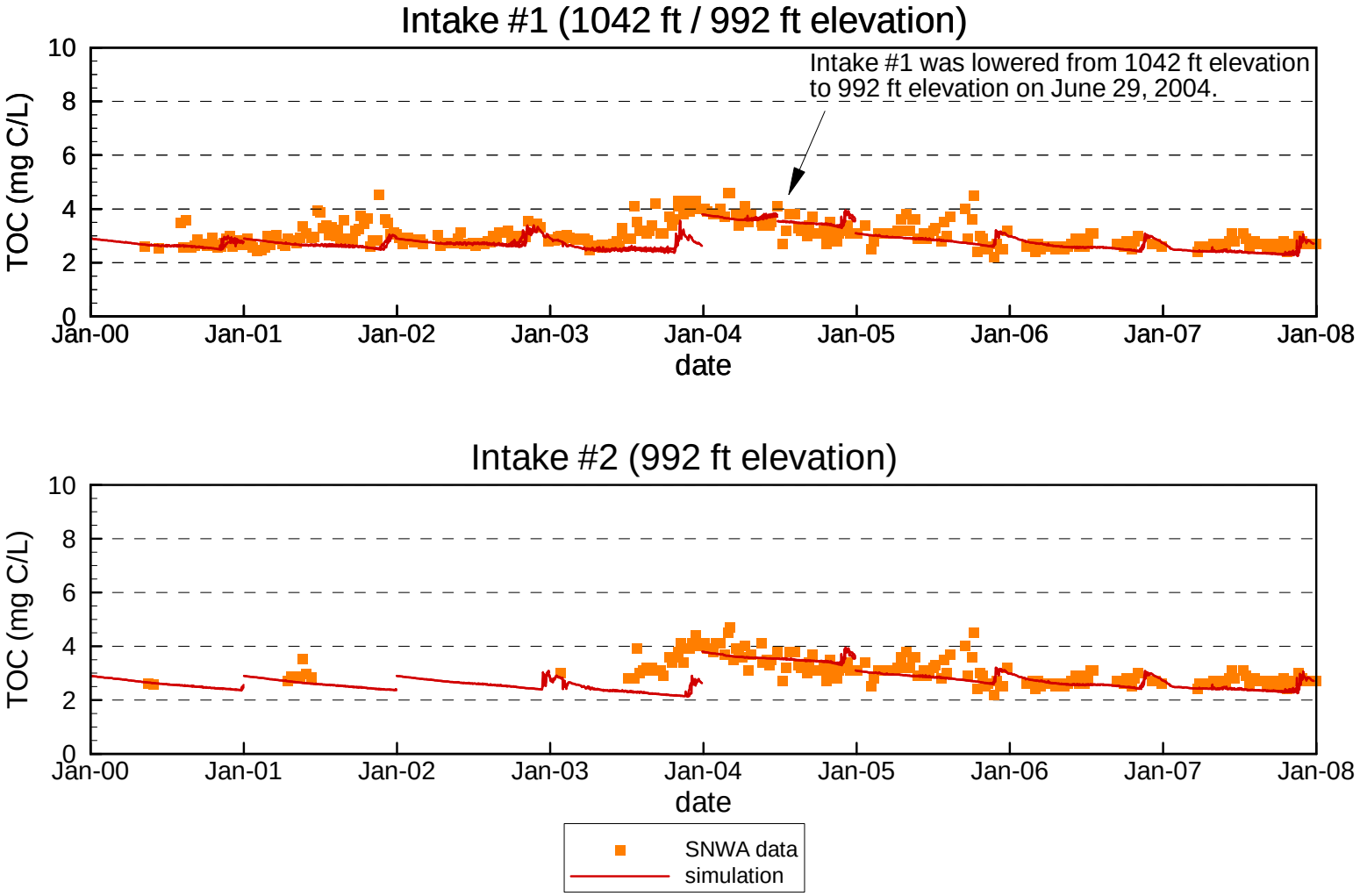

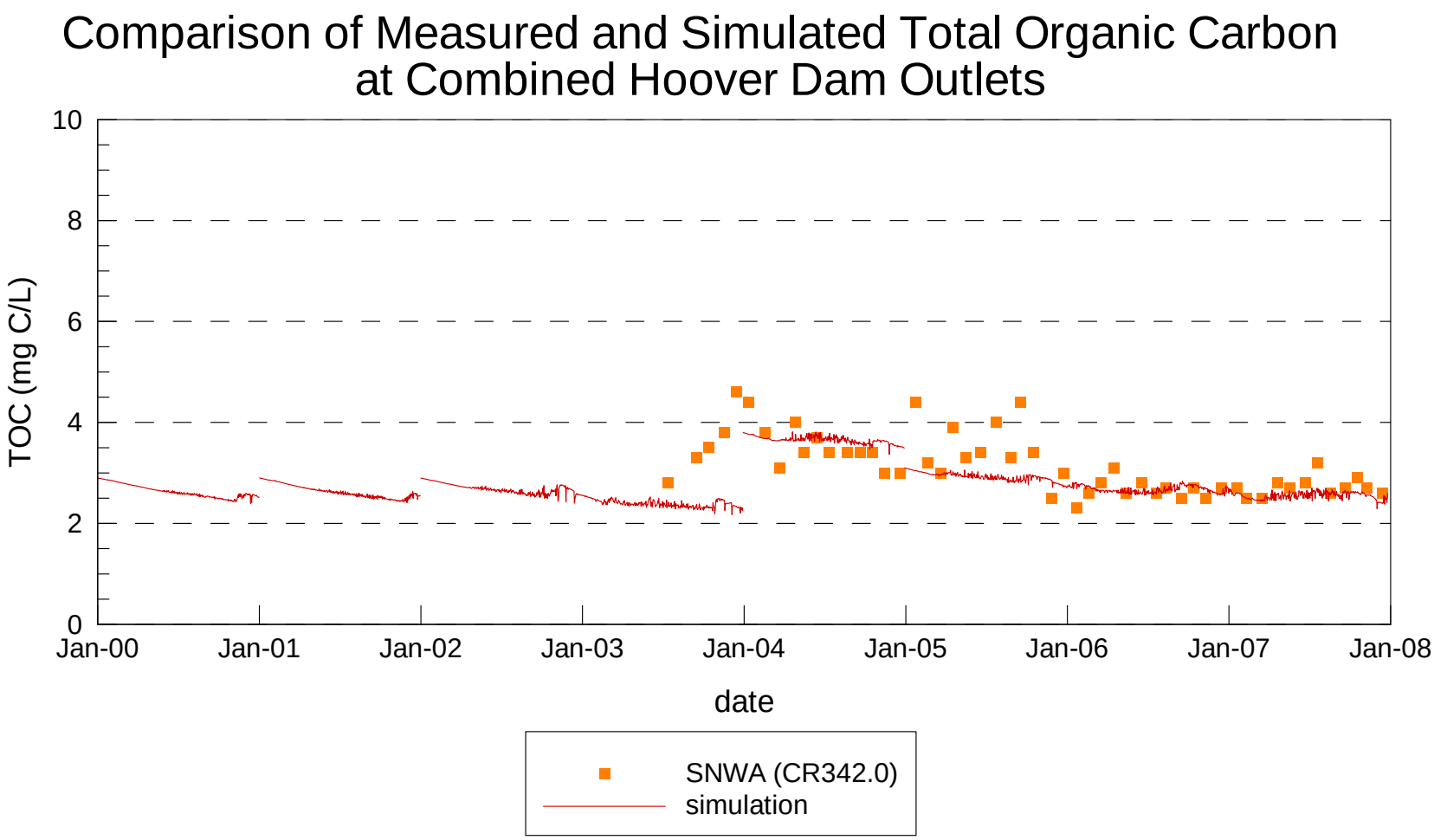
Comparison of Measured and Simulated Total Organic Carbon at Combined Hoover Dam Outlets
TOC (mg C/L)
10
8
6
4
2
0
Jan-00
Jan-01
Jan-02
Jan-03
Jan-04
Jan-05
Jan-06
Jan-07
Jan-08
date
SNWA (CR342.0)
simulation

Figure 4.100

Comparison of Measured and Simulated pH Profiles at Station CR346.4 (2006 – 2007)

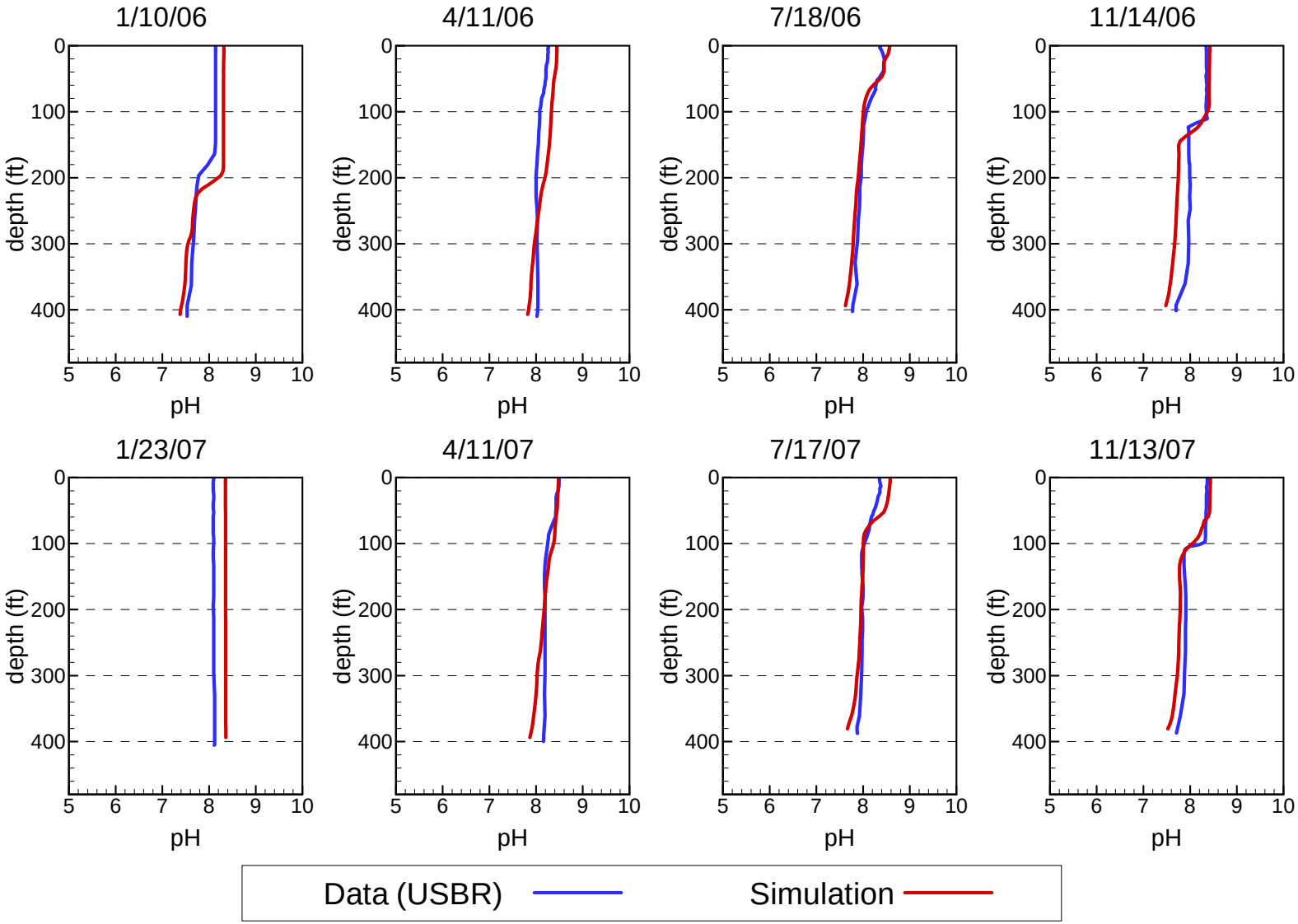

Figure 4.101

Comparison of Measured and Simulated pH at Station CR394.0

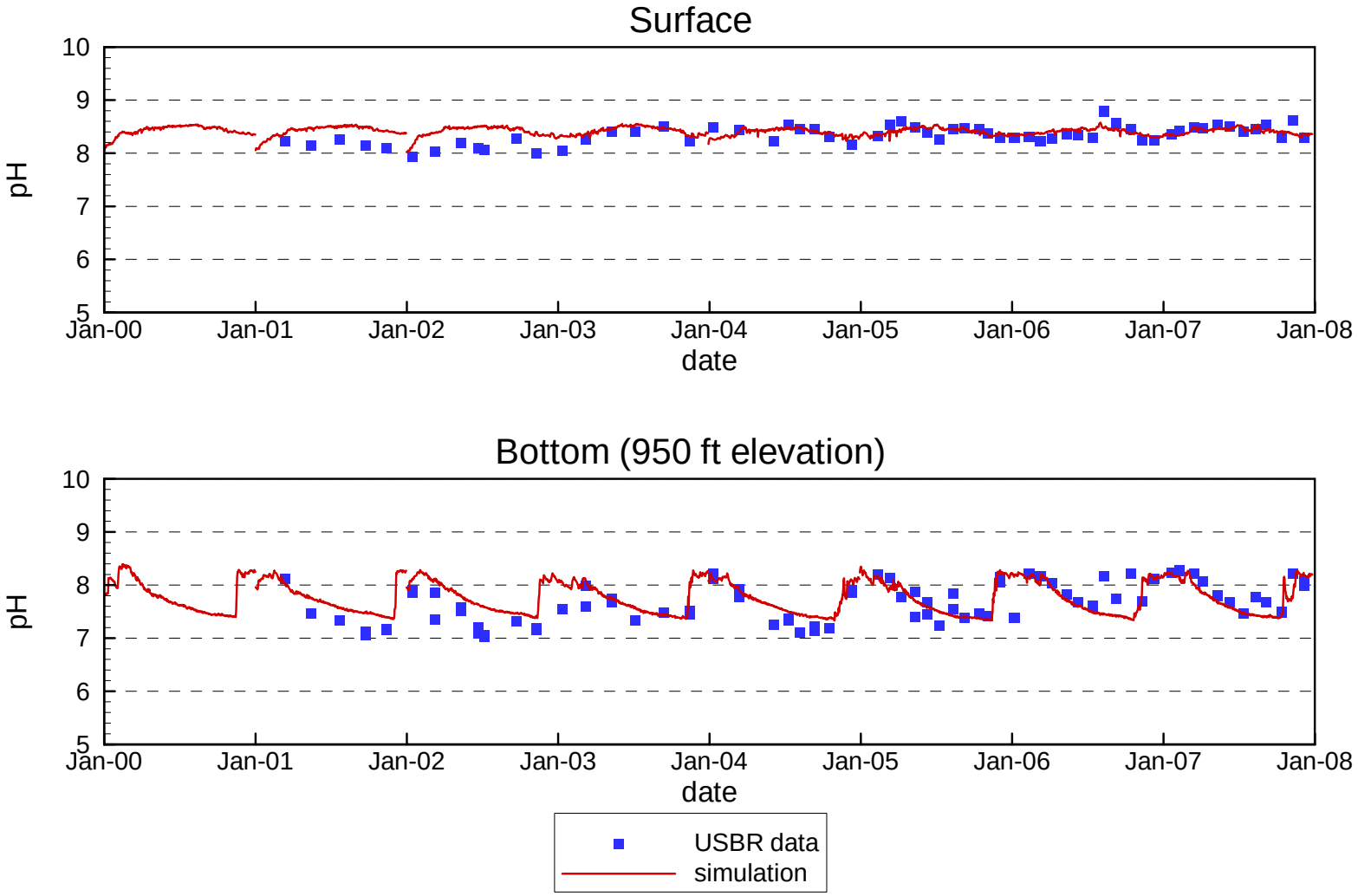

Figure 4.102

Comparison of Measured and Simulated pH at Station VR25.1

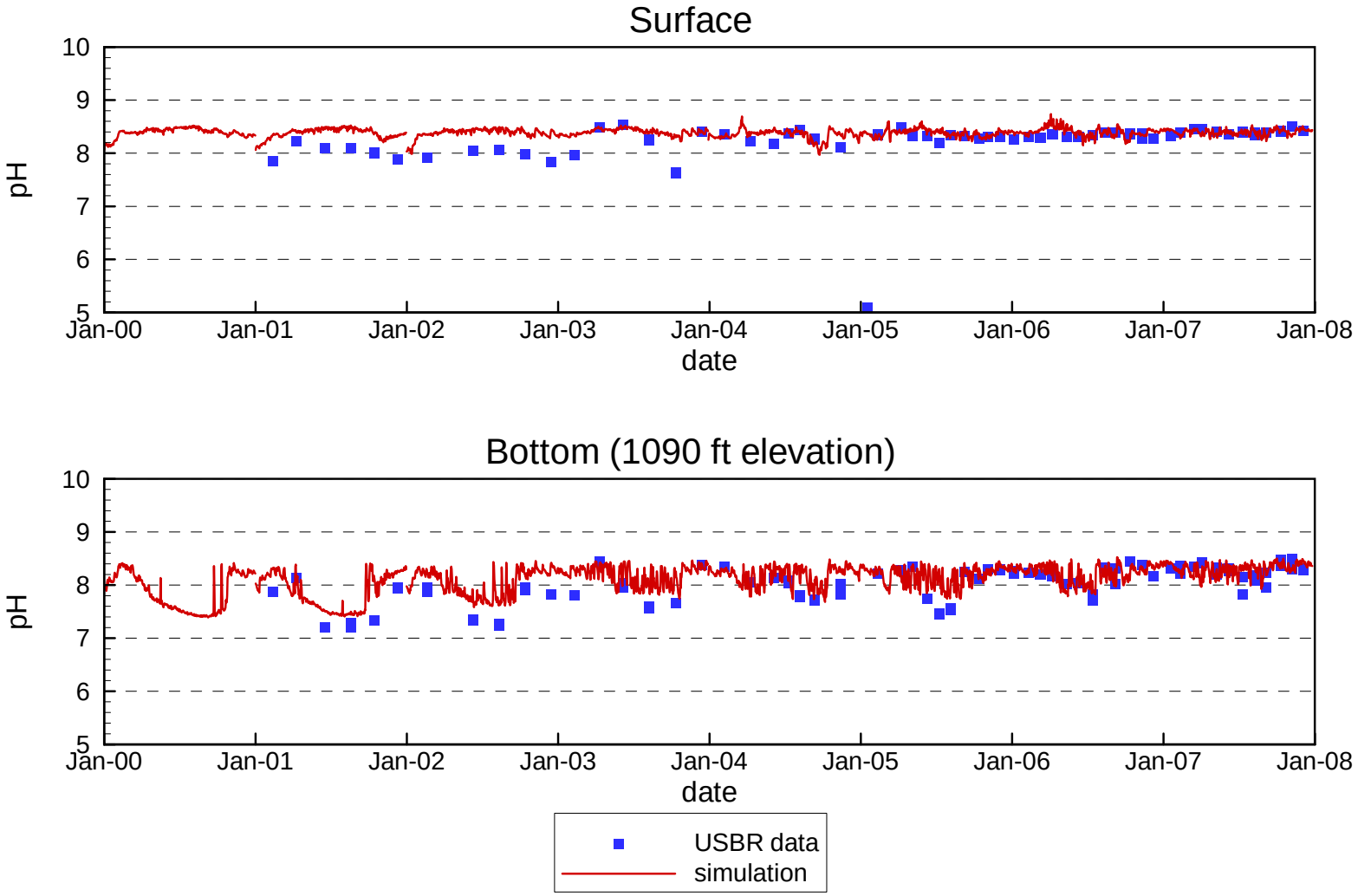

Figure 4.103

Comparison of Measured and Simulated pH at Stations VR12.9 / VR13.0

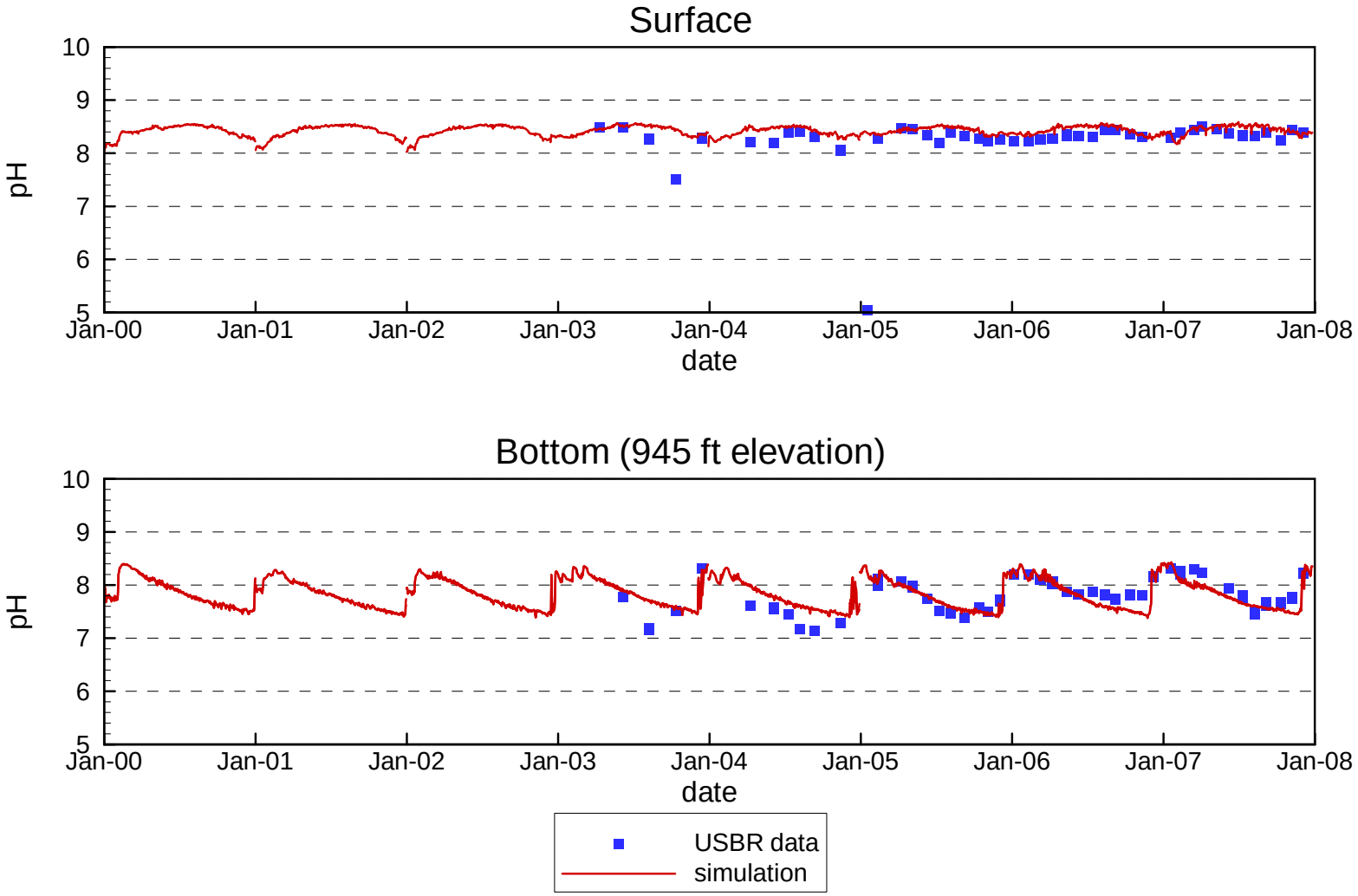

Figure 4.104

Comparison of Measured and Simulated pH at Station CR360.7

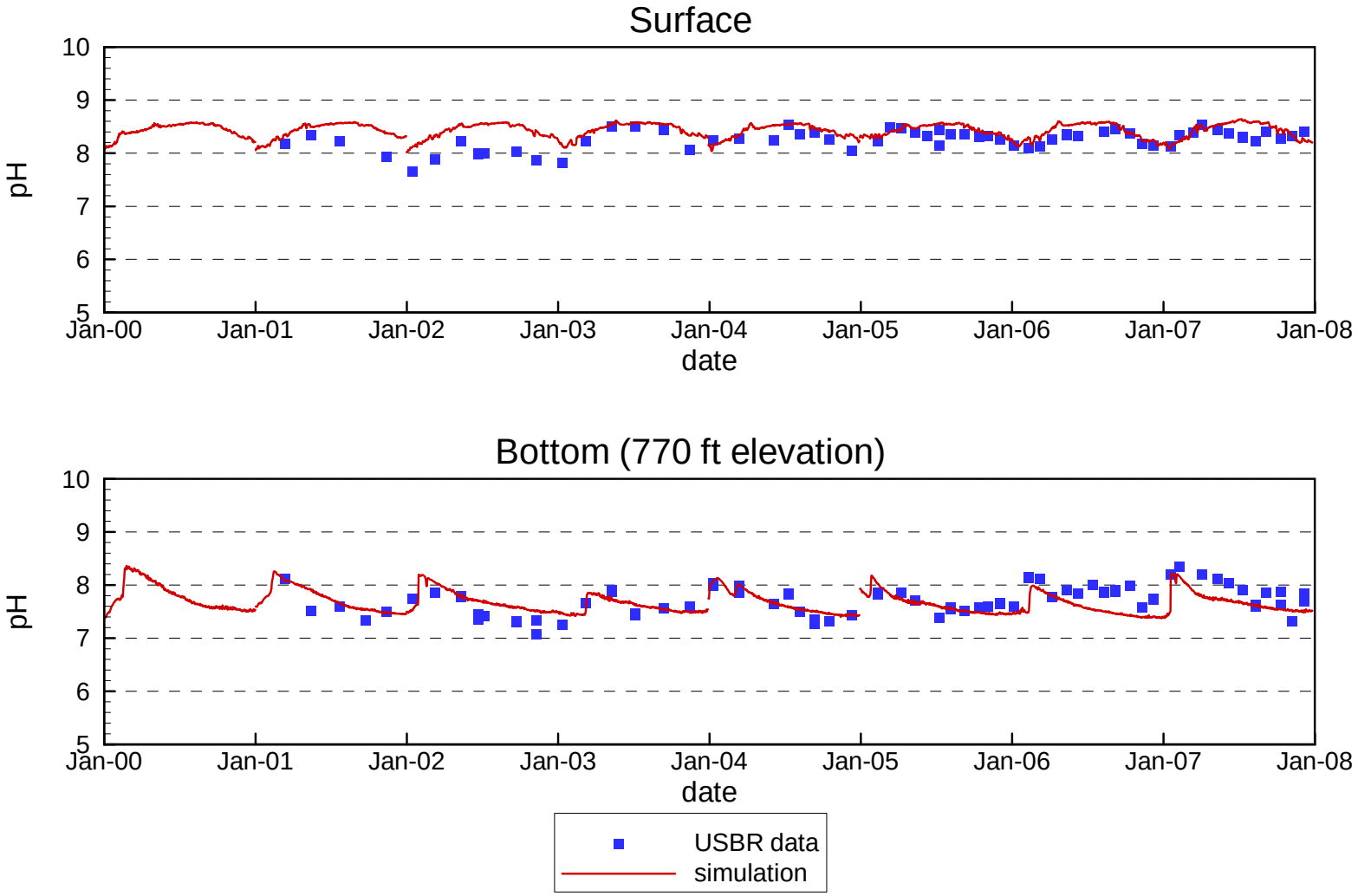

Figure 4.105

Comparison of Measured and Simulated pH at Station LVB3.5

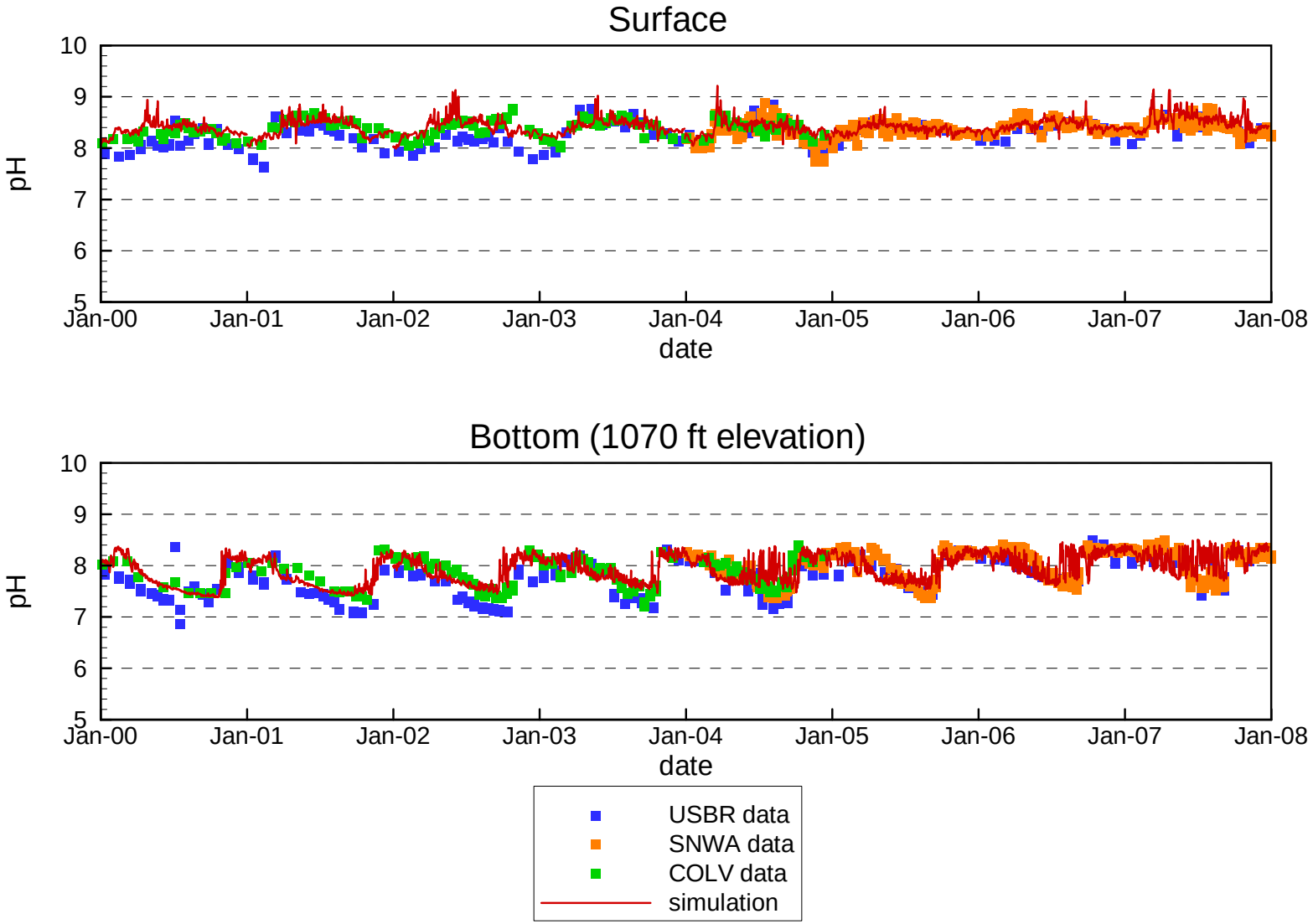

Figure 4.106

Comparison of Measured and Simulated pH at Station CR346.4

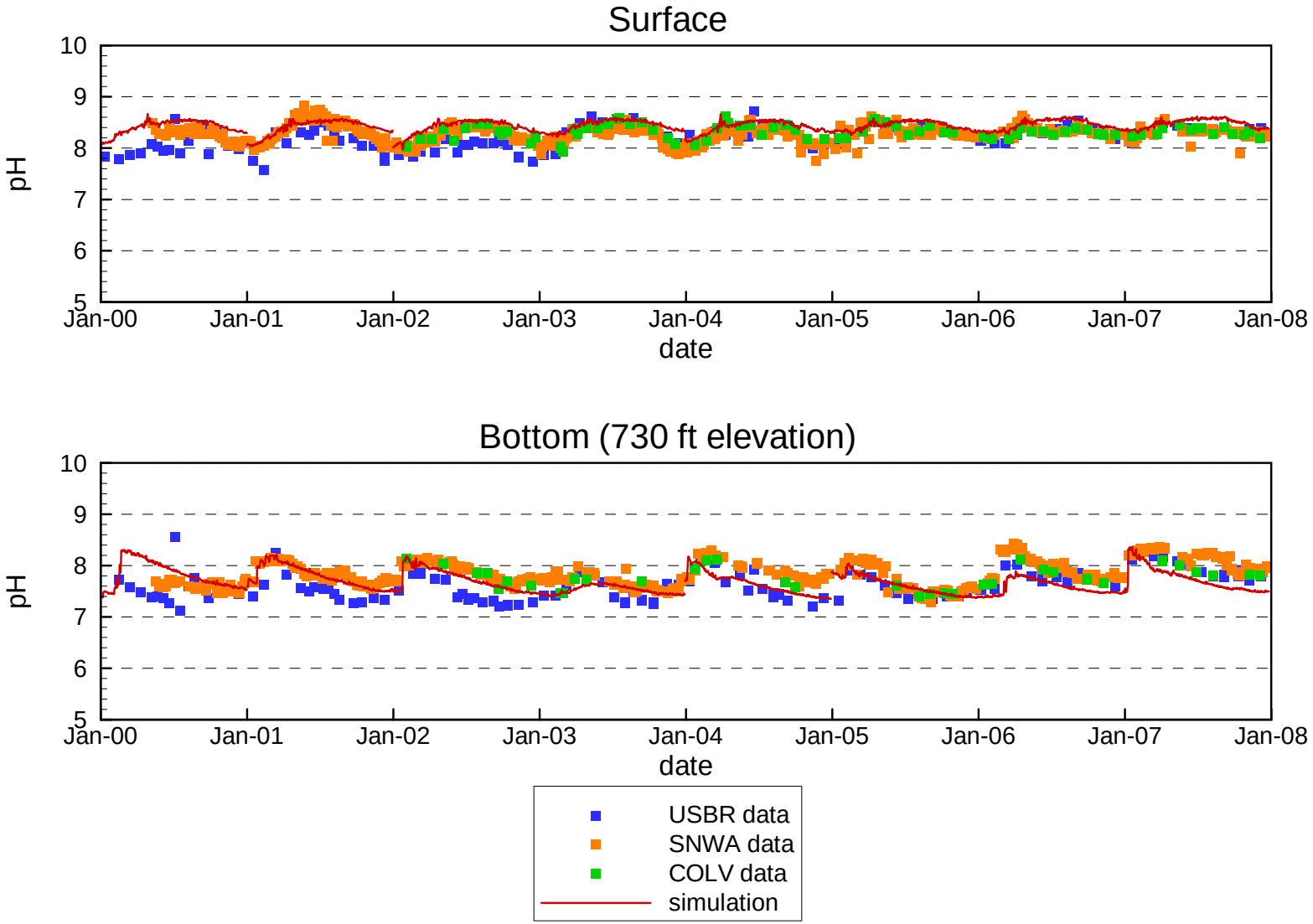

Figure 4.107

Comparison of Measured and Simulated pH at SNWA Intakes #1 and #2

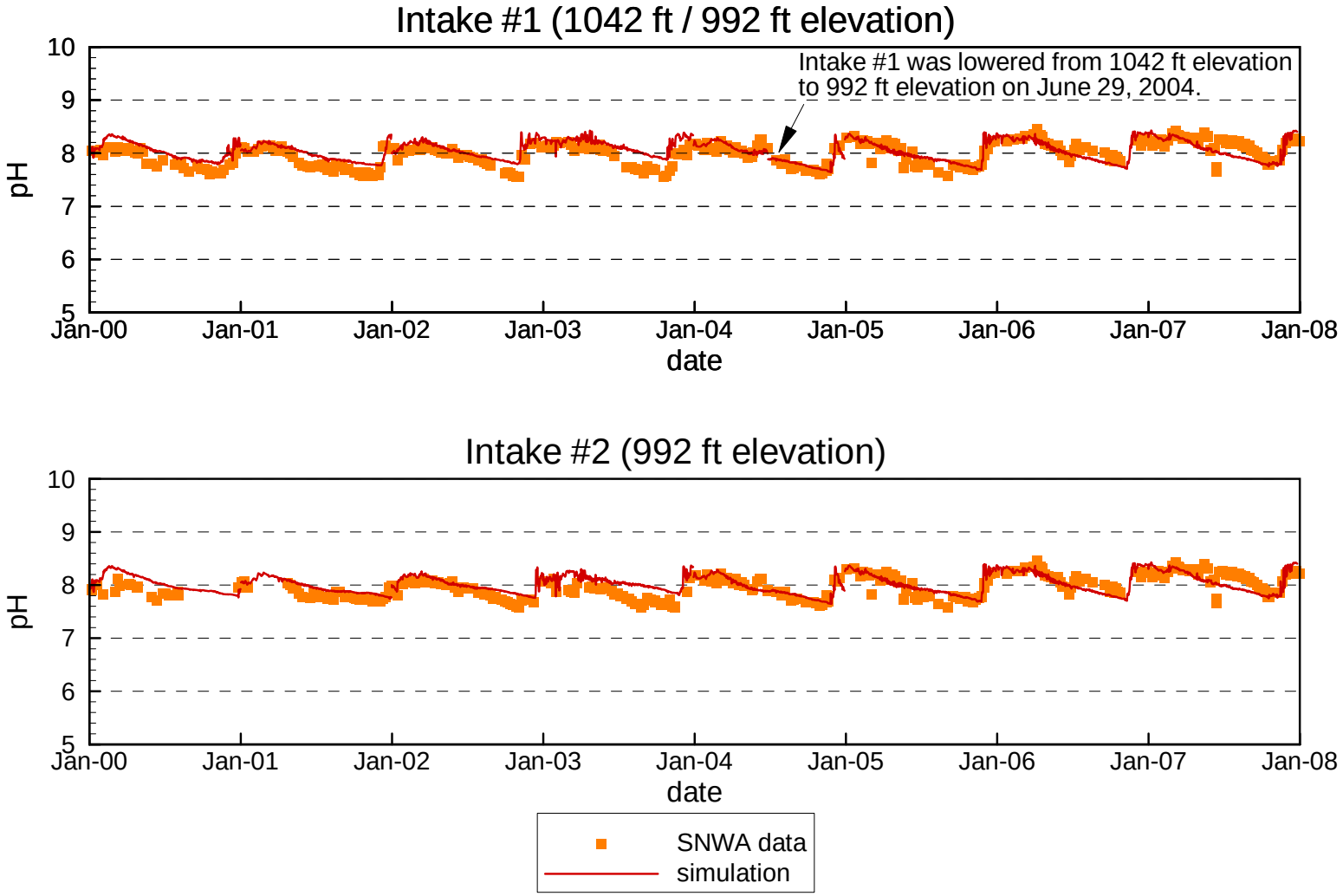

Figure 4.108

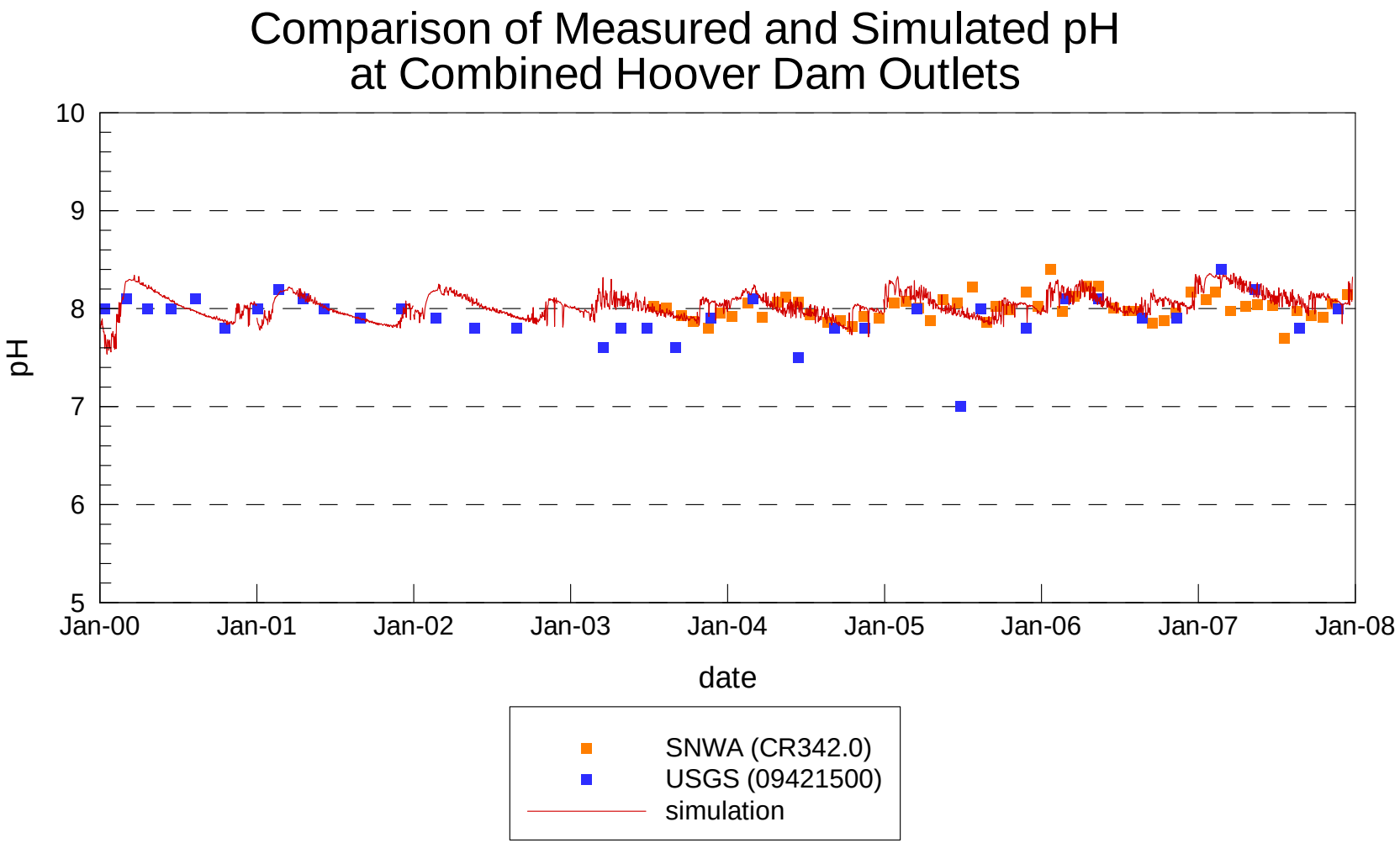
Comparison of Measured and Simulated pH
at Combined Hoover Dam Outlets
pH
10
9
8
7
6
5
Jan-00
Jan-01
Jan-02
Jan-03
Jan-04
Jan-05
Jan-06
Jan-07
Jan-08
date
SNWA (CR342.0)
USGS (09421500)
simulation

Figure 4.109

Comparison of Measured (USBR) and Simulated Dissolved Oxygen on Profile from Hoover Dam to Colorado River

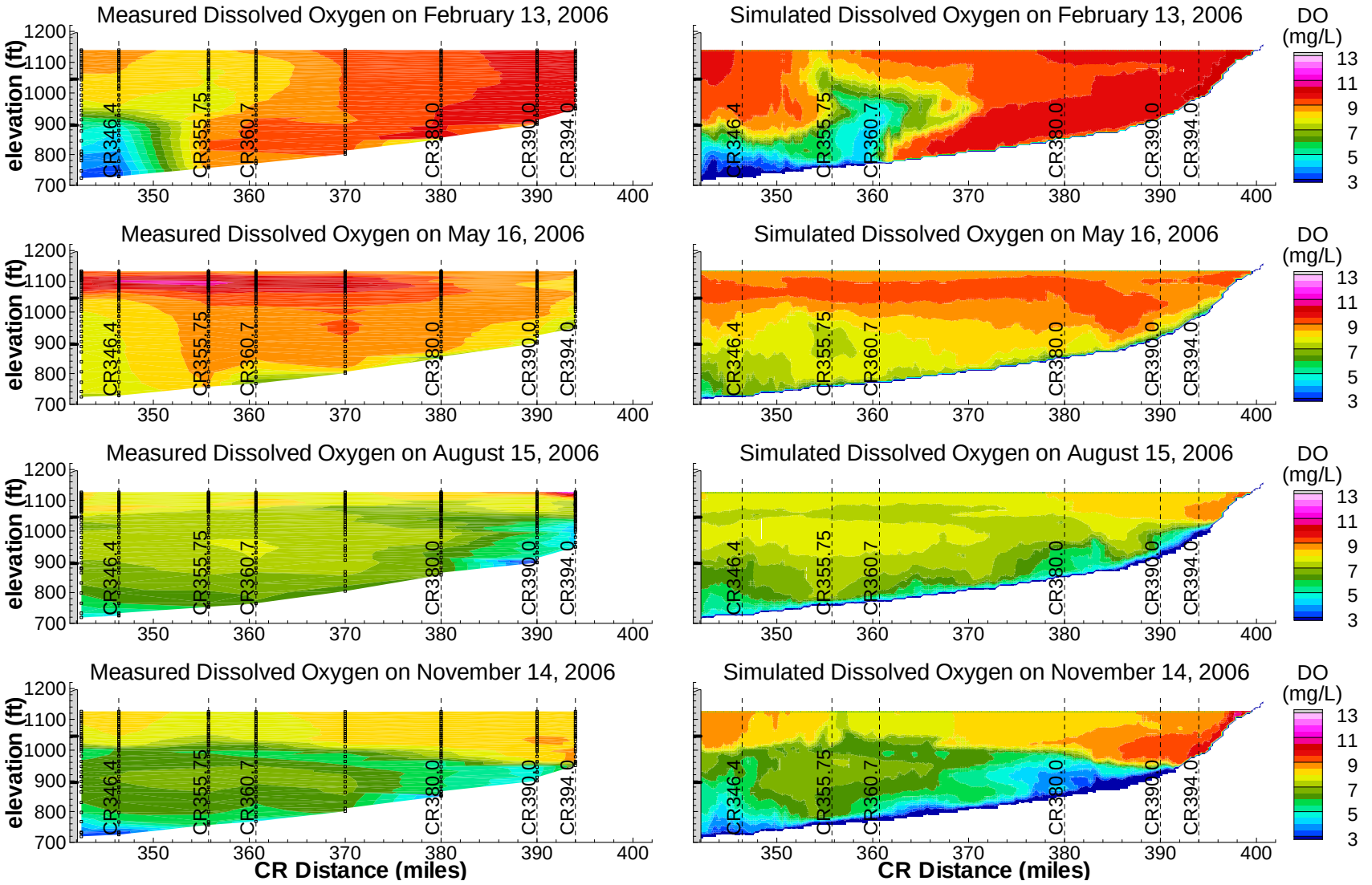

Figure 4.110

FLOW SCIENCE

Comparison of Measured (USBR) and Simulated Dissolved Oxygen on Profile from Hoover Dam to Colorado River

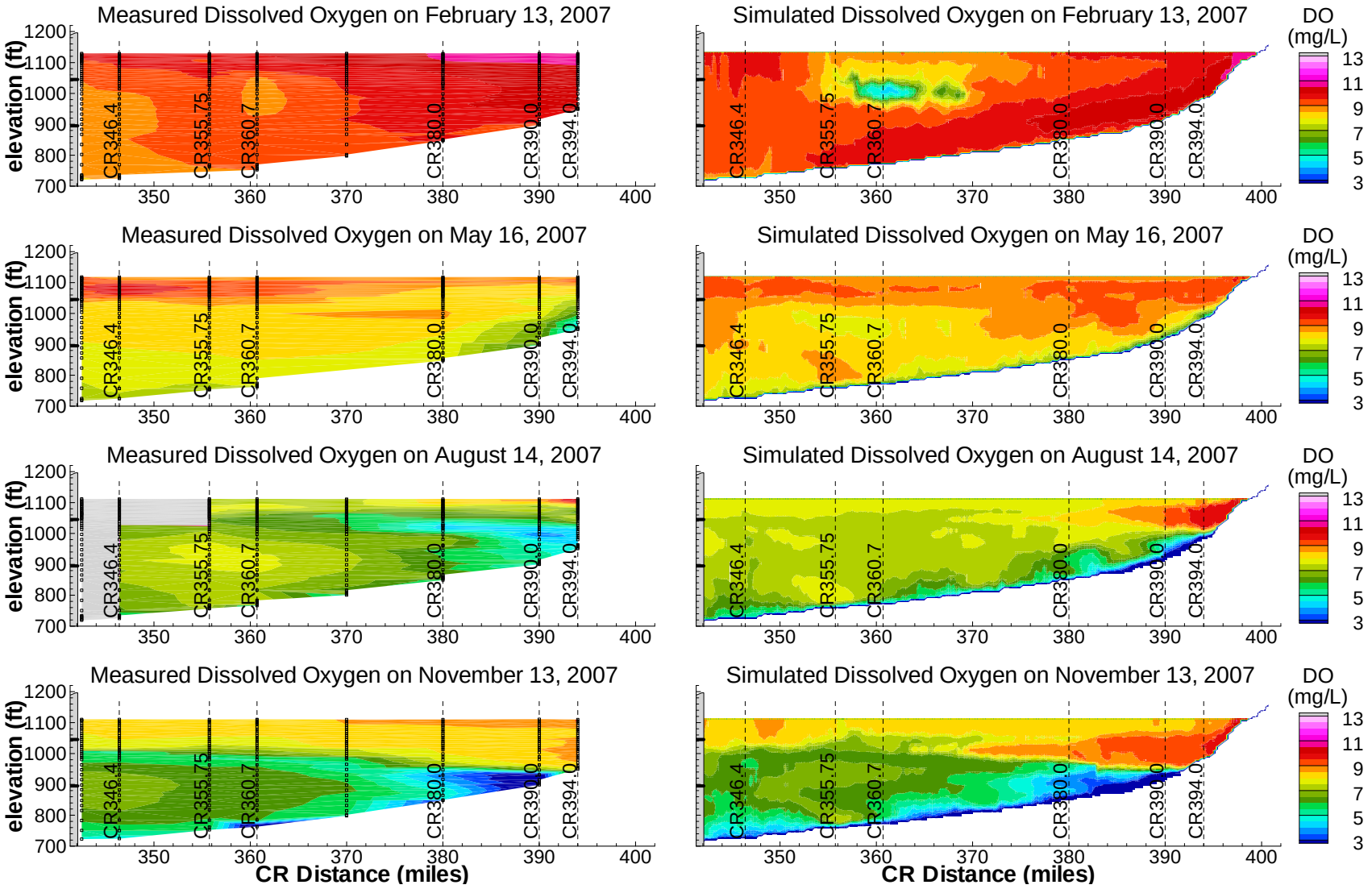

Ch4_Figures.ppt
FSI V064081 & V084015
December 9, 2010

Figure 4.111

FLOW SCIENCE

Comparison of Measured (USBR) and Simulated Dissolved Oxygen on Profile from Hoover Dam to Virgin River

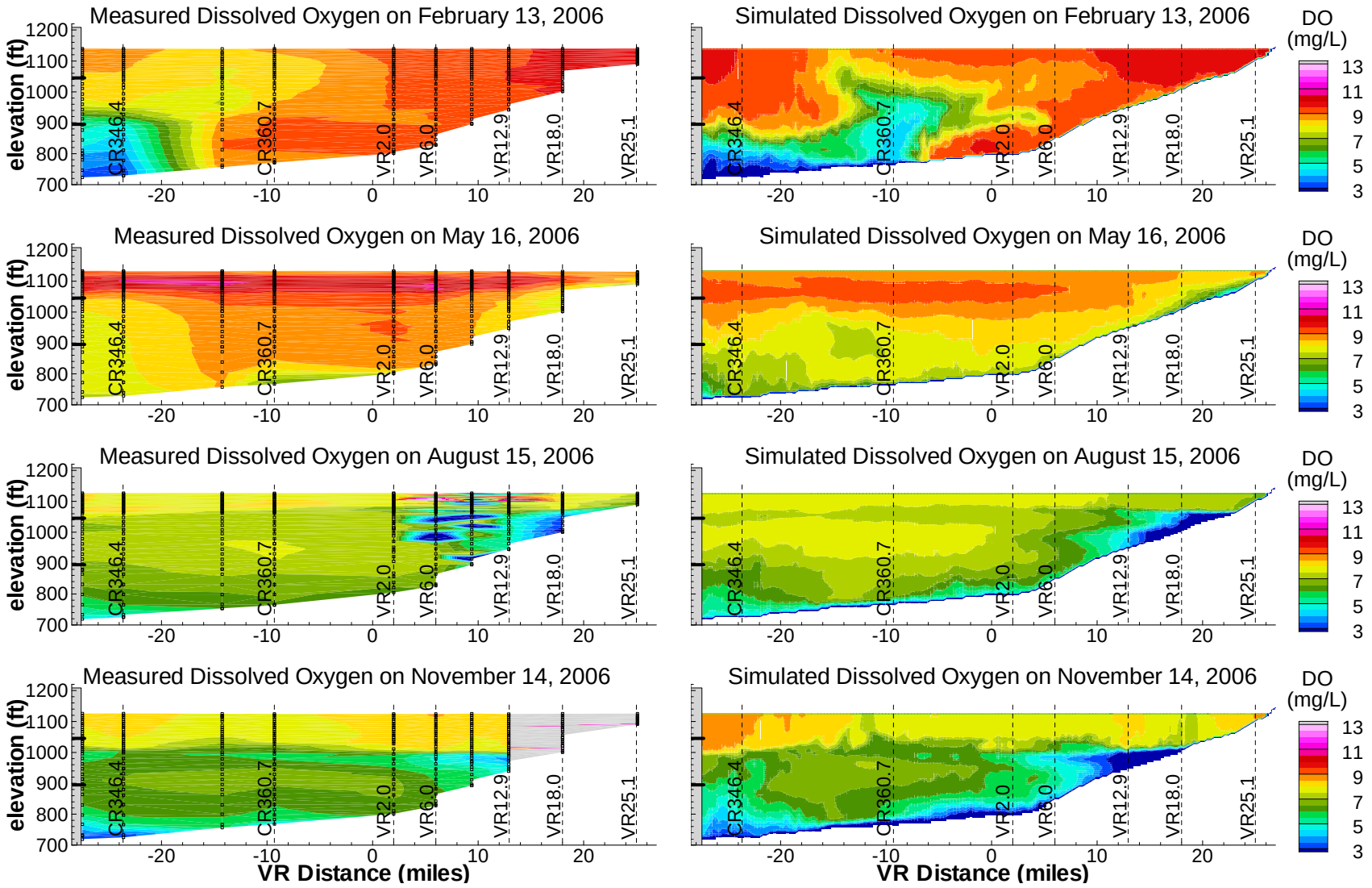

Ch4_Figures.ppt
FSI V064081 & V084015
December 9, 2010

Figure 4.112

FLOW SCIENCE

Comparison of Measured (USBR) and Simulated Dissolved Oxygen on Profile from Hoover Dam to Virgin River

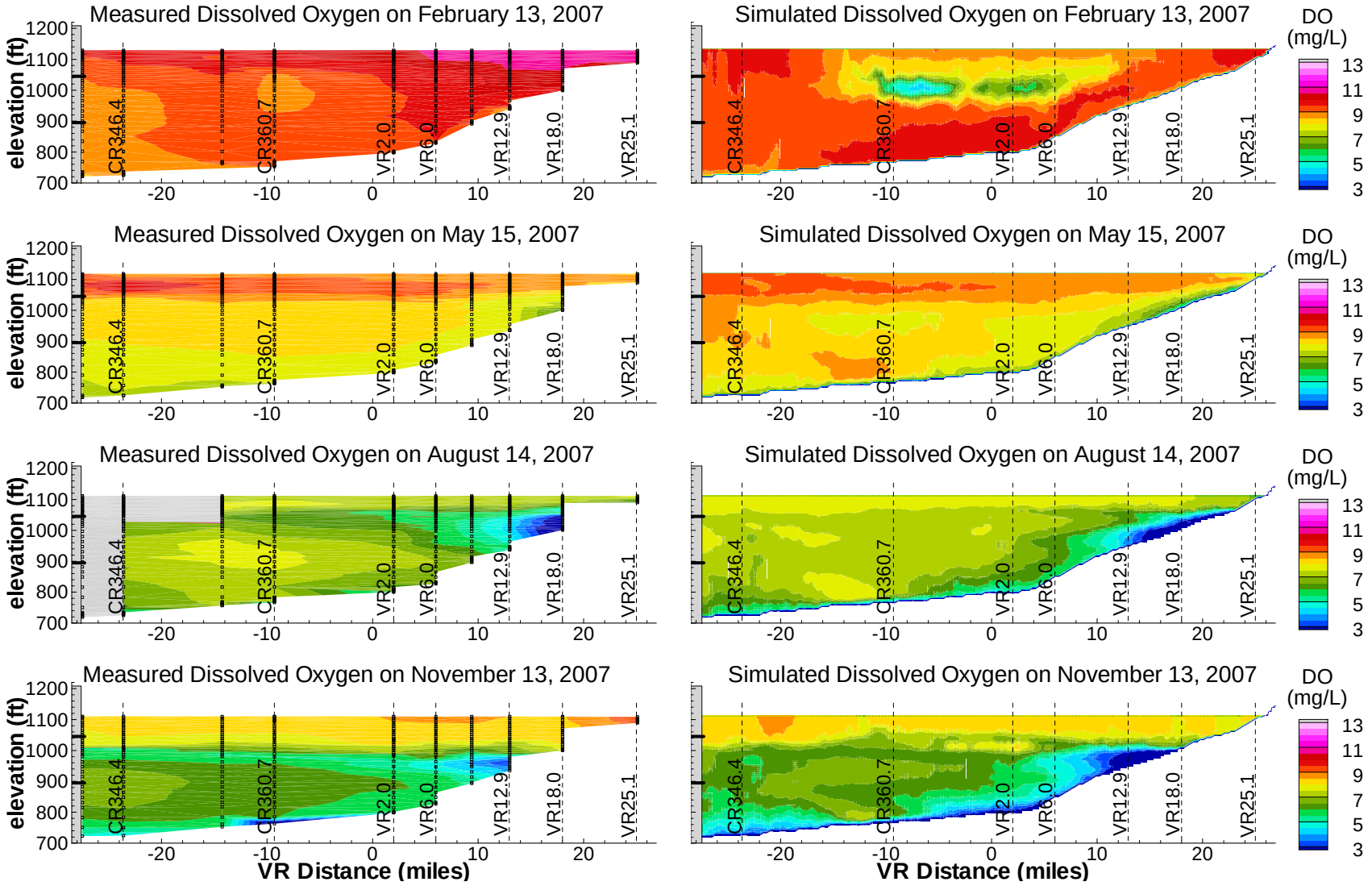

Ch4_Figures.ppt
FSI V064081 & V084015
December 9, 2010

Figure 4.113

FLOW SCIENCE

Comparison of Measured and Simulated Dissolved Oxygen on Profile from Las Vegas Wash to Hoover Dam

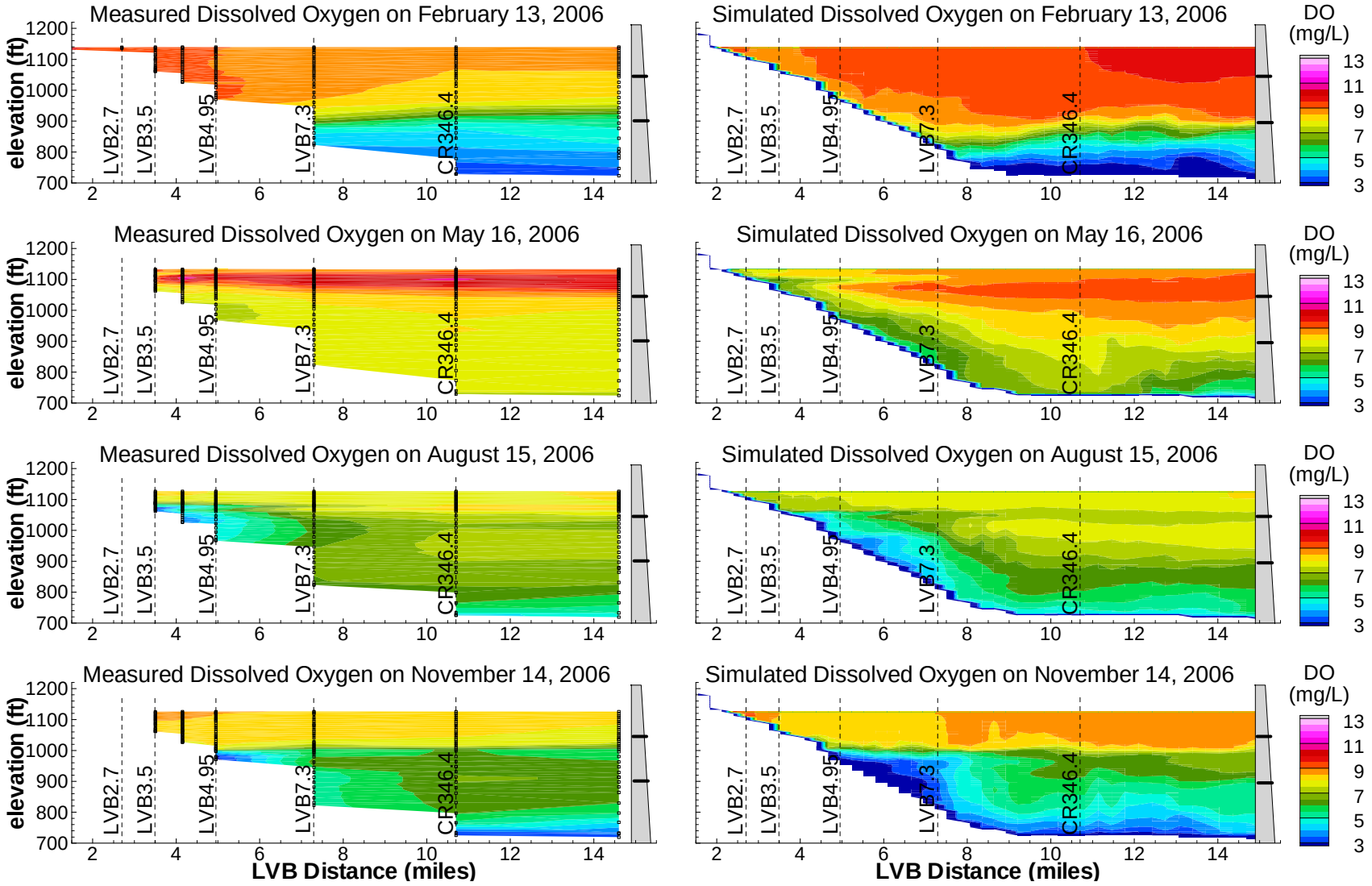

Ch4_Figures.ppt
FSI V064081 & V084015
December 9, 2010

Figure 4.114

FLOW SCIENCE

Comparison of Measured and Simulated Dissolved Oxygen on Profile from Las Vegas Wash to Hoover Dam

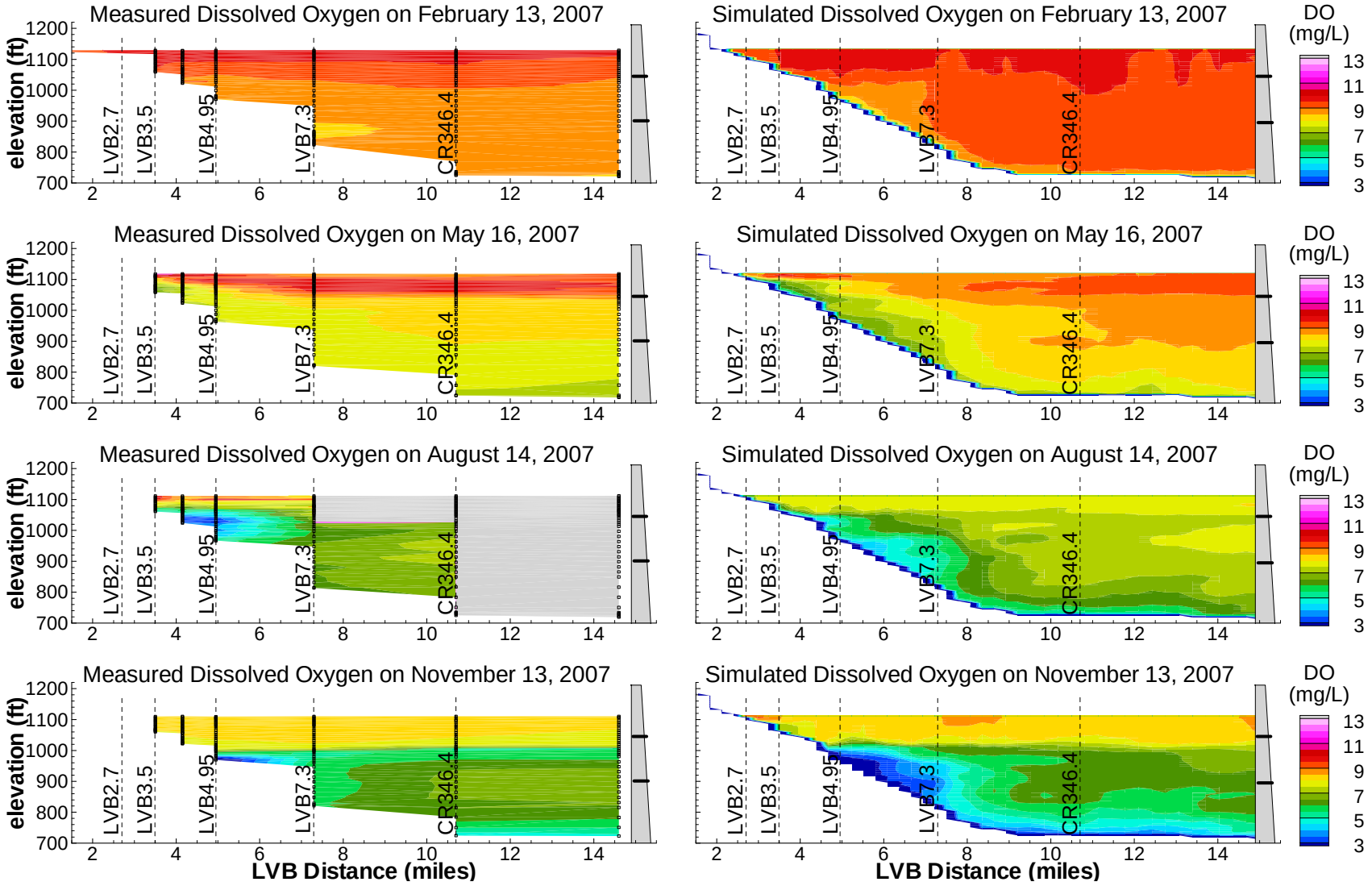

Ch4_Figures.ppt
FSI V064081 & V084015
December 9, 2010

Figure 4.115

FLOW SCIENCE

Comparison of Measured and Simulated Dissolved Oxygen Profiles at Station CR346.4 (2006 – 2007)

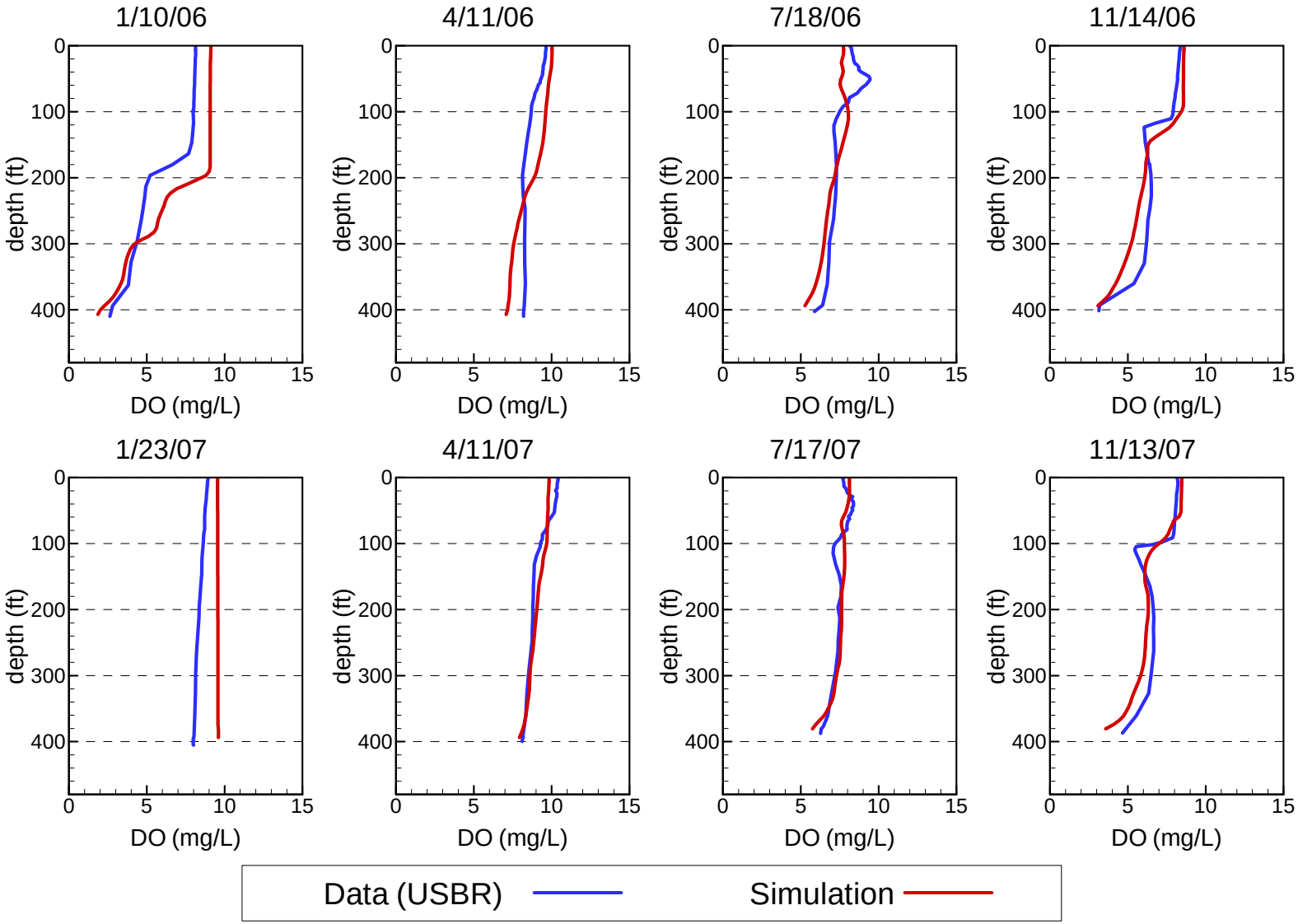

Figure 4.116

Comparison of Measured and Simulated Dissolved Oxygen at Station CR394.0

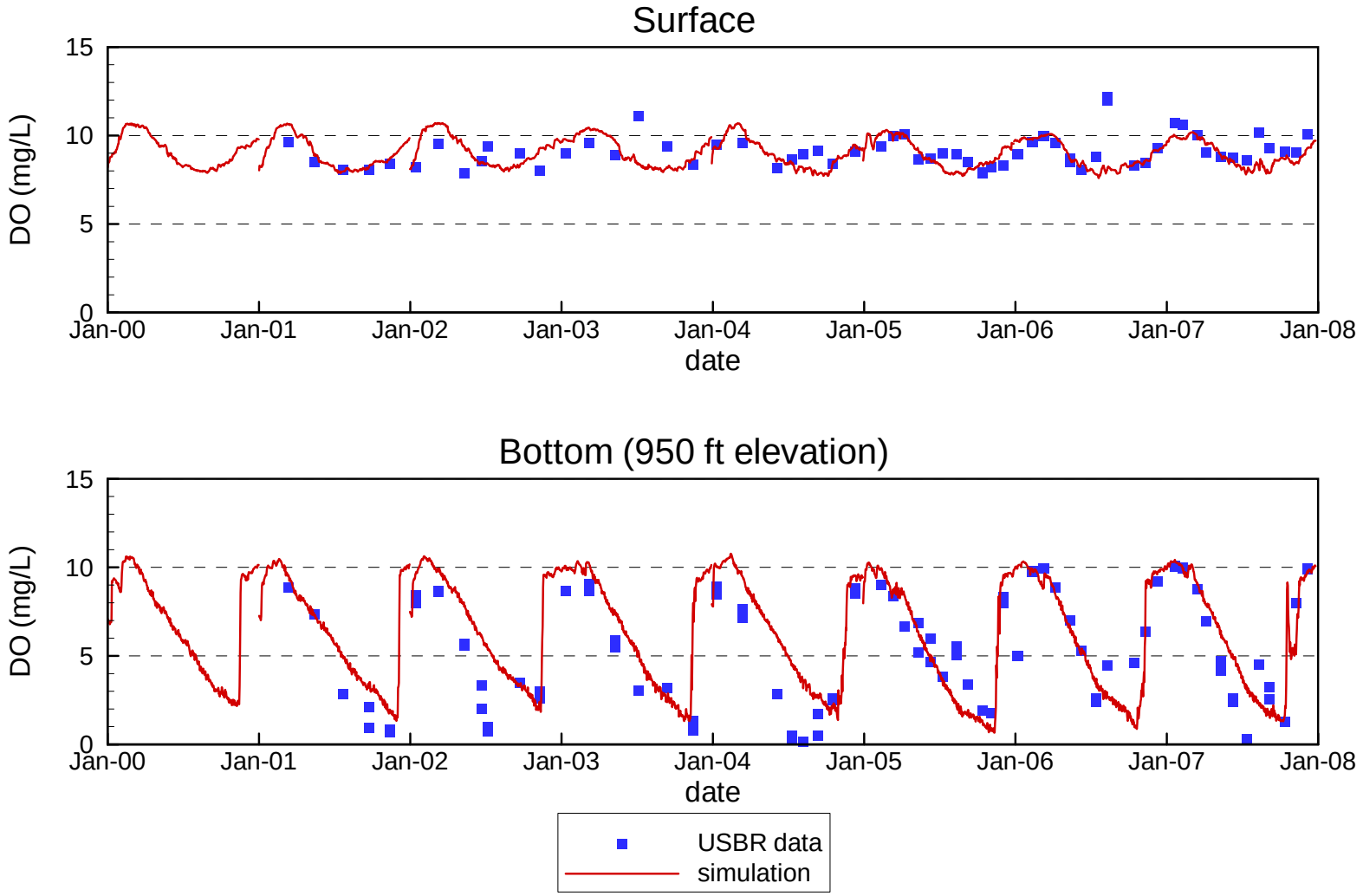

Figure 4.117

Comparison of Measured and Simulated Dissolved Oxygen at Station VR25.1

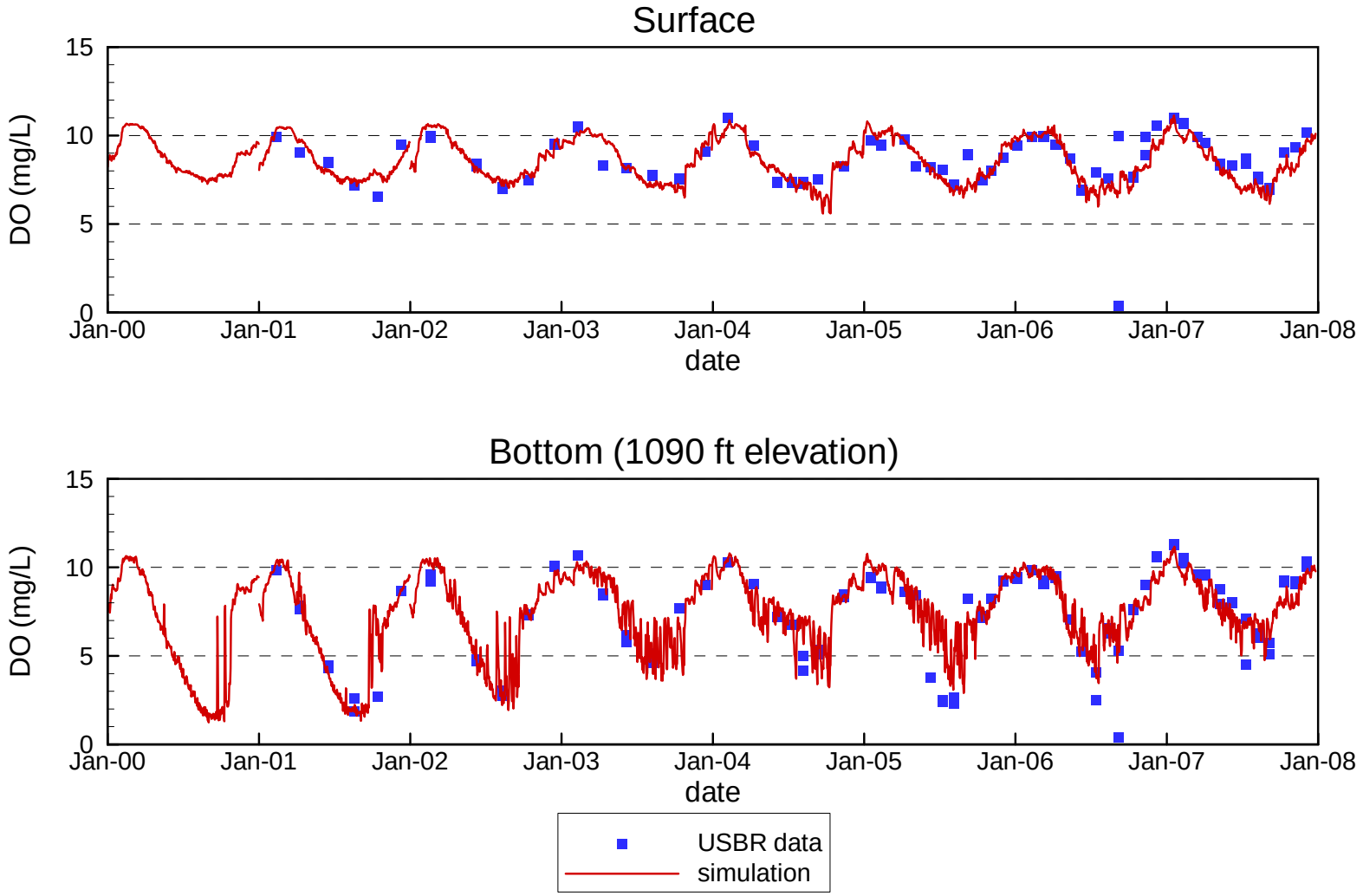

Figure 4.118

Comparison of Measured and Simulated Dissolved Oxygen at Stations VR12.9 / VR13.0

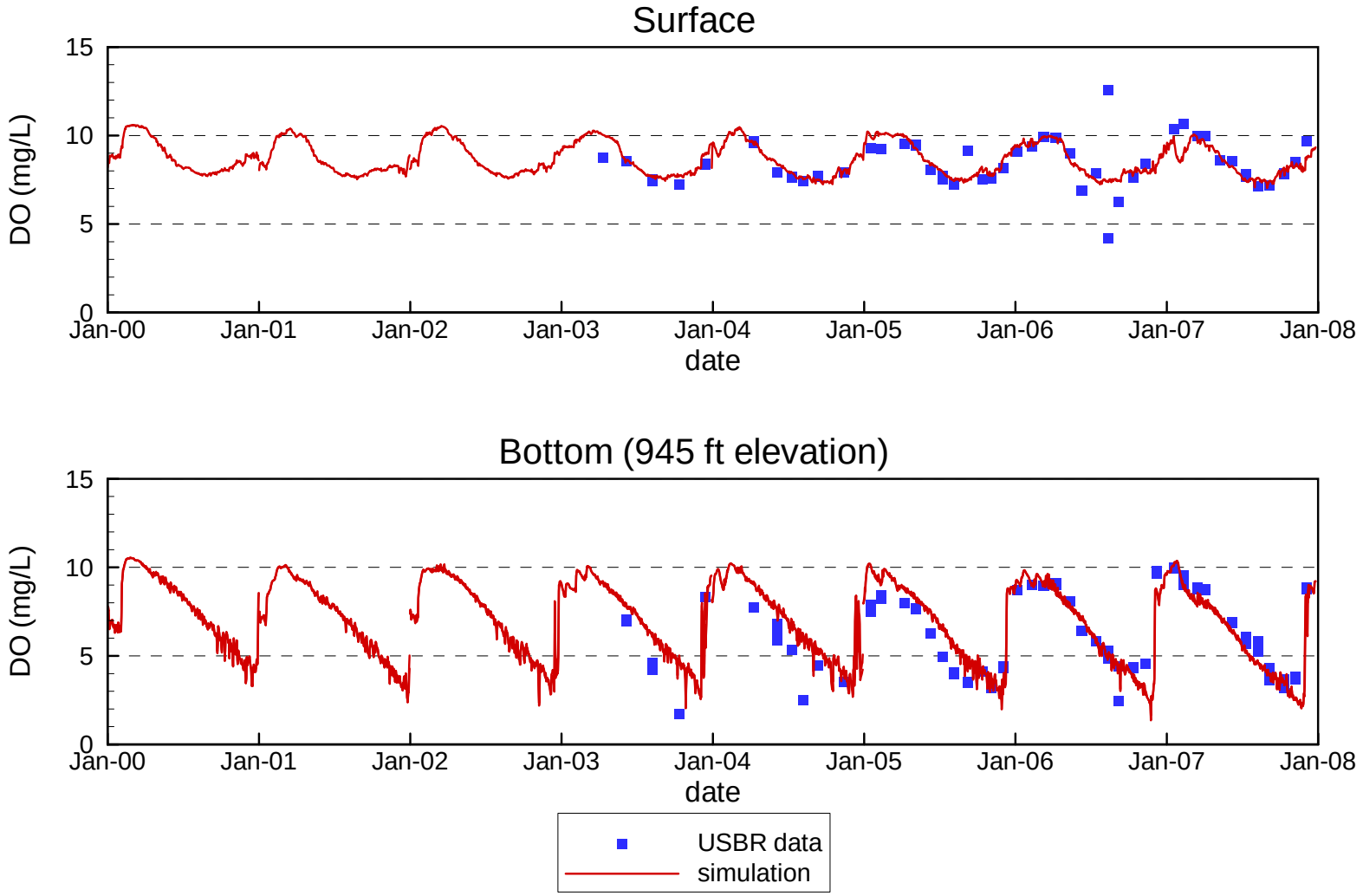

Figure 4.119

Comparison of Measured and Simulated Dissolved Oxygen at Station CR360.7

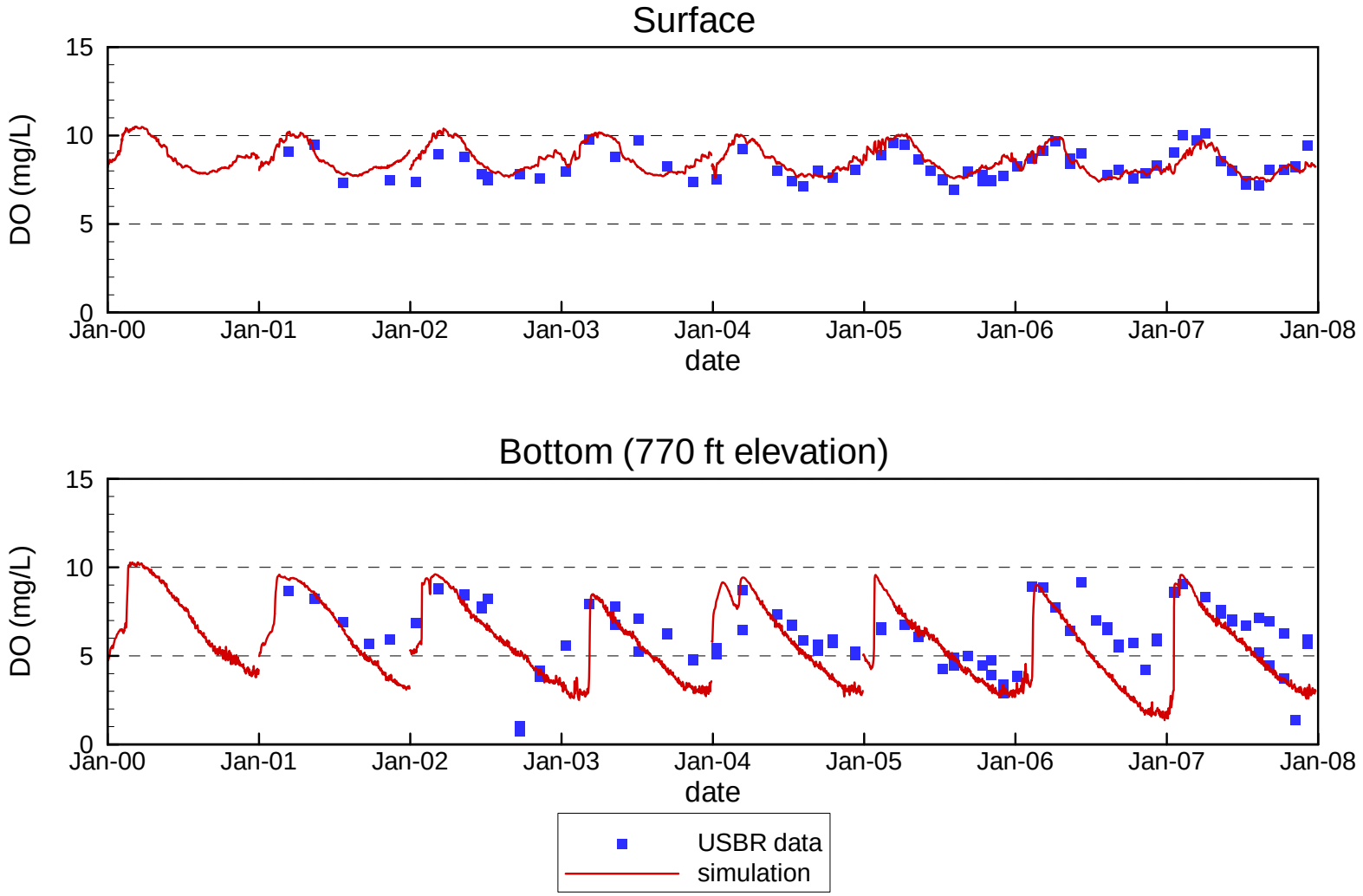

Figure 4.120

Comparison of Measured and Simulated Dissolved Oxygen at Station LVB3.5

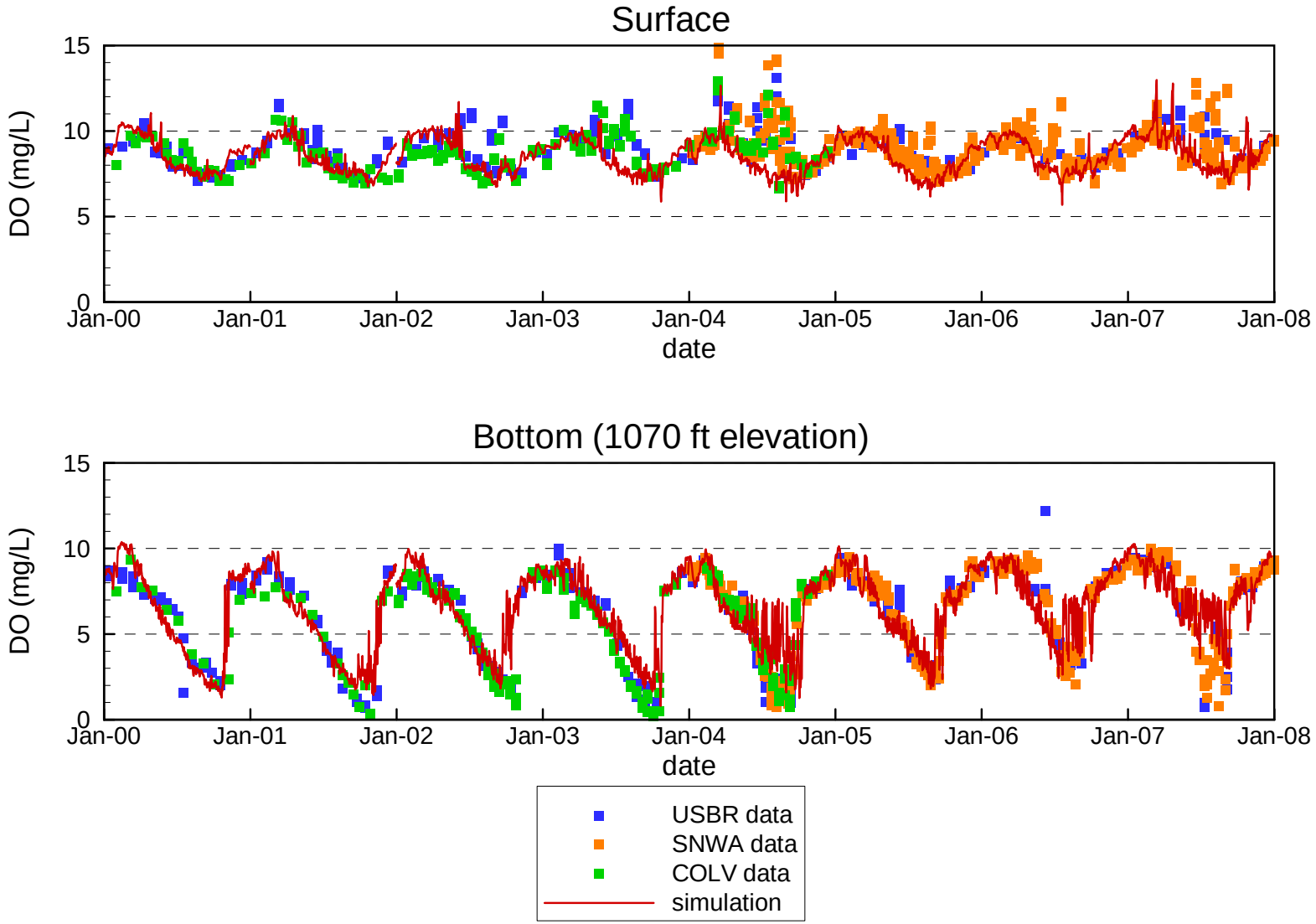

Figure 4.121

Comparison of Measured and Simulated Dissolved Oxygen at Station CR346.4

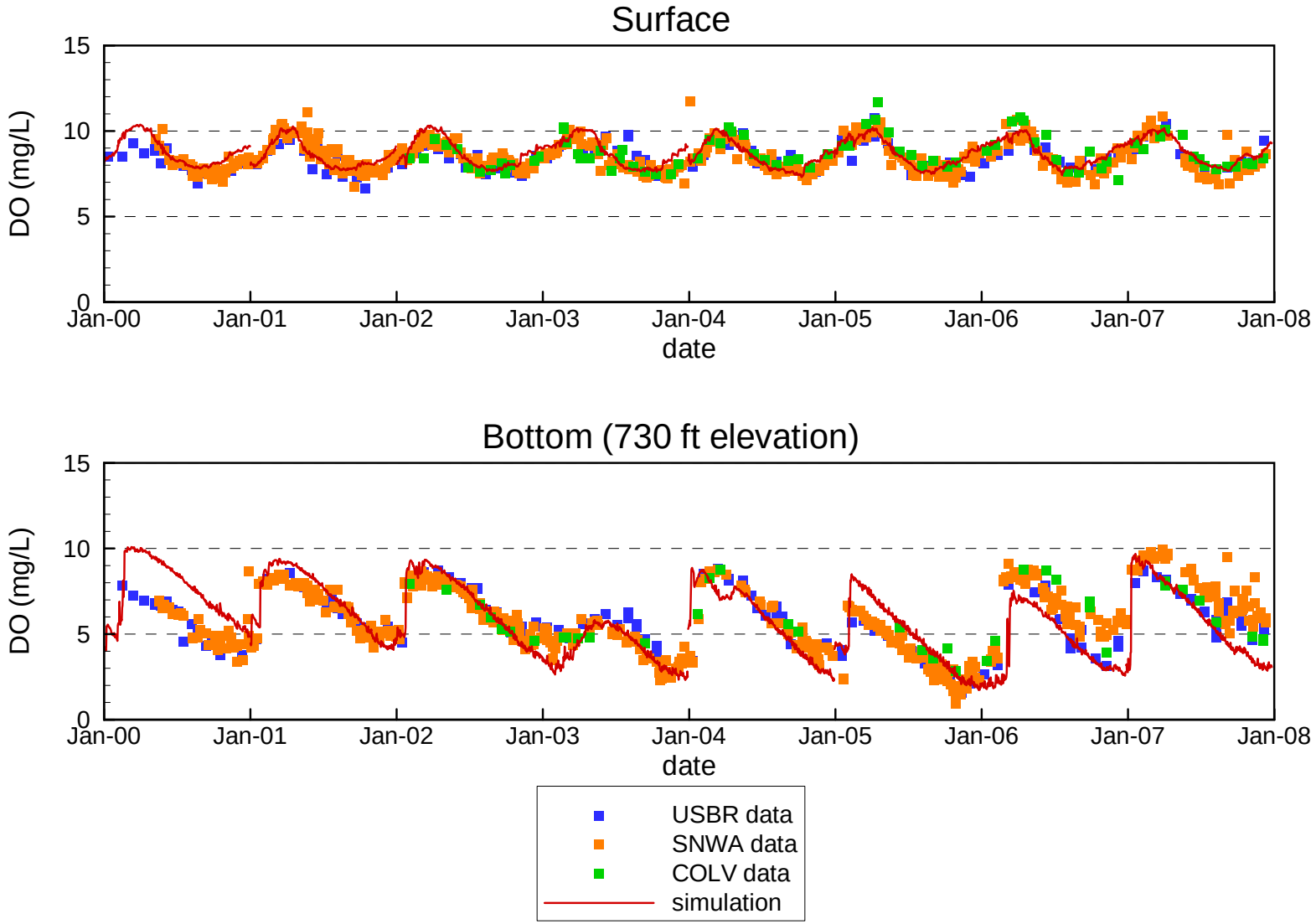

Figure 4.122

Comparison of Measured and Simulated Dissolved Oxygen at SNWA Intakes #1 and #2

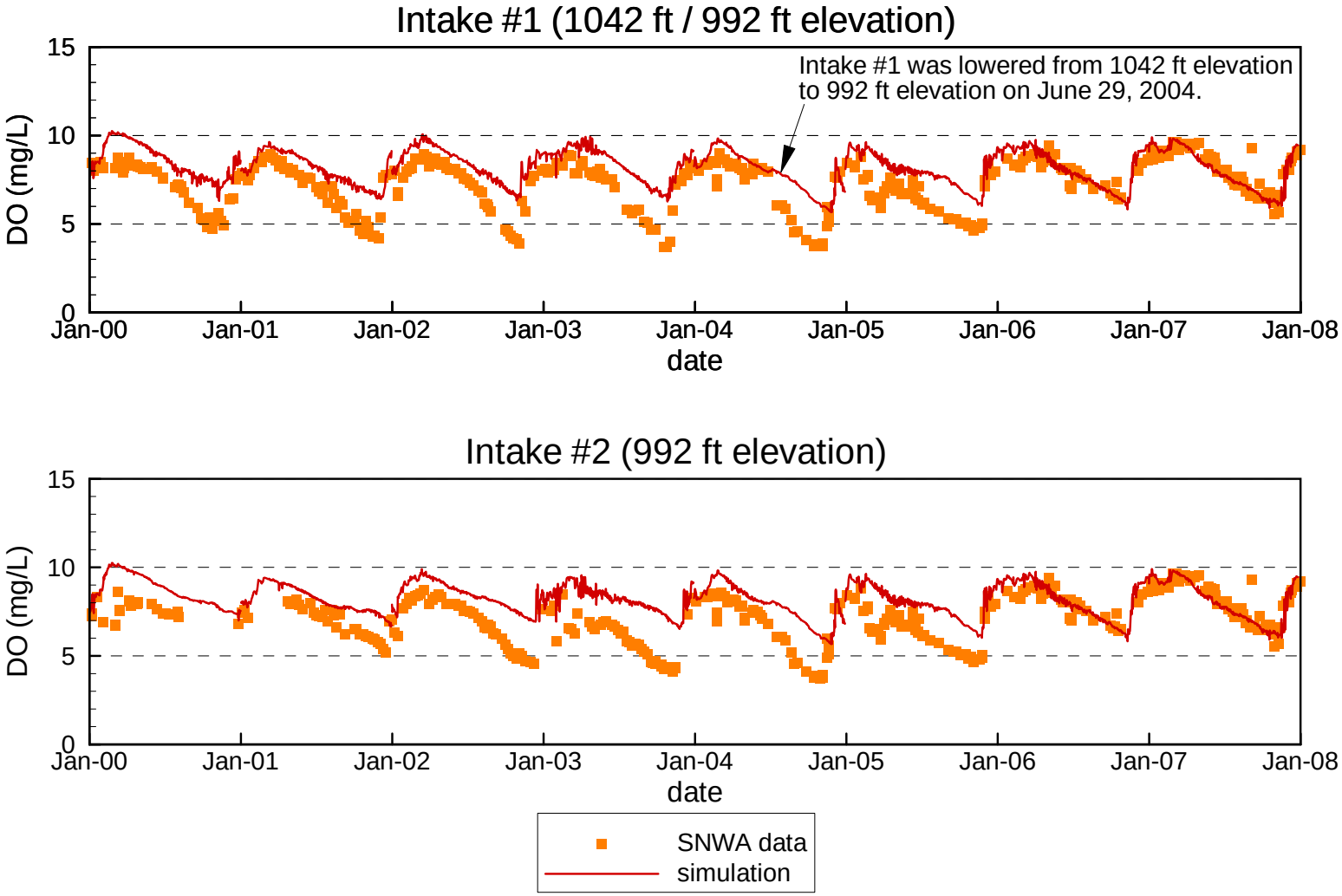

Figure 4.123

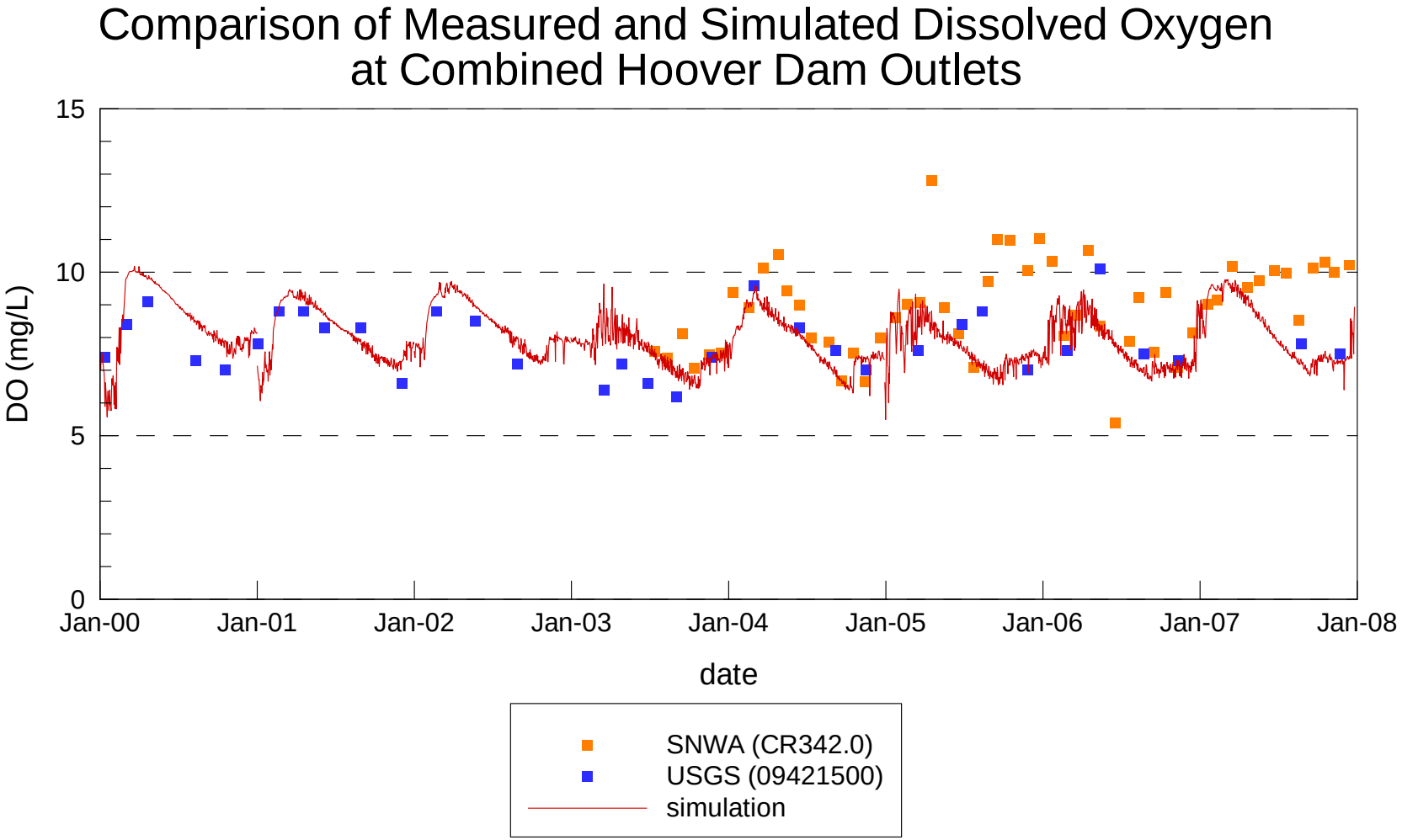
Comparison of Measured and Simulated Dissolved Oxygen
at Combined Hoover Dam Outlets
DO (mg/L)
15
10
5
0
Jan-00
Jan-01
Jan-02
Jan-03
Jan-04
Jan-05
Jan-06
Jan-07
Jan-08
date
SNWA (CR342.0)
USGS (09421500)
simulation

Figure 4.124

5 ANIMATIONS

The simulations yield data at all time steps and locations in the lake, and as such, they are useful to visualize many aspects that may not be able to be readily seen in the significantly less dense measured field data. The most intuitive way of presenting the large amounts of data that are generated by the simulation is through animations. These are provided on the included DVD. These animations include the distributions of water temperature, conductivity, perchlorate, bromide, chlorophyll *a*, TP, NO3, TOC, and DO for the continuous 2005 through 2007 simulation. Animations of the original Whole Lake Model (years 2000 through 2005) were presented in the previous report (Flow Science, 2007). While there have been some changes to the original calibration (Section 3.4) the overall features and trends illustrated by the animations have not changed, and thus the 2000 through 2004 animations are not provided here.

Each animation includes colored contours of the simulated variable in five frames:

1. Plan view of the lake.

2. Along a vertical section that curves along the CR thalweg from Hoover Dam to the CR inflow.

3. Along a vertical section that curves along the LVW thalweg from the LVW to the CR thalweg.

4. Along a vertical section that curves along the VR thalweg from the CR thalweg to the VR inflow.

5. Along a vertical section that curves along the MR thalweg from the VR thalweg to the MR inflow.

The contours shown in the plan view are at the surface for temperature and chlorophyll *a* concentrations, at the bottom for DO concentrations, and at the depth of maximum value for all other variables (to enable visualization of plumes). A wind vector is also plotted on the plan view frame.

It is recommended that the PowerPoint file titled, "Animations.ppt" and located in the "Animations" folder on the included DVD be used to play the animations. Keyboard commands for controlling the playback of the animations are provided in the PowerPoint file. Note that PowerPoint needs to be in "Slide Show" mode for the links to the animations to work. PowerPoint can be switched to "Slide Show" mode by pressing the F5 key.

The following sections briefly describe some of the trends and highlights from these animations. Specific details of each individual animation are in general not provided.

5.1 WATER TEMPERATURE

The animations of water temperature are generally quite similar from year-to-year. Near the beginning of each year the lake is cool with weak stratification. The cold CR underflow can be seen in the first few months of the year, and usually reaches into Boulder Basin. A notable exception was in 2005, when the CR underflow was impeded by the cold and high conductivity underflow from the large VR and MR storm flows in that year. This is illustrated by the animation of conductivity (Section 5.2).

During the spring and summer the surface layers warm up and the epilimnion increases in thickness. At times the simulation indicates that there are upwellings of cold water on the south-eastern shores of the lake. These upwellings occur when there is a sustained wind blowing predominantly in one direction (usually towards the north-west). The warm surface waters are blown to the leeward portions of the lake, where they "pile up". The resulting pressure gradient acts to cause a flow opposite to the wind direction at deeper depths. As a result cooler water from these depths appears on the wind-ward shores of the lake. Additional discussions are provided in the previous report (Flow Science, 2007).

During the summer and fall the "double thermocline" caused by the inflow from the CR can be seen near Station CR394.0 (see Sections 2.4.1 and 4.1.2). In the animations this appears as a region of near uniform temperature water with thermoclines above and below. This feature can persist into the lake as far as about 15 miles from the CR inflow.

During the fall the surface layers cool down and the epilimnion thickens and mixes downwards. By year end, the lake is weakly stratified with a weak thermocline at approximately 200 ft depth.

5.2 CONDUCTIVITY

The animations of conductivity clearly illustrate the high conductivity inflows of the LVW, VR, and MR, and the low conductivity inflow of the CR.

In the winter of 2005, the cold and high conductivity storm flows from the VR and MR entered Boulder Basin prior to the CR underflow, and initially prevented the CR underflow from reaching Boulder Basin. The storms in the VR and MR were discussed in more detail in the previous modeling report (Flow Science, 2007).

In the winters of 2006 and 2007, the low conductivity underflow from the CR extends into Boulder Basin. This is an important mechanism for replenishing the DO in Boulder Basin, which was discussed in Section 2.4.3, and is further illustrated by animation in Section 5.9.

The high conductivity LVW and VR/MR underflows are also apparent in the winters. In the spring and summer, the underflows become interflows and near-surface flows. The animations of the simulations allow the *transitions* between the different types of flows to be visualized more clearly than can be done with measured field data alone.

During the stratified period, and at times of low wind, the animations clearly indicate interflows from the LVW and VR, which insert the inflow horizontally along the thermocline. These thin regions of high conductivity may persist for a few days, but are eventually mixed upwards into the epilimnion by a high wind-mixing event. Such processes can also be examined using measured field data (see, for example, Flow Science, 2005), but the animations provide clearer and more detailed visualizations.

5.3 PERCHLORATE

The animations of perchlorate concentration indicate similar conclusions about the types of inflows from the LVW as those indicated by the conductivity. Inflows other than the LVW are not visible, since no perchlorate has been detected in those inflows.

The perchlorate is largely confined to Boulder Basin, and is generally highest in the epilimnion. On occasion, the animations indicate that perchlorate may travel upstream through the Narrows and into Virgin Basin. The reverse flow in the Narrows that causes this upstream movement was discussed in the previous modeling report (Flow Science, 2007).

5.4 BROMIDE

The animations indicate generally similar trends in the bromide concentration as those for conductivity. This is a result of similar trends in the inflow bromide concentrations and inflow conductivities. That is, the LVW and VR have higher bromide concentrations and conductivities (than the bulk reservoir water), while the CR generally has lower bromide concentrations and conductivities.

There are several durations of a few days to weeks where the simulated bromide concentration in the CR was higher than normal. At these times, the trends in the distribution of bromide concentrations in the lake differ from those for conductivity, with increased concentrations near the CR inflow.

5.5 CHLOROPHYLL *A*

The animations of chlorophyll *a* concentrations clearly illustrate the temporal variations with low concentrations in the winter, moderate concentrations in the summer,

and the highest concentrations in the spring (due to the spring algae bloom). The spatial variations are also well illustrated, with the highest chlorophyll *a* concentrations consistently occurring in Boulder Basin near the LVW, and in the northern part of Overton Arm near the VR and MR inflows. There are also times of elevated chlorophyll *a* concentrations in Gregg Basin near the CR inflow.

The animations also illustrate how the algae on the surface can be quickly transported by the wind, particularly in Boulder Basin. During much of the growing season the prevailing wind from the southeast keeps the algae primarily in the LVB near the LVW. However, when the wind changes direction and blows from the west, the algae can quickly be transported into the open water of Boulder Basin, where the result is an increase in the concentration of chlorophyll *a*. At a fixed location in open water (e.g., Station CR346.4) the changes in chlorophyll *a* concentrations caused by wind transport of algae can occur rapidly. This was briefly discussed in Section 4.2.1. More details on these phenomena are available in the Boulder Basin modeling report (Flow Science, 2005).

5.6 TOTAL PHOSPHORUS

The animations indicate that the highest TP concentrations consistently occur near the LVW inflow. The TP concentrations near the LVW do not fluctuate a great deal due to the relatively consistent phosphorus loading in the LVW from the WWTPs (see Section 2.3.6). By contrast, the TP concentrations near the other inflows (i.e., the CR, VR and MR) fluctuate more. Most of the time the TP concentrations from these inflows are higher than the concentrations of the ambient lake water, but at other times they are lower, particularly for the CR.

During the algae growing season, the TP concentrations within the lake decrease near the surface, as phosphorus is depleted by algae uptake.

5.7 NITRATE

The animations indicate that the highest NO3 concentrations occur in the epilimnion of Boulder Basin near the LVW. This is due to the relatively-higher NO3 concentrations in the LVW inflow. During the algae growing season, the NO3 concentrations decrease slightly near the surface, as nitrogen is used by algae uptake.

5.8 TOTAL ORGANIC CARBON

The animation indicates that the TOC concentrations throughout the lake increase near the surface during the algae growing season, as TOC is generated by algae growth.

The highest TOC concentrations generally occur in the epilimnion near each of the inflows. This is due to the increased algal growth at these locations, as reflected in the simulation by the higher chlorophyll *a* concentrations (Section 5.5).

TOC concentrations in the LVB near the LVW are generally higher than near the other inflows, due to the increased algal growth in this location, as well as the direct impact of the TOC concentrations in the LVW generally being higher than in the other inflows (Section 2.3.8).

5.9 DISSOLVED OXYGEN

Unlike the other animations, the plan view in the DO animation shows contours of the DO concentration on the lake bottom. This was done to enable a clear evaluation of the DO on the lake bottom, since it is here where issues with hypoxia (low DO concentrations) may arise.

The animation of the DO concentrations indicates many similarities between each of the simulation years. In the winters the DO concentrations are generally high throughout all locations and depths in the lake. As the lake becomes stratified in the spring and summer, the DO concentrations in the hypolimnion decrease, particularly above the sediments and even more so above the sediments near the inflows. Meanwhile the DO in the epilimnion remains relatively higher.

As the epilimnion deepens during the fall and into the winter, the DO near the lake bottom may be replenished from the epilimnion by the "top down" mixing process. Additionally, the DO may be replenished directly by inflows, particularly the underflow from the CR. These mechanisms have been discussed in Sections 2.4.3 and 4.2.8, and are clearly illustrated by the animation.

Importantly, the simulation is able capture many aspects of the subtle differences in the DO replenishment mechanisms in the winters of 2006 and 2007. Specifically, in the winter of 2006 the simulation illustrates that the high DO water of the CR underflow reaches the bottom of Station CR346.4 on approximately March 15. This is also visible in the animations of temperature and conductivity (Sections 5.1 and 5.2, respectively) as a cold, high conductivity underflow. The animation of DO concentration indicates at that time (March 15, 2006), that the epilimnion in Boulder Basin had not mixed down to the bottom of the reservoir. That is, in the winter of 2006, the animation indicates that the DO at the bottom of Boulder Basin was replenished by the CR underflow in mid-March,

rather than by a top-down mixing process. This is precisely the mechanism that was also illustrated by the measured field data as discussed in Section 2.4.3.

By contrast, the animation of DO concentration in the winter of 2007 indicates that the DO at the bottom of Station CR346.4 is replenished by a top-down mixing process on approximately January 15. At this time, the animation indicates that the CR underflow has barely reached as far as the Virgin Basin. Thus, in the winter of 2007, the animation indicates that the DO at the bottom of Boulder Basin was replenished by a top-down mixing process. This too was also illustrated by the measured field data as discussed in Section 2.4.3.

By mid-February 2007, the animation indicates that the DO from the CR inflow has progressed through Virgin Basin and the Narrows to reach Boulder Basin. At this time the simulation predicts a region of low DO at about 1000 ft elevation, and 50 to 100 ft thick, and extending from the downstream end of the Narrows, through Station CR360.7 to about Station VR2.0. This region of low DO is not present in the measured field data, and is thought to be a result of the simulation under-estimating the vertical mixing in the hypolimnion. This under-estimation of vertical mixing was discussed in Section 4.1.3, and is generally thought to be limited to regions with high flow rates through narrow channels.

Despite the occasional under-estimation of vertical mixing, the simulation is able capture the important aspects of the subtle differences in the DO replenishment mechanisms in the winters of 2006 and 2007. Furthermore, due to the high resolution output (both spatially and temporally) of the simulation results, the animations enable the dynamics of these mechanisms to be identified more clearly than if field data alone are used.

6 SUMMARY AND CONCLUSIONS

The ELCOM/CAEDYM model previously developed for the entire Lake Mead, including the Upper Basins and covering years 2000 through 2005, has been extended to include years 2006 and 2007. In addition, enhancements have been made to the model to improve the model capability and calibration over the entire 2000 through 2007 modeling period. Relevant field data from in and around Lake Mead in 2006 and 2007 were gathered, analyzed and appended to the previous 2000 through 2005 data-sets. These were then used to calibrate and validate the three-dimensional model over the entire eight years.

This section presents a summary of the main conclusions that can be drawn from the modeling and analysis processes. First, the model enhancements that have been implemented in the recent work are summarized; then the results of the ELCOM and CAEDYM model calibrations are presented. This is followed by conclusions about the general limnology of Lake Mead that can be drawn from interpretation of both the field data analysis and modeling results. Finally, potential improvements and refinements to the calibrated model are discussed.

6.1 MODEL ENHANCEMENTS

During the original 2000 through 2005 modeling a number of possible modeling refinements were identified that could lead to potential enhancements in the model calibration and utility. Many of these enhancements, as well as additional subsequently identified enhancements, have been implemented in the present work. These enhancements are summarized as follows:

- Continuous model simulation over three years (2005 through 2007). This demonstrates the ability of the model to be used for multiple-year simulations, as well as enabling subtleties such as complete or incomplete destratification in each winter to be examined using the model.

- Use of wind data from multiple locations within Lake Mead in 2006 and 2007. This results in a more realistic representation of the on-lake wind patterns and wind speeds and their effect on lake dynamics.

- Use of more accurate Virgin River flow rate due to availability of flow rate data from a location close to Lake Mead from April 2006 onwards. Based upon these new data, additional corrections were also made to the summer flows in years 2000 through 2005.

- Use of spatially variable initial conditions for phosphorus and nitrogen. This enabled different initial concentrations to be specified in Boulder Basin and the Upper Basins, which improved the calibration results.

- Use of spatially-variable sediment oxygen demand. This enabled higher sediment oxygen demand rates to be specified near the inflows, which resulted in a vastly improved DO simulation.

- Re-calibration of phosphorus and algae computational routines. This was motivated by the more recent phosphorus data measured within Lake Mead. Specifically, the USBR samples collected in 2007 were analyzed for phosphorus by the High Sierra Laboratory, using methods with low detection limits. This altered the understanding of the phosphorus processes in the lake, which necessitated a re-calibration.

- Model calibration over an eight-year period. The present calibration spans eight years (2000 through 2007), compared to six years for the previous Whole Lake Model, and four years for the earlier Boulder Basin Model. The longer calibration period provides more confidence in the model.

6.2 MODEL CALIBRATION AND VALIDATION

The performance of the ELCOM/CAEDYM model was evaluated by comparing the simulation results with data collected at stations near the CR inflow (CR394.0), near the VR and MR inflows (VR25.1), in Overton Arm (VR12.9/13.0), near the Narrows (CR360.7), near the LVW inflow in the LVB (LVB3.5), in the open water of Boulder Basin (CR346.4), at the SNWA intakes, and at the Hoover Dam outlets. In certain instances, comparisons at additional locations were made in order to illustrate the simulated and measured spatial trends. In general, the model adequately reproduced most of the observed water quality features within the entire lake and provided added insight into lake mixing processes. In the following, a summary of the calibration/validation process is provided.

Overall, the results of the ELCOM calibration are summarized as follows:

- ELCOM captures the lake water temperature variation, including stratification and thermocline depth, reasonably well over the eight year model period. Overall, time series comparisons of the simulated and measured data show good agreement at all of the measuring stations.

- ELCOM is able to capture the incomplete lake destratification in the winter of 2006 and the complete destratification in the winter of 2007.

- The intrusion (insertion) depths of all the inflows (i.e., CR, VR, MR and LVW) are generally well predicted, indicating that the simulation is ultimately able to predict the fate of each inflow with regard to their relationship to the epilimnion and hypolimnion.

- The spatial and temporal distributions of conductivity throughout the reservoir are well-predicted by the simulation.

- ELCOM captures the variation of perchlorate and bromide concentrations well. Overall, time series comparisons of the simulated and measured data show good agreement at all of the measuring stations.

The CAEDYM calibration process focused on identifying and reproducing the key water quality characteristics within Lake Mead related to the timing of algal blooms (represented by chlorophyll *a*), nutrient concentrations (phosphorus and nitrogen), TOC concentrations, DO concentrations, and pH.

During the calibration process for the previous 2000 through 2005 model, Dr. David Hamilton, Professor of Biological Sciences at the University of Waikato, New Zealand, and the author of CAEDYM, was consulted to assist and review the model calibration and provide ranges of accepted values of the parameters for Lake Mead. In the present work, the parameters used in the re-calibration of the phosphorus and algae routines were determined to fall within the provided range of accepted values for Lake Mead. Overall, the results of the CAEDYM calibration are summarized as follows:

- The model is able to capture the general temporal trends of algae growth and decay during the growing season. The algal growth in the winters is often under-predicted by the simulation, although the measured chlorophyll *a* concentrations are near the method detection limit and may not be representative of the true (but low) concentrations in the winters.

- The simulated chlorophyll *a* results indicate reasonable agreement when plotted directly against the measured field data. There is considerable data scatter, but much of this can be attributed to substantial variation within the field data.

- The model is able to capture the spatial trends and overall magnitudes of the chlorophyll *a* growing season average. In particular, the large spatial gradients near the LVW and VR, and the differences in concentrations between Boulder Basin and the Upper Basins, are generally well replicated. However, the model overestimates the chlorophyll *a* levels in 2000, and underestimates them in 2001.

- The simulated chlorophyll *a* growing season average indicates good agreement when plotted directly against growing season averages computed directly from the field data. There is substantial scatter between the simulation and field data, which has been quantified as illustrated by error bars. Additionally, the variation among the field data of the different agencies (i.e., USBR, COLV and SNWA), has been quantified and illustrated by error bars. While the simulation error bars are larger than the error bars for the field

data, they are of similar magnitude, which indicates that the variation among field data impacts the error of the simulation.

- Due to the difficulty of measuring phosphorus at extremely low concentrations, direct phosphorus concentration comparisons between the data and the model results were difficult. Still, CAEDYM captured the primary characteristics of the spatial variation of phosphorus in the lake, as well as some seasonal trends in the FRP concentrations within the epilimnion.

- The agreement between the simulated and measured NO3 concentrations is good in Boulder Basin. The NO3 simulation was vastly improved in the Upper Basins compared with the previous 2000 through 2005 simulation, as a result of the implementation of spatially variable initial conditions.

- The agreement between the simulated and measured TOC concentrations is reasonable throughout the lake.

- The agreement between the simulated and measured pH is good throughout the lake.

- The agreement between the simulated and measured DO concentrations is good throughout the lake. The DO simulation was vastly improved compared with the previous 2000 through 2005 simulation, as a result of the implementation of spatially-variable sediment oxygen demand.

- The simulation is able to capture the replenishment of the DO in the hypolimnion of Boulder Basin by the CR underflow in winter. This is particularly important in the simulation of the winter of 2006, when the lake did not completely destratify.

Overall, there is good agreement between model results and measured field data. The discrepancies tend to be attributed to difficulties in data sampling, uncertainties in chemical analysis, highly variable biochemical and aquatic processes, and limited model spatial resolution.

6.3 LIMNOLOGICAL CONCLUSIONS

Many limnological conclusions may be drawn from the analysis of the gathered field data. The simulation results can complement these conclusions (e.g., through the use of animations) as well as lead to new conclusions and understanding. This section summarizes the conclusions that have been made from the data analysis and the simulation results.

Many of the general limnological conclusions that were drawn from the present study were also identified in the previous 2000 through 2005 modeling effort. For completeness these are provided here as follows:

- The LVW, VR and MR flow insertion elevations vary from season to season. Between April and October these inflows generally enter the lake as interflows and travel along the thermocline, where they can be vertically mixed within the epilimnion by strong winds. In winter, these inflows generally enter as underflows that travel along the bottom of the reservoir. In November and March, the density currents are in a transition period and can intrude into both the epilimnion and the hypolimnion.

- The CR inflow is colder and generally tends to insert lower in the water column than the other inflows. However, there are times when it can insert near the surface. When the CR inserts at mid-depths during the stratified period, a "double thermocline" structure near the inflow can result.

- Typically, the LVW inflow has the highest conductivities and constituent concentrations (i.e., bromide, perchlorate, TP, NO3, and TOC), followed by the VR and MR. The CR has the lowest conductivities and constituent concentrations. In particular, the CR inflow FRP concentrations are typically an order of magnitude lower than those for the other inflows.

- During most winters the lake is vertically mixed, although on occasion a weak thermocline may persist at depth in the lake, particularly within Boulder Basin.

- The insertion elevations, and the relative conductivities and constituent concentrations of the inflows, result in spatial distributions of conductivity and constituent concentrations that are generally consistent from year to year. In the winters there are higher conductivities/concentrations in Boulder Basin (and near the LVW in particular) and in the northern half of Overton Arm (near the VR and MR). During the stratified period the higher conductivities/concentrations remain at these locations, but are also mainly confined to the epilimnion.

- When the lake is stratified persistent winds prevailing from the southeast can drive the warm surface waters to the northwest portions of the lake, resulting in upwellings of cold water on the southeastern shores.

- DO is lower at the lake bottom near each of the inflows (i.e., LVW, CR, VR and MR), most likely as a result of deposition and decay of particulate organic matter.

- Chlorophyll *a* concentrations are generally higher in Boulder Basin than in the Upper Basins.

- Chlorophyll *a* concentrations are generally higher near the inflows, particularly the LVW.

The addition of model years 2006 and 2007, as well as the availability of additional data sources enabled new general limnological conclusions to be drawn. These are summarized here as follows:

- The wind speeds in the Upper Basins are consistently lower than in Boulder Basin.

- The DO in the bottom of Boulder Basin can be directly replenished by inflow from the CR in the winter. This was identified in the measured field data, and highlighted by the simulation through animations. This mechanism of DO replenishment is particularly important in the years that Lake Mead does not completely destratify.

- There is a correlation between the fluorescence measured at the USGS platform in the LVB, and the chlorophyll *a* data measured at Station LVB3.5. However, this correlation seemed to shift in mid-2007. Additional analysis of the data-sets over longer time periods is required.

6.4 POSSIBLE FUTURE MODELING REFINEMENTS

The model is generally capable of adequately reproducing the water quality in the lake, and a number of modeling refinements have been implemented since the original 2000 through 2005 model. Nevertheless, additional refinements have been identified that could further improve the calibration and model utility.

The possible modeling refinements are identified as follows:

5. Continuous multiple year simulations over the *entire* modeling period. At present the model is initialized in year 2000, and again in years 2001, 2002, 2004 and 2005. Ideally the model would be initialized only once in year 2000, and then run continuously through all simulation years.

6. Improved treatment of particulate phosphorus settling in CAEDYM. Measurements of the particle size distributions of the inflows would be useful to aid in the understanding of particulate settling within Lake Mead, and to enable modifications to CAEDYM in order to improve the settling of particulate phosphorus.

7. Finer grids (e.g., CAEDYM on 300-m grid, or increased vertical resolution) as computational power increases. This would improve the resolution near to the inflows.

8. Statistical metrics of "goodness-of-fit" between the simulation results and measured field data. The error analysis of the model error in chlorophyll *a* concentrations needs to be extended to include other parameters of interest.

In summary, the ELCOM/CAEDYM modeling package has been shown to be a powerful tool that can provide an accurate analysis of the hydrodynamics and water quality within Lake Mead. Many model enhancements have been made since the original 2000 through 2005 modeling, including the addition of years 2006 and 2007. Despite the fact that, as noted, there are some improvements that can further enhance the model's utility, in its current form it still provides the capability of comprehensive resolution of spatial and temporal predictions of the lake response to future changes in inputs or operations.

7 REFERENCES

Flow Science Incorporated, 2005. "Lake Mead ELCOM/CAEDYM Modeling", prepared for Black & Veatch on behalf of Clean Water Coalition. FSI Project No. S014004.1. Pasadena, CA.

Flow Science Incorporated, 2006. "Lake Mead ELCOM/CAEDYM Joint Modeling Study, Alternative SNWA Intake Locations", prepared for Black & Veatch on behalf of Southern Nevada Water Authority. FSI Project No. S014004.1. Pasadena, CA.

Flow Science Incorporated, 2007. "Lake Mead ELCOM-CAEDYM Model, Extension to Entire Lake", prepared for Black & Veatch on behalf of Clean Water Coalition and Southern Nevada Water Authority. FSI Project No. 054145. Pasadena, CA.

Flow Science Incorporated, 2007a. "Lake Mead Pre-Design Lake Diffuser", prepared for Black & Veatch on behalf of Clean Water Coalition. FSI Project No. V054145. Pasadena, CA.

Flow Science Incorporated, 2009. "Lake Mead Phosphorus Budget", Draft Technical Memorandum prepared for Clean Water Coalition. FSI Project No. V084015. Pasadena, CA.

APPENDIX A

Model Input Data Verification and Reconstruction

A MODEL INPUT DATA VERIFICATION AND RECONSTRUCTION

This appendix presents a primarily graphical summary of the model input data and the field data measurements that were collected and used to construct the model inputs. The plots present model input and field data over the entire 2000 through 2007 modeling period. Generally the model input for 2000 through 2005 is the same as was used in the original Whole Lake Model (Flow Science, 2007). However, in the following instances, and as elaborated on in the following sections, the model input for the original 2000 through 2005 period was adjusted as a result of better understanding of processes in Lake Mead:

- Wind/water drag coefficient increased by 15 percent
- VR flow rates set to zero in the summers (July through September)
- CR inflow phosphorus concentrations altered to reflect improved understanding resulting from more recent phosphorus data with lower detection limits than previous data
- Chlorophyll *a* concentrations for all inflows were considered to equal 1 µg/L (due to lack of frequent data in the inflows)
- Data sources for CR inflow TOC concentrations and pH 2005 were switched to more representative sources

It should be noted that not all of the gathered field data are presented in each plot: in instances where there are numerous data sets (e.g., the LVW) the less useful data have been omitted for clarity. However, enough of the data are retained in the plots to enable data sets to be verified against each other and allow outlying data points to be identified and possibly removed from the model input.

In addition to the plots, brief descriptions summarizing the methods used to cleanse the data and reconstruct periods where data are missing are provided where necessary. These descriptions focus on methodologies and data sets that are different to those used in the set-up of the original Whole Lake Model (for model years 2000 through 2005). More complete descriptions of the model input data for the original model are provided in a previous report (Flow Science, 2007).

A.1 ELCOM INPUT DATA

This section discusses inputs for the physical model (ELCOM), which encompasses meteorology, water inflow and outflow rates, temperatures and conductivities of the inflows, and inflow concentrations of perchlorate and bromide.

A.1.1 Meteorology

The original Whole Lake Model used meteorological data from the USGS Sentinel Island station located in open water in Boulder Basin (**Figure A.1**) for all model years (2000 through 2005). The data consist of wind speed and direction, solar radiation, air temperature and relative humidity. Rainfall data were obtained from McCarran International Airport. The air temperature, relative humidity and rainfall data had minimal gaps and therefore the data sets required minimal reconstruction. The wind and solar radiation data did have significant gaps and required adjustments and reconstruction as detailed in a previous report (Flow Science, 2007).

The same data sets and methodologies were used to construct input for the 2006 and 2007 model years, except for the wind speed and direction data. The model input for wind used data from additional USGS meteorological stations at Virgin Basin and Overton Arm (**Figure A.1**), which were installed in Lake Mead in late 2005. The new data sources had some minimal gaps, which were filled with data from surrounding days. The reconstructed data from the three USGS stations (Sentinel Island, Virgin Basin and Overton Arm) were then applied to different "wind-areas" of Lake Mead (as described in Section 3.4.2), for model years 2006 and 2007. The use of multiple wind-areas results in a more realistic representation of the on-lake wind patterns.

In addition to using multiple data-sets for wind speed and direction, the wind/water drag coefficient for the entire 2000 through 2007 simulation period was increased by 15 percent throughout the lake, which resulted in improved prediction of thermocline depth and wind-mixing.

A.1.2 Water Inflow and Outflow Rates

The inflow rates for the LVW, CR, VR and MR were obtained from the USGS gauging stations as summarized in **Table A.1**. The locations of these stations are indicated on **Figure A.2**. The gauging station data had minimal gaps and therefore required minimal reconstruction. As such, graphs of the data are not provided here (plots of model input inflows and outflows are provided in Section 2.3.1).

The gauging Stations 0941500 and 09419000 (used for the VR and MR, respectively) were chosen because they were the only ones that had data spanning the entire modeling period. However, these stations are located at significant distances upstream of Lake Mead (**Figure A.2**) and as a result of water use between the stations and the lake, the flow rates had to be adjusted, as summarized in **Table A.1**.

Table A.1: Gauging Stations used for Model Input Inflow Rates

Inflow	USGS gauging station	Notes	Frequency
LVW	09419800 (near LW0.55)	Used directly	Hourly average of 15-minute data
CR	09404200	Used directly	15-minute data
VR (prior to 4/21/06)	09415000	Adjusted based upon regression relationship with station 09415230, and set to zero in summers (July through September)	Hourly average of 15-minute data
VR (4/21/06 onwards)	09415250	Used directly	Daily average data
MR	09419000	Adjusted based upon flow exceedance method	Hourly average of 15-minute data

In April 2006 Station 0941520 on the VR was re-established. This station is located close to Lake Mead (**Figure A.2**), and is a much better representation of the flow rate into the lake than the data from Station 09415000. At the time of data gathering the 15-minute data were not available, and as such daily average data are used in the model from April 21, 2006 onwards (**Table A.1**). Analysis of the new data together with observations from USGS personnel, indicated that the summer flow rates of the VR into Lake Mead were close to zero in most years. Thus, in the present modeling, the VR flow rate was set to zero from July through September of 2000 through 2005, as summarized in **Table A.1**.

The Hoover Dam outflow rates used hourly-averaged data from USGS. Occasional flow rates greater than 40,260 cfs were identified as erroneous and removed. Since only minimal data corrections were required graphs are not provided here (plots of model input inflows and outflows are provided in Section 2.3.1).

The SNWA outflow rates used hourly-averaged data from SNWA. The small Basic Water Company (BWC) flow rate was also combined with the SNWA data, since the intakes are located close together. Again, only minimal data corrections were required, and as such graphs are not provided here (plots of model input inflows and outflows are provided in Section 2.3.1).

A.1.3 Water Temperature

The measured field data and model input temperatures for the LVW, CR, VR and MR are plotted in **Figures A.3** through **A.6**, respectively.

The 20-minute Hydrolab data at LW0.8 were used for the majority of the model input LVW temperatures (**Figure A.3**). These data were first averaged on an hourly basis (to reduce the size of the data set), and then cleaned and reconstructed. This process involved removing seemingly erroneous data, filling gaps with interpolated or reconstructed data, and applying corrections to data that are measured at some distance from the lake when appropriate (such as heating of an inflow). For the original 2000 through 2005 modeling period the data were cleaned and reconstructed in a time-consuming manual process (Flow Science, 2007). For the 2006 and 2007 modeling years a Fortran program was developed that performed the cleaning and reconstruction automatically. Importantly, both methodologies maintained the diurnal temperature variation of the LVW, which has been identified as having a critical role in the lake insertion level of the LVW inflow (Flow Science, 2005).

The model input CR temperature for 2006 and 2007 used sub-daily data measured at RM246 (**Figure A.4**). This station is located some distance upstream of Lake Mead (see **Figure A.2**), and as such, a correction had to be made to account for additional warming. The correction was the same as used in the original 2000 through 2005 modeling (Flow Science, 2007).

The model input temperatures for the VR and MR (**Figures A.5** and **A.6**) used 20-minute Hydrolab data measured at VR49.3 and MR8.0, respectively (see **Figure A.2** for station locations). Data gaps in 2006 and 2007 were filled following the methods used previously for 2000 through 2005 (Flow Science, 2007).

A.1.4 Conductivity

The measured field data and model input conductivities for the LVW, CR, VR and MR are plotted in **Figures A.7** through **A.10**, respectively.

The 20-minute Hydrolab data at LW0.8 were used for the majority of the model input LVW conductivity (**Figure A.7**). These data were first averaged on an hourly basis (to reduce the size of the data set), and then cleaned and reconstructed. For the original 2000 through 2005 modeling period the data were cleaned and reconstructed in a time-consuming manual process (Flow Science, 2007). For the 2006 and 2007 modeling years a Fortran program was developed that performed the cleaning and reconstruction automatically.

The model input CR conductivity (**Figure A.8**) in 2006 was mostly constructed from sub-daily RM226 data, using a slight correction that was developed in the original 2000 through 2005 modeling (Flow Science, 2007) to account for the distance upstream from the lake to RM226. From August through October, 2006, the RM226 conductivity data was either missing or inconsistent with other data-sets (**Figure A.8**). During this time,

the model input was constructed from a mixture of sparse data points from CRLM and 09404200. From November, 2006 onwards, new hourly conductivity data from 09404200 became available. This was used to construct the model input, using the same correction as was used for the RM226 data (since RM226 and 09404200 are located close together (**Figure A.2**)).

The measured and model input conductivities and the flow rate for the VR and MR are shown in **Figures A.9** and **A.10**, respectively. In 2006 and 2007 the Hydrolab data were used for model input, after being cleaned using the same method that was used for the original modeling (Flow Science, 2007).

A.1.5 Perchlorate

The measured field data and model input perchlorate concentrations for the LVW are plotted in **Figure A.11**. Following the original 2000 through 2005 modeling (Flow Science, 2007), the LW0.55 data were used directly for most of the model input. However, from August 2006 onwards, the LW0.8 data were used directly, since the LW0.55 data were not available at the time of model set-up. Analysis of the two data-sets during the overlapping period indicated only small differences between the LW0.55 and LW0.8 data.

The model input perchlorate concentrations for the CR, VR and MR inflows were assumed to be zero, since all of the perchlorate originates in the LVW (Flow Science, 2005).

A.1.6 Bromide

The measured field data and model input bromide concentrations for the LVW, CR, VR and MR are plotted in **Figures A.12** through **A.15**, respectively. The 2006 and 2007 model input for all four inflows uses the same data-sets as were used in the original 2000 through 2005 modeling (Flow Science, 2007).

A.2 CAEDYM INPUT DATA

This section discusses inputs for the biogeochemical model (CAEDYM), which encompasses inflow concentrations of chlorophyll *a*, phosphorus, nitrogen, carbon, pH and DO.

A.2.1 Chlorophyll a

Measurements of chlorophyll *a* taken directly in the inflows were scarce, and generally measurements taken in Lake Mead near each of the inflows (i.e., LWLVB, CRLM_B, VRLM_B and MRLM_B) were used for the model input in the original 2000 through 2005 modeling (Flow Science, 2007). It is likely that these measurements differ from the true inflow concentrations due to direct mixing with ambient lake water, and to algae growing (or dying) within the lake waters. The new modeling therefore simply set the inflow chlorophyll *a* concentration to a nominal "seed value" of 1 µg/L in all inflows.

Experiments with the model indicate that results are not very sensitive to the seed value that is used; rather it is the amount of available nutrients that impacts the modeled chlorophyll *a* concentrations.

A.2.2 Phosphorus

The measured field data and model input filterable reactive phosphorus (FRP) concentrations for the LVW, CR, VR and MR are plotted in **Figures A.16** through **A.19**, respectively.

The FRP measurements in the LVW indicate good agreement across all the data sets (**Figure A.16**). Following the original 2000 through 2005 modeling (Flow Science, 2007), the data measured at LW0.55 were used for model input for all years.

The original 2000 through 2005 modeling used the FRP data measured at Station 09404200 for the model input CR concentrations (Flow Science, 2007). However, these data are mostly below detection limits, and are not deemed particularly reliable. The model input FRP concentrations for the present modeling have subsequently been adjusted based upon an improved understanding of processes in Lake Mead.

Specifically, the model input FRP in the CR was assumed to be 3 µg P/L through September 2003, and 4 µg P/L from October 2003 through December 2004 (**Figure A.17**). These numbers were based upon model results, and are consistent with results of a phosphorus budget that was conducted for Lake Mead, which used more recent data with lower detection limits (Flow Science, 2009). The use of a higher concentration in late 2003 and 2004 is consistent with the higher inflow conductivities at the same time (**Figure A.8**), which are thought to be related to a lower WSEL in Lake Powell (upstream of Lake Mead). The phosphorus budget also resulted in an improved understanding of the phosphorus loading and settling in Lake Mead, and motivated a re-calibration of the phosphorus and algae models (see Section 3.4.6).

From 2005 onwards the model input FRP in the CR was constructed of a combination of CRLM (SNWA) and CRLM_B (USBR) data-sets (**Figure A.17**). These data have lower detection limits, and are deemed more reliable than earlier data-sets.

The VR model input FRP concentrations used data measured at VR49.3 in years 2006 and 2007 (**Figure A.18**). This is the same data-set that was used for year 2005 in the original modeling (Flow Science, 2007).

Prior to 2005 there were limited FRP field data available for the MR. As a result, the original 2000 through 2005 model used available TP data to estimate FRP, by assuming that FRP was equal to 50 percent of the TP (Flow Science, 2007). The present model uses the same FRP input through 2004, but from 2005 onwards the FRP data that were measured at MR8.0 were used directly (**Figure A.19)**.

The measured field data and model input TP concentrations for the LVW, CR, VR and MR are plotted in **Figures A.20** through **A.23**, respectively.

The TP measurements in the LVW indicate good agreement across all the data sets (**Figure A.20**). Following the original 2000 through 2005 modeling (Flow Science, 2007), the data measured at LW0.55 were used for model input for all years.

Figure A.21 indicates large variability in the TP measurements of the CR. However, it is understood that most of the particulate phosphorus in the CR inflow settles out within the first few miles of Lake Mead. This is evident by the large depth of sediment in Gregg Basin (see Section 3.2), as well as from results of a detailed phosphorus budget of Lake Mead (Flow Science, 2009). Since no data for particulate size were available, the model was not able to be configured to perform this settling within the lake. Instead, the model was adapted to effectively use a fictitious land cell at the location of the CR inflow to remove much of the particulate phosphorus. After the removal of particulate phosphorus the resultant TP concentrations entering the first wet cell of the model were equal to four-times the model input FRP concentrations (see **Figure A.17** for the model input FRP concentration) for the entire simulation period, and this is plotted in **Figure A.21**.

It is noted that in the original 2000 through 2005 modeling more particulate phosphorus was removed than at present (Flow Science, 2007). The revised methodology was based upon analysis of more recent phosphorus data with lower detection limits (Flow Science, 2009). Various rate parameters in the phosphorus and algae routines were also adjusted during the re-calibration, in light of the better understanding (see Section 3.4.6).

The model input TP concentrations for the VR used a similar methodology to remove particulate phosphorus as was used for the CR inflow. However, for the VR, the resultant TP concentrations entering the first wet cell of the model were approximately equal to twice the model input FRP concentrations (see **Figure A.18** for the model input FRP concentration) for the entire simulation period. This is the same as was used in the original 2000 through 2005 modeling (Flow Science, 2007). The inputs for the VR are illustrated in **Figure A.22**.

The model input TP concentrations for the MR for years 2006 and 2007 were constructed using the same methods and data-sets as were used in the original 2000 through 2005 modeling (Flow Science, 2007). The input for the MR is illustrated in **Figure A.23**.

A.2.3 Nitrate

The measured field data and model input NO3 concentrations for the LVW, CR, VR and MR are plotted in **Figures A.24** through **A.27**, respectively.

The agreement between the multiple sets of field data at the LVW is very good (**Figure A.24**), and as such, any of the data sets could reasonably be used for the model

input. Following the original 2000 through 2005 modeling (Flow Science, 2007), the data measured at LW0.55 were used for model input for all years.

The data measured at the USGS Station 09404200 were used for the CR model inputs in 2006 and most of 2007 (**Figure A.25**). This directly followed the methodology that was developed in the original 2000 through 2005 modeling (Flow Science, 2007). From August 2007 onwards the model input switched to the CRLM_B (SNWA) data, since the USGS data collection was discontinued. The CRLM_B (SNWA) data were chosen in preference to other available data-sets, due to it being consistent with the USGS data (**Figure A.25**).

The data measured at the USGS Station 09415000 were used for the VR model inputs in 2006 and 2007 (**Figure A.26**). This directly followed the methodology that was developed in the original 2000 through 2005 modeling (Flow Science, 2007).

There was only one data source for the MR, the data from which were used directly for the model input (**Figure A.27**).

A.2.4 Ammonium

The measured field data and model input NH4 concentrations for the LVW, CR, VR and MR are plotted in **Figures A.28** through **A.31**, respectively.

To maintain consistency, the same data sources that were used for NO3 were also used for NH4 where available (i.e., LVW, CR and VR). An exception to this is for the CR from August 2007 onwards, where the NH4 concentration was simply set to 0.01 mg N/L rather than switching to the CRLM_B (SNWA) data-set. This is because the CRLM_B (SNWA) data are not consistent with the previously used USGS data (**Figure A.30**).

For most of the simulation period there were no NH4 field data available for the MR. As a result, the available NO3 data were used to estimate NH4, by assuming that NH4 was equal to 10 percent of the NO3 (Flow Science, 2007). **Figure A.31** illustrates the resulting input. It is noted that NH4 data did become available in 2005. These data were not used for the model input, because the agreement of the crude model with the new data was reasonable (see **Figure A.31**) and the MR inflow is so small relative to the nearby VR inflow.

A.2.5 Total Organic Carbon

The measured field data and model input TOC concentrations for the LVW, CR, VR and MR are plotted in **Figures A.32** through **A.35**, respectively.

In model years 2006 and 2007 the LW0.8 data were used for the model input LVW TOC concentrations (**Figure A.32**). Prior to 2006, the LW0.8 data were not available, and LW5.5 and adjusted LWLVB data were used (Flow Science, 2007).

The original 2000 through 2005 modeling used the CRLM data for the model input CR TOC concentrations (Flow Science, 2007). However, from 2005 a new data-set at CRLM_B became available, and the model input was switched to this data-set (in years 2005, 2006 and 2007) (**Figure A.33**) since this resulted in improved model results.

Following the original 2000 through 2005 modeling (Flow Science, 2007), the SNWA data were used for model input for all years for the VR and MR inflow TOC concentrations (**Figures A.34** and **A.35**, respectively).

A.2.6 pH

The measured field data and model input pH for the LVW, CR, VR and MR are plotted in **Figures A.36** through **A.39**, respectively.

Following the original 2000 through 2005 modeling (Flow Science, 2007), the data measured at LW0.55 were used for model input LVW pH for all years (**Figure A.36**).

The original 2000 through 2005 modeling used the Station 09402400 data for the model input CR TOC concentrations (Flow Science, 2007). However, the new modeling switched to using CRLM_B data from 2005 onwards (**Figure A.37**) since this resulted in improved model results.

The 2006 and 2007 model input pH uses the same data-sets as were used in the original 2000 through 2005 modeling (Flow Science, 2007) for the VR and MR inflows (**Figures A.38** and **A.39**, respectively).

A.2.7 Dissolved Oxygen

The measured field data and model input DO concentrations for the LVW, CR, VR and MR are plotted in **Figures A.40** through **A.43**, respectively. The 2006 and 2007 model input uses the same data-sets as were used in the original 2000 through 2005 modeling (Flow Science, 2007) for all four inflows.

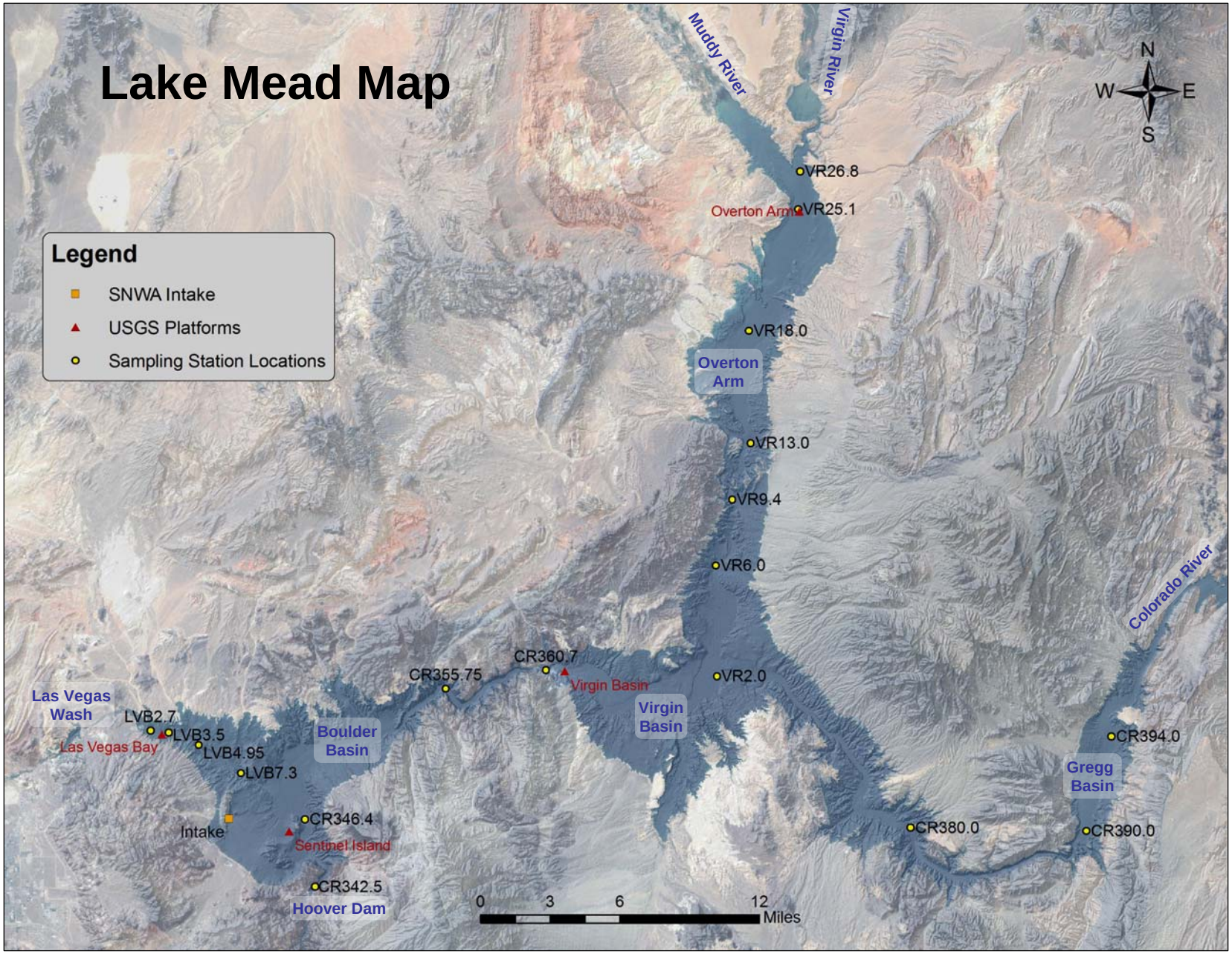
Lake Mead Map
Muddy River
Virgin River
N
W
E
S
Legend
SNWA Intake
USGS Platforms
Sampling Station Locations
VR26.8
Overton Arm
VR25.1
VR18.0
Overton Arm
VR13.0
VR9.4
VR6.0
Colorado River
CR360.7
CR355.75
Virgin Basin
VR2.0
Virgin Basin
Las Vegas Wash
LVB2.7
LVB3.5
Las Vegas Bay
LVB4.95
LVB7.3
Boulder Basin
CR394.0
Gregg Basin
CR346.4
Intake
Sentinel Island
CR380.0
CR390.0
CR342.5
Hoover Dam
0
3
6
12
Miles

Figure A.1

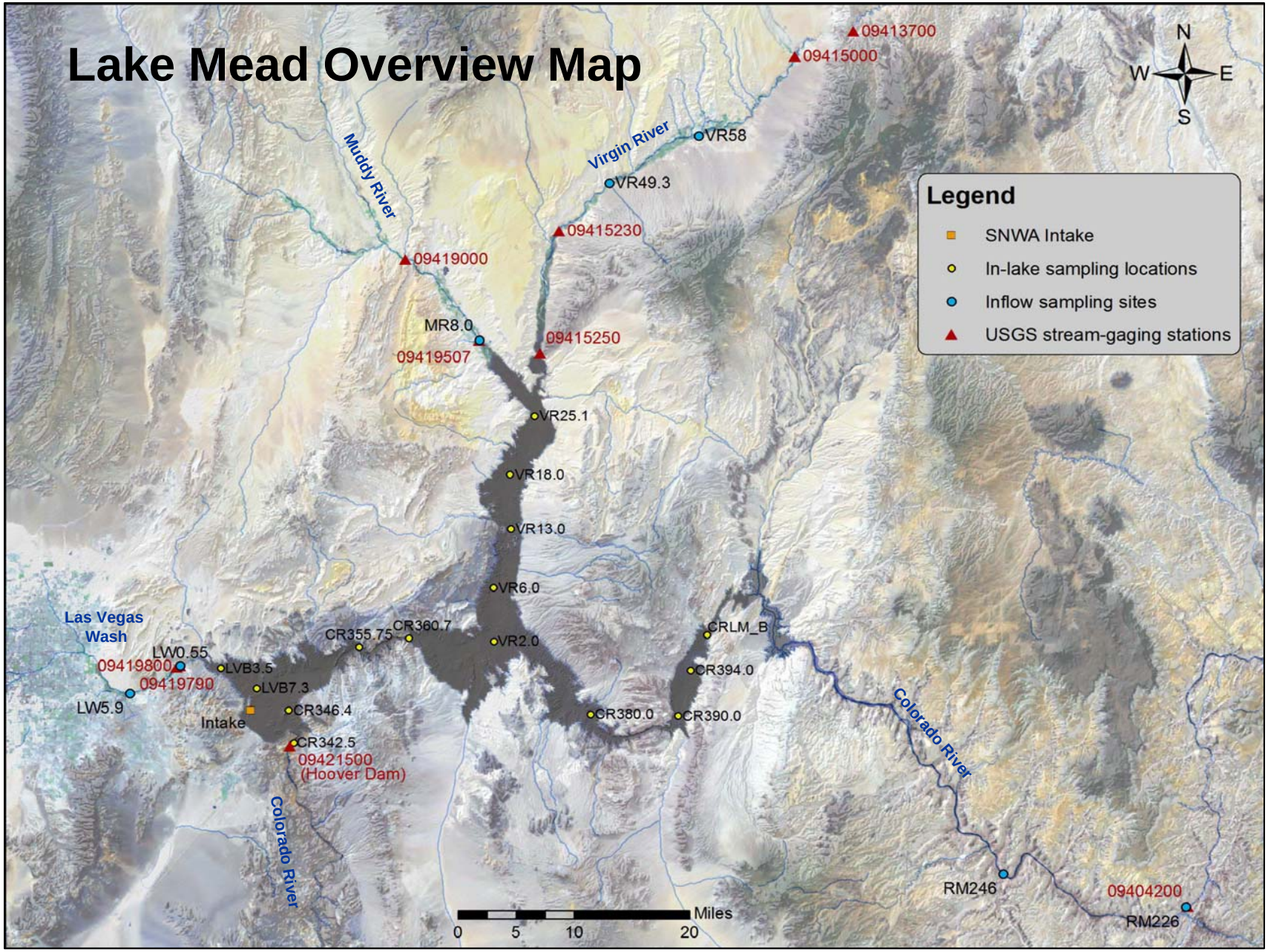

AppA_Figures.ppt
FSI V064081 & V084015 Task 1
December 9, 2010

Figure A.2

FLOW SCIENCE

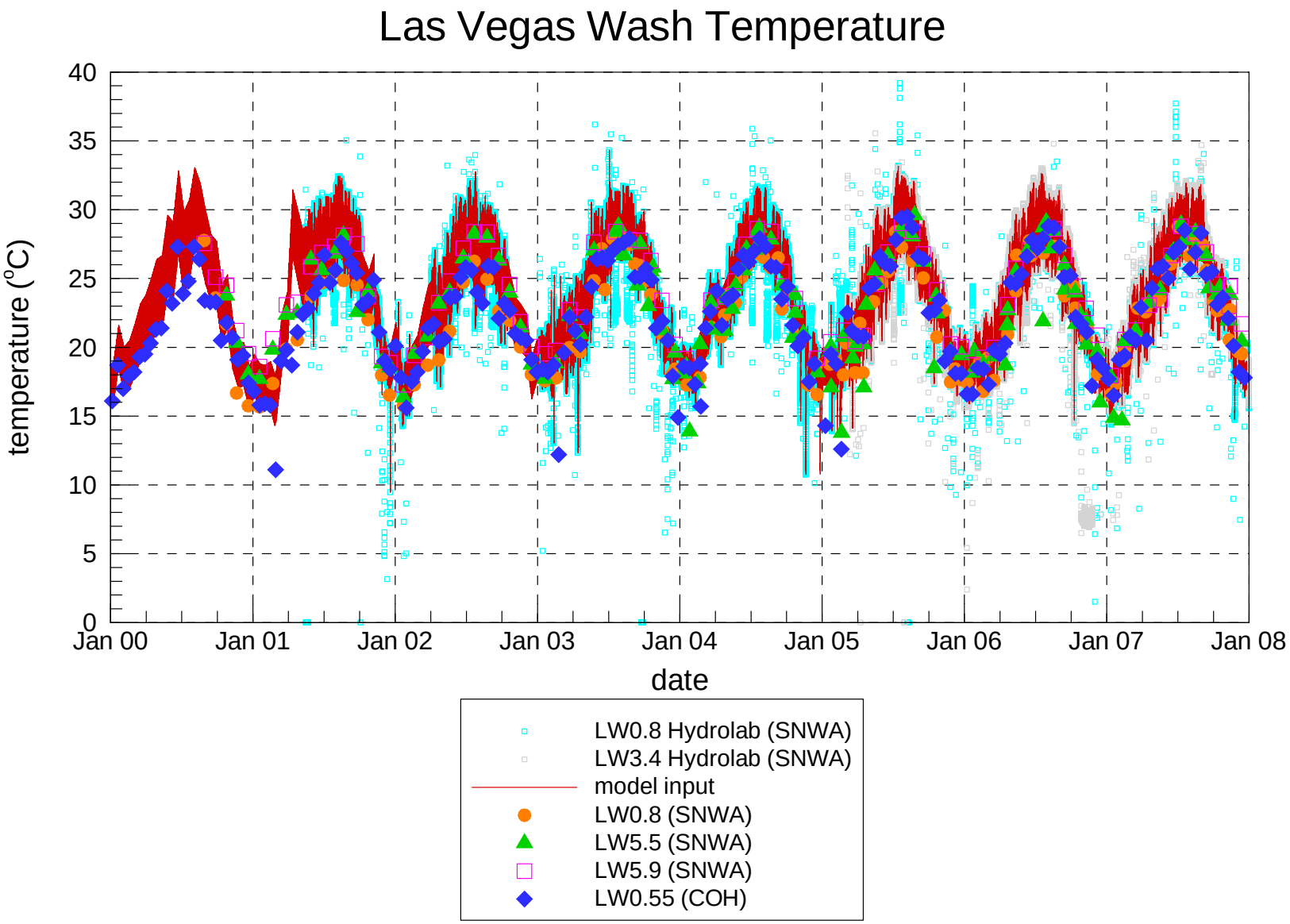
Las Vegas Wash Temperature
temperature (°C)
40
35
30
25
20
15
10
5
0
Jan 00
Jan 01
Jan 02
Jan 03
Jan 04
Jan 05
Jan 06
Jan 07
Jan 08
date
LW0.8 Hydrolab (SNWA)
LW3.4 Hydrolab (SNWA)
model input
LW0.8 (SNWA)
LW5.5 (SNWA)
LW5.9 (SNWA)
LW0.55 (COH)

Figure A.3

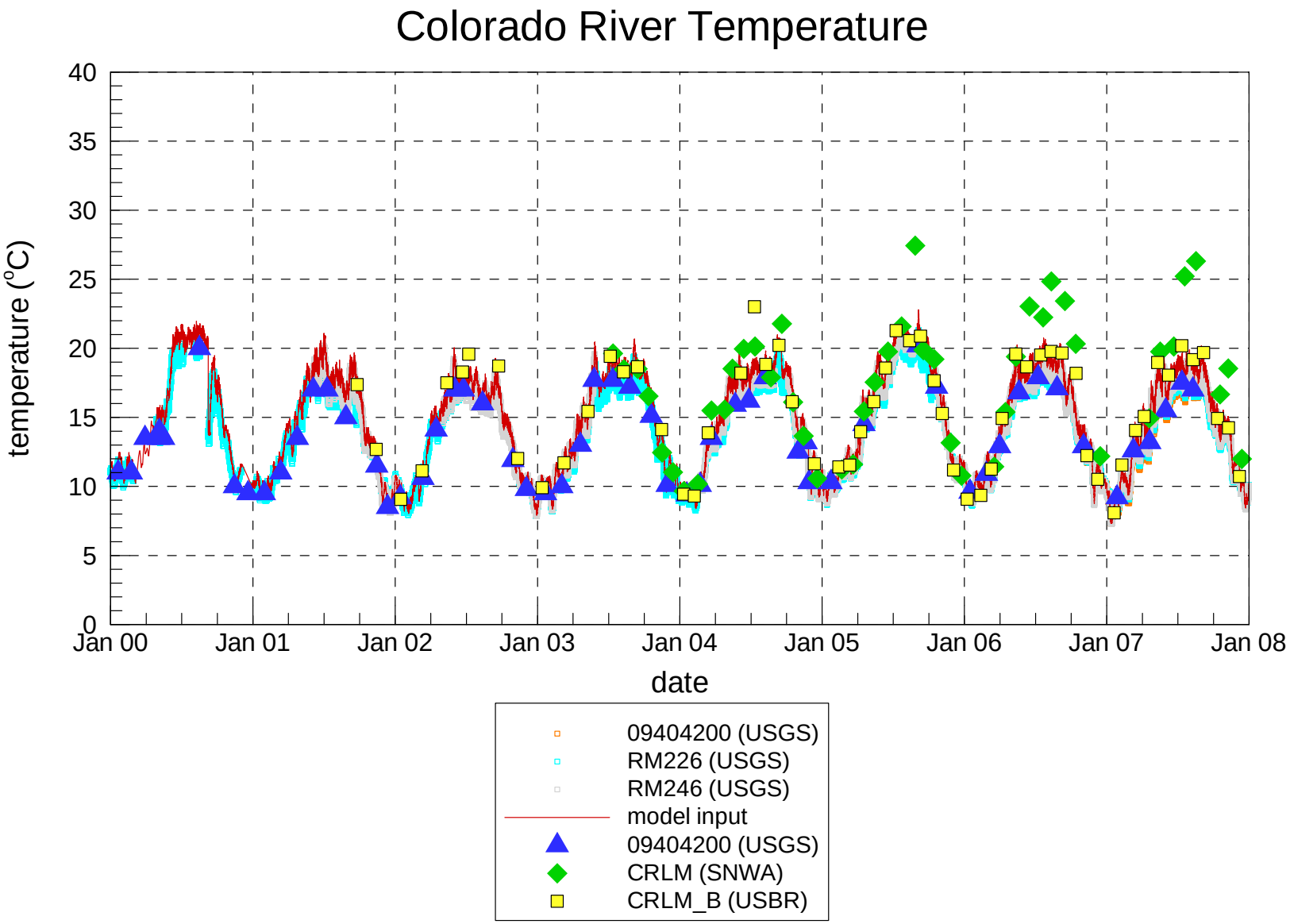
Colorado River Temperature
temperature (°C)
40
35
30
25
20
15
10
5
0
Jan 00
Jan 01
Jan 02
Jan 03
Jan 04
Jan 05
Jan 06
Jan 07
Jan 08
date
09404200 (USGS)
RM226 (USGS)
RM246 (USGS)
model input
09404200 (USGS)
CRLM (SNWA)
CRLM_B (USBR)

Figure A.4

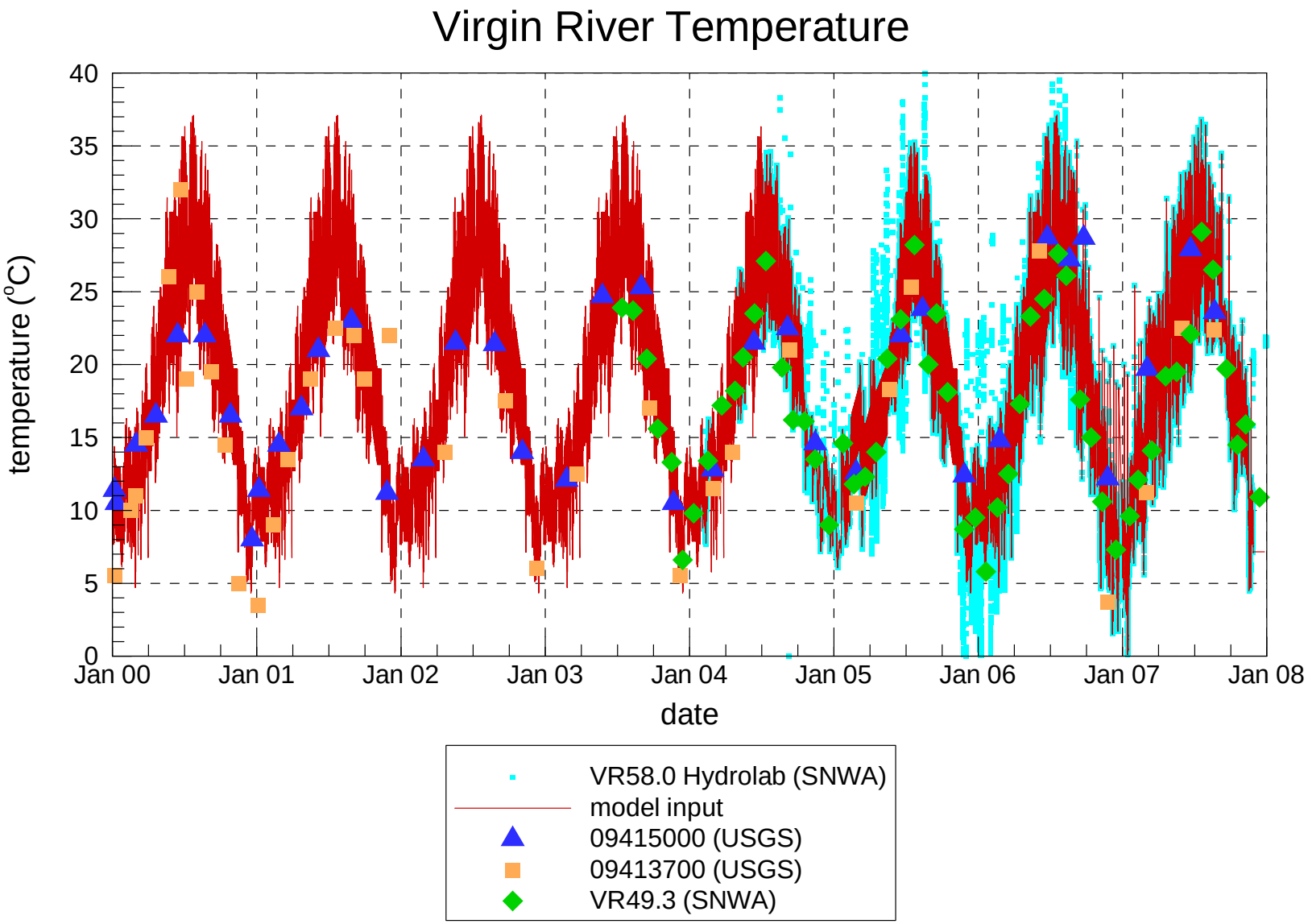
Virgin River Temperature
temperature (°C)
0
5
10
15
20
25
30
35
40
Jan 00
Jan 01
Jan 02
Jan 03
Jan 04
Jan 05
Jan 06
Jan 07
Jan 08
date
VR58.0 Hydrolab (SNWA)
model input
09415000 (USGS)
09413700 (USGS)
VR49.3 (SNWA)

Figure A.5

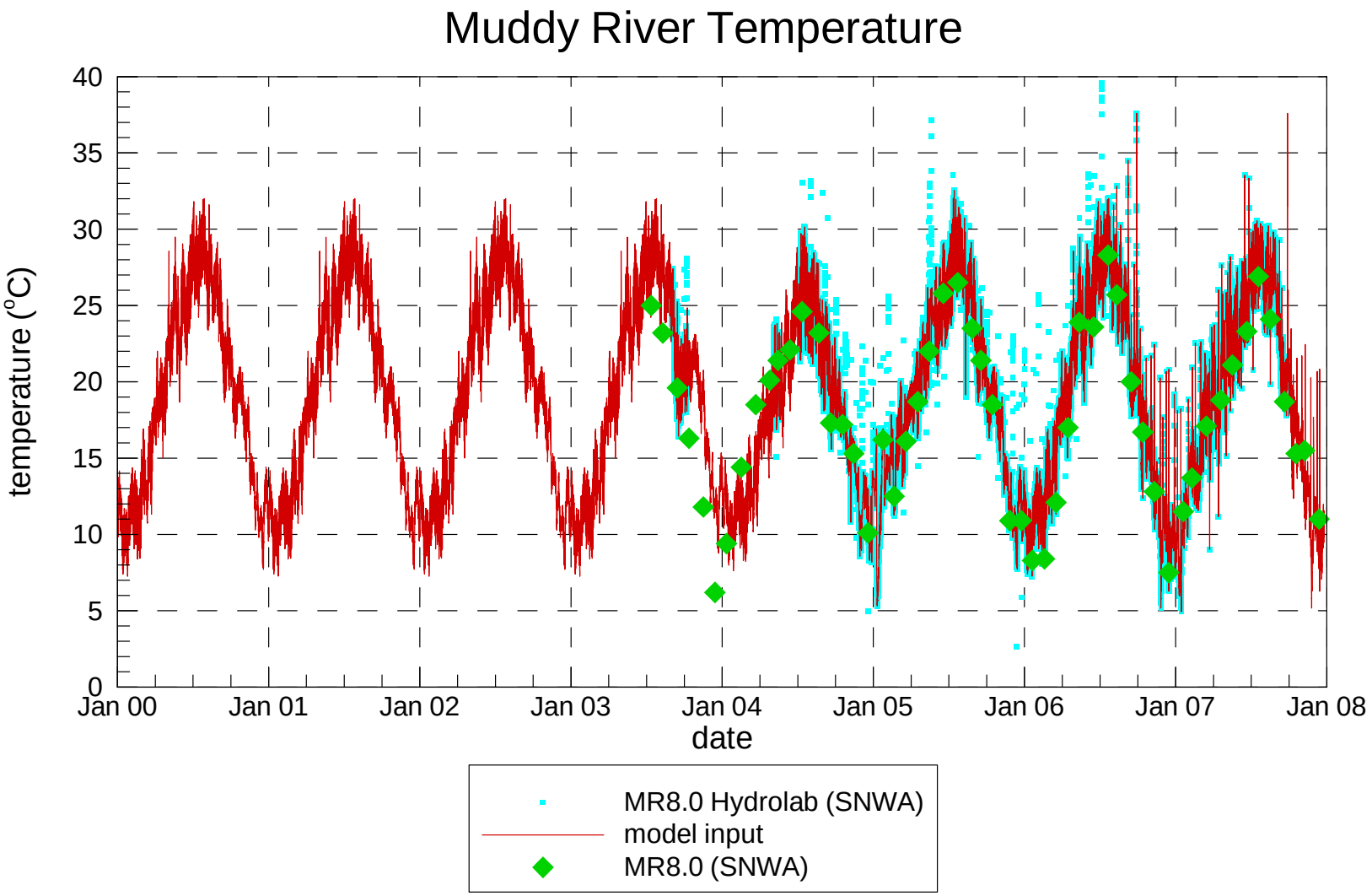
Muddy River Temperature
temperature (°C)
0
5
10
15
20
25
30
35
40
Jan 00
Jan 01
Jan 02
Jan 03
Jan 04
Jan 05
Jan 06
Jan 07
Jan 08
date
MR8.0 Hydrolab (SNWA)
model input
MR8.0 (SNWA)

Figure A.6

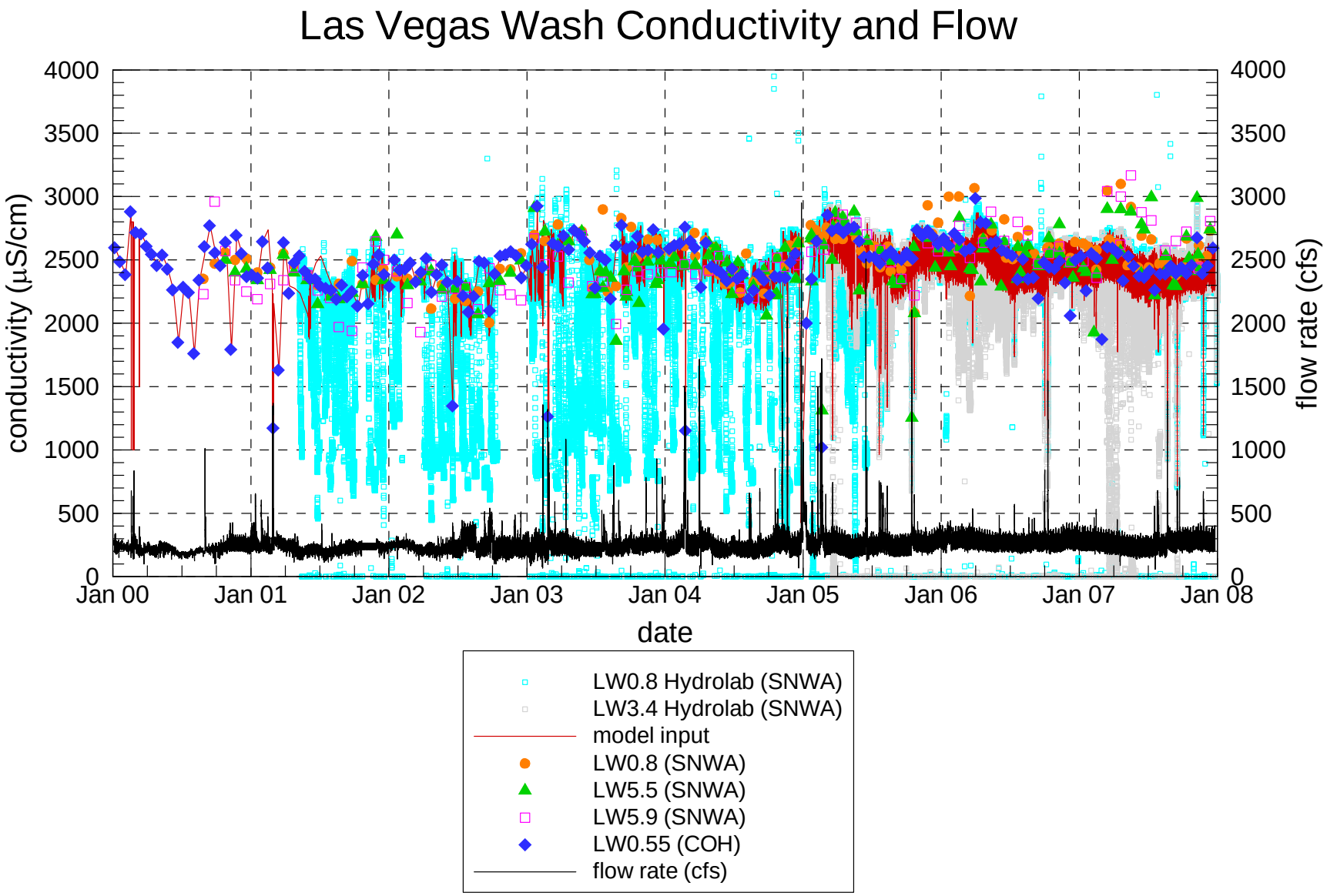
Las Vegas Wash Conductivity and Flow
conductivity (µS/cm)
flow rate (cfs)
4000
3500
3000
2500
2000
1500
1000
500
0
Jan 00
Jan 01
Jan 02
Jan 03
Jan 04
Jan 05
Jan 06
Jan 07
Jan 08
date
LW0.8 Hydrolab (SNWA)
LW3.4 Hydrolab (SNWA)
model input
LW0.8 (SNWA)
LW5.5 (SNWA)
LW5.9 (SNWA)
LW0.55 (COH)
flow rate (cfs)

Figure A.7

Colorado River Conductivity

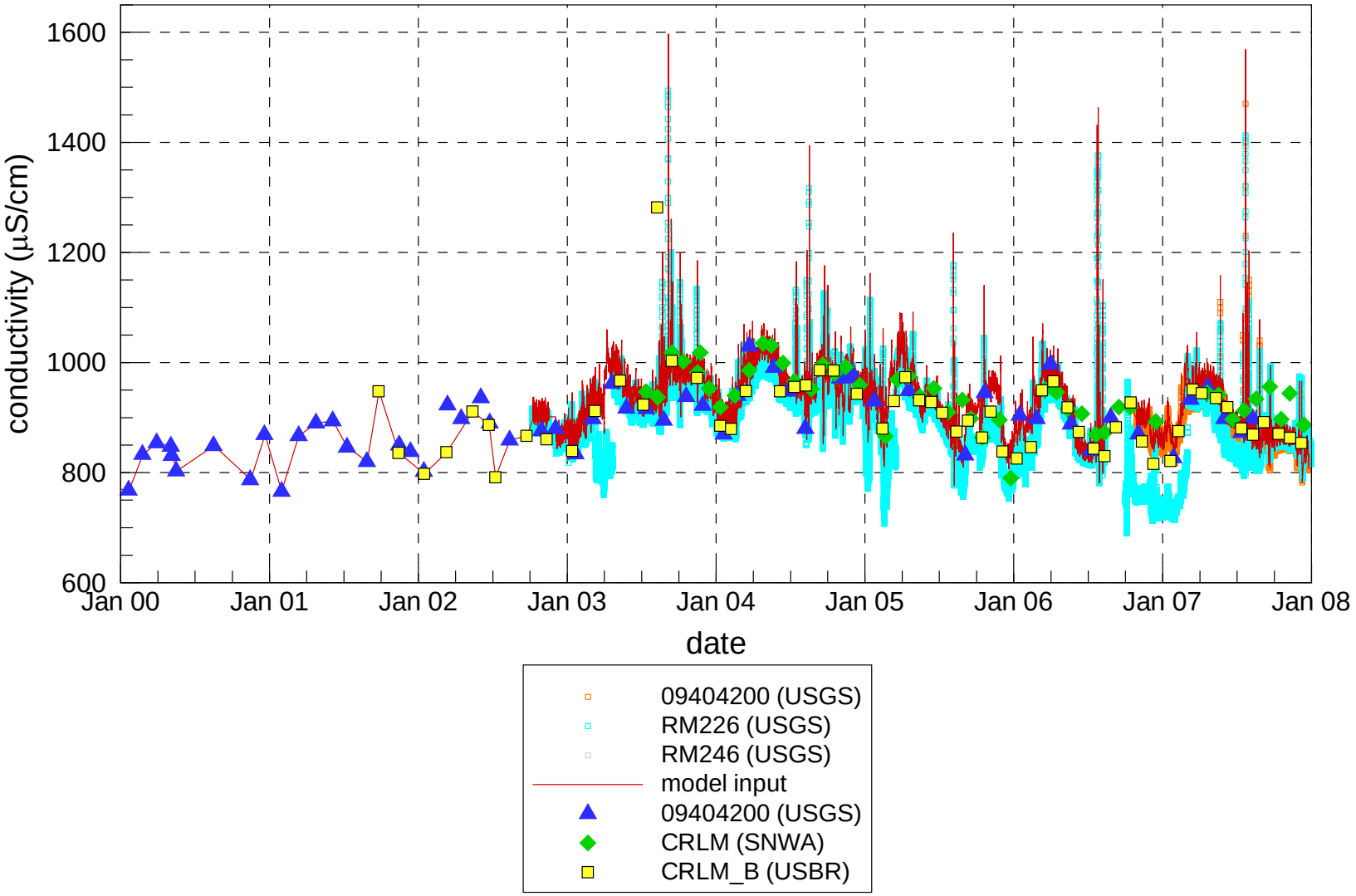

Figure A.8

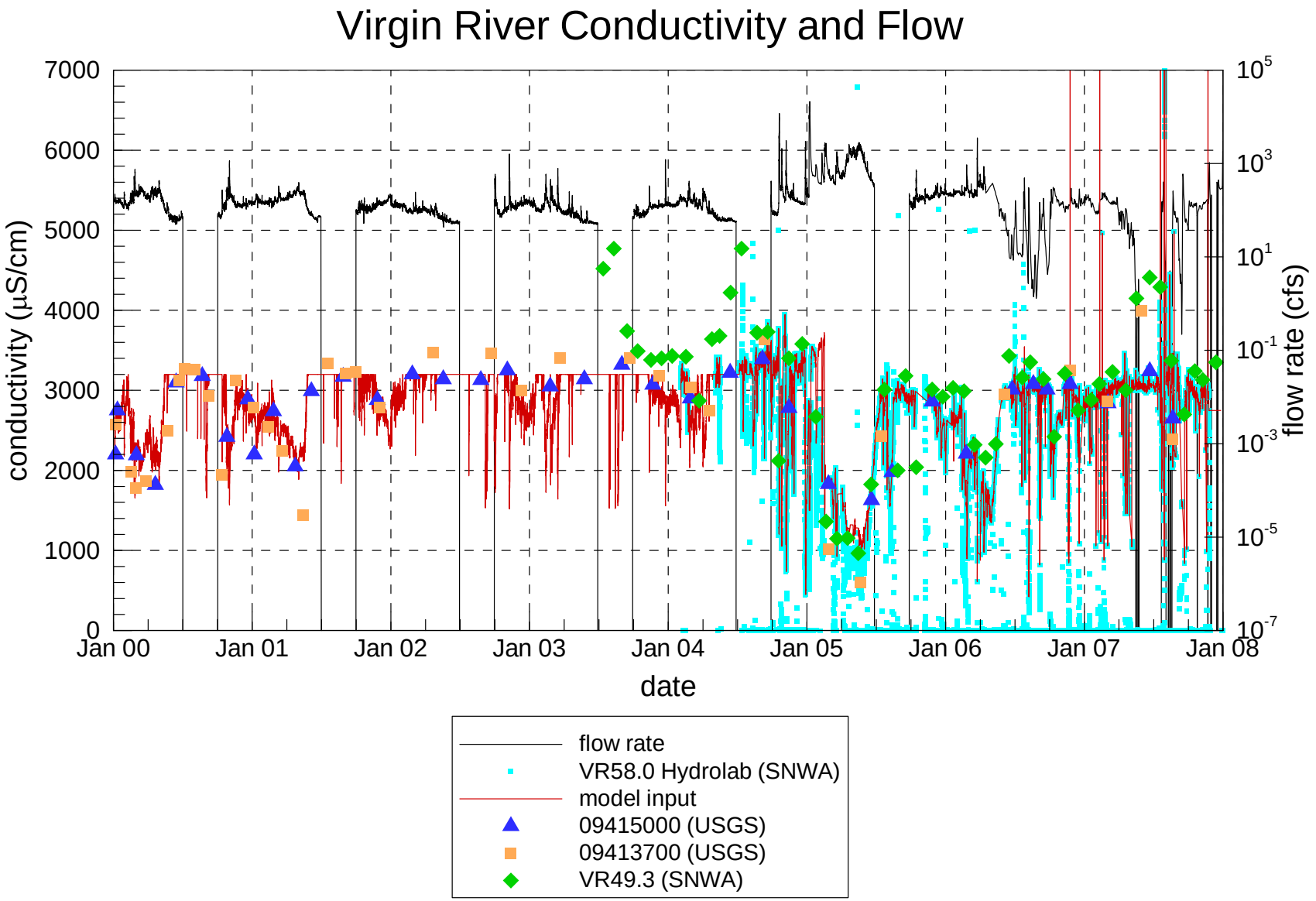
Virgin River Conductivity and Flow
conductivity (µS/cm)
flow rate (cfs)
date
7000
6000
5000
4000
3000
2000
1000
0
10^{5}
10^{3}
10^{1}
10^{-1}
10^{-3}
10^{-5}
10^{-7}
Jan 00
Jan 01
Jan 02
Jan 03
Jan 04
Jan 05
Jan 06
Jan 07
Jan 08
flow rate
VR58.0 Hydrolab (SNWA)
model input
09415000 (USGS)
09413700 (USGS)
VR49.3 (SNWA)

Figure A.9

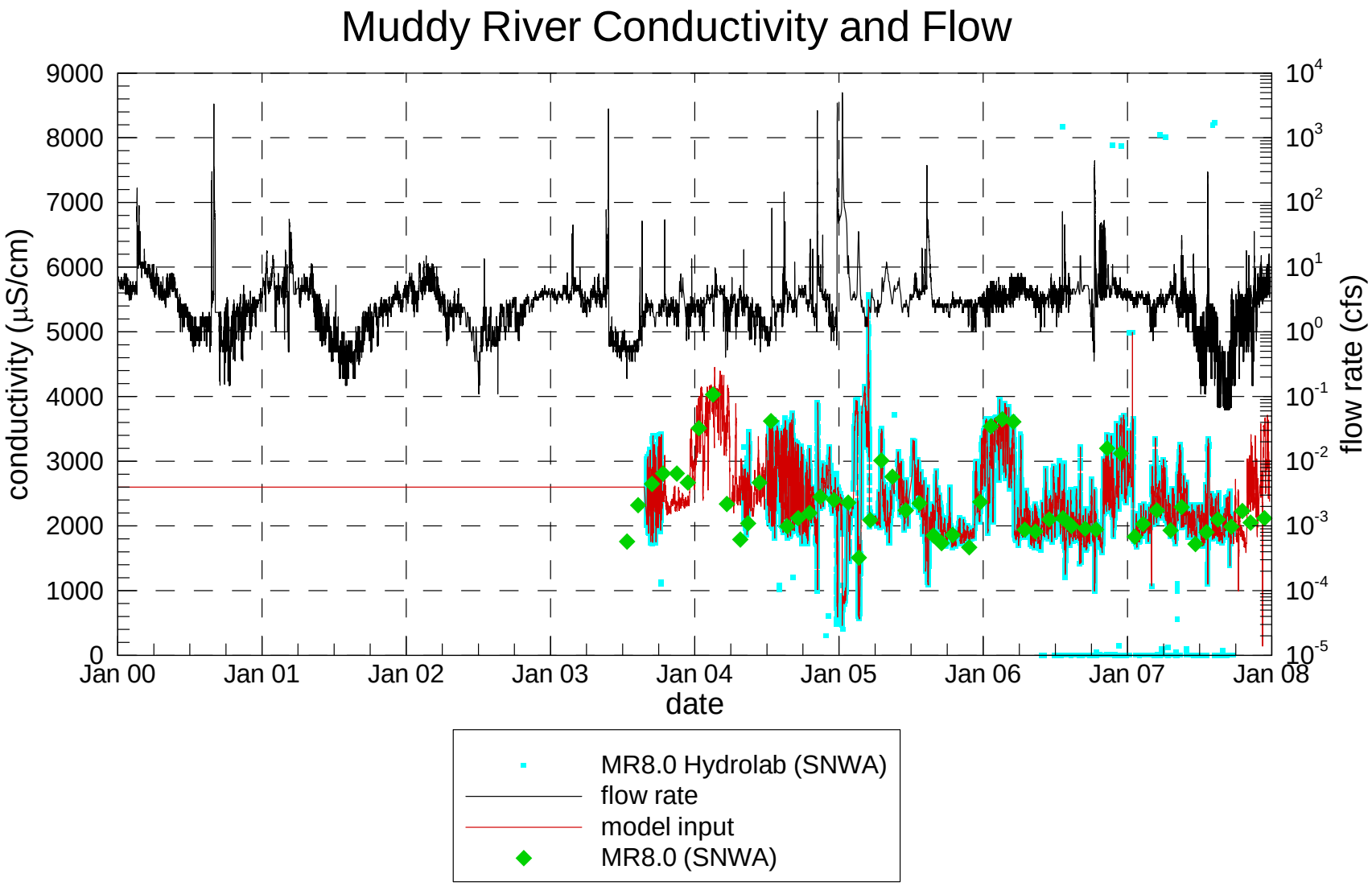
Muddy River Conductivity and Flow
conductivity (µS/cm)
flow rate (cfs)
date
9000
8000
7000
6000
5000
4000
3000
2000
1000
0
10^4
10^3
10^2
10^1
10^0
10^{-1}
10^{-2}
10^{-3}
10^{-4}
10^{-5}
Jan 00
Jan 01
Jan 02
Jan 03
Jan 04
Jan 05
Jan 06
Jan 07
Jan 08
MR8.0 Hydrolab (SNWA)
flow rate
model input
MR8.0 (SNWA)

Figure A.10

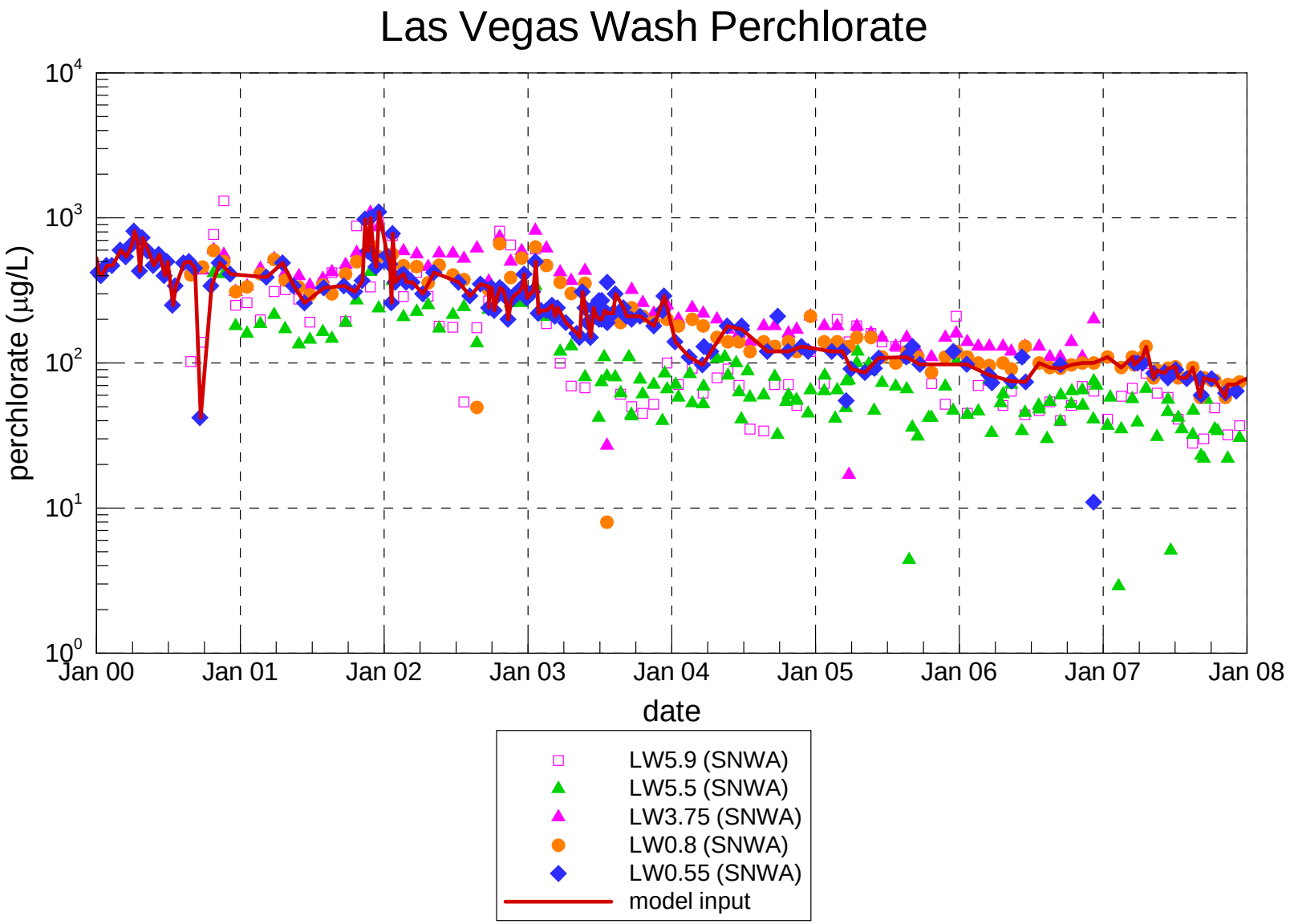
Las Vegas Wash Perchlorate
perchlorate (µg/L)
10^4
10^3
10^2
10^1
10^0
Jan 00
Jan 01
Jan 02
Jan 03
Jan 04
Jan 05
Jan 06
Jan 07
Jan 08
date
LW5.9 (SNWA)
LW5.5 (SNWA)
LW3.75 (SNWA)
LW0.8 (SNWA)
LW0.55 (SNWA)
model input

Figure A.11

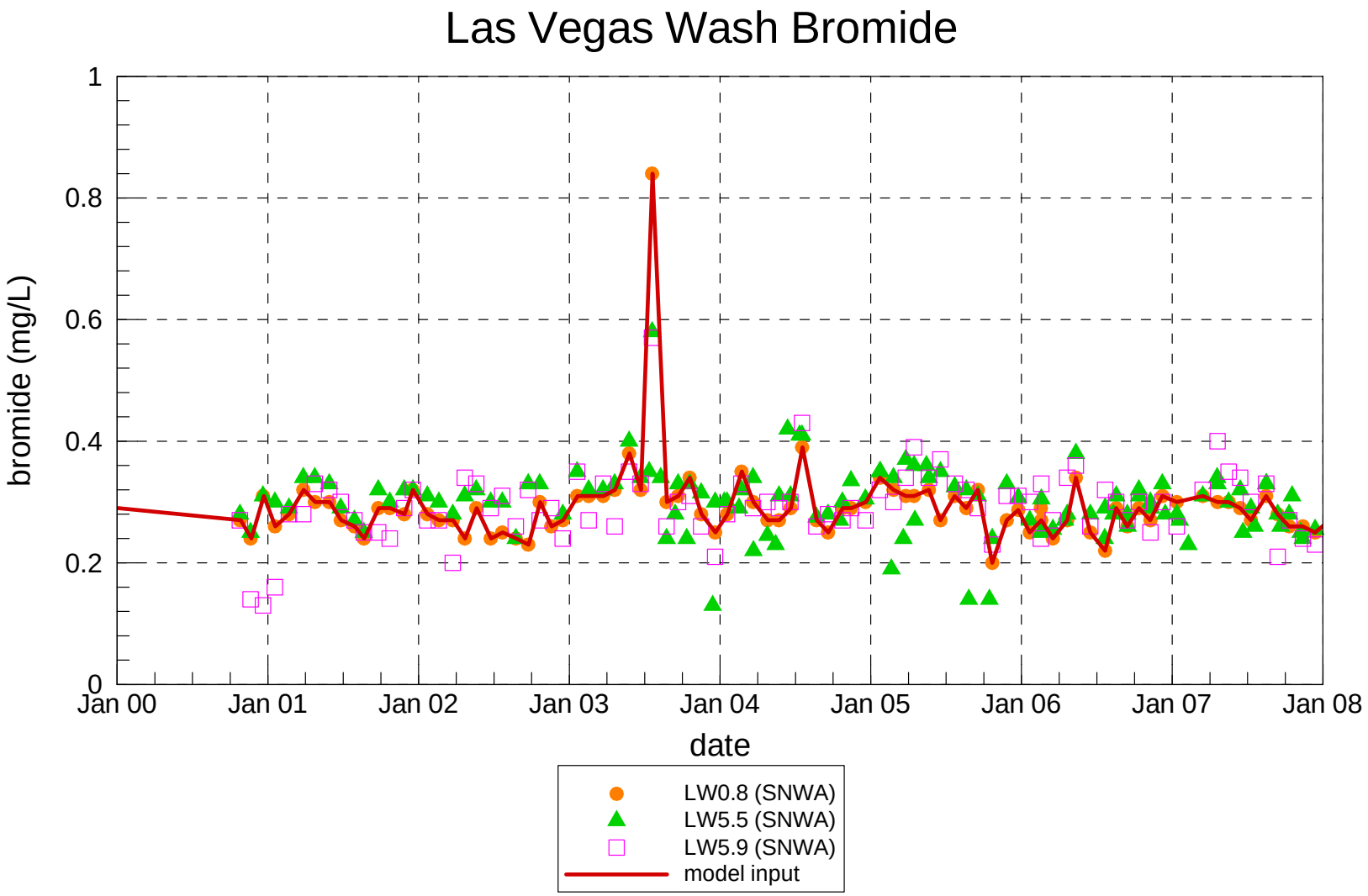
Las Vegas Wash Bromide
bromide (mg/L)
1
0.8
0.6
0.4
0.2
0
Jan 00
Jan 01
Jan 02
Jan 03
Jan 04
Jan 05
Jan 06
Jan 07
Jan 08
date
LW0.8 (SNWA)
LW5.5 (SNWA)
LW5.9 (SNWA)
model input

Figure A.12

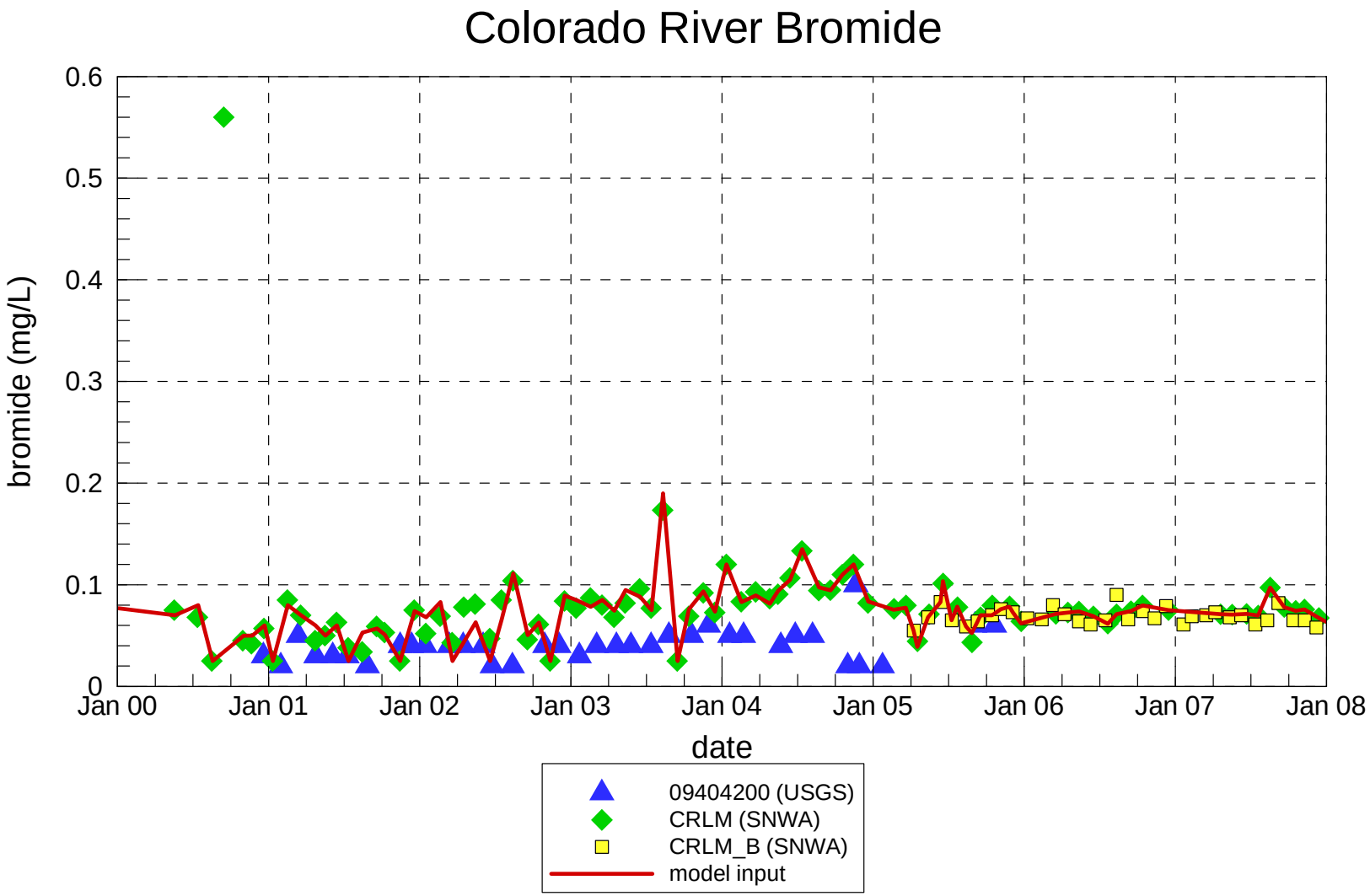
Colorado River Bromide
bromide (mg/L)
0.6
0.5
0.4
0.3
0.2
0.1
0
Jan 00
Jan 01
Jan 02
Jan 03
Jan 04
Jan 05
Jan 06
Jan 07
Jan 08
date
09404200 (USGS)
CRLM (SNWA)
CRLM_B (SNWA)
model input

Figure A.13

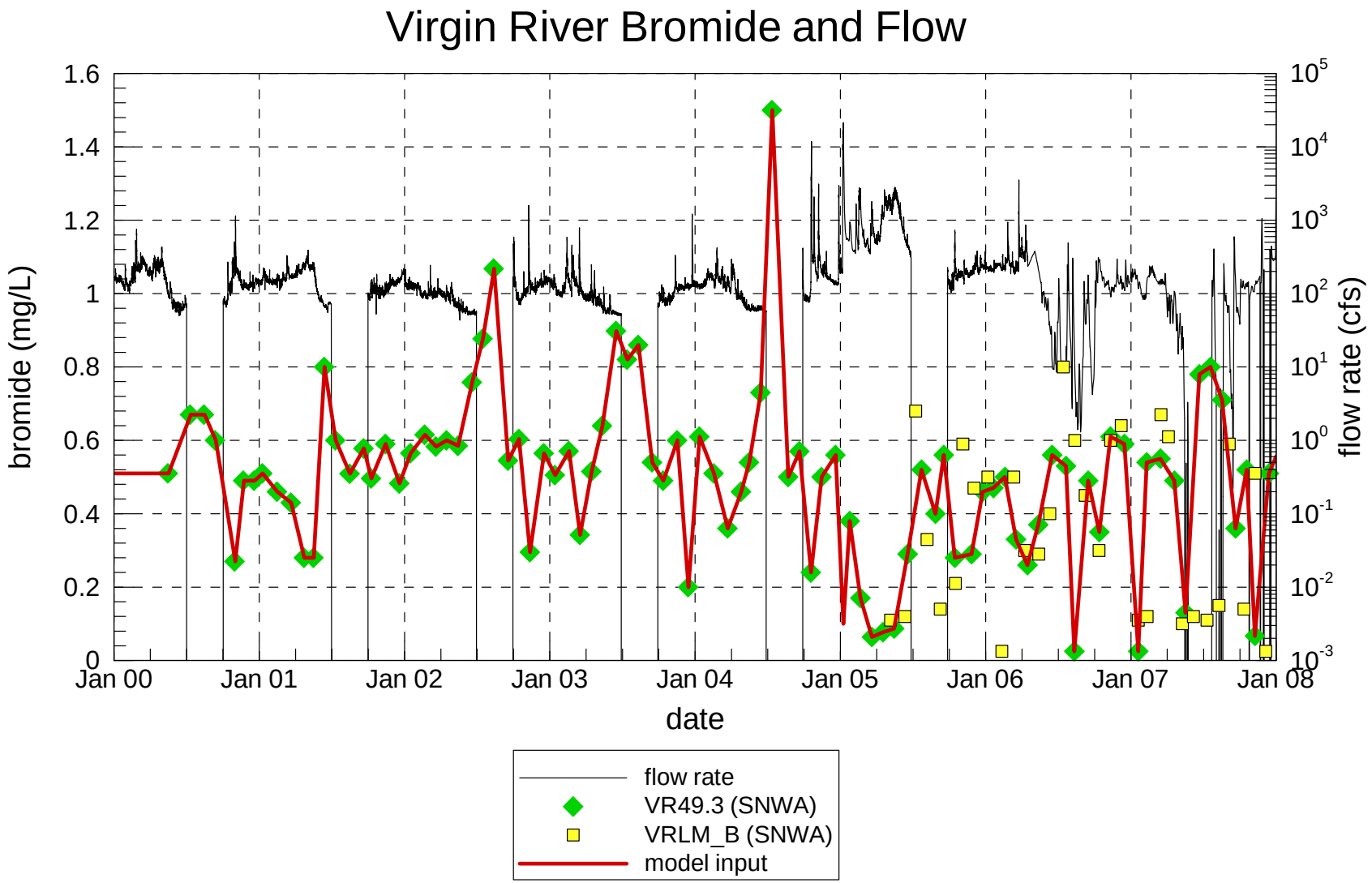
Virgin River Bromide and Flow
bromide (mg/L)
flow rate (cfs)
date
Jan 00
Jan 01
Jan 02
Jan 03
Jan 04
Jan 05
Jan 06
Jan 07
Jan 08
flow rate
VR49.3 (SNWA)
VRLM_B (SNWA)
model input

Figure A.14

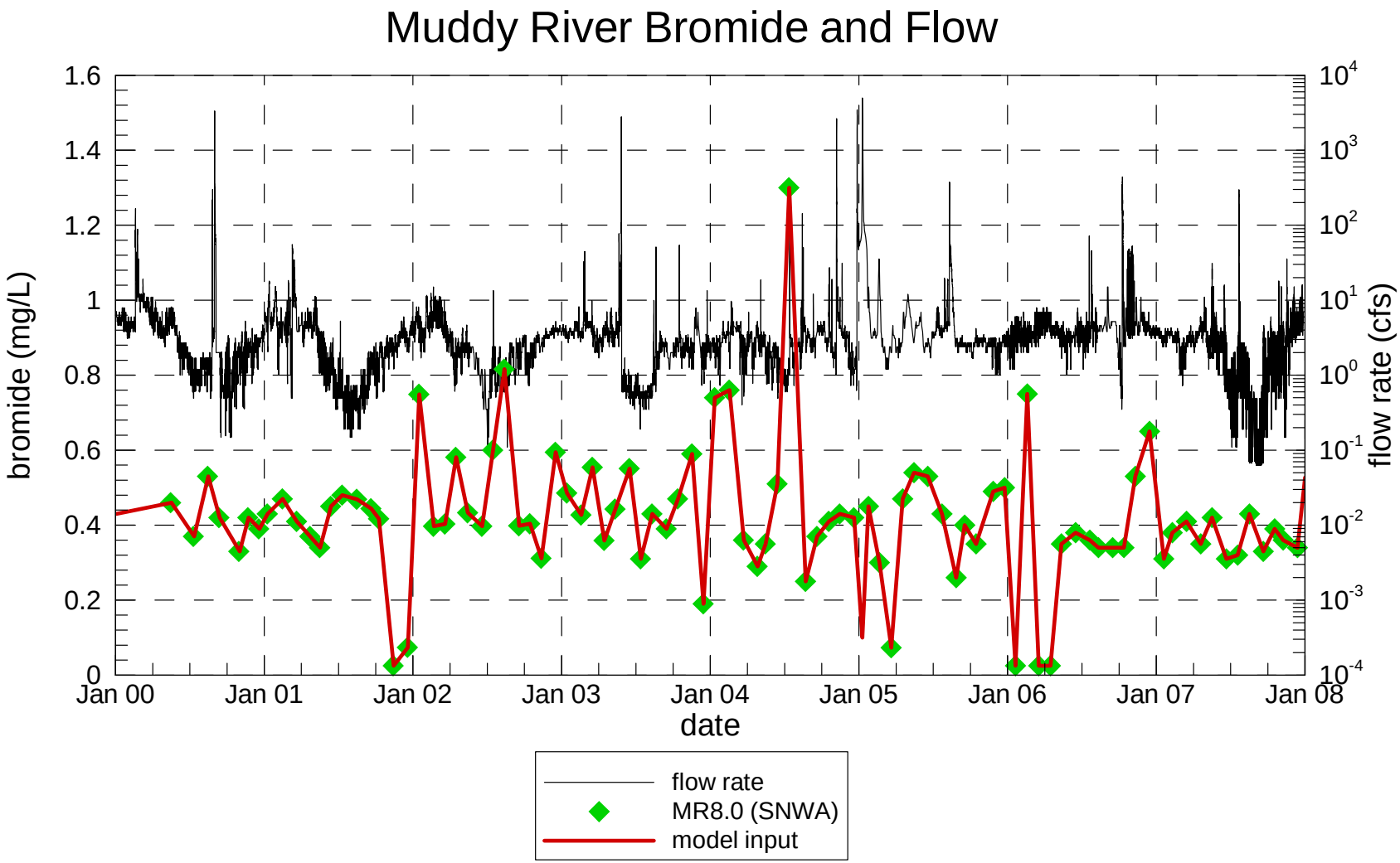
Muddy River Bromide and Flow
bromide (mg/L)
flow rate (cfs)
1.6
1.4
1.2
1
0.8
0.6
0.4
0.2
0
10^4
10^3
10^2
10^1
10^0
10^{-1}
10^{-2}
10^{-3}
10^{-4}
Jan 00
Jan 01
Jan 02
Jan 03
Jan 04
Jan 05
Jan 06
Jan 07
Jan 08
date
flow rate
MR8.0 (SNWA)
model input

Figure A.15

Las Vegas Wash Filterable Reactive Phosphorus

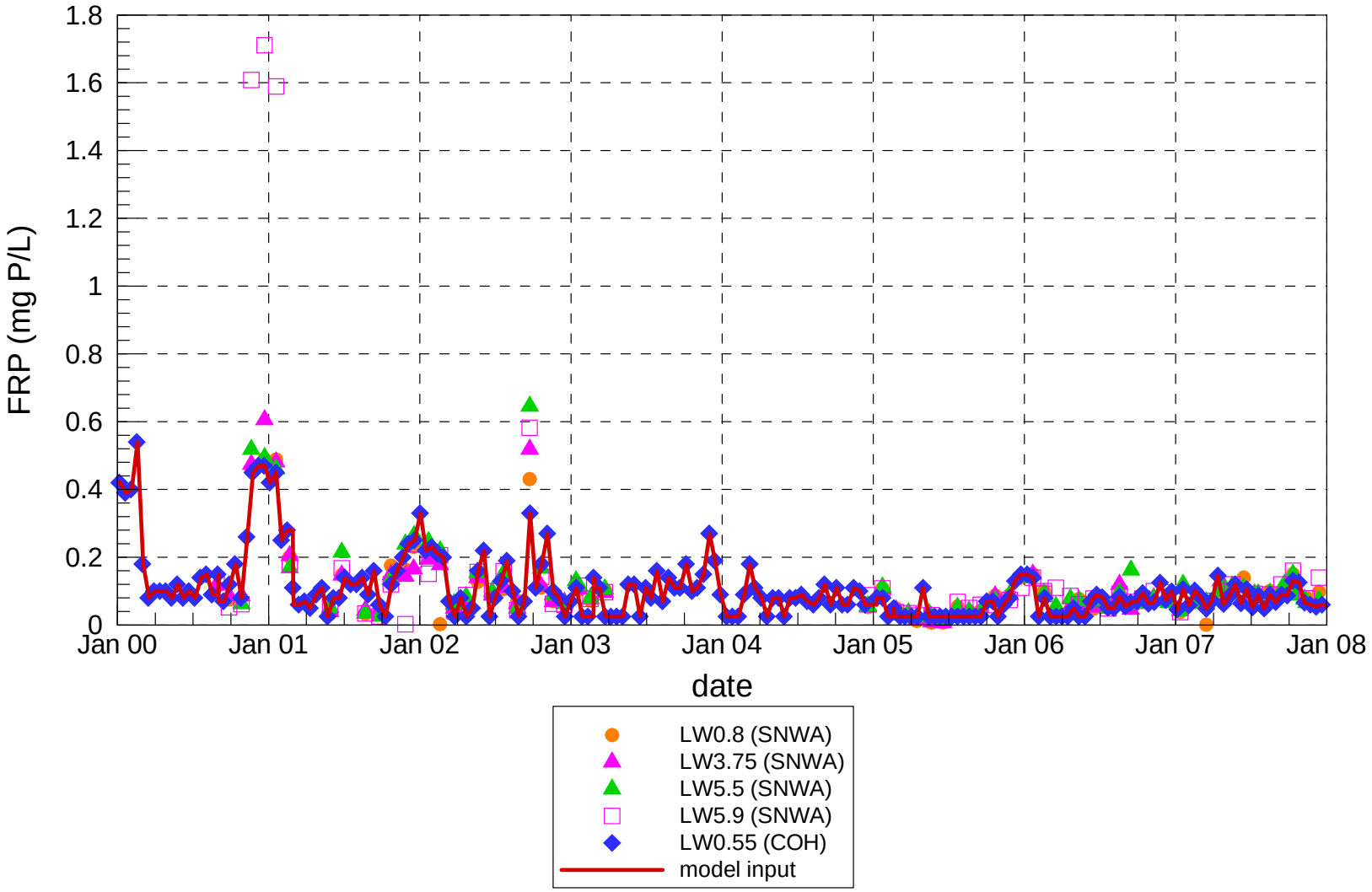

Figure A.16

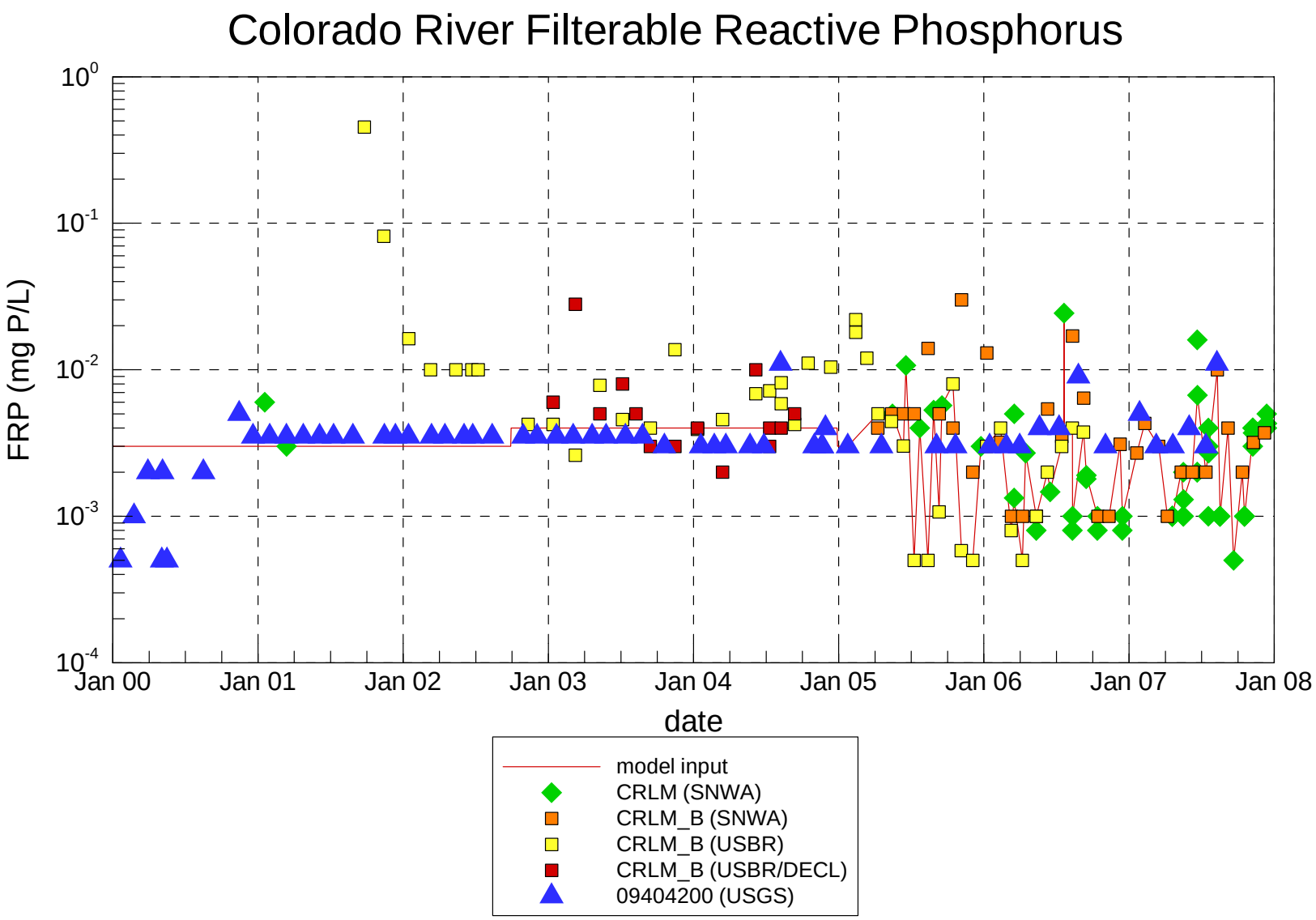
Colorado River Filterable Reactive Phosphorus
FRP (mg P/L)
10^0
10^-1
10^-2
10^-3
10^-4
Jan 00
Jan 01
Jan 02
Jan 03
Jan 04
Jan 05
Jan 06
Jan 07
Jan 08
date
model input
CRLM (SNWA)
CRLM_B (SNWA)
CRLM_B (USBR)
CRLM_B (USBR/DECL)
09404200 (USGS)

Figure A.17

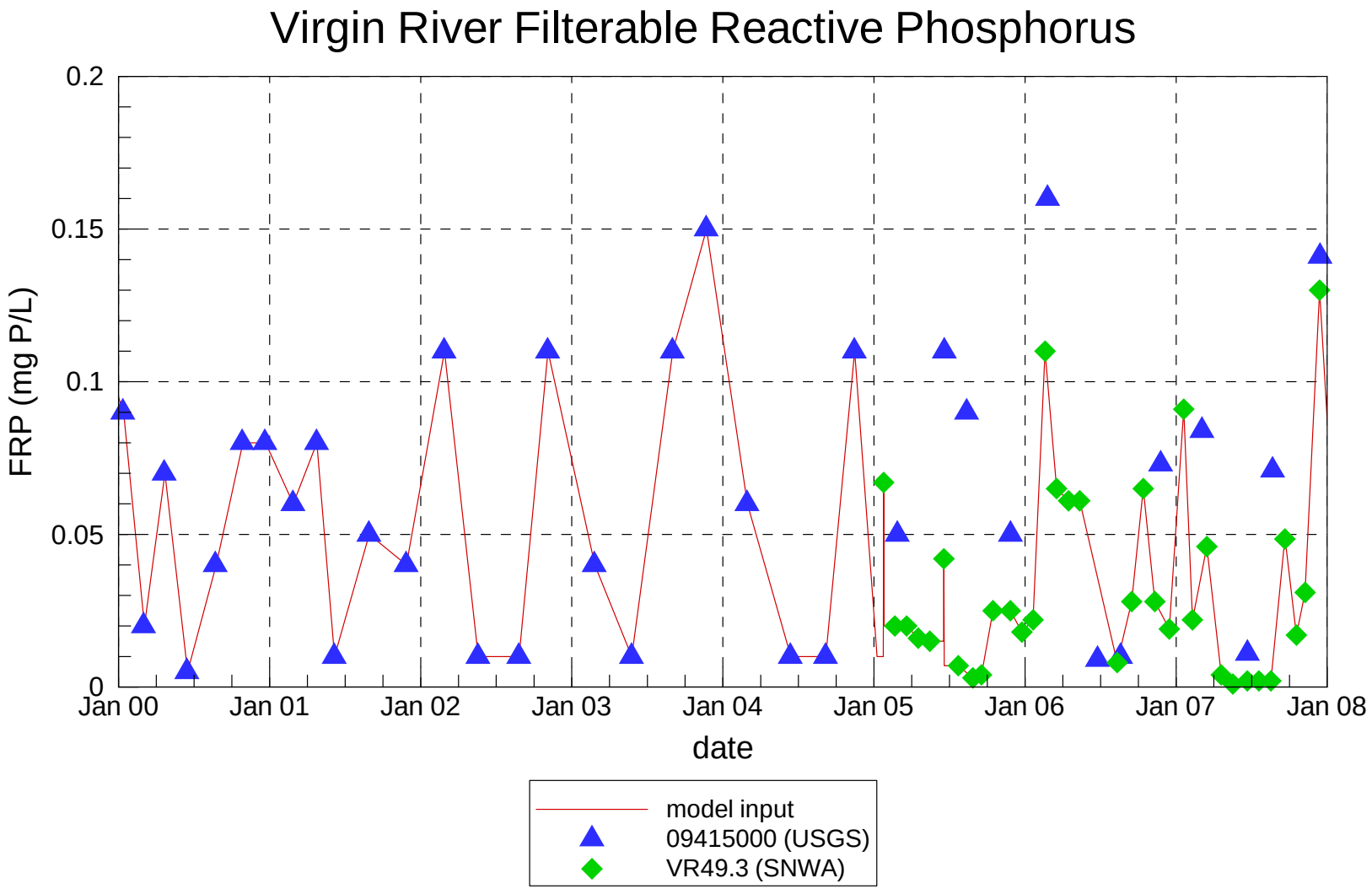
Virgin River Filterable Reactive Phosphorus
FRP (mg P/L)
0.2
0.15
0.1
0.05
0
Jan 00
Jan 01
Jan 02
Jan 03
Jan 04
Jan 05
Jan 06
Jan 07
Jan 08
date
model input
09415000 (USGS)
VR49.3 (SNWA)

Figure A.18

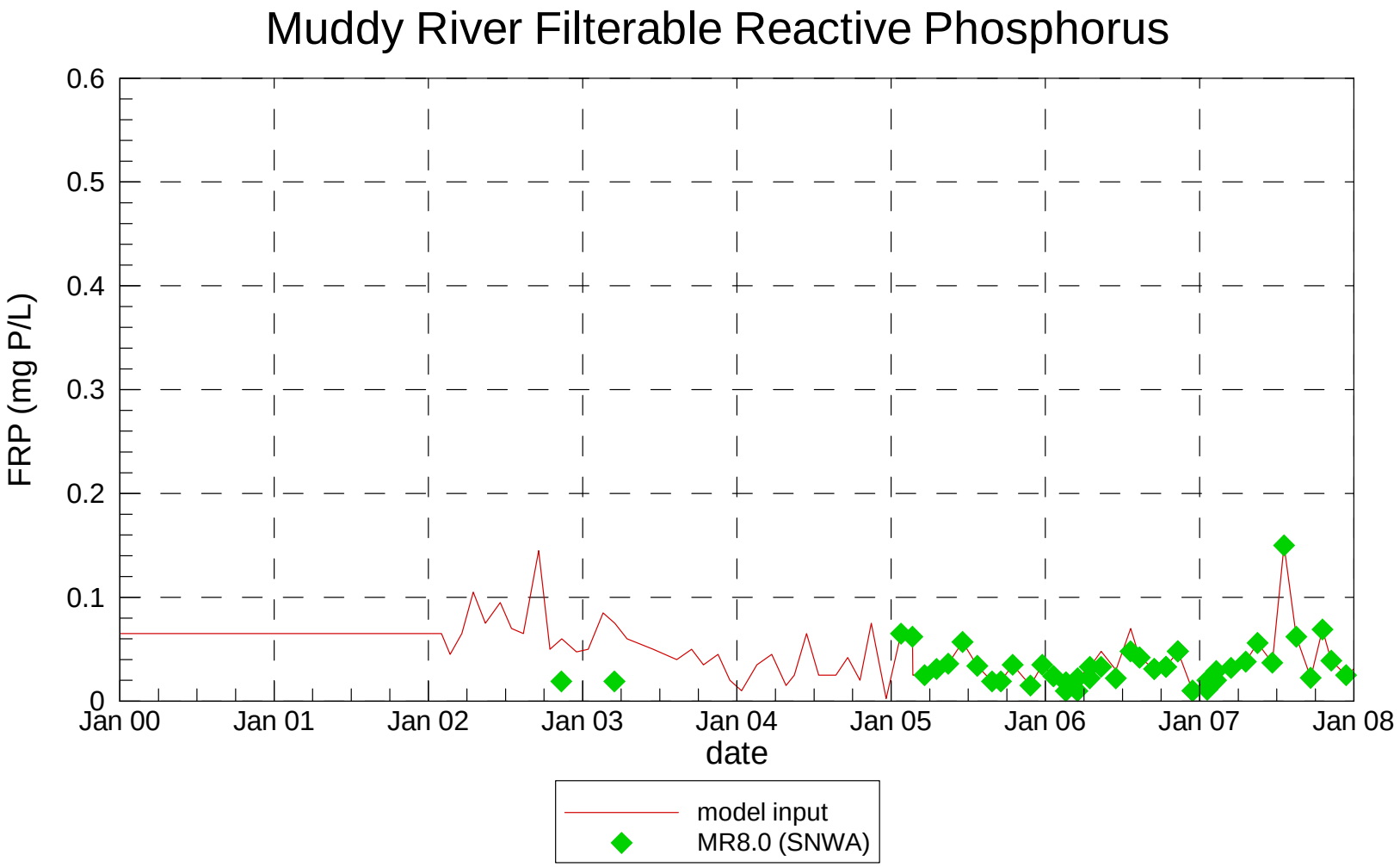

* Prior to 2005, FRP for model input was set equal to half of TP.

Figure A.19

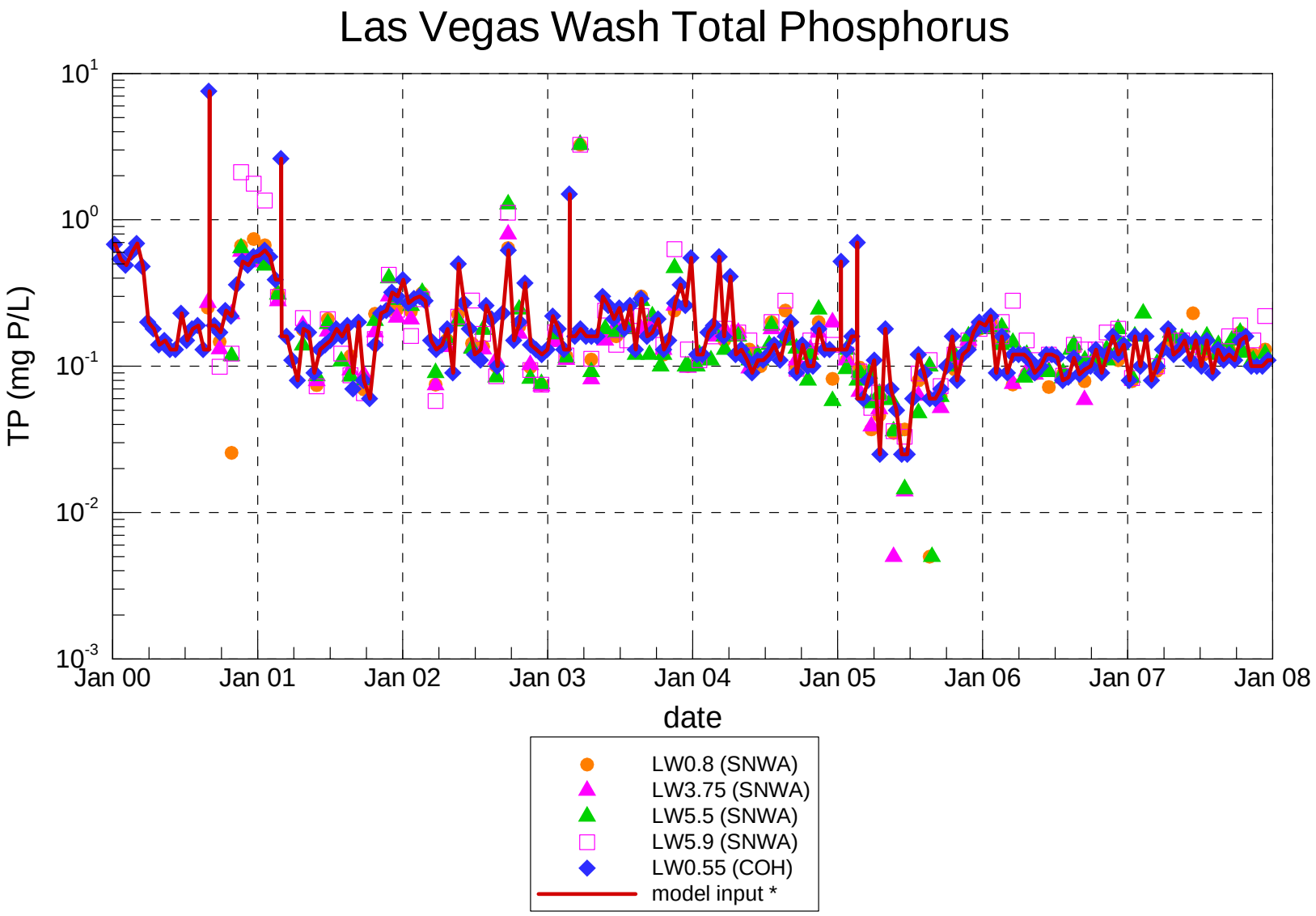

* TP entered the model as the sum of FRP, DOP, POP and IP_CHL.

Figure A.20

Colorado River Total Phosphorus

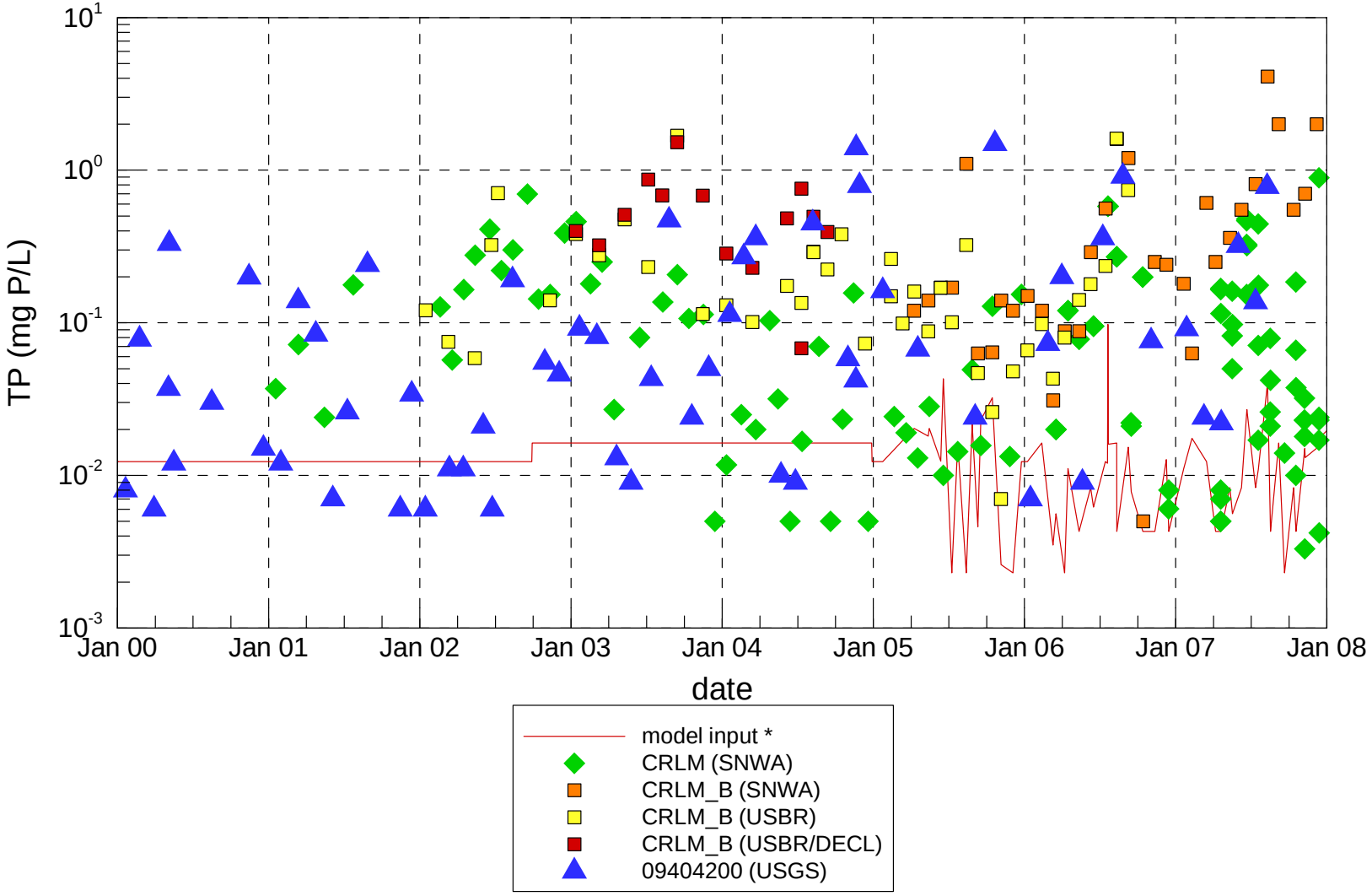

* TP entered the model as the sum of FRP, DOP, POP and IP_CHL.

Figure A.21

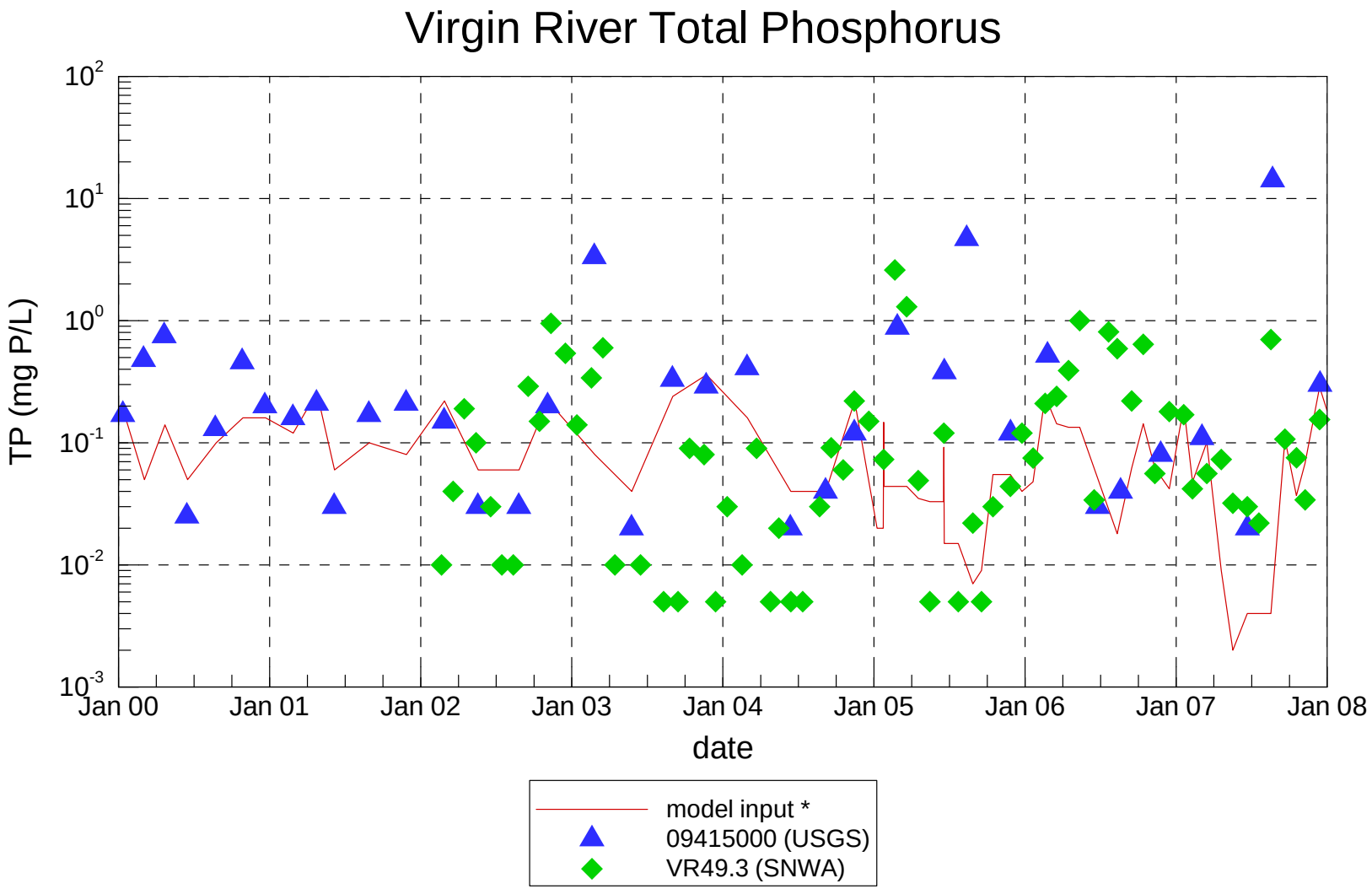

* TP entered the model as the sum of FRP, DOP, POP and IP_CHL.

Figure A.22

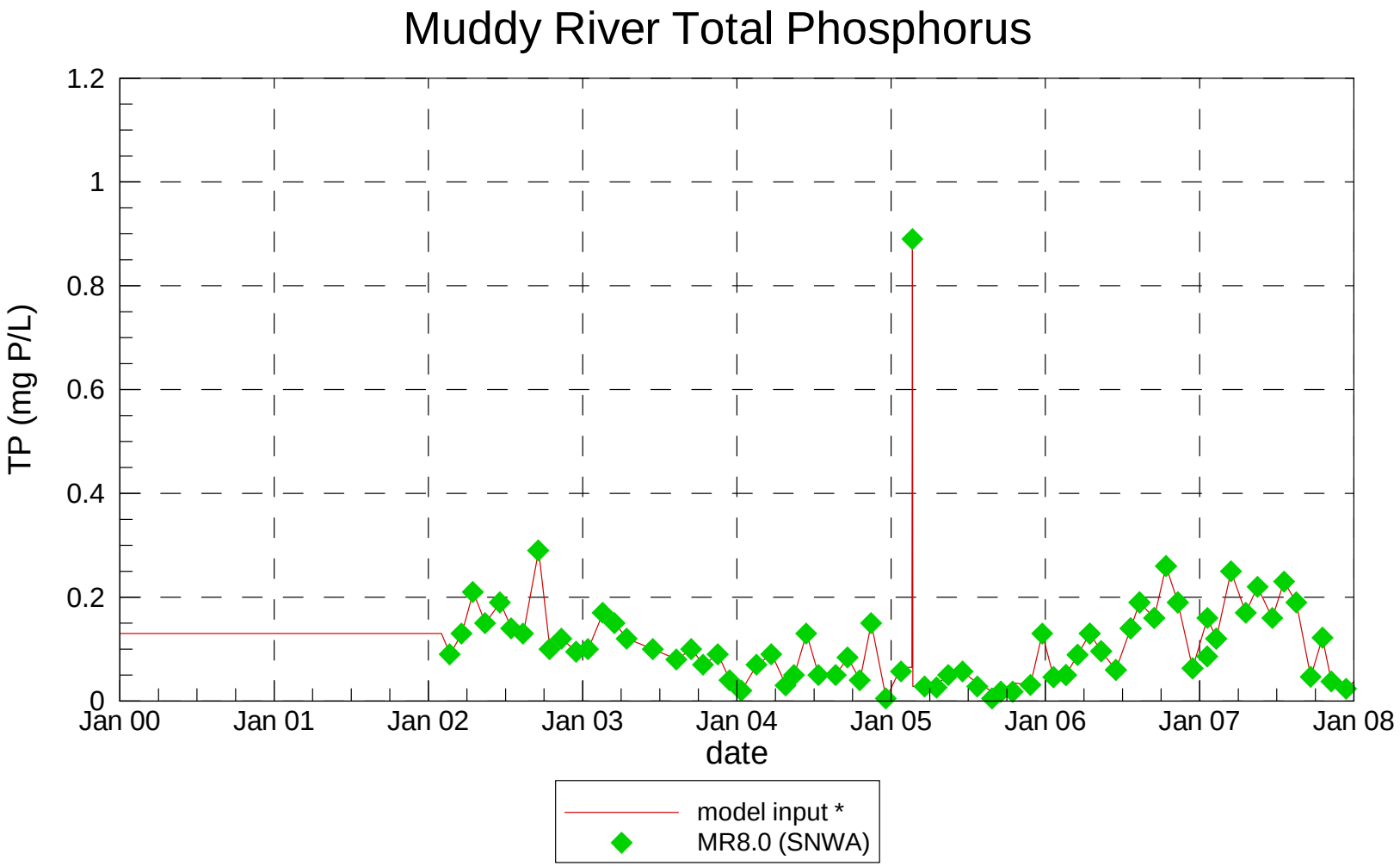

* TP entered the model as the sum of FRP, DOP, POP and IP_CHL.

Figure A.23

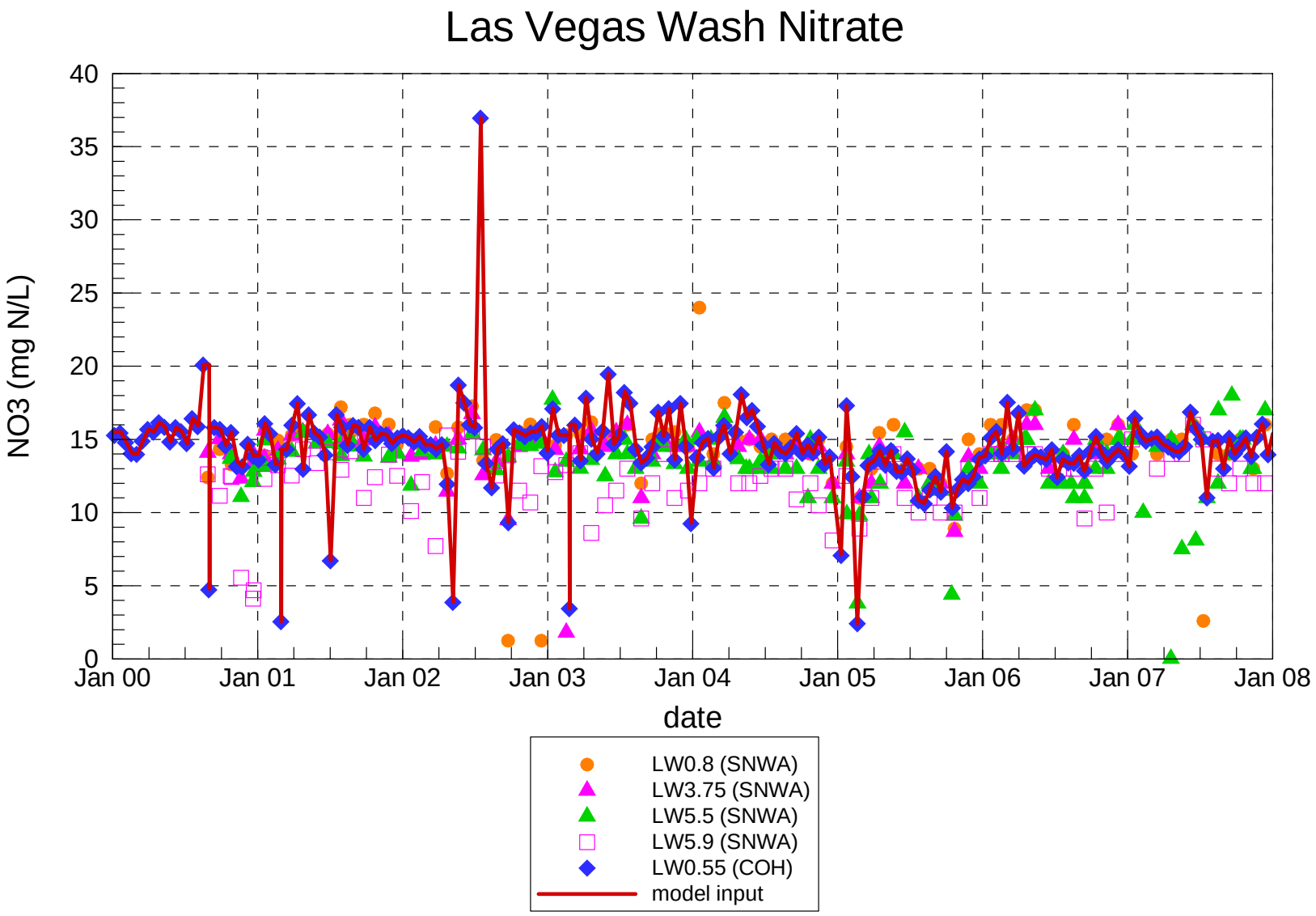
Las Vegas Wash Nitrate
NO3 (mg N/L)
0
5
10
15
20
25
30
35
40
Jan 00
Jan 01
Jan 02
Jan 03
Jan 04
Jan 05
Jan 06
Jan 07
Jan 08
date
LW0.8 (SNWA)
LW3.75 (SNWA)
LW5.5 (SNWA)
LW5.9 (SNWA)
LW0.55 (COH)
model input

Figure A.24

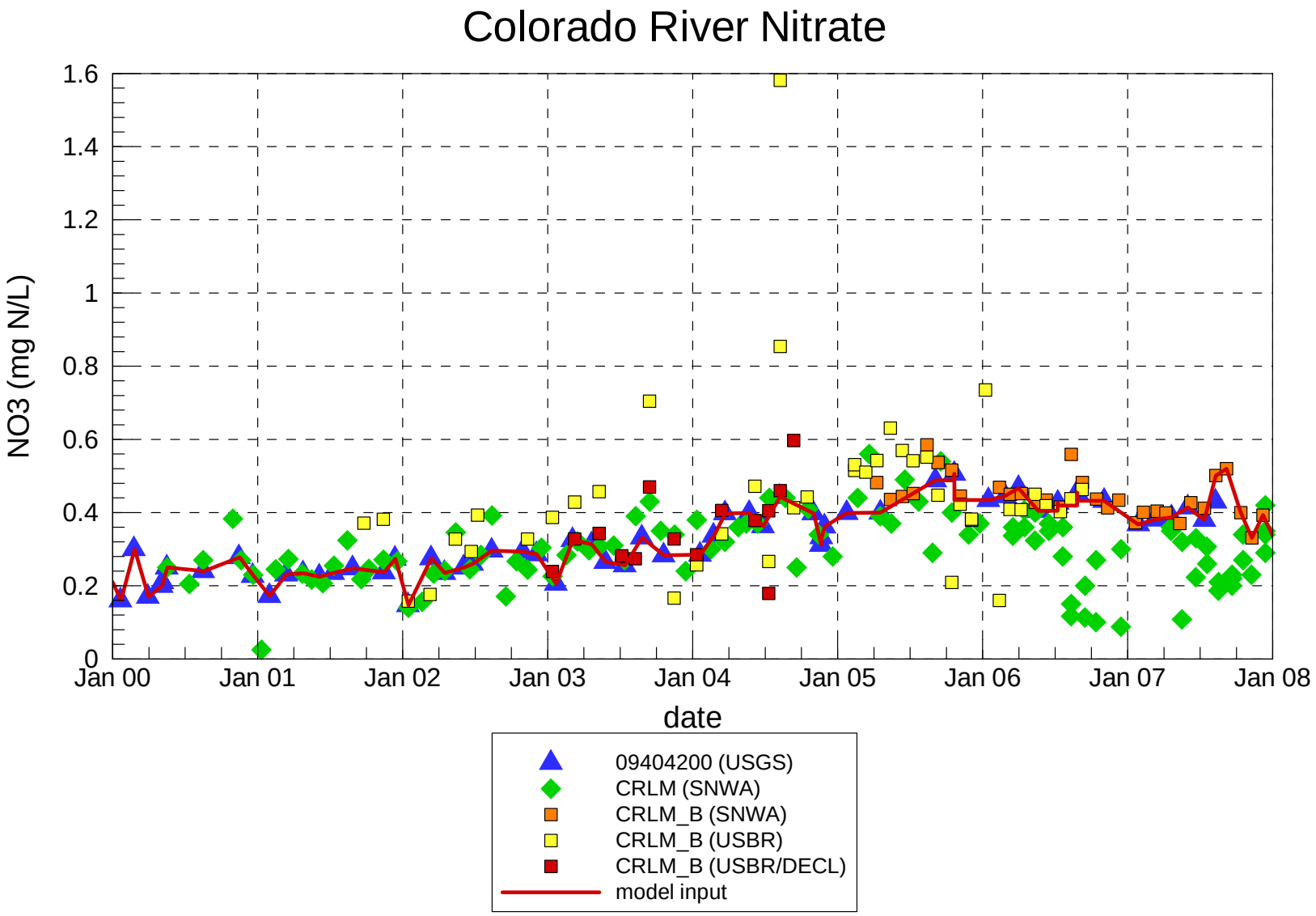
Colorado River Nitrate
NO3 (mg N/L)
1.6
1.4
1.2
1
0.8
0.6
0.4
0.2
0
Jan 00
Jan 01
Jan 02
Jan 03
Jan 04
Jan 05
Jan 06
Jan 07
Jan 08
date
09404200 (USGS)
CRLM (SNWA)
CRLM_B (SNWA)
CRLM_B (USBR)
CRLM_B (USBR/DECL)
model input

Figure A.25

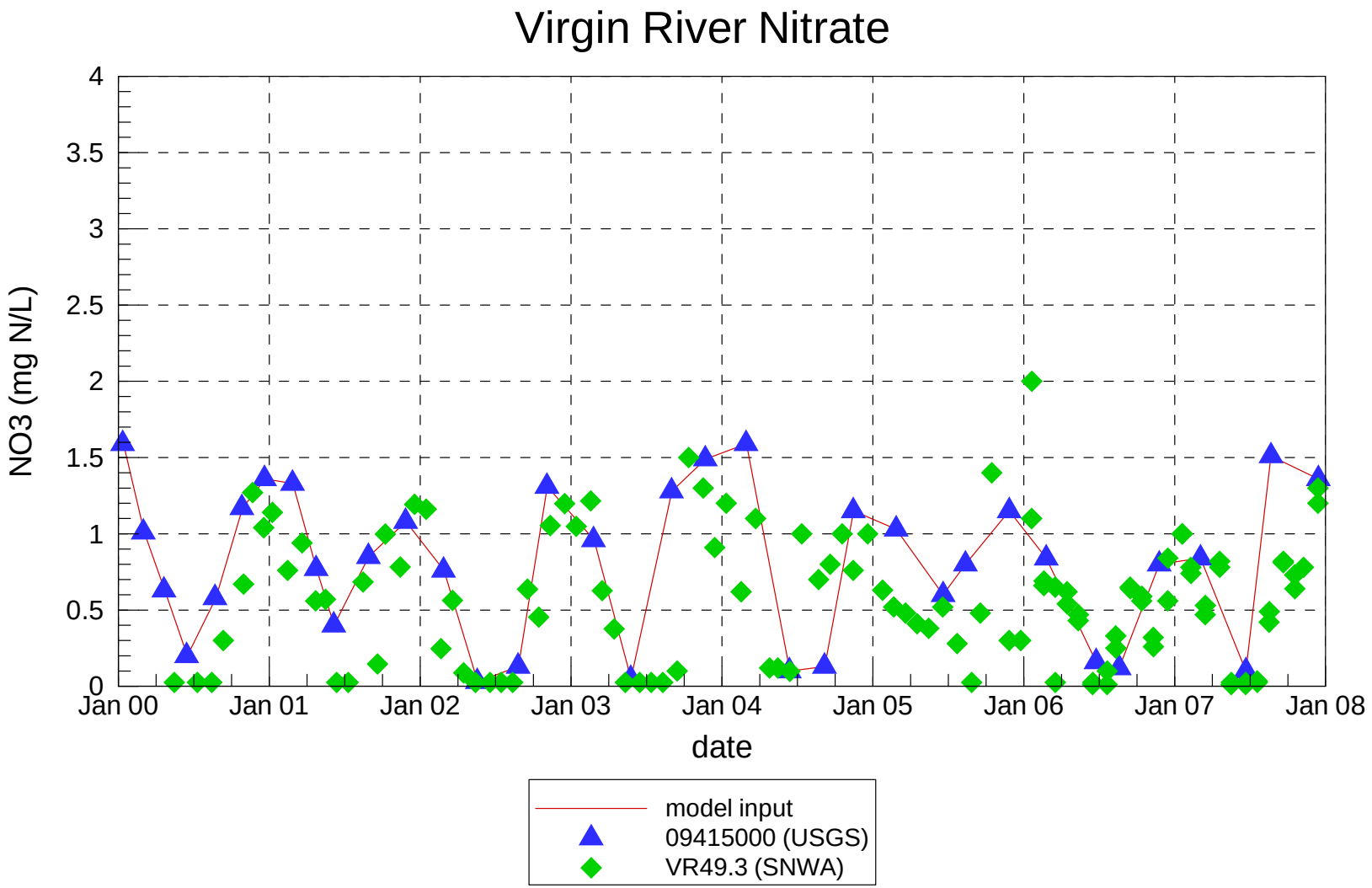
Virgin River Nitrate
NO3 (mg N/L)
4
3.5
3
2.5
2
1.5
1
0.5
0
Jan 00
Jan 01
Jan 02
Jan 03
Jan 04
Jan 05
Jan 06
Jan 07
Jan 08
date
model input
09415000 (USGS)
VR49.3 (SNWA)

Figure A.26

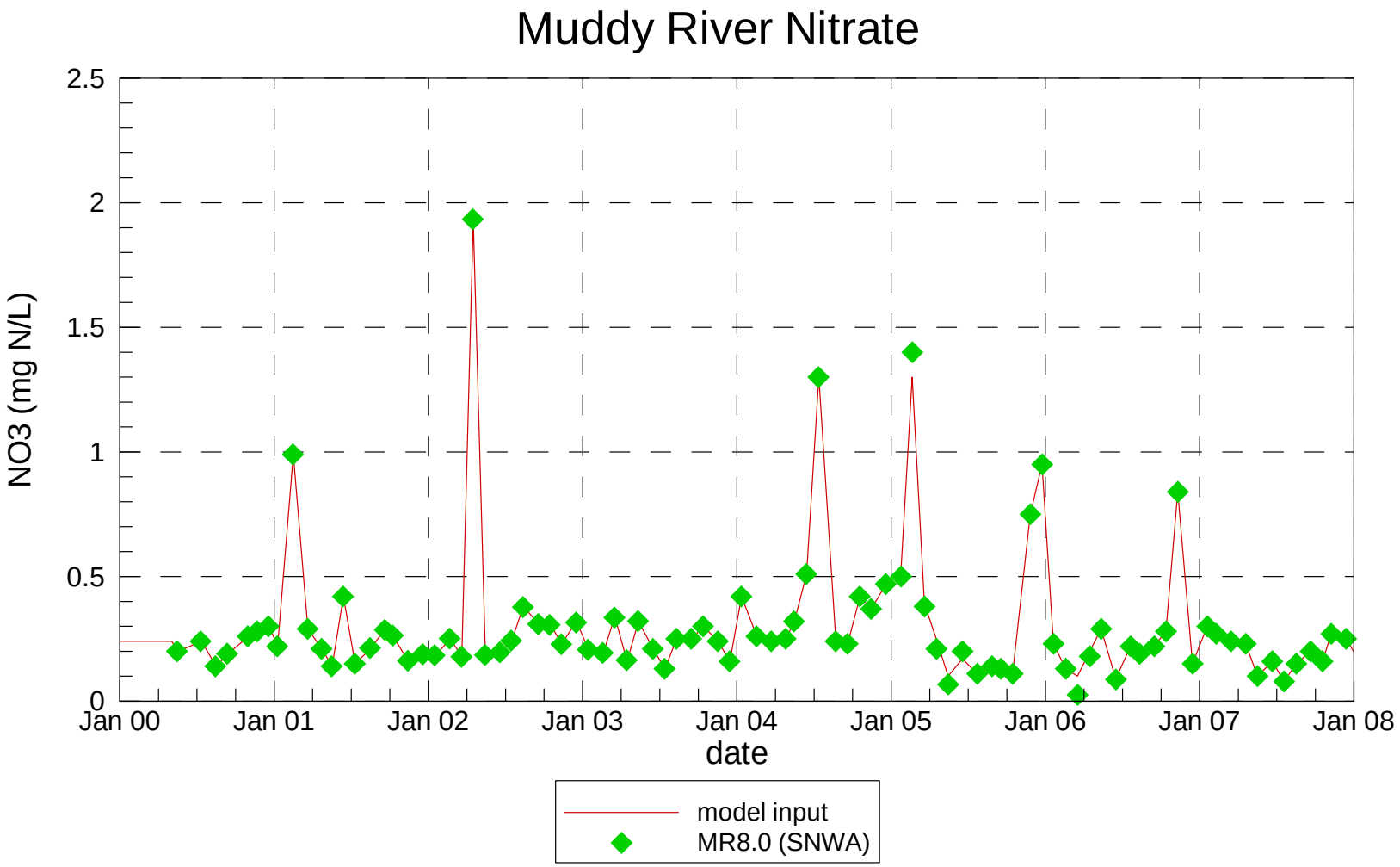
Muddy River Nitrate
NO3 (mg N/L)
2.5
2
1.5
1
0.5
0
Jan 00
Jan 01
Jan 02
Jan 03
Jan 04
Jan 05
Jan 06
Jan 07
Jan 08
date
model input
MR8.0 (SNWA)

Figure A.27

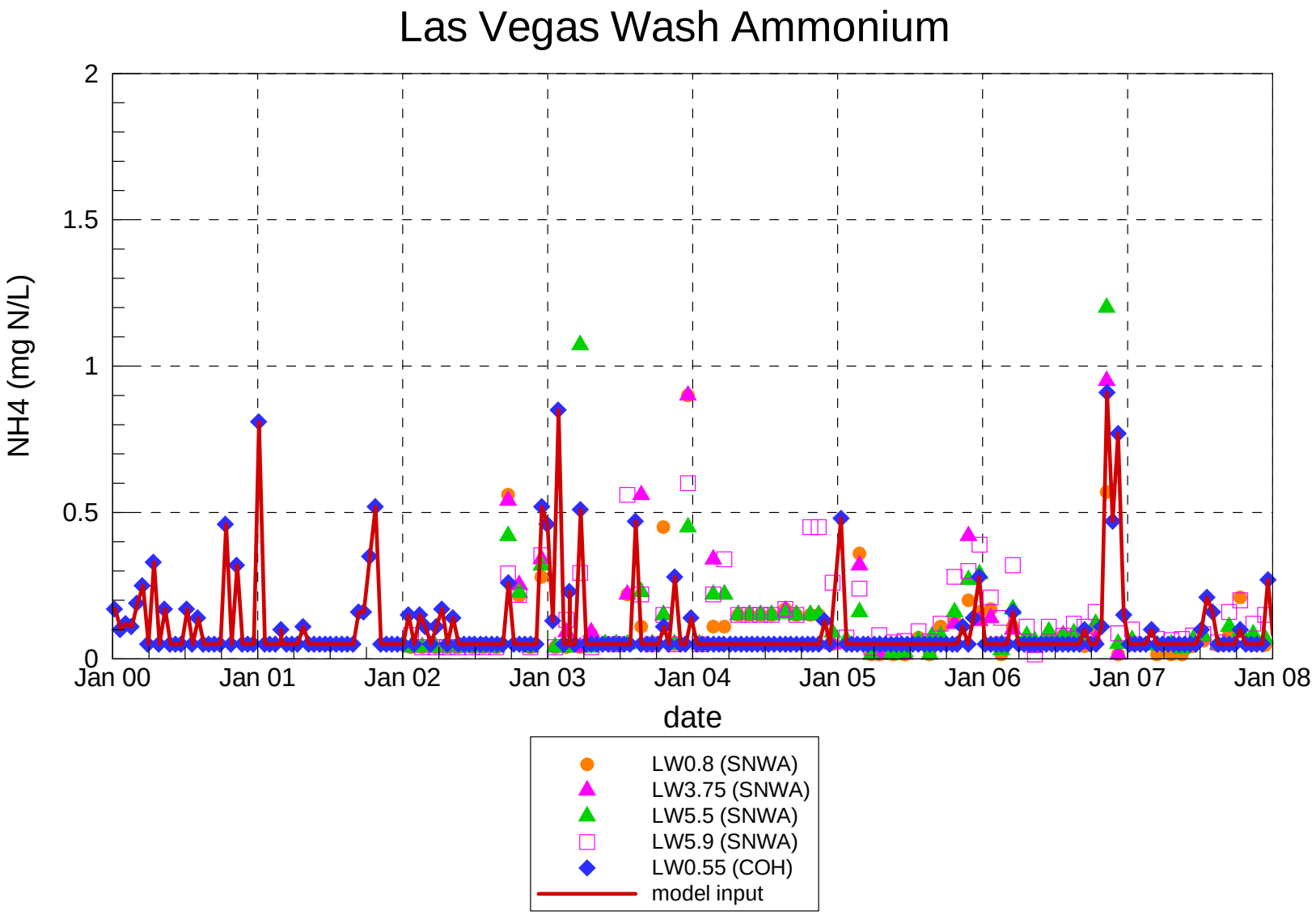
Las Vegas Wash Ammonium
NH4 (mg N/L)
2
1.5
1
0.5
0
Jan 00
Jan 01
Jan 02
Jan 03
Jan 04
Jan 05
Jan 06
Jan 07
Jan 08
date
LW0.8 (SNWA)
LW3.75 (SNWA)
LW5.5 (SNWA)
LW5.9 (SNWA)
LW0.55 (COH)
model input

Figure A.28

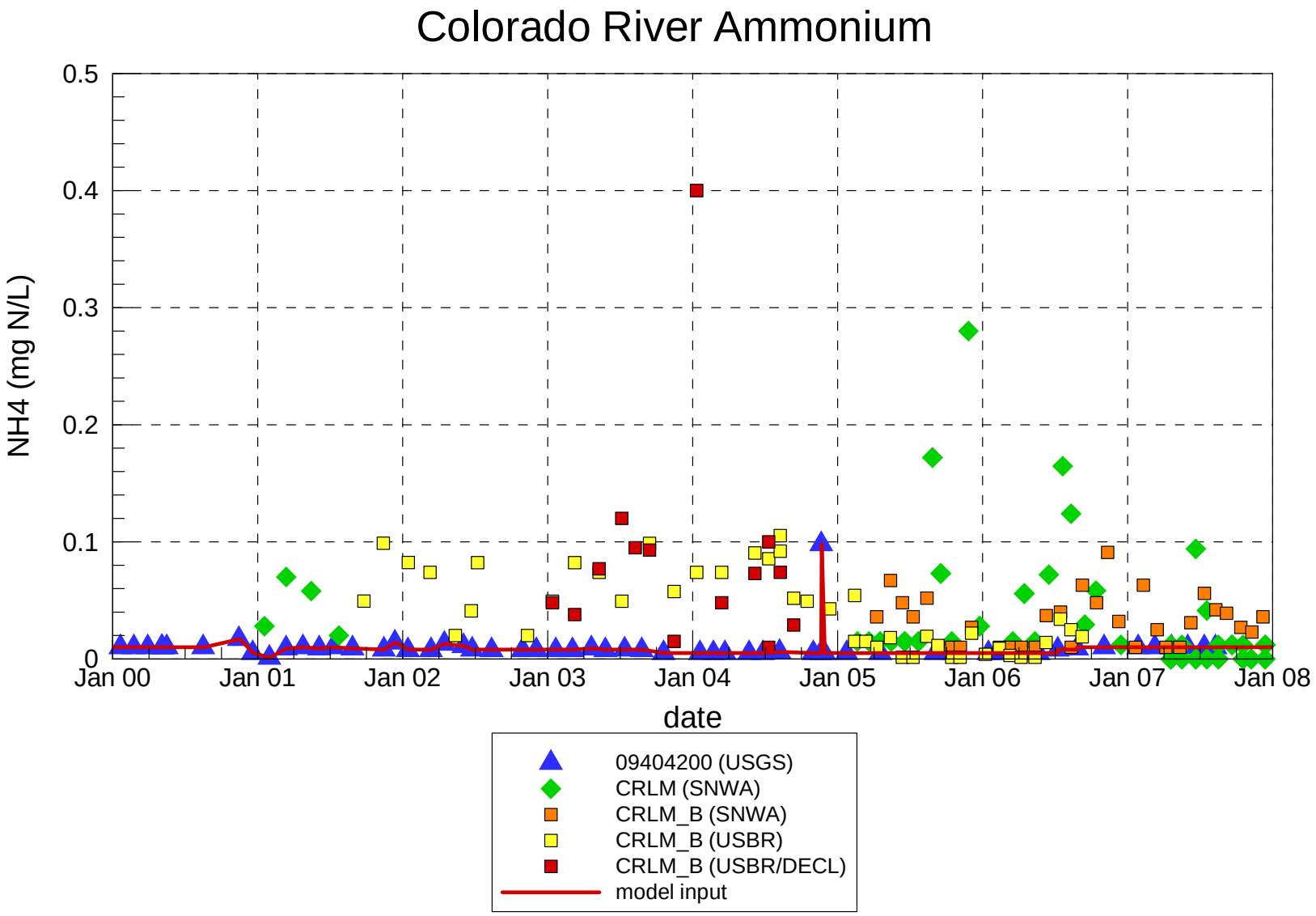
Colorado River Ammonium
NH4 (mg N/L)
0.5
0.4
0.3
0.2
0.1
0
Jan 00
Jan 01
Jan 02
Jan 03
Jan 04
Jan 05
Jan 06
Jan 07
Jan 08
date
09404200 (USGS)
CRLM (SNWA)
CRLM_B (SNWA)
CRLM_B (USBR)
CRLM_B (USBR/DECL)
model input

Figure A.29

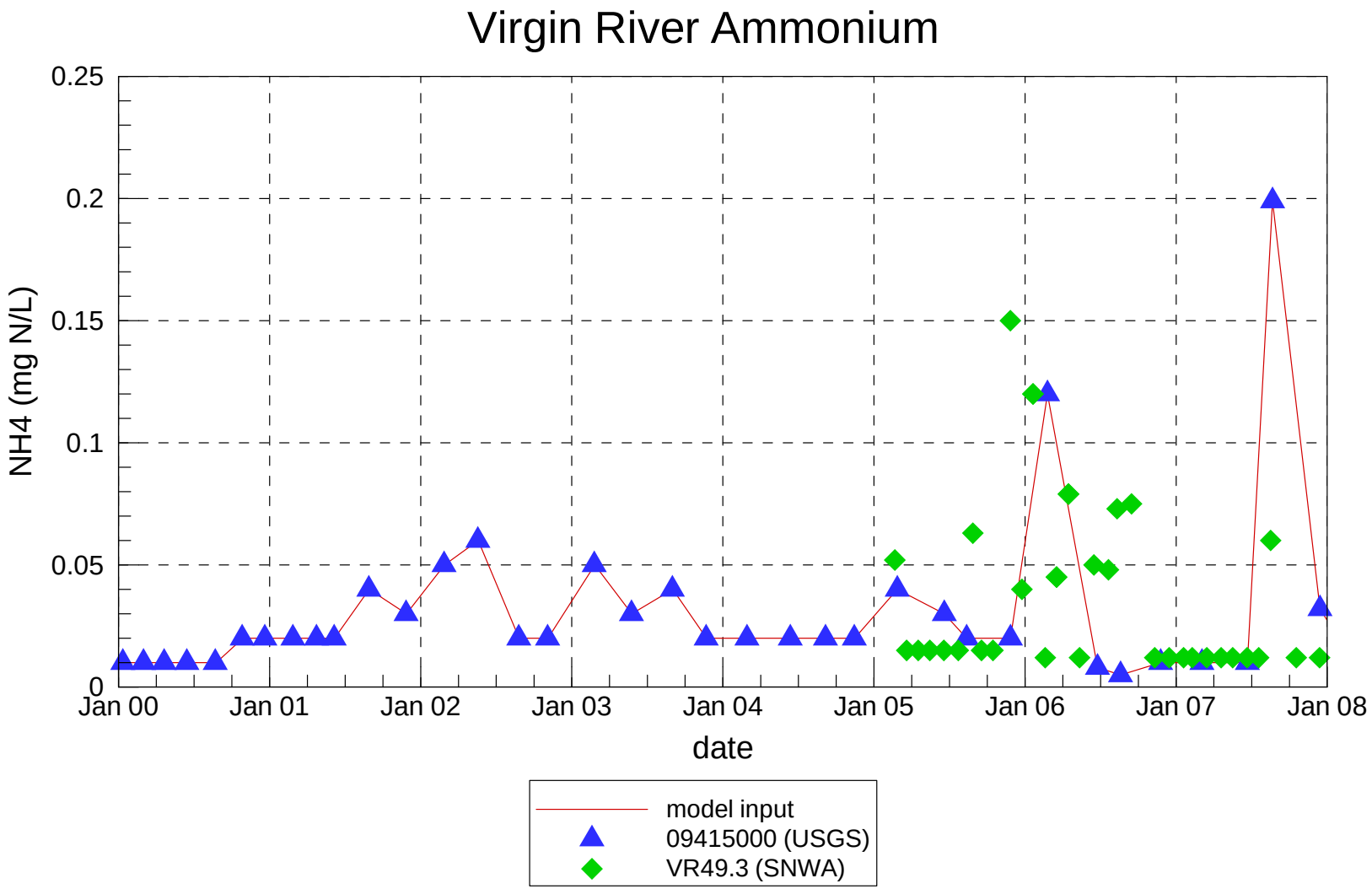
Virgin River Ammonium
NH4 (mg N/L)
0.25
0.2
0.15
0.1
0.05
0
Jan 00
Jan 01
Jan 02
Jan 03
Jan 04
Jan 05
Jan 06
Jan 07
Jan 08
date
model input
09415000 (USGS)
VR49.3 (SNWA)

Figure A.30

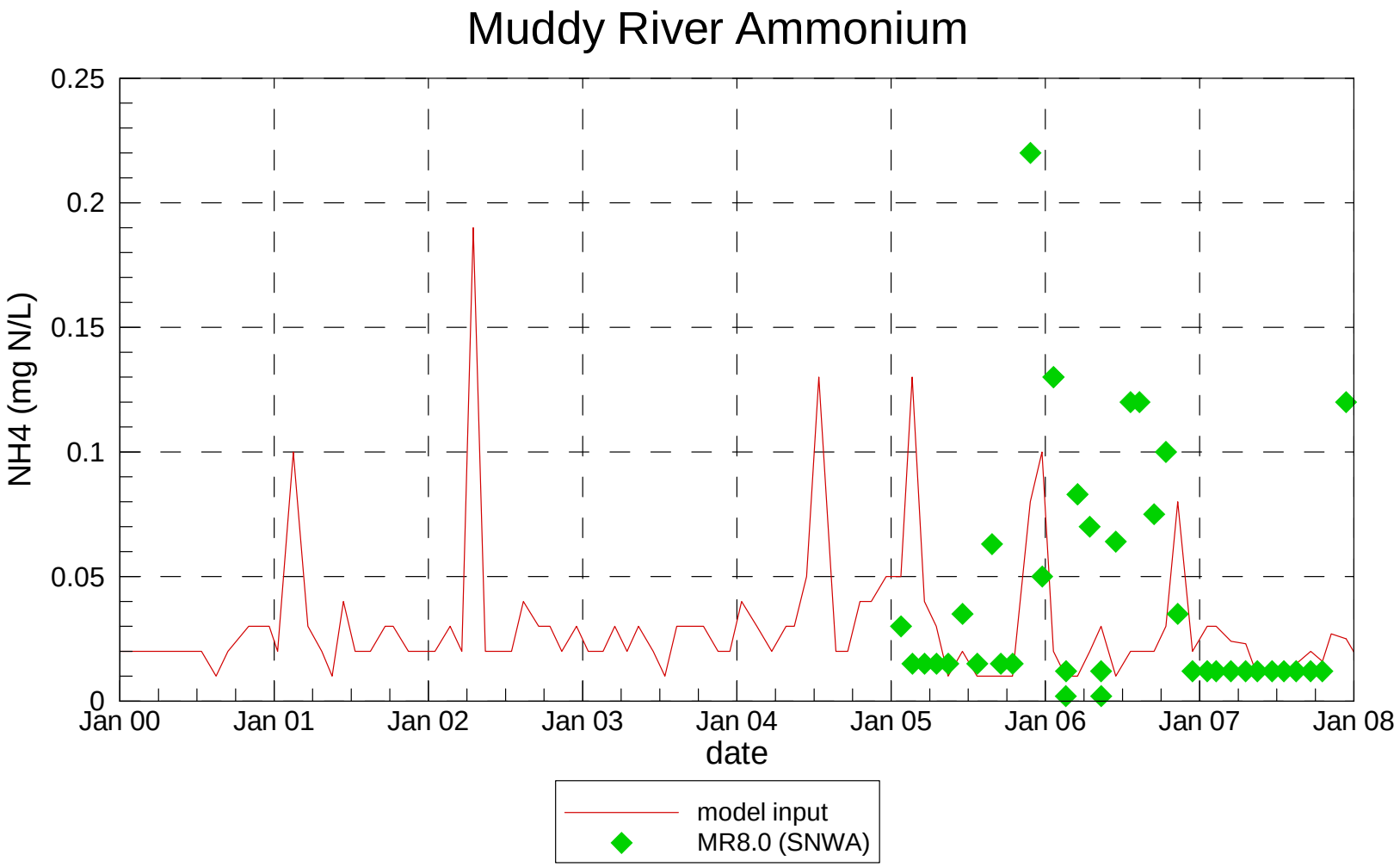

* NH4 for model input was set equal to one-tenth of NO3.

Figure A.31

Las Vegas Wash Total Organic Carbon

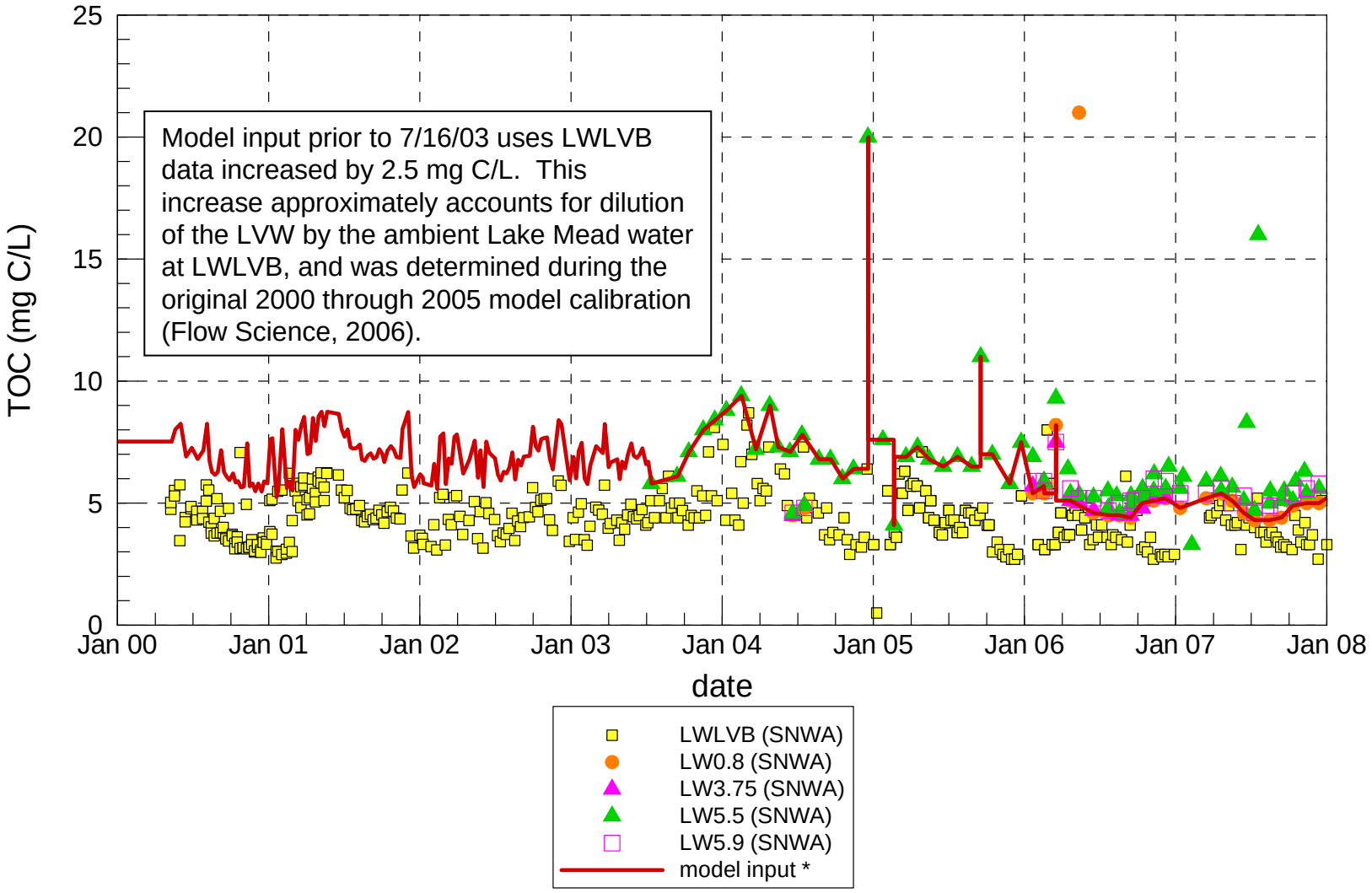

* TOC entered the model as the sum of DOC, POC and IC_CHL.

Figure A.32

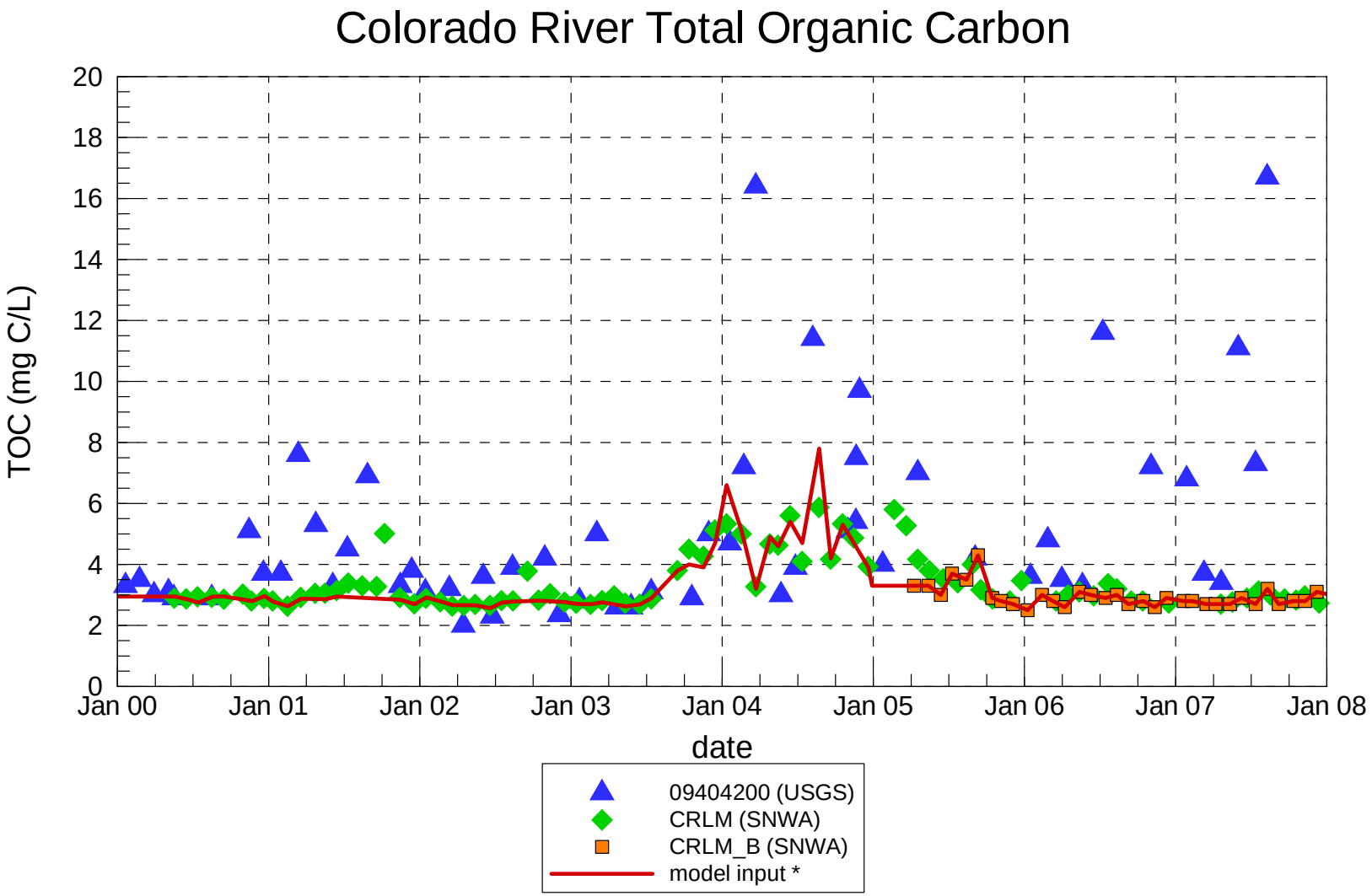

* TOC entered the model as the sum of DOC, POC and IC_CHL.

Figure A.33

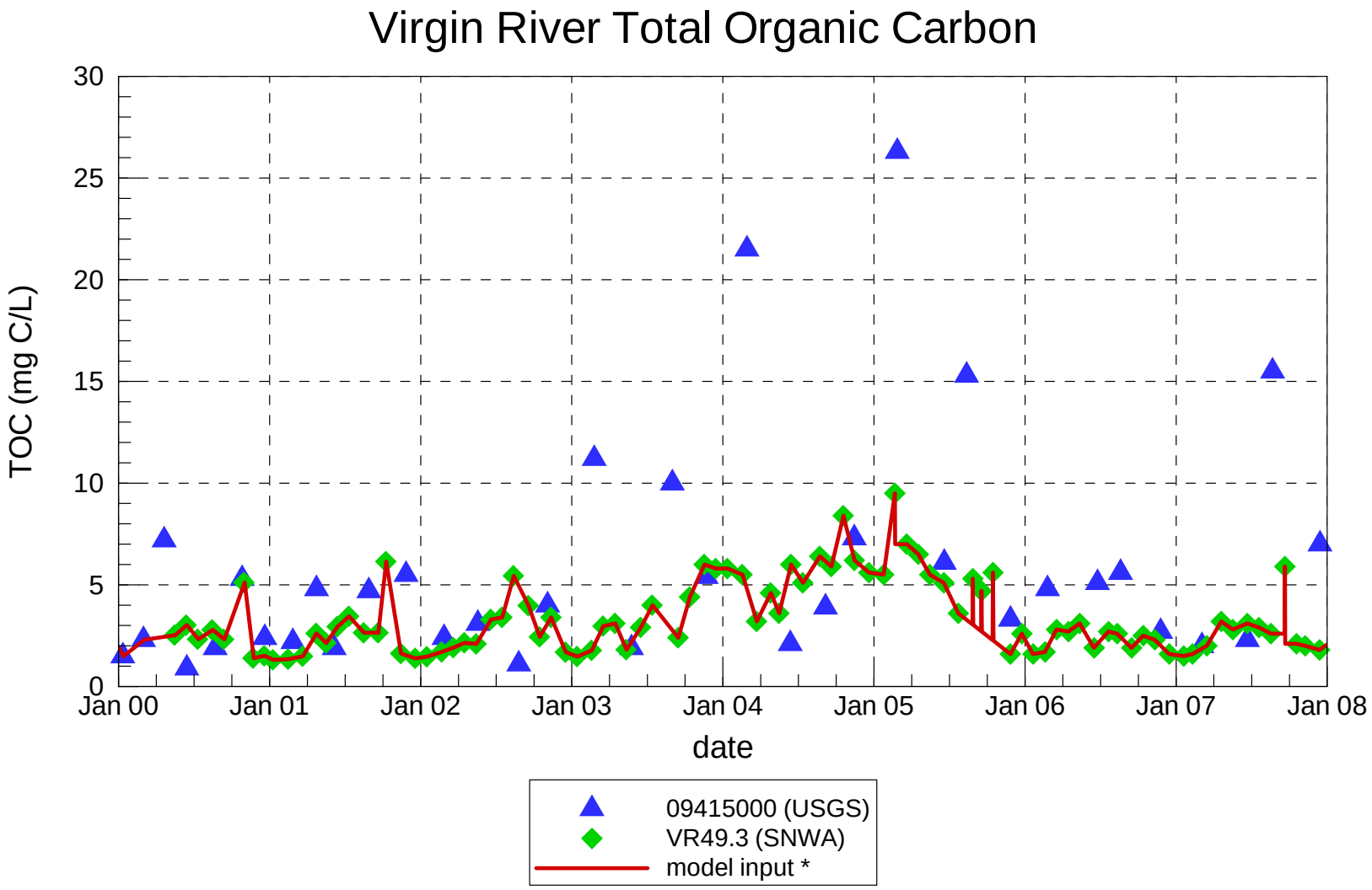

* TOC entered the model as the sum of DOC, POC and IC_CHL.

Figure A.34

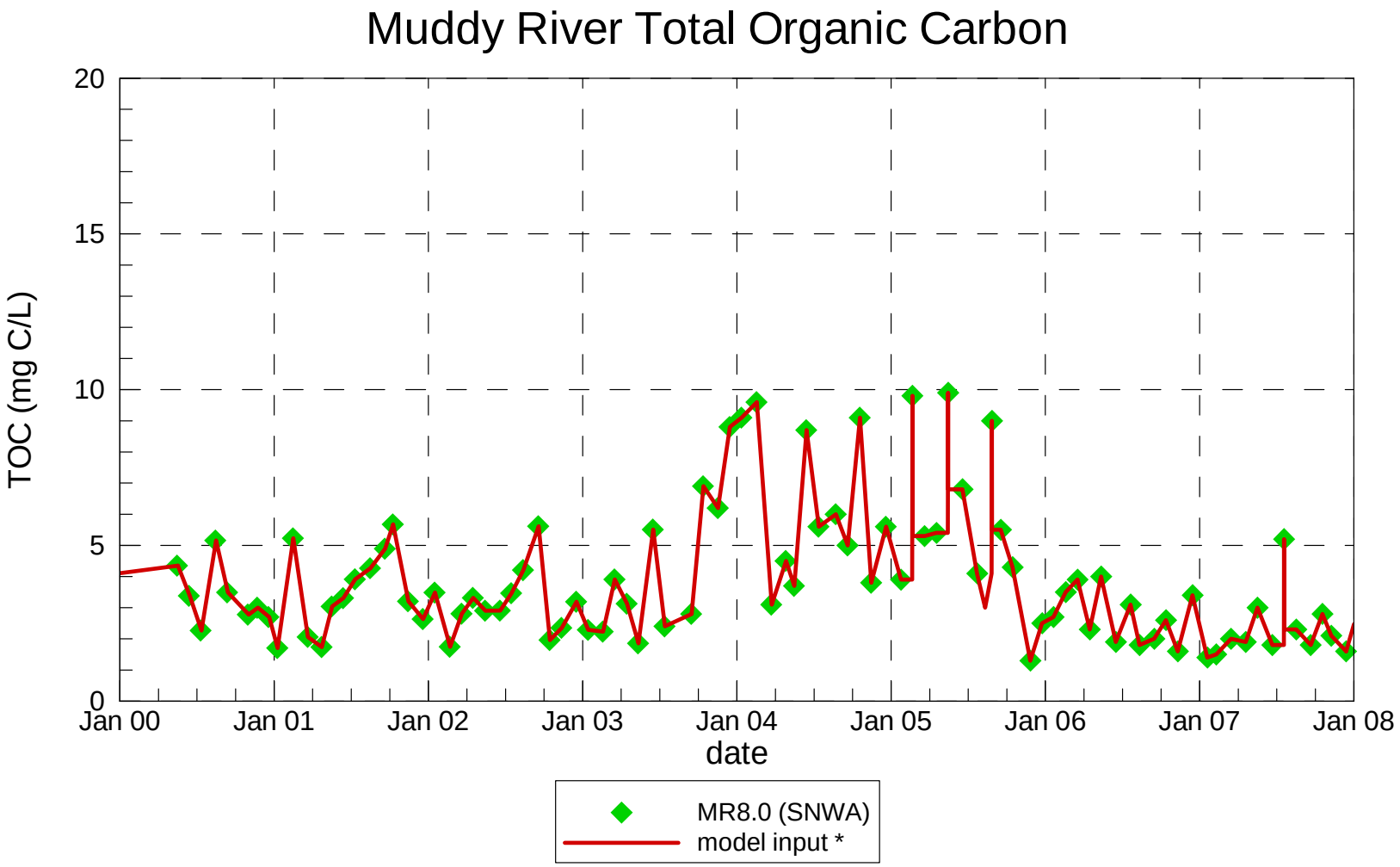

* TOC entered the model as the sum of DOC, POC and IC_CHL.

Figure A.35

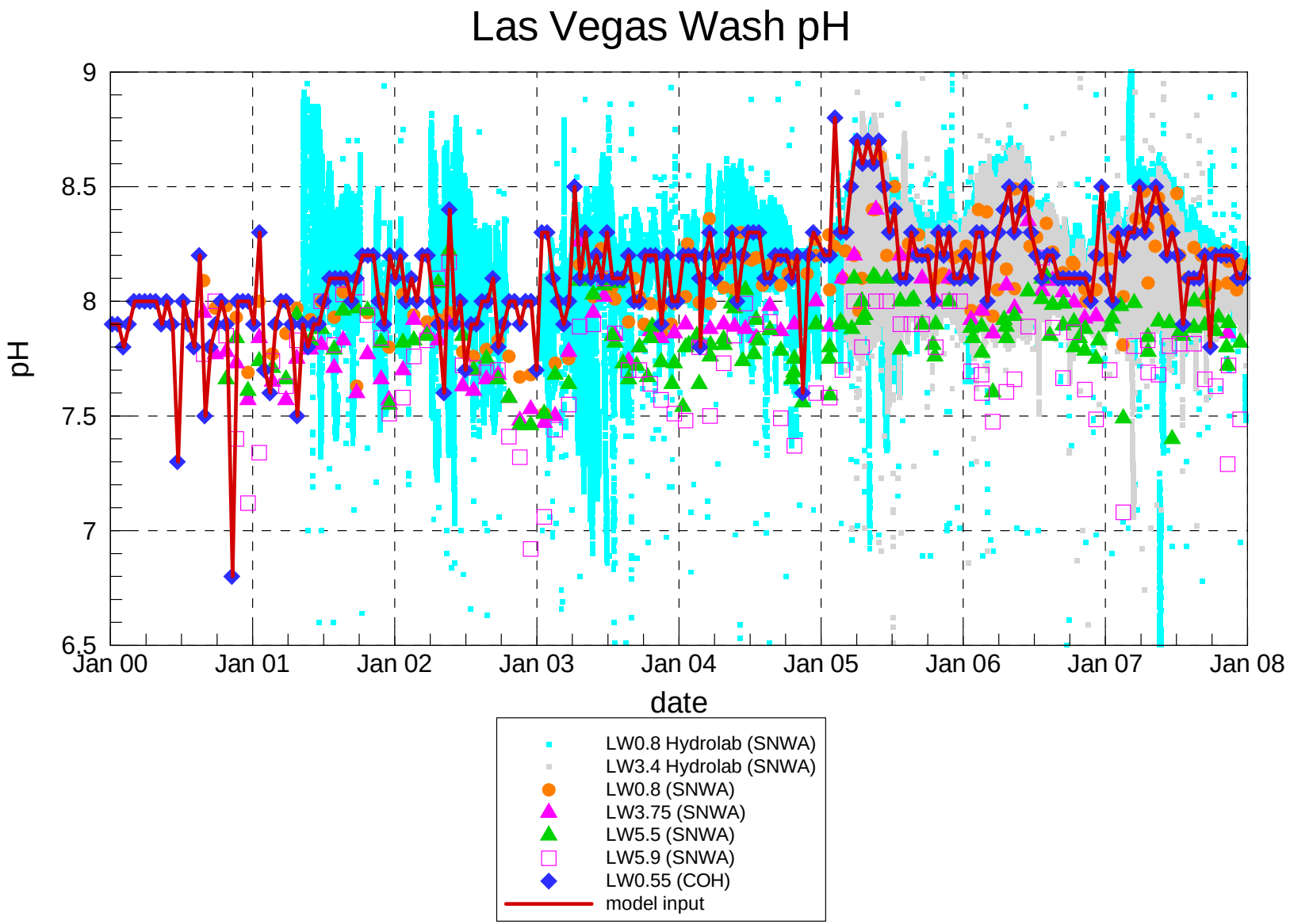
Las Vegas Wash pH
9
8.5
8
7.5
7
6.5
pH
Jan 00
Jan 01
Jan 02
Jan 03
Jan 04
Jan 05
Jan 06
Jan 07
Jan 08
date
LW0.8 Hydrolab (SNWA)
LW3.4 Hydrolab (SNWA)
LW0.8 (SNWA)
LW3.75 (SNWA)
LW5.5 (SNWA)
LW5.9 (SNWA)
LW0.55 (COH)
model input

Figure A.36

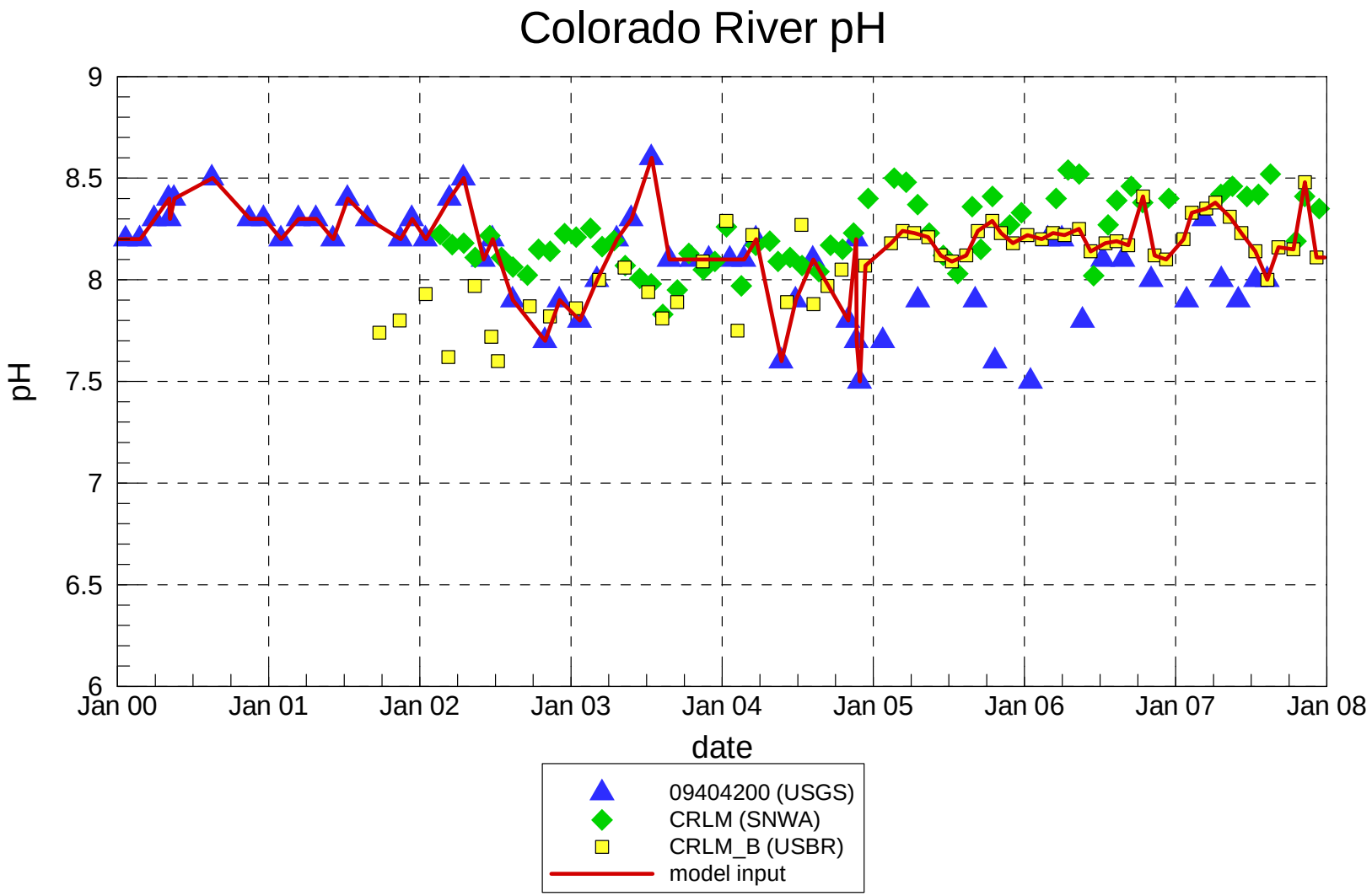
Colorado River pH
9
8.5
8
7.5
7
6.5
6
pH
Jan 00
Jan 01
Jan 02
Jan 03
Jan 04
Jan 05
Jan 06
Jan 07
Jan 08
date
09404200 (USGS)
CRLM (SNWA)
CRLM_B (USBR)
model input

Figure A.37

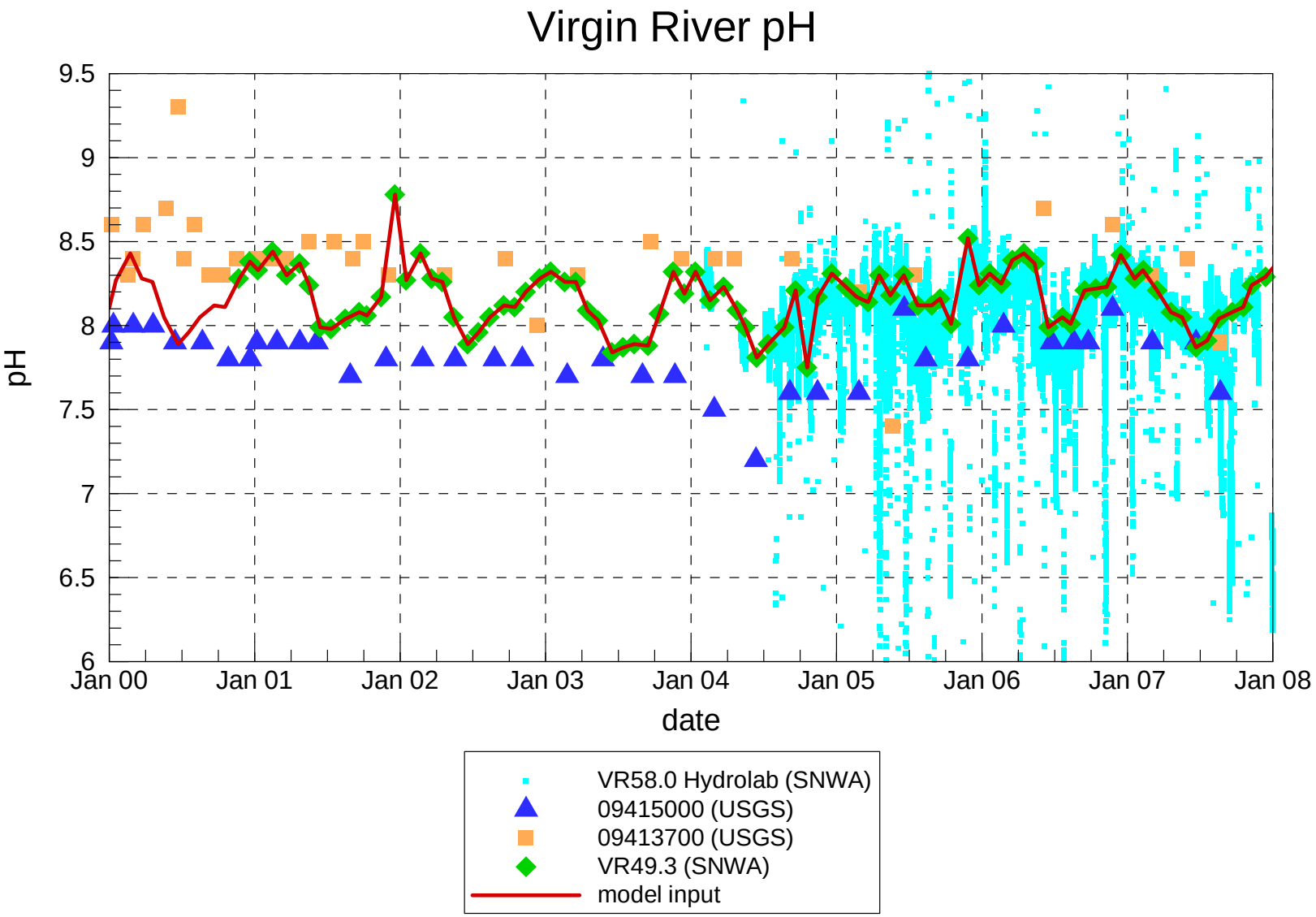
Virgin River pH
9.5
9
8.5
8
7.5
7
6.5
6
pH
Jan 00
Jan 01
Jan 02
Jan 03
Jan 04
Jan 05
Jan 06
Jan 07
Jan 08
date
VR58.0 Hydrolab (SNWA)
09415000 (USGS)
09413700 (USGS)
VR49.3 (SNWA)
model input

Figure A.38

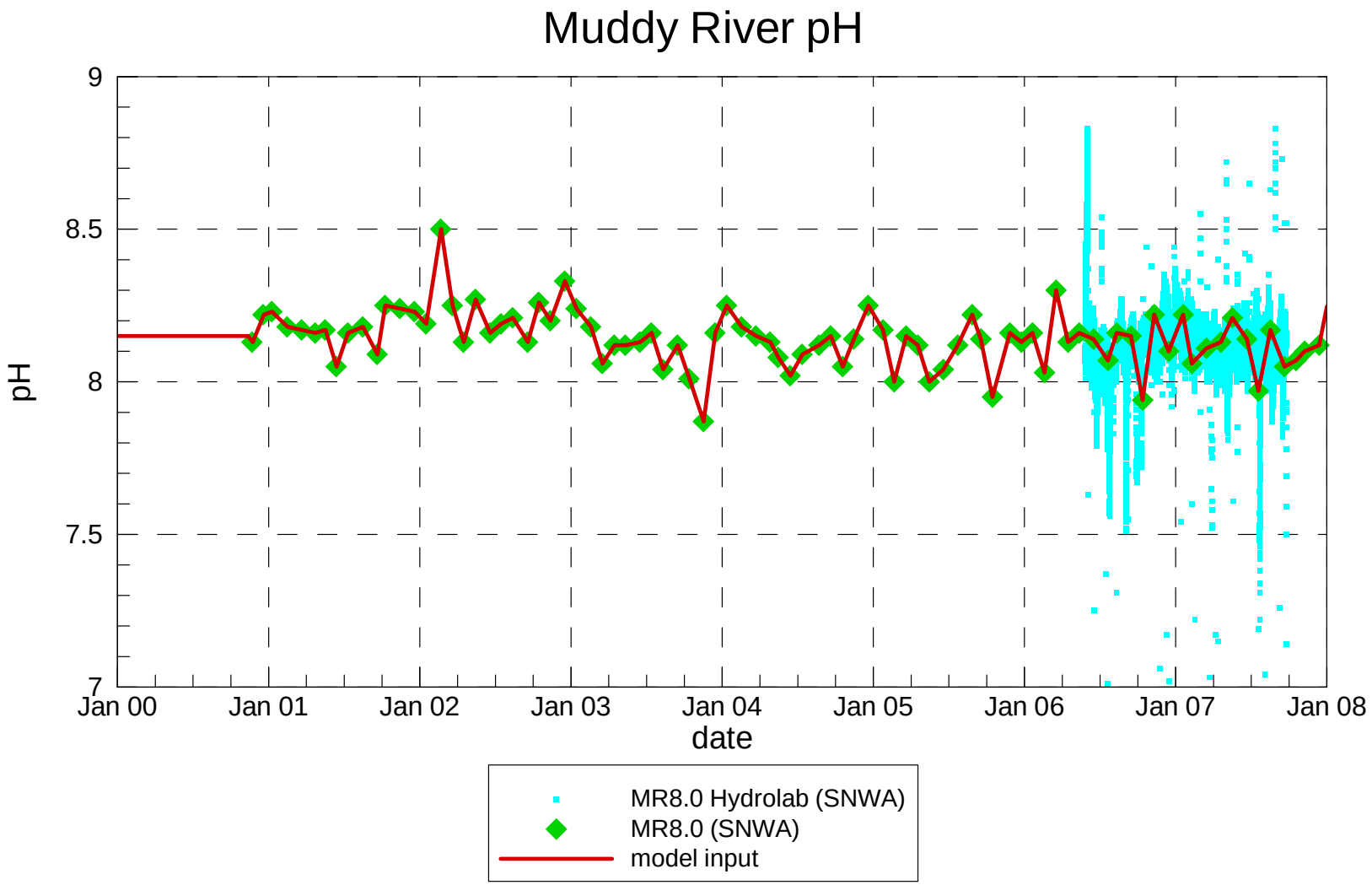
Muddy River pH
9
8.5
8
7.5
7
pH
Jan 00
Jan 01
Jan 02
Jan 03
Jan 04
Jan 05
Jan 06
Jan 07
Jan 08
date
MR8.0 Hydrolab (SNWA)
MR8.0 (SNWA)
model input

Figure A.39

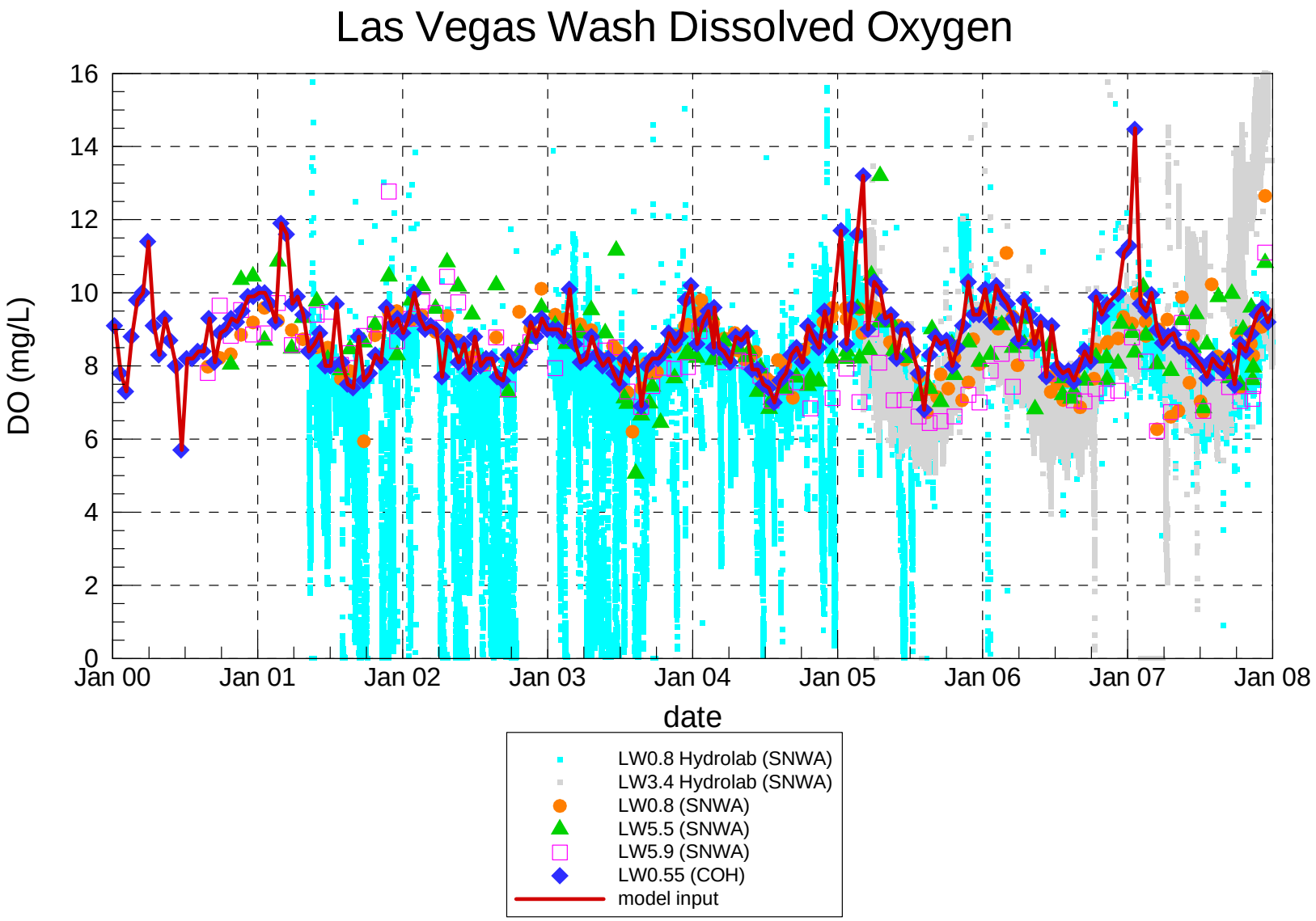
Las Vegas Wash Dissolved Oxygen
DO (mg/L)
0
2
4
6
8
10
12
14
16
Jan 00
Jan 01
Jan 02
Jan 03
Jan 04
Jan 05
Jan 06
Jan 07
Jan 08
date
LW0.8 Hydrolab (SNWA)
LW3.4 Hydrolab (SNWA)
LW0.8 (SNWA)
LW5.5 (SNWA)
LW5.9 (SNWA)
LW0.55 (COH)
model input

Figure A.40

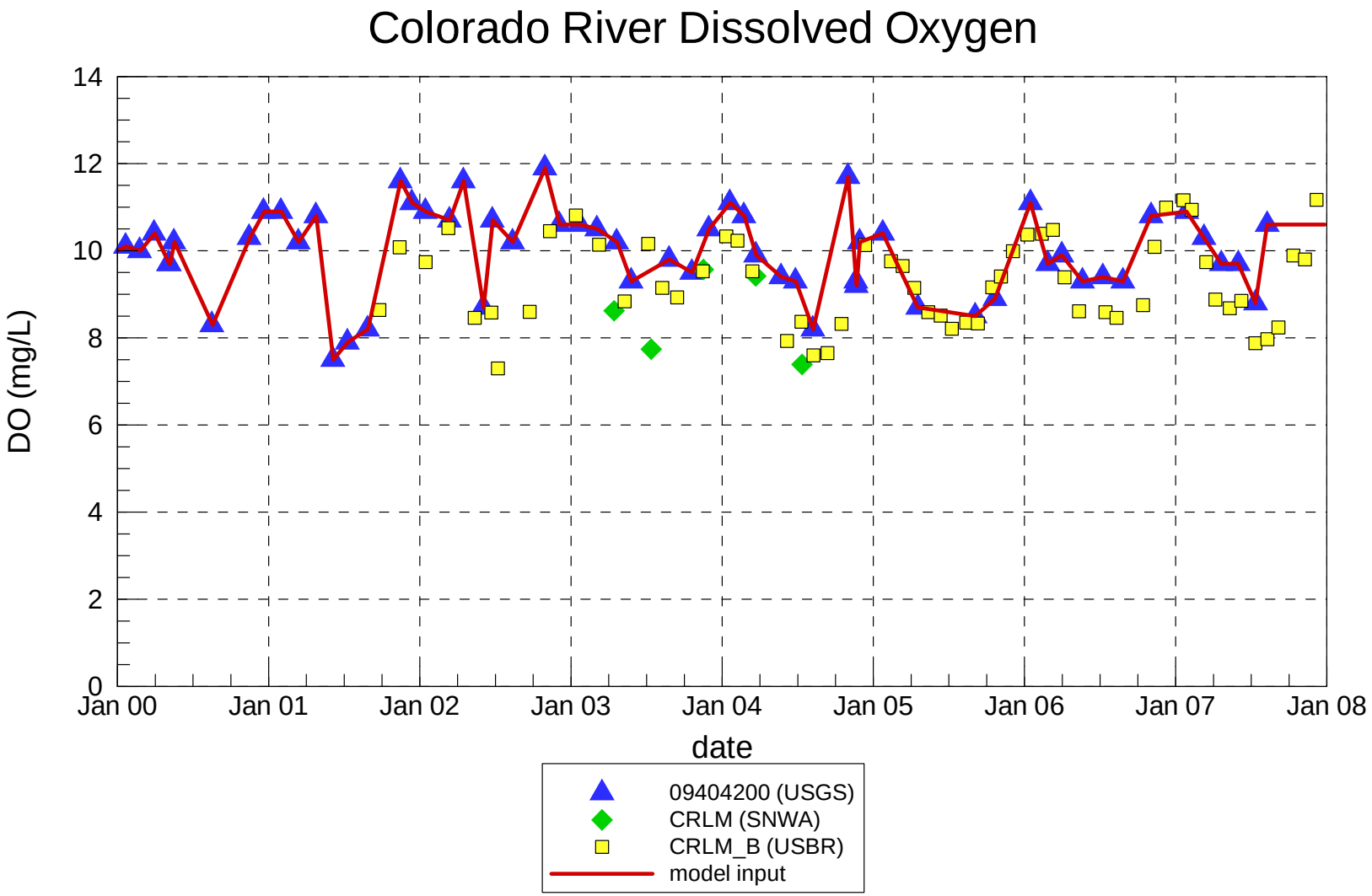
Colorado River Dissolved Oxygen
DO (mg/L)
14
12
10
8
6
4
2
0
Jan 00
Jan 01
Jan 02
Jan 03
Jan 04
Jan 05
Jan 06
Jan 07
Jan 08
date
09404200 (USGS)
CRLM (SNWA)
CRLM_B (USBR)
model input

Figure A.41

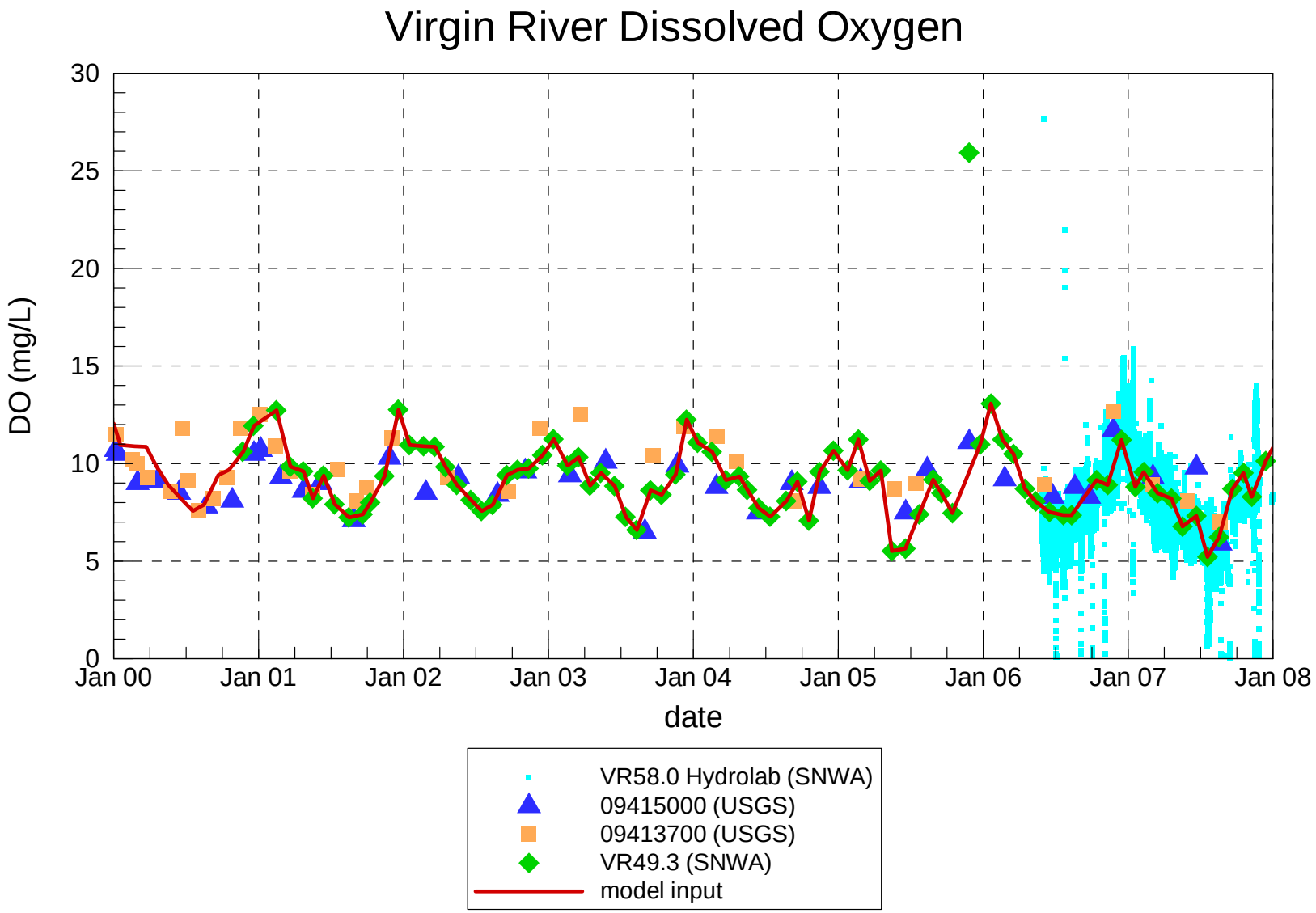
Virgin River Dissolved Oxygen
DO (mg/L)
30
25
20
15
10
5
0
Jan 00
Jan 01
Jan 02
Jan 03
Jan 04
Jan 05
Jan 06
Jan 07
Jan 08
date
VR58.0 Hydrolab (SNWA)
09415000 (USGS)
09413700 (USGS)
VR49.3 (SNWA)
model input

Figure A.42

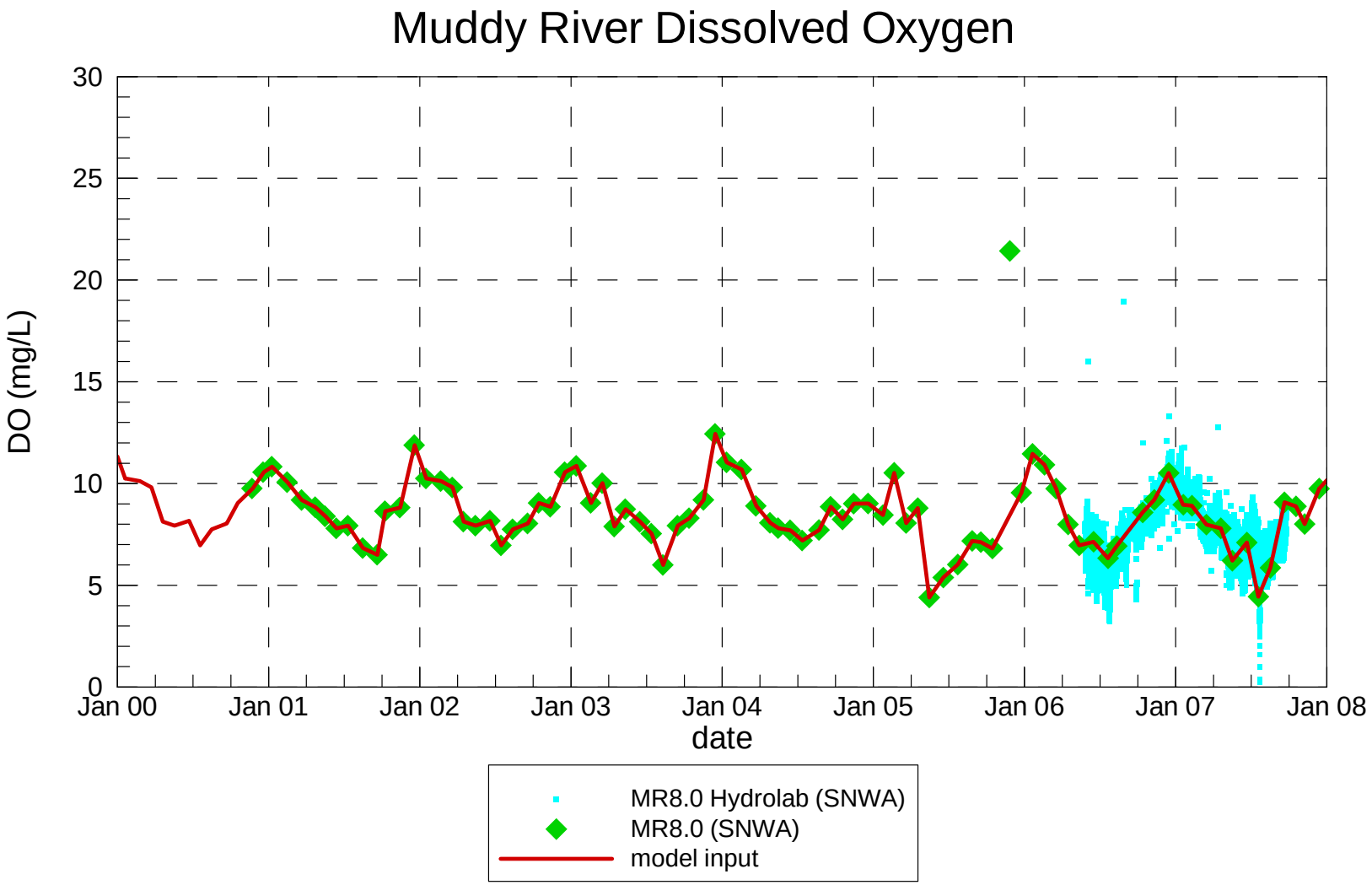
Muddy River Dissolved Oxygen
DO (mg/L)
30
25
20
15
10
5
0
Jan 00
Jan 01
Jan 02
Jan 03
Jan 04
Jan 05
Jan 06
Jan 07
Jan 08
date
MR8.0 Hydrolab (SNWA)
MR8.0 (SNWA)
model input

Figure A.43

APPENDIX B

Description of ELCOM/CAEDYM Models and Evidence of Validation

B DESCRIPTION OF ELCOM/CAEDYM MODELS AND EVIDENCE OF VALIDATION

The coupling of biogeochemical and hydrodynamic processes in numerical simulations is a fundamental tool for research and engineering studies of water quality in coastal oceans, estuaries, lakes, and rivers. A modeling system for aquatic ecosystems has been developed that combines a three-dimensional hydrodynamic simulation method with a suite of water quality modules that compute interactions between biological organisms and the chemistry of their nutrient cycles. This integrated approach allows for the feedback and coupling between biogeochemical and hydrodynamic systems so that a complete representation of all appropriate processes can be included in an analysis. The hydrodynamic simulation code is the Estuary Lake and Coastal Ocean Model (ELCOM) and the biogeochemical model is the Computational Aquatic Ecosystem Dynamics Model (CAEDYM).

The purpose of this appendix is to demonstrate that ELCOM and CAEDYM are accepted models that have been systematically tested and debugged, and then successfully validated in numerous applications. A history of the models is provided, followed by an outline of the general model methodology and evolution that emphasizes the basis of the ELCOM/ CAEDYM codes in previously validated models and research. Then the process of code development, testing, and validation of ELCOM/CAEDYM is detailed. Specific model applications are described to illustrate how the ELCOM/CAEDYM models have been applied to coastal oceans, estuaries, lakes, and rivers throughout the world and the results successfully validated against field data. Finally, a general description of the governing equations, numerical models, and processes used in the models is provided along with an extensive bibliography of supporting material.

A comprehensive description of the equations and methods used in the models is provided in the "Estuary Lake and Coastal Ocean Model: ELCOM v2.2 Science Manual" by Hodges and Dallimore (2006), "Estuary Lake and Coastal Ocean Model: ELCOM v2.2 User Manual" by Hodges and Dallimore (2007), "Computational Aquatic Ecosystem Dynamics Model: CAEDYM: v2.2 Science Manual" by Hipsey, Romero, Antenucci and Hamilton (2005), and the "Computational Aquatic Ecosystem Dynamics Model: CAEDYM: v2.2 User Manual" by Hipsey, Romero, Antenucci and Hamilton (2005).

B.1 MODEL HISTORY

The ELCOM/CAEDYM models were originally developed at the Centre for Water Research (CWR) at the University of Western Australia, although the hydrodynamics code ELCOM is an outgrowth of a hydrodynamic model developed earlier by Professor Vincenzo Casulli in Italy and now in use at Stanford University

under the name TRIM-3D. The CAEDYM model was essentially developed at CWR as an outgrowth of earlier water quality modules used in the one-dimensional model, Dynamic Reservoir Simulation Model - Water Quality (DYRESM-WQ, Hamilton and Schladow, 1997).

The original ELCOM/CAEDYM models, as developed by CWR, were implemented in Fortran 90 (with F95 extensions) on a UNIX computer system platform. In 2001, the codes for both models were ported to a personal computer (PC) platform through an extensive recompiling and debugging effort by Flow Science Incorporated (Flow Science) in Pasadena, California.

B.2 MODEL METHODOLOGY

ELCOM is a three-dimensional numerical simulation code designed for practical numerical simulation of hydrodynamics and thermodynamics for inland and coastal waters. The code links seamlessly with the CAEDYM biogeochemical model undergoing continuous development at CWR, as shown graphically in **Figure B.1**. The combination of the two codes provides three-dimensional simulation capability for examination of changes in water quality that arise from anthropogenic changes in either quality of inflows or reservoir operations.

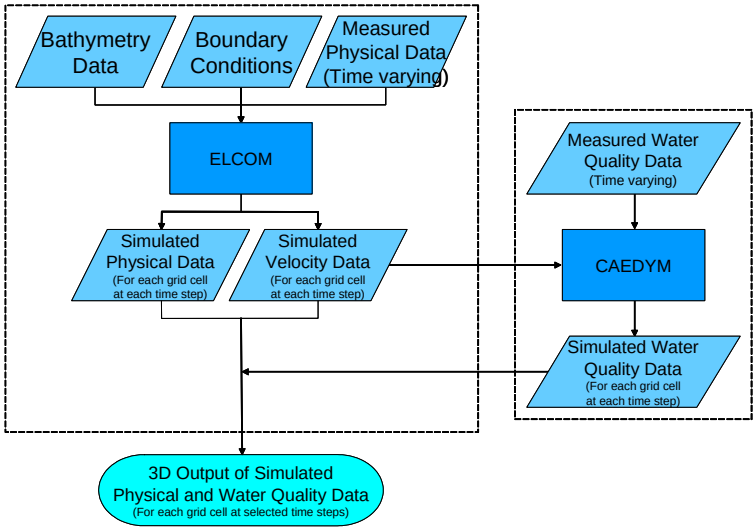

Figure B.1 Flow chart showing the integration of the linked ELCOM/CAEDYM models.

The numerical method used in ELCOM is based on the TRIM-3D model scheme of Casulli and Cheng (1992) with adaptations made to improve accuracy, scalar conversion, numerical diffusion, and implementation of a mixed-layer model. The ELCOM model also extends the TRIM-3D scheme by including conservative advection of scalars. The unsteady Reynolds-averaged, Navier-Stokes equations, and the scalar transport equations serve as the basis of ELCOM. The pressure distribution is assumed hydrostatic and density changes do not impact the inertia of the fluid (the Boussinesq approximation), but are considered in the fluid body forces. There is an eddy-viscosity approximation for the horizontal turbulence correlations that represent the turbulent momentum transfer. Vertical momentum transfer is handled by a Richardson number-based diffusion coefficient. Since numerical diffusion generally dominates molecular processes, molecular diffusion in the vertical direction is neglected in ELCOM.

Both ELCOM and TRIM-3D are three-dimensional, computational fluid dynamics (CFD) models. CFD modeling is a validated and well-established approach to solving the equations of fluid motions in a variety of disciplines. Prior to the development of TRIM-3D, there were difficulties in modeling density-stratified flows and such flows required special numerical methods. With TRIM-3D, Casulli and Cheng (1992) developed the first such successful method to model density-stratified flows, such as occur in the natural environment. Since then, TRIM-3D has been validated by numerous publications. ELCOM is based on the same proven method, but incorporates additional improvements as described above. Furthermore, the ELCOM model is based on governing equations and numerical algorithms that have been used in the past (e.g., in validated models such as TRIM-3D), and have been validated in refereed publications. For example:

- The hydrodynamic algorithms in ELCOM are based on the Euler-Lagrange method for advection of momentum with a conjugate gradient solution for the free-surface height (Casulli and Cheng, 1992).

- The free-surface evolution is governed by vertical integration of the continuity equation for incompressible flow applied to the kinematic boundary condition (e.g., Kowalik and Murty, 1993).

- The numerical scheme is a semi-implicit solution of the hydrostatic Navier-Stokes equations with a quadratic Euler-Lagrange, or semi-Lagrangian (Staniforth and Côté, 1991).

- Passive and active scalars (i.e., tracers, salinity, and temperature) are advected using a conservative ULTIMATE QUICKEST discretization (Leonard, 1991). The ULTIMATE QUICKEST approach has been implemented in two-dimensional format and demonstration of its effectiveness in estuarine flows has been documented by Lin and Falconer (1997).

- Heat exchange is governed by standard bulk transfer models found in the literature (e.g., Amorocho and DeVries, 1980; Imberger and Patterson, 1981; Jacquet, 1983).

- The vertical mixing model is based on an approach derived from the mixing energy budgets used in one-dimensional lake modeling as presented in Imberger and Patterson (1981), Spigel et al (1986), and Imberger and Patterson (1990). Furthermore, Hodges presents a summary of validation using laboratory experiments of Stevens and Imberger (1996). This validation exercise demonstrates the ability of the mixed-layer model to capture the correct momentum input to the mixed-layer and reproduce the correct basin-scale dynamics, even while boundary-induced mixing is not directly modeled.

- The wind momentum model is based on a mixed-layer model combined with a model for the distribution of momentum over depth (Imberger and Patterson, 1990).

The numerical approach and momentum and free surface discretization used in ELCOM are defined in more detail in Hodges, Imberger, Saggio, and Winters (1999). Similarly, the water quality processes and methodology used in CAEDYM are described in more detail in Hamilton and Schladow (1997). Further technical details on ELCOM and CAEDYM are provided in Sections B.4 and B.5 below.

B.3 VALIDATION AND APPLICATION OF ELCOM/CAEDYM

Since initial model development, testing and validation of ELCOM and/or CAEDYM have been performed and numerous papers on model applications have been presented, written, and/or published as described in more detail below. In summary:

- ELCOM solves the full three-dimensional flow equations with small approximations.

- ELCOM/CAEDYM was developed, tested, and validated over a variety of test cases and systems by CWR.

- Papers on ELCOM/CAEDYM algorithms, methodology, and applications have been published in peer reviewed journals such as the *Journal of Geophysical Research*, the *Journal of Fluid Mechanics*, the *Journal of Hydraulic Engineering*, the *International Journal for Numerical Methods in Fluids*, and *Limnology and Oceanography*.

- ELCOM/CAEDYM was applied by Flow Science to Lake Mead, Nevada. As part of this application, mass balances were verified and results were presented to a model review panel over a two-year period. The model review panel, the National Park Service, the Bureau of Reclamation, the Southern

Nevada Water Authority, and the Clean Water Coalition (a consortium of water and wastewater operators in the Las Vegas, Nevada, region) all accepted the ELCOM/CAEDYM model use and validity.

- There are numerous applications of ELCOM/CAEDYM in the literature that compare the results to data, as summarized in Section B.3.2.

The process of code development, testing, and validation of ELCOM/CAEDYM by CWR, and the ongoing validation and refinement of the codes through further application of the models are detailed in the following subsections. The major components of the development, testing, and validation process are summarized in **Figure B.2**.

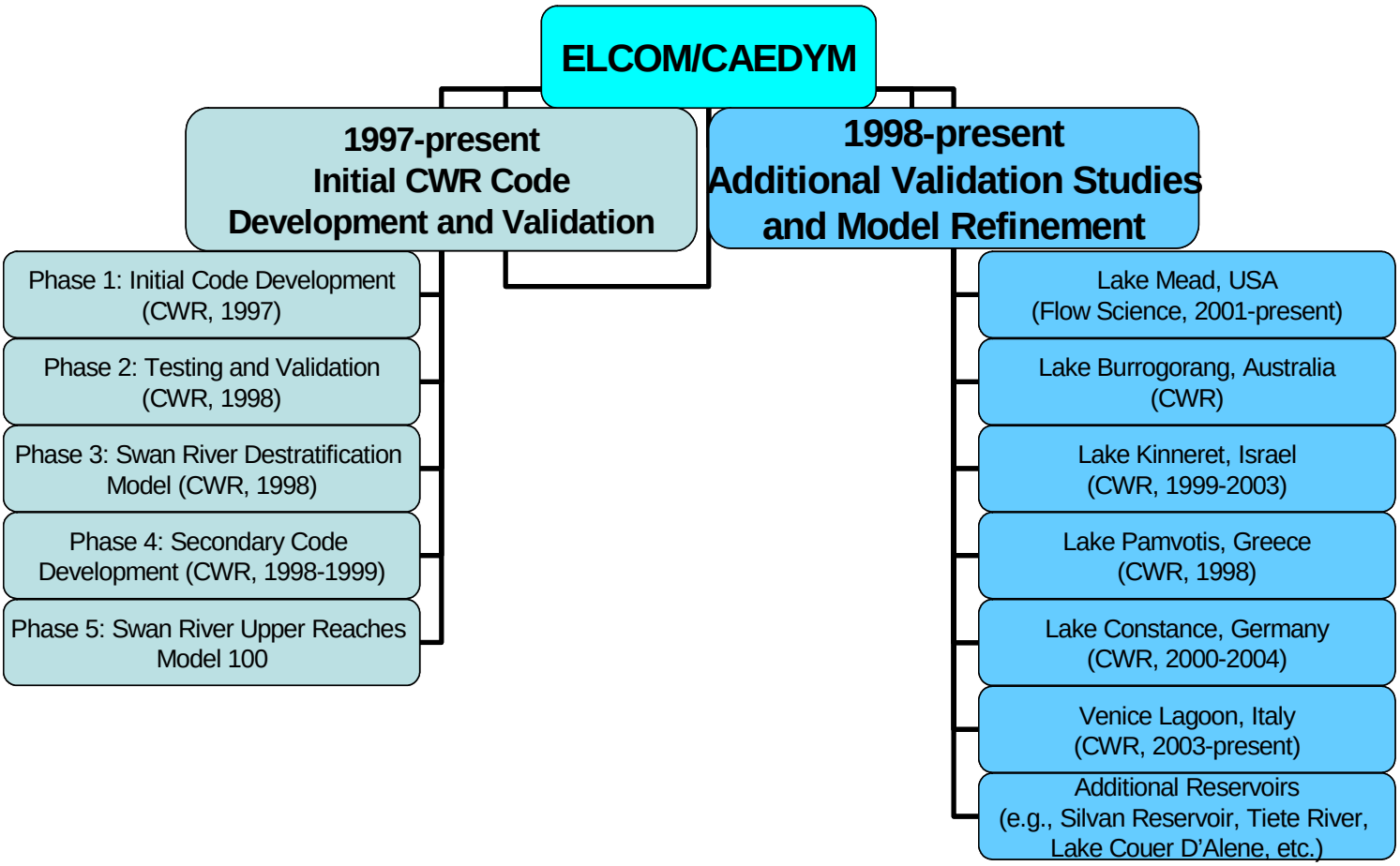

Figure B.2 ELCOM/CAEDYM code development, testing, validation, and applications by CWR and Flow Science Incorporated.

B.3.1 CWR Code Development, Testing, and Validation

Initial development of the code by CWR occurred from March through December 1997 (Phase 1), followed by a period of testing and validation from January through April 1998 (Phases 2 and 3). Secondary code development by CWR occurred from September 1998 through February 1999 (Phase 4). Testing and validation were performed over a variety of test cases and systems to ensure that all facets of the code were tested. In addition, Phase 5 modeling of the Swan River since 1998 has been used to gain a better understanding of the requirements and limitations of the model (Hodges et al, 1999).

B.1.1.1. Phase 1: Initial Code Development

The ELCOM code was initially conceived by CWR as a Fortran 90/95 adaptation of the TRIM-3D model of Casulli and Cheng (1992) in order to: 1) link directly to the CAEDYM water quality module developed concurrently at CWR and 2) provide a basis for future development in a modern programming language. Although written in Fortran 77, TRIM-3D is considered a state-of-the-art numerical model for estuarine applications using a semi-implicit discretization of the Reynolds-averaged hydrostatic Navier-Stokes equations and an Euler-Lagrange method for momentum and scalar transport.

During development of ELCOM, it became clear that additional improvements to the TRIM-3D algorithm were required for accurate solution of density-stratified flows in estuaries. After the basic numerical algorithms were written in Fortran 90, subroutine-by-subroutine debugging was performed to ensure that each subroutine produced the expected results. Debugging and testing of the entire model used a series of test cases that exercised the individual processes in simplified geometries. This included test cases for the functioning of the open boundary condition (tidal forcing), surface wave propagation, internal wave propagation, scalar transport, surface thermodynamics, density underflows, wind-driven circulations, and flooding/drying of shoreline grid cells. Shortcomings identified in the base numerical algorithms were addressed during secondary code development (Phase 4).

Towards the end of the initial code development, ELCOM/CAEDYM were coupled and test simulations were run to calibrate the ability of the models to work together on some simplified problems. Results showing the density-driven currents induced by phytoplankton shading were presented at the Second International Symposium on Ecology and Engineering (Hodges and Herzfeld, 1997). Further details of modeling of density-driven currents due to combinations of topographic effects and phytoplankton shading were presented at a joint meeting of the American Geophysical Union (AGU) and the American Society of Limnology and Oceanography (ASLO) by Hodges et al. (1998), and at a special seminar at Stanford University (Hodges 1998). Additionally, presentations by Hamilton (1997), Herzfeld et al. (1997), and Herzfeld and

Hamilton (1998) documented the concurrent development of the CAEDYM ecological model.

B.1.1.2. Phase 2: Testing and Validation

The simplified geometry tests of Phase I revealed deficiencies in the TRIM-3D algorithm including the inability of the TRIM-3D Euler-Lagrange method (ELM) to provide conservative transport of scalar concentrations (e.g., salinity and temperature). Thus, a variety of alternate scalar transport methods were tested, with the best performance being a flux-conservative implementation of the ULTIMATE filter applied to third-order QUICKEST discretization based on the work of Leonard (1991).

Model testing and validation against simple test cases was again undertaken. In addition, a simulation of a winter underflow event in Lake Burragorang in New South Wales, Australia, was performed to examine the ability of the model to capture a density underflow in complex topography in comparison to field data taken during the inflow event. These tests showed that the ability to model underflows is severely constrained by the cross-channel grid resolution.

B.1.1.3. Phase 3: Swan River Destratification Model

Phase 3 involved examining a linked ELCOM/CAEDYM destratification model of the Swan River system during a period of destratification in 1997 when intensive field monitoring had been conducted. The preliminary results of this work were presented at the Swan-Canning Estuary Conference (Hertzfeld et al, 1998). More comprehensive results were presented at the Western Australian Estuarine Research Foundation (WAERF) Community Forum (Imberger, 1998).

B.1.1.4. Phase 4: Secondary Code Development

In conducting the Phase 3 Swan River destratification modeling, it became clear to CWR that long-term modeling of the salt-wedge propagation would require a better model for mixing dynamics than presently existed. Thus, the availability of an extensive field data set for Lake Kinneret, Israel, led to its use as a test case for development of an improved mixing algorithm for stratified flows (Hodges et al, 1999).

A further problem appeared in the poor resolution of momentum terms using the linear ELM discretization (i.e., as used in the original TRIM-3D method). Since the conservative ULTIMATE QUICKEST method (used for scalar transport, see Phase 1 above) does not lend itself to efficient use for discretization of momentum terms in a semi-implicit method, a quadratic ELM approach was developed for more accurate discretization of the velocities.

B.1.1.5. Phase 5: Swan River Upper Reaches Model

Phases 1-4 developed and refined the ELCOM code for accurate modeling of three-dimensional hydrodynamics where the physical domain is well resolved. Phase 5 is an ongoing process of model refinement that concentrates on developing a viable approach to modeling longer-term evolution hydrodynamics and water quality in the Swan River where fine-scale resolution of the domain is not practical. The Swan River application is also used for ongoing testing and calibration of the CAEDYM water quality module.

The Swan River estuary is located on the Swan Coastal Plain, Western Australia. It is subject to moderate to high nutrient loads associated with urban and agricultural runoff and suffered from *Microcystis aeruginosa* blooms in January 2000. In an effort to find a viable means of conducting seasonal to annual simulations of the Swan River that retain the fundamental along-river physics and the cross-channel variability in water quality parameters, CWR has developed and tested ELCOM/CAEDYM extensively. A progress report by Hodges et al (1999) indicates that ELCOM is capable of accurately reproducing the hydrodynamics of the Swan River over long time scales with a reasonable computational time.

Furthermore, studies conducted by Robson and Hamilton (2002) proved that ELCOM/CAEDYM accurately reproduced the unusual hydrodynamic circumstances that occurred in January 2000 after a record maximum rainfall, and predicted the magnitude and timing of the *Microcystis* bloom. These studies show that better identification and monitoring procedures for potentially harmful phytoplankton species could be established with ELCOM/CAEDYM and will assist in surveillance and warnings for the future.

B.3.2 Model Applications

In addition to the initial code development, testing, and validation by CWR, numerous other applications of ELCOM/CAEDYM have been developed by CWR and validated against field data. Additionally, Flow Science has applied ELCOM/CAEDYM extensively at Lake Mead (USA) and validated the results against measured data. The results of numerous ELCOM/CAEDYM model applications are presented below.

B.1.1.1. Lake Mead (Nevada, USA)

An ELCOM/CAEDYM model of Boulder Basin, Lake Mead near Las Vegas, Nevada, is being used to evaluate alternative discharge scenarios for inclusion in an Environmental Impact Statement (EIS) for the Clean Water Coalition (CWC), a consortium of water and wastewater operators in the Las Vegas region. **Figure B.3** is a cut-away of the three-dimensional model grid used for Boulder Basin, showing the varying grid spacing in the vertical direction. **Figure B.4** is an example of the model output, showing the isopleths of a tracer plume within the reservoir for a sample case.

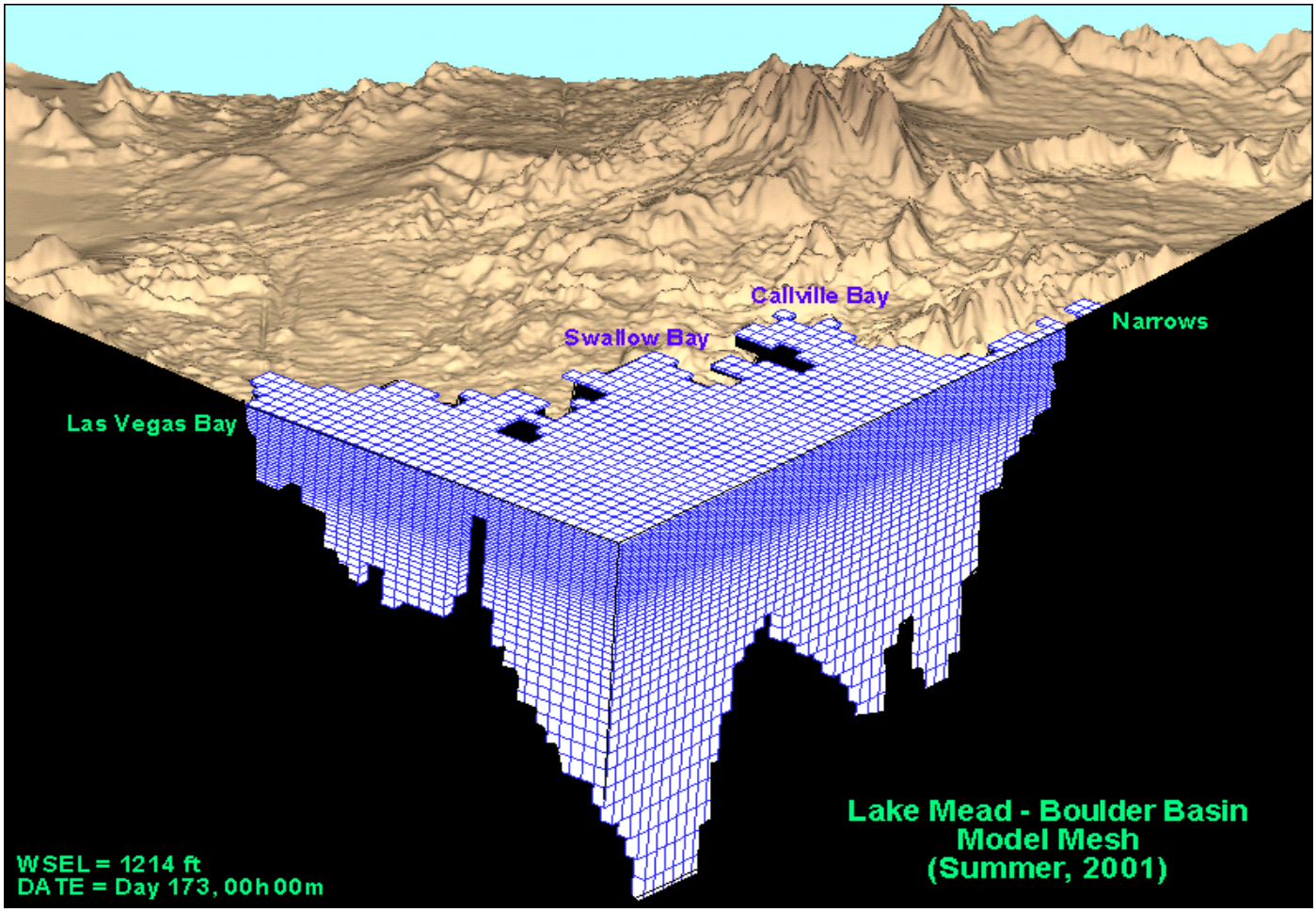

Figure B.3 Model Grid for Lake Mead.

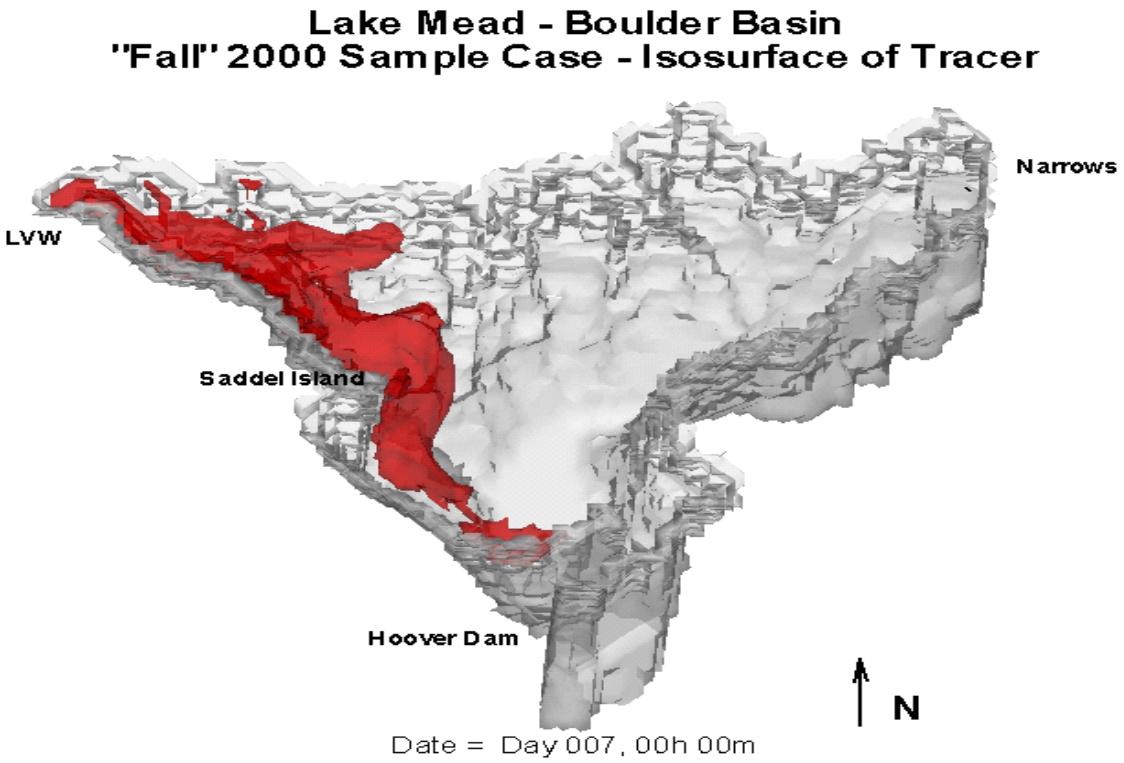

Figure B.4 Boulder Basin isopleths of tracer for a fall 2000 sample case.

As part of the EIS process, a model review panel met monthly for two years to review the validation of the ELCOM/CAEDYM model, its calibration against field data, and its application. The modeling committee approved the use of the model.

Subsequently, a scientific Water Quality Advisory Panel concluded that the ELCOM/CAEDYM model was applicable and acceptable. The members of the Water Quality Advisory Panel were diverse and included Jean Marie Boyer, Ph.D., P.E. (Water Quality Specialist/Modeler, Hydrosphere), Chris Holdren, Ph.D., CLM (Limnologist, United States Bureau of Reclamation), Alex Horne, Ph.D. (Ecological Engineer, University of California Berkeley), and Dale Robertson, Ph.D. (Research Hydrologist, United States Geological Survey).

More specifically, the Water Quality Advisory Panel agreed on the following findings:

- The ELCOM/CAEDYM model is appropriate for the project.

- There are few three-dimensional models available for reservoirs. ELCOM is one of the best hydrodynamic models and has had good success in the Boulder Basin of Lake Mead and other systems.

- The ELCOM model accurately simulates most physical processes.

- The algorithms used in CAEDYM are widely accepted (a biological consultant, Professor David Hamilton of The University of Waikato, New Zealand, has been retained to review the CAEDYM coefficients and algorithms).

The Boulder Basin ELCOM/CAEDYM model was calibrated against four years of measured data for numerous physical and water quality parameters including temperature, salinity, conductivity, dissolved oxygen, pH, nutrients (nitrogen and phosphorus), chlorophyll *a*, perchlorate, chloride, sulfate, bromide, and total organic carbon. Detailed results of this calibration and the subsequent evaluation of alternative discharge scenarios were made available in late 2005 in the CWC EIS that was being prepared for this project. An example of the calibration results for chlorophyll *a* for 2002 is presented in **Figure B.5** below. In this figure, simulated concentrations are compared against field data measured in the lake by the United States Bureau of Reclamation (USBR) and the City of Las Vegas (COLV).

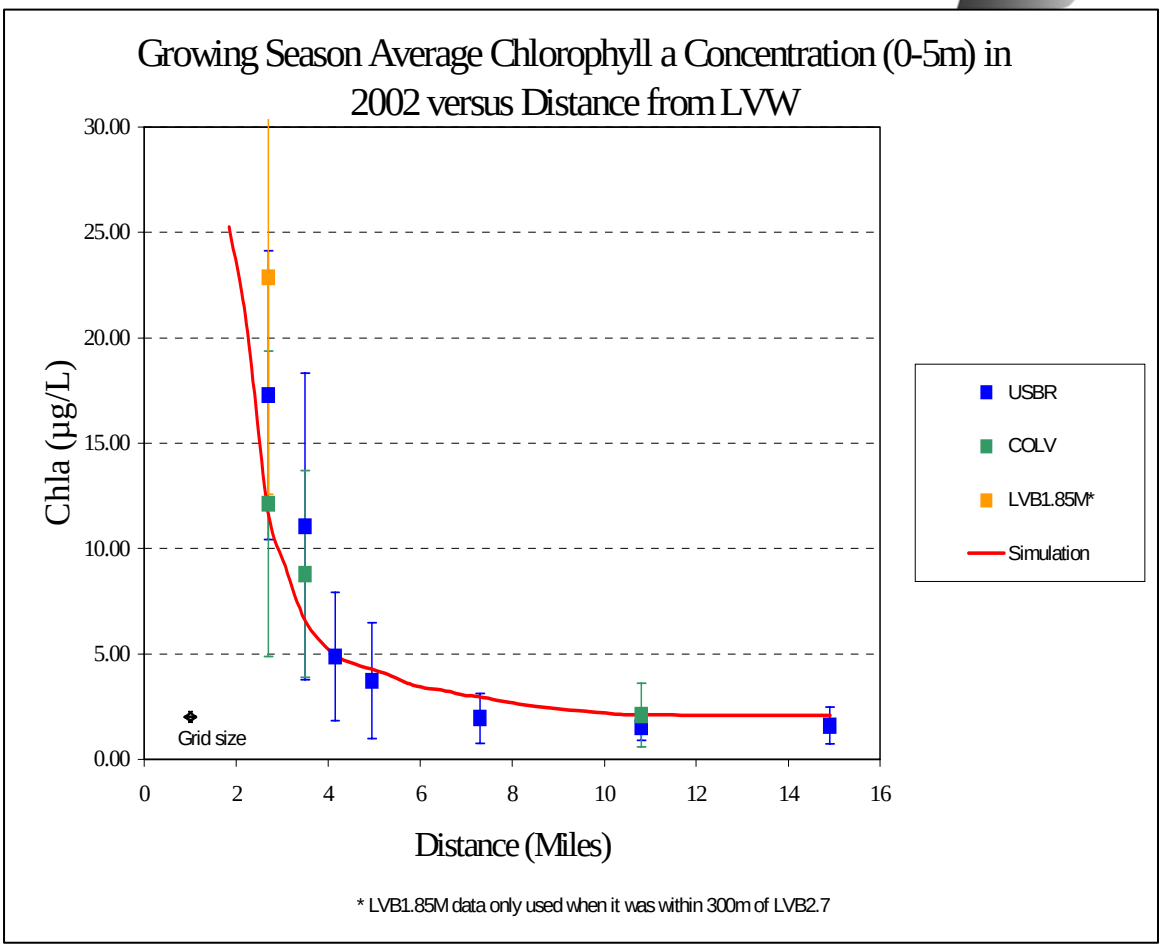

Figure B.5 ELCOM/CAEDYM calibration results for chlorophyll a for 2002 as a function of distance from the inflow at Las Vegas Wash.

In addition to the good agreement between the model and field data and the acceptance of the model by the review committees, Flow Science also performed a mass balance on the model to ensure conservation of tracer materials. As a result of such tests and debugging, Flow Science and the CWR have made continuous improvements to the model as necessary including refinements to the ULTIMATE QUICKEST scheme and boundary cell representations.

B.1.1.2. Lake Burragorang (New South Wales, Australia)

ELCOM was applied and validated for Lake Burragorang in order to rapidly assess the potential impacts on water quality during an underflow event (CWR).

Underflows usually occur during the winter when inflow water temperature is low compared to the reservoir. This causes the upheaval of hypolimnetic water at the dam wall, and as a result it transports nutrient rich waters into the euphotic zone.

The thermal dynamics during the underflow event were reproduced accurately by ELCOM for the case with idealized bathymetry data with coarse resolutions (straightened curves and rotating the lake in order to bypass the resolution problem), but not for the simulation with the complex, actual bathymetry. This is because the model tests showed that the ability to model underflows is severely constrained by the cross-channel grid resolution. When the cross-channel direction is poorly resolved at bends and curves, an underflow is unable to propagate downstream without a significant loss of momentum. Nevertheless, the simulations with the coarse idealized domain certainly can be used as aids and tools to visualize the behavior of reservoirs. Particularly, ELCOM was able to capture the traversal of the underflow down the length of Lake Burragorang and then had sufficient momentum to break against the wall causing the injection of underflow waters into the epilimnion near the dam. This simulated dynamic was in agreement with what was measured in the field.

B.1.1.3. Lake Kinneret (Israel)

ELCOM was applied to model basin-scale internal waves that are seen in Lake Kinneret, Israel, since understanding of basin-scale internal waves behaviors provide valuable information on mixing and transport of nutrients below the wind-mixed layer in stratified lakes. In studies done by Hodges et al. (1999) and Laval et al (2003), the ELCOM simulation results were compared with field data under summer stratification conditions to identify and illustrate the spatial structure of the lowest-mode basin-scale Kelvin and Poincare waves that provide the largest two peaks in the internal wave energy spectra. The results demonstrated that while ELCOM showed quantitative differences in the amplitude and steepness of the waves as well as in the wave phases, the basin-scale waves were resolved very well by ELCOM. In particular, the model captures the qualitative nature of the peaks and troughs in the thermocline and the depth of the wind-mixed layer at relatively coarse vertical grid resolutions (Hodges et al, 1999).

B.1.1.4. Lake Pamvotis (Greece)

ELCOM/CAEDYM was applied to Lake Pamvotis, a moderately sized (22 km^2), shallow (4 m average depth) lake located in northwest Greece. Since the lake has undergone eutrophication over the past 40 years, many efforts are directed at understanding the characteristics of the lake and developing watershed management and restoration plans.

Romero and Imberger (1999) simulated Lake Pamvotis over a one month period during May to June, 1998, and compared the simulated thermal and advective dynamics of the lake with data obtained from a series of field experiments. The simulation results

over-predicted heating; however, diurnal fluctuations in thermal structures were similar to those measured. Since the meteorological site was sheltered from the winds, the wind data used in the simulation was believed to be too low, causing insufficient evaporative heat-loss and subsequent over-heating by ELCOM. An increase in the wind speed by a factor of three gave temperature profiles in agreement with the field data. Moreover, the study demonstrated that the model is capable of predicting the substantial diurnal variations in the intensity and direction of both vertical and horizontal velocities. Romero and Imberger were also able to illustrate the functionality of ELCOM when coupled to the water quality model, CAEDYM, and confirmed that the model could be used to evaluate the effect of various strategies to improve poor water quality in localized areas in the lake.

B.1.1.5. Lake Constance (Germany, Austria, Switzerland)

Appt (2000) and Appt et al. (2004) applied ELCOM to characterize the internal wave structures and motions in Lake Constance [Bodensee] since internal waves are a key factor in understanding the transport mechanisms for chemical and biological processes in a stratified lake such as Lake Constance. Lake Constance is an important source of drinking water and a major tourism destination for its three surrounding countries of Germany, Austria, and Switzerland. Due to anthropogenic activities and climatic changes, Lake Constance water quality has deteriorated and its ecosystem has changed.

It was shown that ELCOM was able to reproduce the dominant internal wave and major hydrodynamic processes occurring in Lake Constance. For instance, three types of basin-scale waves were found to dominate the wave motion: the vertical mode-one Kelvin wave, the vertical mode-one Poincare waves, and a vertical mode-two Poincare wave. Moreover, an upwelling event was also reproduced by ELCOM suggesting that the width and length ratio of the basin, spatial variations in the wind, and Coriolis effects play critical roles in the details of the upwelling event. This on-going research has shown that ELCOM can be used as a tool to predict and understand hydrodynamics and water quality in lakes.

B.1.1.6. Venice Lagoon (Italy)

ELCOM/CAEDYM is being used to develop a hydrodynamic and sediment transport model of Venice Lagoon, Italy, since future gate closures at the mouth of the lagoon are likely to impact flushing patterns. This project is an integral part of the Venice Gate Projects in Italy that was launched in May 2003 to prevent flooding.

ELCOM was validated for the tidal amplitude and phase using the data obtained from 12 tidal stations located throughout the lagoon (Yeates, 2004). Remaining tasks include model validation of temperature, salinity, and velocity against measurements made in the major channels of the lagoon.

B.1.1.7. Silvan Reservoir (Australia)

ELCOM is currently being applied to reproduce the circulation patterns observed in Silvan Reservoir, Australia, during a field experiment that was conducted in March 2004 to determine the transport pathways in the lake. This experiment confirmed the upwelling behavior of the lake and the strong role of the inflows in creating hydraulic flows in the reservoir (Antenucci, 2004).

B.1.1.8. Billings and Barra Bonita Reservoirs (Brazil)

ELCOM/CAEDYM is being applied to Billings and Barra Bonita Reservoirs in Brazil. Billings Reservoir is an upstream reservoir that feeds Barra Bonita via the Tiete River. The objective of the project is to develop an integrated management tool for these reservoirs and river reaches for use in the future planning of water resource utilization in Sao Paulo, Brazil (Romero and Antenucci, 2004).

B.1.1.9. Lake Coeur D'Alene (Idaho, USA)

ELCOM/CAEDYM is being applied to investigate the trade-off between reducing heavy metal concentrations and a potential increase in eutrophication due to remediation procedures in Lake Coeur D'Alene, Idaho. In order to investigate heavy metal fate and transport, CAEDYM is being improved further to include heavy metals and a feedback loop to phytoplankton based on metal toxicity (Antenucci, 2004).

B.1.1.10. Lake Perris (California, USA)

ELCOM was applied to Lake Perris in order to compare the impacts of several recreational use strategies on measured fecal coliform concentrations at the outlet tower. The physical results of the simulation were validated against measured temperature and salinity data over a one-year period. The comparison of fecal coliform concentrations against measured data was fair due to a lack of data describing the timing and magnitude of loading and the settling and re-suspension of fecal matter.

B.1.1.11. Other Applications

Other ELCOM/CAEDYM applications and development in on-going research at CWR include:

- Plume dynamics and horizontal dispersion (Marmion Marine Park, Australia).
- Inflow and pathogen dynamics (Helena, Myponga and Sugarloaf Reservoirs, Australia).

- Mixing and dissipation in stratified environments (Tone River, Japan, and Brownlee Reservoir, USA).

- Tidally forced estuaries and coastal lagoons (Marmion Marine Park and Barbamarco Lagoon, Italy).

- Three-dimensional circulation induced by wind and convective exchange (San Roque Reservoir, Argentina, and Prospect Reservoir, Australia).

- Sea-surface temperature fluctuation and horizontal circulation (Adriatic Sea).

- Response of bivalve mollusks to tidal forcing (Barbamarco Lagoon, Italy).

- Impacts of the additional withdrawals and brine discharge into the ocean from a proposed desalination facility co-located with an existing power plant in the City of Carlsbad (California, USA).

- Design of a new ocean outfall system to discharge 44 m^3/sec of treated wastewater into the Pacific Ocean off Palos Verdes (California, USA).

B.4 TECHNICAL DESCRIPTION OF ELCOM

As outlined above, ELCOM solves the unsteady, viscous Navier-Stokes equations for incompressible flow using the hydrostatic assumption for pressure. ELCOM can simulate the hydrodynamics and thermodynamics of a stratified system, including baroclinic effects, tidal forcing, wind stresses, heat budget, inflows, outflows, and transport of salt, heat and passive scalars. Through coupling with the CAEDYM water quality module, ELCOM can be used to simulate three-dimensional transport and interactions of flow physics, biology, and chemistry. The hydrodynamic algorithms in ELCOM are based upon the proven semi-Lagrangian method for advection of momentum with a conjugate-gradient solution for the free-surface height (Casulli and Cheng, 1992) and a conservative ULTIMATE QUICKEST transport of scalars (Leonard, 1991). This approach is advantageous for geophysical-scale simulations since the time step can be allowed to exceed the Courant-Friedrichs-Lewy (CFL) condition for the velocity without producing instability or requiring a fully-implicit discretization of the Navier-Stokes equations.

B.4.1 Governing Equations

Significant governing equations and approaches used in ELCOM include:

- Three-dimensional simulation of hydrodynamics (unsteady Reynolds-averaged Navier-Stokes equations).

- Advection and diffusion of momentum, salinity, temperature, tracers, and water quality variables.

- Hydrostatic approximation for pressure.
- Boussinesq approximation for density effects.
- Surface thermodynamics module accounts for heat transfer across free surface.
- Wind stress applied at the free surface.
- Dirichlet boundary conditions on the bottom and sides.

B.4.2 Numerical Method

Significant numerical methods used in ELCOM include:

- Finite-difference solution on staggered-mesh Cartesian grid.
- Implicit volume-conservative solution for free-surface position.
- Semi-Lagrangian advection of momentum allows time steps with CFL > 1.0.
- Conservative ULTIMATE QUICKEST advection of temperature, salinity, and tracers.
- User-selectable advection methods for water quality scalars using upwind, QUICKEST, or semi-Lagrangian to allow trade-offs between accuracy and computational speed.
- Solution mesh is Cartesian and allows non-uniformity (i.e. stretching) in horizontal and vertical directions.

The implementation of the semi-Lagrangian method in Fortran 90 includes sparse-grid mapping of three-dimensional space into a single vector for fast operation using array-processing techniques. Only the computational cells that contain water are represented in the single vector so that memory usage is minimized. This allows Fortran 90 compiler parallelization and vectorization without platform-specific modification of the code. A future extension of ELCOM will include dynamic pressure effects to account for nonlinear dynamics of internal waves that may be lost due to the hydrostatic approximation.

Because the spatial scales in a turbulent geophysical flow may range from the order of millimeters to kilometers, it is presently impossible to conduct a Direct Navier-Stokes (DNS) solution of the equations of motion (i.e. an exact solution of the equations). Application of a numerical grid and a discrete time step to a simulation of a geophysical domain is implicitly a filtering operation that limits the resolution of the equations.

Numerical models (or closure schemes) are required to account for effects that cannot be resolved for a particular grid or time step. There are four areas of modeling in the flow physics: (l) turbulence and mixing, (2) heat budgets, (3) hydrodynamic boundary conditions, and (4) sediment transport.

B.4.3 Turbulence Modeling and Mixing

ELCOM presently uses uniform fixed eddy viscosity as the turbulence closure scheme in the horizontal plane (in future versions a Smagorinsky 1963 closure scheme will be implemented to represent subgrid-scale turbulence effects as a function of the resolves large-scale strain-rates). These methods are the classic "eddy viscosity" turbulence closure. With the implementation of the Smagorinsky closure, future extensions will allow the eddy-viscosity to be computed on a local basis to allow improvements in modeling local turbulent events and flow effects of biological organisms (e.g., drag induced by macroalgae or seagrass).

In the present code, the user has the option to extend the eddy-viscosity approach to the vertical direction by setting different vertical eddy-viscosity coefficients for each grid layer. However, in a stratified system, this does not adequately account for vertical turbulent mixing that may be suppressed or enhanced by the stratification (depending on the stability of the density field and the magnitude of the shear stress). To model the effect of density stratification on turbulent mixing the CWR has developed a closure model based on computation of a local Richardson number to scale. The latter is generally smaller than the time step used in geophysical simulations, so the mixing is computed in a series of partial time steps. When the mixing time-scale is larger than the simulation time step, the mixing ratio is reduced to account for the inability to obtain mixing on very short time scales. This model has the advantage of computing consistent mixing effects without regard to the size of the simulation time-step (i.e. the model produces mixing between cells that is purely a function of the physics and not the numerical step size).

B.4.4 Heat Budget

The heat balance at the surface is divided into short-wave (penetrative) radiation and a heat budget for surface heat transfer effects. The surface heat budget requires user input of the net loss or gain through conduction, convection, and long wave radiation in the first grid layer beneath the free surface. The short wave range is modeled using a user-prescribed input of solar radiation and an exponential decay with depth that is a function of a bulk extinction coefficient (a Beer's law formulation for radiation absorption). This coefficient is the sum of individual coefficients for the dissolved organics ("gilvin"), phytoplankton biomass concentration, suspended solids, and the water itself. The extinction coefficients can either be computed in the water quality module (CAEDYM) or provided as separate user input.

B.4.5 Hydrodynamic Boundary Conditions

The hydrodynamic solution requires that boundary conditions on the velocity must be specified at each boundary. There are six types of boundary conditions: (1) free surface, (2) open edge, (3) inflow-outflow, (4) no-slip, (5) free-slip, and (6) a Chezy-Manning boundary stress model (the latter is presently not fully implemented). For the free surface, the stress due to wind and waves is required. The user can either input the wind/wave stress directly, or use a model that relates the surface stress to the local wind speed and direction *via* a bulk aerodynamic drag coefficient. Open boundaries (e.g. tidal inflow boundaries for estuaries) require the user to supply the tidal signature to drive the surface elevation. Transport across open boundaries is modeled by enforcing a Dirichlet condition on the free-surface height and allowing the inflow to be computed from the barotropic gradient at the boundary. Inflow-outflow boundary conditions (e.g. river inflows) are Dirichlet conditions that specify the flow either at a particular boundary location *or inside the domain*. Allowing an inflow-outflow boundary condition to be specified for an interior position (i.e. as a source or sink) allows the model to be used for sewage outfalls or water outlets that may not be located on a land boundary. Land boundaries can be considered zero velocity (no-slip), zero-flux (free-slip) or, using a Chezy-Manning model, assigned a computed stress.

B.4.6 Sediment Transport

While sediment transport is fundamentally an issue of flow physics, the algorithms for the sediment transport are more conveniently grouped with the water quality algorithms in CAEDYM. Settling of suspended particulate matter is computed using Stokes law to obtain settling velocities for the top and bottom of each affected grid cell. This allows the net settling flux in each cell to be computed. A two-layer sediment model has been developed that computes resuspension, deposition, flocculation, and consolidation of sediment based on (1) the shear stress at the water/sediment interface, (2) the type of sediment (cohesive/non-cohesive), and (3) the thickness of the sediment layer. Determination of the shear stress at the water/sediment interface requires the computation of bottom shear due to current, wind, and waves. A model has been developed to account for the effects of small-scale surface waves that cannot be resolved on a geophysical-scale grid. This model computes the theoretical wave height and period for small-scale surface waves from the wind velocity, water depth, and domain fetch. From these, the wavelength and orbital velocities are calculated. The wave-induced shear stress at the bottom boundary resulting from the wave orbital velocities is combined with a model for the current-induced shear stress to obtain the total bottom shear that effects sediment resuspension. The cohesiveness of the sediment determines the critical shear stresses that are necessary to resuspend or deposit the sediments. A model of consolidation of the sediments is used to remove lower sediment layers from the maximum mass that may be resuspended.

B.5 TECHNICAL DESCRIPTION OF CAEDYM

CAEDYM is an outgrowth of previous CWR water quality modules in DYRESM-WQ and the Estuary Lake Model - Water Quality (ELMO-WQ) codes. CAEDYM is designed as a set of subroutine modules that can be directly coupled with one, two, or three-dimensional hydrodynamic "drivers", catchment surface hydrological models, or groundwater models. Additionally, it can be used in an uncoupled capacity with specification of velocity, temperature, and salinity distributions provided as input files rather than as part of a coupled computation. The user can specify the level of complexity in biogeochemical process representation so both simple and complex interactions can be studied. Direct coupling to a hydrodynamic driver (e.g. ELCOM) allows CAEDYM to operate on the same spatial and temporal scales as the hydrodynamics. This permits feedbacks from CAEDYM into ELCOM for water quality effects such as changes in light attenuation or effects of macroalgae accumulation on bottom currents. **Figure B.6** shows an illustration of the interactions of modeled parameters in CAEDYM. Being an “N-P-Z” (nutrient-phytoplankton-zooplankton) model, CAEDYM can be used to assess eutrophication. Unlike the traditional general ecosystem model, CAEDYM serves as a species- or group-specific model (i.e. resolves various phytoplankton species). Furthermore, oxygen dynamics and several other state variables are included in CAEDYM.

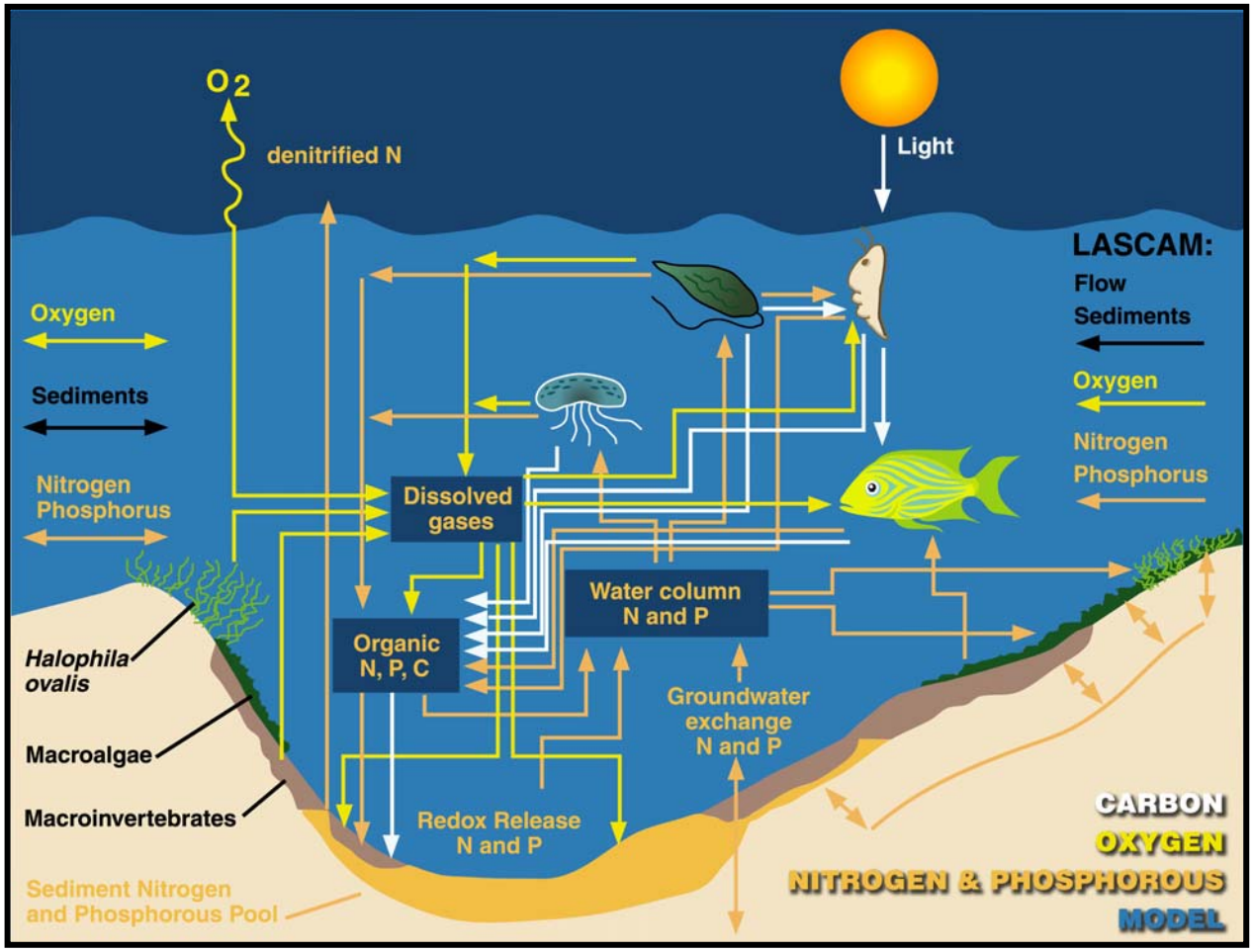

Figure B.6 Illustration of interactions of modeled parameters in CAEDYM.

The representation of biogeochemical processes in ecological models has, historically, been treated in a simple manner. In fact, the pioneering work on modeling marine ecosystems (Riley et al, 1949; Steel, 1962) is still used as a template for many of the models that are currently used (Hamilton and Schladow, 1997). The level of sophistication and process representation included in CAEDYM is of a level hitherto unseen in any previous aquatic ecosystem model. This enables many different components of the system to be examined, as well as providing a better representation of the dynamic response of the ecology to major perturbations to the system (e.g. the response to various management strategies). **Figure B.7** shows the major state variables included in the CAEDYM model. Using CAEDYM to aid in management decisions and system understanding requires (1) a high level of process representation, (2) process interactions and species differentiation of several state variables, and (3) applicability

over a spectrum of spatial and temporal scales. The spectrum of scales relates to the need for managers to assess the effects of temporary events, such as anoxia at specific locations, through to understanding long-term changes that may occur over seasons or years. There is considerable flexibility in the time step used for the ecological component. Long time steps (relative to the hydrodynamic advective scale) may be used to reduce the frequency of links to ELCOM when long-term (i.e. seasonal or annual) simulations are run.

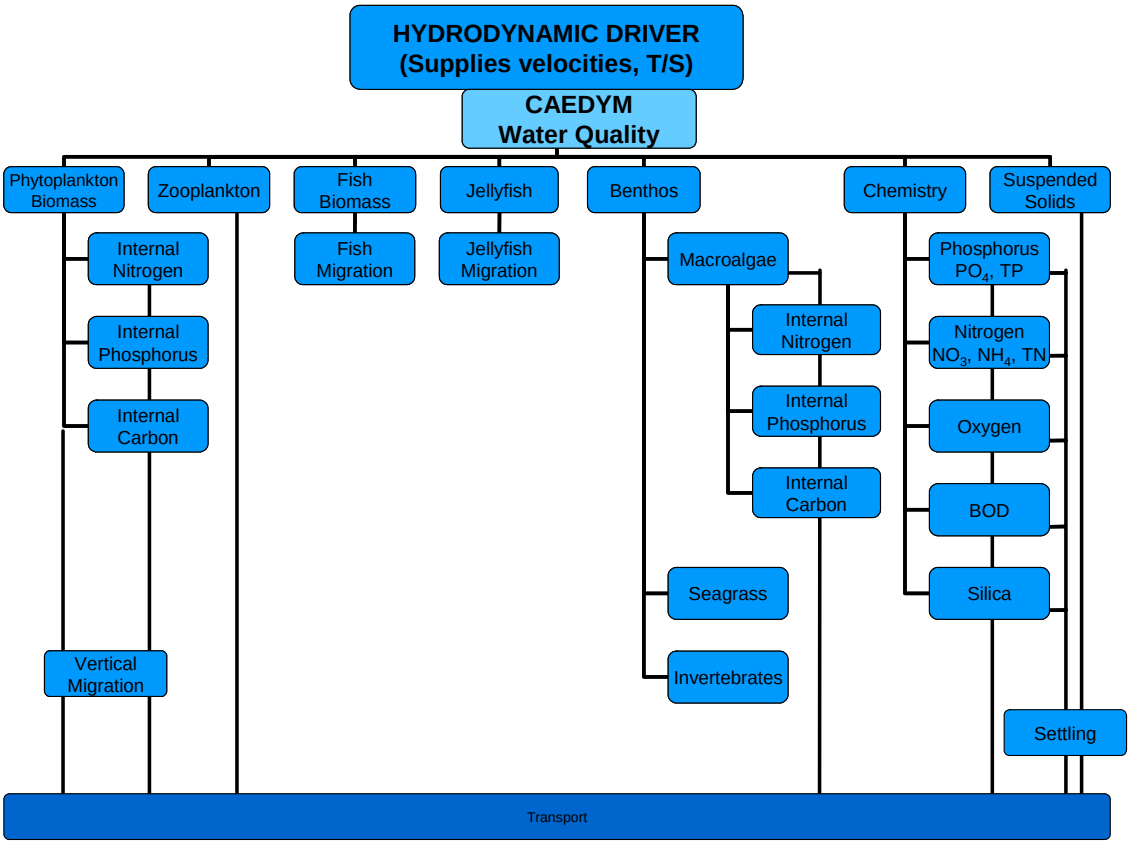

Figure B.7 Major state variables included in the CAEDYM model.

B.5.1 Biological Model

The biological model used in CAEDYM consists of seven phytoplankton groups, five zooplankton groups, six fish groups, four macroalgae groups and three invertebrate groups, as well as models of seagrass and jellyfish. This set will be expanded as biological models are developed, tested, and calibrated to field data. There is flexibility for the user in choosing which species to include in a simulation. Vertical migration is simulated for motile and non-motile phytoplankton, and fish are migrated throughout the model domain according to a migration function based on their mortality. A weighted grazing function is included for zooplankton feeding on phytoplankton and fish feeding on zooplankton. The biomass grazed is related to both food availability and preference of the consumer for its food supply. Improved temperature, respiration and light limitation functions have been developed to represent the environmental response of the organisms. The benthic processes included a self-shading component and beach wrack function for macroalgae, sediment bioturbation and nutrient cycling by polychaetes, and effects of seagrass on sediment oxygen status.

In particular, the seven phytoplankton groups modeled are dinoflagellates, freshwater diatoms, marine/estuarine diatoms, freshwater cyanobacteria, marine estuarine cyanobacteria, chlorophytes, and cryptophytes. Phytoplankton biomass is represented in terms of chlorophyll *a*. Phytoplankton concentrations are affected by the following processes:

- Temperature growth function
- Light limitation
- Nutrient limitation by phosphorus and nitrogen (and when diatoms are considered, silica)
- Loss due to respiration, natural mortality, excretion, and grazing
- Salinity response
- Vertical migration and settling

B.5.2 Nutrients, Metals, and Oxygen Dynamics

The transport and chemical cycling of nutrients is an important part of simulating the interaction of biological organisms in an ecosystem. CAEDYM includes as state variables the following:

- Nutrients (dissolved inorganic phosphorus, total phosphorus, total nitrogen, ammonium nitrate, and silica).
- Dissolved oxygen and biochemical oxygen demand.
- Metals (dissolved and particulate forms of iron and manganese).
- Suspended sediment (the particulate and colloidal fractions).
- pH

The model incorporates oxygen dynamics and nutrient cycling in both the sediments and water column. A sediment pool of organic detritus and inorganic sediments, both of which may be resuspended into the water column, is included. Redox-mediated release of dissolved nutrients is simulated from the sediments to the water column.

Processes included in the water and sediment oxygen dynamics include:

- Atmospheric exchange (Wanninkhof, 1992).
- Oxygen production and consumption through phytoplankton, macroalgae, and seagrass/macrophyte photosynthesis and respiration, respectively.
- Utilization of dissolved oxygen due to respiration of higher organisms such as zooplankton and fish and due to photosynthesis and respiration in jellyfish
- Water column consumption of oxygen during nitrification.
- Biochemical oxygen demand due to mineralization of organic matter in the water column and in the sediments.

Oxygen flux from the water column to the sediments, sediment oxygen demand (SOD), as developed from Fick's law of diffusion.

The last two processes are used together with a sediment porosity and diffusion coefficient (Ullman and Aller, 1982) in order to define the depth of the toxic layer in the sediments.

Nutrient processes included in the sediment and water column dynamics include:

- Phytoplankton nutrient uptake, with provision for luxury storage of nutrients.
- Release of dissolved inorganic nutrients from phytoplankton excretion.
- Excretion of nutrients as fecal material by zooplankton.
- Nitrification and denitrification by bacterial mediated action.

- Generation of inorganic nutrients from organic detritus.
- Transfer of nutrients through the food chain (e.g. phytoplankton--zooplankton--fish).
- Uptake of nutrients by macroalgae and seagrasses.
- Adsorption/desorption of nutrients from inorganic suspended sediments.
- Sediment/water transfer of nutrients (*via* such processes as sediment resuspension, sedimentation, redox-mediated nutrient release, and bioturbation).

In essence, CAEDYM represents the type of interactive processes that occur amongst the ecological and chemical components in the aquatic ecosystem. As a broad generalization, one component of the system cannot be manipulated or changed within the model without affecting other components of the system. Similarly in nature, changing an integral component in the aquatic system will have wide-ranging and follow-on effects on many of the other system components. CAEDYM is designed to have the complexity and flexibility to be able to handle the continuum of responses that will be elicited as components of a system that are manipulated. Thus, the model represents a valuable tool to examine responses under changed conditions, as for example, when new approaches to managing an ecosystem are adopted.

B.6 BIBLIOGRAPHY

B.6.1 Referenced in Text

Amorocho, J. and DeVries, J.J. (1980). "A new evaluation of the wind stress coefficient over water surfaces," Journal of Geophysical Research, 85:433-442.

Antenucci, Jason (2004). "Tracing Short-Circuiting Potential," from CWR Models: Bytes and Nybbles, Autumn 2004, Issue 10, page 2.

Antenucci, Jason (2004). "New Metals Model for CAEDYM," from CWR Services: Bytes and Nybbles, December 2004, Issue 11, page 1.

Appt, Jochen (January 2000), "Review on the modeling of short period internal waves in lakes with focus on Lake Constance," Pfaffenwaldring 61, D-70550 Stuttgart, Universität Stuttgart, Institut für Hydraulik und Grundwasser, Stuttgart.

Appt, J., Imberger, J., Kobus, H. (2004), "Basin-scale motion in stratified Upper Lake Constance," Limnology and Oceanography, 49(4), 919-933

Casulli, Vincenzo and Cheng, Ralph T. (1992), "Semi-implicit finite difference methods for three-dimensional shallow water flow," *International Journal for Numerical Methods in Fluids,* **15**, 629-48.

CWR, "Limnological Study of Lake Burragorang," Centre For Water Research, The University of Western Australia, Chapter 4 excerpt from report, pp. 104-126.

Hamilton, D. (1997). "An integrated ecological model for catchment hydrology and water quality for the Swan and Canning Rivers," presented at the 2nd International Symposium on Ecology and Engineering, 10-12 November 1997, Freemantle, Australia. IAHR Eco-Hydraulics section.

Hamilton, D.P. and S.G. Schladow (1997), "Prediction of water quality in lakes and reservoirs: Part I: Model description," *Ecological Modelling, 96,* 91-110.

Herzfeld, M. and Hamilton, D. (1998), "A computational aquatic ecosystem dynamics model for the Swan River," *EOS Trans. AGU*, **79**(1), Ocean Sciences Meet. Suppl. OS11P-02.

Herzfeld, M.; Hodges, B.R.; and Hamilton, D. (1998), "Modelling the Swan River on small temporal and spatial scales," The Swan Canning Estuary conference, York, Australia, Apr., 1998.

Herzfeld, M.; Hamilton, D.; and Hodges, B.R. (1997), "Reality vs. management: The role of ecological numerical models," *2nd International Symposium on Ecology and Engineering*, 10-12 November 1997, Fremantle, Australia, IAHR Eco-Hydraulics section.

Hipsey, M.R., Romero, J.R., Antenucci, J.P. and Hamilton, D. (2005) "Computational Aquatic Ecosystem Dynamics Model: CAEDYM: v2.2 Science Manual", Centre for Water Research, The University of Western Australia.

Hipsey, M.R., Romero, J.R., Antenucci, J.P. and Hamilton, D. (2005) "Computational Aquatic Ecosystem Dynamics Model: CAEDYM: v2.2 User Manual", Centre for Water Research, The University of Western Australia.

Hodges, B.R. (1998), "Hydrodynamics of differential heat absorption," *Environmental Mechanics Laboratory Seminar*, Dept. of Civil Eng., Stanford University, Feb. 1998.

Hodges, B.R. and Dallimore C (2006), "Estuary Lake and Coastal Ocean Model: ELCOM v2.2 Science Manual", Centre for Water Research, The University of Western Australia.

Hodges, B.R. and Dallimore C (2007), "Estuary Lake and Coastal Ocean Model: ELCOM v2.2 User Manual", Centre for Water Research, The University of Western Australia.

Hodges, B.R. and Herzfeld, M. (1997), "Coupling of hydrodynamics and water quality for numerical simulations of Swan River," *2nd International Symposium on Ecology and Enginnering*, 10-12 November, Fremantle, Australia, IAHR Eco-Hydraulics section.

Hodges, B.R.; Herzfeld, M.; Winters, K.; and Hamilton, D. (1998), "Coupling of hydrodynamics and water quality in numerical simulations," *EOS Trans. AGU*, **79**(1), Ocean Sciences Meet. Suppl. OS11P-01.

Hodges, B.R., Imberger, J., Saggio, A., and K. Winters (1999), "Modeling basin-scale internal waves in a stratified lake," *Limnology and Oceanography*), **45**(7), 1603-20.

Hodges, B.R., Yue, N., and Bruce, L. (May 27, 1999), "Swan River hydrodynamic model progress report," Centre For Water Research, The University of Western Australia, 14pp.

Jacquet, J. (1983). "Simulation of the thermal regime of rivers," In Orlob, G.T., editor, Mathematical Modeling of Water Quality: Streams, Lakes and Reservoirs, pages 150-176. Wiley-Interscience.

Kowalik, Z. and Murty, T.S. (1993). "Numerical Modeling of Ocean Dynamics," World Scientific.

Laval, B., Imberger, J., Hodges, B.R., and Stocker, R. (2003), "Modeling circulation in lakes: spatial and temporal variations," Limnology and Oceanography 48(3), 983-994.

Leonard, B.P. (1991), "The ULTIMATE conservative difference scheme applied to unsteady one-dimensional advection," *Computational Methods in Applied Mechanics and Engineering*, **88**, 17-74.

Lin, B. and Falconer, R.A. (1997). "Tidal flow and transport modeling using ULTIMATE QUICKEST," Journal of Hydraulic Engineering, 123:303-314.

Robson, B.J. and Hamilton, D. P. (2002). "Three-Dimensional Modeling of a Microcystis bloom event in a Western Australian Estuary." Centre For Water Research, The University of Western Australia, 491- 496 pp.

Romero, J.R. and Antenucci, J. (2004). "The Tiete River: Supply for Sao Paolo, Brazil," from CWR Models: Bytes and Nybbles, Autumn 2004, Issue 10, page 4.

Romero, J.R. and Imberger, J. (1999). "Lake Pamvotis Project-Final report", ED report WP 1364 JR, Centre for Water Research, Crawley, Western Australia, Australia.

Spigel, R.H.; Imberger, J.; and Rayner, K.N. (1986), "Modeling the diurnal mixed layer," *Limnology and Oceanography*, **31**, 533-56.

Staniforth, A. and Côté, J. (1991). "Semi-Lagrangian integration schemes for atmospheric models – a review," Monthly Weather Review, 119:2206-2223.

Stevens, C. and Imberger, J. (1996). "The initial response of a stratified lake to a surface shear stress," Journal of Fluid Mechanics, 312:39-66.

Ullman, W.J. and R.C. Aller (1982), "Diffusion coefficients in nearshore marine sediments," *Limnol. Oceanogr., 27*, 552-556.

Wanninkhof, R. (1992), "Relationship between wind speed and gas exchange over the ocean," *J. Geophys. Res., 97(C5)*, 7373-7382.

Yeates, Peter (2004). "ELCOM in the Venice Lagoon," from CWR Models: Bytes and Nybbles, Autumn 2004, Issue 10, page 2.

B.6.2 Supplemental References

(November 1999), "Course notes, Computational aquatic ecosystem dynamics model, CAEDYM, Special introduction work session," TTF/3/Nov99, Centre for Water Research, University of Western Australia, 51pp.

(January 2000), "Course notes, Estuary & lake computer model, ELCOM, Special introduction training session," TTF/3/JAN2000, Centre for Water Research, University of Western Australia, 21pp+app.

(January 21, 2000) "Instructions for the use of the graphical user interface *modeler* in the configuration & visualization of DYRESM-CAEDYM," Draft version 2, 42pp.

Antenucci, J. and Imberger, J. (1999), "Seasonal development of long internal waves in a strongly stratified lake: Lake Kinneret," *Journal of Geophysical Research* (in preparation).

Antenucci, J. and Imberger, J. (2000), "Observation of high frequency internal waves in a large stratified lake," *5th International Symposium on Stratified Flows, (ISSF5)*, Vancouver, July 2000, **1**, 271-6.

Bailey, M.B. and Hamilton, D.H. (1997), "Wind induced sediment re-suspension: a lake wide model," *Ecological Modeling*, **99**, 217-28.

Burling, M.; Pattiaratchi, C.; and Ivey, G. (1996), "Seasonal dynamics of Shark Bay, Western Australia," *3rd National AMOS Conference*, 5-7 February 1996, University of Tasmania, Hobart, 128.

Chan, C.U.; Hamilton, D.P.; and Robson, B.J. (2001), "Modeling phytoplankton succession and biomass in a seasonal West Australian estuary," *Proceedings, SIL Congress XXVIII* (in press).

Chan, T. and Hamilton, D.P. (2001), "The effect of freshwater flow on the succession and biomass of phytoplankton in a seasonal estuary," *Marine and Freshwater Research* (in press).

De Silva, I.P.D.; Imberger, J.; and Ivey, G.N. (1997), "Localized mixing due to a breaking internal wave ray at a sloping bed," *Journal of Fluid Mechanics,* **350**, 1-27.

Eckert, W.; Imberger, J.; and Saggio, A. (1999), "Biogeochemical evolution in response to physical forcing in the water column of a warm monomictic lake," *Limnology and Oceanography* (submitted).

Gersbach, G.; Pattiaratchi, C.; Pearce, A.; and Ivey, G. (1996), "The summer dynamics of the oceanography of the south-west coast of Australia – The Capes current" *3rd National AMOS Conference*, 5-7 February 1996, University of Tasmania, Hobart, 132.

Hamilton, D.P. (1996), "An ecological model of the Swan River estuary: An integrating tool for diverse ecological and physico-chemical studies," *INTECOL's V International Wetlands Conference 1996 "Wetlands for the Future,"* September 1996, Perth, Australia.

Hamilton, D.P.; Chan, T.; Hodges, B.R.; Robson, B.J.; Bath, A.J.; and Imberger, J. (1999), "Animating the interactions of physical, chemical and biological processes to understand the dynamics of the Swan River Estuary," Combined Australian-New Zealand Limnology Conference, Lake Taupo.

Hamilton, D.P. (2000), "Record summer rainfall induces first recorded major cyanobacterial bloom in the Swan River," *The Environmental Engineer*, **1**(1), 25.

Hamilton, D.; Hodges, B.; Robson, B.; and Kelsey, P. (2000), "Why a freshwater blue-green algal bloom occurred in an estuary: the Microcystis bloom in the Swan River Estuary in 2000," Western Australian Marine Science Conference 2000, Path, Western Australia.

Hamilton, D.P.; Chan, T.; Robb, M.S.; Pattiaratchi, C.B.; Herzfeld, M.; and Hodges, B. (2001), "Physical effects of artificial destratification in the upper Swan River Estuary," *Hydrological Processes*.

Heinz, G.; Imberger, J.; and Schimmele, M. (1990), "Vertical mixing in Überlinger See, western part of Lake Constance," *Aquat. Sci.*, **52**, 256-68.

Herzfeld, M. (1996), "Sea surface temperature and circulation in the Great Australian bight," Ph.D. Thesis, School of Earth Science, Flinders University, South Australia.

Herzfeld, M. and Hamilton, D. (1997), "A computational aquatic ecosystem dynamics model for the Swan River, Western Australia," *MODSIM '97, International Congress on Modeling and Simulation Proceedings,* 8-11 December, 1997, University of Tasmania, Hobart, **2**, 663-8.

Herzfeld, Michael (May 28, 1999), "Computational aquatic ecosystem dynamics model (CAEDYM), An ecological water quality model designed for coupling with hydrodynamic drivers, Programmer's guide," Centre for Water Research, The University of Western Australia, Nedlands, Australia, 133pp.

Hodges, Ben R. (July 1991), "Pressure-driven flow through an orifice for two stratified, immiscible liquids," M.S. thesis, The George Washington University, School of Engineering and Applied Science.

Hodges, Ben R. (March 1997), "Numerical simulation of nonlinear free-surface waves on a turbulent open-channel flow," Ph.D. dissertation, Stanford University, Dept. of Civil Engineering.

Hodges, Ben R. (June 9, 1998), "Heat budget and thermodynamics at a free surface: Some theory and numerical implementation (revision 1.0c)," Working manuscript, Centre for Water Research, The University of Western Australia, 14pp.

Hodges, Ben R. (1999), "Numerical techniques in CWR-ELCOM," Technical report, Centre for Water Research, The University of Western Australia. (in preparation)

Hodges, Ben R. (2000), "Recirculation and equilibrium displacement of the thermocline in a wind-driven stratified lake," *5th International Symposium on Stratified Flows, (ISSF5)*, Vancouver, July 2000, **1**, 327-30.

Hodges, B.R., Herzfeld, M., and Hamilton, D. (1998), "A computational aquatic ecosystem dynamics model for the Swan River," *EOS Trans. AGU*, **79**(1), Ocean Sciences Meet. Suppl. OS11P-02.

Hodges, B.; Herzfeld, M.; Winters, K.; and Hamilton, D. (1998), "Interactions of a surface gravity waves and a sheared turbulent current," *EOS Trans. AGU*, **79**(1), Ocean Sciences Meet. Suppl. OS53.

Hodges, B.R. and Street, R.L. (1999), "On simulation of turbulent nonlinear free-surface flow," *Journal of Computational Physics*, **151**, 425-57.

Hodges, B.R.; Imberger, J.; Laval, B.; and Appt, J. (2000), "Modeling the hydrodynamics of stratified lakes," *Fourth International conference on HydroInformatics*, Iowa Institute of Hydraulic Research, Iowa City, 23-27 July 2000.

Hodges, B.R. and Imberger, J. (2001), "Simple curvilinear method for numerical methods of open channels," *Journal of Hydraulic Engineering*, **127**(11), 949-58.

Hodges, Ben R. and Street, Robert L. (1996), "Three-dimensional, nonlinear, viscous wave interactions in a sloshing tank," *Proceedings of the Fluid Engineering Summer Meeting 1996*, Vol. **3**, FED-Vol. **238**, ASME, 361-7.

Hodges, Ben R. and Street, Robert L. (1998), "Wave-induced enstrophy and dissipation in a sheared turbulent current," *Proceedings of the Thirteenth Australian fluid Mechanics Conference*, M.C. Thompson and K. Hourigan (eds.), Monash University, Melbourne, Australia, 13-18 December 1998, Vol. **2**, 717-20.

Hodges, B.R., Street, R.L., and Zang, Y. (1996), "A method for simulation of viscous, non-linear, free-surface flows," *Twentieth Symposium on Naval Hydrodynamics*, National Academy Press, 791-809.

Hollan, E. (1998), "Large inflow-driven vortices in Lake Constance," in J. Imberger (ed.), *Physical Processes in Lakes and Oceans. Coastal and Estuarine Studies*, **54,** American Geophysical Union, 123-36.

Hollan, E.; Hamblin, P.F.; and Lehn, H. (1990), "Long-term modeling of stratification in Large Lakes: Application to Lake Constance," in: Tilzer, M.M. and C. Serruya (eds.). *Large Lakes, Ecological Structure and Function***,** Berlin: Springer Verlag, 107-24.

Horn, D.A.; Imberger, J.; and Ivey, G.N. (1999), "Internal solitary waves in lakes – a closure problem for hydrostatic models," *Proceedings of 'Aha Halikoa Hawaiian Winter Workshop*, January 19-22, 1999, University of Hawaii, Manoa.

Horn, D.A.; Imberger, J.; and Ivey, G.N. (1999), "The degeneration of large-scale interfacial gravity waves in lakes," under consideration for publication in *Journal of Fluid Mechanics*.

Horn, D.A.; Imberger, J.; Ivey, G.N.; and Redekopp, L.G. (2000), "A weakly nonlinear model of long internal waves in lakes," *5th International Symposium on Stratified Flows, (ISSF5)*, Vancouver, July 2000, **1**, 331-6.

Imberger, J. (1985), "The diurnal mixed layer," *Limnology and Oceanography,* **30**(4), 737-70.

Imberger, J. (1985), "Thermal characteristics of standing waters: an illustration of dynamic processes," *Hydrobiologia*, **125,** 7-29.

Imberger, J. (1994), "Mixing and transport in a stratified lake," Preprints of *Fourth International Stratified on Flows Symposium*, Grenoble, France, June-July 1994, **3** 1-29.

Imberger, J. (1994), "Transport processes in lakes: a review," in R. Margalef (ed.), *Limnology Now: A Paradigm of Planetary Problems,* Elsevier Science, 99-193.

Imberger, J. (1998), "Flux paths in a stratified lake: A review," in J. Imberger (ed.), *Physical Processes in Lakes and Oceans. Coastal and Estuarine Studies,* **54,** American Geophysical Union, 1-18.

Imberger, J. (1998), "How does the estuary work?" WAERF Community Forum, 25 July 1998, The University of Western Australia.

Imberger, J.; Berman, T; Christian, R.R.; Sherr, E.B.; Whitney, D.E.; Pomeroy, L.R.; Wiegert, R.G.; and Wiebe, W.J. (1983), "The influence of water motion on the distribution and transport of materials in a salt marsh estuary," *Limnology and Oceanography*, **28**, 201-14.

Imberger, J. and Hamblin, P.F. (1982), "Dynamics of lakes, reservoirs, and cooling ponds," *Journal of Fluid Mechanics,* **14**, 153-87.

Imberger, J. and Head, R. (1994), "Measurement of turbulent properties in a natural system," reprinted from *Fundamentals and Advancements in Hydraulic Measurements and Experimentation*.

Imberger, J. and Ivey, G.N. (1991), "On the nature of turbulence in a stratified fluid. Part II: Application to lakes," *Journal of Physical Oceanography,* **21**(5), 659-80.

Imberger, J. and Ivey, G.N. (1993), "Boundary mixing in stratified reservoirs," *Journal of Fluid Mechanics,* **248**, 477-91.

Imberger, J. and Patterson, J.C. (1981), "A dynamic reservoir simulation model – DYRESM: 5," In H.B. Fischer (ed.) *Transport Models for Inland and Coastal Waters,* Academic Press, 310-61.

Imberger, J. and Patterson, J.C. (1990), "Physical limnology," In: *Advances in Applied Mechanics,* **27**, 303-475.

Ivey, G.N. and Corcos, G.M. (1982), "Boundary mixing in a stratified fluid," *Journal of Fluid Mechanics,* **121**, 1-26.

Ivey, G.N. and Imberger, J. (1991), "On the nature of turbulence in a stratified fluid. Part I: The energetics of mixing," *Journal of Physical Oceanography,* **21**(5), 650-8.

Ivey, G.N.; Imberger, J.; and Koseff, J.R. (1998), "Buoyancy fluxes in a stratified fluid," in J. Imberger (ed.), *Physical Processes in Lakes and Oceans. Coastal and Estuarine Studies,* **54,** American Geophysical Union, 377-88.

Ivey, G.N.; Taylor, J.R.; and Coates, M.J. (1995), "Convectively driven mixed layer growth in a rotating, stratified fluid," *Deep-Sea Research I.,* **42**(3), 331-49.

Ivey, G.N.; Winters, K.B; and De Silva; I.P.D. (1998), "Turbulent mixing in an internal wave energized benthic boundary layer on a slope," submitted to *Journal of Fluid Mechanics*.

Jandaghi Alaee, M.; Pattiaratchi, C.; and Ivey, G. (1996), "The three-dimensional structure of an island wake," *8th International Biennial Conference. Physics of Estuaries and coastal Seas (PECS)* 9-11 September 1996, the Netherlands, 177-9.

Javam, A; Teoh, S.G.; Imberger, J.; and Ivey, G.N. (1998), "Two intersecting internal wave rays: a comparison between numerical and laboratory results," in J. Imberger (ed.), *Physical Processes in Lakes and Oceans. Coastal and Estuarine Studies*, **54,** American Geophysical Union, 241-50.

Kurup, R.; Hamilton, D.P.; and Patterson, J.C. (1998), "Modeling the effects of seasonal flow variations on the position of a salt wedge in a microtidal estuary," Estuarine Coastal *and Shelf Science*, **47**(2), 191-208.

Kurup, R.G.; Hamilton, D.P.; and Phillips, R.L. (2000), "Comparison of two 2-dimensional, laterally averaged hydrodynamic model applications to the Swan River Estuary," *Mathematics and Computers in Simulation*, **51**(6), 627-39.

Laval, B.; Hodges, B.R.; and Imberger, J. (2000), "Numerical diffusion in stratified lake," *5th International Symposium on Stratified Flows, (ISSF5)*, Vancouver, July 2000, **1**, 343-8.

Lemckert, C. and Imberger, J. (1995), "Turbulent benthic boundary layers in fresh water lakes," Iutam Symposium on Physical Limnology, Broome, Australia, 409-22.

Maiss, M.; Imberger, J.; and Münnich, K.O. (1994), "Vertical mixing in Überlingersee (Lake Constance) traced by SF6 and heat," *Aquat. Sci.*, **56**(4), 329-47.

Michallet, H. and Ivey, G.N. (1999), "Experiments on mixing due to internal solitary waves breaking on uniform slopes," *Journal of Geophysical Research*, **104**, 13467-78.

Nishri, A; Eckert, W.; Ostrovosky, I.; Geifman, J.; Hadas, O.; Malinsky-Rushansky, N.; Erez, J.; and Imberger, J. (1999), "The physical regime and the respective biogeochemical processes in Lake Kinneret lower water mass," *Limnology and Oceanography*, (in press).

Ogihara, Y.; Zic, K.; Imberger, J.; and Armfield, S. (1996), "A parametric numerical model for lake hydrodynamics," *Ecological Modeling*, **86**, 271-6.

Patterson, J.C; Hamblin, P.F.; and Imberger, J. (1984), "Classification and dynamic simulation of the vertical density structure of lakes," *Limnology and Oceanography*, **29**(4), 845-61.

Pattiaratchi, C.; Backhaus, J.; Abu Shamleh, B.; Jandaghi Alaee, M.; Burling, M.; Gersbach, G.; Pang, D.; and Ranasinghe, R. (1996), "Application of a three-dimensional numerical model for the study of coastal phenomena in south-western Australia," *Proceedings of the Ocean & Atmosphere Pacific International Conference*, Adelaide, October 1995, 282-7.

Riley, G.A., H. Stommel and D.F. Bumpus, "Quantitative ecology of the plankton of the Western North Atlantic," *Bull. Bingham Oceanogr. Coll., 12(3)*, 1-69, 1949.

Robson, B.J.; Hamilton, D.P.; Hodges, B.R.; and Kelsey, P. (2000), "Record summer rainfall induces a freshwater cyanobacterial bloom in the Swan River Estuary," *Australian Limnology Society Annual Congress*, Darwin, 2000.

Saggio, A. and Imberger, J. (1998), "Internal wave weather in a stratified lake," *Limnology and Oceanography*, **43**, 1780-95.

Schladow, S.G. (1993), "Lake destratification by bubble-plume systems: Design methodology," *Journal of Hydraulic Engineering*, **119**(3), 350-69.

Smagorinsky, J. (1963) "General circulation experiments with the primitive equations, ´*Monthly Weather Review, 91*, 99-152.

Spigel, R.H. and Imberger, J. (1980), "The classification of mixed-layer dynamics in lakes of small to medium size," *Journal of Physical Oceanography*, **10**, 1104-21.

Steele, J.H. (1962), "Environmental control of phytosynthesis in the sea," *Limnol. Oceanogr., 7*, 137-150.

Taylor, J.R. (1993), "Turbulence and mixing in the boundary layer generated by shoaling internal waves," *Dynamics of Atmospheres and Oceans*, **19**, 233-58.

Thorpe, S.A. (1995), "Some dynamical effects of the sloping sides of lakes," *IUTAM Symposium on Physical Limnology*, Broome, Australia, 215-30.

Thorpe, S.A. (1998), "Some dynamical effects of internal waves and the sloping sides of lakes," in J. Imberger (ed.), *Physical Processes in Lakes and Oceans. Coastal and Estuarine Studies*, **54,** American Geophysical Union, 441-60.

Thorpe, S.A. and Lemmin, U. (1999), "Internal waves and temperature fronts on slops," *Annales Geophysicae*, **17**(9), 1227-34.

Unlauf, L; Wang, Y.; and Hutter, K. (1999), "Comparing two topography-Following primitive equation models for lake circulation," *Journal of Computational Physics*, **153**, 638-59.

Winter, K.B. and Seim, H.E. (1998), "The role of dissipation and mixing in exchange flow through a contracting channel," submitted to *Journal of Fluid Mechanics*.

Winter, K.B.; Seim, H.E.; and Finnigan, T.D. (1998), "Simulation of non-hydrostatic, density-stratified flow in irregular domains," submitted to *International Journal of Numerical Methods in Fluids*.

Zhu, S. and Imberger, J. (1994) "A three-dimensional numerical model of the response of the Australian North West Shelf to tropical cyclones," in: *J. Austral. Math. Soc. Ser.*, **B 36,** 64-100.